



MONASH University



The University of
Nottingham

Kinetic studies of dopamine D₂ receptor molecular pharmacology

Alastair Charles Keen
BSci (Hons), MSci (Biotech)

A thesis submitted for the degree of Doctor of Philosophy at Monash University and the
University of Nottingham in 2020

Drug Discovery Biology / Cell Signalling

Copyright notice

© Alastair Charles Keen (2020).

I certify that I have made all reasonable efforts to secure copyright permissions for third-party content included in this thesis and have not knowingly added copyright content to my work without the owner's permission.

Contents

Copyright notice	2
Abstract.....	8
Publications during enrolment	10
Thesis including published works declaration	11
Acknowledgements	13
Abbreviations.....	15
Chapter 1: General introduction	17
1.1 G protein-coupled receptors	18
1.1.1 GPCR classification and architecture	18
1.1.2 GPCR signalling.....	19
1.1.3 GPCR regulation and G protein independent signalling.....	22
1.2 Ligand binding kinetics at GPCRs	25
1.2.1 The importance of ligand binding kinetics.....	25
1.2.2 Molecular determinants of ligand binding kinetics.....	26
1.3 Biased agonism	28
1.3.1 General introduction	28
1.3.2 Quantification of biased agonism	29
1.3.3 The influence of binding kinetics on observations of biased agonism	32
1.4 The dopamine D ₂ receptor.....	34
1.4.1 Background.....	34
1.4.2 Dopamine D ₂ receptor expression.....	35
1.4.3 Dopamine D ₂ receptor physiological functions.....	36
1.4.4 High resolution D ₂ -like structures	36
1.4.5 Molecular determinants of ligand binding at the dopamine D ₂ receptor	37
1.4.6 Dopamine D ₂ receptor G protein signalling.....	38
1.4.7 D ₂ R regulation and G protein-independent signalling	40
1.5 The dopamine D ₂ receptor in Schizophrenia.....	40
1.5.1 Dopamine hypothesis of schizophrenia	40
1.5.2 Antipsychotic drugs	41
1.5.3 The potential of biased agonism within the dopamine hypothesis	42
1.5.4 The role of D ₂ R-ligand binding kinetics in Schizophrenia.....	43
1.6 The dopamine D ₂ receptor in Parkinson's disease.....	44
1.6.1 Background.....	44
1.6.2 Pathogenesis	44
1.6.3 Current treatment.....	45
1.6.4 Scope for improving D ₂ R targeted therapy	46
1.7 Scope of thesis	48

Chapter 2: Towards characterisation of dopamine D ₂ receptor ligand binding pathways through kinetic studies on receptor mutants	50
Abstract	51
2.1 Introduction.....	52
2.2 Methods	55
Materials	55
Mutagenesis	56
Stable cell line production	56
Terbium cryptate labelling	57
Membrane preparation.....	57
HTRF kinetic binding assay	57
Data analysis	58
2.3 Results	59
Determination of ligand kinetics at the wild-type D ₂ R	59
The Trp100 ^{EL1} Ala mutation markedly impacts ligand binding kinetics.....	62
The effects of the Leu94 ^{2.64} Ala mutation and the Trp100 ^{EL1} Ala mutation show similarities	67
No large consequences in ligand binding kinetics are caused by an Ile184 ^{EL2} Ala mutation.....	69
Some ligand's association kinetics can be influenced by a Tyr379 ^{7.35} Ala mutation.....	71
2.4 Discussion	72
2.5 Supplementary Materials	78
Chapter 3: A systematic exploration of the relationship between agonist binding kinetics and observations of biased agonism at dopamine D ₂ receptor proximal signalling events	80
Abstract	81
3.1 Introduction.....	82
3.2 Methods	85
Materials	85
Kinetic binding assays.....	85
Cell culture.....	85
G protein activation	85
GRK2 and arrestin recruitment.....	87
Trafficking	87
Data analysis	88
3.3 Results	89
Measurement of the binding kinetics of agonists at the D ₂ R.....	89
Functional characterisation of agonist action over time	92
Slow agonist dissociation is not essential for an increase in potency over time.....	95
Quantitative assessment of agonist action at a single timepoint at proximal functional events	97

No clear relationship between biased agonism and differences in agonist dissociation rate	110
Assessment of agonist induced D ₂ R trafficking over time	112
Agonist efficacy for G protein activation, GRK2 recruitment, β -arrestin-2 recruitment and receptor trafficking correlates	114
3.4 Discussion	117
3.5 Supplementary Materials	123
Chapter 4: New phospho-site-specific antibodies to unravel the role of GRK phosphorylation in dopamine D ₂ receptor regulation and its modulation by biased agonists	135
Abstract	137
4.1 Introduction	138
4.2 Methods	139
Plasmids	139
Antibodies	140
Drugs	141
Cell culture and transfection	141
Small interfering RNA (siRNA) silencing of gene expression	141
Western blotting analysis	142
G protein activation assay	142
Membrane potential assay	143
GRK2 and β -arrestin-2 recruitment	143
Data Analysis	144
4.3 Results	145
The development of novel phospho-site-specific antibodies for the D ₂ R	145
GRKs 2 & 3 phosphorylate Ser317/Thr318 and enhance β -arrestin-2 recruitment	146
Ser317/Thr318 phosphorylation occurs rapidly after D ₂ R activation	149
D ₂ R agonists vary broadly in their ability to stimulate the recruitment of GRK2, phosphorylation of Ser317/Thr318 and recruitment of β -arrestin-2	150
A putative arrestin-biased agonist displays robust activity in measurements of G protein signalling	154
Analysis of signalling data using an operational model of agonism allows quantitative evaluation of bias between G protein and regulatory events	157
4.4 Discussion	161
Acknowledgements	165
Funding	165
Author contributions	165
Conflict of Interest	165
4.5 Supplementary Materials	166
Chapter 5: Evidence for kinetically distinct dopamine D ₂ receptor G protein signalling waves	171
Abstract	172

5.1 Introduction.....	173
5.2 Methods	174
Materials	174
Mutagenesis	175
Cell culture and transfection.....	175
G protein activation assay	176
cAMP inhibition assay	177
Western blotting analysis	177
Data analysis	178
5.3 Results	178
Monitoring G protein activation at the D ₂ R	178
Temporal patterns of G protein activation change depending on the agonist and the G α subunit.....	181
G α subunit-specific cAMP inhibition reflects G protein activation	182
Observed G protein activation rate at the D ₂ R is influenced by agonist efficacy	184
G α_z remains active for an extended period.....	186
The unique signalling pattern of G α_z is dependent on serine 42.....	188
A mutation that decreases the GTP hydrolysis rate of G α_{i2} confers changes in agonist potency over time.....	190
Co-expression of RGS proteins alters agonist potency over time.....	192
5.4 Discussion	194
5.5 Supplementary Materials	199
Chapter 6: A pertussis toxin-like protein tool for occluding inhibitory G protein signalling including G α_z	201
Abstract.....	202
6.1 Introduction.....	203
6.2 Methods	205
Materials	205
Plasmids	206
Cell culture	206
Transfection	207
G protein activation	207
cAMP production inhibition.....	208
Arrestin recruitment.....	209
Data analysis	209
6.3 Results	209
OZITX treatment abolishes GPCR mediated activation of all G α_i subfamily members, including G α_z	209
G α_{i2} , G α_{oA} and G α_z mediated cAMP production inhibition is inhibited by OZITX.....	212
OZITX does not ablate G α_s , G α_q or G α_{12} subfamily coupling.....	213

The active A subunit of OZITX can be transfected into mammalian cells to act as an inhibitor	216
Gα _i subunits can be made OZITX insensitive.....	217
6.4 Discussion	218
6.5 Supplementary Materials	223
Chapter 7: General Discussion	226
References	236
Appendix 1: Molecular determinants of the intrinsic efficacy of the antipsychotic aripiprazole	262
Appendix 2: Distinct inactive conformations of the dopamine D2 and D3 receptors correspond to different extents of inverse agonism	308

Abstract

The dopamine D₂ receptor (D₂R) is a G protein-coupled receptor (GPCR) that is the primary target of drugs treating the symptoms of Parkinson's disease and schizophrenia. However, drugs acting at the D₂R to manage these diseases often display efficacy for only a subset of their symptoms and have poor side effect profiles. Therefore, it is desirable to rationally design drugs that better manage disease symptoms and reduce side effects. This would be greatly aided by gaining a detailed understanding of the kinetic aspects of D₂R ligand binding, signalling, regulation and trafficking.

Differences in binding kinetics at the D₂R results in varying side effect profiles between antipsychotics. In chapter 2, a time resolved-fluorescence resonance energy transfer competition kinetic ligand binding assay is optimised at the D₂R. The assay is used in combination with D₂R mutants to determine the contribution of selected residues in the extracellular regions of the D₂R in modulating binding kinetic association and dissociation rates. Findings showed that different residues in this region are important determinants of binding kinetics in a ligand-dependent manner.

Some agonists with slow dissociation rates have been shown to display apparent biased agonism at the D₂R. In chapter 3, it is investigated whether the length of time an agonist binds the D₂R influences observations of biased agonism. Within the selected panel of ligands, for which both binding kinetic rates and functional effects were determined, no clear relationship between agonist dissociation rate and apparent biased agonism could be established.

D₂R G protein signalling is regulated through phosphorylation by G protein receptor kinases (GRKs). In chapter 4, antibodies specific for GRK2/3 phosphorylation sites on the D₂R were generated and characterised. A GRK2/3 phosphorylation site within intracellular loop 3 was identified that is phosphorylated on agonist activation of the D₂R. Phosphorylation of this site predicts arrestin recruitment. Measurements of D₂R phosphorylation were included with other measurements of G protein activation and receptor regulation to profile selected D₂R agonists.

The D₂R can couple pleiotropically to G proteins of the G $\alpha_{i/o}$ subfamily. In chapter 5 the kinetics of D₂R mediated activation of individual G $\alpha_{i/o}$ protein subtypes was investigated. Increases in agonist potency were observed when the D₂R activated G α_z . This was shown to be dependent on the slow guanosine triphosphate (GTP) hydrolysis rate of G α_z by either

mutation of serine 42 within the GTP binding site or co-expression with regulator of G protein signalling 20.

Investigating GPCR and D₂R biased agonism in the relevant cell type has been challenging due to the lack of molecular tools. A useful method for interrogating GPCR signalling functions is using bacterially derived toxins, such as pertussis toxin, to inhibit their coupling and then evaluate the downstream changes. In chapter 6 we developed a new pertussis toxin-like protein tool that can inhibit all of the G $\alpha_{i/o}$ subfamily, including G α_z . Ga subunits that are insensitive to the toxin were characterised to serve as tools in combination with the toxin.

Finally, chapter 7 discusses the key implications of the findings in the context of the current literature and future research recommendations.

Publications during enrolment

Klein Herenbrink, C., Verma, R., Lim, H. D., Kopinathan, A., **Keen, A. C.**, Shonberg, J., Draper-Joyce, C. J., Scammells, P. J., Christopoulos, A., Javitch, J. A., Capuano, B., Shi, L., and Lane, J. R. (2019) Molecular Determinants of the Intrinsic Efficacy of the Antipsychotic Aripiprazole. *ACS Chemical Biology* 14, 1780-1792

Lane, J. R., Abramyan, A. M., Adhikari, P., **Keen, A. C.**, Lee, K.-H., Sanchez, J., Verma, R. K., Lim, H. D., Yano, H., and Javitch, J. A. (2020) Distinct inactive conformations of the dopamine D₂ and D₃ receptors correspond to different extents of inverse agonism. *eLife* 9, e52189

Thesis including published works declaration

I hereby declare that this thesis contains no material which has been accepted for the award of any other degree or diploma at any university or equivalent institution and that, to the best of my knowledge and belief, this thesis contains no material previously published or written by another person, except where due reference is made in the text of the thesis.

This thesis includes no original papers published in peer reviewed journals and one submitted publications. The core theme of the thesis is dopamine D₂ receptor molecular pharmacology. The ideas, development and writing up of all the papers in the thesis were the principal responsibility of myself, the student, working within Drug Discovery Biology under the supervision of A/Prof. J. Robert Lane, Prof. Steven Charlton & Dr. Daniel Scott.

The inclusion of co-authors reflects the fact that the work came from active collaboration between researchers and acknowledges input into team-based research.

In the case of Chapter 4 my contribution to the work involved the following:

Thesis Chapter	Publication Title	Status	Nature and % of student contribution	Co-author name(s) Nature and % of Co-author's contribution*	Co-author(s), Monash student
Chapter 4	New phospho-site-specific antibodies to unravel the role of GRK phosphorylation in dopamine D ₂ receptor regulation and its modulation by biased agonists	Submitted	Designed experiments, acquired data, analysed data, wrote first draft of manuscript and subsequent input - 50%	AM designed experiments, acquired data, wrote manuscript - 12.5% HM acquired data - 2% PD acquired data, analysed data - 2% JAJ reviewed and edited manuscript - 1% MC reviewed and edited manuscript - 5% SS designed experiments, reviewed and edited manuscript - 10% JRL designed experiments, analysed data, wrote manuscript, reviewed and edited manuscript - 17.5%	No co-authors are Monash students

I have renumbered sections of submitted or published papers in order to generate a consistent presentation within the thesis.

Student name: Alastair Charles Keen

Student signature:

Date: 14/5/2020

I hereby certify that the above declaration correctly reflects the nature and extent of the student's and co-authors' contributions to this work. In instances where I am not the responsible author I have consulted with the responsible author to agree on the respective contributions of the authors.

Main Supervisor name: Dr. Daniel J. Scott

Main Supervisor signature:

Date: 14/5/2020

Acknowledgements

To my primary supervisor A/Prof. J. Robert Lane, thank you so much for your consistent intellectual mentorship throughout the whole PhD - even when in different countries. I also have appreciated your kindness and the fact that you ask awesome scientific questions.

To my co-supervisors Dr. Daniel J. Scott and Prof. Steven J. Charlton, thank you for your huge commitment and enduring support.

I would like to thank my panel members, Prof. Meritxell Canals, Dr. Michelle Halls, Prof. MacDonald Christie and Dr. Angus Johnston, for practical advice and engaging questions at the many panel meetings.

I greatly appreciate all our collaborators; this would never have been done without all of you. Dr. David Sykes for acquiring some the kinetic binding data in chapter 3. Prof. Stefan Schultz and his laboratory members for their expertise and data in the phosphorylation site antibody manuscript in chapter 4. Dr. Benjamin Capuano, Dr. Anita Yates and Dr. Timothy Fyfe for their insight in laboratory meetings and synthesis of compounds. I would also like to acknowledge Prof. Jonathan Javitch and Dr. Maria Hauge Pederson for experiments and guidance in chapter 6. Prof. Lei Shi for molecular modelling and discussions.

I would like to acknowledge the past and present members of my immediate laboratory, Dr. Herman Lim, Dr. Chris Draper-Joyce, Dr. Carmen Klein-Herenbrink, Dr. Arisbel Batista Gondin, Dr. Julie Sanchez, Dr. Amy Chen, Dr. Srgjan Chivchiristov. Each one of these people have helped me tremendously both directly in laboratory techniques as well as in developing general research ideas.

I would like to acknowledge the wider drug discovery biology colleagues and friends. Dr. Quynh Mai, Dr. Alice Berizzi, Dr. Eevon Moo, Dr. Sheng Yu Ang, Dr. Saori Mukaida, Lachlan Chlydesdale, Dr. Thomas Coudrat, Dr. Pradeep Rajeskhari, Samantha McNeill and the Neurogenic Mechanisms laboratory group for being great companions in this journey.

I would like to acknowledge the Nottingham Cell Signalling group. Dr. Elizabeth Rosethorne, Dr. Maxine Roberts, Jack Lochray, Desislava Nesheva, Nicola Dijon, Dr. Chloe Peach, Hannah Comfort, Charles Lay, Lydia Ogrodzinski, Edward Wragg, Dr. Nick Holliday, Dr. Laura Kilpatrick, Dr. Mark Soave, Dr. Joelle Goulding, Prof. Steve Hill for taking me in and keeping my morale high all the time!

The people from the Florey institute when I conducted my honours year. I have you all to thank for getting me started on this great journey. Prof. Ross Bathgate, Dr. Bradley Hoare, Dr. Kelvin Yong, Dr. Fabian Bumbak, Sharan Layfield, Tania Ferraro, Riley Cridge and Dr. Nick Smith.

I wish to acknowledge the Wurundjeri people, the traditional custodians of the land where I was able to do most of my fun experiments.

Finally, I would like to thank my family and friends for your support through the last four years. Especially to Naomie Young for just being there for me.

This research was supported by an Australian Government Research Training Program (RTP) Scholarship

Abbreviations

β_2 AR	β_2 adrenergic receptor
ANOVA	analysis of variance
ADP	adenosine diphosphate
ACTH	adrenocorticotrophic hormone
AP-2	adaptor protein-2
AT ₁ R	Angiotensin II receptor 1
ATP	adenosine triphosphate
BRET	bioluminescence resonance energy transfer
cAMP	cyclic adenosine monophosphate
CAMYEL	cAMP sensor using YFP-Epac-RLuc
CTX	Cholera toxin
D ₂ R	dopamine D ₂ receptor
DA	dopamine
DAMGO	(D-Ala ² , N-Me-Phe ⁴ , Gly-ol ⁵)-enkephalin
DNA	deoxyribonucleic acid
DMEM	Dulbecco's modified eagle medium
EL/ECL	extracellular loop
ET _A R	endothelin A receptor
FBS	Foetal bovine serum
FSK	forskolin
GAP	GTPase activating protein
G protein	heterotrimeric GTP binding protein
GDP	guanosine diphosphate
GEF	guanine nucleotide exchange factor
GIRK	G protein-coupled inwardly rectifying potassium channel
GPCR	G protein coupled receptor
GRK	G protein-protein coupled receptor kinase
GTP	guanosine triphosphate
HEK	human embryonic kidney
HBSS	Hank's balanced salt solution

IL/ICL – intracellular loop
M₂R – muscarinic acetylcholine receptor 2
MAP – mitogen activated protein
MOPR – μ opioid receptor
NLuc – Nano-luciferase
NT8-13 – neurotensin peptide residues 8 to 13
NTS₁R – neurotensin receptor 1
OZITX – $G\alpha_o$, $G\alpha_z$ and $G\alpha_i$ inhibiting toxin
PBS – phosphate buffered saline
PEI – polyethylenimine
PTX – pertussis toxin
RGS – regulator of G protein signalling
RLuc – Renilla luciferase
RNA – ribonucleic acid
SEM – standard error from the mean
TM – transmembrane domain
TR-FRET – time-resolved fluorescence resonance energy transfer
WT – wild type

Chapter 1:

General introduction

1.1 G protein-coupled receptors

1.1.1 GPCR classification and architecture

G protein coupled receptors (GPCRs) are integral membrane proteins consisting of seven α -helical transmembrane domains (TMs) connected by three intracellular loops (ICL1-3) and three extracellular loops (ECL1-3). The topology of GPCRs is such that the amino-terminus is directed into the extracellular space and the transmembrane domains snake through the membrane with the carboxy-terminus oriented into the cytosol (1). GPCRs are generally localised to the cell surface where they serve as the main mechanism for mammals to carry extracellular messages across the plasma membrane and into the cell. GPCRs do this by being activated by diverse agonists, including neurotransmitters, peptides, hormones or light photons in the case of the GPCR rhodopsin, and subsequently transducing signals intracellularly via coupling to heterotrimeric GTP-binding (G) proteins. Due to this ability, GPCRs are harnessed as the targets of around 30% of currently approved therapeutics (2).

GPCRs represent one of the largest protein superfamilies encoding over 800 different human proteins (3). They are classified phylogenetically into five major families that are the rhodopsin, secretin, adhesion, glutamate and frizzled/taste2 families (Fig.1.1) (4). Each of the GPCRs share common characteristics and structural features within their respective families. The rhodopsin family are the largest family of GPCRs within the human genome. Being the largest family of GPCRs, most approved GPCR drugs target the rhodopsin family (5). This family is generally identified by having a ligand binding site located within the TMs to bind small neurotransmitters or peptides (Fig. 1.1). Moreover, there are fifteen members of the secretin family and these can be defined by their extracellular hormone binding domain of around 70 amino acid residues (Fig. 1.1) (5). The secretin family GPCRs use their hormone binding domain to bind different agonist polypeptides such as parathyroid hormone (PTH), calcitonin and vasoactive intestinal polypeptide (VIP). The adhesion family earn their name by often binding molecules in the extracellular matrix appearing to play an adhesive role. Due to these functions, they usually have very long and richly glycosylated amino-termini. In addition, they are distinguished by a GPCR proteolytic site (GPS) motif as well as often containing several other common protein domains within their amino-terminus (4). The glutamate family differ from other GPCR families by their amino-terminal venus flytrap domain that is used to bind agonists and translate the signal through their cysteine-rich domain into the TMs (6). Another characteristic of the glutamate family is their quaternary structure as obligate dimers (Fig 1.1) (6). The frizzled/taste2 family consist of the smoothened receptor, the frizzled

receptors activated by their Wnt glycoprotein agonists and important in development, and the taste 2 subfamily of receptors that widely function as bitter taste receptors (5).

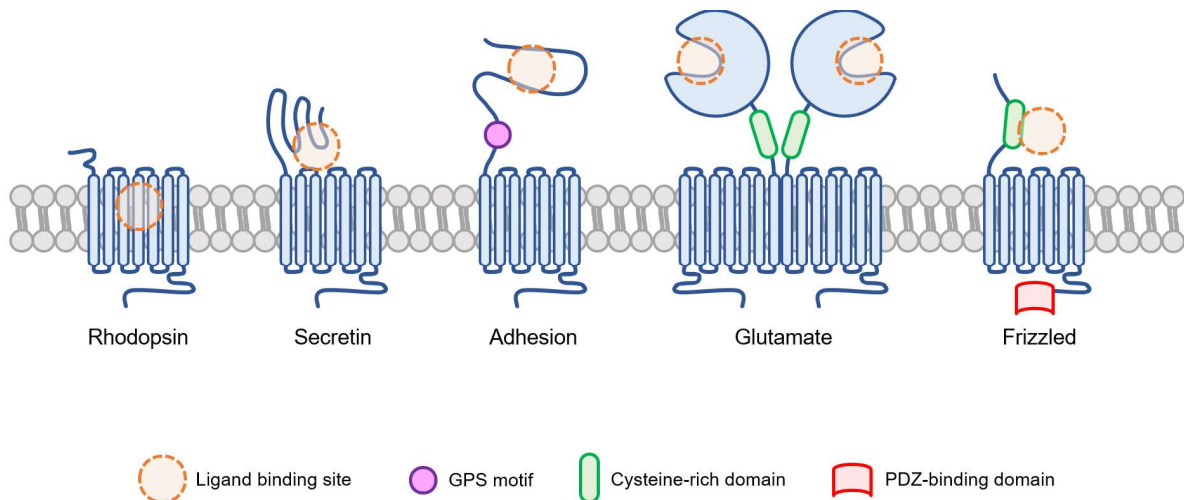


Figure 1.1: Structural differences between GPCR classes.

1.1.2 GPCR signalling

Activation of a GPCR by an agonist results in a conformational change in the TM bundle. The most noticeable structural change upon GPCR activation is the outward movement of intracellular end of TM VI (Fig. 1.2A & B). TM V also moves in concert with TMVI as well as smaller changes and rotations in the other TMs, resulting in an opening of the intracellular TM core of the GPCR (7). This then permits coupling of heterotrimeric G proteins (G proteins). G proteins are comprised of a $G\alpha$ subunit that binds guanine nucleotides and a $G\beta$ and $G\gamma$ subunit that function together as a single entity. The $G\alpha$ subunit is composed of an α -helical domain and a ras-like domain whereas the $G\beta$ subunit contains a β -propeller domain (Fig. 1.2B). Upon coupling, the G protein makes key interactions with the $G\alpha$'s carboxy-terminal $\alpha 5$ helix extending into the intracellular TM core of the GPCR (Fig. 1.2B) (8,9). Having bound a heterotrimeric G protein, the GPCR then has the function of a guanine nucleotide exchange factor (GEF) acting on the $G\alpha$ subunit of the G protein whereby the $G\alpha$ subunit exchanges its bound guanine diphosphate (GDP) for guanine triphosphate (GTP) (Fig. 1.3). This results in the $G\alpha$ subunit transitioning to an active conformation which dissociates from, or rearranges relative to, the $G\beta\gamma$ complex (10,11). Once active, the $G\alpha$ subunit and $G\beta\gamma$ complex can then further activate downstream signalling cascades. When the G protein subunits dissociate to bind downstream effectors, they allow access for other heterotrimeric G proteins to the active GPCR again which can be activated. Furthermore, the $G\alpha$ subunit has native GTPase activity that permits the $G\alpha$ subunit to exist in an active conformation for an amount of time before its

GTP is hydrolysed back to GDP (Fig. 1.3). Thus, the now-inactive $G\alpha$ subunit is capable of re-associating with free $G\beta\gamma$ complexes. This means that the G protein heterotrimer is re-formed and can bind again to the active GPCR to start the signalling cycle again (for review see (12)). Furthermore, the G protein cycle can be accelerated by regulators of G protein signalling (RGS) proteins that act as GTPase activating proteins (GAPs) on the active $G\alpha$ subunit to increase the rate of GTP-hydrolysis (13).

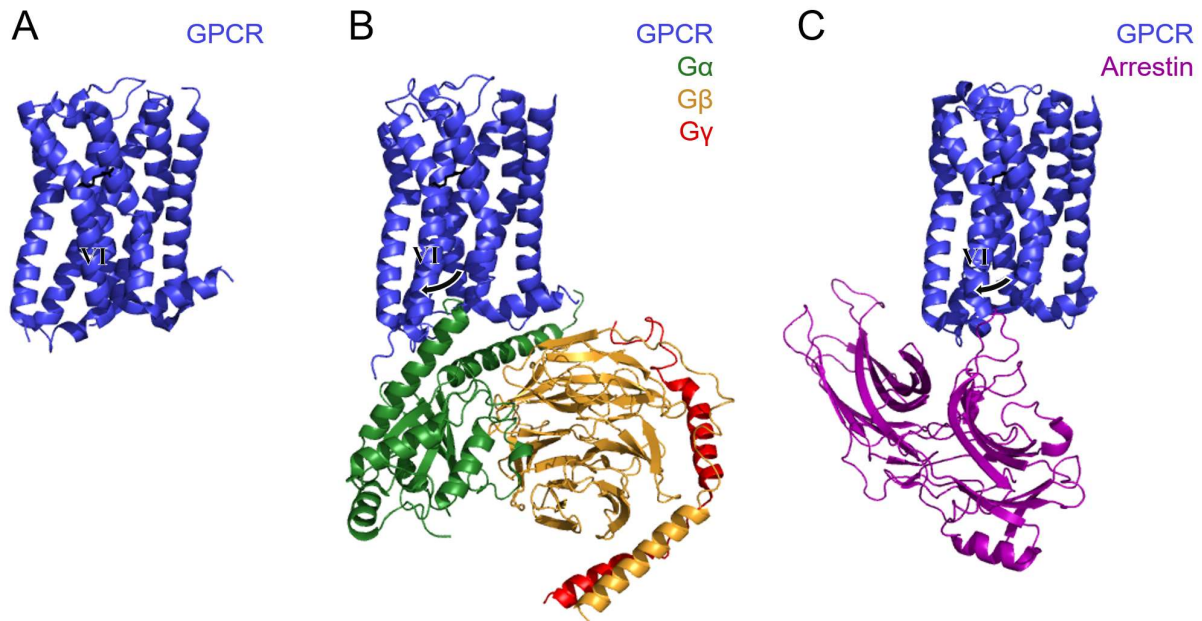


Figure 1.2: Atomic structures of an inactive GPCR, an active G protein-bound GPCR and an arrestin-bound GPCR. (A) Inactive structure of a GPCR – the M_2R . The bottom of transmembrane helix VI is positioned in towards the centre of the protein occluding effector coupling. (PDB code: 3UON) (B) Active structure of a GPCR (the M_2R) bound to a G protein heterotrimer. TM VI moves outwards (black arrow) upon activation, opening the intracellular side of the receptor. The $\alpha 5$ helix of the $G\alpha$ subunit interacts with the intracellular core of the transmembrane domains of the GPCR. The M_2R is bound to $G\alpha_{oA}\beta_1\gamma_2$. (PDB code: 6OIK). (C) Active structure of the M_2R bound to β arrestin-1. TM VI is rotated outwards relative to the inactive structure (black arrow). The finger loop of the arrestin protein engages the intracellular core of the transmembrane domains of the GPCR. (PDB code: 6U1N). M_2R is shown in blue cartoons, $G\alpha_{oA}$ is shown in green cartoons, $G\beta_1$ is shown in orange cartoons, $G\gamma_2$ is shown in red cartoons and β arrestin-1 is shown in purple cartoons.

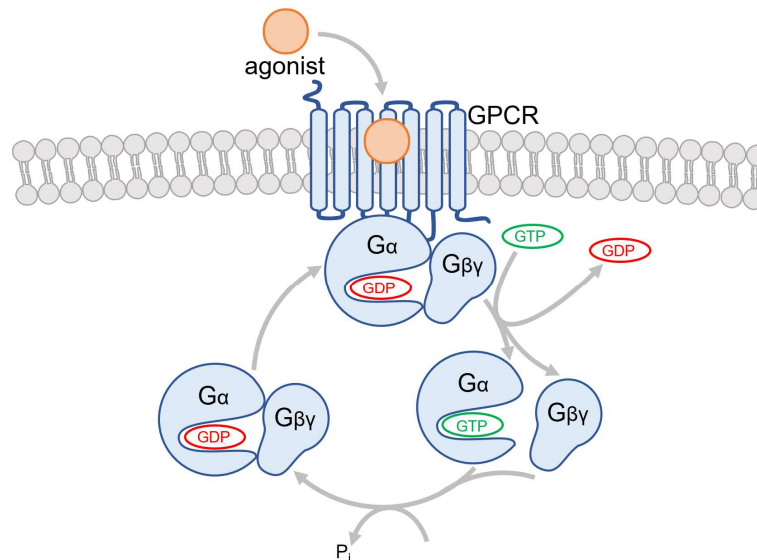


Figure 1.3: Schematic of the G protein cycle. An agonist binds and activates a GPCR. The active GPCR can then bind a heterotrimeric G protein. The heterotrimeric G protein consists of a $G\beta\gamma$ dimer subunit and $G\alpha$ subunit that binds guanine nucleotides. The G protein is initially in its inactive conformation and bound to GDP. Upon G protein coupling, the GPCR promotes the exchange of the bound GDP for GTP and also permits the separation, or rearrangement, of the active GTP bound $G\alpha$ subunit and the $G\beta\gamma$ subunit. The G protein signalling is then terminated when the active $G\alpha$ subunit hydrolyses its GTP back to GDP and the inactive GDP bound $G\alpha$ subunit re-associates with $G\beta\gamma$. The cycle can then begin again by the inactive heterotrimeric G protein recoupling to the GPCR.

There are a huge variety of possible heterotrimeric G protein combinations as there are sixteen different $G\alpha$ subunits, six different $G\beta$ subunits and twelve different $G\gamma$ subunits encoded in the human genome (14). The different $G\alpha$ subunits are categorised into four subfamilies ($G\alpha_{i/o}$, $G\alpha_{s/olf}$, $G\alpha_{q/11}$ and $G\alpha_{12/13}$) and each subfamily often activates the same secondary messengers. The $G\alpha_{s/olf}$ subfamily activates adenylate cyclases that catalyse the production of cyclic adenosine monophosphate (cAMP), $G\alpha_{i/o}$ subunits inhibit adenylate cyclase activation which results in a reduction in cytosolic cAMP (15), an activated $G\alpha_{q/11}$ subunit binds to phospholipase C- β leading to an increase in intracellular Ca^{2+} levels (16) and $G\alpha_{12/13}$ subunits cause activation of Rho guanine nucleotide exchange factors (RhoGEFs) which activate RhoA (17). The $G\alpha_{i/o}$ subfamily is the largest $G\alpha$ subfamily, consisting of $G\alpha_{i1}$, $G\alpha_{i2}$, $G\alpha_{i3}$, $G\alpha_o$, $G\alpha_z$ and also the taste and visual $G\alpha$ subunits; $G\alpha_{gust}$, $G\alpha_{t1}$ and $G\alpha_{t2}$ (18). Members within the $G\alpha_{i/o}$ subfamily can be ADP-ribosylated by pertussis toxin rendering them unable to couple to GPCRs. However, it should be noted that $G\alpha_z$ is insensitive to PTX as it lacks the conserved cysteine substrate site (19). Moreover, after G protein activation the $G\beta\gamma$ subunit is also capable of acting on downstream effectors. For example, different $G\beta\gamma$ subunits can modulate voltage-gated calcium channels, G protein coupled inwardly rectifying potassium (GIRK) channels and particular adenylate cyclases (14). Overall, the specificity of a GPCR for

different G proteins will determine the G proteins that are activated and hence the downstream responses that are mediated within the cell.

1.1.3 GPCR regulation and G protein independent signalling

Once GPCRs are activated, numerous proteins are involved in regulating a GPCR's signalling response over time and within distinct intracellular domains. After having coupled to G proteins, many GPCRs are phosphorylated on the carboxy-terminal tail or ICL3 by a family of serine/threonine kinases called G protein-coupled receptor kinases (GRKs) (Fig. 1.3A & B). There are a total of seven GRKs (GRK1-7) in the human genome with GRK2 and 3 being the most widely expressed in the body (20). Other serine/threonine kinases such as protein kinase C (PKC) can also phosphorylate some GPCRs to regulate their function. Following binding and phosphorylation by a GRK, the negatively charged phosphorylation sites on the GPCR can be recognised by members from the arrestin family, that comprises β -arrestin-1 (arrestin-2), β -arrestin-2 (arrestin-3) and also the visual arrestins, arrestin-1 and arrestin-4. (Fig. 1.3C). Arrestins are structurally characterised by two domains, each containing seven β -strands that form curved lobes (Fig. 1.2C) (21). When arrestins are initially recruited, the phosphorylated carboxy-tail of the GPCR binds to a crevice within the curved amino-terminal domain of the arrestin. Subsequently, arrestins compete with G proteins by binding via their finger loop to an overlapping site located within the intracellular side of the GPCR's TM bundle (Fig 1.2C) (22,23). It is through this competition and steric occlusion of G proteins that β -arrestins earned their name on account of the initial discovery in their ability to *arrest* the signalling of the β_2 -adrenergic receptor (β_2 AR) (24). Furthermore, having bound to the GPCR, arrestins can serve as recruiters of the adapter protein AP-2 which can then allow access of clathrin to mediate budding of a clathrin-coated pit (25,26). Subsequently, dynamin is recruited to enable endocytosis of the GPCR by "pinching off" the clathrin coated pit from the plasma membrane to form an endocytic vesicle. Following this, GPCRs generally follow two distinct pathways: GPCRs can be trafficked from early endosomes into late endosomes and then lysosomes where they are degraded, or, GPCRs can enter recycling endosomes where they are trafficked back to the cell surface (27). While the former trafficking pathway leads to a sustained termination of the GPCR signal until new protein is translated, the latter trafficking pathway is important for rapid re-sensitisation of the GPCR.

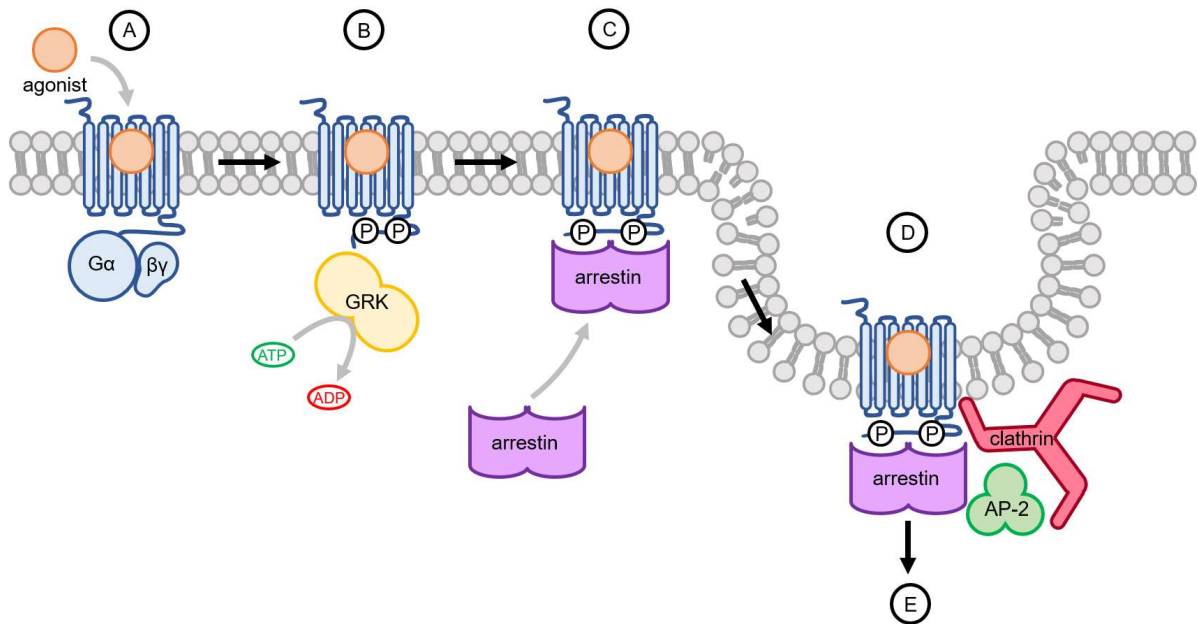


Figure 1.3: Arrestin mediated endocytosis of GPCRs. (A) GPCRs are activated upon agonist binding permitting their coupling to heterotrimeric G proteins producing a downstream signalling response. (B) GPCRs are then phosphorylated on their intracellular loops and carboxy-tail by GRKs. (C) Phosphorylation by GRKs allows recruitment of arrestins to the intracellular side that sterically hinder the coupling of G proteins. (D) Arrestins then allow the recruitment of the adaptor protein-2 (AP-2) followed by clathrin and dynamin which enable endocytosis of the GPCR. (E) GPCRs are then internalised into endosomes where they are either recycled back to the cell surface or it trafficked into lysosomes where they are degraded.

GPCR trafficking is generally associated with desensitisation or re-sensitisation, however, trafficking can also be employed by the cell to elicit the desired signalling outcome. It is now appreciated that GPCRs can be trafficked to particular endocytic compartments where they can continue to signal from after having internalised. These observations have brought about the area of compartmentalised signalling at GPCRs whereby different responses may be elicited from a GPCR depending on the cellular localisation of the GPCR. Such compartmentalised signalling has been heavily investigated in regions such as endosomes, specific membrane microdomains and the nucleus (28-30).

Of the different non-canonical intracellular signalling compartments, endosomes are the most well appreciated compartment to mediate the signalling of GPCRs. Some of the first evidence of endosomal G protein signalling came from observations of prolonged G protein dependent responses from the sphingosine-1 phosphate (S1P₁) receptor, parathyroid hormone (PTH1) receptor and thyrotropin (TSH) receptor (31-33). The prolonged responses mediated by these GPCRs were either sustained or only partially reversed after agonist washout or addition of a competing antagonist. Importantly, it was shown that G protein responses could be abolished using inhibitors of endocytosis (32). Indicating that agonist internalised GPCRs

can mediate responses and hence that GPCRs can have additional G protein signalling waves after their initial acute plasma membrane localised signalling. Furthermore, direct visual evidence of active GPCRs in internal endomembrane compartments has also been confirmed. To demonstrate this, researchers made use of nanobodies that were initially developed to stabilise active conformations of GPCRs for structural studies and repurposed these into biosensors. By tagging these different biosensors with GFP, they were able to sense the active state of GPCRs in live cells via fluorescence microscopy. It could be observed upon agonist addition that β_2 AR can be activated in endosomes, and, using a different nanobody, that the μ opioid receptor (MOPR) can be activated on endosomes and the golgi apparatus (29,34).

Upon activation, GPCRs can also couple to other proteins to initiate G protein independent signalling. Some of the most intensely studied proteins involved in G protein independent signalling are arrestins. Once arrestins have recruited and activated, they are thought to be capable of scaffolding to enhance existing signalling processes or, potentially, to mediate their own signalling events (35,36). This arrestin-dependent signalling may often occur from internal endocytic compartments. Arrestins can act as signalling scaffolds to recruit and activate several proteins such as mitogen activated protein (MAP) kinases including extracellular signal related kinase (ERK) 1/2 and c-Jun N-terminal kinases (JNKs) (37). There are now known to be over one hundred different proteins that can interact with the non-visual arrestins, many of which are known cellular signalling transducers (38). Moreover, GRKs are activated by GPCRs and can serve as signalling molecules eliciting further effects (39). In addition to kinase domains, GRKs possess other domains to elicit or modify signalling. For example, the GRK2/3 family contain an RGS domain and pleckstrin homology (PH) domain that can modulate $G\alpha_q$ subunits and $G\beta\gamma$ respectively (39).

GPCRs can exist in pre-formed complexes with scaffolding proteins and effector proteins, termed signalosomes, that are primed to elicit a response to an agonist. Some of the first evidence of GPCRs existing in a signalosome was as early as 1978 suggesting GPCR can complex with adenylate cyclase (40). Such signalosomes have been extensively studied at several GPCRs such as the dopamine D_4 receptor (D_4R) and the relaxin family peptide receptor 1 (RXFP1) (41,42). There is also increasing documentation of the propensity of GPCRs to form homodimers, including at the dopamine D_2 receptor (D_2R) (43,44). GPCRs may also form heterodimers with other GPCRs. One of the most well studied class A GPCR heterodimers to date is the canonical D_2R dimer consisting of the D_2R and the adenosine A_{2A} receptor ($A_{2A}R$). Multiple levels of experimental evidence support the idea of D_2R - $A_{2A}R$ heterodimers. Early work showed that activation of the $A_{2A}R$ modulates the affinity of ligands at the D_2R ; indicating

allosteric interactions between the two receptors (45). Subsequently, biophysical studies using FRET and BRET techniques further supported the existence of D₂R-A_{2A}R dimers (46). Ex vivo and in vivo studies have also confirmed both the presence and the functional role of D₂R-A_{2A}R dimers in the striatum (47,48). In addition, there has been a considerable amount of research into the existence and functional importance of D₂R - neurotensin receptor 1 (NTS₁R) heterodimers as well as D₂R – dopamine D₁ receptor (D₁R) heterodimers (49-51).

1.2 Ligand binding kinetics at GPCRs

1.2.1 The importance of ligand binding kinetics

Ligands binding a protein, such as a GPCR, have an association rate and a dissociation rate for the protein that are denoted k_{on} (M⁻¹ s⁻¹) and k_{off} (s⁻¹) respectively. These two rates at equilibrium determine the binding affinity of the ligand for the protein, which is given by the dissociation constant (K_d) that is defined by the following equation:

(1.1)

$$K_d = \frac{k_{off}}{k_{on}}, (nM)$$

This is the concentration of the ligand required to occupy half of the proteins (GPCRs) at equilibrium. Pharmacologists often use this number when describing the avidity with which a ligand binds to a GPCR. This is important as the affinity of a ligand lead is often increased through medicinal chemistry in the drug discovery process because a consequential potency increase in vivo is predicted. This process is commonly referred to as determining structure-activity relationships (SAR). However, the affinity (or dissociation constant (K_d)) may be a poor predictor of drug action as the concentration in vivo will be in a constant flux governed by processes such as dosing regime, hepatic clearance and membrane absorption. Hence, the drug is unlikely to reach equilibrium in the target tissue or compartment (52). Therefore, a drug's kinetic binding rate parameters may better predict its in vivo activity. Indeed, both the association rate and dissociation rate can shape the pharmacodynamics and micro-pharmacokinetics of the drug (53-57).

The dissociation rate is important as it determines the lifetime of the ligand-GPCR complex. The lifetime of the ligand-GPCR complex can also be termed the residence time (RT) of the ligand for the protein, (58) which is given by:

(1.2)

$$RT = \frac{1}{k_{off}}, (s)$$

This measure is useful as a drug only elicits its effects when bound to the GPCR. The residence time can also be expressed as the half-life of the ligand-receptor complex ($t_{1/2}$) which is given by $\ln 2/k_{\text{off}}$. As mentioned above, the residence time or $t_{1/2}$ may be a better predictor of in vivo drug efficacy. This is because at non-equilibrium conditions such as when drugs are rapidly cleared in the body, a drug's action may be prolonged by having a long residence time. In agreement with this, the prolonged duration of action of candesartan at the angiotensin II receptor 1 (AT₁R) is thought to be due to its slow dissociation from the receptor (59). Similarly, slow dissociation, or prolonged residence, time may sometimes contribute to the sustained signalling of agonists acting at their receptors (60).

The ligand association rate is also an equally important consideration in lead optimisation. The association rate can contribute to rebinding, where rebinding is the ability of a ligand to remain in a close vicinity with the GPCR after having dissociated such that it cannot escape and therefore is more likely to re-associate with the receptor (54). Consequently, the association rate, similar to the dissociation rate, can increase the target occupancy by effectively prolonging the lifetime of the interaction. This occurs particularly in instances when rebinding effects are more pronounced in a tissue compartment that has reduced diffusion such as a synapse (55,61).

1.2.2 Molecular determinants of ligand binding kinetics

Understanding the molecular determinants of binding kinetic rates is important so that one can tailor a small molecule to have the desired binding kinetics. Miller and colleagues (62), collated data from over 2000 distinct compounds and showed that some common features broadly influence ligand binding kinetics at all proteins. Particularly, ligands that slowly associate were found to often have a slow dissociation rate. They additionally presented a correlation between the drug size and the residence time of the ligand-protein complex. However, simply increasing the molecular weight of a compound will have reduced penetration in vivo. Therefore, information specifically regarding the molecular determinants of each GPCR's ligand kinetics are required to rationally modulate drug efficacy and potency. Yet, studies investigating GPCR-ligand binding have been historically dominated by performing mutagenesis around a proposed binding site and subsequent assessment of the equilibrium affinity. Although these studies have given insight into the amino acid residues that govern the orthosteric site, they provide no understanding of the influence these residues have on the rate of ligand association or dissociation. While reports investigating structure kinetics relationships (SKR) on drugs that bind GPCRs are increasing, only a handful of studies have

thoroughly explored this to date. Of note, a report investigating the binding kinetics of ZM241385 derivatives to the adenosine A_{2A} receptor (A_{2A}R), identified that some derivatives displayed markedly different dissociation rates while having very little change in binding affinity (63). Another study at the prostanoid DP₂ receptor showed that the orientation of a hydrogen bond acceptor positioned at the tail of antagonists was critical for extending the dissociation rate (64). Together these studies demonstrated that association and dissociation rates can be adjusted based on structure.

Technical advances have led to a rapid expansion in the number of GPCR x-ray crystal and cryo-electron microscopy structures being reported. These structures are only capable of providing static or averaged poses of the particular ligand bound. Nonetheless, the structures of GPCRs have provided useful data for molecular modellers to investigate the molecular basis of ligand binding kinetics at different GPCRs. In doing so, Dror and colleagues (65), provided the first evidence that GPCRs can contain an extracellular vestibule that makes initial contacts with the ligand before it traverses into the deep binding pocket between the TMs. This work also showed that the initial binding of the drug to the extracellular vestibule was enabled through dehydration of the residues on the extracellular vestibule. This ‘de-solvation’ presented the largest energy barrier to overcome for binding to occur, surprisingly larger than any subsequent process occurring before entry into the final binding pose. Additionally, the crystal structures of the muscarinic acetylcholine M₂ receptor and M₃ receptors (M₂R and M₃R) allowed for indirect information on ligand binding kinetics via molecular dynamics simulations (66,67). The two crystal structures were unable to provide a mechanism as to why tiotropium displays a residence time of 34.7h at the M₃R but only 3.6h at the M₂R (68), as the M₂R and M₃R structures exhibited a highly conserved orthosteric binding site for the co-crystallised antagonists. However, by using the crystal structures to perform virtual ligand dissociation dynamics experiments, it was observed that ECL2 of the M₂R displays increased flexibility which allows key residues to rotate, opening an exit for tiotropium to dissociate more readily than at the M₃R. Soon after, Tautermann *et al* (69) followed up these observations with more extensive wet lab binding experiments and molecular simulations to thoroughly map the residues important in determining tiotropium’s dissociation rate.

1.3 Biased agonism

1.3.1 General introduction

Biased agonism is the phenomenon of one agonist that acts to preferentially activate one signalling pathway more than another signalling pathway relative to another agonist at the same receptor (70) (Fig. 1.5). It is widely accepted that GPCRs are capable of existing in multiple conformational states (71,72). Hence, having this natural capability, biased ligands are thought to act via stabilising distinct states of the GPCR. The different conformational states then presumably lead to the differential coupling of heterotrimeric G proteins or other effectors (e.g. arrestins) and thus lead to signalling pathways being activated to different extents. Therefore, biased agonism can be explained through allostery at a GPCR (73) if one envisions a biased agonist acting allosterically to modulate a GPCR into distinct conformations that translate through to its “primary” intracellular G protein binding site to have different abilities to bind or activate G proteins and other intracellular effectors. Among some of the evidence showing the structural allosteric basis as the mechanism of bias are studies on the μ -opioid receptor (MOPR) (74), β 2AR (75), AT1R (76) and the serotonin 5-HT_{2B} receptor (77).

The appeal of signalling bias is novel drugs can be designed which are highly targeted as they only activate the specific signalling pathways that are desired. For example, drugs such as morphine for acute pain relief target the MOPR, however their use is associated with severe adverse effects including respiratory depression, analgesic tolerance, hyperalgesia, constipation, and addiction. In the late 1990s it was shown that knockout mice that lacked the β -arrestin-2 (arrestin-3) subtype displayed enhanced morphine-induced analgesia but attenuated tolerance, respiratory depression and constipation suggesting that β -arrestin-2 mediated signaling underlies these adverse effects (78). This suggested when the MOPR is activated by these drugs, it is the signalling through arrestins that leads to these limiting side effects. This infers that the best pain relief drugs may be ones that are biased towards activating G proteins but negligibly recruit arrestins. This finding stimulated efforts to identify biased MOPR agonists that would activate G protein but not arrestin pathways as safer analgesics. One such apparent G protein biased ligand, TRV130, developed by the biotechnology company Trevena Inc. was reported to have an improved pre-clinical profile over morphine and underwent clinical trials in treating moderate to severe acute pain (79). Other biased MOPR agonists have been identified but remain experimental compounds (80,81).

Recent contradictory reports, however, suggest that the abuse potential of these drugs is similar to morphine and that they can still cause respiratory depression and constipation (82).

Further, morphine was found to induce respiratory depression, constipation and withdrawal in a mouse in which the MOPR was replaced by a mutant MOPR that cannot activate β -arrestin-2 (83). Finally, a more recent study using the β -arrestin-2 knockout mouse found that morphine could still cause respiratory depression in a manner indistinguishable from that observed for the wild-type (84). This illustrates that the clinical development of these biased agonists is challenging because it remains unclear how distinct downstream signalling pathways in different MOPR expressing cells and tissues control the therapeutic and adverse physiological effects of opioid analgesics. Determining which signalling pathways need to be activated and to what magnitude to have the desired physiological outcome is a major hurdle that the field faces (85).

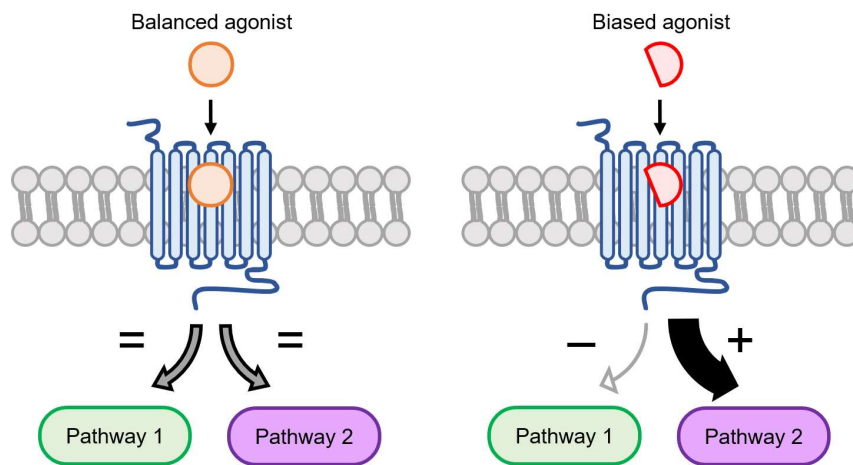


Figure 1.5: GPCR biased agonism. The balanced agonist (orange) binds the GPCR (blue), inducing an active conformation or conformations that lead to even relative activation of signalling pathways one and two. The biased agonist (red) is a chemically distinct agonist that binds and stimulates the same GPCR, yet, it preferentially activates signalling pathway two more so than pathway one (relative to the balanced agonist). By activating signalling pathways to different extents, the biased agonist produces a unique downstream cellular and physiological response.

1.3.2 Quantification of biased agonism

To determine whether an agonist displays bias, it is essential to have robust methods to quantify biased agonism. Measuring biased agonism is usually conducted by accurately detecting multiple signalling pathways in cellular assays, constructing concentration-response curves (Fig. 1.6A), fitting the data to a suitable model to quantify agonist action and then comparing to determine relative efficiency with which an agonist activates a particular pathway relative to another. While there are many methods for quantifying biased agonism, the most common is to use a method based on an operational model of agonism proposed by Black and Leff (86) to derive ratios of the agonists' efficacy (τ) and functional affinity (K_A), and then

compare the ratios between agonists. The equation re-arranged to fit to functional data is defined below:

(1.3)

$$E = \frac{E_m \tau^n [A]^n}{([A] + K_A)^n + \tau^n [A]^n}$$

Where, E is the pharmacological effect (or response), E_m is the maximal effect (or maximal response) of the system, τ is termed the transducer ratio and is the agonist's operational efficacy which is comprised of the receptor density ($[R_t]$) divided by the intrinsic efficacy (K_E) of the agonist at the particular signalling pathway; $[R_t]/K_E$, $[A]$ is the agonist concentration, K_A is the agonist's dissociation constant for the receptor when acting at the particular signalling effector/pathway, and, n is the slope of the transducer function that links the agonist's concentration to pharmacological effect (or response).

The transducer slope (n) and the maximal effect (E_m) are shared by all agonists. Therefore, parameters describing the agonist activity at a particular signalling pathway include both the functional affinity (K_A) and the operational efficacy (τ) values. These values are usually, combined into a ratio called the transduction coefficient ($\text{Log}(\tau/K_A)$) (Fig. 1.6B) (87). Importantly, the transduction coefficients need to be normalised to a reference agonist before attempting to determine bias. This is because the transduction coefficient incorporates the differences in the coupling efficiency, cell type and signalling effector stoichiometry (system bias) as well as differences in the sensitivity and assay conditions (observational bias). Accordingly, an agonist is chosen to be the reference agonist and its transduction coefficient is subtracted from the agonists of interest in that particular pathway to determine their relative transduction coefficient ($\Delta \text{Log}(\tau/K_A)$) (Fig. 1.6C). A further normalisation can then be made between two pathways of interest to graphically assess biased agonism as $\Delta\Delta\text{Log}(\tau/K_A)$ values between the two desired pathways (Fig. 1.6D).

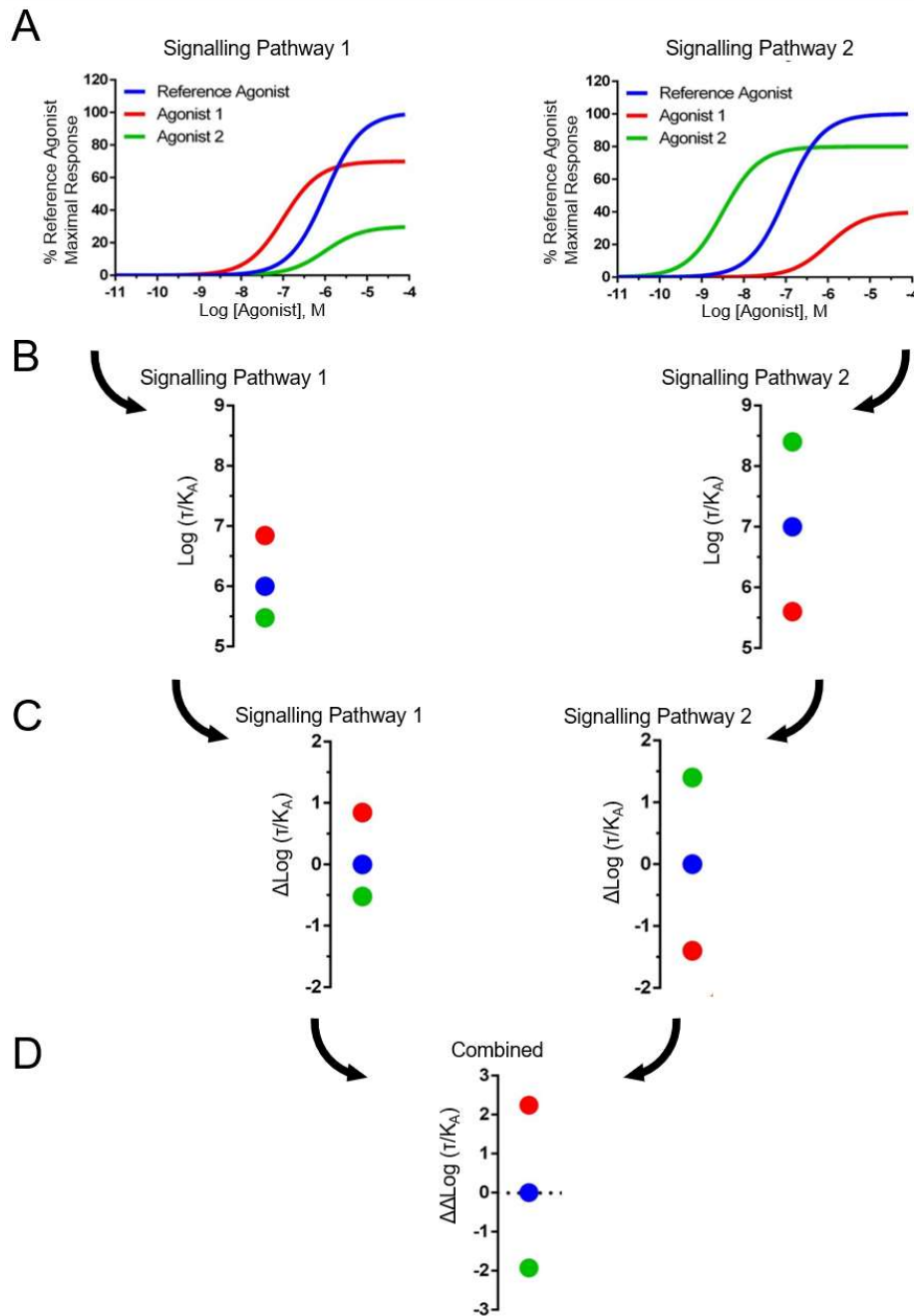


Figure 1.6: Biased agonism quantification based on the Black-Leff operational model. (A) Agonist concentration response curves are determined for two separate signalling pathways or endpoints. Note that agonist 1 (red) is more potent and efficacious than agonist 2 (green) in signalling pathway 1, however, this pattern is reversed in signalling pathway 2. (B) Agonist concentration response curves are fit to the operational model equation described in detail above to determine the $\text{Log}(\tau/K_A)$ values (also called transduction coefficients). (C). The $\text{Log}(\tau/K_A)$ values of the reference agonist (shown in blue) from each signalling pathway are subtracted from the corresponding $\text{Log}(\tau/K_A)$ values of the other agonists of interest to give $\Delta\text{Log}(\tau/K_A)$ values. (D) The $\Delta\text{Log}(\tau/K_A)$ values of one signalling pathway are subtracted from another signalling pathway to determine the $\Delta\Delta\text{Log}(\tau/K_A)$ values (also called LogBias). Shown here, agonist 1 is biased towards signalling pathway 1 whereas agonist 2 is biased towards signalling pathway 2 – importantly the bias is all relative to the reference agonist.

1.3.3 The influence of binding kinetics on observations of biased agonism

A key feature of allosteric communication is the ability of one ligand to modulate the affinity of the other. Likewise, a change in the binding kinetics at a receptor may indicate a change in the conformational state of that receptor such that the ligand has a different affinity for this state. For example, Birdsong et al. (88) showed that after prolonged agonist exposure to the MOPR, the binding affinity of the receptor for agonists is increased. This suggests that pre-exposing the receptor to an agonist may allow intracellular effectors to couple to the receptor, resulting in different conformational states being stabilised. In addition, a group was able to decrease the rate of dissociation of ligands by titrating in the concentration of G proteins to a purified receptor system (89), thus showing that increasing the concentration of proteins which interact with the GPCR will allosterically modulate the GPCR in vitro. These studies indicate that the kinetics of both the agonist and the effector at the receptor have a fundamental part in determining the response together. While the studies showing this are relatively recent, the concept that ligand binding kinetics can influence efficacy is not new. Indeed, one of the classic models of pharmacological action is Paton's rate "theory of drug action" (90). Paton used different drugs on guinea-pig intestine and observed that their response onset rate was proportional to the magnitude of their response. It was therefore postulated that the a drug's intrinsic efficacy would be proportional to the number of agonist-receptor interactions and as such, dependent on the association rate (90). Contrasting with Paton's rate theory are many other studies demonstrating the opposite relationship. Studies at the M₃R from two separate groups have shown that agonists with an increased residence time display increased agonist efficacy assessed at multiple endpoints (91,92). Similar findings have also been observed at the A_{2A}R and the α_{2A} -adrenoreceptor (93,94). Additionally, the β_2 AR agonist C26, displayed higher efficacy than adrenaline and isoprenaline which was thought to be due to its extended residence time (95). While these reports are elegant, overall the relationship between agonist binding kinetics and its influence on signalling efficacy remain incomplete.

Our group recently extended these studies from kinetic studies on efficacy to kinetic studies on biased agonism. Interestingly, we reported that the kinetics of agonists can also lead to observations of apparent biased agonism (96). This was an important step for the field because distinct agonist-induced conformations are generally the assumed to be the molecular mechanism of biased agonism when examining pharmacological data. However, without any direct structural evidence this assumption may be problematic because biased agonism observations can occur through system bias, observational bias or potentially other molecular

mechanisms (87). Furthermore, our finding was exemplified at the dopamine D2 receptor (D₂R) whereby agonists with different dissociation rates, meaning different agonist-GPCR residence times, displayed biased agonism between different pathways in a manner that changed over time. Depending on the pathway being measured, agonists with a fast dissociation rate such as dopamine and ropinirole either displayed no change in potency over time or a decrease in potency over time. In contrast, agonists with slower dissociation rates such as bifeprunox exhibited a concomitant increase in potency over time due to an increase in receptor occupancy over time. Therefore, one would presume that differences in receptor occupancy between distinct pathways would result in bias between pathways. Yet, while the apparent bias emerged from slow dissociating agonists relative to fast dissociating agonists, the bias was not entirely due to changes in receptor occupancy over time. Therefore, Klein-Herenbrink et al. (96) suggested that the interplay between the agonist binding kinetics, the kinetics of signalling and the kinetics of the regulatory processes all are responsible for the apparent bias. Following this work, other reports have followed examining the relationship between agonist binding kinetics and biased agonism. It appears that at some serotonin receptors arrestin recruitment, but not G protein mediated pathways, can be altered by changing the drugs binding kinetics through receptor mutagenesis (97). In addition, neuropeptide Y₁ receptor biased agonists appear to increase the relative lifetime of the G protein with the GPCR and by doing so impart their G protein bias relative to arrestins (98). Overall, these reports can lead one to hypothesise that agonists with a slow dissociation rate or extended residence time could permit different effectors, such as G proteins or arrestins, to engage the receptor for different amounts of time through inducing a different conformational landscape in the GPCR for an extended amount period and thus produce biased agonism (Fig. 1.7). Certainly, more evidence is required including studies on more distinct ligands and pathways in order to determine whether biased agonism through this mechanism can occur.

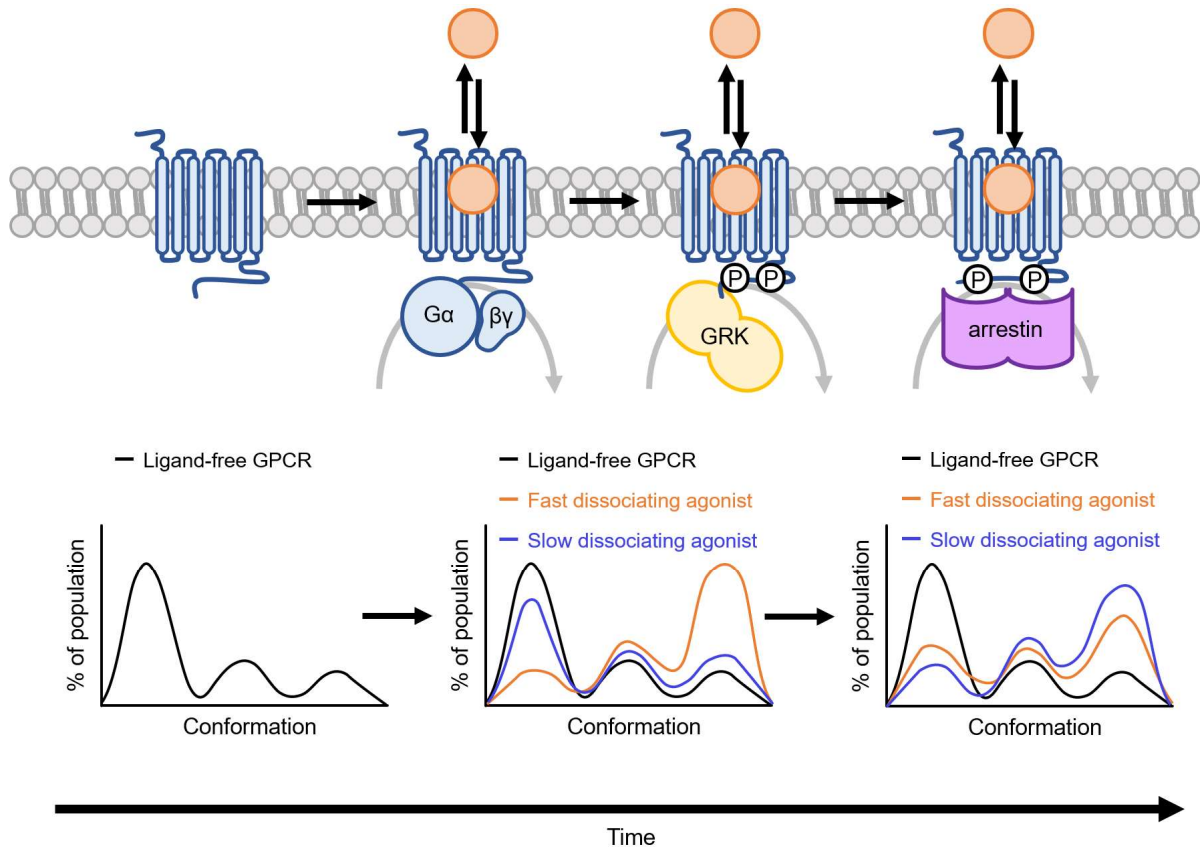


Figure 1.7: A potential mechanism of kinetic bias at a GPCR. GPCR's can constantly sample multiple different conformations. Upon binding of an agonist, the agonist will induce the GPCR to exist in different conformational ensembles that have increased propensity to bind and activate downstream effectors. Agonists can have differing dissociation rates that determine the lifetime of the drug-receptor complex or residence time. An agonist with a slow dissociation rate may allow the receptor to remain in active conformations for an extended period as it has a long residence time. This in turn could lead to the ability of the GPCR to engage distinct G proteins, regulatory proteins or other effectors over time or engage these proteins for differing amounts of time. Subsequently, the GPCR will then explore a different repertoire of active conformations by engaging these proteins differently. (Figure adapted from Klein-Herenbrink et al. (96)).

1.4 The dopamine D₂ receptor

1.4.1 Background

The dopamine D₂ receptor (D₂R) is a constituent of a subfamily of five closely related GPCRs (D₁-D₅) within the broader rhodopsin (Class A) family of GPCRs. Receptors within the dopamine receptor subfamily share the monoamine dopamine as their endogenous agonist and thus have many similarities to other rhodopsin family monoamine receptors such as the adrenergic, histamine and serotonin receptors. The dopamine D₁ and D₅ receptors are termed the D₁-like receptors and are coupled to the G $\alpha_{s/olf}$ subfamily of G proteins that stimulate adenylate cyclases. The D₂-like receptors comprise the D₂, D₃ and D₄ receptors that couple to

inhibitory $G\alpha_{i/o}$ subfamily G proteins. Interestingly, the two D₁-like receptors are encoded by a single exon whereas the D₂-like receptor genes consist of multiple exons and introns, allowing for translation of multiple isoforms due to alternative splicing (99). There are two splice variants of the D₂R, termed D₂ short isoform (D_{2s}R) and D₂ long isoform (D_{2L}R), the D_{2s}R lacks 29 amino acid residues in ICL3 compared to the D_{2L}R and acts as an presynaptically autoreceptor (100,101). The D₂R differs from most GPCRs in that it has no carboxy-terminal tail but instead has a very large ICL3. This large ICL3 is thought to reproduce the functions of the carboxy-tail in other GPCRs (102). The D₂R has the widest expression in the central nervous system and modulates most of the effects of dopamine in the brain (103). Moreover, the D₂R is the most intensely investigated dopamine receptor for drug discovery. The D₂R is a key target for Parkinson's disease, schizophrenia, restless legs syndrome, hyperprolactinaemia, depression, nausea and bipolar disorder (103-107).

1.4.2 Dopamine D₂ receptor expression

The D₂R has an extensive expression pattern in the central nervous system (CNS) and more restricted expression in the peripheral nervous system and other tissues. Of note, expression of the D₂R has often been determined using radioligand binding or immunodetection, both of which are subject to cross-reactivity with other D₂-like receptors. Nonetheless, the D₂R is most abundant in the central nervous system where it is enriched in the striatum, the olfactory tubercle and nucleus accumbens (108,109). Within the striatum, D₂Rs are located on medium spiny neurons (MSNs). More moderate labelling of the D₂R has also been observed in many other brain regions including the substantia nigra pars compacta, olfactory bulb, superior colliculus and subthalamic nucleus (103,110). In addition, the D₂R is expressed in smaller regions including the retina and arcuate nucleus (103). As is the case for all dopamine receptors, the majority of D₂-like receptors are found on non-dopamine neurons (103,109). Moreover, Jang and colleagues (111), demonstrated in the substantia nigra pars compacta, that most expression of the D₂R is the long isoform (D_{2L}R) as opposed to the presynaptic D_{2s}R (101). Furthermore, the D₂R is also expressed in some endocrine tissues including the anterior pituitary and pancreatic β -cells (108,112). The D₂R also appears to be expressed in the gut, for example, expression has been identified in the enteric nervous system of mice (113). Moreover, in rats, it has been determined by immunofluorescence and reverse transcription-polymerase chain reaction that the D₂R is present in the gastric mucosa (114). The D₂R has further been documented in the lymphocytes, implicating it in immune system function (115).

1.4.3 Dopamine D₂ receptor physiological functions

The most heavily investigated physiological functions of the D₂R are those mediated by D₂Rs expressed in different dopamine pathways in the CNS. Some examples of D₂R functions include locomotor responses, motivation, cognition, reward behaviours, temperature regulation, learning and sexual behaviour. Many of these D₂R functions are often overlapping with other dopamine receptors or dependent on their activity.

One of the best characterised D₂R functions is its role in locomotor activity. While locomotor activity is also regulated by the D₁R and D₃R, activation of the D₂R has the largest effect (110). Specifically, activation of presynaptic D₂R autoreceptors, that regulate dopamine release by dopaminergic neurons, by drugs of abuse such as amphetamine and cocaine produce a reduction in the locomotion (103). In contrast, post-synaptic D₂Rs oppose these functions and stimulate locomotor responses. Post-synaptic receptors generally activate signalling at higher concentrations than autoreceptors, therefore, locomotor activity can often be dependent on the concentration of the agonist. Moreover, learning and memory retention are also an important functions driven by the D₂R. D₂-like subtype selective agonists increase memory consolidation and subtype selective antagonists impairing this process (116). However, a similar relationship is also observed for the D₁R. Drug reward is a neurobiological process associated with memory that is also influenced by the D₂R. Mice lacking the D₂R display a reduced preference to seek and consume ethanol (117). These types of process do not appear to be limited to addictive drugs and may be extended to general non-specific motivated behaviours. For example, an increase in the expression of the D₂R in the nucleus accumbens is associated with increased motivation such as increased effort to obtain a goal (118). Moreover, there are a number of neuroendocrine duties of the D₂R. In the pituitary, dopamine released from the hypothalamus acts at D₂Rs on lactotrophs of the anterior pituitary to inhibit the production of prolactin and the subsequent lactation and developmental processes (119). Sexual behaviour can also be driven by the D₂R through activation in the hypothalamus and interaction with the oxytocin system(120). Efficacious D₂R agonists are well known to elicit hypothermia, demonstrating that the D₂R regulates body temperature (110). The overarching roles that the receptor plays in many neurobiological and neuroendocrine functions highlights the reason why it has become such a common drug target.

1.4.4 High resolution D₂-like structures

Recently there has been an explosion in the number of high-resolution structures of GPCRs including those of D₂-like receptors. The D₃R was the first dopamine receptor to have

its structure solved and was crystallised bound to the high affinity antagonist eticlopride (121). Subsequent structures were then solved of the D₄R, followed by the D₂R bound to risperidone (Fig. 1.8) (122,123). There are currently two reported structures of the D₂R, with the second, most recent, structure solved bound to the typical antipsychotic haloperidol (123,124). These crystal structures revealed a very similar structure to other rhodopsin family (class A) GPCRs consisting of seven transmembrane domains positioned around in an anti-clockwise manner followed by a short helix 8 that runs parallel with the plasma membrane. Moreover, the D₄R structure was solved at high enough resolution to visualise a conserved sodium site important for modulating ligand affinity and function at D₂-like receptors (122). The D₂-like structures confirmed work from previous radioligand binding and mutagenesis studies demonstrating that orthosteric ligands bind deep within the TM bundle. However, the structures have also aided further binding and molecular modelling studies to fine-tune our understanding of ligand-receptor interactions (125,126).

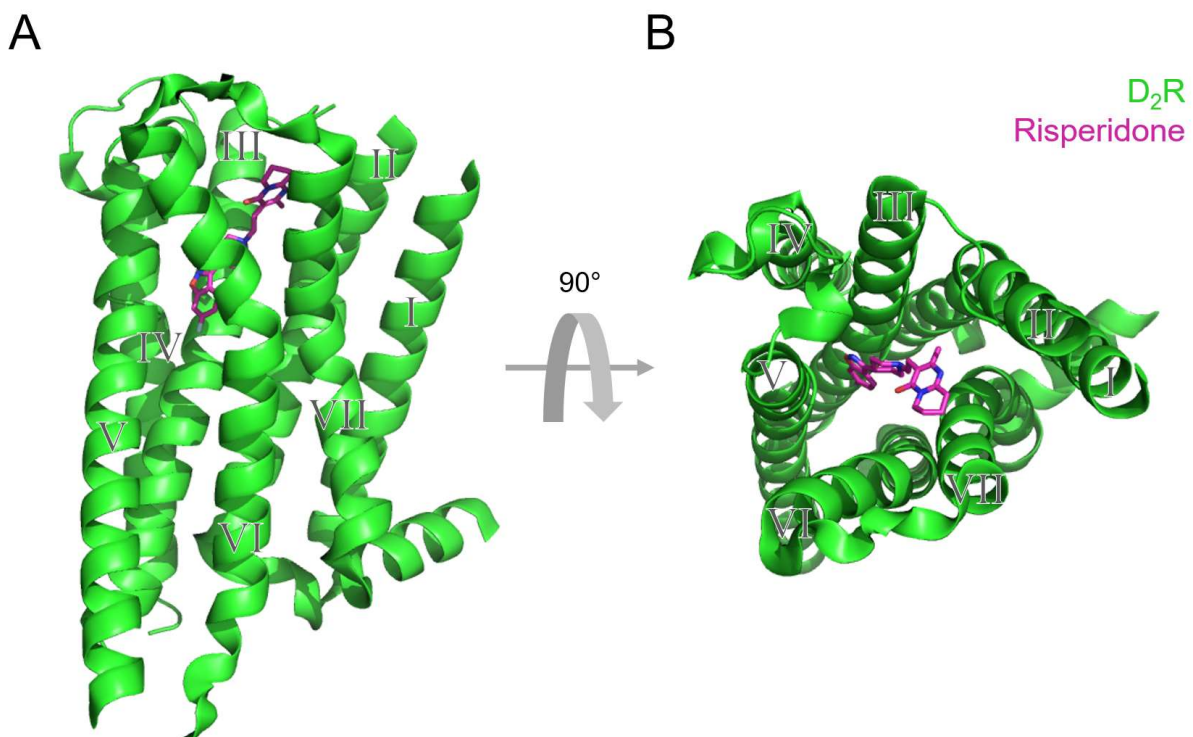


Figure 1.8: X-ray crystal structure of the D₂R bound to risperidone. (A) Side view parallel to the plasma membrane of the D₂R (green cartoon) bound to risperidone (magenta sticks). (B) Top view from the extracellular space of the D₂R (green cartoon) bound to risperidone (magenta sticks). (PDB code: 6CM4)

1.4.5 Molecular determinants of ligand binding at the dopamine D₂ receptor

Our understanding of the molecular processes that influence binding kinetics at the D₂R is building. It is well appreciated that D₂R ligands, such as dopamine, bind in the orthosteric

site comprising residues such as aspartate 114 located deep within the TMs (127). The orthosteric pocket is highly conserved among D₂-like receptors, however, residues in the extracellular tips of the TMs and ECLs of GPCRs can form secondary binding sites and extracellular “vestibules” (65,67). These residues that constitute these sites are less conserved and hence can confer selectivity for specific ligands. While most studies investigating binding at the D₂R have traditionally assessed effects on equilibrium affinity, an increasing number of studies are starting to reveal the intricacies of the whole binding and unbinding process. Tresadern et al (128) have investigated the influence of some physicochemical properties on the rate of dissociation of a large number of antagonists from the D₂R. It was observed that increasing lipophilicity and larger molecular weight was related to slower dissociation rate from the receptor. Additionally, more targeted analysis on smaller sets of ligands has also been performed. One study examined the kinetics of a series of compounds at the D₂R and suggested that a particular agonist-like moiety that the compounds shared was important for their fast dissociation rates from the D₂R (129). However, this finding is only relevant for the particular moiety and cannot be extended to other compounds with different agonist moieties such as the agonist bifeprunox that is one of the slowest dissociating D₂R ligands reported to date (96). Furthermore, Fyfe et al. (130) reported that modification of different moieties on the scaffold of haloperidol can significantly alter both the association and dissociation rates at the D₂R. Together such studies have illustrated that ligands can be altered through medicinal chemistry to tune their D₂R binding kinetics. Some studies have also started to explore the particular interactions ligands make with the receptor amino acid residues upon ligand binding. Early work by Shi and Javitch showed through substituted-cysteine accessibility that ECL2 lines the ligand binding site ‘crevice’ of the D₂R (131). While the association and dissociation rates of ligands were not investigated, certain residues such as isoleucine 184 within ECL2 may be likely to influence binding kinetics. Interestingly, the structure of the D₂R bound to risperidone (Fig. 1. 8) revealed a novel conformation of a tryptophan residue within ECL1 that is highly conserved among aminergic GPCRs. The tryptophan 100 residue was extended out over the top of the binding site. The tryptophan residue in this pose was suggested to be important for determining the residence time of risperidone (123).

1.4.6 Dopamine D₂ receptor G protein signalling

The main effectors for the D₂R are G $\alpha_{i/o}$ subfamily heterotrimeric G proteins. The D₂R can activate all members of the non-visual G $\alpha_{i/o}$ family which are G α_{i1} , G α_{i2} , G α_{i3} , G α_o , and

$G\alpha_z$ (132,133). Downstream effects of D_2R $G\alpha_{i/o}$ coupling include decreases in cAMP production by inhibition of adenylate cyclases (134), inhibition of P/Q-type and N-type calcium channels (135), activation of G protein-coupled inwardly rectifying potassium (GIRK) channels leading to increases in cytosolic potassium, and potentiation of stimulated arachidonic acid release (136).

It is known that the D_2R couples more strongly to $G\alpha_o$ isoforms ($G\alpha_{oA}$ and $G\alpha_{oB}$) than the $G\alpha_i$ subtypes (137-139). In agreement with its G protein selectivity, the D_2R is generally considered to elicit most of its effects in the brain through $G\alpha_o$ (140). Although, the method used to determine that $G\alpha_o$ coupling is the predominant form of coupling by the D_2R was based on detecting the high affinity state of an agonist for the receptor-G protein complex. This needs to be taken into consideration given that $G\alpha_o$ is the most plentiful G protein subtype in the central nervous system (141,142), such that, the experiment would be less sensitive at detecting other G protein subtypes expressed at lower levels. Certainly in pituitary cells it is appreciated that multiple $G\alpha_{i/o}$ subunits are involved in D_2R mediated signalling responses such as inhibition of prolactin release (143). Additionally, Marcott and colleagues (144), provided evidence that the weaker coupling to $G\alpha_i$ subtypes may function to allow the D_2R to display reduced sensitivity to dopamine in particular striatal sub-regions or cell types. While it was reported that multiple mechanisms likely explain differences in the kinetics of signalling between brain regions, the differences in signalling sensitivity in the nucleus accumbens relative to the dorsal striatum could be attributed to coupling to $G\alpha_o$ subunits in the nucleus accumbens compared to $G\alpha_i$ subunits in the dorsal striatum (144).

In addition to $G\alpha_o$ and $G\alpha_i$ coupling, there is also evidence that the D_2R can couple to $G\alpha_z$ to mediate some of its physiological effects. In contrast to other $G\alpha_{i/o}$ subtypes that are ubiquitously expressed, $G\alpha_z$'s expression is largely specific to neuronal and some endocrine cell types, including regions enriched with the D_2R such as the striatum and pituitary (145). The D_2R and $G\alpha_z$ are also co-expressed in pancreatic islets (146,147). It has been hypothesised that the D_2R mediates PTX-insensitive signalling through $G\alpha_z$ as determined by experiments performed on *ex vivo* rat pituitary tissue (148). Moreover, a well characterised behavioural reflex response mediated through D_2R is the disruption to prepulse inhibition upon dopaminergic stimulation with drugs such as amphetamine (149). Interestingly, $G\alpha_z$ knockout mice display an increased disruption to prepulse inhibition upon stimulation with dopaminergic drugs (150). In addition, $G\alpha_z$ is also required for D_2R mediated inhibition of dopamine release in the nucleus accumbens and its resultant suppression of locomotor activity (151). D_2R

mediated adrenocorticotrophic hormone (ACTH) secretion and hypothermia is also dependent on $G\alpha_z$ (151).

1.4.7 D₂R regulation and G protein-independent signalling

Upon agonist activation of the D₂R, several proteins other than G proteins are involved in regulating and coordinating the signalling response. The rate and magnitude of D₂R G protein signalling can be regulated in the striatum by regulator of G protein signalling 9-2 (RGS9-2) (152). Subsequently GRK2 and 3 are recruited and phosphorylate the receptor (102,153). In the case of the D₂R, GRK recruitment is required for arrestin recruitment to the receptor although, interestingly, the phosphorylation of the receptor which occurs on ICLs has been shown to be not critical for arrestin recruitment (102). This observation goes against the current dogma within the GPCR field, as classically it is thought that arrestins recognise the phosphorylated serines and threonines on the receptor due to the GRK. The phosphorylation by GRK2 or 3 is instead thought to be important in recycling of the D₂R back to the cell surface (102,153). Nonetheless, β -arrestin-2 is thought to be the main arrestin that binds to the D₂R to sterically hinder G protein activation (154). The D₂R is a relatively poor arrestin recruiter, this usually results in the receptor being recycled back to the plasma membrane instead of being trafficked into lysosomes for degradation. Moreover, one group has provided evidence of arrestin scaffolding at the D₂R mediating a novel signalling cascade comprising protein phosphatase 2A (PP2A), Akt and GSK3 β (155). In addition to agonist dependent regulation, heterologous desensitisation can occur at the D₂R through activation of PKC (156). PKC can phosphorylate the receptor on intracellular loops, resulting in reduced G protein mediated responses and receptor trafficking. Finally, while it is beyond the scope of this thesis, it should be noted that many other proteins interact with the D₂R to regulate or mediate their own signalling such as GIPC (157), NCS-1 (158,159), Spinophilin (160), Dysbindin-1 (161), and S100B (162). These proteins are termed dopamine receptor interacting proteins or DRIPs.

1.5 The dopamine D₂ receptor in Schizophrenia

1.5.1 Dopamine hypothesis of schizophrenia

Schizophrenia is a chronic mental illness with a prevalence of approximately 5 in 1000 in the global population (163). The precise aetiology of the disease is poorly understood, however, there are a number of known risk factors involving parental age, ethnicity, birth issues, immune disorders, and cannabis usage (164). The disease is characterised by positive

symptoms such as delusion and hallucinations, negative symptoms such as social withdrawal and depression and cognitive symptoms including impaired working memory (165).

The dopamine hypothesis of schizophrenia has evolved over time although broadly the fundamental assumption of the hypothesis is that schizophrenia is associated with a dysregulation of dopamine in the brain (166). Initially, antipsychotic drugs were extemporaneously discovered in the 1950s and found to treat the positive symptoms of the disease. Soon after this, the existence of dopamine receptors was starting to be established through work by Carlsson, Greengard and Kebabian (167-169). However, the “antipsychotic receptor” was not confirmed until 1976 by illustrating that the clinically used concentrations of all antipsychotics correlated with the concentration needed to inhibit binding of [³H] haloperidol to 50% in brain striatal tissue (170). This finding was made possible by the creation of [³H] haloperidol, that could specifically label what was later termed the dopamine D₂ receptor (171,172). Having achieved this, the dopamine hypothesis of schizophrenia was born.

1.5.2 Antipsychotic drugs

Since the first antipsychotic drug, some newer and improved drugs have been approved yet their ability to block dopamine agonism at the D₂R remains essential for robust efficacy (173). First generation antipsychotics are antagonists at the D₂R. These first generation antipsychotics are largely a group of phenothiazines, of note is the first discovered antipsychotic chlorpromazine (174). After chlorpromazine, other first generation antipsychotics that were developed including ones with differing scaffolds such as the butyrophenone haloperidol (174).

The first approved second generation antipsychotic was clozapine, which remains the gold standard treatment for schizophrenia today (175). Second generation antipsychotics are D₂R and serotonin 5-HT_{2A} receptor antagonists. The second generation antipsychotics have a reduced propensity to cause side effects such as extrapyramidal side effects due to differences in their binding kinetics at the D₂R discussed in a following section (1.5.4) (61,176).

The main feature of third generation antipsychotics is that they are weak partial agonists at the D₂R (173). Although, they additionally display partial agonism at the serotonin 5-HT_{1A} and 5-HT_{2B} receptors. These antipsychotics currently include aripiprazole, cariprazine and brexpiprazole. These antipsychotics were originally proposed to act as dopamine stabilisers by functioning as agonists at the presynaptic autoreceptor but antagonists at the postsynaptic heteroreceptor (177). However, subsequent studies demonstrated that they act as partial agonists at postsynaptic receptors (178). Therefore, being partial agonists, they likely function

by reducing D₂R signalling when there is too much dopamine released and increasing dopamine signalling when too little is released. In, addition the serotonin receptor agonism may also be advantageous through possibly boosting mood or reducing extrapyramidal side effects (179). Moreover, it has been suggested that the third generation antipsychotics may act through a mechanism involving biased agonism although this is not the current consensus in the field (173,180).

1.5.3 The potential of biased agonism within the dopamine hypothesis

The generally accepted hypothesis for pharmaceutical intervention in schizophrenia is that antipsychotics are antagonists or partial agonists which work by blockade of the D₂R. However, recent work by Caron and colleagues have suggested that partial agonists that preferentially activate the arrestin pathways may be more efficacious. Inferring that this may be an example where biased agonism (or biased antagonism) may provide improved drug efficacy in vivo. However, the basis for arrestin biased agonism and antipsychotic efficacy is convoluted. Early studies showed that activation of β -arrestin-2 by the D₂R in the striatum leads to specific dopamine-dependent behaviours in mice (181), demonstrating that not all D₂R mediated effects in vivo are dependent on G protein cAMP/PKA. This work further developed into a mechanism of G protein independent activation of the Akt/GSK-3 β /PP2A pathway whereby β -arrestin-2 recruitment by the D₂R leads to deactivation of Akt which in turn promotes activation of GSK-3 β (155,182). Additionally, it was shown that Akt protein levels are downregulated in patients with schizophrenia, suggesting a potential role for specifically pharmacologically antagonising β -arrestin-2 via D₂Rs to increase Akt activity (182). Follow-up studies by the Caron group then aligned with this hypothesis through molecular pharmacology by using clinically efficacious antipsychotics in mammalian cells and showing that they antagonise arrestin recruitment (183). However, more recent studies by the same group now oppose this view, whereby ligands that antagonise G protein mediated events but still retain the ability to recruit β -arrestin-2 are preferred. This was suggested through administration of an apparent arrestin-biased partial agonists in mouse models of psychosis as well as studies between arrestin knock-out and wild-type mouse models (184,185). Therefore, the relationship between arrestin bias and antipsychotic efficacy currently remains unclear. More recently, a separate group has investigated arrestin dependent effects at the D₂R by using an engineered arrestin biased mutant receptor (186). Through these studies it was possible to discern that arrestin recruitment can independently enhance locomotion but not motivation behaviours. While it is unclear which downstream signalling pathways or mechanisms may be

involved, the work demonstrates that D₂R mediated physiological effects could potentially be separated through biased agonism.

1.5.4 The role of D₂R-ligand binding kinetics in Schizophrenia

Seminal work by Kapur and Seeman (176,187) lead to the “fast off” hypothesis for atypical antagonist antipsychotics at the D₂R. Second generation (atypical) antipsychotics display less side effects such as hyperprolactinaemia, motor symptoms, and extrapyramidal side effects compared to first generation (typical) antipsychotics. Kapur and Seeman postulated that second generation antipsychotics produce less on-target side effects because they have a faster dissociation rate from the D₂R. The fast dissociation rate of the second-generation antagonists then leads to a lower receptor occupancy in the striatum compared to first generation antipsychotics. The idea was further supported by the fact that at high doses of a second generation antipsychotic, which produce high receptor occupancy, on-target symptoms start to present akin to those of the first generation antipsychotics (188).

Extending this work, Sykes et al (61), reassessed the both the association rate and the dissociation rate in regards to the side effects associated with different first and second generation antipsychotics. While an identical relationship was found between the dissociation rate and the propensity to induce hyperprolactinaemia, a different correlation emerged between the association rate and the tendency to cause extrapyramidal side effects (61). It was further suggested that this was due to rebinding of the antipsychotic inside the diffusion limited compartment of a synapse.

Later investigations by Carboni and colleagues (189) took a similar approach to these studies to investigate the newer third generation antipsychotics. The third-generation antipsychotics are weak partial agonists at the D₂R that include cariprazine, aripiprazole and brexpiprazole. Carboni et al. (189) investigated the agonist efficacy and binding kinetics in relation to prolactin release into the bloodstream in rats. The measurement was used as a surrogate to predict the likelihood of hyperprolactinamia in humans. Interestingly, they demonstrated with aripiprazole and several other partial agonists synthesised in-house, that slower dissociation of partial agonists produced a smaller increase in prolactin compared to the other partial agonists with similar efficacy. One key observation to come out of this study was that agonist maximal response did not correlate with prolactin release, suggesting that in vitro agonist efficacy may not be the best predictor of in vivo efficacy. Additionally, this relationship between kinetics for partial agonist antipsychotics was effectively the opposite of the work by

Kapur and Seeman as well as Sykes et al. with antagonist antipsychotics. This suggests then that the partial agonists may have a separate mechanism of action to antagonists.

1.6 The dopamine D₂ receptor in Parkinson's disease

1.6.1 Background

Parkinson's disease is a continual progressive neurodegenerative disorder. It is the second most prevalent neuropathological disorder after Alzheimer's disease (190). The disease usually begins in a person's 50s or 60s, although in rare cases early-onset Parkinson's can occur before the age of 40. The high societal and economic impact of the disease is expected to grow substantially as the prevalence grows due to an aging global population (191). The disease is featured by motor symptoms including tremors, bradykinesias, muscular rigidity and reduction of postural balance. While in the community it is primarily thought of as a movement disorder, it is important to recognise that the disease is also associated with several non-motor symptoms including orthostatic hypotension, depression, skin conditions, anxiety, dementia, sleep problems and sensory impairments (192). Parkinson's disease pathology is characterised by the progressive loss of dopaminergic neurons in the substantia nigra pars compacta (193). As the neurons die over time this results in a loss of dopamine in the posterior striatum, where the dopaminergic neurons of the substantia nigra project to. It is this loss of dopaminergic tone that then leads to the motor symptoms observed in patients (194). This pathology is usually coupled with characteristic protein aggregate inclusions called Lewy bodies in certain regions of the brain (195).

1.6.2 Pathogenesis

Parkinson's disease has been historically considered an idiopathic disorder. While it is still often unclear which components are responsible for initiating, spreading or worsening the disease, multiple environmental and genetic factors have become evident over time. Increasing age is the highest risk factor for the disease. This may be due in part to dopaminergic neurons in the substantia nigra being more susceptible to processes like mitochondrial dysfunction than other neurons. Moreover, there are also many other triggers or risk factors including, exposure to some pesticides (196), brain trauma, some bacterial and viral pathogens, changes in the gut microbiome (197) ethnicity, geography and sex (198).

Specific genes were not identified as risk factors until mutations in the α -synuclein encoding gene SNCA were identified in a family with Parkinson's disease in 1997 (199).

Shortly after identifying that mutations in α -synuclein can cause rare forms of the disease, it was shown that α -synuclein is a major component of Lewy bodies. This more directly linked the genetics to the pathogenesis because Lewy bodies are thought to be a toxic species to organelles. These results lead to several genome wide association studies (GWAS) and meta-analyses to identify genetic risk factors. Now, there is an ever-increasing list of upwards of 20 genes associated with the disease that display varying functions within the cell. The most common heritable form of the disease being due to genetic differences in leucine-rich repeat kinase 2 (LRRK2) (200,201). Other commonly associated genes are PTEN-induced kinase 1 (PINK1) (202) and glucocerebrosidase (GBA)(203).

1.6.3 Current treatment

At present, pharmacological treatment mainly manages the motor symptoms of the disease, having efficacy towards only some of the non-motor symptoms (204). Using different small molecule approaches, all treatments aim to restore dopamine signalling in the striatum. This is managed by treatment with either L-dihydroxyphenylalanine (L-DOPA), a D₂R agonist, a monoamine oxidase B (MAO-B) inhibitor, or a combination of these.

L-DOPA is still the mainstay medical treatment for Parkinson's disease (205). L-DOPA is converted by DOPA decarboxylase to dopamine and is the body's natural dopamine precursor. Thus, in Parkinson's treatment L-DOPA functions as a prodrug through which it can cross the blood brain barrier where it is then converted into dopamine to have its effect. Moreover, L-DOPA is usually taken in combination with a decarboxylase inhibitor such as carbidopa. This is to prevent conversion of dopamine outside of the brain because dopamine plays a dual role as a hormone in the periphery and a neurotransmitter in the brain. This then allows the use of lower initial doses of L-DOPA. Once treatment with L-DOPA has started, MAO-B inhibitors are often used in combination to enhance the effect and D₂R agonists have also historically been used in combination.

Taken orally or with a transdermal patch, small molecule D₂R agonists cross the blood-brain-barrier where they can act to enhance some dopamine receptor signalling in the striatum. These agonists generally have selectivity for the D₂R and the D₃R. First generation D₂R agonists for Parkinson's disease include lisuride, bromocriptine, pergolide and cabergoline that are derived from ergots. Some of these agonists have fallen out of favour due to their increased risk of cardiac valvular disease and fibrosis of other connective tissues (206,207). In particular, cabergoline and pergolide have been withdrawn from the market due to their serotonin 5-HT_{2B} receptor agonism which leads to valvular pathologies (208). Bromocriptine remains a marketed

drug however it is mainly prescribed for other indications such as the treatment of hyperprolactinemia and acromegaly. Second generation agonists such as ropinirole, pramipexole, apomorphine, rotigotine and piribedil vary in structure and hence do not have the side effects common to some of the ergot-derived agonists. While these D₂R agonists are generally considered to be less efficacious than L-DOPA, they can be used after L-DOPA shows “escape” or to delay the need for L-DOPA because they may have reduced risk for motor-related complications such as dystonia, dyskinesia and motor fluctuations (209). Moreover, MAO-B inhibitors may be used for similar reasons in early stages of disease. In contrast to direct activation of D₂Rs, MAO-B inhibitors boost dopamine signalling by permitting the body’s naturally produced dopamine to persist for longer in the synapse. After being released in the brain, dopamine is taken up by neurons or glia where it then undergoes oxidative deamination. MAO-B is the enzyme that is chiefly responsible for this action on dopamine (210). Therefore, in early stages of the disease a MAO-B inhibitor such as selegiline or rasagiline may be prescribed to enhance dopamine signalling in the nigrostriatal system.

1.6.4 Scope for improving D₂R targeted therapy

It should be noted that there are numerous promising approaches targeting proteins other than the D₂R that are being developed. However, any disease modifying therapy is only likely to be approved over the long term as these therapies are generally in the early clinical or pre-clinical stages. Some examples include drugs targeting other GPCRs (211,212), therapies designed to immunise against α -synuclein (213), modalities targeting other proteins such as LRRK2 and PINK1 (214), dopaminergic cell-based therapies (215), and gene therapies to restore dopamine production (216).

In the shorter term, it may be more realistic to improve D₂R targeting through detailed pharmacological characterisation of existing D₂R agonists or through targeting the D₂R via novel mechanisms such as biased agonism. Indeed, there is considerable scope in identifying the most efficacious existing drugs through post-approval research. Particularly in the case of the early stage of the disease where current therapeutic strategies vary, with a wide use of different agonists that display varying efficacies and binding kinetics. Current thinking suggests that the D₂Rs simply need “switching on”, however we now know the agonists being prescribed are not equivalent. Indeed, ergot agonists are usually not prescribed by doctors anymore as mentioned earlier. Additionally, other D₂R agonists could potentially display partial agonism or biased agonism with respect to dopamine. Therefore, it may be important to investigate the signalling properties of prescribed agonists in more detail to better understand

which drugs are the most efficacious or reduce side effects. In addition, investigating the molecular determinants of signalling and binding kinetics of D₂R agonists could identify whether new small molecule D₂R agonists can be developed with differing pharmacology to the currently available options. Altogether, this could improve the doctors guidelines as well as advise the dosing regimens of D₂R agonists as it is somewhat complicated due to the existing drugs having different potencies (217).

1.7 Scope of thesis

The dopamine D₂ receptor (D₂R) is a key target for various neuropsychiatric and neurological diseases. However, drugs acting at the D₂R for these diseases often have limited efficacy and poor side effect profiles. Understanding the molecular mechanisms of binding and signalling of the D₂R, including their kinetic rates will provide the foundation for the design of the next generation of improved D₂R-targeted drugs.

There are quite clear differences in the binding kinetics of clinically relevant ligands acting at the D₂R. The work of Seeman and colleagues (187,218) and later by Sykes and colleagues (61) has highlighted the importance of binding kinetics in the side effect profile of antagonist antipsychotics at the D₂R. Additionally, Klein-Herenbrink and co-workers (96) as well as Carboni and colleagues (189), have demonstrated that the functional differences of agonists can sometimes be attributed to differences in their binding kinetics. In **chapter 2** we optimise a novel time resolved fluorescence resonance energy transfer (TR-FRET) competition kinetic binding assay to measure unlabelled ligands binding rates. We then use mutagenesis to understand the influence of distinct residues in the extracellular vestibule of the D₂R on the binding kinetics of clinically relevant antagonists and agonists.

In Klein-Herenbrink and colleagues' study, it was found that some slowly dissociating partial agonists acting at the D₂R can display apparent bias relative to fast dissociating agonists in a manner that changes over time. Based on this work, we hypothesise that agonists with a slow dissociation rate and hence a longer residence time may lead to observations of biased agonism through potentially allowing the receptor to sample different effector bound states. In **chapter 3**, we therefore extend the work of Klein-Herenbrink and colleagues (96) with several different approaches. We test a greater number of agonists, including agonists that display high efficacy and slow dissociation from the D₂R. We expand the functional assessment to multiple receptor-proximal events and receptor trafficking to subcellular compartments.

Continuing with our research on the mechanisms of D₂R biased agonism, we investigate the relationship between biased agonism and D₂R phosphorylation. This is important because GRK phosphorylation is often thought of as the “switch point” between G protein mediated signalling and arrestin recruitment (219). In **chapter 4**, we develop novel phosphorylation-site antibodies that target the intracellular loops of the D₂R. We then use the antibodies coupled with bioluminescence resonance energy transfer signalling and proximity assays to assess D₂R

regulation and its modulation by agonists, including those that display apparent biased agonism. We are able to further clarify the role GRKs play in these processes.

Through our work investigating the biased agonism in chapters 3 and 4 it is appreciated that the pharmacological system needs to be understood in order to determine the mechanisms of biased agonism observations. The D₂R's main signalling effectors are G proteins of the $G\alpha_{i/o}$ subfamily and it is known to promiscuously couple to multiple different $G\alpha_{i/o}$ subunits. In **chapter 5**, we therefore simplify the system and focus in on signalling only at the level of different G proteins. We characterise and investigate the drivers of the kinetics of agonist induced D₂R G protein activation. We describe kinetically distinct G protein signalling waves that are mediated by the D₂R. The kinetically distinct waves are shown to be due to a generally unappreciated role for the GTP hydrolysis rate of the $G\alpha$ subunits in determining agonist responses over time.

In chapters 3, 4 and 5 we identify that D₂R biased agonism is heavily dependent on the system in which it is studied in. In an ideal scenario, one would study D₂R biased agonism in a tissue or animal model that is relevant to the disease to reduce this dependence. However, investigating biased agonism in the relevant setting has been challenging due to the lack of molecular tools. Consequently, in **chapter 6**, the final experimental results chapter, we develop and characterise a new tool for helping discern, *in vivo* or *ex vivo*, the dependence of different $G\alpha_{i/o}$ proteins and arrestins on particular signalling responses and physiological outcomes. We show that this tool has the novel property of abolishing all $G\alpha_{i/o}$ signalling including $G\alpha_z$. We further develop G protein mutants that are not inhibited by this toxin that can complement this tool and suggest the means in which the toolkit can be utilised.

Overall, this thesis provides a detailed molecular understanding of the determinants of ligand binding kinetics and receptor function at the D₂R. The findings fundamentally help to clarify potential mechanisms of biased agonism.

Chapter 2:

Towards characterisation of dopamine D₂ receptor ligand binding pathways through kinetic studies on receptor mutants

Abstract

The dopamine D₂ receptor (D₂R) is a prototypical GPCR as it has been a long-standing target for drugs that relieve the symptoms of Parkinson's disease and schizophrenia. Multiple studies have highlighted the clinical importance of drug binding kinetics at the D₂R. Therefore, the rational design of drug binding kinetics at the D₂R is desired. In order to do this, an understanding of the molecular interactions involved in the binding process are required. Recent x-ray crystal structures are not able to completely explain the molecular mechanisms of differing binding kinetic rates between ligands. Additionally, many amino acid residues in the extracellular regions of the D₂R are likely quite dynamic and as such cannot be fully appreciated in crystal structures. Therefore, temporal studies are required to provide sufficiently detailed molecular insight into the binding entry and exit pathways of ligands at the D₂R. In this study we optimise a time resolved-fluorescence resonance energy transfer competition kinetic binding assay at the D₂R. We subsequently use the assay on some mutants in the extracellular regions of the D₂R to determine the contribution these residues have in modulating binding kinetic association and dissociation rates. We show that amino acid residue mutations in these regions, such as Trp100^{EL1}Ala, can alter ligand binding kinetics and that distinct ligands are more sensitive than others depending on the residue. Overall, these studies demonstrate that one can use competition kinetic binding experiments to start to understand the binding pathways of the D₂R with molecular detail.

2.1 Introduction

G protein coupled receptors (GPCRs) are cell surface receptors characterised by seven α -helical transmembrane domains (TMs) that are connected by three extracellular loops (EL1-3) and three intracellular loops (IL1-3). They bind agonists such as hormones, peptides and neurotransmitters on their extracellular side, permitting them to couple to heterotrimeric G proteins on their intracellular interface to transduce signals within cells. Drugs can be used to hi-jack GPCR signalling systems, in turn, altering cellular processes to modify the pathophysiology or symptoms of diseases. As a result of this, GPCRs represent the largest protein class of drug targets, accounting for around a third of all marketed small molecule drugs (220).

Describing the relationships between small molecule leads and their GPCR target is essential to drug discovery efforts. To describe a particular ligands' affinity for a GPCR, pharmacologists determine the dissociation constant (K_d). The dissociation constant is defined as the concentration of a ligand required to occupy half of the GPCRs at equilibrium. As such, the dissociation constant is typically determined through binding experiments such as saturation binding assays. Saturation binding assays are performed by mixing increasing concentrations of a ligand with a constant concentration of GPCR and measuring the bound population at equilibrium. Most studies perform these experiments due to their simplicity and practicality. However, a ligands' dissociation constant for a GPCR is fundamentally comprised of the dissociation rate of the binding reaction (k_{off}) divided by the association rate (k_{on}). Indeed, determining the dissociation rates and association rates of ligand leads can provide a deeper understanding of the binding process. Binding kinetic rates can be determined by methods such as the one reported by Motulsky and Mahan (221) where a tracer ligand is co-added with increasing concentrations of a competitor ligand and tracked over time. Knowing the binding kinetics then allows one to incorporate these parameters when developing ligand leads in the drug discovery pipeline.

It has been suggested that a drug's binding kinetics, as opposed to its affinity, may better explain the *in vivo* efficacy in some instances (53,56). This is because a drugs' concentration in the body does not reach equilibrium due to a several processes such as drug distribution and hepatic clearance. Therefore, effects related to a drugs' binding kinetics can modulate the pharmacodynamics of the drug. For example, the slow dissociation rate of tiotropium at the muscarinic acetylcholine M_3 receptor leads to prolonged duration of action, allowing for less frequent dosing compared to other chronic obstructive pulmonary disease

drugs (222). In addition, a fast-association rate may also produce sustained drug action due to an increased likelihood of rebinding (223,224), where rebinding describes the phenomenon whereby a drug that does not completely escape the receptor's vicinity after its dissociation and subsequently rebinds (54). Therefore, there is significant scope for improvement of drugs by designing them with the desired binding kinetics.

It is vital to understand the molecular basis of ligand binding kinetics at GPCRs. In particular, it is beneficial to understand the contribution that specific ligand-amino acid residue contacts have on ligand binding kinetics. Gaining knowledge on the roles of these binding contacts permits efforts to rationally design drugs with the desired binding kinetics. Consequently, a drug developed with the desired binding kinetic profile could be more efficacious or have a longer duration of action. Our understanding of GPCR structure has been greatly improved in recent years largely due to X-ray crystallography and cryo-electron microscopy (225). Through use of this structural data, the relationships between receptor structure and ligand binding kinetics have been amenable to investigations using molecular dynamics simulations. Dror and colleagues showed using long timescale simulations of the β_2 receptor that ligands entering the binding site first encounter a metastable site within the extracellular loops and the top of the transmembrane domains termed the extracellular vestibule (65). It is thought that when the ligand gets to this position there is a large energy barrier due to the significant de-wetting that occurs. Following this, the ligand can then enter the orthosteric site deep within the transmembrane domains. Molecular dynamics simulations on additional GPCRs have continued to support these observations of metastable ligand binding sites in the extracellular regions (126,226). Indeed, molecular dynamics simulations implicated the EL2 in the histamine H₁ receptor and the adenosine A_{1A} receptor as important for initial ligand contacts (226,227). Furthermore, a similar phenomenon has also been documented upon ligand exit at the adenosine A_{2A} receptor (228). While these simulations have proven useful, the findings often remain to be validated by wet laboratory experiments.

The dopamine D₂ receptor (D₂R) is a member of the dopamine family of GPCRs, consisting of the D₁-like receptors (D₁ and D₅) and the D₂-like receptors (D₂, D₃ and D₄). The dopamine D₁-like receptors couple to the G α_s subfamily to increase adenylate cyclase activity and the dopamine D₂-like receptors couple to the G α_i subfamily to decrease adenylate cyclase activity (103). Expression of the D₂R is enriched in many central nervous system regions such as the striatum, ventral tegmental area and substantia nigra pars compacta (109). While all dopamine receptors are important for many neurophysiological functions, the D₂R is necessary for the majority of the roles of dopamine in vivo such as reward behaviours and locomotor

activity (229,230). The D₂R is one of the most well-known GPCRs as it is the main target for drugs that relieve the symptoms of schizophrenia and Parkinson's disease (231,232). Small molecule D₂R antagonists or partial agonists are used to treat schizophrenia whereas efficacious agonists are used for the treatment of Parkinson's disease.

The importance of drug binding kinetics at the D₂R has been highlighted by several studies. Kapur and Seeman have established the fast-off hypothesis of antipsychotic drugs acting at the D₂R, positing that antipsychotics with fast dissociation rates have reduced side effects (187,218). In agreement with this hypothesis, we observe that the dissociation rate of an antagonist antipsychotic correlates with hyperprolactinaemia – a common side effect of these drugs. However, we observed that antagonists with faster association rates appeared to have increased likelihood of causing extrapyramidal side effects (61). Our group proposed that this is due to the rebinding within the diffusion limited compartment of a dopaminergic synapse. Moreover, the relationship between D₂R agonist binding kinetics and clinical effect in Parkinson's disease has not been thoroughly explored. Yet, D₂R agonists with slow dissociation rates can also display differing functional profiles, including observations of biased agonism (96,189). Together, these studies indicate that ligand binding kinetics at the D₂R may be tuned to have the desired therapeutic outcome.

Our knowledge of the molecular determinants of binding kinetics at the D₂R is still in its infancy. Some progress has been made towards understanding ligands' structural elements that influence binding kinetics at the D₂R. General trends are that higher molecular weight and increasing lipophilicity correlates with a slower antagonist dissociation rate at the D₂R (128). More recently, Fyfe et al. have shown that structural modification of the scaffold of the antipsychotic haloperidol can yield a ligand with differing kinetics at the D₂R (130). This work has demonstrated that ligand-receptor structure kinetic relationships can be optimised at the D₂R. However, the interactions ligand moieties make with particular D₂R amino acid residues upon entry and exit is largely unexplored. Traditional equilibrium binding studies coupled with site directed mutagenesis have established the main residues important for ligand binding such as Asp114^{3.32} that sits within the orthosteric binding pocket (233). Yet, whether a residue is more important for ligand association or dissociation is often unclear. For example, Shi and Javitch have previously shown that Ile184 within EL2 (Ile184^{EL2}) was important for the binding of ³[H]N-methylspiperone as this residue lines the top of the binding site (234). Whether this residue plays a role in granting access or egress of ³[H]N-methylspiperone is unclear.

There have been a number of recent reports of X-ray crystal structures of D₂-like receptors that have helped drive investigations of ligand binding kinetics. Indeed, the first D₂-like structure of the D₃R bound to eticlopride has been subsequently used to model the D₂R and perform molecular dynamics simulations of ligand interactions on multiple occasions (121,125,126,235). Thomas et al. (126) used long timescale molecular dynamics simulations of a D₂R that was based on the D₃R-eticlopride structure to understand the association of two antipsychotics, clozapine and haloperidol. In doing so, they presented that Tyr379^{7,35} may be important for the ligand entry pathway of both ligands (126). Their simulations additionally indicated that haloperidol and clozapine also frequently interacted with Ile184^{EL2} along their binding entry pathway. Moreover, later structures of the D₂R and D₄R have also enabled additional molecular dynamics simulations and binding studies to improve our understanding of ligand entry and exit (122-124,236). In particular, Trp100^{EL1} was highlighted as an influential residue in the D₂R-risperidone structure by potentially acting as a hydrophobic “lid” to increase the lifetime of ligands once bound (123).

In this study, we aimed to use time resolved-fluorescence resonance energy transfer (TR-FRET) competition kinetic binding assays on extracellular vestibule mutants of the D₂R to identify and characterise the roles these residues play in determining ligand binding rates. We identified that some residues in the extracellular vestibule are important drivers of the ligand binding kinetic rates. We showed that amino acid residue mutants in these regions can alter ligand binding kinetics in a ligand-specific manner. Generally, these residues appeared to alter the dissociation rate more so than the association rate. We noted that the effects of particular D₂R residues on kinetic binding rates of different ligands cannot be easily predicted from the existing structural information. This study shows that TR-FRET competition kinetic binding represents a suitable platform for analysis of the molecular determinants of ligand binding kinetics at GPCRs to enable the design of drugs with the preferred kinetic profile.

2.2 Methods

Materials

Dulbecco's phosphate buffered saline (DPBS), Hank's balanced salt solution (Cat. No. H8264) (HBSS), pluronic acid-F127, Gpp(NH)p, Quikchange primers, risperidone, spiperone, haloperidol and bromocriptine were purchased from Sigma-Aldrich. Saponin was from Fluka (now Sigma-Aldrich). Eticlopride hydrochloride was purchased from Tocris Bioscience (Bio-Techne Corp Ltd.) 384-well white optiplate LBS-coated were purchased from PerkinElmer.

Bifeprunox and aripiprazole (>95% pure) were synthesised in the Medicinal Chemistry department at Monash Institute of Pharmaceutical Sciences, Monash University Parkville Campus as described previously (96). Polyethylenimine (PEI) MW 25,000 was purchased from Polysciences, Inc. Clozapine-Cy5 was synthesised in the Centre for Biomolecular Sciences at the University of Nottingham as described previously (237). 5 x SNAP/CLIP-tag labelling medium (Part No. LABMED), SNAP-Lumi4-Tb (terbium cryptate, Part No. SSNPTBC) and fluorescent Spiperone-d2 (Part No. L0002RED) were acquired from Cisbio (PerkinElmer).

Mutagenesis

Quikchange technique was used to perform site directed mutagenesis. This method was performed using Phusion® High-Fidelity DNA polymerase (New England BioLabs). Quikchange was carried out using DNA template of FLAG-SNAP-D₂sR encoded in a pEF5-DEST-FRT plasmid. Primers used for the mutagenesis were as follows:

SNAP-D₂sR-L94^{2,64}A:

Fwd; 5'-CTGGGTTGTCTACGCGGAGGTGGTAGGTGAG-3',

Rev; 5'-CTCACCTACCACCTCCGCGTAGACAACCCAG-3'.

SNAP-D₂sR-W100^{EL1}A:

Fwd; 5'-GGAGGTGGTAGGTGAGGCGAAATTCAGCAGGATTC-3',

Rev; 5'-GAATCCTGCTGAATTTGCCTCACCTACCACCTCC-3'.

SNAP-D₂sR-II84^{EL2}A:

Fwd; 5'-CAGAACGAGTGCATCGCTGCCAACCCGGCCTTC-3',

Rev; 5'-GAAGGCCGGGTTGGCAGCGATGCACTCGTTCTG-3',

this mutant construct has been previously described by our group (235).

SNAP-D₂sR-Y379^{7,35}A:

Fwd; 5'-CAACATCCCGCCTGTCCTGGCGAGCGCCTTCACGTG-3',

Rev; 5'-CACGTGAAGGCGCTCGCCAGGACAGGCGGGATGTTG-3'.

After Quikchange mutagenesis, the full coding region was demonstrated to be correct and containing the desired mutations through Sanger sequencing method by the DNA Sequencing Laboratory, D98 Medical School, Queens Medical Centre.

Stable cell line production

Generations of stably expressing mutant D₂R cell lines was achieved using the Flp-In™ system (ThermoFisher Scientific). Mutant SNAP-D₂sR constructs were transfected into parental Flp-In CHO-K1 cells. The parental Flp-In CHO-K1 cells were grown in Dulbecco's Modified Eagle's Medium (DMEM)/F12 supplemented with 10% FBS, 100µg/mL

penicillin/streptomycin and 100µg/mL zeocin. The FlpIn CHO-K1 cells were seeded into T75 flasks to be approximately 30% confluent the following day in complete media lacking zeocin. The next day, the cells were transfected with pOG44 together with the mutant pEF5-DEST-FRT-FLAG-SNAP-D₂S_R construct in a DNA ratio of 9:1 (w/w) using polyethylenimine (PEI). 48 hours after transfection, selection of genomic integration by replacing the media with DMEM/F12 supplemented with 10% FBS, 100µg/mL penicillin/streptomycin and 700µg/mL hygromycin B (Corning). Cells were then expanded into T175 flasks and passaged three times before freezing and storing. SNAP-D₂S_R mutant expression was confirmed by a functional G protein activation assay described in detail the following chapters. previously reported Flp-In CHO-K1 cells stably expressing SNAP-D₂S_R mutants were subsequently grown in DMEM/F12 supplemented with 10% FBS, 100µg/mL penicillin/streptomycin and 600µg/mL hygromycin B.

Terbium cryptate labelling

Terbium cryptate labelling of SNAP-tagged receptors in live Flp-In CHO-K1 cells was performed identically to our previously described method in Appendix 2 (125).

Membrane preparation

Membrane preparations were performed on terbium cryptate labelled thawed cell pellets identical to our previously described method in Appendix 2 (125).

HTRF kinetic binding assay

The kinetic binding assay was performed almost identically to our previously described method, for specific details please see this work (125). This method was adapted from our group's earlier publications using the same technique (61,96). Briefly, 20µL of different ligand cocktails diluted in Hanks Balanced Salt Solution + 20mM HEPES + 0.02% Pluronic-F127 + 1% dimethyl sulfoxide, pH 7.4 (with KOH) was added to each well of a 384-well white bottom optiplate LBS coated. After incubating the ligand cocktail in the plate and the membrane preparation in the injector system at 37°C, the PHERAstar FS (BMG Labtech) was then set to inject 20µL of cell membrane preparation in the same buffer +100µM Gpp(NH)p and 50µg/mL saponin at 400µL/s. The HTRF filter module detected the terbium cryptate at 337nm and the fluorescent ligand at 665nm simultaneously. The focal height was set to 10.4mm. The excitation source was set to laser and the number of flashes varied between 5-9 depending on the particular experiment and cycle time. Integration start: 60µs, Integration time: 400µs. Cycle

time varied between 2-5 seconds depending on experiment. All experiments were performed a minimum of four times and in singlet wells.

Data analysis

The TR-FRET binding values were determined by dividing the 665nm (fluorescent ligand acceptor) channel values by the 337nm (terbium cryptate donor) channel and multiplying by 10,000. This was then subtracted by the non-specific binding determined in each experiment providing the “specific HTRF ratio x 10,000”. All laboratory data was analysed with the curve-fitting software GraphPad Prism 8.2 using nonlinear regression.

To determine kinetic binding parameters of fluorescent ligands in association binding experiments equation (2.1) was used. In GraphPad Prism this is named as the ‘Association kinetics – Two or more conc. of hot.’ model. L is the fluorescent ligand - either spiperone-d2 or clozapine-Cy5 (concentration in M).

(2.1)

$$k_{ob} = [L] \times k_{on} + k_{off}$$

To determine the affinity of the fluorescent ligands at each mutant equation (2.2) was then used. Where K_D is the equilibrium dissociation constant.

(2.2)

$$K_d = \frac{k_{off}}{k_{on}}$$

To determine the kinetic binding parameters of unlabelled competitor ligands, the data was fit to equation (2.3) for the kinetics of competitive binding described by Motulsky and Mahan (221). In GraphPad Prism this is named the ‘Kinetics of competitive binding’ model. Where; k_1 , k_{on} of fluorescent ligand ($M^{-1}min^{-1}$); k_2 , k_{off} of fluorescent ligand (min^{-1}); k_3 , k_{on} of unlabelled competitor ligand ($M^{-1}min^{-1}$); k_4 , k_{off} of unlabelled competitor ligand (min^{-1}); L , the fluorescent ligand (concentrations are in nM); I , the unlabelled competitor ligand (concentrations are in nM); Y , specific binding of the fluorescent ligand with the receptor (HTRF ratio x 10,000); X , time (minutes).

(2.3)

$$K_A = k_1[L] \times 10^{-9} + k_2$$

$$K_B = k_3[I] \times 10^{-9} + k_4$$

$$S = \sqrt{(K_A - K_B)^2 + 4 \times k_1 \times k_3 \times [L] \times [I] \times 10^{-18}}$$

$$K_F = 0.5(K_A + K_B + S)$$

$$K_S = 0.5(K_A + K_B - S)$$

$$Q = \frac{B_{max} \times K_1 \times [L] \times 10^{-9}}{K_F - K_S}$$

$$Y = Q \times \left(\frac{k_4 \times (K_F - K_S)}{K_F \times K_S} + \frac{k_4 - K_F}{K_F} \times e^{(-K_F \times X)} - \frac{k_4 - K_S}{K_S} \times e^{(-K_S \times X)} \right)$$

2.3 Results

Determination of ligand kinetics at the wild-type D₂R

We initially aimed to determine the binding kinetics of several diverse ligands at the wild-type D₂R. We subsequently aimed to assess the binding kinetics of these ligands at D₂R mutants. Therefore, we were only able to assess a handful of ligands due to assay throughput constraints. Further, we selected high affinity ligands that would remain amenable to quantification with the assay despite a significant loss of affinity at a receptor mutant. In addition, we were interested in assessing agonists as well as antagonists to determine whether agonist efficacy may influence binding kinetic rates. We therefore selected three agonists; aripiprazole, bifeprunox and bromocriptine, as well as three antagonists; eticlopride, risperidone and spiperone (Fig. 2.1). The three agonists were chosen due to their clinical relevance, structural variability and variation in efficacy. Aripiprazole is the first of a novel class of antipsychotics that display very low levels of agonism (238). Bifeprunox is a partial agonist with a very slow dissociation rate that was initially under development for the treatment of schizophrenia but later discontinued (239). Aripiprazole and bifeprunox are both phenylpiperazine derivatives although they are structurally quite different from each other (Fig. 2.1). Bromocriptine is a high efficacy agonist derived from ergots. It is prescribed for Parkinson's disease and hyperprolactinemia among other indications (240). The three antagonists that we selected in this study were chosen based on their distinct chemotypes that we hypothesised may confer different D₂R amino acid contacts upon binding. In addition, we chose to assess eticlopride and risperidone because these antagonists had both been solved in

high resolution structures of D₂-like receptors. This is important as it enables the first attempt to independently assess the accuracy of the reported structures as well as to relate accurate kinetic data to the static structures. Eticlopride is used primarily for research and was bound to the D₃R in the only solved D₃R crystal structure at the time of writing (121). Eticlopride has a similar substituted benzamide scaffold to other D₂-like antagonists such as sulpiride and nemonapride. Risperidone is a benzisoxazole derivative that is an atypical antipsychotic and was reported bound to the D₂R in the first D₂R crystal structure (123,241). Spiperone is from the butyrophenone class of typical antipsychotics, a class that includes haloperidol that was bound in the second reported crystal structure of the D₂R (124,242).

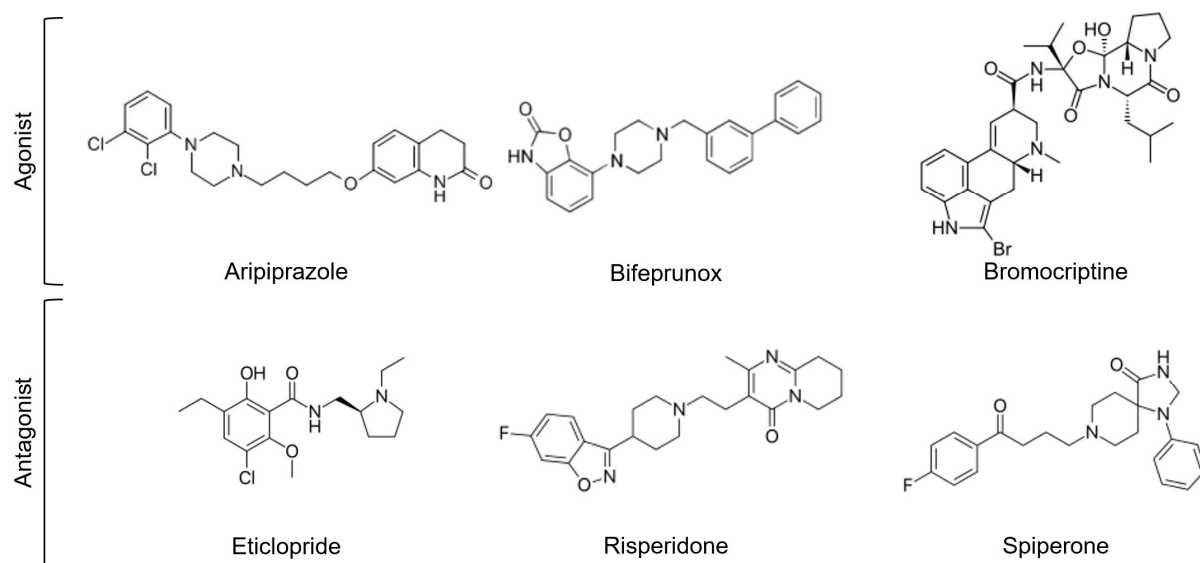


Figure 2.1: Chemical structures of the D₂R ligands assessed in this study.

To determine the binding kinetics of our set of diverse ligands it was first necessary to characterise the fluorescent tracer ligands. We used two fluorescent tracers in this study; the high affinity tracer spiperone-d2 and a lower affinity tracer clozapine-Cy5. The binding kinetics of these two tracers were successfully determined using association kinetic binding assays at the wild type D₂S_R (Fig. S2.1A & B, Fig. S2.2A & B and Table 2.1). The binding kinetic parameters of the unlabelled ligands of interest were then obtained using the two tracers separately in competition kinetic binding experiments following the method of Motulsky and Mahan (Figure S2.1 & S2.2) (221). Importantly, the values determined with each tracer were in close agreement with each other (Table 2.1). Indeed, no significant differences were observed between the k_{on} , k_{off} or K_d values of unlabelled ligands when using clozapine-Cy5 as a tracer instead of spiperone-d2 as determined by unpaired t-test ($P < 0.05$). Aripiprazole, bifeprunox, risperidone and spiperone have previously had their binding kinetics determined by our group (61,96). The results here closely matched our previous results despite using

different fluorescent tracer ligands from our previous work. For example, bifeprunox dissociated slowly ($2.92 \times 10^{-2} \text{ min}^{-1}$ using Spiperone-d2) from the D₂R whereas risperidone dissociated at a moderate pace ($8.49 \times 10^{-1} \text{ min}^{-1}$) (Table 2.1). Moreover, bromocriptine displayed the slowest association rate out of the ligands that we determined ($6.69 \times 10^6 \text{ M}^{-1} \text{ min}^{-1}$), whereas eticlopride displayed the fastest association rate ($1.31 \times 10^9 \text{ M}^{-1} \text{ min}^{-1}$). Both bromocriptine and eticlopride also displayed relatively slow dissociation rates (Table 2.1).

Table 2.1: Kinetic binding parameters of ligands at the SNAP-D₂S_R-WT.

Tracer	Spiperone-d2				Clozapine-Cy5			
	k_{on} , M ⁻¹ min ⁻¹	k_{off} , min ⁻¹	K_d , M (pK _d) ^b	n	k_{on} , M ⁻¹ min ⁻¹	k_{off} , min ⁻¹	K_d , M (pK _d) ^b	n
Spiperone-d2^a	3.89 ± 0.62 x10 ⁷	9.81 ± 1.28 x10 ⁻²	2.52 ± 0.52 x10 ⁻⁹ (8.60)	9	-	-	-	-
Clozapine-Cy5^a	-	-	-	-	1.76 ± 0.31 x10 ⁶	1.96 ± 0.21	1.11 ± 0.23 x10 ⁻⁶ (5.95)	7
Aripiprazole	9.47 ± 2.55 x10 ⁷	1.57 ± 0.12 x10 ⁻¹	1.66 ± 0.46 x10 ⁻⁹ (8.78)	8	6.52 ± 1.88 x10 ⁷	1.50 ± 0.07 x10 ⁻¹	2.29 ± 0.67 x10 ⁻⁹ (8.64)	7
Bifeprunox	3.79 ± 0.44 x10 ⁷	2.92 ± 0.54 x10 ⁻²	7.71 ± 1.69 x10 ⁻¹⁰ (9.11)	8	2.86 ± 0.44 x10 ⁷	3.91 ± 0.28 x10 ⁻²	1.36 ± 0.23 x10 ⁻⁹ (8.87)	7
Bromocriptine	6.69 ± 1.20 x10 ⁶	5.54 ± 0.71 x10 ⁻²	8.29 ± 1.83 x10 ⁻⁹ (8.08)	8	6.37 ± 1.57 x10 ⁶	6.10 ± 0.40 x10 ⁻²	9.59 ± 2.44 x10 ⁻⁹ (8.02)	7
Eticlopride	1.31 ± 0.06 x10 ⁹	7.52 ± 0.86 x10 ⁻²	5.73 ± 0.70 x10 ⁻¹¹ (10.2)	8	8.04 ± 1.81 x10 ⁸	6.93 ± 0.24 x10 ⁻²	8.62 ± 1.96 x10 ⁻¹¹ (10.1)	6
Risperidone	4.25 ± 0.36 x10 ⁸	8.49 ± 0.31 x10 ⁻¹	2.00 ± 0.18 x10 ⁻⁹ (8.70)	7	3.16 ± 0.26 x10 ⁸	6.75 ± 0.46 x10 ⁻¹	2.14 ± 0.23 x10 ⁻⁹ (8.67)	4
Spiperone	9.59 ± 0.91 x10 ⁸	6.46 ± 0.82 x10 ⁻²	6.74 ± 1.07 x10 ⁻¹¹ (10.2)	8	8.78 ± 1.73 x10 ⁸	8.21 ± 0.91 x10 ⁻²	9.35 ± 2.11 x10 ⁻¹¹ (10.0)	5

All values are expressed as the mean ± SEM from 'n' number of experiments performed in singlet wells. ^aSpiperone-d2 and clozapine-Cy5 parameters were determined from association kinetic binding experiments. ^bK_d and pK_d values were calculated from the mean k_{on} and k_{off} values determined via competition kinetic binding experiments.

The Trp100^{EL1}Ala mutation markedly impacts ligand binding kinetics

By determining the binding kinetics of several ligands at the D₂R-WT, we established a reference dataset to then investigate the effects of mutations in extracellular vestibule residues. Due to the low affinity of clozapine-Cy5 it became inadequate as a tracer on mutant D₂Rs. We ascertained that higher concentrations of clozapine-Cy5 were required when its affinity was reduced due to mutation of the D₂R, this resulted in appreciable non-specific binding at these concentrations possibly through bystander FRET. The high non-specific

binding markedly increased the noise when acquiring temporal data (data not shown). Therefore, competition kinetic binding experiments were carried out using the higher affinity tracer spiperone-d2.

Trp100^{EL1} in the D₂R-risperidone structure is positioned over the top of the binding site suggesting that it could potentially act as a hydrophobic “lid” over the orthosteric binding site (Fig. 2.2A) (123). Another D₂R structure, with haloperidol bound, shows disparity in its position of Trp100^{EL1} whereby it is rotated away from the orthosteric site and its sidechain pyrrole ring appears to make polar contacts with Ser103^{3,21} (superscript numbers indicate Ballesteros-Weinstein numbering (243)) on the very top of transmembrane domain (TM) III (Fig. 2.2B) (124). Trp100^{EL1} in this position would likely have less of an effect on ligand binding. Likewise, the corresponding Trp96^{EL1} in the closely related D₃R-eticlopride structure is also in this position (Fig. 2.2C) (121), and the same pose of the Trp^{EL1} is observed in two separate D₄R structures and other aminergic receptor structures (67,122,236,244). We therefore were interested in understanding what role Trp100^{EL1} plays in influencing ligand binding rates.

We first assessed the effect of the Trp100^{EL1}Ala mutation on the fluorescent tracer spiperone-d2. (Table 2.2). The dissociation rate of spiperone-d2 was significantly increased and its affinity was reduced (Fig. 2.2D). Plotting the observed association rate against the concentration of spiperone-d2 demonstrated that a linear relationship remained, indicating that the ligand-receptor binding reaction followed the law of mass action and hence spiperone-d2 could continue to be used as a tracer on this mutant (Fig. 2.2E). Upon performing competition kinetic binding experiments using spiperone-d2 we observed that the mutation significantly reduced the affinity of all the ligands tested (Table 2.2). The three agonists; aripiprazole, bifeprunox and bromocriptine all displayed an accelerated dissociation rate with the largest change occurring on bifeprunox’s dissociation rate which increased approximately 112-fold (Fig. 2.2F). Moreover, bromocriptine was the only ligand to display a significantly increased association rate relative to that at the WT (2.5-fold Δ). In contrast to bromocriptine, the association rates of the antagonists eticlopride and risperidone were significantly decreased (eticlopride 0.17-fold Δ , risperidone 0.37-fold Δ), and spiperone’s association rate was not significantly changed ($P = 0.057$, one-way ANOVA with Dunnett’s multiple comparisons test). Risperidone’s dissociation rate and affinity were less attenuated relative to the other small molecules tested (Table 2.2 and Fig. 2.2G)). The sample size of the ligands is relatively small yet, overall, the loss of affinity at Trp100^{EL1}Ala for the three agonists can be attributed to increases in dissociation rate, whereas for the antagonists, loss of affinity emerges from both a decrease in association rate and an increase in dissociation rate.

Table 2.2: Kinetic binding parameters of ligands at SNAP-D_{2S}R mutants.

	L94A^{2.64}					W100A^{EL1}					I184A^{EL2}					Y379A^{7.35}				
	<i>k</i> _{on} , M ⁻¹ min ⁻¹ (foldΔ ^c)	<i>k</i> _{off} , min ⁻¹ (foldΔ ^c)	<i>K</i> _d ^b , M (foldΔ ^c)	<i>pK</i> _d ^b	<i>n</i>	<i>k</i> _{on} , M ⁻¹ min ⁻¹ (foldΔ ^c)	<i>k</i> _{off} , min ⁻¹ (foldΔ ^c)	<i>K</i> _d ^b , M (foldΔ ^c)	<i>pK</i> _d ^b	<i>n</i>	<i>k</i> _{on} , M ⁻¹ min ⁻¹ (foldΔ ^c)	<i>k</i> _{off} , min ⁻¹ (foldΔ ^c)	<i>K</i> _d ^b , M (foldΔ ^c)	<i>pK</i> _d ^b	<i>n</i>	<i>k</i> _{on} , M ⁻¹ min ⁻¹ (foldΔ ^c)	<i>k</i> _{off} , min ⁻¹ (foldΔ ^c)	<i>K</i> _d ^b , M (foldΔ ^c)	<i>pK</i> _d ^b	<i>n</i>
Spiperone-d2^a	7.99 ± 1.01 x10 ⁷ (2.1) *	1.59 ± 0.15 (16) *	1.99 ± 0.31 x10 ⁻⁸ (7.9) *	7.70	5	5.36 ± 0.64 x10 ⁷ (1.4)	2.01 ± 0.19 (21) *	3.75 ± 0.57 x10 ⁻⁸ (14.9) *	7.43	9	4.41 ± 0.56 x10 ⁷ (1.1)	5.77 ± 0.67 x10 ⁻² (0.59)	1.31 ± 0.23 x10 ⁻⁹ (0.52)	8.88	5	9.17 ± 1.31 x10 ⁷ (2.4) *	4.28 ± 0.23 x10 ⁻¹ (4.36)	4.67 ± 0.71 x10 ⁻⁹ (1.9)	8.33	5
Aripiprazole	9.85 ± 4.04 x10 ⁷ (1.0)	4.26 ± 0.96 (27) *	4.32 ± 2.02 x10 ⁻⁸ (26)	7.36	4	4.60 ± 1.12 x10 ⁷ (0.49)	14.5 ± 2.2 (92) *	3.15 ± 0.90 x10 ⁻⁷ (190) *	6.50	5	8.62 ± 2.11 x10 ⁷ (0.91)	3.58 ± 0.40 x10 ⁻¹ (2.3)	4.15 ± 1.11 x10 ⁻⁹ (2.5)	8.38	5	1.79 ± 0.44 x10 ⁸ (1.9)	8.64 ± 1.27 x10 ⁻¹ (5.5)	4.82 ± 1.38 x10 ⁻⁹ (2.9)	8.32	5
Bifeprunox	6.70 ± 1.54 x10 ⁷ (1.8)	1.03 ± 0.18 (35) *	1.53 ± 0.44 x10 ⁻⁸ (20)	7.81	5	3.77 ± 0.61 x10 ⁷ (1.0)	3.26 ± 0.21 (112) *	8.64 ± 1.50 x10 ⁻⁸ (112) *	7.06	8	2.56 ± 0.57 x10 ⁷ (0.67)	1.05 ± 0.10 x10 ⁻¹ (3.6)	4.12 ± 1.00 x10 ⁻⁹ (5.3)	8.39	5	6.84 ± 1.53 x10 ⁷ (1.8)	1.57 ± 0.22 x10 ⁻¹ (5.4)	2.29 ± 0.60 x10 ⁻⁹ (3.0)	8.64	5
Bromocriptine	1.61 ± 0.19 x10 ⁷ (2.4) *	2.41 ± 0.80 (43) *	1.50 ± 0.53 x10 ⁻⁷ (18) *	6.82	5	1.66 ± 0.28 x10 ⁷ (2.5) *	4.34 ± 0.82 (78) *	2.62 ± 0.66 x10 ⁻⁷ (32) *	6.58	4	2.61 ± 0.38 x10 ⁶ (0.39)	3.02 ± 0.63 x10 ⁻¹ (5.5)	1.16 ± 0.30 x10 ⁻⁷ (14)	6.94	5	1.71 ± 0.32 x10 ⁷ (2.6) *	1.63 ± 0.30 (29)	9.53 ± 2.50 x10 ⁻⁸ (12)	7.02	4
Eticlopride	4.01 ± 0.30 x10 ⁸ (0.31) *	3.16 ± 0.53 x10 ⁻¹ (4.2) *	7.88 ± 1.46 x10 ⁻¹⁰ (14)	9.10	4	2.17 ± 0.09 x10 ⁸ (0.17) *	1.38 ± 0.15 (18) *	6.37 ± 0.76 x10 ⁻⁹ (111) *	8.20	4	1.24 ± 0.15 x10 ⁹ (0.95)	4.55 ± 0.38 x10 ⁻¹ (6.0) *	3.66 ± 0.54 x10 ⁻¹⁰ (6.4)	9.44	4	4.56 ± 0.33 x10 ⁸ (0.35) *	1.79 ± 0.09 x10 ⁻¹ (2.4)	3.92 ± 0.34 x10 ⁻¹⁰ (6.8)	9.41	4
Risperidone	1.73 ± 0.35 x10 ⁸ (0.41) *	1.85 ± 0.44 (2.2)	1.07 ± 0.33 x10 ⁻⁸ (5.3)	7.97	5	1.55 ± 0.28 x10 ⁸ (0.37) *	3.62 ± 0.44 (4.3) *	2.33 ± 0.51 x10 ⁻⁸ (12) *	7.63	7	3.66 ± 0.14 x10 ⁸ (0.86)	1.56 ± 0.15 x10 ⁻¹ (0.18)	4.25 ± 0.45 x10 ⁻¹⁰ (0.21)	9.37	5	1.87 ± 1.02 x10 ⁸ (0.44) *	2.00 ± 0.37 (2.4)	1.07 ± 0.61 x10 ⁻⁸ (5.3)	7.97	5
Spiperone	3.73 ± 0.99 x10 ⁸ (0.39) *	1.45 ± 0.30 (22) *	3.87 ± 1.31 x10 ⁻⁹ (58) *	8.41	5	6.17 ± 0.82 x10 ⁸ (0.64)	1.95 ± 0.12 (30) *	3.17 ± 0.46 x10 ⁻⁹ (47) *	8.50	7	6.93 ± 0.89 x10 ⁸ (0.72)	8.09 ± 0.81 x10 ⁻² (1.3)	1.17 ± 0.19 x10 ⁻¹⁰ (1.7)	9.93	5	8.89 ± 1.65 x10 ⁸ (0.93)	2.78 ± 0.38 x10 ⁻¹ (4.3)	3.13 ± 0.73 x10 ⁻¹⁰ (4.6)	9.50	5

All values are expressed as the mean \pm SEM from 'n' number of experiments performed in singlet wells. ^aSpiperone-d2 parameters were determined from association kinetic binding experiments. ^b K_d and pK_d values were calculated from the mean k_{on} and k_{off} values determined with competition kinetic binding experiments. ^cfold change as compared to the parameters obtained at the wild type D₂R using spiperone-d2 as a tracer. * Statistically significant ($P < 0.05$) from WT value determined with spiperone-d2 by one-way ANOVA and Dunnet's multiple comparison's test.

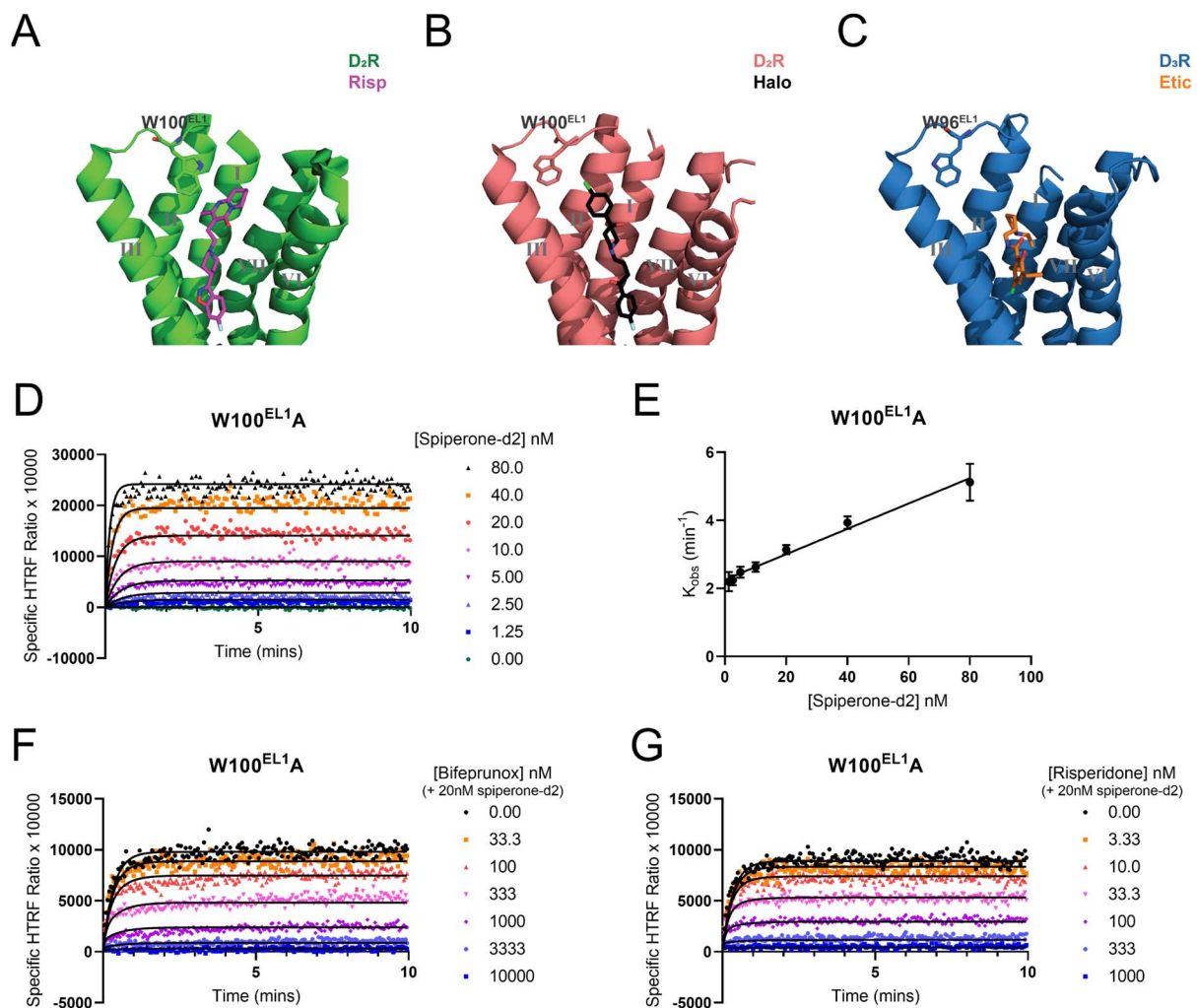


Figure 2.2: Assessment of ligand binding kinetics at the SNAP-D_{2s}R-W100^{EL1}A mutant. (A) Position of Trp100^{EL1} within the D₂R structure (green cartoon) bound to risperidone (Risp) (magenta sticks) (PDB code 6CM4). (B) Position of Trp100^{EL1} within the D₂R structure (red cartoon) bound to haloperidol (halo) (black sticks) (PDB code 6LUQ). (C) Position of Trp96^{EL1} within the D₃R structure (blue cartoon) bound to eticlopride (etic) (orange sticks) (PDB code 3PBL). (D) A representative association kinetic binding trace of increasing concentrations of spiperone-d2 to SNAP-D_{2s}R-W100^{EL1}A (experiment was performed in singlet and representative of 9 separate experiments). (E) Observed association rate vs. concentration plot displays a linear relationship. Observed association rates were determined from one phase association fits at each spiperone-d2 concentration. Data represent the mean \pm SEM (n=9). (F) A single representative competition kinetic binding trace with increasing concentrations of unlabelled competitor bifeprenox (representative of 8 separate experiments performed in singlet wells). (G) A single representative competition kinetic binding trace with increasing concentrations of unlabelled competitor risperidone (representative of 7 separate experiments performed in singlet wells).

The effects of the Leu94^{2.64}Ala mutation and the Trp100^{EL1}Ala mutation show similarities

Leu94^{2.64} is positioned at the top of TM II where, in the D₂R-risperidone structure, it appears to help coordinate Trp100^{EL1} over the top of the orthosteric binding site by making hydrophobic interactions (Fig. 2.3A) (123). In contrast, Leu94^{2.64} in the D₂R-haloperidol structure and Leu89^{2.64} in the D₃R-eticlopride structure do not appear to make large contacts with Trp100^{EL1} or Trp96^{EL1} respectively as this residue is turned away from the orthosteric site (Fig. 2.3A & B) (121,124). Consequently, we next examined the effects of a Leu94^{2.64}Ala mutation on several ligands to see whether this had related effects to the Trp100^{EL1}Ala mutation.

The Leu94^{2.64}Ala mutation significantly increased both the rate of association and dissociation for spiperone-d2 (Table 2.2 and Fig. 2.3D). The net effect was a reduction in spiperone-d2's affinity. In competition kinetic experiments, the Leu94^{2.64}Ala mutation slowed the association rate of all the unlabelled antagonists while the agonists were either unchanged or increased in their association rate. For example, eticlopride's association rate was significantly decreased by 0.31-fold (~30%), while aripiprazole's association rate was unchanged (Fig. 2.3F & G). Furthermore, the effects on dissociation rate were more pronounced than effects on association rate. Indeed, the Leu94^{2.64}Ala mutation increased the rate of dissociation of all ligands tested, with the notable exception of risperidone that displayed a small increase that was not statistically significant. The largest increases in dissociation rate were observed for the agonists, all increasing more than 20-fold. On the whole, it could be seen that there was a broad relationship between the effects at the Leu94^{2.64}Ala mutant with those effects observed at the Trp100^{EL1}Ala mutant. Dissociation rate was considerably increased for the agonists at Leu94^{2.64}Ala and even more so at Trp100^{EL1}Ala. Antagonist association rates were often slowed at these two residues whereas for agonists they were either unchanged or accelerated.

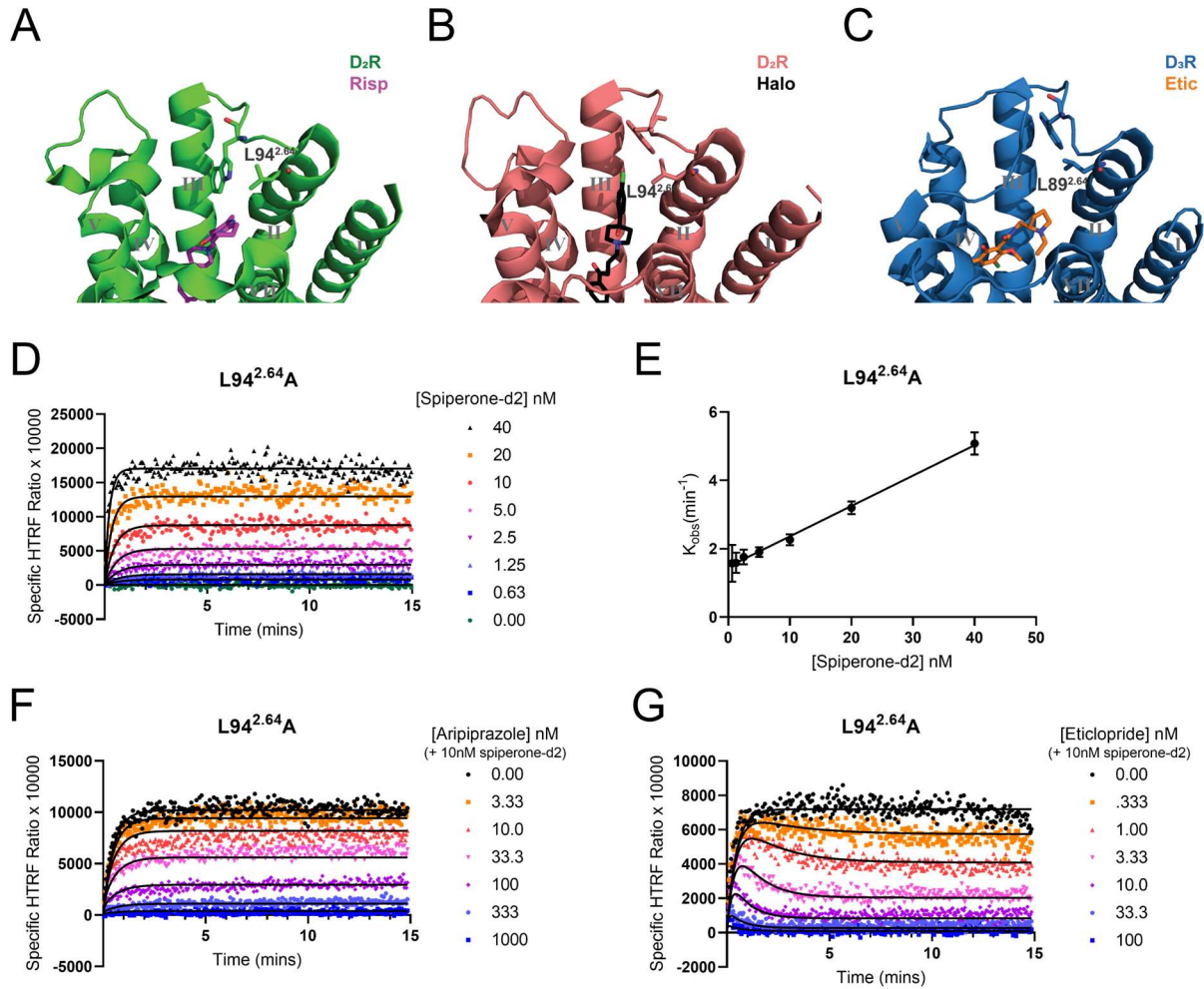


Figure 2.3: Assessment of ligand binding kinetics at the SNAP-D₂sR-L94^{2.64}A mutant. (A) Position of Leu94^{2.64} within the D₂R structure (green cartoon) bound to risperidone (risp) (magenta sticks) (PDB code 6CM4). (B) Position of Leu94^{2.64} within the D₂R structure (red cartoon) bound to haloperidol (halo) (black sticks) (PDB code 6LUQ). (C) Position of Leu89^{2.64} within the D₃R structure (blue cartoon) bound to eticlopride (etic) (orange sticks) (PDB code 3PBL). (D) A representative association kinetic binding trace of increasing concentrations of spiperone-d2 to SNAP-D₂sR-L94^{2.64}A (experiment was performed in singlet and representative of 5 separate experiments). (E) Observed association rate vs. concentration plot displays a linear relationship. Observed association rates were determined from one phase association fits at each spiperone-d2 concentration. Data represent the mean \pm SEM (n=5). (F) A single representative competition kinetic binding trace with increasing concentrations of unlabelled competitor aripiprazole (representative of 4 separate experiments performed in singlet wells). (G) A single representative competition kinetic binding trace with increasing concentrations of unlabelled competitor eticlopride (representative of 4 separate experiments performed in singlet wells).

No large consequences in ligand binding kinetics are caused by an Ile184^{EL2}Ala mutation

We next examined the effect of an Ile184^{EL2}Ala mutation on ligand binding kinetics. In the D₂R-risperidone structure, Ile184^{EL2}'s side chain extends from its short α -helix in EL2 across to the top of the orthosteric binding pocket and interacts with Trp100 on EL1 (Fig. 2.4A, 2.2A & 2.3A) (123). However, in the D₂R-haloperidol structure Trp100^{EL1} is turned away and thus does not interact with Ile184^{EL2} (Fig. 2.4B and 2.3B) (124). Additionally, the Ile^{EL2} in the D₃R structure (Ile183^{EL2}) is in a different pose whereby EL2 is disordered, resulting in Ile183^{EL2} being directed downwards and the Ile183^{EL2} backbone hydrogen bonding with His349^{6.55} (His393^{6.55} in D₂R) (Fig. 2.4C) (121). While these interactions of Ile184^{EL2} would suggest it may be important for ligand entry and egress, the Ile184^{EL2}Ala mutation generally influenced ligand kinetics the least out of all amino acid residue mutants in this study (Table 2.2). However, very little statistically significant differences were determined between this mutant and the WT. For example, risperidone's dissociation rate did not significantly change at the Ile184^{EL2}Ala mutant ($P = 0.39$, one-way ANOVA with Dunnett's multiple comparisons test). Eticlopride was the only ligand significantly affected with its dissociation rate being increased approximately six-fold.

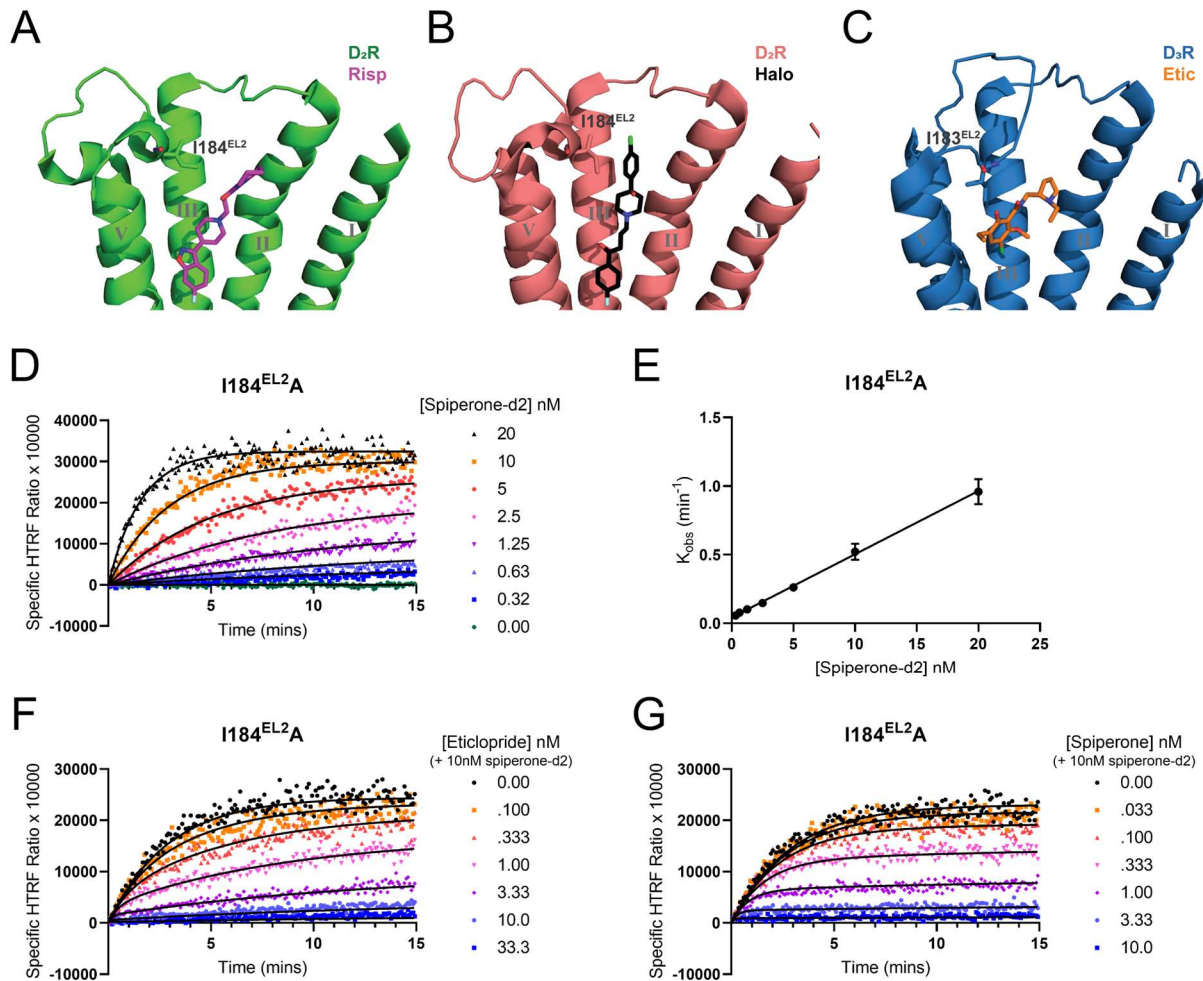


Figure 2.4: Assessment of ligand binding kinetics at the SNAP-D₂sR-I184^{EL2}A mutant. (A) Position of Ile184^{EL2} within the D₂R structure (green cartoon) bound to risperidone (risp) (magenta sticks) (PDB code 6CM4). (B) Position of Ile184^{EL2} within the D₂R structure (red cartoon) bound to haloperidol (halo) (black sticks) (PDB code 6LUQ). (C) Position of Ile183^{EL2} within the D₃R structure (blue cartoon) bound to eticlopride (etic) (orange sticks) (PDB code 3PBL). (D) A representative association kinetic binding trace of increasing concentrations of spiperone-d2 to SNAP-D₂sR- I184^{EL2}A (experiment was performed in singlet and representative of 5 separate experiments). (E) Observed association rate vs. concentration plot displays a linear relationship. Observed association rates were determined from one phase association fits at each spiperone-d2 concentration. Data represent the mean \pm SEM (n=5). (F) A single representative competition kinetic binding trace with increasing concentrations of unlabelled competitor eticlopride (representative of 4 separate experiments performed in singlet wells). (G) A single representative competition kinetic binding trace with increasing concentrations of unlabelled competitor spiperone (representative of 5 separate experiments performed in singlet wells).

Some ligand's association kinetics can be influenced by a Tyr379^{7.35}Ala mutation

Tyr379^{7.35} (Tyr408^{7.35} in D₂L_R) sits at the top of TM VII and makes a hydrogen bond with His393^{6.55}. Broadly, Tyr379^{7.35} exists in two different poses in current D₂-like X-ray crystal structures. In the D₂R-risperidone structure, the Tyr379^{7.35} sidechain is positioned across towards TM VI (Fig. 2.5A)(123). Tyr379^{7.35} in the D₂R-haloperidol structure is positioned with its side chain pointing in towards the orthosteric binding site and the hydroxy group hydrogen bonds with haloperidol (Fig. 2.5B) (124). This same pose is also observed in the D₃R-eticlopride (Tyr365^{7.35}) structure and other reported D₄R structures (Fig. 2.5C)(121,122,236). The position Tyr379^{7.35} adopts in the D₂R-haloperidol structure and D₃R-eticlopride structure would in fact clash with risperidone as positioned in the D₂R-risperidone structure. This indicates that the side chain of Tyr379^{7.35} is likely quite dynamic.

Upon mutation of tyrosine 379^{7.35} to alanine, spiperone-d₂'s association rate was increased. This increase was likely an effect of the attached fluorophore because unlabelled spiperone was unchanged in its association rate (Table 2.2 and Fig. 2.5A & B). Eticlopride (0.35-fold Δ) and risperidone (0.44-fold Δ) were both significantly slowed in their association rate at the Tyr379^{7.35}Ala mutant. The Tyr379^{7.35}Ala mutant significantly increased the association rate of bromocriptine approximately 2.6-fold (Table 2.2 and Fig. 2.5G). Additionally, no ligands displayed any significant differences in their dissociation rate or the affinity (Fig. 2.5F). Overall, Tyr379^{7.35} may be an important mediator of the association for some, but not all, agonists and antagonists.

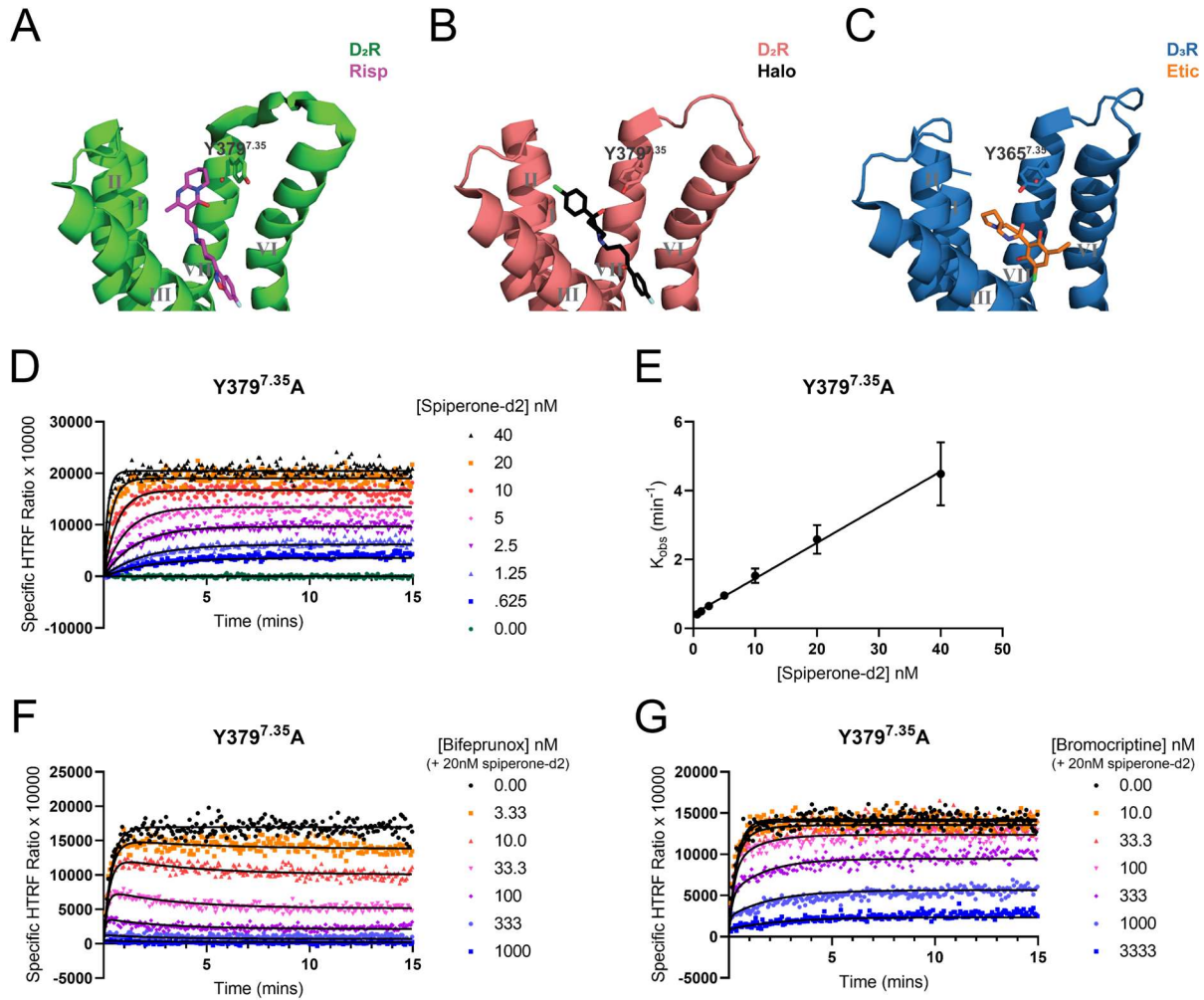


Figure 2.5: Assessment of ligand binding kinetics at the SNAP-D₂sR-Y379^{7.35}A mutant. (A) Position of Tyr379^{7.35} within the D₂R structure (green cartoon) bound to risperidone (risp) (magenta sticks) (PDB code 6CM4). (B) Position of Tyr379^{7.35} within the D₂R structure (red cartoon) bound to haloperidol (halo) (black sticks) (PDB code 6LUQ). (C) Position of Tyr365^{7.35} within the D₃R structure (blue cartoon) bound to eticlopride (etic) (orange sticks) (PDB code 3PBL). (D) A representative association kinetic binding trace of increasing concentrations of spiperone-d2 to SNAP-D₂sR-Y379^{7.35}A (experiment was performed in singlet and representative of 5 separate experiments). (E) Observed association rate vs. concentration plot displays a linear relationship. Observed association rates were determined from one phase association fits at each spiperone-d2 concentration. Data represent the mean \pm SEM (n=5). (F) A single representative competition kinetic binding trace with increasing concentrations of unlabelled competitor bifeprunox (representative of 5 separate experiments performed in singlet wells). (G) A single representative competition kinetic binding trace with increasing concentrations of unlabelled competitor bromocriptine (representative of 4 separate experiments performed in singlet wells).

2.4 Discussion

In this study, we made some of the first efforts towards understanding the roles residues in the extracellular regions of the D₂R play in determining ligand binding kinetics. We demonstrated that some selected amino acid residues in the extracellular regions of the D₂R

can dramatically alter ligand binding association and dissociation in a ligand-dependent fashion. This suggests that small molecule drugs can be rationally designed based on particular metastable binding sites as they enter and exit from the D₂R. Hence, medicinal chemistry of ligands targeting the D₂R can be guided by these new contact sites identified upon entry and exit of the receptor in addition to the ligand contacts in the final binding pose within the orthosteric site as is classically done. Furthermore, we highlighted the importance of measuring ligand binding kinetics at GPCRs by the fact that often the association rate and/or dissociation rate of a ligand was altered without the affinity being altered. Therefore, these changes in binding would not be detected in traditional equilibrium binding assays. Moreover, through selecting a panel of structurally diverse ligands including antipsychotics from different classes and agonists with varying efficacy, we were able to show that the same mutation can influence the binding kinetics of agonists and antagonists in a distinct manner. Indeed, at the Trp100^{EL1}Ala mutation and the Leu94^{2,64}Ala mutation, agonists' dissociation rates were increased whereas for antagonists both the association rates and dissociation rates were negatively impacted. This may reflect distinct binding pathways between agonists and antagonists at the D₂R or possibly different conformational equilibria of the receptor.

Our results on the Trp100^{EL1}Ala mutant revealed that Trp100^{EL1} is critical for determining the binding kinetics of all the six ligands that were tested. This indicates that Trp100^{EL1} is likely important for the binding of most D₂R ligands. The results at this mutant are consistent with Wang and colleagues radioligand binding experiments reporting that Trp100^{EL1} was an important residue for prolonging the dissociation rate of risperidone and some additional ligands (123). Indeed, in our experiments the Trp100^{EL1}Ala mutation had a larger impact on dissociation rates than association rates. Moreover, Wang and colleagues first singled out the Trp100^{EL1} residue due to the unique “lid” position it adopts in the D₂R-risperidone structure (Fig. 2.2A & 2.3A). However, out of all the ligands tested in our study, risperidone's dissociation rate and its affinity were the least impacted by the Trp100^{EL1}Ala mutation (k_{off} 4.3-fold Δ , K_d 12-fold Δ). It is not clear as to why this is the case for risperidone, although, future assessment of additional ligands at this mutant may further our knowledge of the mechanisms behind this observation. Moreover, bifeprunox displayed the slowest dissociation rate out of the ligands tested. Interestingly, the dissociation rate of bifeprunox was considerably impacted (112-fold Δ) by the Trp100^{EL1}Ala mutation. Bifeprunox is a bitopic drug (Fig. 2.1), therefore the fact that Trp100^{EL1}Ala influences its dissociation to such an extent may be evidence for bifeprunox's benzyl group extending out and making contacts with Trp100^{EL1} that helps maintain bifeprunox in the binding site for an extended period.

The changes in binding kinetics at the Leu94^{2.64}Ala mutant appeared to follow a similar trend to the Trp100^{EL1}Ala effects. Certainly, most ligands' dissociation rates were significantly increased at the Leu94^{2.64}Ala, this was consistent with previous research showing that the Leu94^{2.64}Ala mutation increases the dissociation rate of nemonapride from the D₂R (123). The two mutants having similar effects suggests that Leu94^{2.64} and Trp100^{EL1} interact. Given that ligand dissociation rates were often impacted suggests that one of these interactions is likely to be Leu94^{2.64} stabilising Trp100^{EL1} in a position that extends the lifetime of the drug-receptor complex after the ligand has bound in some manner. For Trp100^{EL1} to exchange between the position in the D₂R-risperidone structure and the D₂R-haloperidol structure it may have to cross Leu94^{2.64}. However, whether the important pose of Trp100^{EL1} is Trp100^{EL1} in its “lid” position as shown in the D₂R-risperidone structure or the outward position in the D₂R-haloperidol structure or a completely different pose are unclear from these experiments. What is clear is that Leu94^{2.64} likely contributes through coordinating Trp100^{EL1} and the region is likely quite dynamic because ligands display differing sensitivity to these mutations. Future work incorporating molecular dynamics simulations would help disentangle the poses and interactions that occur at these residues.

There were limited changes in the binding kinetics of each of the ligands at the Ile184^{EL2}Ala mutant. The only statistically significant finding was that of an increase in eticlopride's dissociation rate. This is interesting considering that the analogous Ile183^{EL2} in the D₃R-eticlopride structure appears to be coordinated downwards towards the ligand relative to the current D₂R structures (Fig. 2.4A, B & C) (121). One could speculate tentatively that eticlopride may direct this residue along with EL2 into a different orientation as opposed to other ligands. Moreover, the overall observation that there were little effects at the Ile184^{EL2}Ala mutant initially appears inconsistent with previous research, for example, early work by Shi and Javitch (234) identified this residue as important when scanning D₂R EL2 residues with the substituted cysteine accessibility method. In this previous work, Ile184^{EL2} was substituted for cysteine and allowed to react with methanethiosulfonate substrate derivatives. Having a bulky methanethiosulfonate substrate derivative attached lead to the inhibition of the binding of the antagonist ³[H]N-methylspiperone, indicating that the residues' side chain is directed towards the binding site (234). Indeed, the position of Ile184^{EL2} was directly observed upon solving the D₂R-risperidone X-ray crystal structure where it was shown to be positioned inwards over the orthosteric binding site (Fig. 2.4A)(123). From the crystal structure, Wang and colleagues suggested that Ile184^{EL2} was important for ligand binding kinetics by making contacts with Trp100^{EL1}. However, Wang and colleagues did not observe any significant effect

of the Ile184^{EL2}Ala mutation on risperidone's dissociation rate unless the mutation was combined with the Leu94^{2.64}Ala mutation (123). Together this suggests that Leu94^{2.64} is probably more important for the correct coordination of Trp100^{EL1} than Ile184^{EL2} is. Certainly, in our experiments the Ile184^{EL2}Ala effects did not relate to those of the Trp100^{EL1}Ala like the Leu94^{2.64}Ala effects did. Therefore, our data illustrates that Ile184^{EL2} does not play a substantial role in determining ligand binding kinetics even though it can line the top of the binding site. In agreement with this, we previously showed that the Ile184^{EL2}Ala mutation did not impact the equilibrium binding affinity of aripiprazole with radioligand binding assays (235). Additionally, we have demonstrated in a separate study using molecular dynamics simulations that the EL2 of the D₂R is can be disordered and has a propensity spontaneously unwind from its largely α -helical nature (125) (Fig. 2.4C). Accordingly, if EL2 is unwound then IL184^{EL2} may be oriented differently and hence play a less important role in ligand binding. In addition, it is worth noting that the chemical divergence between the isoleucine to alanine mutation may not have been distinct enough to notice an effect. Future research could assess the effects upon mutation to a polar residue.

The data on the Tyr379^{7.35}Ala mutant suggests that Tyr379^{7.35} may be important for the association of some antagonists. A previous molecular dynamics study provided evidence that Tyr379^{7.35} can make initial contacts with clozapine and haloperidol, allowing these ligands to gain entry into the extracellular vestibule before entering into their final binding pose deeper in the orthosteric site (126). Therefore, the results here are in agreement with these previous molecular dynamics simulations and that eticlopride and risperidone may have a similar passageway of association as that proposed for clozapine and haloperidol. It is important to note, however, that spiperone's association rate was not significantly decreased even though it shares a butyrophenone moiety with haloperidol. The specific lack of impact on spiperone warrants follow up studies on additional antagonists because it indicates that not all antagonists follow the same entry pathway. Indeed, antagonists following different entry pathways may permit the fine-tuning of antagonist association rates which is an major factor for determining an antipsychotic's propensity to cause extrapyramidal side effects (61).

We have shown that understanding the role of extracellular vestibule residues in determining ligand binding kinetics requires extensive dynamic experiments that cannot easily be predicted from a stationary crystal structure. Certainly, the Ile184^{EL2} residue would appear to be important for binding of many ligands based on its position in D₂R receptor structures. However, X-ray crystal structures reflect only a single snapshot of one binding pose of a ligand in the receptor. In addition, the currently available D₂R structures were solved by using

identical constructs that harbour the same thermostabilising mutations (123,124). Consequently, there could be constraints in these structures that do not represent the multiple different conformations that the D₂R can adopt. Determining D₂R structures with different receptor constructs as well as in apo- and active-states would provide a wider picture in understanding the possible roles different residues play in influencing ligand entry and exit.

We encountered some technical challenges in this study that may explain why there has only been a handful of reports assessing the effects mutagenesis on the ligand binding kinetics of GPCRs. We identified that clozapine-Cy5, that has low D₂R affinity, would not be a suitable tracer ligand at a number of the mutants due to an inability to use it at higher concentrations. We also identified that differing concentrations of ligands and measurement timescales were often required depending on the D₂R mutant. Therefore, the assay throughput is reduced owing to the amount of optimisation required for each mutant and ligand combination. In addition to this, low affinity and fast dissociating unlabelled competitor ligands could not have their binding kinetics determined at mutant receptors because their binding kinetics were above the temporal limits of assay detection (245).

While performing competition kinetic binding experiments is excellent for aiding drug discovery efforts due to its ease and throughput, there is also a limitation in that the kinetic rates of association and dissociation are average rates of potentially multiple binding pathways. Hence, there may be far more complexity in the entry and exit pathways of different ligands that is overlooked with this approach. Fitting with this idea, the dissociation of miroviroc at the CCR5 was argued to be a multi-step event as it displayed a two-phase fit that indicated that there is possibly two receptor bound states; one with tighter binding and one that dissociates faster (246). Therefore, coupling the data in this study with single molecule studies or molecular dynamics simulations would deepen our understanding of these processes. Single molecule fluorescent ligand binding studies could reveal multiple different populations that correspond to multiple different binding pathways or processes (247). In addition, molecular dynamics simulations would also allow for the high-resolution visualisation of the multiple different binding pathways.

In summary, we have taken the first steps towards identifying amino acid residues that may be important in lining the ligand entry and exit pathways of the D₂R. The results in this study may be used towards guiding design of D₂R ligands with the appropriate kinetics for the particular indication of interest. In addition, we have provided a framework for interrogating ligand binding kinetics of mutant GPCRs with TR-FRET competition kinetic binding. Hence,

our study here and studies following our framework will be crucial to deepening our knowledge of the molecular determinants of binding kinetics at GPCRs to enhance rational drug design.

2.5 Supplementary Materials

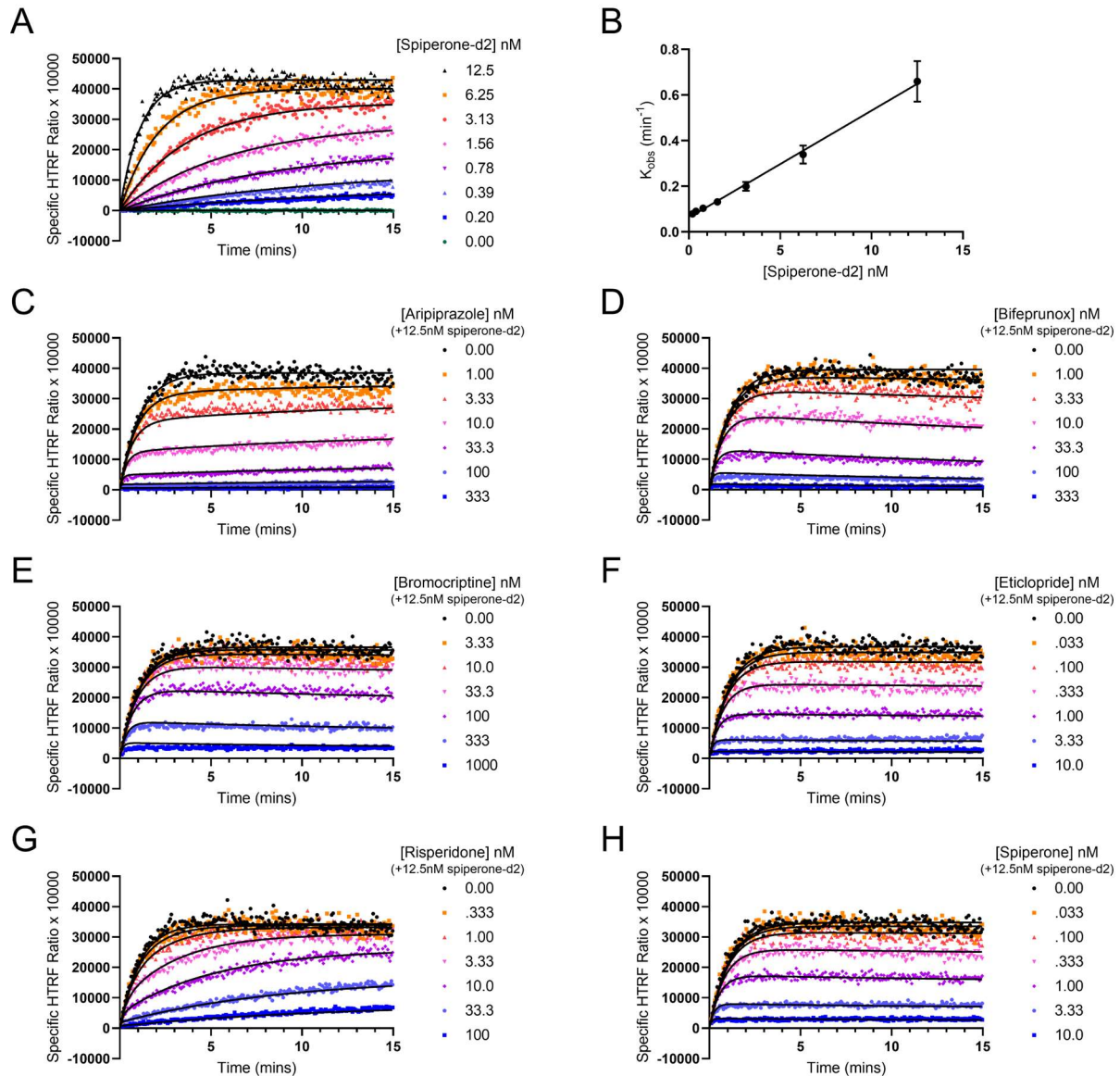


Figure S2.1: SNAP-D₂sR-WT membrane binding with spiperone-d2 fluorescent ligand tracer. (A) Representative association kinetic binding trace of increasing concentrations of spiperone-d2 to SNAP-D2SR-WT (n=9). (B) Observed association rate vs. concentration plot displays a linear relationship. Observed association rates were determined from one phase association fits at each spiperone-d2 concentration. Data represent the mean \pm SEM (n=9). (C-H) Single representative competition kinetic binding traces with increasing concentrations of unlabelled; aripiprazole (n=8) (C), bifeprunox (n=8) (D), bromocriptine (n=8) (E), eticlopride (n=8) (F), risperidone (n=7) (G) and spiperone (n=8) (H).

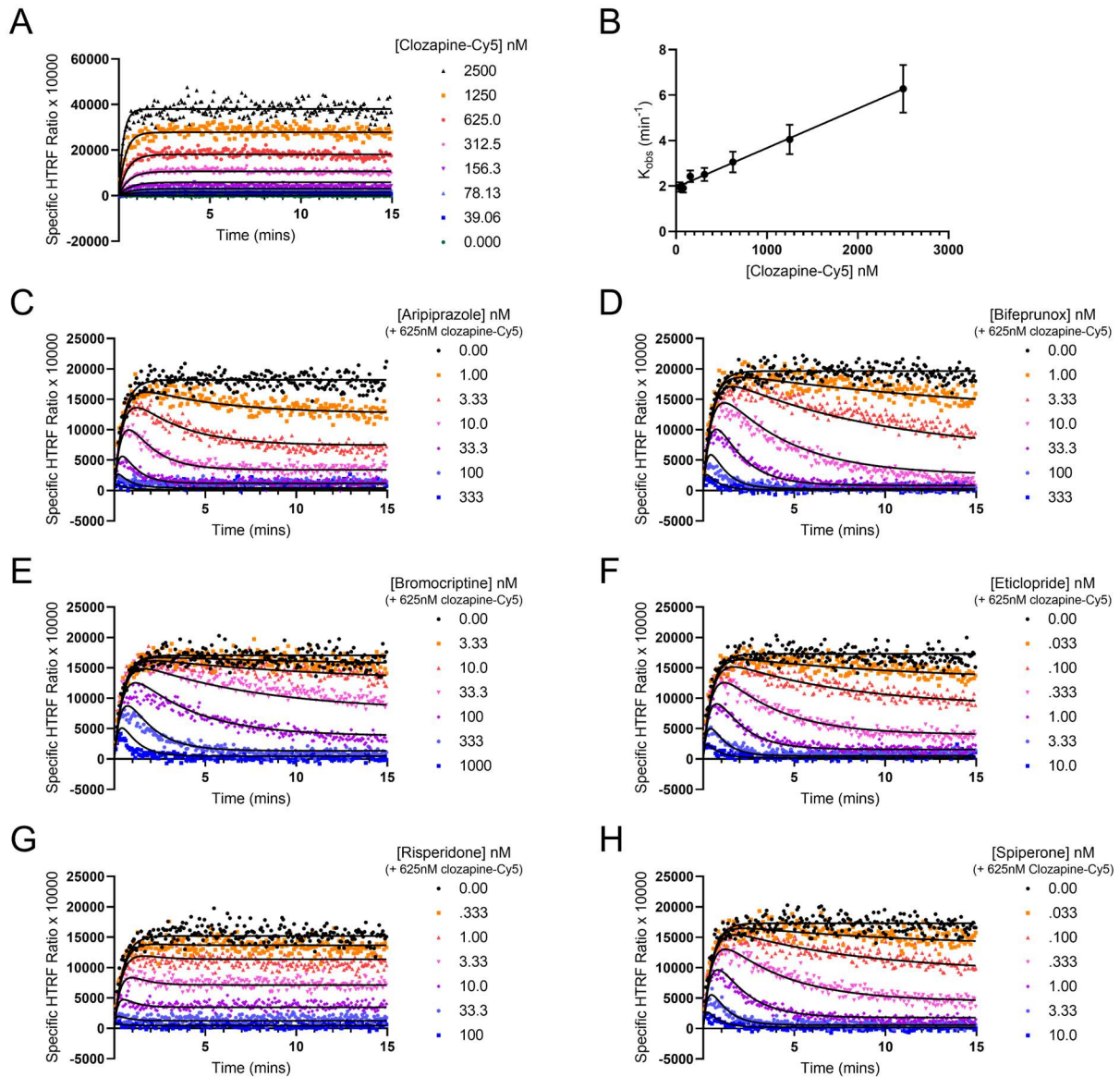


Figure S2.2: SNAP-D₂S_R-WT membrane binding with clozapine-Cy5 fluorescent ligand tracer. (A) Representative association kinetic binding trace of increasing concentrations of clozapine-Cy5 to SNAP-D₂S_R-WT (n=7). (B) Observed association rate vs. concentration plot displays a linear relationship. Observed association rates were determined from one phase association fits at each clozapine-Cy5 concentration. Data represent the mean \pm SEM (n=7). (C-H) Single representative competition kinetic binding traces with increasing concentrations of unlabeled; aripiprazole (n=7) (C), bifeprunox (n=7) (D), bromocriptine (n=7) (E), eticlopride (n=6) (F), risperidone (n=4) (G) and spiperone (n=5) (H).

Chapter 3:

A systematic exploration of the relationship between agonist binding kinetics and observations of biased agonism at dopamine D₂ receptor proximal signalling events

Abstract

In the previous chapter it was highlighted that ligands binding the D₂R can have quite different binding kinetics. In this chapter, we investigated what differing binding kinetics of agonists may mean for the functional effects of those agonists. It is well appreciated that GPCRs, including the D₂R, can elicit pluri-dimensional signalling waves mediated by different G proteins, regulatory proteins and other signalling effectors. Moreover, some agonists are capable of preferentially activating one signalling pathway over another, a phenomenon termed biased agonism. By selectively activating the desired pathway, harnessing biased agonism can potentially reduce a drugs' on-target side effects while maintaining the therapeutic benefit. However, the mechanisms responsible for biased agonism are largely unknown. Establishing the mechanisms of biased agonism allows for the rational design of biased agonists. Therefore, we aimed to investigate whether the length of time an agonist binds the D₂R may influence its signalling and manifest biased agonism. Time resolved-fluorescence resonance energy transfer competition kinetic binding assays were used to determine the binding kinetics of a panel of ligands. The agonist's functional effects were then assessed at multiple receptor-proximal events including G protein activation, regulatory protein recruitment and D₂R trafficking using bioluminescence resonance energy transfer. Responses were quantified with an operational model of agonism and compared to their binding kinetic parameters. Modest biased agonism was detected mainly between well coupled G proteins and poorly coupled regulatory proteins. Agonist dissociation rate did not consistently correlate with biased agonism and no clear relationship between agonist dissociation rate and apparent biased agonism could be established. Both association rate and dissociation rate may partly contribute to biased agonism observations. Differences in the functional affinity of agonists may be responsible for most observations of bias at the D₂R. Overall, further studies involving a larger number of agonists and providing more mechanistic insight are warranted to understand whether binding parameters influence D₂R biased agonism detection.

3.1 Introduction

G protein-coupled receptors (GPCRs) are the largest drug target in the world, accounting for approximately 30% of all marketed drugs (2). GPCRs are characterised by seven α -helical transmembrane domains that snake through the plasma membrane. They receive extracellular signals in the form of agonists such as hormones, neurotransmitters and odorants, that induce conformational changes in the GPCR, permitting signal transduction into the cell.

Recent research has provided increasing examples of the multifaceted nature of GPCR signalling. Once activated, GPCRs can couple to heterotrimeric G proteins, consisting of a G α subunit and a G $\beta\gamma$ obligate dimer. GPCRs can couple to multiple distinct G proteins, described according to the different G α subfamilies that can act on different downstream signalling effectors (248). Having coupled to G proteins, GPCRs commonly bind G protein coupled-receptor kinases (GRKs) and arrestins to regulate the G protein mediated signalling (249). In addition, arrestins may also act as a signalling scaffold to help elicit a distinct wave of signalling (250). Considerable efforts have been made to understand and harness this multifaceted nature of GPCR signalling in an effort to design improved drugs. This has spawned the notion of biased agonism. Biased agonism is the phenomenon of one agonist that acts to preferentially activate one signalling pathway more than another signalling pathway at the same receptor (70). It is widely accepted that GPCRs are capable of existing in multiple conformational states (71,72). Hence, having this natural capability, biased ligands are thought to act via stabilising distinct states of the GPCR (76). These different conformational states then presumably lead to the differential coupling of heterotrimeric G proteins or other effectors (e.g. arrestins) and thus lead to signalling pathways being activated to different extents.

A GPCR at which biased agonism has previously been investigated is the dopamine D₂ receptor (D₂R). The D₂R has long been a validated therapeutic target for neuropsychiatric and neurological diseases. The D₂R is known to promiscuously couple to all members of the G $\alpha_{i/o}$ family (132). While it is thought that the D₂R mainly couples to the G α_o isoforms; G α_{oA} and G α_{oB} , in the brain (140), there is also strong evidence of D₂R coupling to other G proteins. For example, the D₂R may couple to a G α_i subtype (G α_{i1} , G α_{i2} or G α_{i3}) in the dorsal striatum where the receptor has reduced sensitivity to dopamine (144). Similarly, coupling to G α_z may be important for D₂R dependent hyperlocomotion, adrenocorticotrophic hormone secretion and hypothermia (150,151). Furthermore, some D₂R mediated behaviours may be dependent on arrestin scaffolding to mediate a signalling pathway distinct from those mediated by G proteins involving protein phosphatase 2, Akt and GSK3 β (155). Therefore, by selectively biasing the

coupling towards different G proteins or arrestin, a D₂R drug may have differential effects. For this reason, such drugs that display apparent bias at the D₂R have already been generated including those that display bias between G proteins and arrestins and those that display bias between different G protein subtypes (184,251,252). Understanding how such agonists engender bias at the D₂R is important because then one may be able to extend the mechanism to other GPCRs. If mechanisms are shared across GPCRs, such as agonists displaying a particular biochemical property or characteristic that is responsible for manifesting bias, then this would enable the rational design of biased agonists at other GPCRs, and in turn, greatly improve the efficiency of the drug discovery process.

Ligand binding kinetics has long been implicated in efforts aiming to understand the functional effects of agonists. One of the early attempts to relate the binding kinetics to the action of drugs was proposed by Paton in 1961 (90). Paton's "rate theory of drug action" was based on experiments with a range of ligands performed on guinea-pig ileum. It was observed that the magnitude of the response was proportional to the rate of the offset of the response. Paton concluded that a ligand must dissociate from the receptor before another ligand could bind and exert its effects, hypothesising that agonists act effectively as competitive antagonists after having induced signalling at the receptor. Hence, the theory states that agonist action is dependent on the number of interactions an agonist makes with the receptor. Following this, kinetic models have been developed based on the idea that an agonist can allosterically activate a GPCR that essentially acts as an enzyme to facilitate guanine nucleotide exchange on the G protein (253,254). It could be conceived from these models that a slower agonist dissociation rate may lead to higher efficacy because more productive G protein cycle events are able to occur before agonist dissociation. Following this logic, Sykes and colleagues were able to show a correlation between agonist efficacy and dissociation rate at the muscarinic acetylcholine M₃ receptor (91). Likewise, the same correlation has also been observed at the adenosine A_{2A} receptor (93).

While our laboratory did not observe any clear relationship between ligand binding kinetics and efficacy, we recently reported that the differing binding kinetics of agonists can lead to observations of apparent biased agonism (96). This was exemplified using the D₂R as a prototypical GPCR, agonists with slow dissociation rates were shown to display biased agonism between distinct signalling endpoints in a manner that changed over time. The apparent bias emerged from slow dissociating agonists relative to fast dissociating agonists, and Klein-Herenbrink *et al.* (96) provided evidence that the interplay between agonist binding kinetics, the kinetics of cell signalling events and the kinetics of regulatory/desensitization

pathways altogether lead to apparent bias. Subsequent studies on the serotonin 5-HT_{2A} and 5-HT_{2B} receptor used mutagenesis to alter the binding kinetics of agonists and by doing so, showed that β -arrestin-2 recruitment could be selectively modulated with minimal effects on G protein dependent pathways (97). Moreover, biased agonists acting at the Y₁ receptor may impart their bias by increasing the relative residence time of the G protein with the Y₁ receptor (98). Together these studies may indicate that agonists with a long residence time may induce a different conformational landscape in the GPCR for an extended amount of time and thus permit different effectors, such as G proteins or arrestins, to engage the receptor for different amounts of time, leading to biased signalling. In addition, other mechanisms may explain the bias observations due to differences in agonist dissociation rate. For example, Woolf and Linderman (255) used a kinetic two-dimensional Monte Carlo model to suggest that differently sized enrichment zones can be created on the plasma membrane due to differing dissociation rates of agonists, this in turn can result in GRK recruitment becoming partially disconnected from G protein signalling.

Our groups' previous work had some limitations that we sought to address in this study. Our previous research used a finite number of agonists in which all the slowly dissociating agonists were also partial agonists with a similar bitopic piperazine derivative structure. Additionally, all the higher efficacy agonists that were tested dissociated quickly from the D₂R. Moreover, we only measured the activation of a subset of G $\alpha_{i/o}$ proteins and we measured the activation of downstream signalling events that may be more prone to cellular system effects such as cAMP inhibition, cellular impedance and ERK1/2 phosphorylation. To address these concerns in this study, we selected a larger panel of agonists with greater structural diversity and a wider range of agonist efficacy. This allowed us to draw stronger conclusions on relationships between agonist kinetics and particular functional measurements. In addition, we measured proximal signalling and regulatory events at the D₂R, encompassing G $\alpha_{i/o}$ subfamily activation including G α_z activation, GRK2 recruitment, arrestin recruitment and D₂R trafficking. By doing so, we allow for less kinetic steps to occur between ligand binding and the signalling response. We identified that while agonist dissociation rate may play a role in bias observations, agonist association rate may also play an equally important role – possibly through rebinding. Our results show that, even at proximal receptor events, high affinity agonists that increase in occupancy over time may display some apparent bias relative to agonists that have a relatively constant occupancy over time. Considering differing changes in agonist occupancy over time will be a critically important step for pre-clinical biased agonism drug discovery moving forward.

3.2 Methods

Materials

Drugs: aripiprazole, bifeprunox, cariprazine and pardoprunox were synthesised in house as previously reported (96,256). Brexpiprazole was synthesised in house. Ropinirole was sourced from BetaPharma Shanghai. Dopamine, S-3PPP, bromocriptine, rotigotine and spiperone were sourced from Sigma-Aldrich Corporation. ST-836 was a generous gift from Thomas P. Blackburn. PPHT-Red was from Cisbio. Clozapine-Cy5 was synthesised in house as previously described (237).

Kinetic binding assays

The terbium labelling of receptors, fluorescent ligand binding assays, determination of fluorescent ligand binding kinetics, competition kinetic binding assays and data analysis were performed as previously described (61), also as outlined in the previous chapter and in appendix 2. Determination of kinetic parameters for ST-836 were performed identically except that clozapine-Cy5 was used as the fluorescent tracer.

Cell culture

Parental Flp-In HEK 293 cells and Flp-In HEK 293 cells stably expressing the human D_{2L}R were cultured in plastic T175 flasks with DMEM + 10% FBS (+ 600µg/mL G418 for D_{2L}R expressing cells). Cells were split 1/10 with 1xVersene + trypsin (0.5%) every 2 days and were not passaged beyond 30 passages.

G protein activation

G protein activation was measured by means of a bioluminescence resonance energy transfer (BRET) assay that has been described earlier (132,257). The mechanism by which the BRET technique functions is through the ability of the pleckstrin homology domain of GRK3 to reversibly bind free Gβγ subunits such that when the Gα subunit becomes active (GTP bound conformation) the Gα subunit dissociates from Gβγ and then the BRET donor; masGRK3ct-Rluc8, binds dissociated Gβ₁γ₂-venus subunits – the BRET acceptor. The BRET sensors were adapted from earlier FRET constructs, both first published by Hollins and colleagues (258).

Flp-In HEK 293 cells recombinantly expressing the human D₂L_R were initially harvested and plated into 10cm dishes at a density of 2.5 million cells. 24 hours after transferring the cells to dishes the cells were co-transfected with the different plasmid DNA constructs using polyethylenimine (PEI) at a ratio of 1:6 (μ g DNA: μ g PEI). The following constructs (in pcDNA3.1) were transfected in a ratio of 1:1:1:2 (μ g): masGRK3ct-Rluc8, venus-156-239-G β ₁, venus-1-155-G γ ₂, and either G α _{i1}/G α _{i3}/G α _{oA}/G α _{oB}-C351I, G α _{i2}-C352I or G α _z-WT. MasGRK3ct-Rluc8, venus-156-239-G β ₁ and venus-1-155-G γ ₂ constructs were kind gifts from Nevin Lambert (Augusta University, USA). PTX insensitive mutant G α subunits and G α _z were from the cDNA resource centre, cDNA.org. The following morning, the transfected cells were collected from the dishes and plated into poly-D-lysine coated white-bottom 96 well optiplates. That night, the cells were treated in their plates with pertussis toxin (100ng/mL) in DMEM + 10% FBS for 16 hours. The next day the plates were taken out of the cell culture incubator and the media was aspirated, washed with Hank's balanced salt solution (HBSS) pH 7.4 and replaced with 80 μ L HBSS. The plate was returned to 37°C for the remainder of the experiment. The cells were then left to equilibrate for 15 minutes in HBSS. 10 μ L of coelenterazine-h (final concentration of 5 μ M) was then added to the wells with an electronic Eppendorf multi-step pipette and the plate was incubated for another 15 minutes before addition of the drugs. The plate was then detected in a PHERAstar® FS microplate reader (BMG LABTECH GmbH, Germany). The PHERAstar® FS is equipped for simultaneous dual emission detection of the donor 465-505nm and acceptor 505-555nm. The plate was continuously measured with a 30s cycle time, 2.5 minutes occurred before addition of the D₂L_R agonist of interest using a 12 channel Eppendorf electronic multi-pipette. The measurements from the acceptor channel were then divided by the donor channel to determine the BRET ratio. The BRET ratio was then normalised with the maximal effect produced by dopamine set to 100%. The setup of experiments measuring the functional re-association kinetics of G α _{oB} heterotrimers was kept identical up until the day of the assay with the exception of cells being devoid of treatment with pertussis toxin. After washing the cells with HBSS on the day of the assay, 140 μ L of HBSS was added to each well and a cocktail of 40 μ L of coelenterazine-h was co-added with 100nM ropinirole, 33nM cariprazine, 100nM aripiprazole, 1nM rotigotine and 100nM bifeprunox 12.5 minutes before addition of 20 μ L of spiperone to make a final concentration of 20 μ M. For these experiments the data was normalised to wells with the particular agonist followed by the vehicle set to 100%.

GRK2 and arrestin recruitment

GRK2 and arrestin recruitment experiments were performed essentially the same as previously described by our group and others with minor modifications (96,102,259). Briefly, 2 million Flp-In HEK 293 cells were first plated into 10cm dishes. The following day after transferring the cells to dishes the cells were transfected using PEI in a ratio of 1:6 (μ g DNA: μ g PEI). The cells were transfected with pcDNA3.1+ encoding human D₂L_R-Nluc (0.25 μ g). Then, depending on the particular assay the cells were co-transfected with the additional constructs as follows: For GRK2 recruitment, the cells were additionally transfected with GRK-venus (4 μ g) and pcDNA3.1+ (3.5 μ g). For β -arrestin-1 recruitment, the cells were additionally transfected with GRK2 (2 μ g) and YFP- β -arrestin-1 (5.5 μ g). For β -arrestin 2 recruitment, the cells were additionally transfected with GRK2 (2 μ g) and YFP- β -arrestin 2 (5.5 μ g). The following day after transfection, the cells were harvested from the dishes and plated into poly-D-lysine coated white-bottom 96 well optiplates. The next day after the cells were transferred to plates, the assay was conducted keeping the buffers, incubators and plate reader at 37°C. The plate was first taken out of the incubator and the media was aspirated, washed once with HBSS and replaced with HBSS to 80 μ L. The cells were then left to equilibrate for 15 minutes at 37°C in the HBSS before addition of 10 μ L of 1/100 Nano-Glo substrate (Promega) was added to each well of the 96 well plate with an electronic pipette. The plate was then left for an additionally 15 minutes at 37°C before then being measured using the PHERAstar® FS microplate reader (BMG LABTECH GmbH, Germany). Individual wells were simultaneously measured for the luminescence emission signal of the luciferase Nluc (465-505nm) and the acceptor fluorescent protein YFP/venus (505-555nm). The plate was measured at 37°C over a 30-minute time-course upon addition of each D₂L_R agonist with a 12-channel electronic-pipette for quick addition of compounds. The BRET was then quantified identically to the G protein activation assays.

Trafficking

D₂L_R trafficking assays were performed using cellular compartment BRET sensors described by Lan and colleagues (260). Trafficking for the D₂R using this method has been performed and characterised by another group (261). The basis of the assay requires different endomembrane compartments to be tagged with a yellow fluorescent protein venus to serve as BRET acceptor and the D₂L_R is tagged with Nluc to serve as BRET donor. The changes in BRET are then monitored to indicate movement towards or away from various compartments.

First, 2 million Flp-In HEK 293 cells were harvested and dispersed evenly into a 10cm dish. The following day after the cells had adhered, the media was changed and the cells were transfected with PEI:DNA complexes in a ratio of 1:6 ($\mu\text{g}/\mu\text{g}$). The cells were transfected in a dropwise manner with D₂L_R-Nluc (0.25 μg), GRK2 (2 μg), β -arrestin-2 (4 μg) and either KRas-venus (1 μg), Rab5a-venus (1 μg) or Rab11-venus (1 μg). The following day the cells were lifted off the dishes and plated in poly-D-lysine coated 96 well white bottom optiplates at 100 μL per well. The next day the assay was started and performed as described for the GRK2 and arrestin recruitment assays with a PHERAstar® FS plate reader at 37°C in HBSS pH 7.4. The plates for the trafficking experiments were measured over a one-hour time course collecting data simultaneously with a 465-505nm (donor) channel and a 505-555nm (acceptor) channel. The BRET ratio was determined by dividing the acceptor channel by the donor channel. The raw BRET ratio was then plotted for five independent experiments. A one phase exponential equation was fit to the hour-long time course data to determine the trafficking rates for each agonist.

Data analysis

Data was analysed using GraphPad prism version 8. Concentration response curves were fit with a three-parameter fit to determine potency and maximal effect values. For quantifying bias parameters, an operational model of agonism described previously was used, this is also outlined in the subsequent chapter in more detail (86,87).

3.3 Results

Measurement of the binding kinetics of agonists at the D₂R

We have previously determined the binding kinetics of several D₂R agonists using TR-FRET competition kinetic binding on cell membranes (96). To build on this work and obtain a more comprehensive panel of agonists with known binding kinetic parameters for the D₂R, we set out to use this method again on some additional agonists. We initially characterised PPHT-Red, the fluorescent tracer to be used for competition kinetic binding studies. In equilibrium saturation binding experiments, the fluorescent tracer behaved essentially as we had determined before (61,96); with low non-specific binding and a dissociation constant (K_d) of approximately 14.7 ± 1.8 nM (Fig. 3.1A). The binding kinetics of PPHT-Red were then determined using increasing concentrations of the ligand in association kinetic binding experiments (Fig. 3.1B). PPHT-Red displayed an association rate (k_{on}) of $2.3 \pm 0.2 \times 10^7$ M⁻¹min⁻¹ and a dissociation rate (k_{off}) of 0.29 ± 0.02 min⁻¹. These binding kinetic parameters also fit well with what we have previously described. When using the binding kinetic parameters to calculate an affinity ($K_d = 12.6$ nM), this calculation agreed with the affinity that was determined from saturation binding at equilibrium.

We were then able to determine the kinetics of some additional agonists through competition kinetic binding experiments. The binding kinetics of brexpiprazole, a relatively new antipsychotic drug with low agonist efficacy at the D₂R, was determined (262). We observed that brexpiprazole displayed a high affinity for the D₂R, associating very quickly and dissociating slowly relative to the other agonists (Table 3.1). We also determined the binding kinetics of bromocriptine and rotigotine, two efficacious agonists approved for the treatment of Parkinson's disease (Table 3.1 & Fig. 3.1D & E)(263-265). The binding kinetics of bromocriptine and rotigotine varied substantially even though these two agonists are prescribed for the same indication. Bromocriptine dissociated quite slowly from the D₂R ($k_{off} = 0.02 \pm 0.007$ min⁻¹) whereas rotigotine dissociated relatively quickly ($k_{off} = 1.20 \pm 0.21$) (Table 3.1 & Fig. 3.1D & E). Additionally, we characterised a new investigational agonist for Parkinson's disease – ST-836 (266). This agonist was the only ligand where the binding kinetics were determined with a different fluorescent tracer - clozapine-Cy5. We have previously demonstrated that using clozapine-Cy5 as a tracer instead of PPHT-Red in these assays leads to no noticeable difference in binding kinetics (237). ST-836 dissociated very rapidly from the D₂R although it also displayed quite a fast association rate to the D₂R that maintained its

binding affinity in the nanomolar range (Table 3.1). With these new agonists characterised, along with the previously characterised agonists, we then had a suite of eleven D₂R agonists with varying binding kinetics and chemical structure (Fig. 3.1F & Table 3.1).

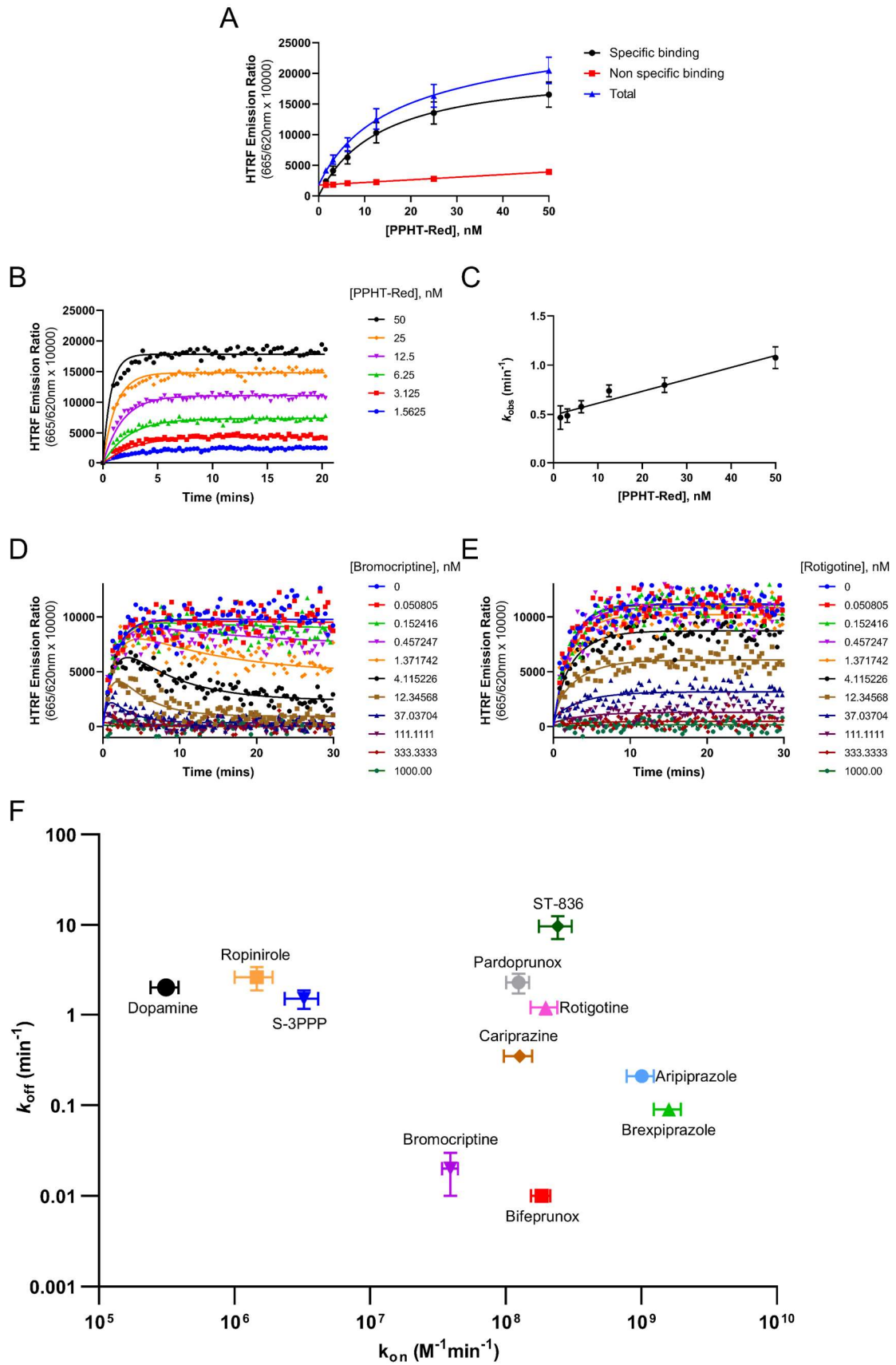


Figure 3.1: Determination of the binding kinetics of additional D₂R agonists with tr-FRET. (A) Saturation binding of SNAP-D₂R membranes with the fluorescent ligands PPHT-Red. Data represents the mean \pm SEM, n=9. (B) Association kinetic binding of increasing concentrations of PPHT-Red to the SNAP-D₂R. Data represents the mean, n=9. (C) A one phase association curve was fit to the binding of each concentration of PPHT-Red (shown in panel B) to determine the observed association rate (k_{obs}). Each concentration of PPHT-Red is shown on the x-axis the k_{obs} is plotted on the y-axis. The relationship between the two follows a linear relationship giving a y-intercept (k_{off}) of $0.47 \pm 0.04 \text{ min}^{-1}$. Data represents the mean \pm SEM, n=9. (D & E) Single representative competition kinetic binding experiments with PPHT-Red and bromocriptine (D) or rotigotine (E) are shown. (F) The binding kinetic parameters of agonists used in this study. Data represents the mean \pm SEM. Agonists binding kinetic parameters were determined in this study and also from our groups previous published work (96).

Table 3.1: Kinetic binding parameters of selected agonists for the human D₂R.

Data are expressed as the mean \pm SEM

Agonist	$k_{off} (\text{min}^{-1})$	$k_{on} (\text{M}^{-1} \text{min}^{-1})$	pK_d
Aripiprazole ^a	0.21 ± 0.02	$1.01 \pm 0.23 \times 10^9$	9.66
Bifeprunox ^a	0.01 ± 0.00	$1.84 \pm 0.30 \times 10^8$	10.3
Brexipiprazole	0.09 ± 0.01	$1.60 \pm 0.36 \times 10^9$	10.2
Bromocriptine	0.02 ± 0.01	$3.93 \pm 0.52 \times 10^7$	9.40
Cariprazine ^a	0.35 ± 0.05	$1.27 \pm 0.30 \times 10^8$	9.53
Dopamine ^a	2.00 ± 0.30	$3.14 \pm 0.73 \times 10^5$	5.18
Pardoprunox ^a	2.28 ± 0.56	$1.25 \pm 0.24 \times 10^8$	7.75
Ropinirole ^a	2.60 ± 0.75	$1.46 \pm 0.46 \times 10^6$	5.73
Rotigotine	1.20 ± 0.21	$1.97 \pm 0.44 \times 10^8$	8.21
S-3PPP ^a	1.51 ± 0.35	$3.25 \pm 0.90 \times 10^6$	6.11
ST-836 ^b	9.66 ± 2.81	$2.42 \pm 0.66 \times 10^8$	7.40

^a Determined in a previous study by our group (96). ^b determined using clozapine-Cy5 as the fluorescent tracer.

Functional characterisation of agonist action over time

We next monitored the functional effects of the panel of agonists. We used HEK 293 cells and transiently transfected bioluminescence resonance energy transfer (BRET) sensors, enabling us to monitor the responses in live cells and in real time. The D₂R mediated activation of six different inhibitory G proteins; G α_{i1} , G α_{i2} , G α_{i3} , G α_{oA} , G α_{oB} , and G α_z , was monitored with a sensor that measures the release of G $\beta\gamma$ (258). The detection method utilises the pleckstrin homology domain of GRK3 as a BRET donor that binds dissociated G $\beta\gamma$ -Venus subunits. Therefore, the wild type D₂R and unlabelled G α subunits are used, reducing the likelihood of altering the native G protein activation kinetics (257). In addition to this, we measured the recruitment of GRK2, β -arrestin-1 and β -arrestin-2 to the D₂R. The direct recruitment of these three regulatory proteins was measured by tagging the D₂R with a BRET donor (Nluc) and each one of the regulatory proteins with a BRET acceptor (YFP/Venus). In

general, all agonists inducing G protein activation or recruitment of regulatory proteins displayed signals that were sustained for over 30 minutes (Fig. S3.1-S3.11). Efficacious agonists, such as dopamine, produced large responses at all effectors (Fig. S3.6). Efficacious agonist responses were rapid and sustained when activating G proteins, however, when recruiting arrestins a peak followed by a smaller plateau was observed. Contrastingly, agonists with low efficacy, such as bifeprunox, produced weak responses over time when activating G α_{i1} , G α_{i2} , G α_{i3} (Fig. S3.2). The greater potency and maximal effect of agonists acting at G α_{oA} and G α_{oB} relative to G α_{i1} , G α_{i2} and G α_{i3} was expected from previous studies demonstrating that the D₂R is more efficiently coupled to these G proteins (138,139,267). Moreover, low efficacy agonists also very weakly induced the recruitment of GRK2, β -arrestin-1 and β -arrestin-2 and no initial peak in recruitment was observed.

Knowing each agonist's binding kinetic parameters and having determined the functional effects over time, we then aimed to investigate how these two characteristics relate. We used the binding kinetic values and the different concentrations of each agonist that were used in our functional assays to simulate their expected receptor occupancy over time (Fig. 3.2A, B & C). From these simulations, we observed that sub-saturating concentrations of the agonist had either a constant occupancy over time if the agonist dissociated quickly (e.g. dopamine) (Fig. 3.2A), or sub-saturating concentrations of agonist increased in occupancy over time if the agonist dissociated slowly (e.g. bifeprunox) (Fig. 3.2B). Therefore, we predicted that, when fitting concentration response curves for each measurement timepoint in our functional assays, agonists would either have a constant potency over time if they had a fast dissociation rate or they would increase in potency over time if they had a slow dissociation rate.

When examining G α_{oA} activation or β -arrestin-2 recruitment induced by the fast dissociating agonist dopamine, the relative responses at each concentration remained constant over time (Fig. 3.2D & G and Fig. S3.6). Hence, when fitting concentration response curves at 30 second intervals over a 30-minute time course, dopamine's potency (pEC₅₀) remained constant over time for these pathways (Fig. 3.2J). Two other fast dissociating agonists, ropinirole and S-3PPP, had functional responses over time that fit with this pattern of agonist action (Fig. S3.8 & S3.10). Moreover, slow dissociating agonists including aripiprazole, bifeprunox, brexpiprazole, bromocriptine and cariprazine fit the expected profile whereby low concentrations of the agonist slowly increased in response over time, leading to an increase in potency over time (Fig. 3.2E, H & K and Fig. S3.1-S3.5). However, when we measured the functional responses of rotigotine over time, the temporal profile did not match the simulated

receptor occupancy (Fig. 3.2C, F, I & L & Fig. S3.9). Rotigotine had a relatively fast dissociation rate and hence it was expected to display a constant response at each concentration over time. Unexpectedly, we observed an increase in response over time for the lower concentrations that manifested as an increase in potency of approximately 25-fold at G α_{oA} and 21-fold at β -arrestin-2 (Fig. 3.2F, I & L). Additionally, pardoprunox and ST-836 also displayed a similar increase in potency over time to rotigotine while also having relatively fast dissociation rates from the D₂R (Fig. S3.7 & S3.11). Overall, our temporal functional assays showed that potency changes over time at the D₂R can usually, but not always, be predicted by their binding kinetics measured in membranes.

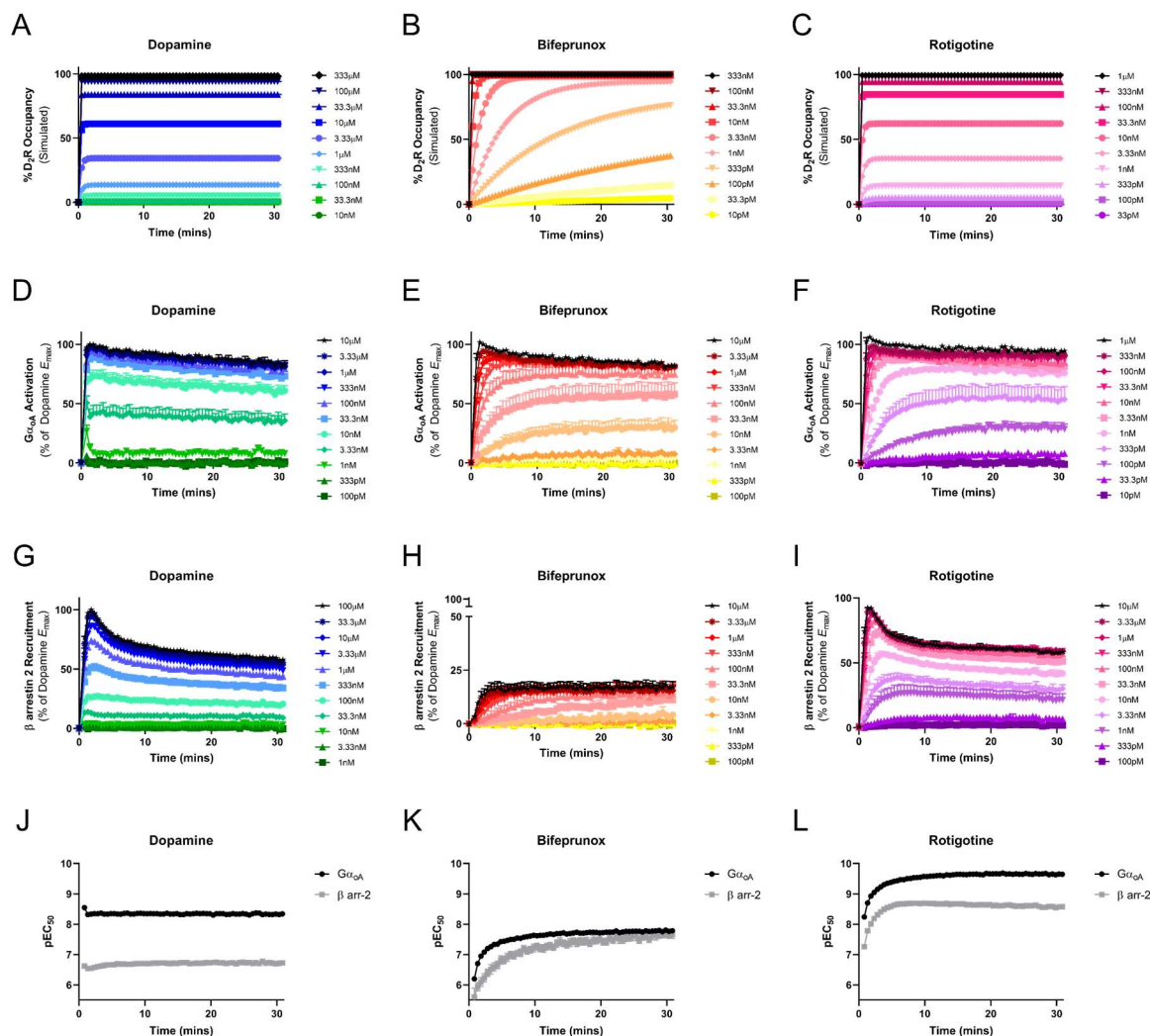


Figure 3.2: Concentration-response time course characterisation of agonists acting at the D₂R. Simulated D₂R occupancy of increasing concentrations of dopamine (A), bifeprunox (B) and rotigotine (C) over time based on the binding kinetics determined by tr-FRET experiments. D₂R mediated G_{αOα} protein activation over time in response to increasing concentrations of dopamine (D), bifeprunox (E) and rotigotine (F). Recruitment of β-arrestin-2 over time by the D₂R upon stimulation with increasing concentrations of dopamine (G), bifeprunox (H) and rotigotine (I). Concentration response curves were taken at each time point for G_{αOα} activation (black circles) and β-arrestin-2 recruitment (grey squares), the potency estimates (pEC₅₀) were then plotted over time for dopamine (J), bifeprunox (K) and rotigotine (L). Data for graphs D-L represent the mean ± SEM of between 3-6 separate experiments.

Slow agonist dissociation is not essential for an increase in potency over time

We further investigated the mechanism through which rotigotine, pardoprunox and ST-836 exhibit an increase in potency over time in a manner that was inconsistent with their fast dissociation rates. Given that Birdsong and colleagues (88) have shown that over time agonists can exhibit an increased affinity at the μ-opioid receptor, we hypothesised that the agonists displaying an increase in potency over time at the D₂R may ‘sense’ a different conformation of

the receptor over time which may lead to a slowed dissociation rate in live cells. Therefore, in a similar experimental design as that used by Birdsong and colleagues, we decided to measure the functional deactivation rate of the D₂R after pre-incubation with a number of agonists, including rotigotine. Although there are obvious differences between the experimental design of this assay and our measurements of ligand binding kinetics above (Fig. 3.1, Table 3.1), we anticipated that this would serve as a good proxy estimate of the ligand binding dissociation rate in our live cell assays. We performed these experiments by initially stimulating cells with the agonist of interest, followed by adding an antagonist at high saturating concentrations to prevent the agonist from re-binding once it dissociated from the D₂R. Before being outcompeted with spiperone, agonists were incubated with the cells for 12.5 minutes - a time that allowed for agonists to increase in potency as well as display a robust response. This experiment is analogous to binding assays in which an isotopic dilution method, using a saturating concentration of cold ligand, is used to visualise ligand dissociation by preventing radioligand rebinding. In this manner, we utilised the same BRET sensor for the earlier G protein activation assays and were able to essentially track the rate at which the G proteins become inactive and re-associate. This assay was chosen because it detects activation directly proximal to the receptor and can be measured with high temporal resolution (132,257). When we performed these experiments, we observed large differences in the deactivation rates between the panel of agonists (Fig. 3.3A). Moreover, the rate of re-association of the G protein heterotrimers correlated strongly with the ligand binding dissociation rate (Fig. 3.3B) (Pearson $r = 0.988$, $P=0.003$). Therefore, the signalling deactivation in live cells can be directly in line with the binding dissociation performed in membranes. Importantly, rotigotine's functional deactivation rate approximated its binding dissociation rate (Fig. 3.3B and Table 3.2). This suggests that the dissociation rate, at least in the case of rotigotine, is not altered at all in the functional assays in this study. Consequently, the increase in potency in all functional events over time for rotigotine, pardoprunox and ST-836 is likely not conferred through a slowed dissociation rate over time.

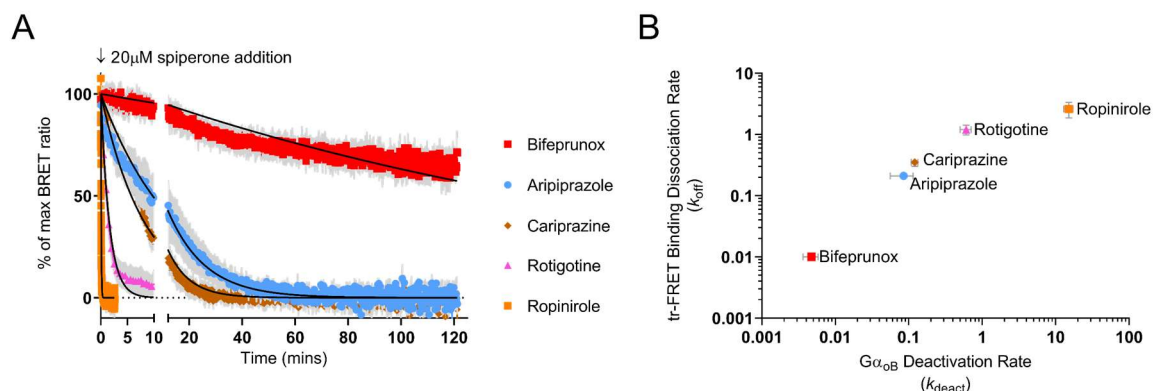


Figure 3.3. The relationship between the agonist-specific G protein deactivation rate in live cells and direct ligand binding dissociation rate. D₂R agonists were added to D₂R expressing Flp-In HEK 293 cells and allowed to activate $G\alpha_{oB}$ heterotrimers followed by being out-competed by a high concentration of the high affinity antagonist spiperone to track the rate of de-activation of $G\alpha_{oB}$ protein signaling. **(A)** 100nM Bifeprunox (red squares), 100nM Aripiprazole (light blue circles), 33nM Cariprazine (brown diamonds) 1nM Rotigotine (pink triangles) and 100nM Ropinirole (orange squares) were incubated for 12.5 minutes before being out-competed with 20 μ M Spiperone. **(B)** Experimentally determined ligand binding dissociation rates (k_{off}) plotted on the y-axis with $G\alpha_{oB}$ protein re-association rate (deactivation – k_{deact}) in this study plotted on the x-axis showed a Pearson correlation with an R^2 of 0.988 ($P=0.003$). Data is plotted on a \log_{10} scale for ease of visualization.

Table 3.2: G protein deactivation rate after stimulation with different agonists.

Data is represented as the mean \pm SEM from three separate experiments.

Agonist	k_{deact} (min^{-1})
Aripiprazole	0.085 ± 0.029
Bifeprunox	0.005 ± 0.001
Cariprazine	0.120 ± 0.013
Ropinirole	15.10 ± 2.206
Rotigotine	0.604 ± 0.104

Quantitative assessment of agonist action at a single timepoint at proximal functional events

We next wanted to quantitatively assess the different agonists' functional responses at each effector. The agonists' responses were assessed by taking a single timepoint and fitting concentration response curves. We chose a time of fifteen minutes after agonist stimulation to examine the responses because a robust window of response was maintained and most of the increases in potency had occurred by this time point. When assessing the activation of the different G proteins at 15 minutes we observed clear differences in the responses generated by each agonist at $G\alpha_{i1}$, $G\alpha_{i2}$ and $G\alpha_{i3}$ as compared to those at $G\alpha_{oA}$, $G\alpha_{oB}$, and $G\alpha_z$. As we had observed in the temporal responses, there were large differences in maximal effect between the

agonists when activating G α_{i1} , G α_{i2} and G α_{i3} but not G α_{oA} , G α_{oB} and G α_z . Regarding G α_{i1} , G α_{i2} and G α_{i3} activation, known low efficacy agonists such as aripiprazole and brexpiprazole produced weak responses (262,268), whereas efficacious agonists such as dopamine and rotigotine produced more full responses (Fig. 3.4A, B & C and Table 3.3)(264). Indeed, the maximal G α_{i2} response induced by brexpiprazole was approximately 23% that of dopamine's response (Table 3.3). In contrast to the responses at G α_{i1} , G α_{i2} and G α_{i3} , the activation of G α_{oA} , G α_{oB} , and G α_z produced more robust responses, with most agonists' effects resembling a full agonist (Fig. 3.4D, E & F and Table 3.3). For example, brexpiprazole induced a maximal response at G α_{oA} that was 89% that of dopamine's response. Agonists were also usually more potent when activating G α_{oA} , G α_{oB} , and G α_z relative to G α_{i1} , G α_{i2} and G α_{i3} . For instance, dopamine was approximately 10-fold more potent at activating G α_{oA} over G α_{i2} (G α_{oA} pEC₅₀ = 8.32 \pm 0.04 (EC₅₀ = 4.79nM), G α_{i2} pEC₅₀ = 7.30 \pm 0.03 (EC₅₀ = 50.1nM)). The stronger responses at G α_{oA} and G α_{oB} reflect the selectivity of the D₂R for these G proteins (138,139).

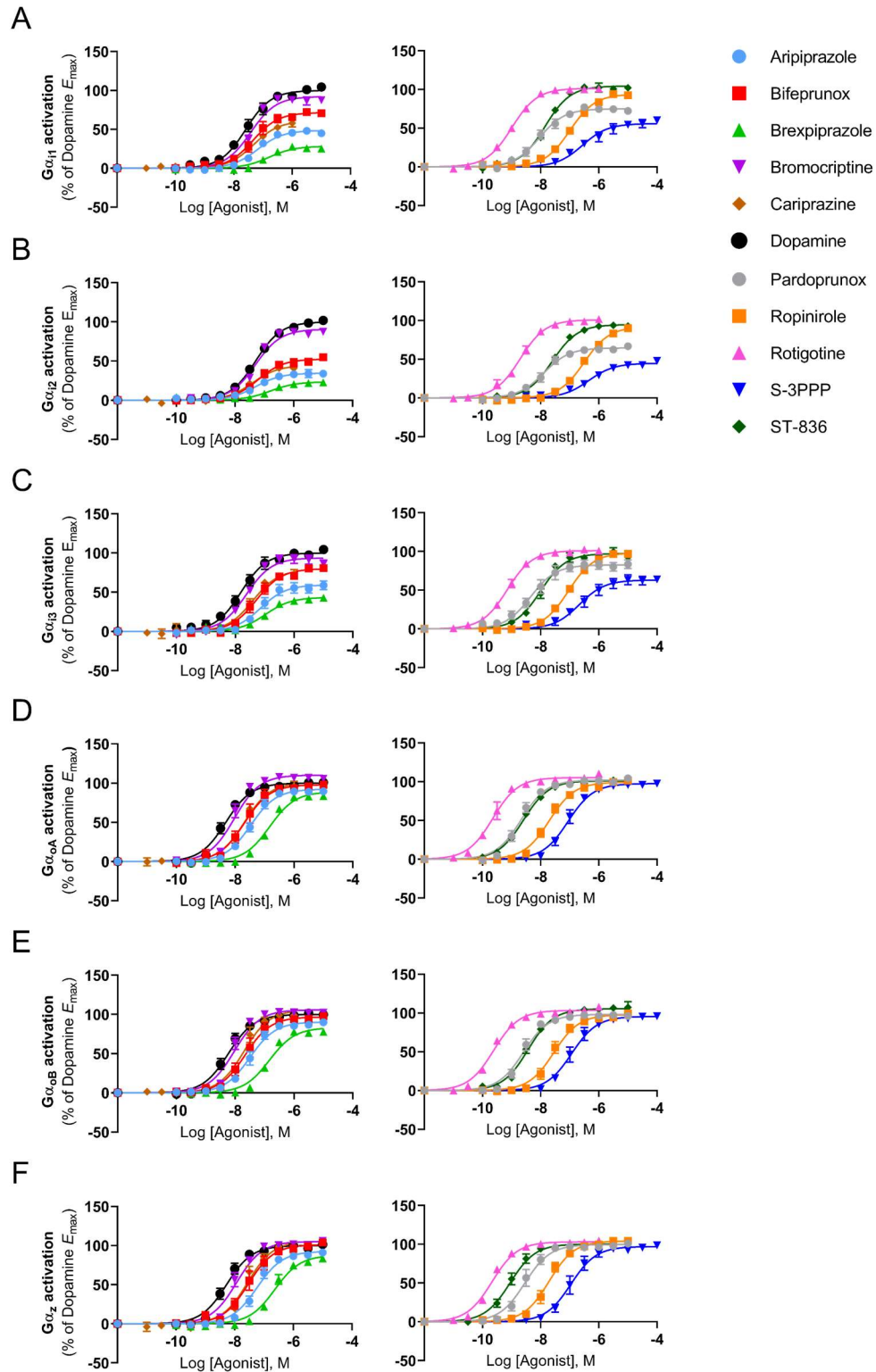


Figure 3.4: Agonist activation of different G protein subtypes by the D₂R. Flp-In HEK 293 cells stably expressing the D₂R were transfected with BRET sensors and the activation of Gα_{i1} (A), Gα_{i2} (B), Gα_{i3} (C), Gα_{oA} (D), Gα_{oB} (E), and Gα_z (F) was monitored in the live cells in response to increasing concentrations of a set of agonists with varying binding kinetics and efficacy. All responses shown were determined 15 minutes after stimulation. Data represents the mean ± SEM of 4-6 separate experiments.

Table 3.3: Functional parameters of various agonists abilities to induce activation of different G proteins by the D₂R.
Activation was measured 15 minutes after stimulation. Data is represented as the mean \pm SEM of 4-6 separate experiments.

	G protein α subunit											
	Gα_{i1}		Gα_{i2}		Gα_{i3}		Gα_{oA}		Gα_{oB}		Gα_z	
Agonist	pEC ₅₀	E _{max}	pEC ₅₀	E _{max}	pEC ₅₀	E _{max}	pEC ₅₀	E _{max}	pEC ₅₀	E _{max}	pEC ₅₀	E _{max}
Aripiprazole	7.18 \pm 0.08	48.6 \pm 1.7	7.30 \pm 0.11	34.5 \pm 1.7	7.14 \pm 0.10	59.2 \pm 2.7	7.48 \pm 0.04	92.3 \pm 1.6	7.50 \pm 0.1	90.4 \pm 1.8	7.24 \pm 0.05	92.5 \pm 2.1
Bifeprunox	7.34 \pm 0.08	71.5 \pm 2.3	7.21 \pm 0.09	52.5 \pm 2.0	7.28 \pm 0.07	79.9 \pm 2.2	7.69 \pm 0.07	98.0 \pm 2.6	7.66 \pm 0.07	96.8 \pm 2.5	7.54 \pm 0.07	101.1 \pm 2.8
Brexipiprazole	6.79 \pm 0.16	28.2 \pm 2.2	6.80 \pm 0.08	23.4 \pm 1.0	6.97 \pm 0.11	43.3 \pm 2.1	6.83 \pm 0.04	89.0 \pm 1.7	6.84 \pm 0.05	83.1 \pm 1.9	6.63 \pm 0.06	87.6 \pm 2.5
Bromocriptine	7.42 \pm 0.06	92.2 \pm 2.3	7.31 \pm 0.04	90.6 \pm 1.6	7.63 \pm 0.06	93.7 \pm 2.3	8.03 \pm 0.05	110.2 \pm 2.1	8.03 \pm 0.05	105.8 \pm 2.0	7.94 \pm 0.05	105.2 \pm 2.0
Cariprazine	6.32 \pm 0.08	60.7 \pm 2.7	7.40 \pm 0.07	44.4 \pm 1.6	7.40 \pm 0.09	78.7 \pm 3.9	7.68 \pm 0.05	100.5 \pm 2.6	7.70 \pm 0.07	105.6 \pm 3.6	7.56 \pm 0.07	105.6 \pm 3.8
Dopamine	7.59 \pm 0.06	100.0 \pm 2.2	7.30 \pm 0.03	100.0 \pm 1.4	7.81 \pm 0.06	100.0 \pm 2.4	8.32 \pm 0.04	100.0 \pm 1.3	8.23 \pm 0.05	100.0 \pm 1.7	8.28 \pm 0.04	100.0 \pm 1.5
Pardoprunox	8.05 \pm 0.07	75.0 \pm 1.9	7.89 \pm 0.06	64.5 \pm 1.5	8.35 \pm 0.09	82.6 \pm 2.4	8.67 \pm 0.04	102.0 \pm 1.4	8.60 \pm 0.05	98.2 \pm 1.5	8.55 \pm 0.05	99.6 \pm 1.8
Ropinirole	7.00 \pm 0.03	94.0 \pm 1.3	6.50 \pm 0.05	92.0 \pm 2.2	7.04 \pm 0.04	98.3 \pm 1.7	7.71 \pm 0.04	99.3 \pm 1.4	7.55 \pm 0.05	97.8 \pm 2.0	7.71 \pm 0.05	104.3 \pm 1.9
Rotigotine	8.99 \pm 0.03	101.4 \pm 1.1	8.71 \pm 0.04	100.9 \pm 1.4	9.15 \pm 0.03	101.1 \pm 1.3	9.65 \pm 0.04	105.3 \pm 1.5	9.62 \pm 0.04	103.3 \pm 1.2	9.67 \pm 0.03	103.1 \pm 1.1
S-3PPP	6.56 \pm 0.10	55.9 \pm 2.2	6.35 \pm 0.08	44.7 \pm 1.5	6.67 \pm 0.10	63.1 \pm 2.6	7.06 \pm 0.05	97.5 \pm 1.7	6.93 \pm 0.06	95.6 \pm 2.0	6.96 \pm 0.07	97.1 \pm 2.4
ST-836	7.85 \pm 0.04	104.4 \pm 1.6	7.60 \pm 0.03	94.7 \pm 1.2	8.01 \pm 0.06	97.3 \pm 2.0	8.59 \pm 0.03	101.1 \pm 1.0	8.43 \pm 0.05	105.4 \pm 1.7	9.05 \pm 0.05	100.3 \pm 1.5

In the G protein cycle, a single GPCR can catalytically activate multiple G proteins that results in the amplification of G protein signalling (269). Arrestin and GRK recruitment by GPCRs does not appear to have this level of amplification. For this reason, there is often a reduction in the potency when measuring the recruitment of arrestins and GRKs to GPCRs relative to the activation of G proteins (96,270). When we assessed the recruitment of GRK2, β -arrestin-1 and β -arrestin-2 our data supported this notion because agonists were generally less potent than they were at activating G proteins (Fig. 3.5A, B & C and Table 3.4). Moreover, when measuring the recruitment of any of the regulatory proteins, weaker efficacy agonists also displayed substantial reductions in the maximal effect they induced relative to dopamine. For example, the aripiprazole induced maximal effects for GRK2, β -arrestin-1 and β -arrestin-2 were all less than 20% of dopamine's response (Table 3.4). Certainly, some partial agonists displayed such weak responses when recruiting GRK2 and β -arrestin-1 that a sigmoidal concentration response curve could not be fit to their responses accurately (Table 3.4, $r^2 < 0.7$ indicated by ND). The fact that weaker efficacy agonists displayed dampened maximal effects may reflect previously published data that, relative to other GPCRs such as the vasopressin V₂ receptor, the D₂R has a weak interaction with arrestins (271,272). In the GRK2 and arrestin recruitment assays, dopamine induced the largest maximal response, and this robust effect matches previous observations in arrestin recruitment assays (270). However, rotigotine was the most potent agonist in these assays as well as in the G protein activation assays.

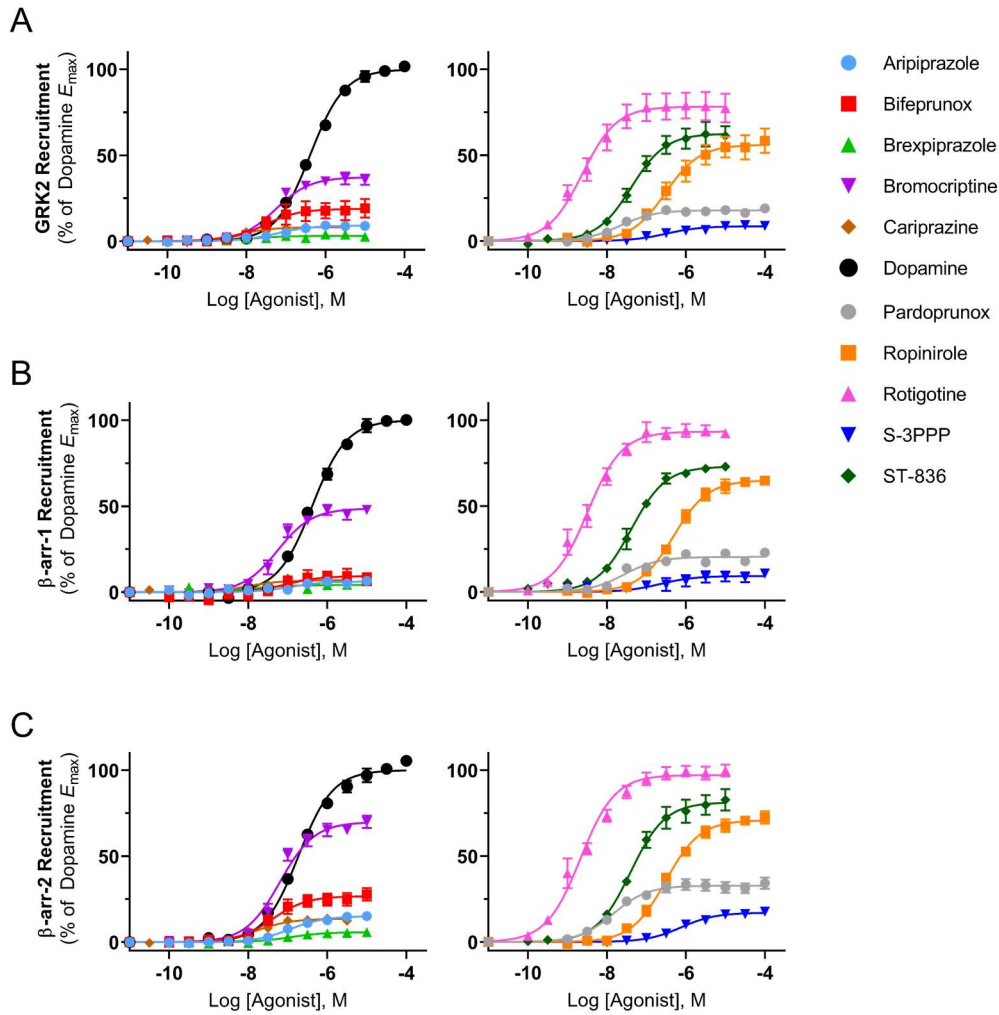


Figure 3.5: Agonist induced recruitment of GRK2, β -arrestin-1 and β -arrestin-2 to the D₂R. Recruitment of GRK2 (**A**), β -arrestin-1 (**B**), and β -arrestin-2 (**C**) to the D₂R was monitored in live Flp-In HEK 293 cells with BRET. Concentration-response curves of different agonists with varying binding kinetics and efficacy at the D₂R were plotted. All responses plotted were determined 15 minutes after stimulation. The data is presented as the mean \pm SEM of 3-4 separate experiments.

Table 3.4: GRK2 and β -arrestin recruitment parameters for different agonists.

Measurements were taken 15 minutes after stimulation. Data represents the mean \pm SEM of 3-4 separate experiments.

Agonist	Regulatory event					
	GRK2		β -arrestin-1		β -arrestin-2	
	pEC ₅₀	E _{max}	pEC ₅₀	E _{max}	pEC ₅₀	E _{max}
Aripiprazole	7.23 \pm 0.15	9.1 \pm 0.6	ND	~6	6.94 \pm 0.07	15.1 \pm 0.5
Bifeprunox	ND	~19	ND	~9	7.39 \pm 0.12	26.8 \pm 1.4
Brexiprazole	ND	~3	ND	~4	6.93 \pm 0.15	5.81 \pm 0.40
Bromocriptine	7.26 \pm 0.07	37.3 \pm 1.1	7.25 \pm 0.07	48.7 \pm 1.4	7.20 \pm 0.06	69.9 \pm 1.8
Cariprazine	8.18 \pm 0.14	8.2 \pm 0.5	ND	~7	7.78 \pm 0.10	13.6 \pm 0.6
Dopamine	6.39 \pm 0.02	100.0 \pm 1.0	6.38 \pm 0.03	100.0 \pm 1.2	6.73 \pm 0.03	100.0 \pm 1.2
Pardoprunox	7.66 \pm 0.10	17.9 \pm 0.6	7.56 \pm 0.09	20.4 \pm 0.7	7.84 \pm 0.08	32.8 \pm 0.9
Ropinirole	6.52 \pm 0.10	56.1 \pm 2.2	6.31 \pm 0.05	65.0 \pm 1.3	6.51 \pm 0.04	70.9 \pm 1.2
Rotigotine	8.62 \pm 0.09	78.2 \pm 2.4	8.49 \pm 0.05	93.4 \pm 1.7	8.67 \pm 0.05	97.2 \pm 1.7
S-3PPP	6.49 \pm 0.22	8.6 \pm 0.8	ND	~9	6.12 \pm 0.07	17.0 \pm 0.5
ST-836	7.38 \pm 0.07	62.5 \pm 1.9	7.38 \pm 0.04	73.0 \pm 1.3	7.40 \pm 0.06	81.3 \pm 1.9

Having determined the potencies at G proteins and regulatory pathways we were then able to compare these values to our determined affinities of the agonists. It is expected that the potency of each compound would not match their affinity due to the intrinsic efficacy of the particular compound. However, we observed very large differences between potencies and affinities, with some potencies much higher and some lower than the respective affinity. Interestingly, the group of bitopic partial agonists including aripiprazole, bifeprunox, brexpiprazole and cariprazine all displayed functional potencies that were orders of magnitude lower than their binding affinities. For example, aripiprazole displayed a kinetic pK_d of 9.66 whereas its potency (pEC_{50}) for $G\alpha_{oA}$ activation and β -arrestin-2 recruitment was 7.48 and 6.94 respectively (Table 3.3 & 3.4). The responses and potencies of these agonists largely reach their maximal point at the 15-minute measurement timepoint (Figure S3.1-S3.11). Therefore, this observation is likely not due to the agonists not reaching equilibrium with the D₂R. Moreover, the ergot agonist bromocriptine also displayed a decrease in its potency values ($pEC_{50} G\alpha_{oA} = 8.03$, $pEC_{50} \beta$ -arrestin-2 = 7.20) relative to its affinity ($pK_d = 9.40$). In contrast, some other agonists displayed higher or similar potencies in the functional assays as compared to their binding affinities, such as dopamine ($pK_d = 5.18$, $pEC_{50} G\alpha_{oA} = 8.32$, $pEC_{50} \beta$ -arrestin-2 = 6.73) and rotigotine ($pK_d = 8.21$, $pEC_{50} G\alpha_{oA} = 9.65$, $pEC_{50} \beta$ -arrestin-2 = 8.67). In these cases, the higher potency in the functional assay relative to the binding affinity is likely due to a combination of receptor reserve, agonist efficacy and signal amplification and such observations are consistent with many previous studies of agonist action at GPCRs (273). However, the lower potency of ligands like aripiprazole as compared to their binding affinity cannot be reconciled with this mechanism. Together this demonstrates that the receptor occupancy of an agonist required to elicit a half-maximal response can be vastly different between distinct D₂R agonists.

While assessing differences in either the maximal effect or potency is useful, each of these measures are subject to differences in both the system and the specific assay detection method. Different functional endpoints can have different levels of amplification due to various phenomenon such as the efficiency of coupling to particular downstream effectors or positive feedback loops. Likewise, differences in detection sensitivity or amplification depending on the level of detection within the signalling cascade can also introduce similar effects. Due to this, observations of relative changes in potency or maximal effect between different pathways may appear as agonist bias. However, once the signalling system and the differences in assays

are taken into account, such bias may be insignificant. Therefore, we were also interested in comparing agonist activity in an integrated manner. We did this by applying an operational model of agonist activity adapted from work by Black and Leff (86,87). This enabled us to determine individual transduction coefficients for each agonist acting at each effector (Table 3.5). The transduction coefficient is a parameter estimated from the concentration response curves that is comprised of the agonists' affinity for the receptor-effector complex (K_A) and the efficacy of the agonist to activate that effector (τ). This analysis showed rotigotine had the most powerful agonist activity, having the largest transduction coefficient for all effectors (Table 3.5). In general, the analysis displayed larger transduction coefficients for the agonists at $G\alpha_{oA}$, $G\alpha_{oB}$ and $G\alpha_z$, indicating that these G proteins were more efficiently coupled to the D₂R relative to other effectors. Therefore, to more accurately assess the relative activities of the agonists acting at each effector, the relative coupling efficiency and/or amplification of each signalling pathway needs to be accounted for. This was achieved by normalising the different transduction coefficients at each effector to that of dopamine - the reference agonist. Having done this, we could then observe that some agonists selectively activated some effectors relative to the action of dopamine. In particular, multiple agonists appeared to preferentially recruit either GRK2, β -arrestin-1 or β -arrestin-2 relative to their activation of $G\alpha_{oA}$ (Table 3.6). That is, several agonists displayed statistically significant biased agonism for these pathways. For example, bromocriptine and rotigotine both showed a significant preference for the recruitment of all three regulatory proteins over $G\alpha_{oA}$.

Table 3.5: Agonist transduction coefficients.Data represents the mean \pm SEM of 3-6 separate experiments.

Agonist	Log (τ/K_A)								
	G α_{i1}	G α_{i2}	G α_{i3}	G α_{oA}	G α_{oB}	G α_z	GRK2	β -arrestin-1	β -arrestin-2
Aripiprazole	6.88 \pm 0.10	6.91 \pm 0.10	6.96 \pm 0.10	7.52 \pm 0.04	7.55 \pm 0.05	7.29 \pm 0.05	6.01 \pm 0.41	ND	5.98 \pm 0.19
Bifeprunox	7.21 \pm 0.07	6.99 \pm 0.07	7.22 \pm 0.07	7.74 \pm 0.04	7.72 \pm 0.04	7.57 \pm 0.04	ND	ND	6.68 \pm 0.11
Brexiprazole	6.27 \pm 0.17	6.25 \pm 0.15	6.67 \pm 0.13	6.87 \pm 0.05	6.89 \pm 0.05	6.70 \pm 0.05	ND	ND	5.60 \pm 0.45
Bromocriptine	7.39 \pm 0.05	7.28 \pm 0.04	7.61 \pm 0.06	8.12 \pm 0.03	8.09 \pm 0.03	8.01 \pm 0.04	6.70 \pm 0.13	6.90 \pm 0.08	6.97 \pm 0.05
Cariprazine	7.12 \pm 0.09	7.11 \pm 0.09	7.33 \pm 0.08	7.70 \pm 0.04	7.76 \pm 0.04	7.64 \pm 0.04	6.89 \pm 0.44	ND	6.76 \pm 0.20
Dopamine	7.57 \pm 0.04	7.30 \pm 0.03	7.80 \pm 0.05	8.33 \pm 0.03	8.25 \pm 0.03	8.31 \pm 0.03	6.37 \pm 0.05	6.37 \pm 0.04	6.71 \pm 0.04
Pardoprunox	7.93 \pm 0.06	7.74 \pm 0.05	8.29 \pm 0.06	8.70 \pm 0.03	8.65 \pm 0.04	8.59 \pm 0.04	6.74 \pm 0.24	6.81 \pm 0.16	7.22 \pm 0.10
Ropinirole	6.97 \pm 0.05	6.49 \pm 0.04	7.05 \pm 0.06	7.77 \pm 0.04	7.62 \pm 0.05	7.77 \pm 0.04	6.16 \pm 0.09	6.09 \pm 0.05	6.29 \pm 0.05
Rotigotine	8.99 \pm 0.04	8.72 \pm 0.03	9.16 \pm 0.05	9.70 \pm 0.03	9.66 \pm 0.03	9.72 \pm 0.04	8.45 \pm 0.06	8.44 \pm 0.03	8.63 \pm 0.03
S-3PPP	6.32 \pm 0.08	6.06 \pm 0.08	6.51 \pm 0.09	7.11 \pm 0.04	7.00 \pm 0.04	7.02 \pm 0.04	5.23 \pm 0.48	ND	5.21 \pm 0.19
ST-836	7.88 \pm 0.05	7.59 \pm 0.04	8.00 \pm 0.06	8.61 \pm 0.04	8.50 \pm 0.04	9.07 \pm 0.04	7.09 \pm 0.08	7.22 \pm 0.05	7.25 \pm 0.04

ND – not determined, could not be calculated due to poor initial non-linear curve fit ($r^2 < 0.7$).

Table 3.6: Relative Transduction coefficients.Data represents the mean \pm SEM of 3-6 separate experiments.

	$\Delta\text{Log} (\tau/K_A)$								
Agonist	$G\alpha_{i1}$	$G\alpha_{i2}$	$G\alpha_{i3}$	$G\alpha_{oA}$	$G\alpha_{oB}$	$G\alpha_z$	GRK2	β -arrestin-1	β -arrestin-2
Aripiprazole	-0.68 \pm 0.10	-0.39 \pm 0.10	-0.84 \pm 0.11	-0.81 \pm 0.05	-0.70 \pm 0.06	-1.01 \pm 0.06	-0.36 \pm 0.41	ND	-0.74 \pm 0.19
Bifeprunox	-0.36 \pm 0.08	-0.32 \pm 0.10 *	-0.59 \pm 0.08	-0.59 \pm 0.05	-0.53 \pm 0.05	-0.73 \pm 0.05	ND	ND	-0.03 \pm 0.12 *
Brexiprazole	-1.30 \pm 0.17	-1.05 \pm 0.15	-1.14 \pm 0.14	-1.46 \pm 0.06	-1.36 \pm 0.06	-1.61 \pm 0.06	ND	ND	-1.11 \pm 0.45
Bromocriptine	-0.18 \pm 0.06	-0.02 \pm 0.05	-0.19 \pm 0.07	-0.22 \pm 0.05	-0.16 \pm 0.05	-0.29 \pm 0.05	0.34 \pm 0.14 *	0.53 \pm 0.09 *	0.25 \pm 0.06 *
Cariprazine	-0.45 \pm 0.10	-0.19 \pm 0.10	-0.48 \pm 0.10	-0.64 \pm 0.05	-0.49 \pm 0.05	-0.66 \pm 0.05	0.53 \pm 0.45 *	ND	0.05 \pm 0.21
Dopamine	0.00 \pm 0.05	0.00 \pm 0.04	0.00 \pm 0.07	0.00 \pm 0.04	0.00 \pm 0.05	0.00 \pm 0.05	0.00 \pm 0.07	0.00 \pm 0.05	0.00 \pm 0.05
Pardoprunox	0.37 \pm 0.07	0.44 \pm 0.06	0.49 \pm 0.08	0.37 \pm 0.05	0.40 \pm 0.05	0.29 \pm 0.05	0.38 \pm 0.25	0.44 \pm 0.16	0.51 \pm 0.11
Ropinirole	-0.60 \pm 0.07	-0.81 \pm 0.05	-0.76 \pm 0.08	-0.56 \pm 0.05	-0.64 \pm 0.06	-0.53 \pm 0.05	-0.20 \pm 0.10 *	-0.28 \pm 0.06 *	-0.43 \pm 0.06
Rotigotine	1.42 \pm 0.06	1.42 \pm 0.04	1.36 \pm 0.07	1.37 \pm 0.05	1.41 \pm 0.05	1.42 \pm 0.05	2.08 \pm 0.08 *	2.07 \pm 0.05 *	1.91 \pm 0.05 *
S-3PPP	-1.24 \pm 0.09	-1.24 \pm 0.08	-1.30 \pm 0.10	-1.23 \pm 0.05	-1.26 \pm 0.05	-1.29 \pm 0.06	-1.14 \pm 0.49	ND	-1.51 \pm 0.19
ST-836	0.32 \pm 0.06	0.29 \pm 0.05	0.20 \pm 0.07	0.27 \pm 0.05	0.25 \pm 0.05	0.77 \pm 0.05 *	0.72 \pm 0.10 *	0.85 \pm 0.06 *	0.54 \pm 0.06 *

* Agonist's $\Delta\text{Log} (\tau/K_A)$ value is significantly different from the corresponding $G\alpha_{oA}$ value within the row, $P < 0.05$ Ordinary one-way ANOVA with Dunnett's multiple comparisons test. ND – not determined, could not be calculated due to poor initial non-linear curve fit ($r^2 < 0.7$).

The majority of D₂Rs in the central nervous system are thought to be coupled to $G\alpha_o$ subunits (140). In addition, more compounds displayed significant bias when using either a $G\alpha_o$ isoform or $G\alpha_z$ as a reference pathway compared to using one of the $G\alpha_i$ subunits (for example $G\alpha_{i2}$). Moreover, using a $G\alpha_i$ subunit as a reference pathway had a similar, albeit reduced, pattern of bias to using $G\alpha_{oA}$ or $G\alpha_z$. Hence, for these reasons, we next normalised the

relative transduction coefficient values to the values at the reference effector $G\alpha_{oA}$ to obtain the final values of biased agonism (Table 3.7). With these values we could construct a web of bias to more easily visualise biased agonism (Fig. 3.6). From this, it could be observed that there was minimal biased agonism between the G protein subtypes, whereas multiple agonists displayed apparent bias towards the recruitment of regulatory proteins and away from $G\alpha_{oA}$. Rotigotine, ST-836 and bromocriptine, that are quite efficacious agonists, displayed significant biased agonism between $G\alpha_{oA}$ activation and all of GRK2, β -arrestin-1 and β -arrestin-2 (Fig. 3.6A & B and Table 3.6 & 3.7). Moreover, multiple partial agonists at the poorly coupled GRK2 and β -arrestin-1 recruitment endpoints produced an inadequate signal to be able to robustly fit the operational model. Consequently, the transduction coefficients of some of the partial agonists and their resultant biased agonism values could not be determined (Table 3.5, 3.6, & 3.7). Nonetheless, the partial agonists cariprazine and bifeprunox displayed significant bias between $G\alpha_{oA}$ and one of the regulatory proteins. Indeed, cariprazine displayed the largest significant difference in relative transduction coefficients of approximately 14-fold between GRK2 recruitment and $G\alpha_{oA}$ activation (Fig. 3.6A and Table 3.6 & 3.7). In comparison, other partial agonists pardoprunox and S-3PPP displayed a consistent lack of bias at each endpoint (Fig. 3.6B). In general, applying this straightforward method of analysis by applying an operational model together with suitable internal references allowed us to observe statistically significant apparent bias primarily, but not exclusively, between the well coupled G proteins and the less efficient regulatory proteins.

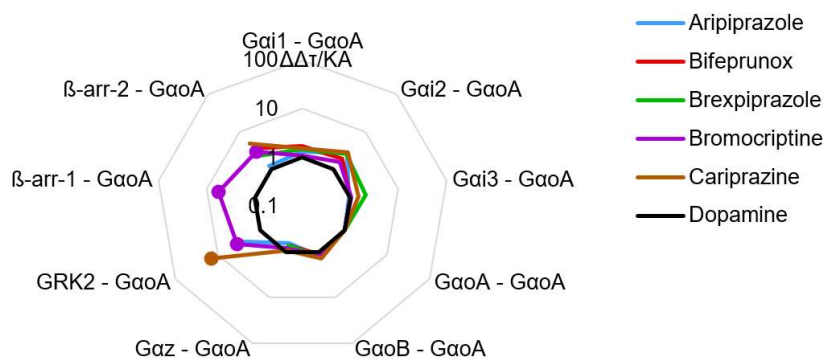
Table 5.7: Bias quantification values relative to Gα_{oA} activation.

Data represents the mean ± SEM of 3-6 separate experiments.

Agonist	ΔΔLog (τ/K _A)								
	Gα _{i1}	Gα _{i2}	Gα _{i3}	Gα _{oA}	Gα _{oB}	Gα _z	GRK2	β-arrestin-1	β-arrestin-2
Aripiprazole	0.13 ± 0.12	0.42 ± 0.12	-0.03 ± 0.12	0.00 ± 0.07	0.11 ± 0.08	-0.20 ± 0.08	0.45 ± 0.42	ND	0.07 ± 0.20
Bifeprunox	0.23 ± 0.09	0.28 ± 0.09	-0.01 ± 0.10	0.00 ± 0.07	0.06 ± 0.07	-0.14 ± 0.07	ND	ND	0.56 ± 0.13
Brexiprazole	0.16 ± 0.18	0.41 ± 0.16	0.32 ± 0.15	0.00 ± 0.08	0.10 ± 0.08	-0.15 ± 0.09	ND	ND	0.35 ± 0.45
Bromocriptine	0.04 ± 0.08	0.19 ± 0.07	0.02 ± 0.09	0.00 ± 0.06	0.05 ± 0.07	-0.08 ± 0.07	0.55 ± 0.15	0.74 ± 0.10	0.47 ± 0.08
Cariprazine	0.19 ± 0.11	0.44 ± 0.11	0.16 ± 0.11	0.00 ± 0.07	0.14 ± 0.07	-0.03 ± 0.07	1.16 ± 0.45	ND	0.68 ± 0.21
Dopamine	0.00 ± 0.07	0.00 ± 0.06	0.00 ± 0.08	0.00 ± 0.06	0.00 ± 0.06	0.00 ± 0.06	0.00 ± 0.08	0.00 ± 0.07	0.00 ± 0.07
Pardoprunox	0.00 ± 0.08	0.08 ± 0.08	0.12 ± 0.09	0.00 ± 0.06	0.03 ± 0.07	-0.08 ± 0.07	0.01 ± 0.25	0.07 ± 0.17	0.15 ± 0.12
Ropinirole	-0.03 ± 0.09	-0.25 ± 0.08	-0.19 ± 0.09	0.00 ± 0.08	-0.07 ± 0.08	0.03 ± 0.08	0.36 ± 0.11	0.28 ± 0.08	0.14 ± 0.08
Rotigotine	0.05 ± 0.07	0.05 ± 0.06	-0.01 ± 0.08	0.00 ± 0.06	0.04 ± 0.07	0.05 ± 0.07	0.71 ± 0.09	0.70 ± 0.07	0.54 ± 0.07
S-3PPP	-0.02 ± 0.10	-0.02 ± 0.10	-0.07 ± 0.11	0.00 ± 0.07	-0.03 ± 0.07	-0.07 ± 0.07	0.09 ± 0.49	ND	-0.28 ± 0.20
ST-836	0.04 ± 0.08	0.02 ± 0.07	-0.08 ± 0.09	0.00 ± 0.07	-0.03 ± 0.07	0.50 ± 0.07	0.45 ± 0.11	0.57 ± 0.08	0.27 ± 0.08

ND – not determined, could not be calculated due to poor initial non-linear curve fit ($r^2 < 0.7$).

A



B

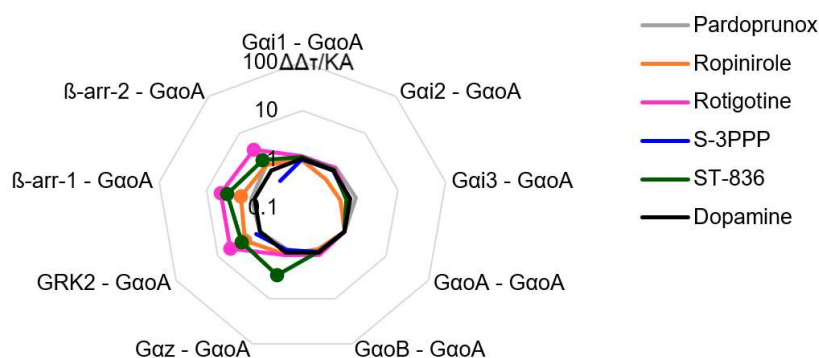


Figure 3.6: Web of biased agonism between the reference pathway $G\alpha_{oA}$ activation and different functional pathways. (A) Web of biased agonism for aripiprazole, bifeprunox, brexpiprazole, bromocriptine and cariprazine. (B) Web of biased agonism for pardoprunox, ropinirole, rotigotine, S-3PPP and ST-836. $\text{Log}(\tau/K_A)$ values were determined for each agonist at each pathway 15 minutes after agonist stimulation. These values were subtracted from the reference agonist dopamine's values to obtain $\Delta\text{Log}(\tau/K_A)$ values. The $\Delta\text{Log}(\tau/K_A)$ values for each pathway were then subtracted from the $\Delta\text{Log}(\tau/K_A)$ values of $G\alpha_{oA}$ activation to give $\Delta\Delta\text{Log}(\tau/K_A)$ values. The anti-logarithm ($\Delta\Delta\tau/K_A$) of these values were then plotted to show a web of bias. The reference agonist dopamine is shown in black in both panels and has a $\Delta\Delta\tau/K_A$ value of 1 between each pathway. Filled in circles denotes where the biased agonism is statistically significant ($P < 0.05$) as determined by a one-way ANOVA between the $\Delta\text{Log}(\tau/K_A)$ values.

No clear relationship between biased agonism and differences in agonist dissociation rate

Having observed the most statistically significant apparent biased agonism between the regulatory proteins and the well coupled $G\alpha_o$ or $G\alpha_z$ proteins, we then sought to examine whether there is a relationship between an agonists' dissociation rate and the bias towards a particular functional event. We plotted the different binding parameters we had determined against the biased agonism between multiple pathways detected at a single timepoint of 15 minutes. A Spearman's correlation was performed on these plots to assess the relationship

between the rank values of each parameter. We chose to perform this type of correlation considering the mechanisms behind the manifestation of bias are not entirely clear, such that one must consider the possibility that biased agonism between any two pathways may saturate at some point. We then examined the relationship between the binding kinetics and bias at GRK2 recruitment relative to $G\alpha_{oA}$ activation because many agonists displayed bias between these two signalling events. We first performed a negative control correlation plot between this bias and the association rate of the agonist (Fig. 3.7A). As anticipated, we observed no correlation between the association rate and the bias at GRK2 recruitment relative to $G\alpha_{oA}$ activation. Moreover, we also observed no statistically significant correlation between the bias towards GRK2 recruitment and the dissociation rate of the agonist (Fig. 3.7D). We next correlated the affinity of the agonist, again to serve as a negative control. Unexpectedly, a correlation was observed between agonist affinity and the bias towards GRK2 recruitment relative to $G\alpha_{oA}$ activation (Fig. 3.7G). We next examined the bias between β -arrestin-2 recruitment and $G\alpha_{oA}$ activation. We observed no significant correlation between either the association rate or the dissociation rate and the bias for β -arrestin-2 recruitment relative to $G\alpha_{oA}$ activation (Fig. 3.7B & E). However, performing a correlation between the affinity and the bias for β -arrestin-2 recruitment relative to $G\alpha_{oA}$ activation displayed a statistically significant Spearman's correlation (Fig. 3.7H). Moreover, some relatively large biased agonism was also observed between β -arrestin-2 recruitment and $G\alpha_z$ activation. When plotting the association rate with the bias between β -arrestin-2 recruitment and $G\alpha_z$ activation, no correlation was observed (Fig. 3.7C). In contrast, robust correlations were observed between both agonist dissociation rate or affinity and the bias of β -arrestin-2 recruitment relative to $G\alpha_z$ activation (Fig. 3.7F & I). In general, there was no clear relationship between bias and the dissociation rate of the agonist. In fact, there was a tendency for higher affinity agonists to display some bias towards the weakly coupled regulatory pathways such as GRK2 or β -arrestin-2 recruitment relative to the strongly coupled $G\alpha_{oA}$ or $G\alpha_z$.

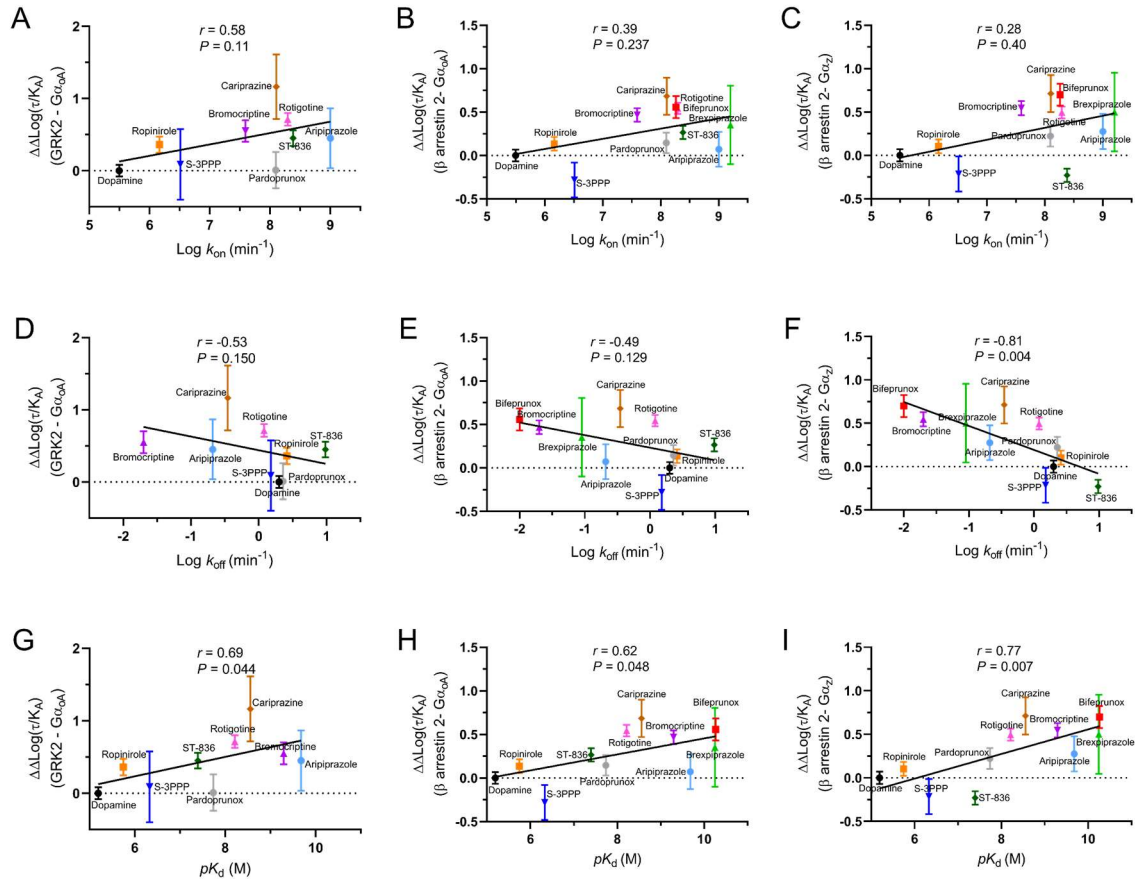


Figure 3.7: Correlation between Log(τ/K_A)/LogBias and different binding parameters. Correlation between $\text{Log } k_{on}$ and the Log bias between: GRK2 recruitment and $G_{\alpha_{O_A}}$ activation (A), β -arrestin-2 recruitment and $G_{\alpha_{O_A}}$ activation (B), and β -arrestin-2 recruitment and G_{α_z} activation (C). Correlation between $\text{Log } k_{off}$ and the Log bias between: GRK2 recruitment and $G_{\alpha_{O_A}}$ activation (D), β -arrestin-2 recruitment and $G_{\alpha_{O_A}}$ activation (E), and β -arrestin-2 recruitment and G_{α_z} activation (F). Correlation between pK_d and the Log bias between: GRK2 recruitment and $G_{\alpha_{O_A}}$ activation (G), β -arrestin-2 recruitment and $G_{\alpha_{O_A}}$ activation (H), and β -arrestin-2 recruitment and G_{α_z} activation (I). All Log bias values were determined at 15 minutes after stimulation. Two-tailed nonparametric Spearman correlation was performed that does not assume the Log bias values to be linear with the different kinetic binding parameters. The Spearman's rank correlation coefficient, r , is shown as well as the P value.

Assessment of agonist induced D₂R trafficking over time

We next assessed the ability of each agonist to induce trafficking of the D₂R. We again decided to take a BRET approach to monitor the trafficking of the D₂R in live cells. The cells were transfected with plasmids encoding the D₂R tagged on the C-terminus with Nluc to serve as a BRET donor and different endomembrane compartment proteins were tagged with venus to serve as BRET acceptors. GRK2 and β -arrestin-2 were also transfected together with the BRET sensors as they are known to aid the internalisation of the D₂R and increase the signal

in these assays (261). We measured the trafficking of the D₂R over time after stimulation with a high concentration of each agonist such that most receptors would be rapidly occupied.

When examining the movement of the D₂R away from the membrane marker KRas-venus, we saw large differences between agonists (Fig. 3.8A & D). The efficacious agonists, dopamine and rotigotine produced the largest decrease in BRET ratio that plateaued approximately 20 minutes after stimulation. Other agonists, such as bromocriptine and pardoprunox produced a weaker decrease in BRET ratio however the rate of the decrease in BRET was similar, reaching a plateau at about 20 minutes (Fig. 3.8G & J). In contrast, the lower efficacy agonists such as aripiprazole and S-3PPP produced no change in BRET ratio from baseline. In contrast to the KRas plasma membrane sensor, we observed an increase in BRET over time when assessing drug induced changes in proximity to Rab5a positive early endosomes (Fig. 3.8B & E). Furthermore, all agonists produced some detectable change in the BRET ratio (Fig. 3.8H). This may indicate that because the endosomes are a smaller compartment relative to the plasma membrane, the stoichiometry of the Rab5a-venus donor to the D₂R-Nluc may be more favourable for sensing small changes in the average localisation of the D₂R. Again, the most efficacious agonists such as, dopamine and rotigotine were the most robust at trafficking the D₂R into early endosomes. These agonists with higher efficacy tended to induce faster observed rates of trafficking into the Rab5a positive endosomes (Fig. 3.8K). The overall rate at which agonists induced trafficking into the early endosomes was similar to the rate that the D₂R moved away from the plasma membrane. Measuring the drug induced changes in proximity of the D₂R with recycling endosomes using the Rab11 marker, agonists generally produced a slow increase in BRET ratio over time (Fig. 3.8C, F, I & L). The increase in proximity into this recycling endosome compartment was significantly slower than the KRas or Rab5a marked compartments, with the BRET ratio not coming to a complete plateau within 60 minutes for any of the agonists tested. The slow increase in BRET ratio may be indicative of the population of receptors slowly recycling back to the plasma membrane after having first been internalised. Again, efficacious agonists such as dopamine produced the largest increase in trafficking into this endomembrane compartment. In general, the temporal trafficking experiments showed marked differences in the magnitude of trafficking between agonists with little difference in the rate of trafficking between agonists.

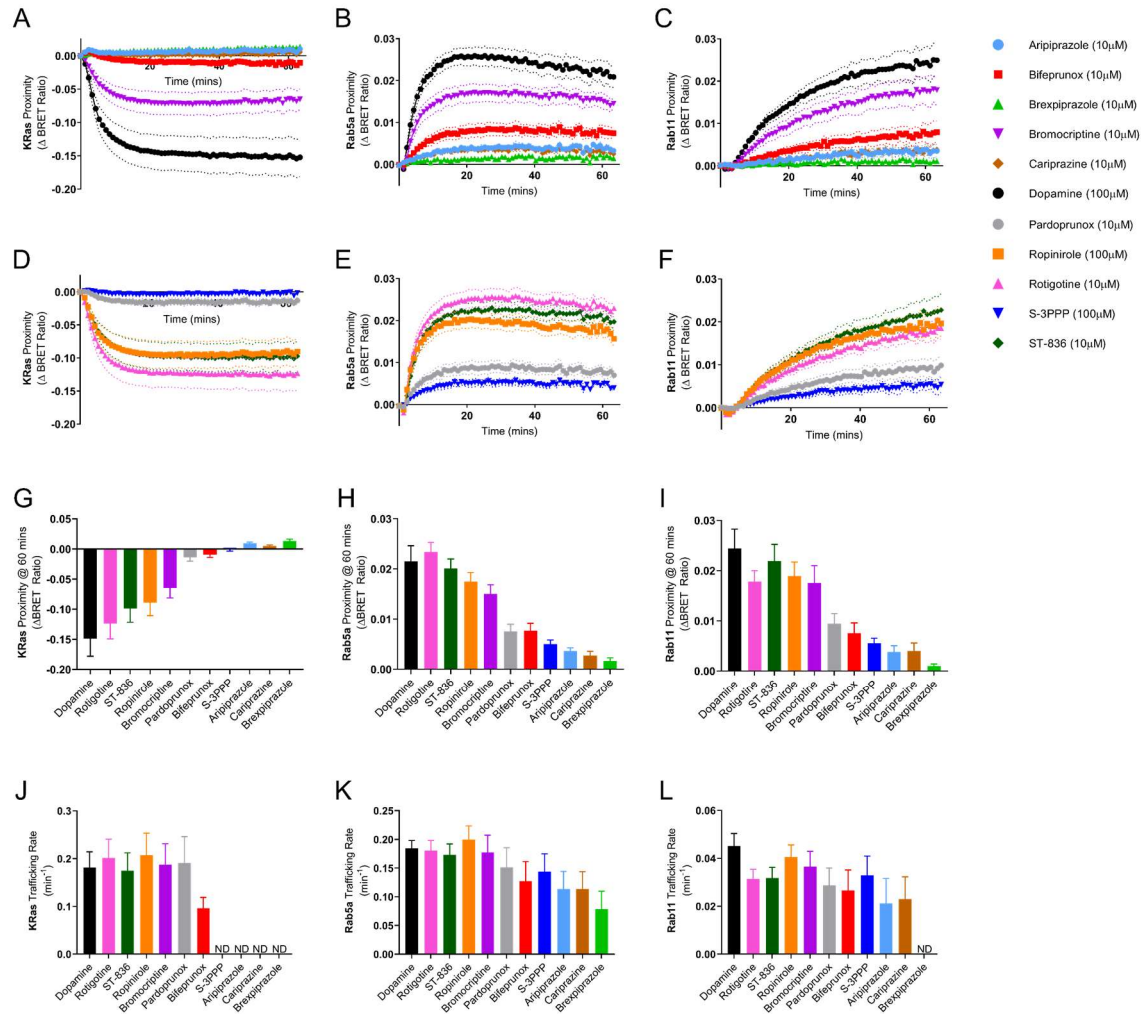


Figure 3.8: Agonist dependent trafficking of the D₂R over time. (A & D) Trafficking of D₂R-Nluc away from the KRas-venus plasma membrane marker over time in response to different agonists. (B & E) Trafficking of D₂R-Nluc towards Rab5a-venus positive early endosomes time in response to different agonists. (C & F) Trafficking of D₂R-Nluc towards Rab11-venus positive recycling endosomes over time in response to different agonists. The agonist induced change in BRET ratio measured 60 minutes after stimulation for D₂R-Nluc trafficking away from the KRas positive plasma membrane (G), Rab5a positive early endosomes (H) and Rab11 positive recycling endosomes (I). The observed rate from a one-phase exponential fit of agonist induced trafficking away from the plasma membrane (J), towards early endosomes (K) and towards recycling endosomes (L). All data represents the mean ± SEM from 5 separate experiments.

Agonist efficacy for G protein activation, GRK2 recruitment, β-arrestin-2 recruitment and receptor trafficking correlates

To understand what drives agonist bias, one must determine the phenomenon that is responsible for differences in transduction coefficients. The parameters that underpin an agonists' transduction coefficient are the efficacy (τ) and the functional affinity (K_A) (86,87). Therefore, relative changes in the transduction coefficient can be driven by differences in either

of these values. Due to this duality, we therefore decided separate the transduction coefficient and investigate a single component separately. The functional affinity values for several agonists change over time in our data as their occupancy and potency changes over time. In addition, we did not use full concentration curves when measuring D₂R trafficking and, as such, we were unable to determine functional affinity values for the D₂R trafficking. Thus, we chose to focus on the estimated operational efficacy of each agonist at each pathway.

Considering some historical models that aimed to relate efficacy to binding kinetics such as rate theory (90), we tested whether agonist efficacy at a particular pathway is influenced by either agonist association rate or dissociation rate. Hypothetically, having a slow agonist dissociation rate could be important to wholly elicit slow functional events including arrestin recruitment, whereas it may be less important for fast responses such as G protein activation. Consequently, some efficacy bias may emerge between fast and slow signalling events based on agonist dissociation rate. We therefore plotted correlations between the binding kinetic parameters and the Log τ values for G α_{i2} activation, GRK2 recruitment and β -arrestin-2 recruitment determined using an operational model described earlier (Fig. S3.12) (86,87). G α_{oA} activation was not included in this analysis because only four agonists could have their τ values accurately determined due to this pathway being efficiently coupled. We observed no statistically significant correlation between either the association rate or the dissociation rate and efficacy at any signalling pathway (Fig. S3.12A-F). We also observed no correlation in the negative control plots examining the relationship between the agonist affinity and efficacy (Fig. S3.12G-I). Therefore, based on this modest panel of agonists, neither association rate nor dissociation rate appear to be the main drivers of efficacy for any tested D₂R proximal event. Thus, bias observations are unlikely to be mediated by a mechanism that involves differences in binding kinetics driving changes in efficacy.

We then sought to elucidate any further insights into the drivers of the efficacy (τ) values with the continued hope that these may in turn help to understand differences in transduction coefficients. Accordingly, we next aimed to identify whether our data describing the agonist efficacy for one signalling event could be used to help predict the agonist efficacy at another signalling event. To do this, we correlated the different agonist efficacies between each pathway. We chose to compare G protein activation values to the other events because G protein coupling has been the canonical function of GPCRs historically. When examining G α_{i2} activation, all ligands except the two most efficacious agonists, dopamine and rotigotine, could have their τ values estimated. We therefore correlated the G α_{i2} activation τ value estimates with the other signalling events. When correlating the Log τ values of G α_{i2} with G α_{oA} , we observed

a statistically significant Pearson's correlation (Fig. 3.9A). We then correlated the τ values for G α_{i2} activation with other pathways. Log τ values of agonists activating G α_{i2} , correlated with the Log τ values for GRK2 (Fig. 3.9B). Additionally, the Log τ values of agonists activating G α_{i2} robustly correlated with the Log τ values for agonists in the β -arrestin-2 recruitment assay (Fig. 3.9C). We did not obtain full concentration response curves in the trafficking assays, such that we were unable to determine operational efficacy τ values. Even so, we were able to observe a strong correlation between the G α_{i2} Log τ values and the increase in BRET when measuring trafficking of the D₂R to Rab5a positive endosomes (Fig. 3.9D). Altogether, this demonstrated that the efficacy of an agonist at one D₂R mediated pathway can be accurately predicted by measuring any other pathway. Moreover, the strong correlations may imply that divergence in efficacy values may not be the main mediators of bias at the D₂R.

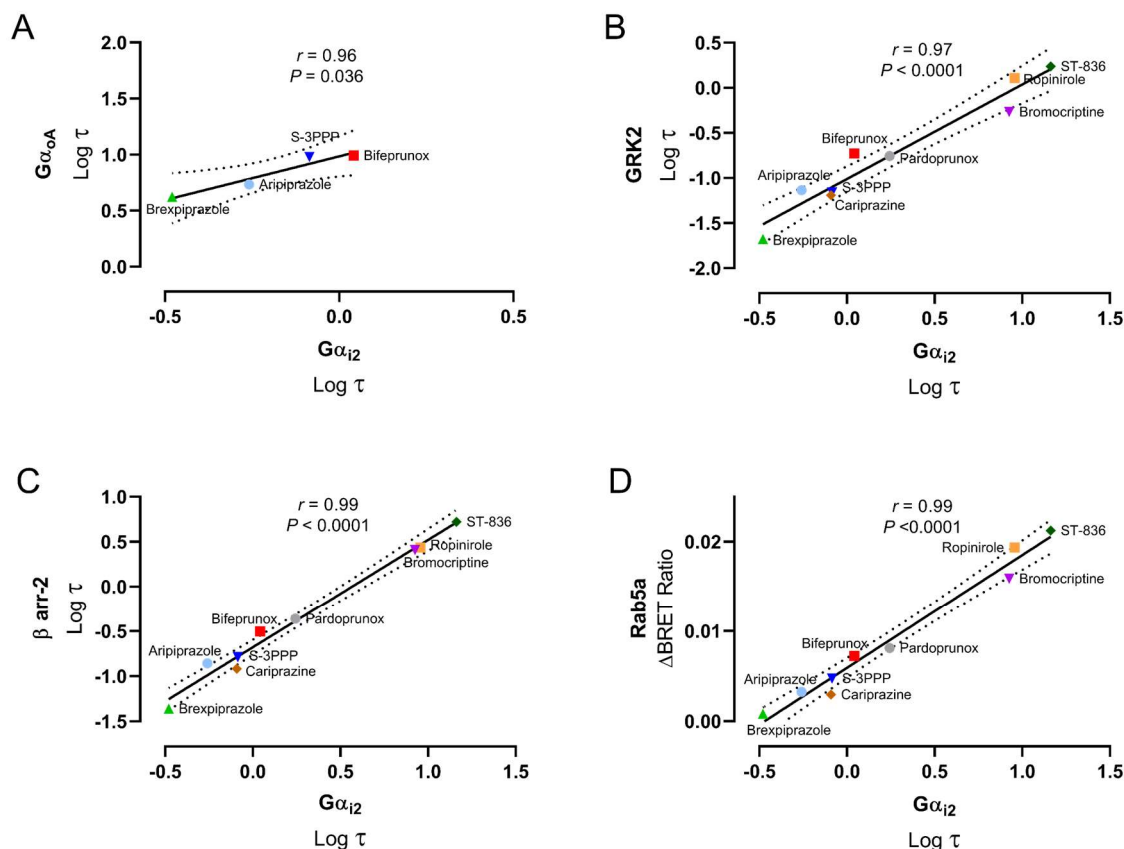


Figure 3.9: Correlation of agonist Log τ values between $G\alpha_{i2}$ activation and other functional pathways. (A) Correlation between agonist Log τ values for $G\alpha_{i2}$ activation and Log τ values for $G\alpha_{oA}$ activation. (B) Correlation between agonist Log τ values for $G\alpha_{i2}$ activation and Log τ values for GRK2 recruitment. (C) Correlation between agonist Log τ values for $G\alpha_{i2}$ activation and Log τ values for β arrestin-2 recruitment. (D) Correlation between agonist Log τ values for $G\alpha_{i2}$ activation and increase in BRET ratio for Rab5a trafficking. All Log τ values were determined from concentration response curves 15 minutes after stimulation. The Rab5a increase in BRET ratio was taken 15 minutes after agonist addition with a saturating concentration. For each panel a Pearson correlation was performed, the Pearson correlation coefficient (r) and P value is shown.

3.4 Discussion

The concept of biased agonism suggests that a drug's on-target side effects can be reduced while maintaining its therapeutic activity. Therefore, new drugs may be developed that have improved therapeutic windows through harnessing biased agonism (274). While this offers great potential, the mechanisms of biased agonism are not entirely clear. Consequently, biased agonism drug discovery efforts have relied on inefficient means such as complex high throughput screens that require multiple drug concentrations and signalling endpoints (251,275,276). Such approaches leave the probability of obtaining a biased agonist to chance and only explore a fraction of the total chemical space available. Understanding how biased

agonism materialises would allow for the rational design of biased agonists. This would greatly aid biased agonist drug discovery by reducing the time and costs associated with the process.

In our previous research we identified a mechanism that may explain some biased agonism observations. We determined that some agonists that slowly dissociate from the D₂R can display bias between proximal signalling measurements and downstream measurements (96). We concluded that this observation is due to the interplay between the differences in the kinetics of binding and the kinetics of signalling. In particular, bias was observed when comparing an upstream or transient signalling endpoint with one further downstream, and when the measurement of each pathway was taken at different timepoints. While this finding helped move forward views on biased agonism, we did not comprehensively explore the kinetic effects on all G protein subtypes, regulatory proteins such as arrestins, and receptor trafficking. In the present study, we aimed to further explore this by determining whether differences in agonist dissociation rate may contribute to apparent biased agonism when assessed at diverse proximal functional events.

We were able to demonstrate that the dissociation rate of the agonist is likely not the sole determinant of biased agonism observations at proximal events at the D₂R. We achieved this by taking a range of agonists with varying binding kinetics and structure, quantifying bias at multiple proximal events, and correlating the bias with the agonist dissociation rate. A correlation was observed between the dissociation rate in only one instance. Furthermore, we additionally performed the same correlations with the association rate and the affinity. In reality, the affinity of the agonist appeared to correlate more strongly than did the dissociation rate. Importantly, affinity is a composite of association rate and dissociation rate. Therefore, this may suggest that large differences in association rate, dissociation rate or a combination of both, may lead to observations of bias by some means.

It could be reconciled that our results altogether provide preliminary evidence for a mechanism by which higher affinity agonists display bias through an increase in receptor occupancy over time. In our temporal functional assays, not only did we observe increases in potency over time for the slow dissociating agonists such as bifeprunox, but we also observed that some other agonists displayed an increase in potency over time. In particular, we observed that rotigotine, pardoprunox and ST-836 increased in potency over time in a manner that was inconsistent with their fast dissociation rate (Fig. S3.7, S3.9 & S3.11). We verified that rotigotine had a fast dissociation rate by measuring the deactivation of G proteins (Fig. 3.3) and a separate group has also determined that rotigotine dissociates from the D₂R faster than aripiprazole and cariprazine through radioligand binding (277). Under further examination of

the properties of rotigotine, pardoprunox and ST-836, it can be seen that these agonists very rapidly associate with the D₂R. This property is important because, along with the receptor density and factors influencing ligand diffusion, agonist association rate is also a major determinant of ligand rebinding (54,224). In this case ligand rebinding describes the action of a ligand, having dissociated from the receptor, remains in the close vicinity to the receptor and as such revisits the receptor binding site or another receptor site nearby. The plausibility of rebinding occurring in this study is supported by reports of the antagonist [³H]-spiperone displaying D₂R rebinding characteristics in assays with a similar setup, and also, that many D₂R ligands are likely to display rebinding propensity in vivo (61,278,279). Therefore, we speculate that fast associating agonists, including rotigotine, pardoprunox and ST-836, may be rebinding in our assays leading to sub-saturating concentrations of the agonist increasing in receptor occupancy over time and in turn producing an increase in potency over time.

The results in the present study agree with our previous work when re-examining the data. As mentioned earlier, our previous research led us to conclude that agonists with slow dissociation rates increased in potency over time that lead to apparent bias (96). We had not previously considered that association rate may also play a role in this process. Our group's publication reported that bifeprunox was by far the slowest dissociating ligand in the study, however, it did not actually display any more bias than cariprazine or aripiprazole (96). The affinity and association rate of cariprazine, aripiprazole and bifeprunox are in a similar range and this may explain why differences in the magnitude of bias between the two ligands was not observed. In the case of cariprazine, aripiprazole and bifeprunox, both the association rate and dissociation rate may be partly involved. Therefore, increases in potency either through slow dissociation or through rebinding due to a fast association rate may explain these observations of bias.

Moving forward, it would be useful to attempt to extend this mechanism to other datasets using additional GPCRs. One GPCR where bias has been extensively investigated is the angiotensin II receptor 1 (AT₁R). There may be a similar trend for the AT₁R as it appears that apparent biased agonists such as DVG and SII have reduced receptor affinity relative to the high affinity reference agonist angiotensin II (280,281). However, for most GPCRs, there is a lack of large datasets that include both ligand affinity and biased agonism. Additionally, there is often no consensus on which ligands are definitively biased. For example, initial reports suggested that PZM21 displayed G protein bias at the μ opioid receptor, however this was not supported by any statistically significant biased agonism when quantified (82). Future studies could design experiments to further explore this idea at other GPCRs.

While there was a trend for high affinity agonists to display bias relative to the low affinity reference agonist dopamine, the biased agonism was repeatedly observed towards the poorly coupled effectors and away from the well coupled effectors. Such bias was observed between the most efficiently coupled $G\alpha_o$ or $G\alpha_z$ proteins and poorly coupled GRK2, β -arrestin-1 or β -arrestin-2. The fact that the bias routinely occurs in the same direction suggests that either each biased agonist is biasing the receptor in a similar fashion or that biased agonism is hard-wired by the system. By using a reference agonist together with the Black and Leff operational model we were able to reduce system bias by accounting for any differences in receptor reserve between pathways. However, we cannot completely rule out system bias if there are very large and irregular patterns of amplification in a particular pathway (282). As a theoretical example, continual increases in receptor occupancy may result in amplified increases in response in one pathway through mechanisms such as positive cooperativity or positive feedback until the response is saturated for one pathway, while having no effect at another pathway. This could result in relative differences in response if one agonist is much higher efficacy than another agonist as smaller occupancy levels may still lead to a very large response. Indeed, Onaran and colleagues (283) have demonstrated that using the Black and Leff operational model of agonism to determine ligand bias can result in a higher number of false positives than other methods. Moreover, when we did observe bias, there was appreciable noise in our final bias calculations resulting in some nonuniform bias patterns. For example, bifeprunox displayed statistically significant bias between $G\alpha_oA$ and β -arrestin-2, however, bifeprunox's transduction coefficient at GRK2 and β -arrestin-1 was not determined due to a poor signal in these assays. Therefore, it is unclear whether bifeprunox would display bias at GRK2 or β -arrestin-1 if there was a robust window in these assays. Similarly, ropinirole displayed very subtle bias at β -arrestin-1 relative to $G\alpha_oA$. However, no statistically significant bias was observed at β -arrestin-2 relative to $G\alpha_oA$. This makes interpretations of the data difficult because β -arrestin-1 and β -arrestin-2 would be expected to share similar patterns of recruitment due to their very high sequence identity (284).

It should be noted that while our goal was to investigate the mechanisms of bias at the D₂R, this task became challenging due to the underwhelming amount of bias that materialised. Having BRET as the sole detection technique and using identical buffers, detection times and temperatures, we expected to reduce the amount of observational bias. Nevertheless, we did not expect to observe few ligands displaying bias and the fold change in bias generally being less than 10-fold. In addition, we did not predict that there would be almost no statistically significant bias between G protein subtypes. GPCR-G protein selectivity is common, hence, if

an agonist induces different conformational states then one could envisage that these different states may have G protein selectivity as well. In agreement with this concept, apparent bias between G protein subtypes at the D₂R has been observed before between G α_{i1} and G α_{oA} (252). Furthermore, G protein subtype bias has been identified at other GPCRs such as the dopamine D₁ receptor and the free fatty acid 2 receptor (285,286). The reasons why we do not widely observe G protein subtype bias cannot yet be explained.

We were able to investigate the drivers of agonist efficacy at the D₂R. While rate theory advocates for association rate being proportional to efficacy (90), we did not observe this with our dataset. Other groups have also observed the opposite of rate theory, whereby slow dissociation leads to increased efficacy (91,93). However, we again did not see any correlation between dissociation rate and efficacy. It is important to note here that some ligands within the dataset have been through a drug discovery process that may have selected for increased or decreased agonist efficacy. Indeed, weak partial agonists are the preferred agonists for schizophrenia whereas efficacious agonists are desired for Parkinson's disease (287). Nonetheless, we also compared the agonist efficacy between all the endpoints. Each endpoints' Log τ showed a robust correlation with G α_{i2} activation (Fig. 3.9). This matches another report at the μ opioid receptor where efficacy between G protein mediated signalling, arrestin recruitment and internalisation all correlated (288). While the number of agonists tested in our study is not totally all-encompassing, our results nevertheless indicate that the ligand-specific properties that determine intrinsic efficacy at the D₂R are in fact identical at all signalling pathways. This has implications for targeting the D₂R because it suggests that the relative maximal effects may be quite challenging to separate based on the agonist. That is, the strong correlation of Log τ values between all pathways may indicate that bias observations (as determined by relative Log(τ/K_A) values) may only be able to be driven by K_A values and not τ values at the D₂R. Thus, further insight into how K_A values can differ would be important to move the field forward. A possible mechanism explaining the manifestation of differences in K_A values that in turn engenders bias may be through agonists having different affinities for the GPCR when bound to different effectors. This mechanism has been proposed by Strachan and colleagues (76), through designing AT₁R fusion proteins of AT₁R-G α_q and AT₁R- β -arrestin-2, they were able to demonstrate that biased agonists have a tighter binding affinity for the fusion protein consisting of the effector in which they are biased towards whereas balanced agonists displayed no preference.

In summary, our study suggests that differences in the binding affinity of agonists may explain some observations of biased agonism. The mechanism accounting for why agonist

affinity appears to sometimes correlate with bias between well coupled G proteins and poorly coupled regulatory proteins may in part be due to increases in receptor occupancy over time. Future research may seek to investigate whether differences in affinity relate to bias at other GPCRs and if so, how it emerges. Understanding this could aid in the rational design of biased agonist therapeutics.

3.5 Supplementary Materials

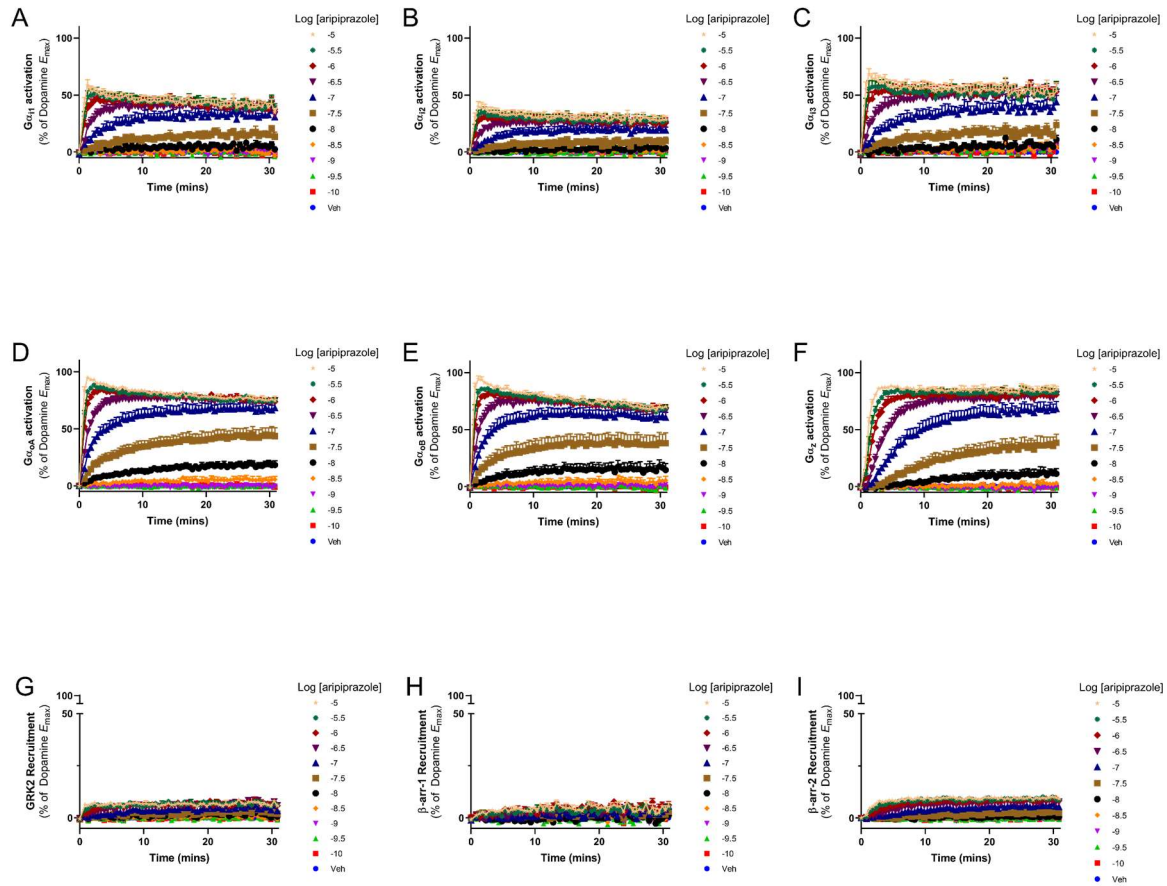


Figure S3.1: Measurement of aripiprazole induced G protein activation and regulatory protein recruitment. Activation over time of $G\alpha_{i1}$ (A), $G\alpha_{i2}$ (B), $G\alpha_{i3}$ (C), $G\alpha_{oA}$ (D), $G\alpha_{oB}$ (E), $G\alpha_z$ (F). Data represents the mean + SEM from 5 separate experiments. Recruitment over time of GRK2 (G), β arrestin-1 (H) and β arrestin-2 (I). Data represents the mean + SEM from 4 separate experiments.

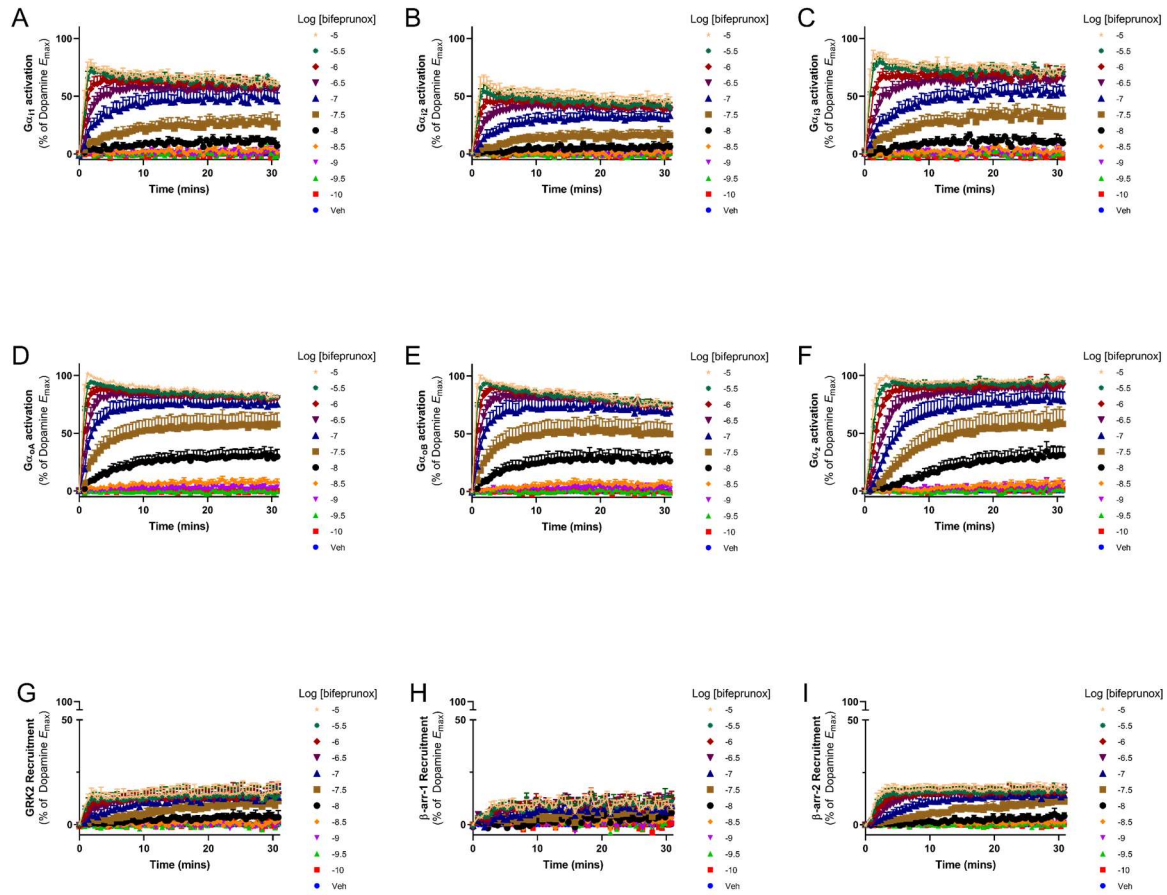


Figure S3.2: Measurement of bifepunox induced G protein activation and regulatory protein recruitment. Activation over time of $G\alpha_{i1}$ (A), $G\alpha_{i2}$ (B), $G\alpha_{i3}$ (C), $G\alpha_{oA}$ (D), $G\alpha_{oB}$ (E), $G\alpha_z$ (F). Data represents the mean + SEM from 5 separate experiments. Recruitment over time of GRK2 (G), β arrestin-1 (H) and β arrestin-2 (I). Data represents the mean + SEM from 4 separate experiments.

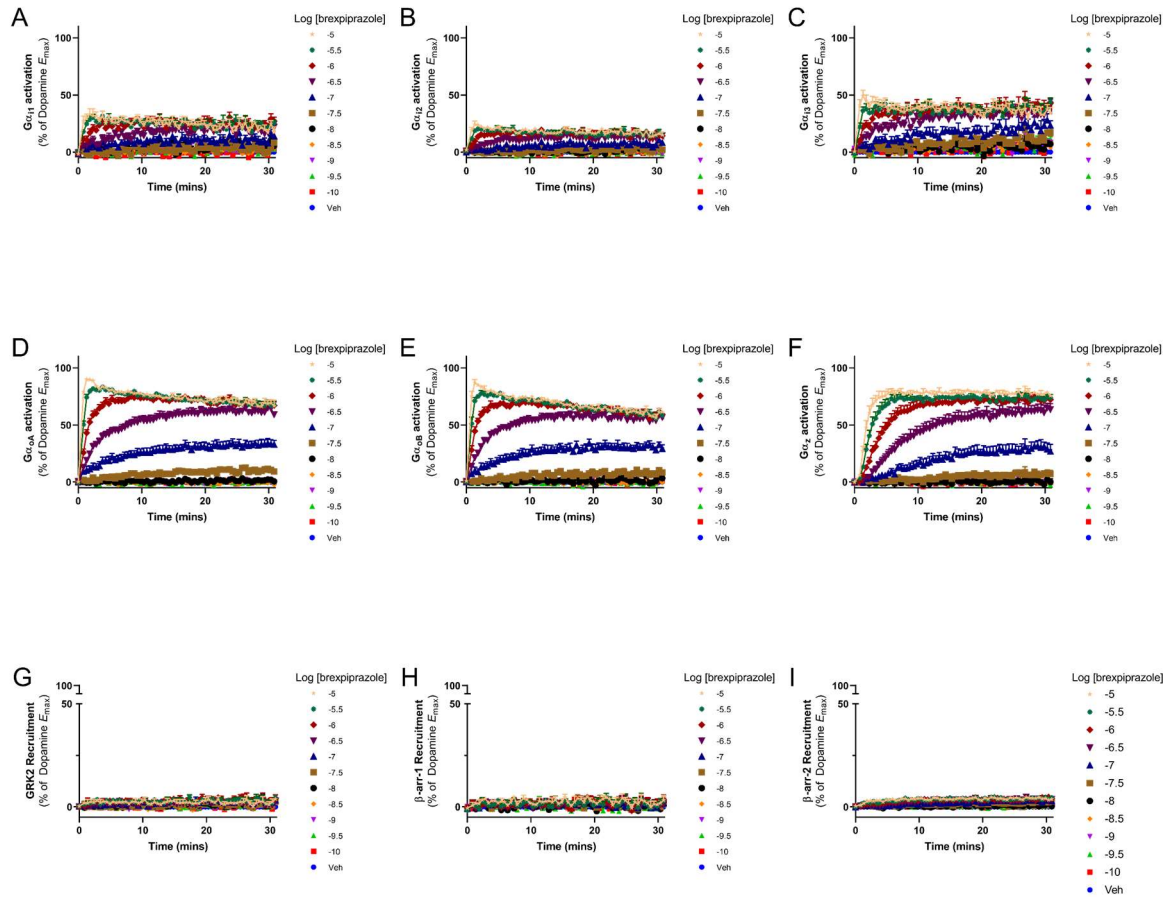


Figure S3.3: Measurement of brexpiprazole induced G protein activation and regulatory protein recruitment. Activation over time of $G\alpha_{i1}$ (A), $G\alpha_{i2}$ (B), $G\alpha_{i3}$ (C), $G\alpha_{oA}$ (D), $G\alpha_{oB}$ (E), $G\alpha_z$ (F). Data represents the mean + SEM from 5 separate experiments. Recruitment over time of GRK2 (G), β arrestin-1 (H) and β arrestin-2 (I). Data represents the mean + SEM from 4 separate experiments.

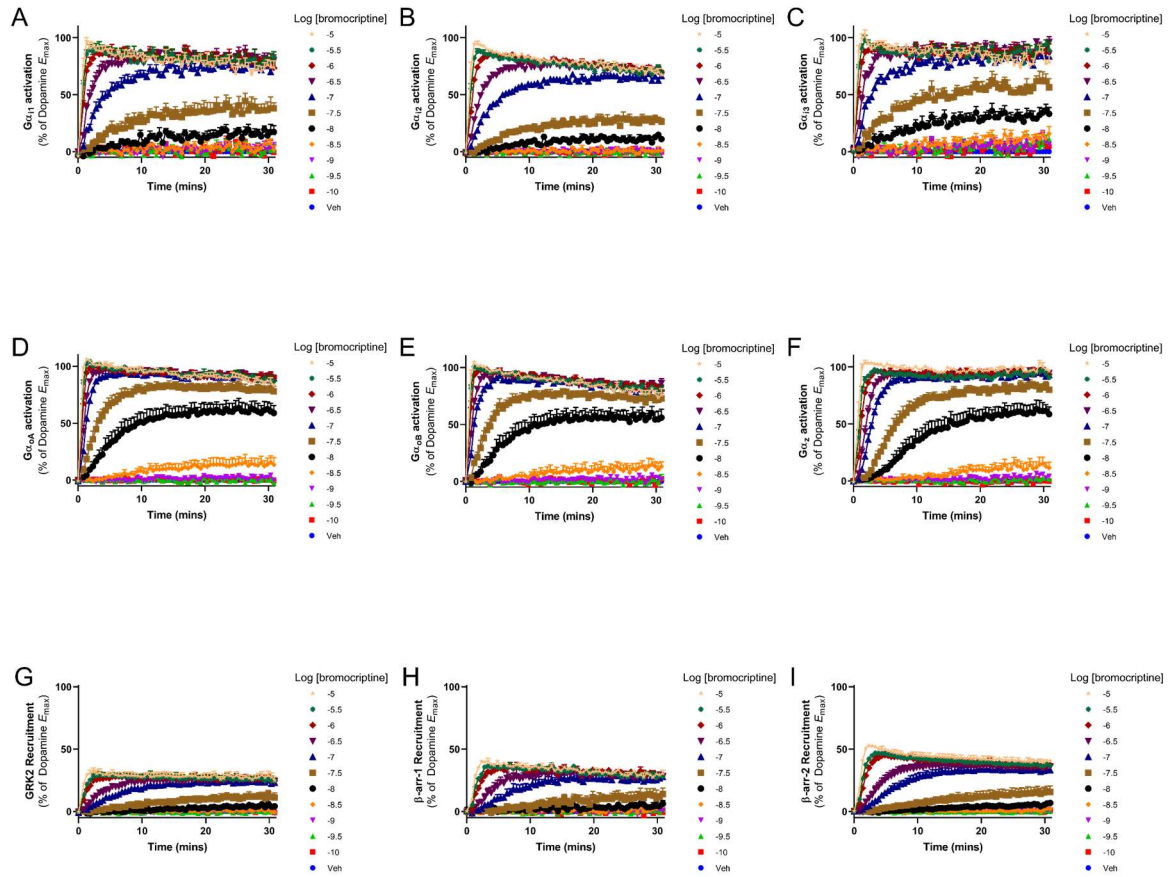


Figure S3.4: Measurement of bromocriptine induced G protein activation and regulatory protein recruitment. Activation over time of $G\alpha_{i1}$ (A), $G\alpha_{i2}$ (B), $G\alpha_{i3}$ (C), $G\alpha_{oA}$ (D), $G\alpha_{oB}$ (E), $G\alpha_z$ (F). Data represents the mean + SEM from 5 separate experiments. Recruitment over time of GRK2 (G), β arrestin-1 (H) and β arrestin-2 (I). Data represents the mean + SEM from 3 separate experiments.

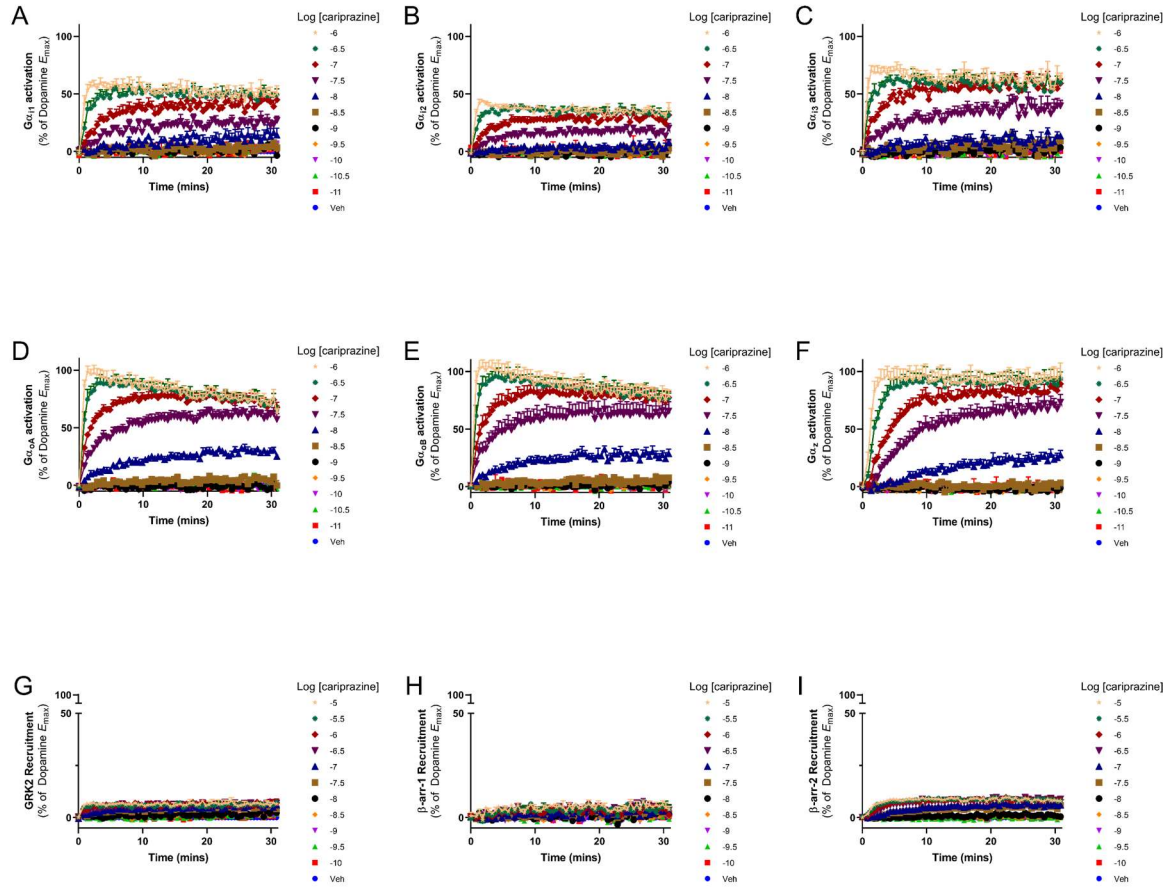


Figure S3.5: Measurement of cariprazine induced G protein activation and regulatory protein recruitment. Activation over time of $G\alpha_{i1}$ (A), $G\alpha_{i2}$ (B), $G\alpha_{i3}$ (C), $G\alpha_{oA}$ (D), $G\alpha_{oB}$ (E), $G\alpha_z$ (F). Data represents the mean + SEM from 4 separate experiments. Recruitment over time of GRK2 (G), β arrestin-1 (H) and β arrestin-2 (I). Data represents the mean + SEM from 4 separate experiments.

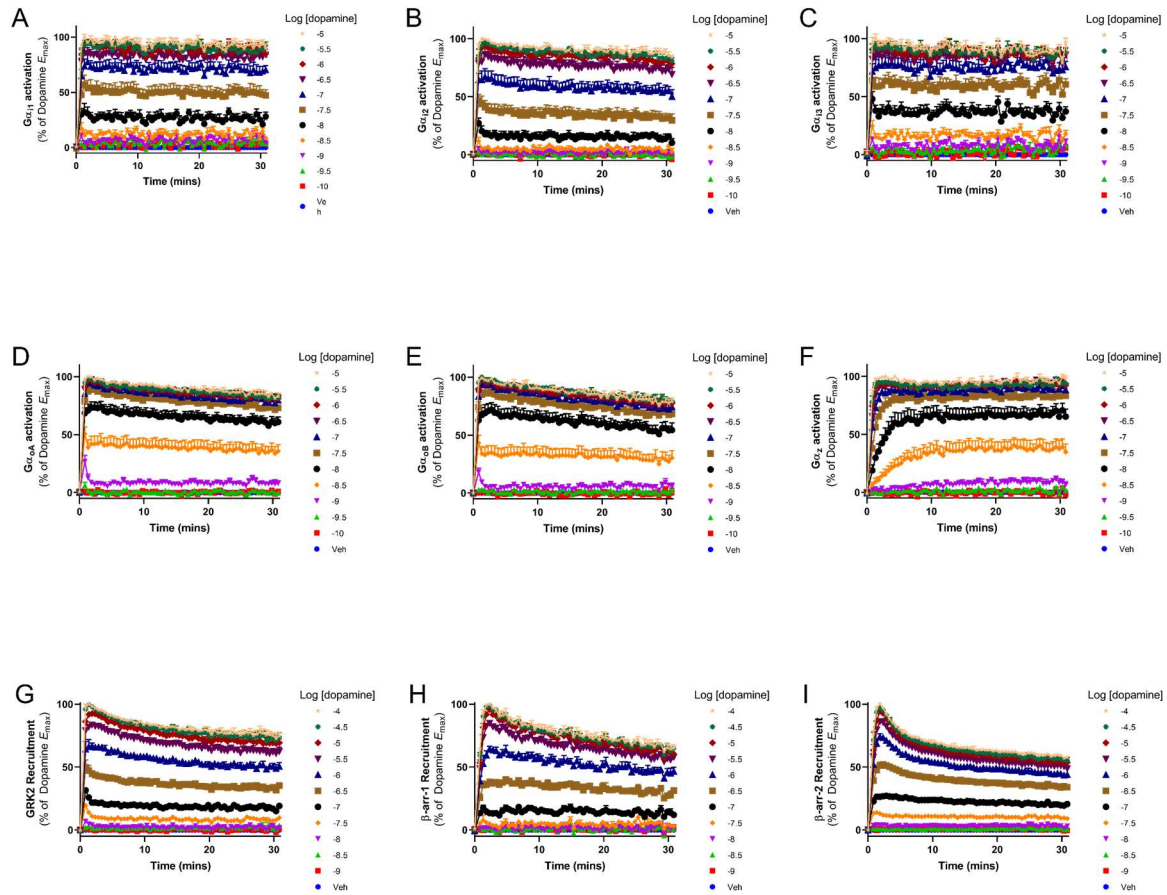


Figure S3.6: Measurement of dopamine induced G protein activation and regulatory protein recruitment. Activation over time of $G\alpha_{i1}$ (A), $G\alpha_{i2}$ (B), $G\alpha_{i3}$ (C), $G\alpha_{oA}$ (D), $G\alpha_{oB}$ (E), $G\alpha_z$ (F). Data represents the mean + SEM from 6 separate experiments. Recruitment over time of GRK2 (G), β arrestin-1 (H) and β arrestin-2 (I). Data represents the mean + SEM from 3 separate experiments.

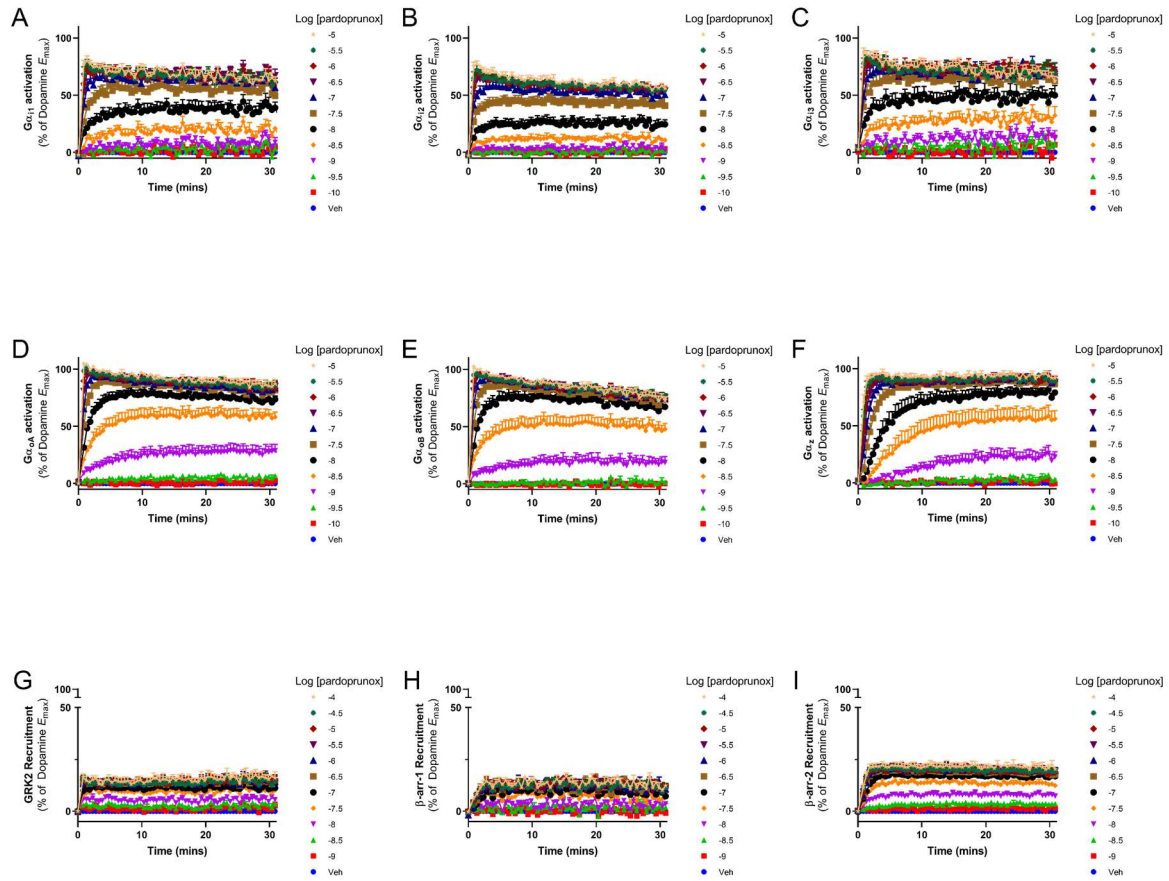


Figure S3.7: Measurement of pardoprunox induced G protein activation and regulatory protein recruitment. Activation over time of $G\alpha_{i1}$ (A), $G\alpha_{i2}$ (B), $G\alpha_{i3}$ (C), $G\alpha_{oA}$ (D), $G\alpha_{oB}$ (E), $G\alpha_z$ (F). Data represents the mean + SEM from 5 separate experiments. Recruitment over time of GRK2 (G), β arrestin-1 (H) and β arrestin-2 (I). Data represents the mean + SEM from 3 separate experiments.

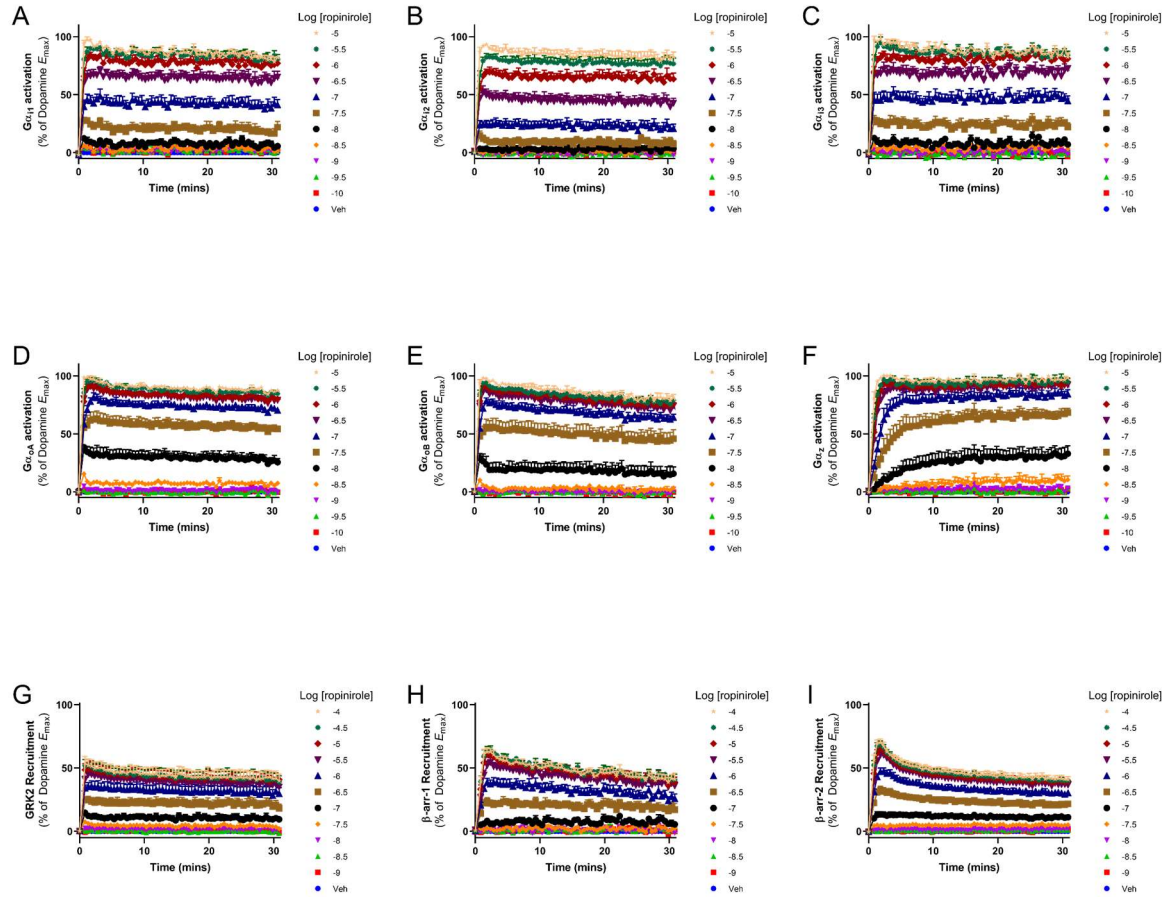


Figure S3.8: Measurement of ropinirole induced G protein activation and regulatory protein recruitment. Activation over time of $G\alpha_{i1}$ (A), $G\alpha_{i2}$ (B), $G\alpha_{i3}$ (C), $G\alpha_{oA}$ (D), $G\alpha_{oB}$ (E), $G\alpha_z$ (F). Data represents the mean + SEM from 4 separate experiments. Recruitment over time of GRK2 (G), β arrestin-1 (H) and β arrestin-2 (I). Data represents the mean + SEM from 4 separate experiments.

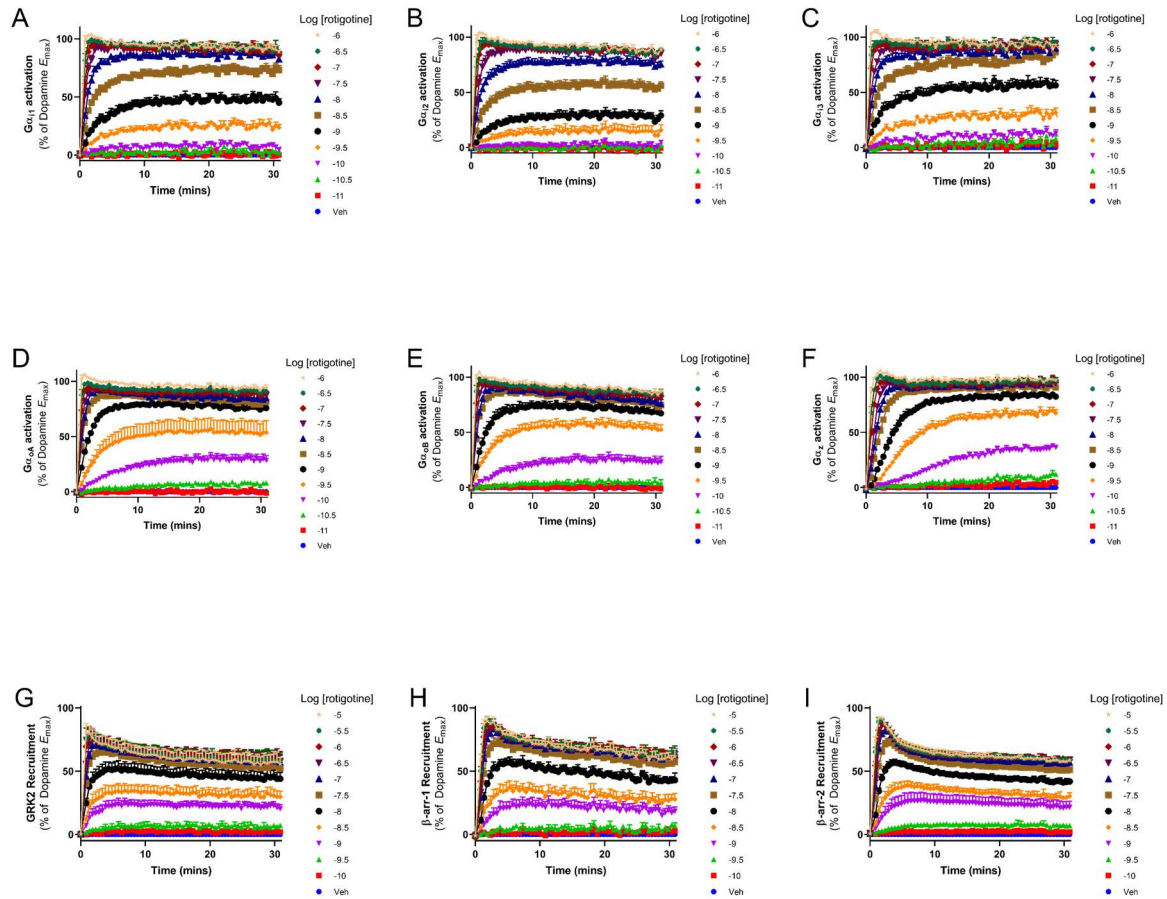


Figure S3.9: Measurement of rotigotine induced G protein activation and regulatory protein recruitment. Activation over time of $G\alpha_{i1}$ (A), $G\alpha_{i2}$ (B), $G\alpha_{i3}$ (C), $G\alpha_{oA}$ (D), $G\alpha_{oB}$ (E), $G\alpha_z$ (F). Data represents the mean + SEM from 5 separate experiments. Recruitment over time of GRK2 (G), β arrestin-1 (H) and β arrestin-2 (I). Data represents the mean + SEM from 4 separate experiments.

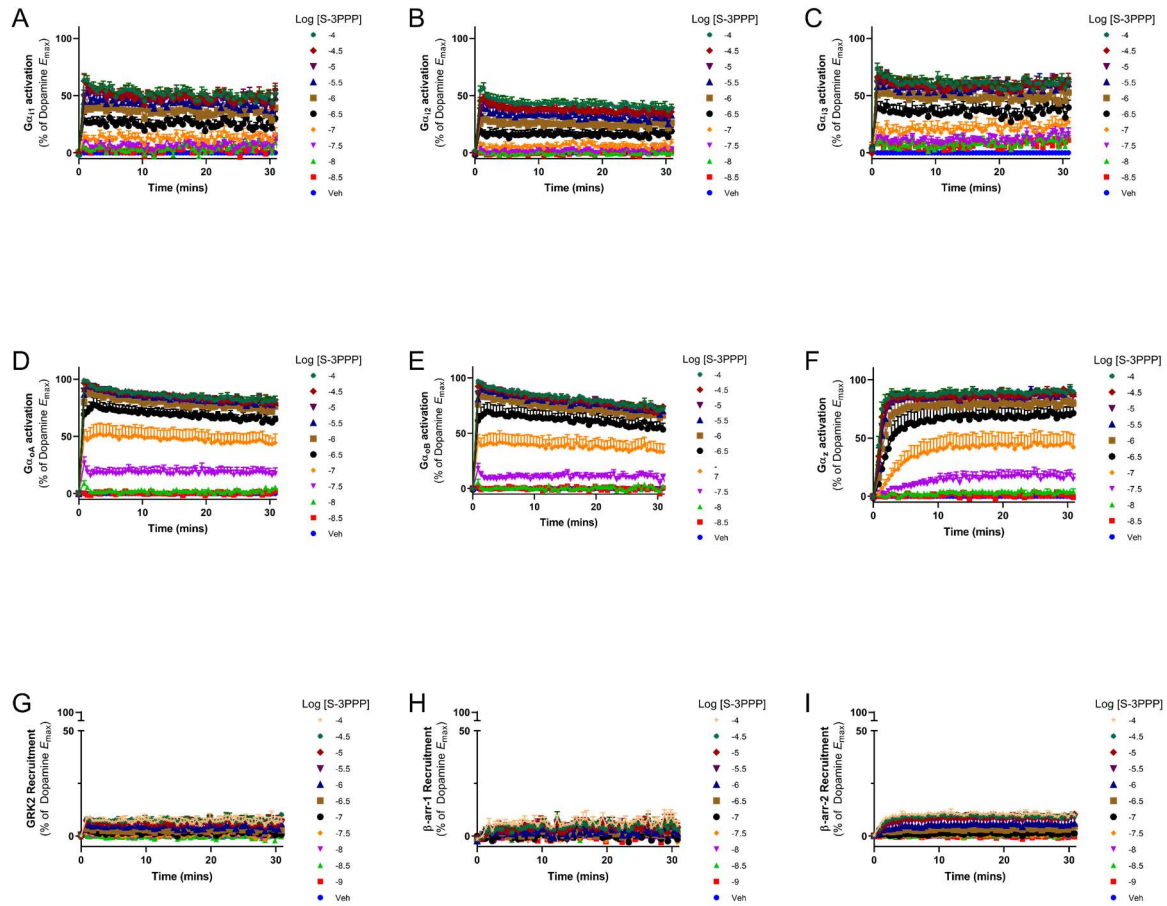


Figure S3.10: Measurement of S-3PPP induced G protein activation and regulatory protein recruitment. Activation over time of $G\alpha_{i1}$ (A), $G\alpha_{i2}$ (B), $G\alpha_{i3}$ (C), $G\alpha_{oA}$ (D), $G\alpha_{oB}$ (E), $G\alpha_z$ (F). Data represents the mean + SEM from 5 separate experiments. Recruitment over time of GRK2 (G), β arrestin-1 (H) and β arrestin-2 (I). Data represents the mean + SEM from 3 separate experiments.

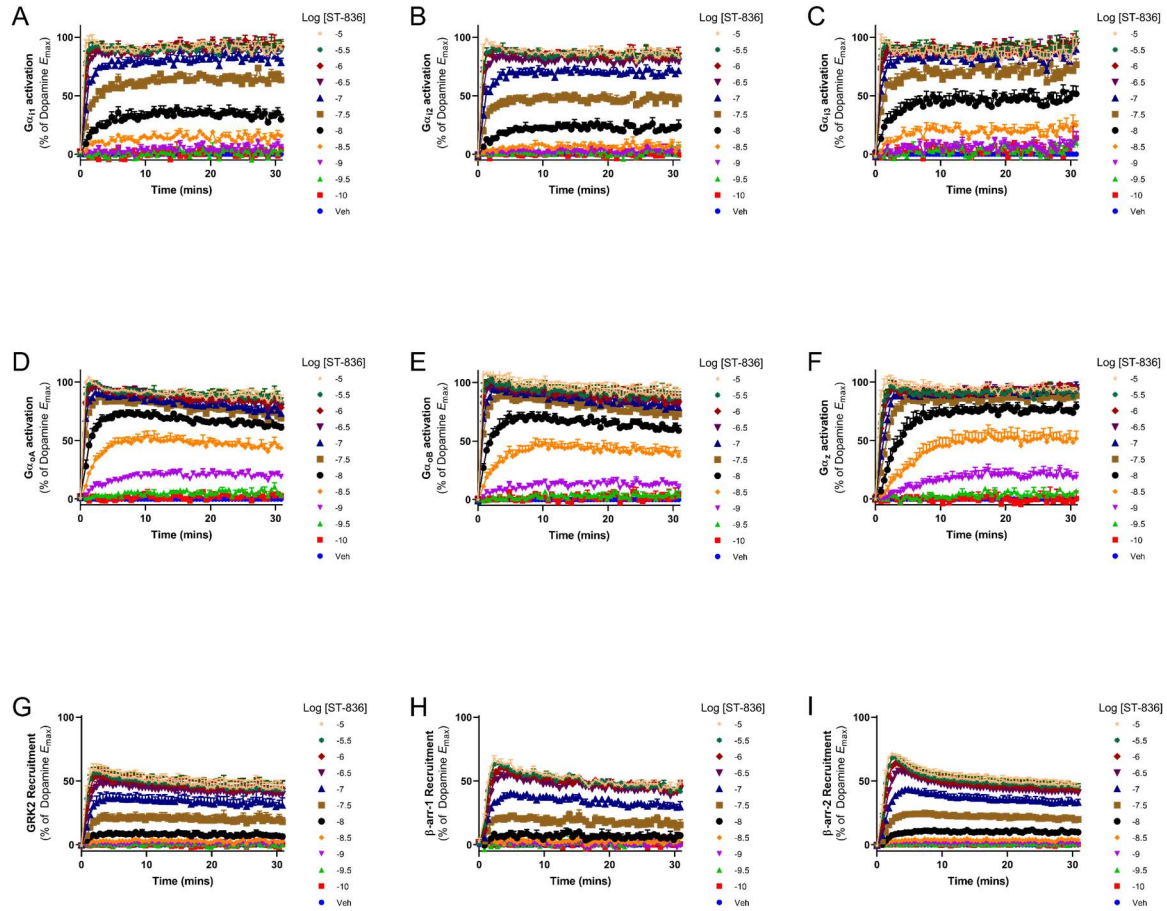


Figure S3.11: Measurement of ST-836 induced G protein activation and regulatory protein recruitment. Activation over time of $G\alpha_{i1}$ (A), $G\alpha_{i2}$ (B), $G\alpha_{i3}$ (C), $G\alpha_{oA}$ (D), $G\alpha_{oB}$ (E), $G\alpha_z$ (F). Data represents the mean \pm SEM from 4 separate experiments. Recruitment over time of GRK2 (G), β arrestin-1 (H) and β arrestin-2 (I). Data represents the mean \pm SEM from 3 separate experiments.

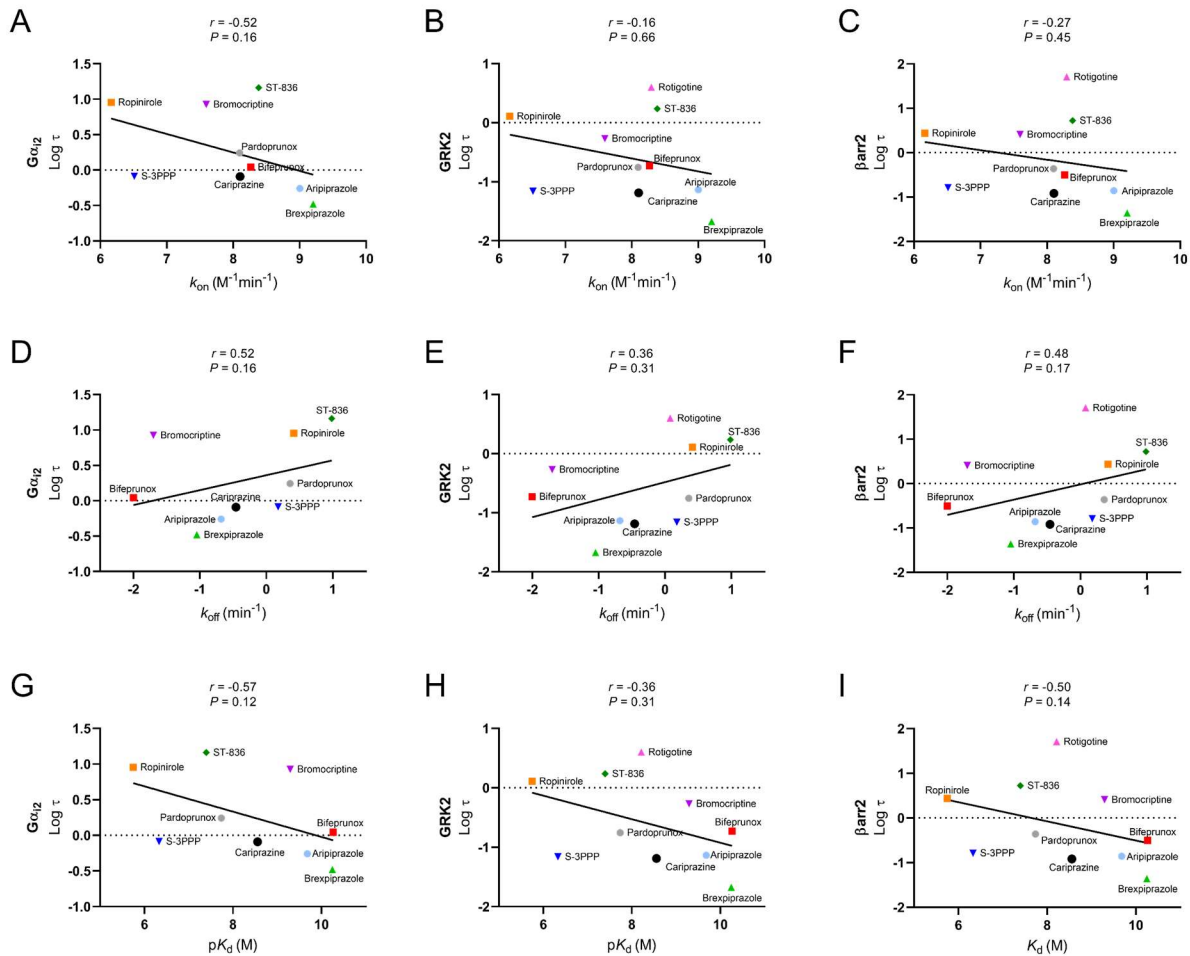


Figure S3.12: Correlations between Log(τ) values at different endpoints and different binding parameters. Correlation of the Log k_{on} with the Log τ for: $G\alpha_{i2}$ activation (A), GRK2 recruitment (B), β arrestin-2 recruitment (C). Correlation of the Log k_{off} with the Log τ for: $G\alpha_{i2}$ activation (D), GRK2 recruitment (E), β arrestin-2 recruitment (F). Correlation of the pK_d with the Log for: $G\alpha_{i2}$ activation (G), GRK2 recruitment (H), β arrestin-2 recruitment (I). All τ values were determined at 15 minutes after stimulation. Two-tailed nonparametric Spearman correlation was performed that does not assume the τ values to be linear with the different kinetic binding parameters. The Spearman's rank correlation coefficient, r , is shown as well as the P value.

Chapter 4:

New phospho-site-specific antibodies to unravel the role of GRK phosphorylation in dopamine D₂ receptor regulation and its modulation by biased agonists

Anika Mann^{1*}, Alastair C Keen^{2,3,4*}, Hanka Mark¹, Pooja Dasgupta¹, Jonathan A. Javitch^{5,6,7}, Meritxell Canals^{3,4}, Stefan Schulz^{1*}, J Robert Lane^{3,4*}

¹Institute of Pharmacology and Toxicology, Jena University Hospital, Friedrich Schiller University Jena, Drackendorfer Str. 1, 07747, Jena, Germany

²Drug Discovery Biology, Monash Institute of Pharmaceutical Sciences, Monash University, Parkville, VIC, Australia.

³School of Life Sciences, Queen's Medical Centre, University of Nottingham, Nottingham, United Kingdom.

⁴Centre of Membrane Proteins and Receptors, University of Birmingham and University of Nottingham, Midlands, United Kingdom.

⁵Department of Psychiatry, Vagelos College of Physicians and Surgeons, Columbia University, United States; ⁶Division of Molecular Therapeutics, New York State Psychiatric Institute, United States; ⁷Vagelos College of Physicians and Surgeons, Columbia University, United States

Abstract

The dopamine D₂ receptor (D₂R) is the target of drugs used to treat the symptoms of Parkinson's disease and schizophrenia. D₂R G protein signalling is regulated through phosphorylation by G protein receptor kinases (GRKs) and interaction with arrestins. In addition, D₂R arrestin mediated signalling has been shown to have physiological functions distinct from those of G protein mediated pathways. Recent studies have explored the action of pathway biased agonists as an avenue for the development of improved antipsychotic treatments. Despite this interest, relatively little is known about the patterns of D₂R receptor phosphorylation that might control these processes. Antibodies that selectively bind intracellular phosphorylation sites have proved useful tools to investigate such mechanisms at other GPCRs. Herein we generate and characterise the first antibodies specific for GRK2/3 phosphorylation sites on the D₂R. We identify a phosphorylation site in ICL3 that is phosphorylated by GRK2/3 on agonist activation of the D₂R. Phosphorylation of this site predicts arrestin recruitment. We incorporate measurements of D₂R phosphorylation with other measurements of G protein activation and receptor regulation to profile selected D₂R agonists including putative biased agonists. These studies demonstrate the utility of these phospho-site-specific antibodies to investigate D₂R regulation, and as part of the characterisation of biased agonists at the D₂R.

4.1 Introduction

The catecholamine neurotransmitter dopamine (DA) is involved in many physiological processes in the central nervous system (CNS) such as cognition, motor control and reward (289). DA effects are mediated by 5 members of the G protein-coupled receptor (GPCR) superfamily. The dopamine D₁ and D₅ receptors (D₁R & D₅R) are coupled to stimulatory G proteins (G α_s or G α_{olf}) whereas the D₂-like DRs (D₂R, D₃R, D₄R) are coupled to inhibitory G proteins (G $\alpha_{i/o/z}$). Dysregulation of dopamine signalling is associated with many CNS disorders and the D₂R is a validated drug target in neurology and psychiatry. D₂R agonists are used to treat the symptoms of Parkinson's disease, whereas D₂R antagonism is a necessary property of all clinically used antipsychotics(290).

G protein signalling is rapidly desensitized by phosphorylation of the receptor by GPCR kinases (GRKs) followed by the recruitment of arrestins to the phosphorylated receptor(24). This inhibits G protein-signalling and leads to receptor internalization, dephosphorylation and recycling of receptors to the cell surface or trafficking to lysosomes for degradation. GRKs 2 and 3 primarily mediate agonist stimulated D₂R phosphorylation (291,292) and over-expression of GRK2 has been shown to enhance D₂R arrestin recruitment(293). The D₂R lacks the long C-terminal tail that is the site of GRK phosphorylation for many GPCRs. Mutagenesis studies from Namkung and colleagues identified eight serine/threonine (Ser/Thr) residues that are phosphorylated by GRK2/3 and a further five residues that are phosphorylated by protein kinase C (PKC) within intracellular loop (ICL) 3(294). A subsequent study by Cho and colleagues identified additional residues in ICL2 and 3 that appear to be important for PKC-mediated desensitisation of the D₂R (292).

In addition to their role in receptor regulation, arrestins may act as scaffolding proteins to initiate signalling pathways (295). Indeed, while G $\alpha_{i/o/z}$ G protein signalling appears to be responsible for many of the physiological consequences of D₂R activation, a β -arrestin-2-mediated signalling cascade involving protein phosphatase 2A, Akt (PKB) and glycogen synthase 3 β may also have an important physiological role (155,296). A global β -arrestin-2 knockout displayed a reduction in DA dependent locomotor activity (155). Two studies that used the expression of mutant D₂Rs, compromised either in the ability to recruit β -arrestin-2 or to activate G protein signalling relative to the other signalling process, in D₂R-expressing medium spiny neurons (D₂R-MSNs), provided evidence that D₂R-arrestin signalling is sufficient for normal locomotor activity but not incentive motivation (297,298). Elimination of

β-arrestin-2 specifically in D₂-MSNs reduced locomotor responses and blunted cocaine reward (299). Together these data suggest that D₂R β-arrestin-2 signalling may mediate physiological functions distinct from those controlled by D₂R Gi/o protein signalling (300). ‘Biased agonism’ describes a phenomenon whereby different ligands stabilise distinct conformations of a single receptor such that they differentially engage distinct signalling effectors (301). By exploiting this concept, one may be able to develop signalling pathway-specific drugs that display a greater level of cell type or tissue specificity (302). Therefore, if the therapeutic and deleterious side effects of a drug are mediated through a single receptor, as is the case for antipsychotics at the D₂R, then biased agonists may provide an approach to avoid such “on-target” side effects. Both arrestin and G protein biased ligands have been identified for the D₂R (293,303). Intriguingly, the action of one series of arrestin-biased ligands both to attenuate amphetamine-induced hyperlocomotion and avoid catalepsy was diminished by global knockout of β-arrestin-2 (293).

Together these studies highlight D₂R phosphorylation by GRK2/3 as a key step in modulating downstream to control distinct physiological responses to dopamine. We and others have shown that antibodies specific to phosphorylated residues of GPCRs are particularly useful in unravelling the complexities of such regulatory processes and in particular the hierarchy of phosphorylation patterns or barcodes (304-306). In this study we develop and characterise the first GRK phosphorylation site (phospho-site)-specific antibodies for the D₂R and identify a site that is phosphorylated by GRK2 in response to D₂R agonists. We compare the action of a number of agonists, including putatively biased agonists, at triggering receptor phosphorylation and correlate this to G protein activation, GRK2 recruitment and arrestin recruitment.

4.2 Methods

Plasmids

DNA for the long splice variant of the hD₂R was generated via artificial synthesis and cloned into pcDNA3.1 by imaGenes. The coding sequence for an amino-terminal HA-tag was added.

Antibodies

Peptide sequences used for generating phosphosite-specific antibodies against individual phosphorylated forms of the long splice variant of the D₂R are shown in Table 4.1, including a phosphorylation-independent antiserum targeting a proximal epitope in the D₂R third intracellular loop. After HPLC purification, the respective peptides were coupled to keyhole limpet haemocyanin. The conjugates were mixed 1:1 with Freund's adjuvant and injected into groups of three rabbits (5095-5097) for anti-pT287/288 antibody production, (5098-5100) for anti-pT293/S296 antibody production, (5101-2103) for anti-pS317/T318 antibody production, and (5104-5106) for anti-D₂R antibody production. The rabbits were injected at 4-week intervals. The serum was obtained 2 weeks after immunizations, beginning with the second injection. Specificity of the antisera was tested using dot blot analysis. Antibodies were affinity-purified against their immunizing peptide, immobilized using the SulfoLink kit (Thermo Scientific), for subsequent analysis. Anti-GRK2 (sc-562), anti-GRK3 (sc-563), anti-GRK5 (sc-518005) and anti-GRK6 (sc-566) antibodies were purchased from Santa Cruz Biotechnology. The anti-HA IgG CF™488A antibody (SAB4600054) was obtained from Sigma-Aldrich, anti-HA IgG CF640R antibody (20240) was purchased from Biotium and the anti-rabbit IgG HRP-coupled antibody (7074) was obtained from Cell Signaling.

Table 4.1: D₂R peptide sequences used for generation of phospho-site-specific antisera. List of peptide sequences used for generating phosphosite-specific antibodies against individual phosphorylated forms of the D₂R and a phosphorylation-independent antiserum targeting the D₂R at the proximal part of the third intracellular loop.

Antiserum Name	Sequence used for immunization	Amino acid position in human D ₂ receptor
T287/S288	EMLSS-T(p)-S(p)-PPER	282-292
T293/S296	PPER-T(p)-RY-S(p)-PIPP	289-300
S317/T318	HHGLH-S(p)-T(p)-PDSP	312-322
D ₂ R (phosphorylation-independent)	VNTRSSRAFRAHLRAPLKGN	223-243

Drugs

Terguride (ab144611) was obtained from Abcam. Aripiprazole (SML-0935), PMA (P8139) and pergolide mesylate (P8828) were purchased from Sigma-Aldrich. Apomorphine hydrochloride (2073), MLS1547 (6171), ropinirole (3680), quinpirole hydrochloride (1061), dopamine hydrochloride (3548), cabergoline (2664), bromocriptine mesylate (0427), forskolin (1099), SCH23390 (0925), PTX (3097), haloperidol hydrochloride (0931), L-741,626 (1003) and roxindole (1559) were obtained from Tocris. UNC9994 (A16087) was purchased from AdooQ[®] Bioscience. Lambda-phosphatase (P0753S) was obtained from Santa Cruz. Compound 101 (HB2840) was obtained from Hello Bio. Terguride, PMA, forskolin, L-741,626, aripiprazole, pergolide, apomorphine, MLS1547, ropinirole, cabergoline, bromocriptine, haloperidol, roxindole, UNC9994 and compound 101 are DMSO-soluble and all the other mentioned compounds are water-soluble.

Cell culture and transfection

Human embryonic kidney 293 (HEK293) cells were obtained from the German Collection of Microorganisms and Cell Cultures GmbH (Deutsche Sammlung von Mikroorganismen und Zellkulturen; DSMZ). Cells were cultured in Dulbecco's modified Eagle's medium (DMEM), supplemented with 10% fetal bovine serum, 2 mM L-glutamine and 100 U/ml penicillin/streptomycin at 37 °C and 5% CO₂. HEK293 cells were stably transfected with TurboFect (ThermoFisher Scientific). Cells stably expressing HA-hD2 receptor were selected in medium supplemented with 400 µg/ml geneticin and cells stably transfected with HA-hD2 receptor and GIRK-eGFP were selected in medium supplemented with 400 µg/ml geneticin and 300 µg/ml hygromycin. To increase the number of HEK293 cells stably expressing HA-hD2 receptor or HA-hD2 receptor in combination with GIRK-eGFP, fluorescence-activated cell sorting was used as described previously (305,307).

Small interfering RNA (siRNA) silencing of gene expression

Chemically synthesized double-stranded siRNA duplexes (with 3'-dTdT overhangs) were purchased from Qiagen for the following targets: *GRK2* (5'-AAGAAAUUCAUUGAGAGCGAU-3'), *GRK3* (5'-AAGCAAGCUGUAGAACACGUA-3'), *GRK5* (5'-AAGCAGTATCGAGTGCTAGGA-3') and *GRK6* (5'-AACACCUUCAGGCAAUACCGA-3') and from GE Dharmacon a non-silencing RNA

duplex (5'-GCUUAGGAGCAUUAGUAAA-3' and 3'-UUUACUAAUGCUCCUAAGC-5'). - HEK293 cells stably expressing HA-hD2 receptor were transfected with 150 nM siRNA for single transfection or with 100 nM of each siRNA for double transfection for 3 days using HiPerFect. All experiments showed target protein abundance reduced by $\geq 80\%$.

Western blotting analysis

HEK293 cells stably expressing the HA-hD2R were plated onto poly-L-lysine-coated 60-mm dishes and grown for 2 days to 80% confluency. Cells were treated with agonists or antagonists and subsequently lysed with detergent buffer (50 mM Tris-HCl, pH 7.4; 150 mM NaCl; 5 mM EDTA; 10 mM NaF; 10 mM disodium pyrophosphate; 1% Nonidet P-40; 0.5% sodium deoxycholate; 0.1% SDS) in the presence of protease and phosphatase inhibitors. Where indicated, cells were preincubated with GRK2/3 inhibitor compound 101 or D2 receptor antagonists for 30 min before agonist treatment. HA-tagged hD2 receptors were enriched using anti-HA-agarose beads after 30 min centrifugation at 4 °C. Samples were inverted for 2 hours at 4 °C. Where indicated, cell lysates were dephosphorylated with lambda protein phosphatase (Santa Cruz) for 1 hour at 30 °C. Following sample washing, proteins were eluted using SDS sample buffer for 30 min at 50 °C. Protein separation was performed on 7.5% or 12% SDS-polyacrylamide gels. After electroblotting, membranes were incubated with 0.1 µg/ml antibodies to pT287/S288 (5095), pT293/S296 (5099) or pS317/T318 (5102) overnight at 4 °C. Enhanced chemiluminescence detection (ECL) was used to detect bound antibodies (Thermo Fisher Scientific). Subsequently, blots were stripped and reprobed with the phosphorylation-independent antibody to the D₂ receptor (5106) to ensure equal loading of the gels.

G protein activation assay

The G protein activation assay was performed based on a previously reported bioluminescence resonance energy transfer (BRET) detection method (257,308). Initially, 2,500,000 Flp-InTM HEK 293 cells stably expressing the human D_{2L}R were harvested into 10cm dishes. 24 hours after harvesting cells, the cells were transfected with cDNA constructs using linear polyethylenimine (PEI) in a ratio of 1µg DNA: 6µg PEI. Cells were transfected with pcDNA3.1 encoding the following constructs: 1µg venus-1-155-G_{γ2}, 1µg venus-156-239-G_{β1}, 1µg masGRK3ct-Nluc and 2µg of either G_{αi1}-C351I or G_{αoA}-C351I. 24 hours after transfection the cells were harvested from dishes and plated into poly-D-lysine coated Greiner white 96-well TC treated plates. The cells were left to adhere for approximately 8 hours and

then treated with 100ng/mL pertussis toxin overnight. The following day the plate was taken out of the incubator, washed once with Hank's balanced salt solution (HBSS) pH 7.4 and left to equilibrate in HBSS 37°C for 30 minutes before BRET detection. 10 minutes prior to addition of agonist, 10µL of Nano-Glo substrate (Promega) was added to each well with a multi-step pipette (final dilution 1 in 1000). BRET was then measured using a PHERAstar FS microplate reader (BMG LABTECH). Luminescence was measured with the BRET¹ plus filter for the emission signal of Nluc (445-505nm) and venus (505-565nm) simultaneously. Measurements were taken 10 minutes after agonist addition. The counts from the venus acceptor (505-555nm) was then divided by the donor Nluc (465-505nm) counts to give a BRET ratio. BRET ratios were then normalised to percent of the dopamine induced maximal responses where indicated.

Membrane potential assay

Membrane potential change was measured as previously described (309). HEK293 cells stably expressing the HA-hD₂ and R GIRK-eGFP transfected HEK293 cells were plated into 96-well plates. After washing with Hank's balanced salt solution (HBSS), buffered with 20 mM HEPES (pH 7.4, containing 1.3 mM CaCl₂; 5.4 mM KCl; 0.4 mM K₂HPO₄; 0.5 mM MgCl₂; 0.4 mM MgSO₄; 136.9 mM NaCl; 0.3 mM Na₂HPO₄; 4.2 mM NaHCO₃; 5.5 mM glucose) cells were incubated with membrane potential dye (FLIPR Membrane Potential kit BLUE, Molecular Devices) for 45 min at 37 °C. Final used injection volume of compounds and vehicle was 20 µl. The initial volume in the wells was 180 µL (90 µL buffer plus 90 µL dye) and 20 µL of compound was added to the cells resulting in a final volume in the well of 200 µL and a 1:10 dilution of the compound. Therefore, the compounds were prepared at 10x concentrations. Compounds or buffer were injected after a baseline reading for 60 sec and measurements were accomplished at 37 °C using a FlexStation 3 microplate reader (Molecular Devices). After data normalization to the baseline, the buffer-only trace for each corresponding data point was subtracted.

GRK2 and β-arrestin-2 recruitment

GRK2 and β-arrestin-2 recruitment assays were measured by means of BRET detection. The BRET assays previously reported by our group (310) and by others (311) were improved by utilising NanoBRET technology. Flp-In™ HEK 293 cells were initially harvested and transferred into plastic 10cm² dishes (Corning®) in DMEM + 10% FBS at a density of

2,000,000 cells. 24 hours after transferring the cells to dishes, the cells were transfected using linear polyethylenimine (PEI) in a 1:6 ratio of DNA:PEI (μ g). For GRK2 recruitment, 0.25 μ g hD₂L_R-NLuc, 4 μ g GRK2-Venus and 3.5 μ g pcDNA3.1 were transfected. For β -arrestin-2 recruitment, 0.25 μ g hD₂L_R-NLuc, 2 μ g GRK2 (untagged) and 5.5 μ g YFP- β -arrestin-2 were transfected. Approximately 30 hours after transfection the cells were harvested from the dishes and plated into poly-D-lysine coated Greiner white 96-well TC treated plates in DMEM + 10% FBS. Approximately 20 hours after cells were transferred to plates, the plate was washed with HBSS pH 7.4 and replaced with 80 μ L HBSS. The cells were then left to equilibrate for 30 minutes at 37°C before agonist addition. 10 minutes prior to agonist addition, 10 μ L of Nano-Glo Luciferase Assay Substrate (Promega) diluted in HBSS was added to each well with a multi-step pipette (final concentration 1 in 1000). Changes in BRET were then detected 10 minutes after agonist addition in a PHERAstar FS microplate reader (BMG LABTECH) set to 37°C. Individual wells were measured for the luminescence emission signal of NLuc (465-505nm) and Venus/YFP (505-555nm) simultaneously. Data was analysed by taking the counts from the acceptor Venus/YFP (505-555nm) and dividing by the donor NLuc (465-505nm) counts to give a BRET ratio. The BRET ratio is baseline-normalised to vehicle wells as well as 100% defined as the maximal BRET ratio obtained by stimulation with dopamine or quinpirole where indicated.

Data Analysis

ImageJ 1.47v software was used for quantification of protein bands detected on western blots. GraphPad Prism 5 software was used for data analyzation. Densitometry of every protein band was carried out with Image J. We used the same area size to perform densitometry for every protein band from the same experiment for every phosphorylation site as well as the total receptor. Accordingly, an equally sized empty area from the blot/film was measured to subtract this value as background signal from every measuring point. Finally, phosphorylation signals were normalized to the total receptor (phosphorylation-independent antibody; D₂R). SCR-controls were defined as 100% and phosphorylation of every target protein was calculated as percentage phosphorylation in comparison to the respective control. Statistical analysis was carried out with one-way ANOVA followed by Bonferroni correction. P values <0.05 were considered statistically significant.

4.3 Results

The development of novel phospho-site-specific antibodies for the D₂R

We set out to develop G protein-coupled receptor kinase (GRK) phospho-site-specific antibodies for the hD₂R. Previous work identified putative GRK2 phosphorylation sites within the intracellular loops of the D₂R using site-directed mutagenesis coupled with autoradiography(292,294). In particular, Namkung and colleagues identified several GRK2 sites in the rat D_{2L}R (rD_{2L}R) including Thr287, Ser288, Thr293 and Ser317(294). Note that in the human D_{2L}R Ser317 is positioned next to another putative GRK site, Thr318, that is substituted for Asn in rD_{2L}R (Fig. S4.1). Taking this work into consideration, we synthesised phosphopeptides corresponding to regions within ICL3 of the hD₂R (Table 4.1, Fig. 4.1A, Fig. S4.1) and used them to raise phospho-site-specific antibodies for the hD₂R, targeting pThr287/pSer288, pThr293/pSer296 and pSer317/pThr318 (Fig. 4.1A). In addition to raising antibodies to distinct phospho-sites we also raised antibodies to a spatially separate region of ICL3 to serve as a hD₂R loading control antibody (Table 4.1, Fig. 4.1A). All sites are conserved in the long (D_{2L}R) and short (D_{2S}R) isoforms of the D₂R.

When used in western blot experiments, all the antibodies detected the hD₂R, showing a diffuse band at approximately 72 kDa consistent with preceding studies of N-terminally glycosylated D₂Rs(312). While previous work suggested that Thr287, Ser288, and Thr293 are GRK2 phosphorylation sites(294), we were unable to detect significant agonist-induced changes in phosphorylation with the pThr287/pSer288 antibody or the pThr293/pSer296 antibody (Fig. 4.1B). The pThr287/pSer288 and pThr293/pSer296 antibody recognition was phosphorylation dependent because the binding was lost when samples were treated with λ -phosphatase (Fig. 4.1C). This indicates that these sites are likely to be constitutively phosphorylated. The antibody recognising pSer317/pThr318 showed a large increase in binding when cells were stimulated with the D₂R-selective agonist quinpirole, and this agonist-induced phosphorylation was lost when samples were treated with λ -phosphatase (Fig. 4.1B & C), or with the D₂R antagonists haloperidol or L741,626 (Fig. S4.2).

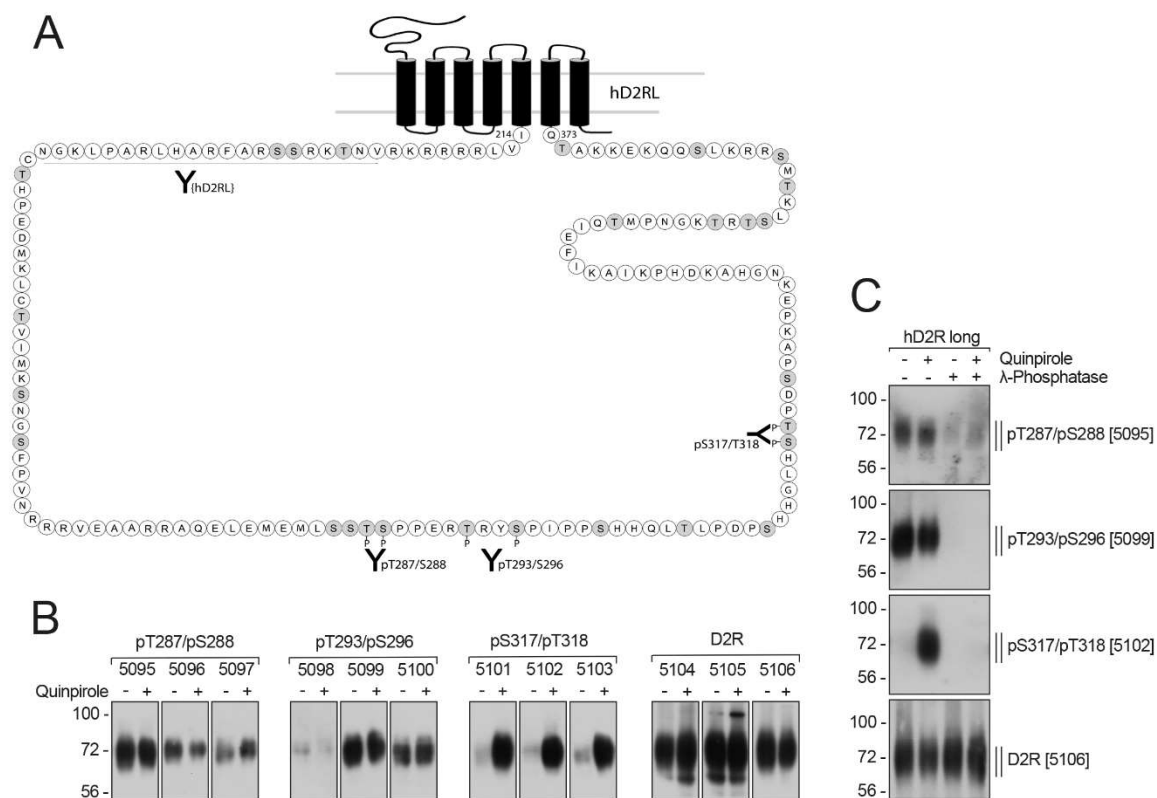


Figure 4.1: Characterisation of phospho-site-specific D₂R antibodies. (A) Schematic representation of the long splice variant of the human dopamine D₂ receptor (hD₂RL). All potential phosphate acceptor sites in the third intracellular loop are indicated (gray). T287/S288, T293/S296 and S317/T318 were targeted for the generation of phospho-site-specific antibodies and the epitope used for generating a phosphorylation-independent antibody (D2RL) is indicated by a black line. (B) HEK293 cells stably expressing HA-tagged D₂R were either untreated (-) or treated (+) with 1 μM quinpirole for 10 min at 37°C. Cells were lysed and immunoblotted with the anti-pT287/288 antibodies (5095-5097), anti-pT293/S296 antibodies (5098-5100) anti-pS317/T318 antibodies (5101-5103) or anti-D₂R antibodies (5104-5106), respectively. Blots are representative, n=3. (C) Characterisation of phospho-site-specific antibodies directed against T287/S288, T293/S296 and S317/T318 using λ-phosphatase. Cells described in (B) were either untreated (-) or treated (+) with 1 μM quinpirole for 10 min at 37°C. Lysates were then either incubated (+) or not (-) with λ-phosphatase and immunoblotted with the phospho-site-specific antibodies to pT287/S288 [5095], pT293/S296 [5099], or pS317/T318 [5102]. Blots were stripped and re-probed with the phosphorylation-independent antibody to D₂R [5106] as a loading control. Blots are representative, n=3. Molecular mass markers (kDa) are indicated, left.

GRKs 2 & 3 phosphorylate Ser317/Thr318 and enhance β-arrestin-2 recruitment

Ser317 has been shown to be phosphorylated by GRK2 in the rD₂R (294). We next wanted to confirm that phosphorylation of Ser317/Thr318 in the hD₂R is also orchestrated by GRK2/3. No phosphorylation of Ser317/Thr318 was detected when cells were stimulated with either phorbol 12-myristate 13-acetate (PMA) or forskolin, that lead to activation of protein

kinase C (PKC) and protein kinase A (PKA) family members, respectively (Fig. 4.2A). Treatment of cells with the ATP-competitive inhibitor of GRK2 and 3, compound 101 (cmpd101) (313), led to a concentration-dependent decrease in quinpirole-induced phosphorylation of Ser317/Thr318 (Fig. 4.2B). We used siRNA to confirm the GRK subtypes involved in phosphorylation of Ser317/Thr318. Transfection of siRNA directed at GRK2 significantly reduced Ser317/Thr318 phosphorylation, as did siRNA directed at GRK3 (Fig. 4.2C). Co-transfection of cells with the siRNAs directed at GRK2 and GRK3 together had a synergistic effect in decreasing the phosphorylation of Ser317/Thr318 further as compared to each siRNA alone (Fig. 4.2C). Moreover, experiments transfecting siRNA directed at the other ubiquitously expressed GRKs; GRK5 and GRK6, had no effect on agonist-induced phosphorylation (Fig. 4.2C and D). Finally, overexpression of GRK2 increased the phosphorylation of Ser317/Thr318 in response to quinpirole (Fig. S4.3). Together these data confirm that GRK2 or 3 activity is required for agonist-induced phosphorylation of Ser317/Thr318.

In the prevalent model of arrestin recruitment to GPCRs, GRK-mediated phosphorylation of intracellular serine and threonine residues drives this process by increasing the affinity of arrestins for the GPCR(24,314). Having shown that GRK2 or 3 mediate agonist-dependent phosphorylation of Ser317/Thr318, we next investigated the role GRK2-mediated phosphorylation plays in β -arrestin-2 recruitment to the D₂R. β -arrestin-2 recruitment assays were performed with or without GRK2 overexpression (Fig. 4.2E & F). Quinpirole-induced β -arrestin-2 recruitment was enhanced upon GRK2 overexpression. Pre-treatment of cells overexpressing GRK2 with compound 101 significantly reduced β -arrestin-2 recruitment (vehicle control $E_{\max} = 100.00 \pm 0.91$, compound 101 $E_{\max} = 28.89 \pm 0.90$, (mean \pm SEM), $P < 0.0001$, Extra sum-of-squares F -test) (vehicle control $pEC_{50} = 7.29 \pm 0.02$, compound 101 $pEC_{50} = 6.89 \pm 0.07$, (mean \pm SEM), $P < 0.0001$, Extra sum-of-squares F -test) (Fig. 4.2E). In cells expressing endogenous levels of GRK2, a more subtle but statistically significant reduction in maximal effect was observed on treatment with compound 101 (vehicle control $E_{\max} = 33.58 \pm 1.33$, compound 101 $E_{\max} = 29.09 \pm 0.98$ (mean \pm SEM), $P = 0.0041$, Extra sum-of-squares F -test) (vehicle control $pEC_{50} = 6.83 \pm 0.08$, compound 101 $pEC_{50} = 6.82 \pm 0.05$, (mean \pm SEM) (Fig. 4.2F). Together these data demonstrate that there are both GRK2/3 phosphorylation -dependent and -independent components of β -arrestin-2 recruitment to the hD₂R.

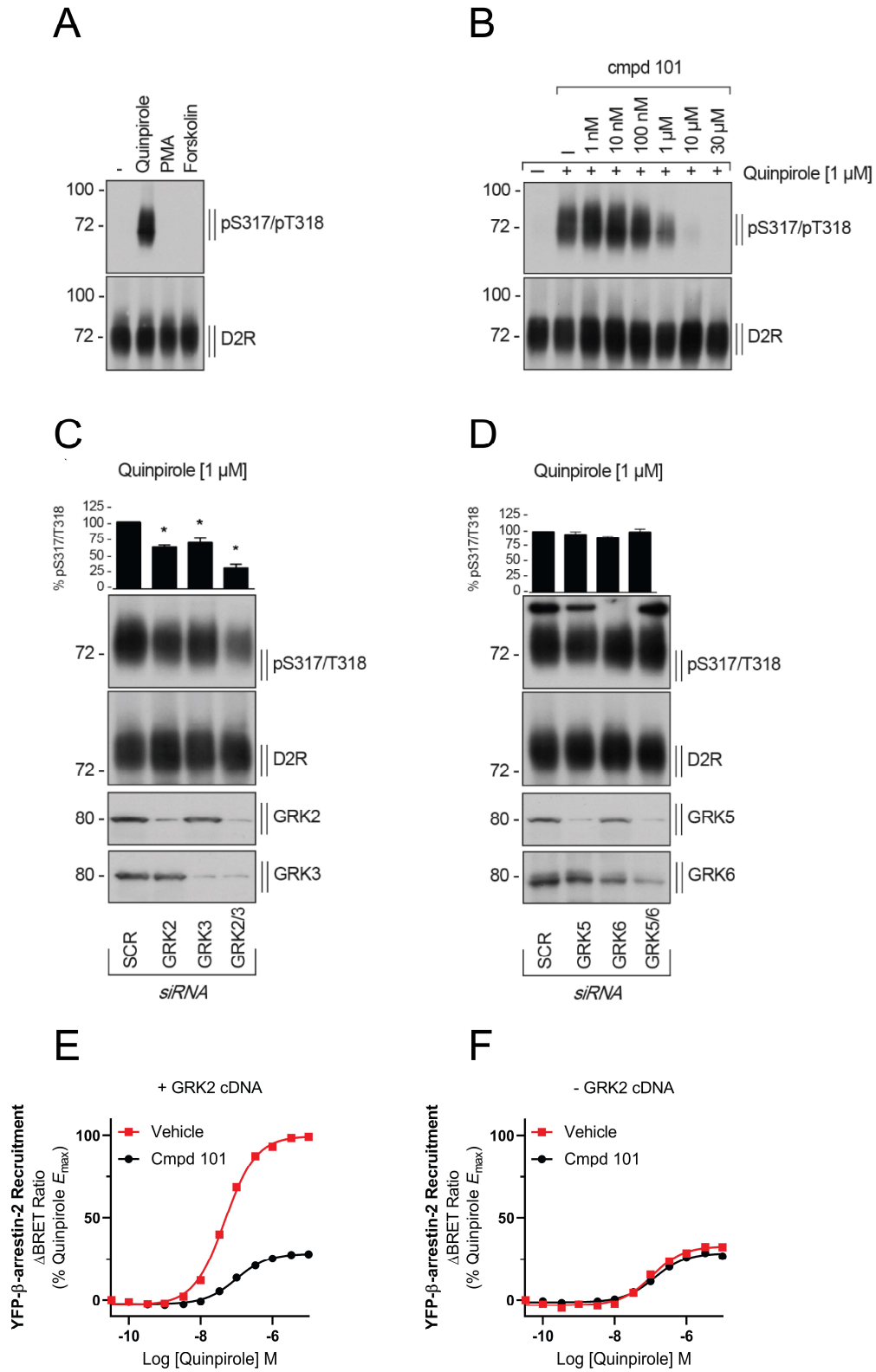


Figure 4.2: GRK2 and GRK3 mediate phosphorylation at Ser317/Thr318 and enhance β -arrestin-2 recruitment. (A) HEK293 cells stably expressing HA-hD₂L_R were stimulated with 1 μ M quinpirole, 1 μ M PMA or 10 μ M forskolin for 10 min at 37 °C. Cell lysates were immunoblotted with anti-pS317/T318 [5102] antibody. Blots were stripped and reprobed for D₂R [5106] to confirm equal loading of the gel. Blots are representative, n=3. (B) Cells described in (A) were pre-incubated with either vehicle (DMSO; control (-)) or the GRK2/3-specific inhibitor compound 101 (cmpd 101) at the indicated concentrations for 30 minutes at 37 °C, then treated with water (-) or 1 μ M quinpirole for 10 min at 37 °C. Lysates were immunoblotted as described in (A). Blots are representative, n=3. (C and D) Cells described in (A) were transfected with siRNAs targeting GRK2, GRK3, or GRK2 and GRK3 (GRK2/3) or a scrambled control (SCR) (C) or with siRNAs targeting GRK5, GRK6 or GRK5 and GRK6 (GRK5/6) or a scrambled control (SCR) (D). 72 hours post-transfection, cells were stimulated with 1 μ M quinpirole for 10 min at 37 °C and cell lysates were immunoblotted as described in (A). Blots were stripped and reprobed for D₂R. Densitometry analysis, shown above the blots, was normalized to the signal obtained in SCR-transfected cells, which was set to 100%. Data are mean \pm SEM from five to six independent experiments. (*p<0.05 vs. SCR by one-way ANOVA with Bonferroni post-test). (E and F) β -arrestin-2 recruitment to the D₂R in the presence and absence of over expressed GRK2. FlpIn™ HEK 293 cells were transfected with cDNA encoding hD₂L_R-Nluc, YFP- β -arrestin-2, and either GRK2 (E) or pcDNA3.1 control (F) as described in the methods section. Transfected cells were then preincubated with either vehicle (DMSO) or 30 μ M cmpd 101 for 30 minutes at 37°C before stimulation with increasing concentrations of quinpirole for 10 minutes before BRET detection at 37°C. Data represents mean \pm SEM from 3-4 separate experiments and are normalised to the maximal effect of quinpirole in the presence of GRK2 overexpression.

Ser317/Thr318 phosphorylation occurs rapidly after D₂R activation

As Ser317/Thr318 is phosphorylated by GRK2/3 (Fig. 4.2), we next monitored GRK2 recruitment to the hD₂R in live cells using BRET. GRK2 was rapidly recruited to the D₂R, within one minute of dopamine addition, and the recruitment remained sustained over time (Fig. 4.3A). We next used the pSer317/pThr318 antibody to monitor the time-course of D₂R phosphorylation at these residues following application of the agonist quinpirole (1 μ M) and observed rapid and sustained phosphorylation over time, with maximal signal obtained within 2.5 minutes (Fig. 4.3B). The kinetic profile of Ser317/Thr318 phosphorylation, then, is rapid and occurs on a timescale similar to that of GRK2 recruitment.

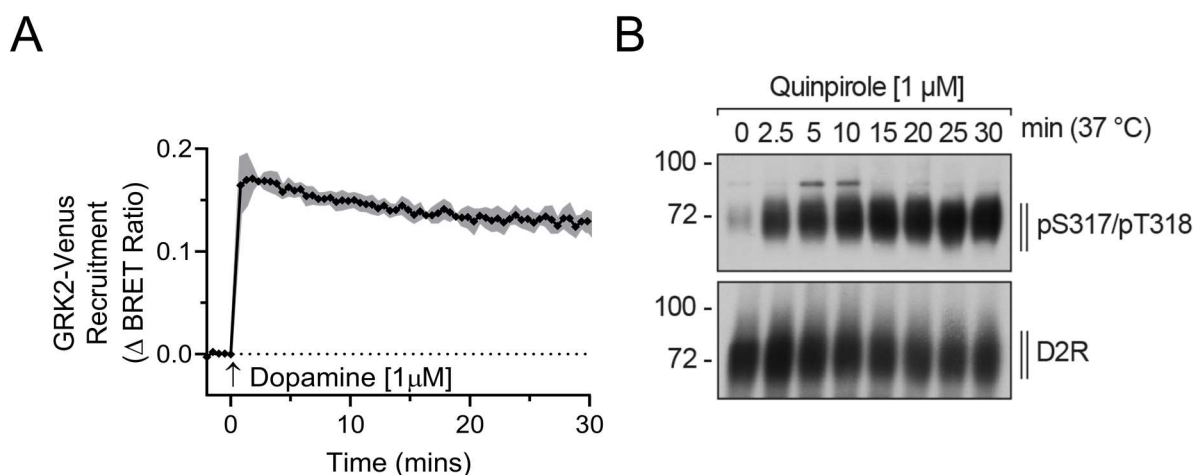


Figure 4.3: Time-course of GRK2 recruitment and Ser317/Thr318 phosphorylation. (A) Agonist-stimulated GRK2 recruitment to the D₂R over time. Flp-In™ HEK 293 cells were transfected with hD₂L-R-NLuc and GRK2-Venus. Dopamine-induced recruitment of GRK2-Venus was measured for 30 minutes at 37°C. The baseline-corrected increase in BRET ratio over time is plotted. Data represents mean ± SD (grey shading) of three separate experiments. **(B)** Agonist stimulated Ser317/Thr318 phosphorylation of the D₂R over time. HEK 293 cells stably expressing HA-hD₂L-R were exposed to 1 μM quinpirole for the indicated times at 37 °C; lysates were immunoblotted with antibody to pSer317/Thr318 [5102]. Blots were stripped and re-probed for D₂R. Blots are representative, n=4.

D₂R agonists vary broadly in their ability to stimulate the recruitment of GRK2, phosphorylation of Ser317/Thr318 and recruitment of β-arrestin-2

Our pSer317/pThr318 antibody is a novel tool with which to measure agonist dependent GRK2/3 mediated phosphorylation of the D₂R and complements our BRET assays to measure GRK2 and β-arrestin-2 recruitment. We next used these tools to measure the ability of 12 structurally distinct D₂R agonists to initiate these processes. This selection included the efficacious agonists pergolide, cabergoline, bromocriptine, ropinirole, apomorphine that are used clinically to treat Parkinson's disease and hyperprolactinaemia. We also included the partial agonists roxindole, terguride and the antipsychotic aripiprazole as well as ligands that have previously been described as G protein (MLS1547) and arrestin (UNC9994) biased agonists(293,303). We have previously shown that the binding kinetics of D₂R agonists can influence comparisons of agonist effect across measurements of different signalling endpoints (310). This effect is driven, to an extent, by measurements of agonist action at different signalling endpoints at distinct timepoints. To negate this effect, the agonist induced regulatory effects were all measured ten minutes after stimulation to allow comparison across all assays. There was a wide range in the maximal response of agonists to induce GRK2 recruitment to

the D₂R (Fig. 4.4A, Table 4.2). Interestingly, DA produced a larger maximal effect than all other agonists tested. We used Schild analysis to determine whether the larger response induced by dopamine was due to action at endogenously expressed dopamine D₁-like receptor subtypes using the selective D₁-type antagonist SCH23390. Increasing concentrations of this antagonist caused a dextral shift of the DA concentration-response curve with no decrease of E_{\max} . Schild analysis of these data gave a Schild slope of approximately unity (1.10 ± 0.04), indicating that SCH23390 inhibits a response mediated by a single receptor type, and an affinity that was consistent with the reported affinity of SCH23390 for the D₂R ($pA_2 = 6.28 \pm 0.06$, Fig. S4.4A and B). Thus, it appears that, with respect to GRK2 recruitment, DA displays superior efficacy to all other tested agonists.

Quinpirole, apomorphine, ropinirole and cabergoline showed robust GRK2 recruitment to 50-60% that of dopamine (Fig. 4.4A & Table 4.2). Bromocriptine and roxindole behaved as less efficacious partial agonists. The antipsychotic and weak partial agonist aripiprazole, stimulated GRK2 recruitment very poorly such that an accurate measurement of maximal effect or potency could be determined. Surprisingly, both the previously reported G protein-biased agonist (MLS1547) and the arrestin biased agonist (UNC9994) induced GRK2 recruitment with similar low potency and efficacy (26.1% and 13.3% of DA, respectively at a concentration of 10 μ M (Fig. 4.4A & Table 4.2). Roxindole and terguride also displayed weak partial agonist efficacy in this assay (E_{\max} 24% and 7% of DA, respectively)

We next determined the level of Ser317/Thr318 phosphorylation induced by the twelve different agonists (Fig. 4.4B, Table 4.2). In general, the ability of the various agonists to stimulate GRK2 recruitment largely predicted their relative ability to induce phosphorylation at Ser317/Thr318 at saturating concentrations. For example, efficacious agonists such as dopamine and quinpirole produced robust phosphorylation whereas roxindole promoted phosphorylation to a lesser degree. To quantify this phosphorylation responses, we performed densitometry analysis in which the intensity of the pSer317/pThr317 bands were normalised to the corresponding intensity of the total D₂R bands. The relative effect of a saturating concentration (10 μ M) of each agonist was then normalised relative to DA. Together these analyses allowed us to plot the concentration-dependent increases in Ser317/Thr318 phosphorylation for each agonist. DA displayed higher intrinsic efficacy relative to all other agonists consistent with the GRK2 recruitment data and while observed potencies were generally lower for Ser317/Thr318 phosphorylation as compared to GRK2 recruitment the order of potencies was consistent (Fig. 4.4A & B, Table 4.2). Importantly, no significant

phosphorylation could be detected after treatment with aripiprazole, MLS1547 or UNC9994 as compared to the control condition (Fig. 4.4B). This is in line with the very low efficacy shown by these ligands in the GRK2 recruitment above.

Next, we evaluated β -arrestin-2 recruitment to the D₂R for the 12 agonists. Of note, β -arrestin-2 recruitment assays were performed in the presence of GRK2 to enable us to observe both the GRK2 phosphorylation dependent and independent components that we previously distinguished (Fig. 4.2E & F). The maximal effects observed for β -arrestin-2 recruitment followed a very similar trend to that observed for GRK2 recruitment and Ser317/Thr318 phosphorylation (Fig. 4.4C, Table 4.2). The more efficacious agonists dopamine, quinpirole and apomorphine produced robust responses whereas partial agonists such as aripiprazole produced weaker responses. DA was more potent in this assay as compared to our measurements of GRK2 recruitment or Ser317/Thr318 phosphorylation and all other agonists followed this trend, indicating. Surprisingly, the arrestin biased agonist UNC9994 displayed only modest β -arrestin-2 recruitment and a reduced maximal effect (23.3 ± 3.3 % DA E_{\max} , Table 4.2) relative to previously reported values in a similar assay (>50 % Quinpirole E_{\max}) (293). We subsequently assessed β -arrestin-2 recruitment in the absence of overexpression of GRK2. In these experiments, however, stimulation with a concentration of up to 10 μ M UNC9994 could not be distinguished from the vehicle control (Fig. S4.7)., In summary, the ability of agonists to stimulate GRK2 recruitment and Ser317/Thr318 phosphorylation predicts their efficacy to drive β -arrestin-2 recruitment, in agreement with the canonical model of GPCR regulation. The pSer317/pThr318 antibody is, therefore, a useful tool with which to measure the action of D₂R agonists to activate these regulatory events.

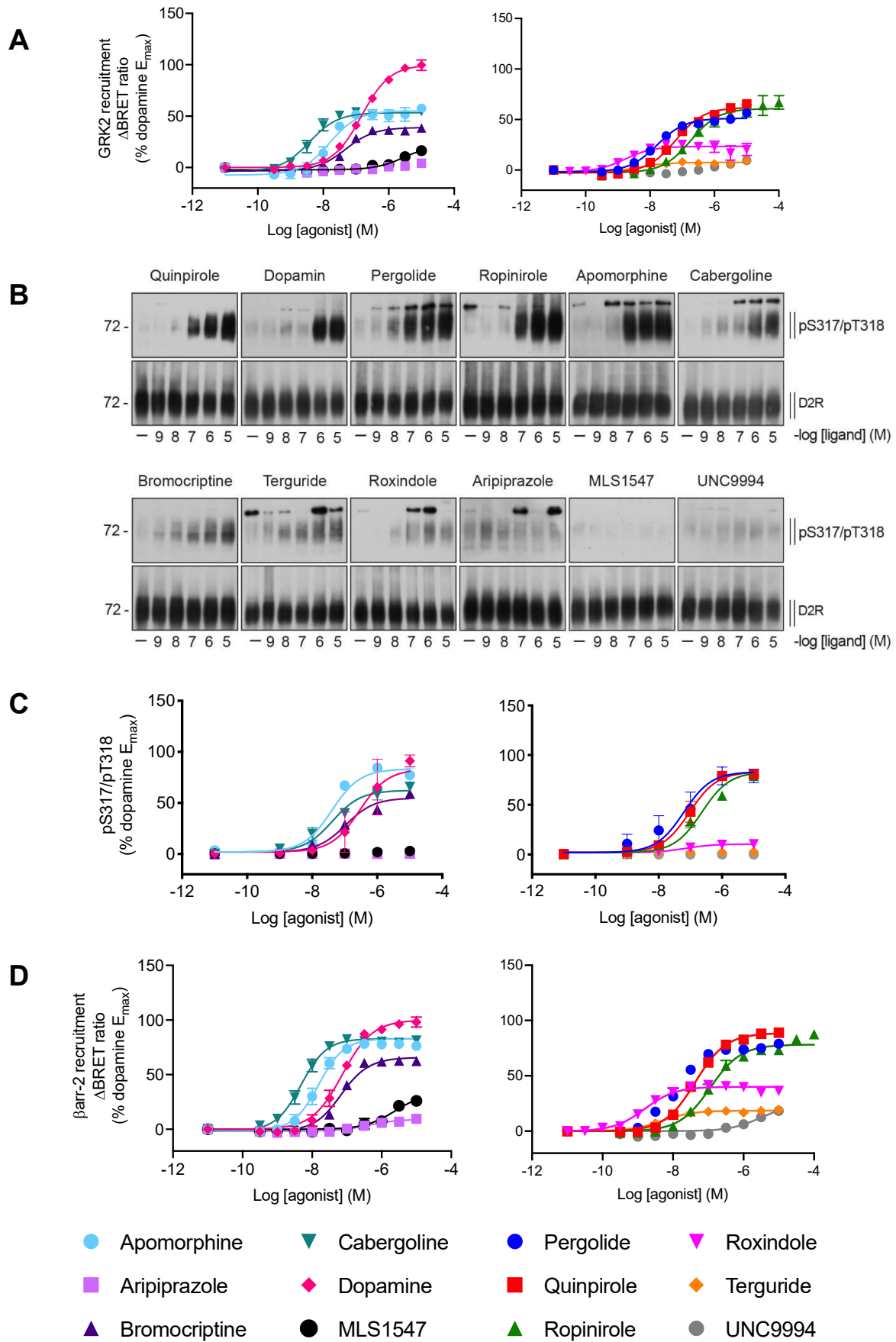


Figure 4.4: Agonist-induced GRK2 recruitment, Ser317/Thr318 phosphorylation and β -arrestin-2 recruitment. (A) Agonist-induced GRK2 recruitment to the D₂R. FlpIn™ HEK 293 cells were transfected GRK2-Venus and hD₂L-R-Nluc. GRK2 recruitment was measured by BRET 10 minutes after agonist addition at 37°C. Data is presented as the increase in BRET ratio normalised to vehicle (0%) and the maximal effect of dopamine (100%). Data represents the mean \pm SEM of 3-6 separate experiments performed in duplicate. (B) HA-hD₂R expressing HEK293 cells were either stimulated with vehicle (solvent) or quinpirole, dopamine, pergolide, ropinirole, apomorphine, cabergoline, bromocriptine, terguride, roxindole, aripiprazole, MLS1547 or UNC9994 at concentrations ranging from 10⁻⁹ to 10⁻⁵ M for 10 min at 37 °C. Lysates were immunoblotted with antibody to pS317/T318 [5102]. Blots were stripped and reprobed for D2R. Blots are representative, n=3-4. (C) Densitometry analysis of Western blots. pS317/pT318 signals were normalised to the total D₂R signal and expressed as a percentage of the signal detected when cells were stimulated with 10 μ M dopamine. These data are presented as concentration response curves. (D) Agonist-induced β -arrestin-2 recruitment to the D₂R. FlpIn™ HEK 293 cells were transfected with hD₂L-R-Nluc, GRK2 and YFP- β -arrestin-2. β -arrestin-2 recruitment was measured by BRET 10 minutes after agonist addition at 37°C. Data is presented as the increase in BRET ratio normalised to vehicle (0%) and the maximal effect of dopamine (100%). Data represents the mean \pm SEM of 3-6 separate experiments performed in duplicate.

Table 4.2: Potency and maximal effect estimates for agonists activating different D₂R pathways.

Responses were analysed using a three-parameter fit. Values represent the mean \pm SEM.

Agonist	pSer317/pThr318		GRK2		β -arr-2	
	pEC ₅₀	E _{max}	pEC ₅₀	E _{max}	pEC ₅₀	E _{max}
Dopamine	6.40 \pm 0.45	100 \pm 7	6.84 \pm 0.04	100.0 \pm 2.1	7.13 \pm 0.05	100.0 \pm 2.3
Apomorphine	7.42 \pm 0.10	84 \pm 3	7.68 \pm 0.09	56.2 \pm 2.1	7.85 \pm 0.05	81.2 \pm 1.7
Aripiprazole	ND	ND	ND	ND	6.23 \pm 0.25	10.3 \pm 1.5
Bromocriptine	6.84 \pm 0.25	57 \pm 2	7.18 \pm 0.06	38.7 \pm 1.1	7.10 \pm 0.05	66.3 \pm 1.3
Cabergoline	7.38 \pm 0.25	61 \pm 2	8.36 \pm 0.07	54.4 \pm 1.4	8.29 \pm 0.04	83.7 \pm 1.2
MLS1547	ND	ND	5.20 \pm 0.27	26.1 \pm 7.8	5.59 \pm 0.13	33.6 \pm 3.8
Pergolide	7.73 \pm 0.46	79 \pm 2	7.67 \pm 0.06	50.8 \pm 1.2	7.83 \pm 0.04	76.7 \pm 1.3
Quinpirole	7.06 \pm 0.17	83 \pm 0.6	7.13 \pm 0.04	62.9 \pm 1.2	7.38 \pm 0.03	88.6 \pm 1.2
Ropinirole	6.77 \pm 0.22	77 \pm 2	6.72 \pm 0.07	59.1 \pm 2.0	6.99 \pm 0.04	76.8 \pm 1.4
Roxindole	7.52 \pm 0.09	10 \pm 0.6	8.73 \pm 0.15	24.3 \pm 1.3	8.83 \pm 0.07	41.0 \pm 1.0
Terguride	ND	ND	8.10 \pm 0.24	7.4 \pm 0.7	8.33 \pm 0.09	18.9 \pm 0.6
UNC9994	ND	ND	5.45 \pm 0.31	13.3 \pm 3.8	5.63 \pm 0.18	23.0 \pm 3.3

ND – Not determined: unable to be determined due to insufficient response to allow accurate fitting of the model.

A putative arrestin-biased agonist displays robust activity in measurements of G protein signalling

Two agonists previously described as arrestin and G protein-biased agonists both acted as low efficacy partial agonists at these regulatory endpoints. It was important, then, to extend our analysis to test the ability of these agonists to activate G protein-mediated pathways. We measured G α_{i1} and G α_{oA} G protein activation using BRET sensors that monitor the dissociation

of the G $\beta\gamma$ subunit from the G α subunit (308,315). All agonists induced robust activation of G α_{i1} (Fig. 4.5A & Table 4.3). Aripiprazole, roxindole and terguride acted as partial agonists for G α_{i1} activation whereas most of the other agonists showed maximal responses equivalent to that of dopamine. Surprisingly, UNC9994, the arrestin biased agonist, displayed robust partial agonism in this assay (81.6% dopamine response) with a similar low potency to that observed in the β -arrestin-2 recruitment assay (Fig. 4.5A & Table 4.3). The D₂R is preferentially coupled to G α_o G proteins (316). Accordingly, in the G α_{oA} activation assay, all agonists displayed a similar maximal response to dopamine and an increase in potency relative to that observed when G α_{i1} activation was measured (Fig. 4.5B & Table 4.3).

Finally, we measured activation of G protein inwardly rectifying potassium (GIRK) channels as a readout of the activation of G $\alpha_{i/o}$ G proteins using a membrane potential sensitive dye (309)(Fig. S4.5). In this case all agonists displayed the same maximal response as dopamine with the exception of terguride which acted as a partial agonist. In addition, while the relative order of potencies for the various agonists was consistent with that obtained in the G protein activation assays, aripiprazole, MLS1547 and UNC9994 displayed low potencies in this assay such that the maximal response was not obtained at the highest (1 μ M) concentration used for each agonist (Fig. 4.5C & Table 4.2).

Overall, all agonists displayed a similar relative trend in their responses in each of the three G protein-dependent signalling measurements. In addition, our observations were largely consistent with previous reports of agonist action, for example apomorphine is known to be a potent and efficacious agonist (317) and induced robust responses in all three G protein signalling endpoints and in measurements of receptor regulatory events. In contrast, aripiprazole is known to be a low efficacy agonist and behaved as such in all assays with the exception of the highly amplified G α_{oA} activation assay (318,319). Interestingly, UNC9994, that was previously reported to be an arrestin biased agonist unable to activate G protein responses or antagonise G protein signalling stimulated by dopamine (293,320), acted as a weak partial agonist in measurements of both G protein activation and receptor regulation. Furthermore, we found that pre-treatment of cells with UNC9994 antagonised GIRK channel activation or pSer317/Thr318 down to a level consistent with its maximal effect in each assay (Fig. S4.6) These observations are in agreement with a previous study that characterised UNC9994 measuring GIRK channel activation in frog oocytes expressing the hD₂R(321).

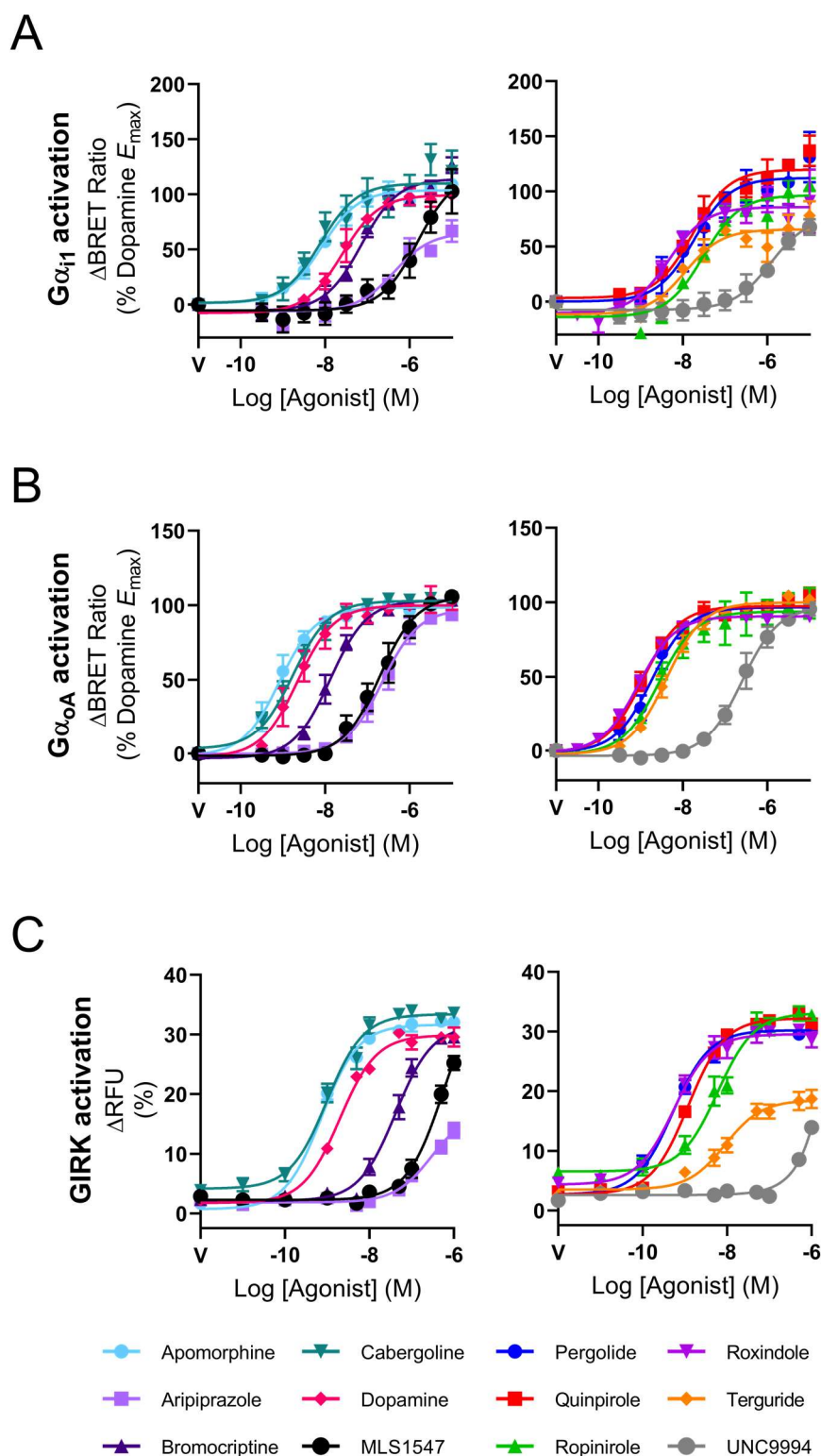


Figure 4.5. D₂R mediated activation of Gα_{i1}, Gα_{oA} and GIRK channels by distinct agonists. FlpIn™ HEK 293 cells stably expressing hD_{2L}R were transfected with BRET sensors for (A) Gα_{i1} activation and for (B) Gα_{oA} activation as described in methods. Agonist responses were determined after 10 minutes at 37°C. The response is plotted as the increase in BRET ratio normalised to the vehicle control (0%) and the maximal response produced by dopamine defined as 100%. The data in (A) and (B) represent the mean ± SEM for 3-6 separate experiments performed in duplicate. (C) GIRK channel activation using a membrane potential kit. Data represents mean ± SEM performed in duplicate.

Table 4.3: Potency and maximal effect estimates for agonists activating different D₂R pathways.Responses were analysed using a three-parameter fit. Values represent the mean \pm SEM.

Agonist	G α_{i1}		G α_{oA}		GIRK	
	pEC ₅₀	E _{max}	pEC ₅₀	E _{max}	pEC ₅₀	E _{max}
Dopamine	7.50 \pm 0.09	100.0 \pm 3.5	8.63 \pm 0.08	100.0 \pm 2.6	8.70 \pm 0.06	100.0 \pm 2.5
Apomorphine	8.10 \pm 0.07	103.6 \pm 2.5	9.07 \pm 0.06	98.6 \pm 1.9	9.13 \pm 0.08	110.0 \pm 3.5
Aripiprazole	6.21 \pm 0.17	67.5 \pm 6.9	6.64 \pm 0.08	97.6 \pm 3.8	6.53 \pm 0.11	54.6 \pm 4.5
Bromocriptine	7.07 \pm 0.08	115.0 \pm 4.1	7.84 \pm 0.05	103.7 \pm 2.0	7.38 \pm 0.08	104.7 \pm 4.3
Cabergoline	8.13 \pm 0.16	109.8 \pm 6.5	8.80 \pm 0.05	102.7 \pm 1.7	9.01 \pm 0.08	104.0 \pm 3.4
MLS1547	5.71 \pm 0.20	123.9 \pm 19.5	6.68 \pm 0.08	106.5 \pm 4.4	6.25 \pm 0.08	129.3 \pm 15.4
Pergolide	7.73 \pm 0.17	112.3 \pm 7.3	8.73 \pm 0.07	96.7 \pm 2.3	9.28 \pm 0.07	97.9 \pm 2.7
Quinpirole	7.81 \pm 0.10	119.3 \pm 4.6	8.93 \pm 0.05	97.4 \pm 1.5	8.98 \pm 0.05	104.9 \pm 2.1
Ropinirole	7.33 \pm 0.13	98.01 \pm 5.2	8.55 \pm 0.13	93.9 \pm 3.7	8.23 \pm 0.07	94.4 \pm 3.4
Roxindole	8.19 \pm 0.12	86.6 \pm 4.2	9.04 \pm 0.04	90.7 \pm 1.1	9.26 \pm 0.06	89.7 \pm 2.2
Terguride	7.76 \pm 0.18	66.2 \pm 4.6	8.36 \pm 0.05	100.1 \pm 1.6	8.05 \pm 0.08	53.3 \pm 2.1
UNC9994	5.74 \pm 0.21	81.6 \pm 13.4	6.55 \pm 0.08	98.0 \pm 4.1	ND	ND

ND – Not determined: unable to be determined due to insufficient response to allow accurate fitting of the model.

Analysis of signalling data using an operational model of agonism allows quantitative evaluation of bias between G protein and regulatory events

In general, our data suggests that the actions of the various agonists appeared, relative to each other, consistent across the various G protein-mediated and regulatory pathways. However, such qualitative comparisons of agonist action across different pathways can be confounded by system bias resulting from, for example, the relative efficiency with which each pathway is coupled to the receptor. Accordingly, we employed a more quantitative approach to determine the relative action of each agonist at each pathway by fitting our concentration response data to an operational model of agonism (322). Using this model, we can determine a transduction coefficient (τ/K_A) that is a composite of the affinity of the agonist for the receptor-effector complex (K_A) and the efficacy with which the agonist acts at that effector (τ) (Table 4.2). We then subtracted the values obtained for each agonist with the values obtained by dopamine to compare the relative transduction coefficients of agonists between pathways ($\Delta\log[\tau/K_A]$), Fig. 4.6 & Table 4.4). The transduction coefficients of apomorphine, aripiprazole, quinpirole, MLS1547, pergolide and ropinirole were not significantly different across the different signalling and regulatory endpoints, noting that the operational model could not be fitted to data describing the action of MLS1547 to stimulate GRK2 recruitment or pSer317/pThr318 likely due to the inefficient coupling of these pathways and the low affinity

and efficacy of this compound. No significant difference was seen across all regulatory endpoints measured for any of the compounds, illustrating that measurement of one of these steps (GRK2 recruitment, pSer317/pThr318 or β -arrestin-2 recruitment) is likely to predict relative agonist action at the others. Moreover, for all agonists, there was no significant difference between the normalised transduction coefficient obtained in the $G\alpha_{i1}$ activation assay and any of the regulatory pathways. However, we did observe differences between the $G\alpha_{oA}$ activation or GIRK activation and the regulatory events for the agonists bromocriptine (GRK2 recruitment, pSer317/pThr318 and β -arrestin-2 recruitment), carbergoline (GRK2 and β -arrestin-2 recruitment), terguride (GRK2 and β -arrestin-2 recruitment) and pergolide (pSer317/Thr318 and β -arrestin-2 recruitment versus $G\alpha_{oA}$ activation, Fig. 4.6, Table 4.4). In all cases, relative to the action of dopamine, these agonists were more efficient at activating the regulatory pathways (Fig. 4.6). While most of these differences were subtle (< 5-fold), bromocriptine displayed a 13-fold and 8-fold preference for GRK2 and β -arrestin-2 recruitment over GIRK activation, respectively. Of particular note, however, is that two agonists previously described as arrestin biased (UNC9994) and G protein biased (MLS1547) did not display these profiles in our hands. UNC9994 acts as a low efficacy partial agonist at all pathways, displaying robust agonist action at more efficiently coupled pathways such as $G\alpha_{oA}$ activation but barely detectable action at less efficiently coupled endpoints such as pSer317/pThr318 or β -arrestin-2 recruitment. MLS1547 was able to stimulate both G protein activation and β -arrestin-2 recruitment. Our analysis revealed that this ligand does not display bias between these two endpoints.

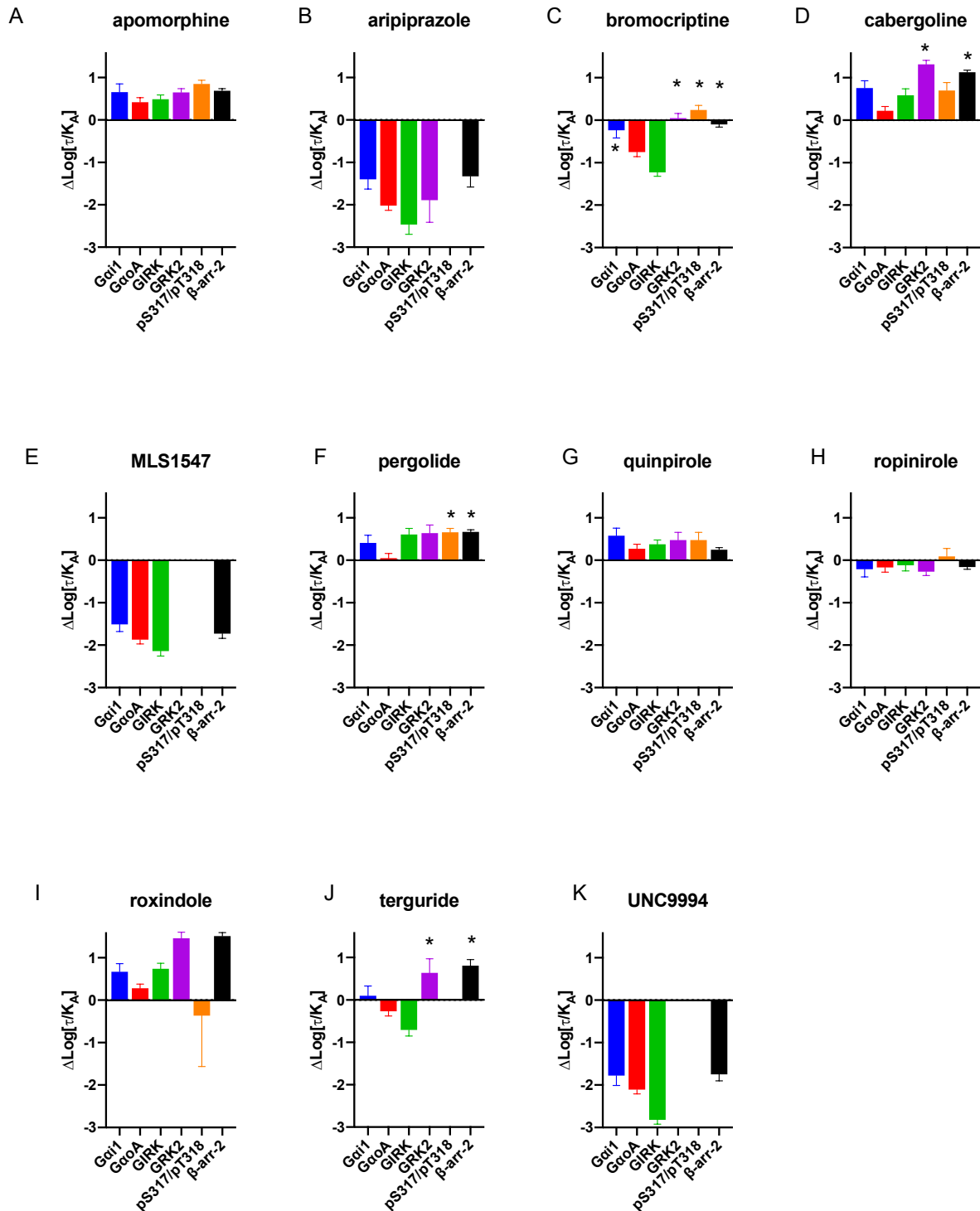


Figure 4.6: Relative transduction coefficients ($\Delta\text{Log}(\tau/K_A)$) for agonists to activate D₂R pathways. Concentration response curves for each endpoint were fit to an operational model of agonism to determine ($\text{Log}(\tau/K_A)$), this was normalised relative to dopamine to determine the relative transduction coefficient ($\Delta\text{Log}(\tau/K_A)$, Table 4.4). Analysis of these data using a one-way ANOVA with Dunnet's post hoc test revealed significant differences between the relative transduction coefficient, normalised to that of dopamine, determined for each agonist in the G α_o assay as compared to that obtained in the other signalling and regulatory endpoints (* = $P < 0.05$, data presented represents the mean \pm SEM of at least 4 independent experiments).

Table 4.4: Estimates of transduction coefficients and relative transduction coefficients for agonists activating D₂R signalling pathways.

Responses were determined and analysed using an operational model of agonism. Values represent the mean \pm SEM.

Agonist	Log (τ/K_A)						Δ Log (τ/K_A)					
	G α_{i1}	G α_{oA}	GIRK	GRK2	pS317/pT318	β -arr-2	G α_{i1}	G α_{oA}	GIRK	GRK2	pS317/pTr18	β -arr-2
Dopamine	7.42 \pm 0.14	8.68 \pm 0.09	8.57 \pm 0.06	6.90 \pm 0.05	6.55 \pm 0.18	7.19 \pm 0.03	0.00 \pm 0.20	0.00 \pm 0.12	0.00 \pm 0.09	0.00 \pm 0.07	0.00 \pm 0.07	0.00 \pm 0.05
Apomorphine	8.08 \pm 0.12	9.09 \pm 0.07	9.06 \pm 0.07	7.55 \pm 0.07	7.38 \pm 0.18	7.87 \pm 0.04	0.66 \pm 0.19	0.42 \pm 0.11	0.49 \pm 0.10	0.65 \pm 0.09	0.85 \pm 0.09	0.69 \pm 0.05
Aripiprazole	6.02 \pm 0.19	6.66 \pm 0.06	6.10 \pm 0.22	5.01 \pm 0.52	ND	5.86 \pm 0.25	-1.40 \pm 0.23	-2.02 \pm 0.11	-2.47 \pm 0.23	ND	ND	-1.33 \pm 0.25
Bromocriptine	7.18 \pm 0.11	7.93 \pm 0.06	7.35 \pm 0.06	6.94 \pm 0.10	6.79 \pm 0.17	7.09 \pm 0.05	-0.24 \pm 0.18	-0.75 \pm 0.11	-1.23 \pm 0.09	0.05 \pm 0.11	0.24 \pm 0.11	-0.10 \pm 0.06
Cabergoline	8.18 \pm 0.10	8.89 \pm 0.06	9.16 \pm 0.14	8.22 \pm 0.07	7.25 \pm 0.17	8.31 \pm 0.03	0.76 \pm 0.17	0.22 \pm 0.10	0.59 \pm 0.15	1.32 \pm 0.09	0.70 \pm 0.19	1.13 \pm 0.05
MLS1547	5.91 \pm 0.10	6.81 \pm 0.06	6.43 \pm 0.11	ND	ND	5.46 \pm 0.11	-1.51 \pm 0.17	-1.87 \pm 0.10	-2.14 \pm 0.12	ND	ND	-1.73 \pm 0.11
Pergolide	7.83 \pm 0.11	8.73 \pm 0.06	9.18 \pm 0.12	7.53 \pm 0.08	7.21 \pm 0.13	7.85 \pm 0.04	0.41 \pm 0.18	0.05 \pm 0.11	0.61 \pm 0.14	0.64 \pm 0.19	0.66 \pm 0.09	0.67 \pm 0.05
Quinpirole	8.00 \pm 0.11	8.94 \pm 0.06	8.95 \pm 0.07	7.06 \pm 0.07	7.02 \pm 0.11	7.44 \pm 0.03	0.58 \pm 0.18	0.27 \pm 0.11	0.38 \pm 0.10	0.48 \pm 0.18	0.48 \pm 0.18	0.25 \pm 0.05
Ropinirole	7.21 \pm 0.11	8.50 \pm 0.07	8.45 \pm 0.11	6.63 \pm 0.07	6.63 \pm 0.14	7.03 \pm 0.04	-0.21 \pm 0.18	-0.17 \pm 0.11	-0.12 \pm 0.13	-0.27 \pm 0.09	0.09 \pm 0.19	-0.16 \pm 0.05
Roxindole	8.08 \pm 0.13	8.95 \pm 0.06	9.31 \pm 0.11	8.36 \pm 0.13	6.17 \pm 1.16	8.69 \pm 0.07	0.67 \pm 0.19	0.28 \pm 0.10	0.74 \pm 0.13	1.46 \pm 0.14	-0.37 \pm 1.2	1.51 \pm 0.08
Terguride	7.52 \pm 0.18	8.40 \pm 0.06	7.87 \pm 0.12	7.54 \pm 0.32	ND	7.99 \pm 0.14	0.10 \pm 0.23	-0.27 \pm 0.11	-0.71 \pm 0.14	0.64 \pm 0.33	ND	0.81 \pm 0.14
UNC9994	5.64 \pm 0.18	6.57 \pm 0.06	5.75 \pm 0.08	ND	ND	5.44 \pm 0.15	-1.78 \pm 0.23	-2.11 \pm 0.10	-2.82 \pm 0.10	ND	ND	-1.75 \pm 0.15

ND – Not determined: unable to be determined due to insufficient response to allow accurate fitting of the model.

4.4 Discussion

GPCR phosphorylation by GRKs is a key process for the regulation of most GPCRs by promoting arrestin binding and, thus, inhibition of G protein mediated signalling. Arrestin mediated signalling has been shown to mediate distinct physiological processes downstream of the D₂R and arrestin-biased agonists have been proposed as an avenue for the development of more efficacious antipsychotic drugs (300). Antibodies raised against GPCR phosphorylation sites have been useful tools with which to understand the hierarchical and sequential pattern of multisite phosphorylation upon agonist stimulation (323,324). In this study we developed and characterised phospho-site-specific antibodies for the D₂R against predicted phosphorylation sites within ICL3 and used them to provide an insight into the role GRK phosphorylation plays in D₂R regulatory processes and how it is controlled by chemically distinct agonists including those thought to have pathway-biased actions. One of these antibodies revealed an increase in Ser317 and Thr318 phosphorylation upon agonist activation mediated by GRK2/3. Comparison of these data with measurements of GRK2 and arrestin recruitment revealed that the relative efficacy of all tested agonists at the level pSer317/pThr318 can predict their efficacy at these other regulatory processes. A challenge associated with measuring these regulatory processes is that such measurements often entail the overexpression of one or more regulatory proteins that are modified with a fluorescent tag such as those used in BRET assays. This may alter the stoichiometry of the different protein components associated with downstream signalling and may be particularly problematic if one wants to compare agonist action across different signalling pathways as is often done in studies aimed at identifying biased agonists. In this regard, the measurement of Ser317/Thr318 phosphorylation can be used in both heterologous expression systems and native tissue without the need for the over-expression of modified proteins. Importantly, the antibodies described in the present study recognise phospho-sites present in both D_{2S}R and D_{2L}R. This is particularly relevant when considering future studies that use these antibodies in tissues or primary neuronal cultures as it will allow the detection of phosphorylation of both, pre- and post-synaptic receptors.

Two other antibodies developed in this study recognised two additional sites, pThr287/pSer288 and pThr293/pSer296, that appear to be constitutively phosphorylated. The role of this constitutive phosphorylation is unclear. Interestingly, GRK2/3 phosphorylation has

been shown to play a role in post-endocytic trafficking and re-sensitisation (291,294,325) and Thr287, Ser288, and Thr293 have been identified as GRK2 phosphorylation sites important for post-endocytic trafficking (294). Interestingly, while Ser317 is conserved in humans and rodents, Thr318 is absent in both mice (*Mus musculus*) and rats (*Rattus norvegicus*) suggesting there may be species differences in the patterns of GRK phosphorylation. Moreover, other kinases have been shown to regulate D₂Rs (326,327), for example PKC has been demonstrated to phosphorylate the D₂R and regulate function through heterologous desensitisation (327,328). An antibody that recognizes a PKC phospho-site in ILC3 of the D₂R has previously been described that, surprisingly, shows differences in phosphorylation between D_{2s}R and D_{2L}R (329). It should be noted that we observed significant arrestin recruitment in the presence of a GRK2/3 inhibitor, meaning that this process can occur independently of Ser317/Thr318 phosphorylation. Future efforts to develop phospho-antibodies targeting other GRK and PKC sites, in combination with receptor mutants in which such phosphorylation sites are removed, will allow us to understand better the broader temporal pattern of D₂R phosphorylation and how it might modulate D₂R signalling.

Recent interest in understanding GPCR regulatory processes such as arrestin recruitment has been driven, to some extent, by the appreciation that arrestin-mediated signalling may drive distinct physiological processes to those mediated by G protein signalling and that one may be able to selectively modulate these processes using biased agonists. GRK phosphorylation has been proposed to be the key event that controls the balance between G protein- and arrestin-mediated signalling. It is suggested that the unique phosphorylation pattern, or barcode, that can then lead to distinct downstream signalling through a mechanism that involves altered β -arrestin recruitment and/or stabilisation of distinct β -arrestin conformations (330). There has been a surge of interest in D₂R biased agonists over the last decade driven by their potential as novel, safer, treatments for schizophrenia and Parkinson's disease (293,331-337). In this study we tested a range of agonists and compared their relative ability to stimulate Ser317/Thr318 phosphorylation to other measures of D₂R activation including measurements of G protein signalling and arrestin recruitment. We included two ligands that have been described as biased agonists, the G protein-biased agonist MLS1547 (331) and the arrestin-biased agonist UNC9994 (293). In addition, the atypical antipsychotic aripiprazole was initially described as a D₂R partial agonist, but subsequent studies suggested it may act as a biased agonist (338,339). Initial reports using MLS1547 suggested that it is a G protein biased agonist that acts as an agonist to activate G protein pathways but antagonises the arrestin pathway (331). In our hands, stimulation with MLS1547 results in recruitment of

β -arrestin-2 as well as GRK2 recruitment and our analysis revealed no bias between G protein activation and β -arrestin-2 recruitment. In agreement with this finding, MLS1547 has previously been shown to induce recruitment of β -arrestin-2 (340), and produce some internalisation in striatal neurons (341), a process that is usually mediated through arrestins. UNC9994 was initially described as an arrestin biased agonist, acting as a robust partial agonist for β -arrestin-2 recruitment but with no apparent activity at G protein signalling pathways (293,342). In this present study, however, we found that even in the presence of over-expressed GRK2 UNC9994 promoted modest recruitment of β -arrestin-2 with both lower maximal effect and potency than that reported in its initial characterisation (293). Consistent with this observation, UNC9994 showed no detectable phosphorylation of Ser317/Thr318 and induced only very weak GRK2 recruitment. Furthermore, in the absence of GRK2 overexpression UNC9994 did not stimulate β -arrestin-2 recruitment. Together these data suggest that UNC9994 has low efficacy for GRK2 phosphorylation, GRK2 recruitment and β -arrestin-2 recruitment. Surprisingly, we found that UNC9994 also acted as a weak partial agonist in G protein activation BRET assays as well as in an assay measuring G protein mediated GIRK channel activation. These observations match previous work by Ågren and co-workers in experiments measuring GIRK channel opening in frog oocytes (321). Analysis of our data to derive bias factors revealed that UNC9994 does not display bias between G protein and arrestin pathways relative to dopamine. Together these data are difficult to reconcile with the initial characterisation of UNC9994 as an arrestin biased agonist. Finally, we also found that aripiprazole did not display bias between G protein signalling and any of the regulatory processes such as arrestin recruitment. In original studies that identified MLS1547 and UNC9994 as biased agonists (293,331), no agonism was detected in the ‘unfavoured’ pathway and, thus, no quantitative measurement of bias could be made whereas in our studies we observed sufficient efficacy in all pathways to enable the quantification of their effect. The difference between these observations likely stems from differences in the sensitivity of the assays used to detect the different endpoints. These results, therefore, are not necessarily contradictory but instead illustrate how experimental conditions and cellular context can influence measurements of agonist action, particularly for very low efficacy partial agonists. Our study illustrates how the measurement of the action of putative biased agonists at multiple steps of a signalling pathway may provide further insight into their mechanism of action, particularly if the different endpoints are associated with different levels of amplification. Measuring this process by using phosphorylation-site specific antibodies, will likely be an effective approach to identify and characterise such ligands.

Beyond their potential therapeutic value, biased agonists that display a preference for one pathway over another can be extremely useful tools with which to interrogate the role of distinct downstream signals in a particular physiological process. In this regard, the utility of such biased agonists as tools is entirely dependent on the robustness of the pathway bias that they display. MLS1547 and UNC9994 have both been used to interrogate the contribution of arrestins and G proteins to D₂R mediated physiological effects (185,293,300,342,343). The interpretation of the above studies that used these drugs as tool compounds should now be revisited considering our data that shows that neither UNC9994 or MLS1547 are biased agonists.

The ability of all ligands to stimulate G α_{i1} activation predicted their effect in the three regulatory endpoints. This observation agrees with β -arrestin recruitment being somewhat dependent on G protein activation through release of G $\beta\gamma$ that binds the pleckstrin homology domain of GRK2/3 recruiting it to the plasma membrane, leading to receptor phosphorylation and β -arrestin recruitment (344-346). G α_o , however, has been proposed to be the primary G protein that the D₂R is coupled to *in vivo*(347). While the relative action of the agonists dopamine, apomorphine, aripiprazole, quinpirole, ropinirole and roxindole, as well as the biased agonists UNC9994 and MLS1547 are consistent between G α_o activation and the regulatory endpoints, this is not the case for bromocriptine, cabergoline, terguride and pergolide. These agonists display a preference for the regulatory pathways as compared to G α_o activation. These agonists are used clinically to treat hyperprolactinaemia and/or Parkinson's disease and, intriguingly, all have an ergoline scaffold. It is not apparent how this bias profile might influence their therapeutic effect, but this observation certainly warrants further investigation.

In summary, we have developed the first antibodies specific for GRK phosphorylation sites on the D₂R. We identify one phosphorylation site (pS317/pT318) within ICL3 that is phosphorylated on agonist activation of the D₂R. The action of agonists to phosphorylate this site predicts their relative action at arrestin recruitment suggesting that phosphorylation of this site is important for arrestin binding to the D₂R. We incorporate measurements of pS317/pT318 with other measurements of G protein activation and receptor regulation to profile a number of D₂R agonists including putative biased agonists. Our findings, in the light of the interest in G protein independent signalling, show the utility of measurements of receptor phosphorylation as part of such characterisations.

Acknowledgements

We thank Stephanie Lange, Ulrike Schiemenz and Heike Stadler for excellent technical assistance.

Funding

This work was supported by the Deutsche Forschungsgemeinschaft grants SFB/TR166-TPC5 and SCHU924/18-1 to S.S and National Health and Medical Research Council (NHMRC) Project Grant APP1049564 to J.R.L.

Author contributions

AM, SS, ACK, JRL designed experiments. AM, HM, PD, ACK acquired the data. AM, HM, PD, ACK, JRL analysed the data. AM, ACK, JRL wrote the manuscript. SS, JRL, JAJ, MC reviewed and edited the draft.

Conflict of Interest

The authors declare that they have no conflict of interest.

4.5 Supplementary Materials

	214 (HUMAN)				263
DRD2_HUMAN	IVLRRRRKRV	NTKRSSRAFR	AHLRAPLKGN	CTHPEDMKLC	TVIMKSNGSF
DRD2_PANTR	IVLRRRRKRV	NTKRSSRAFR	AHLRAPLKGN	CTHPEDMKLC	TVIMKSNGSF
DRD2_BOVIN	IVLRRRRKRV	NTKRSSRAFR	ANLKAPLKGN	CTHPEDMKLC	TVIMKSNGSF
DRD2_RAT	IVLRKRRKRV	NTKRSSRAFR	ANLKTPLKGN	CTHPEDMKLC	TVIMKSNGSF
DRD2_MOUSE	IVLRKRRKRV	NTKRSSRAFR	ANLKTPLKGN	CTHPEDMKLC	TVIMKSNGSF
	264				313
DRD2_HUMAN	PVNRRRVEAA	RRAQELEMEM	LSSTSPPERT	RYSPIPPSHH	QLTLPDPSHH
DRD2_PANTR	PVNRRRVEAA	RRAQELEMEM	LSSTSPPERT	RYSPIPPSHH	QLTLPDPSHH
DRD2_BOVIN	PVNRRRVEAA	RRAQELEMEM	LSSTSPPERT	RYSPIPPSHH	QLTLPDPSHH
DRD2_RAT	PVNRRRMDAA	RRAQELEMEM	LSSTSPPERT	RYSPIPPSHH	QLTLPDPSHH
DRD2_MOUSE	PVNRRRMDAA	RRAQELEMEM	LSSTSPPERT	RYSPIPPSHH	QLTLPDPSHH
	314				362
DRD2_HUMAN	GLHSTPDSPA	KPEKNGHAKD	.HPKIAKIFE	IQTMPNGKTR	TSLKTMSRRK
DRD2_PANTR	GLHSTPDSPA	KPEKNGHAKD	.HPKIAKIFE	IQTMPNGKTR	TSLKTMSRRK
DRD2_BOVIN	GLHSTPDSPA	KPEKNGHAKT	VNPKIAKIFE	IQSMPNGKTR	TSLKTMSRRK
DRD2_RAT	GLHSNPDSA	KPEKNGHAKI	VNPRIAKFFE	IQTMPNGKTR	TSLKTMSRRK
DRD2_MOUSE	GLHSNPDSA	KPEKNGHAKI	VNPRIAKFFE	IQTMPNGKTR	TSLKTMSRRK
	363	373			
DRD2_HUMAN	LSQQKEKKAT	Q			
DRD2_PANTR	LSQQKEKKAT	Q			
DRD2_BOVIN	LSQQKEKKAT	Q			
DRD2_RAT	LSQQKEKKAT	Q			
DRD2_MOUSE	LSQQKEKKAT	Q			

Figure S4.1: Multiple amino acid sequence alignment of mammalian D_{2L}R intracellular loop three. Primary amino acid sequence alignment of intracellular loop three for *Homo sapiens* (Human), *Pan troglodytes* (Chimpanzee), *Bos Taurus* (Bovine), *Rattus norvegicus* (Rat) and *Mus musculus* (mouse). Phosphosite-specific antibody sites (T287/S288, T293/S296 and S317/T318) are highlighted in grey. T318 is not present in rat or mouse D₂R. Sequence absent from the short isoform (D_{2S}R) is highlighted in yellow. Alignment was performed using Clustal Omega version 1.2.4.

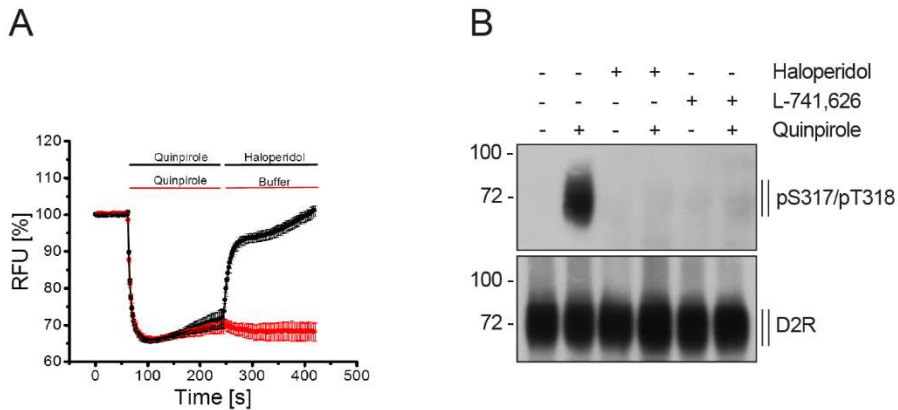


Figure S4.2: Antagonist-selective inhibition of quinpirole-induced phosphorylation and G protein signaling. (A) Reversal of quinpirole-induced hyperpolarization by haloperidol using a fluorescence-based membrane potential assay. After baseline recording for 60 sec, HEK293 cells stably expressing HA-hD2 receptor and GIRK-eGFP were exposed to 1 μ M quinpirole and 240 sec later, 10 μ M haloperidol was added, yielding a final molar quinpirole/haloperidol ratio of 1:10. Shown are representative results from one of four independent experiments performed in triplicate. Vehicle-induced changes in fluorescence signal (background) were subtracted. (B) Stably HA-hD2 receptor expressing HEK293 cells were preincubated (+) or not (-) with 50 μ M haloperidol or L-741,626 for 30 min at 37 °C, then treated with vehicle (water (-)) or with 1 μ M quinpirole (+) for 10 min at 37 °C. Cell lysates were then immunoblotted with anti-pS317/T318 antibody. Blots were stripped and reprobed for D2R. Blots are representative, n=3.

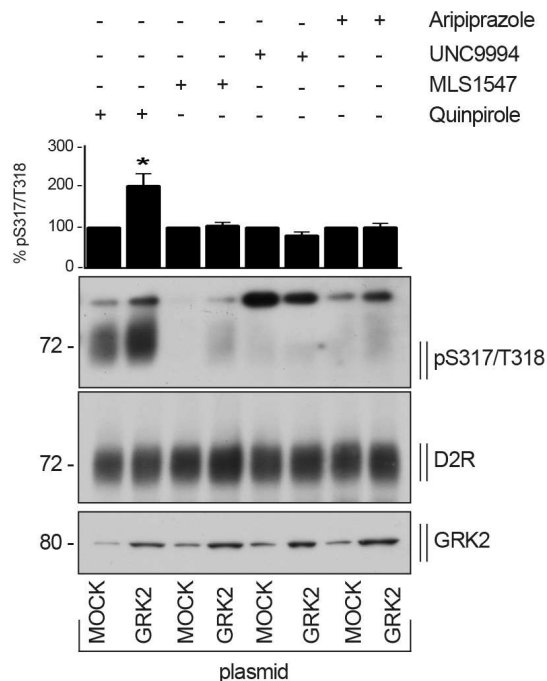


Figure S4.3: D2 receptor phosphorylation is increased by GRK2 overexpression. HEK293 cells stably expressing HA-hD2 receptor were transfected with GRK2 plasmid or empty vector (MOCK) for 48 hours. After stimulation with 1 μ M quinpirole, 10 μ M MLS1547, 10 μ M UNC9994 or 10 μ M aripiprazole for 10 min at 37 °C, lysates were immunoblotted with anti-pS317/T318 antibody. Blots were stripped and reprobed for D2R to confirm equal loading of the gel. Densitometry, above the blots, was normalized to those in MOCK-transfected cells, which were set to 100%. Data are mean \pm SEM from seven independent experiments. (*p<0.05 vs. MOCK by one-way ANOVA with Bonferroni post-test).

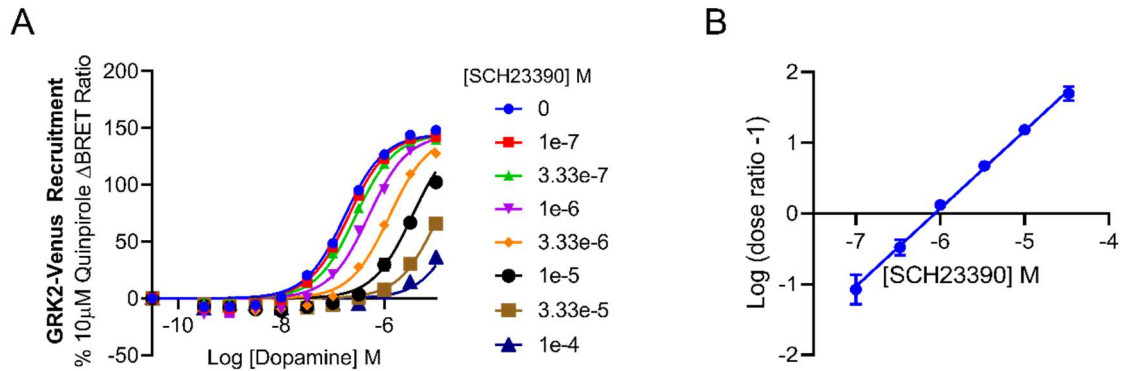


Figure S4.4: Schild analysis of the effect of SCH23390 on dopamine-induced GRK2 recruitment. (A) Recruitment of GRK2-Venus to the D₂R-Nluc in response to dopamine with 30 minutes prior treatment of increasing concentrations of the dopamine D₁-type receptor selective antagonist SCH23390. Schild slope = 1.01 ± 0.03 , $pA_2 = 6.28 \pm 0.06$ (mean \pm SEM) (Analysis using a global fit to the Gaddum/Schild EC₅₀ model with prism 8.1.2) (B) Schild plot linear regression analysis. Slope = 1.10 ± 0.04 , $pA_2 = 6.06 \pm 0.08$. Data is presented as the mean \pm SEM from three separate experiments.

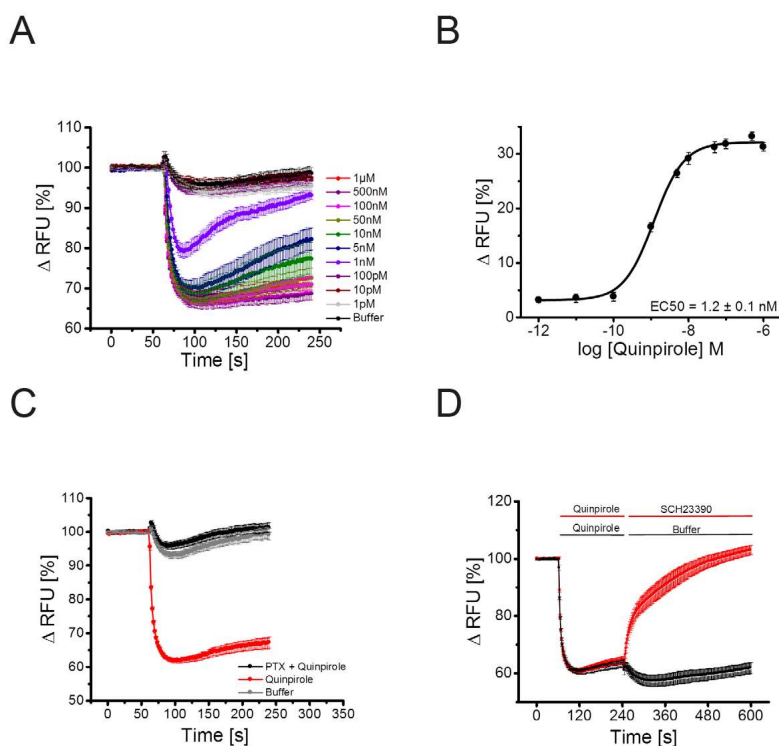


Figure S4.5: Establishment of the membrane potential assay. (A, B) HEK293 cells stably expressing the HA-hD₂R and GIRK-eGFP were stimulated with quinpirole at the indicated concentrations. (C) Cells described in (A and B) were either not treated or treated with 300 ng/ml PTX for 24 hours and then stimulated with 1 μM quinpirole after baseline recording for 60 sec. (D) Cells described in (A and B) were treated with 1 μM quinpirole and subsequently either not treated or treated with 10 μM SCH23390 for 10 min. Shown are representative results of four independent experiments performed in quintuple (mean \pm SEM) for dose-response curves and four to five independent experiments performed in duplicate (mean \pm SEM) for experiments with PTX and SCH23390. Relative changes in fluorescence signal were shown. Background signal (vehicle-induced changes in fluorescence signal) were subtracted from agonist-induced changes at each given concentration. Fitting was performed using a Levensberg-Marquardt Iteration algorithm using a four-parameter nonlinear regression to obtain concentration-response curves with OriginPro software.

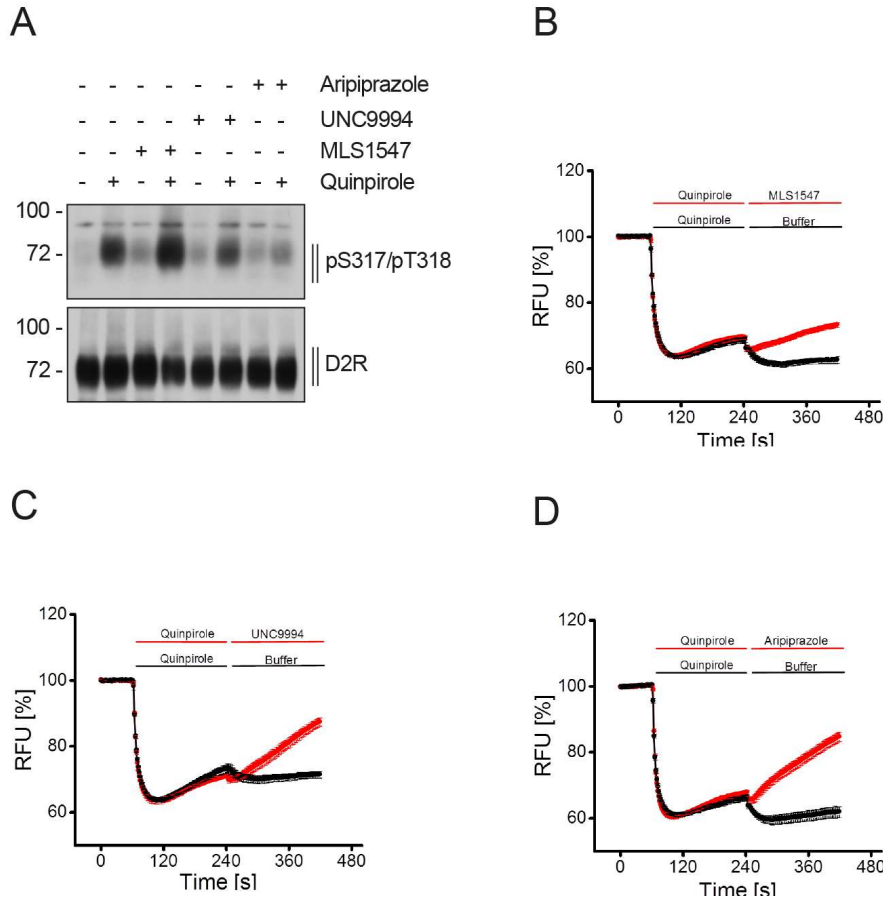


Figure S4.6: Inhibition of quinpirole-induced phosphorylation and G protein signaling. (A) Stably expressing HA-hD₂R HEK293 cells were preincubated (+) or not (-) with 5 μ M MLS1547, UNC9994 or aripiprazole for 30 min at 37 °C, then treated with vehicle (water (-)) or with 1 μ M quinpirole (+) for 10 min at 37 °C. Cell lysates were then immunoblotted with anti-pSer317/Thr318 antibody. Blots were stripped and reprobed for D₂R. Blots are representative, n=3. (B, C, D) After baseline recording for 60 sec, HEK293 cells stably expressing HA-hD₂R and GIRK-eGFP were exposed to 1 μ M quinpirole and 240 sec later, (A) 10 μ M MLS1547, (B) 10 μ M UNC9994 or (C) 10 μ M aripiprazole was added, yielding a final molar quinpirole/MLS1547, quinpirole/UNC9994 or quinpirole/aripiprazole ratio of 1:10. Shown are representative results from one of four independent experiments performed in triplicate. Vehicle-induced changes in fluorescence signal (background) were subtracted.

Chapter 5: Evidence for kinetically distinct dopamine D₂ receptor G protein signalling waves

Abstract

The dopamine D₂ receptor (D₂R) is a G protein-coupled receptor that activates members of the G α_i family of heterotrimeric G proteins. We sought to investigate the kinetics of D₂R mediated activation of individual G α_i protein subtypes to provide a further understanding of the biochemical processes that govern the ability of the D₂R to activate a particular G protein. We used genetically encodable bioluminescence resonance energy transfer-based sensors to monitor either G protein activation or relative concentrations of cAMP in live cells. When the D₂R was stimulated with ropinirole, the D₂R robustly activated G α_o and G α_z proteins more so than G α_{i1} , G α_{i2} and G α_{i3} . Ropinirole induced the activation of all G proteins tested at a significantly faster observed rate than the rate produced by the D₂R agonist antipsychotic aripiprazole. Moreover, the efficient activation of G α_z by the D₂R was shown to be dependent on the slow GTP hydrolysis rate of G α_z . The slow GTP hydrolysis rate lead to an accumulation of active G α_z over time when activated by the D₂R, resulting in increased agonist potency over time. The increased potency over time was abolished by either mutation of serine 42 within the GTP binding site or co-expression with RGS20. Overall, we demonstrate that G protein mediated responses by the D₂R are largely controlled over time by the efficacy and binding kinetics of the agonist as well as the GTP hydrolysis rate of the G α subunit.

5.1 Introduction

G protein-coupled receptors (GPCRs) are integral membrane proteins that transduce cellular signals from a diverse range of extracellular stimuli such as neurotransmitters, hormones and light. Therapeutic exploitation of the ability of GPCRs to transduce such signals has been achieved by designing small molecule binders that can consequently control cellular and physiological outcomes in disease, thus GPCRs represent the largest class of drug targets (348).

GPCRs respond to stimuli by coupling to and activating heterotrimeric G proteins. Heterotrimeric G proteins are comprised of an α subunit ($G\alpha$) that binds guanine nucleotides and a β and γ subunit that act together as a dimer ($G\beta\gamma$). In the G protein cycle, GPCRs function as guanine nucleotide exchange factors (GEFs) by means of inducing a conformational change in the G protein such that the $G\alpha$ subunit exchanges bound guanine diphosphate (GDP) for guanine triphosphate (GTP). This results in $G\alpha$ dissociation, or rearrangement relative to, the $G\beta\gamma$ subunit (10,11). Once active, the $G\alpha$ subunit and $G\beta\gamma$ complex can then further activate downstream signalling cascades. The signalling is then terminated by the $G\alpha$ subunit's native GTPase activity that permits the $G\alpha$ subunit to exist in an active conformation before hydrolysis of the γ -phosphate of GTP, converting it to GDP. The inactive $G\alpha$ subunit then re-associates with free $G\beta\gamma$ and is able to couple to the GPCR and start the cycle again (12).

Despite there being over 800 GPCRs in humans, there are only sixteen genes encoding different $G\alpha$ subunits for GPCRs to transduce signals through. The $G\alpha$ subunits are categorised into four subfamilies ($G\alpha_i$, $G\alpha_s$, $G\alpha_q$ and $G\alpha_{12}$) depending on their sequence homology. $G\alpha$ subunits within the same subfamily often activate similar effectors. For example, the $G\alpha_i$ subfamily members commonly act to inhibit adenylate cyclases and activate G protein-coupled inwardly-rectifying potassium (GIRK) channels (349,350). Because of the restriction in variety of G proteins and downstream effectors, it is thought that GPCRs coordinate a distinct cellular response through discriminating between different G proteins over space and time. One specialised example of spatial coordination is in the retina where activation of $G\alpha_t$ leads to a large portion of $G\alpha_t$ translocating from the rod outer segment to rod intracellular compartments (351). This translocation away from the receptor serves as a means of light adaptation, permitting the retina to work at higher levels of light than usual. Understanding the molecular mechanisms of how GPCRs can process extracellular stimuli and coordinate such a response has been a significant focus of the field.

GPCR signalling can be tuned through activation by agonists with differing efficacy. Ligand efficacy describes the intrinsic 'power' of an agonist to elicit a cellular response in relation to its receptor occupancy (352). While an agonist with high efficacy might robustly activate all responses, an agonist with low efficacy may only poorly activate responses that are less efficiently transduced

by the receptor. Moreover, agonist binding kinetics can shape the texture of the response over time because the association and dissociation rate are responsible for determining the receptor occupancy at any given time. For example, an agonist with slow dissociation from the receptor will often slowly increase its receptor occupancy over time, leading to an increase in potency over time. Interestingly, agonist efficacy and binding kinetics do not appear to be completely independent from each other. Agonist binding kinetics has been proposed to play a role in influencing agonist efficacy and biased agonism at some GPCRs (91,93,95-97,353).

The dopamine D₂ receptor (D₂R) is a GPCR that mediates many of the effects of the catecholamine dopamine in the central nervous system. The D₂R has been the subject of intense study because it is a target for several neuropsychiatric and neurological disorders (104-107). Due to these investigations, there is a wealth of knowledge and pharmacological tools for the D₂R such that it can serve as a good model for investigating GPCR signalling. The D₂R can couple pleiotropically to the non-visual G proteins of the G α_i subfamily (G α_{i1} , G α_{i2} , G α_{i3} , G α_o & G α_z) upon activation. In the brain, the D₂R is thought to mainly couple to the G α_o isoforms (140). However, when specifically examining the nucleus accumbens, where the D₂R displays reduced sensitivity to dopamine, it is thought that D₂R coupling to G α_o may be reduced relative to G α_{i1} , G α_{i2} or G α_{i3} subtype coupling (144). Additionally, there is also evidence that the D₂R couples to G α_z , based on G α_z knockout studies in mice and experiments in rat primary tissue cultures (148,150,151).

Here, we investigated the kinetics of D₂R G protein coupling in live cells. We reconstituted the D₂R signalling system with single G α subunits to assess the activation of individual subunits in real time. We observed differences in maximal effect values and observed rates of activation when assessing the different agonists and G proteins. Potency estimates changed differently over time depending on the agonist and the G protein α subtype. We were able to attribute the changes in potency to disparities in either the agonist dissociation rate or the rate of GTP hydrolysis of the G protein. In doing so, we were able to determine the main molecular determinants responsible for shaping distinct G protein responses by the D₂R.

5.2 Methods

Materials

Ropinirole (>98% pure) was purchased from BetaPharma Co. Ltd. (Wujiang, China). Aripiprazole was synthesised as previously described and shown to be >95% pure (256). Spiperone was purchased from Sigma-Aldrich Pty Ltd (Castle Hill, NSW, AUS). Coelenterazine-h was purchased from Nanolight Technologies a division of Prolume Ltd. (Pinetop, AZ, USA). 96-well

CulturPlates were purchased from PerkinElmer (Beaconsfield, UK). Dulbecco's Modified Eagle Medium (DMEM), Hanks Balanced Salt Solution (HBSS), foetal bovine serum (FBS), trypsin, FlnTM 293 cells, pertussis toxin, geneticin® (G418 Sulfate) and the PierceTM BCA Protein Assay Kit were purchased from Thermo Fisher Scientific (Waltham, MA, USA). Mini-PROTEAN® TGX Stain-FreeTM Gels and Immun-Blot® Low Fluorescence PVDF membranes were purchased from Bio-Rad (Hercules, CA, USA). Anti-Gα_z rabbit polyclonal antibody #3904S and anti-β-actin mouse monoclonal antibody #3700 were purchased from Cell Signalling Technology, Inc. (Danvers, MA, USA). Anti-rabbit 800CW #926-32211 and anti-mouse 680RD #926-68070 IRDye® goat polyclonal antibodies were purchased from LI-COR (Lincoln, NE, USA).

Plasmids encoding masGRK3ct-Rluc8, venus-1-155-G_{γ2} and venus-156-239-Gβ₁ were a generous gift from Prof. Nevin Lambert (Augusta University, GA, USA). pcDNA3L-6xHis-CAMYEL plasmid encoding the BRET sensor was purchased from ATCC (Manassas, VA, USA). pcDNA3.1+ encoding human cDNA of D₂L_R, Gα_{i1}-C351I, Gα_{i2}-C352I, Gα_{i3}-C351I, Gα_{oA}-C351I, Gα_{oB}-C351I, Gα_z, Gβ₅S, RGS9-2 and RGS20 were purchased from the cDNA Resource Centre (Bloomsberg, PA, USA).

Mutagenesis

Mutations were introduced into pcDNA3.1+ encoding wild-type Gα_z or Gα_{i2}-C352I at amino acid position 42 using the Phusion Site-Directed Mutagenesis Kit (Thermo Fisher Scientific). Primers were purchased from Integrated DNA Technologies (Baulkam Hills, NSW, AUS).

Primers are as follows;

Gα_z->S42G;

forward: 5'-CTCCTGCTGGGCACCGGAACTCAGGCAAGAG-3'

reverse: 5'-CTCTTGCCTGAGTTTCCGGTGCCAGCAGGAG-3'.

Gα_{i2}-C352I->G42S;

forward: 5'-CTGCTGTTGGGTGCTAGCGAGTCAGGGAAGAG-3'

reverse: 5'-CTCTTCCCTGACTCGCTAGCACCCAACAGCAG-3'.

Mutagenesis was confirmed by Sanger sequencing of the open reading frame (AGRF, Melbourne, AUS).

Cell culture and transfection

Creation and culture of stable cell line-Cells stably expressing the wild type D₂L_R were generated by initially harvesting 500,000 FlnTM 293 cells into a T25 flask. The following day cells

were transfected with 1µg of pcDNA3.1+ hD₂L_R. The cells were then cultured in DMEM 10% FBS and left to divide to reach 50% confluency in a T75 flask before selection with 600µg/ml G418. After selection, live single cells were then sorted into 96 well plates via fluorescence activated cell sorting (FACS). Individual cells were then cultured to obtain separate colonies and a single colony was selected based on [³H] spiperone radio-ligand binding, and functional receptor detection with the cAMP production inhibition assay. Flp-In™ 293 cells stably expressing the wild type D₂L_R were then aliquoted and frozen for later culturing in DMEM 10% FBS 600µg/mL G418. Cells were split 1 in 10 with 0.5% trypsin in Versene every 2-3 days and were not used past 30 passages.

Transfection for signalling assays and western blotting-2,500,000 Flp-In™ 293 cells stably expressing the D₂L_R were harvested into 10cm dishes. 24 hours after harvesting cells, the DNA constructs were mixed in 250uL PBS and linear polyethylenimine (PEI) was mixed in a separate tube of 250uL PBS in a ratio of 1µg DNA: 6µg PEI. The DNA-PBS mix was then combined with the PEI-PBS mix, vortexed and incubated at room temperature for 10 minutes. In the incubation time, the media was removed from the cell culture dishes and replaced with 10mL DMEM +10% FBS containing penicillin (100U/mL) and streptomycin (100ug/mL). The DNA-PEI-PBS mix was then added drop-wise on top of the cell media and the dishes were returned to the incubator.

G protein activation assay

The G protein activation assay was based on a BRET detection method that has been previously reported (257,258). Initially, Flp-In™ 293 cells stably expressing the D₂L_R were transfected as described above with pcDNA3.1 encoding the following constructs: 1µg venus-1-155-G_γ2, 1µg venus-156-239-G_β1, 1µg masGRK3ct-Rluc8 and 2µg of either G_αi1-C351I, G_αi2-C352I, G_αi3-C351I, G_αoA-C351I, G_αoB-C351I, G_αz, G_αz-S42G, G_αi2-G42S-C352I or empty vector control. For the G protein activation assays where RGS proteins were also transfected, cells were transfected with 1µg venus-1-155-G_γ2, 1µg venus-156-239-G_β1, 1µg masGRK3ct-Rluc8, 2µg of the G_α subunit of interest, 1µg G_β5s and 1µg of either pcDNA3.1+, RGS9-2 or RGS20. 24 hours after transfection, the cells were harvested from dishes and plated into poly-D-lysine coated white 96 well CulturPlates. The cells were left to adhere for approximately 8 hours and then treated with 100ng/mL pertussis toxin overnight. The following day the plate was taken out of the incubator, washed once with Hank's balanced salt solution (HBSS) pH 7.4 and left to equilibrate in HBSS 37°C for 30 minutes before BRET detection. 15 minutes prior to addition of agonist, coelenterazine-h was added to each well with an electronic multi-step pipette to make a final concentration of 5µM. For experiments using PDBu, 333nM PDBu was added 10 minutes before addition of ropinirole. BRET was then measured in a LUMIstar Omega microplate reader (BMG LABTECH). Individual well luminescence was

measured for the emission signal of RLuc8 (445-505nm) and venus (505-565nm) simultaneously. For slow temporal assays, measurements were conducted in 'plate mode' at a cycle time of 30 seconds with five cycles occurring before manual addition of agonist or spiperone with a 12 channel multi-pipette. For fast temporal assays, the plate was measured in 'well mode' with a measurement interval time of 60 milliseconds and a baseline established for 10 seconds before automated injection of 20µL agonist or spiperone at 430µL/s. The counts from the venus acceptor (505-555nm) was then divided by the donor RLuc8 (465-505nm) counts to give a BRET ratio. The BRET ratio values were then subtracted by the vehicle control values to give ΔBRET ratio.

cAMP inhibition assay

Flp-InTM 293 cells stably expressing the D₂L_R were transfected with 3µg of pcDNA3L-6xHis-CAMYEL and 2µg of either pcDNA3.1+ encoding Gα_{i2}-C352I, Gα_{oA}-C351I, Gα_z, Gα_z-S42G or empty vector control. 24 hours later the cells were harvested and transferred into poly-D-lysine coated white 96 well CulturPlates. Approximately 8 hours after the cells were transferred to plates, the cells were treated with 100ng/mL pertussis toxin overnight. The following day the cells were washed once with HBSS (pH 7.4, 37°C) and left to equilibrate in HBSS for 30 minutes before taking luminescence measurements. Addition of coelenterazine-h to make a final concentration of 5µM was carried out 15 minutes before agonist addition. Cells were then treated with 10µM forskolin 10 minutes before addition of increasing concentrations of agonist and detecting BRET at the indicated times. For experiments using spiperone to out-compete ropinirole, coelenterazine-h and ropinirole (100nM final concentration) were co-added 18 minutes before addition of 20µM spiperone. BRET was detected at 37°C measuring luminescence at 445-505nm (RLuc) and 505-565nm (venus) simultaneously using a LUMIstar Omega microplate reader (BMG LABTECH). Plates were measured in 'plate mode' at a cycle time of 30 seconds with a baseline of 5 cycles established before addition of agonist or spiperone. Counts from the 505-555nm channel were then divided by the 465-505 channel to give a BRET ratio. The ratios were then baseline normalised whereby wells treated with 10uM forskolin were set to 0% and vehicle treated wells set to 100%.

Western blotting analysis

While plating transfected cells for G protein activation assays or cAMP inhibition assays the cells were also plated into Corning® Costar® 6 well plates. On the same day as performing signalling assays, protein samples were prepared from the cells for later blotting. Cells were washed with PBS and harvested in 1mL Versene. Cells were spun at 350g for 5 minutes at 4°C and supernatant was

removed. The cell pellet was then lysed in RIPA buffer (150mM NaCl, 1%NP-40, 0.5% sodium deoxycholate, 0.1% SDS, 50mM Tris-HCl, pH8.0, cOmpleteTM protease inhibitor) and left to shake gently on ice for 30 minutes. The sample was then spun at 15,000g for 10 minutes at 4°C, the supernatant was kept and stored at -80°C for analysis. Protein concentration was determined by BCA assay and 30µg of protein in SDS-loading buffer (4% SDS, 10% β-mercaptoethanol, 20% glycerol, 0.004% bromophenol blue, 0.125M Tris-HCl) was loaded for separation by SDS-PAGE (4-15% gradient gel). Samples were transferred onto Immun-Blot® Low Fluorescence PVDF membranes using a Trans-Blot® SD Semi-Dry Transfer Cell (Bio-Rad). Membranes were then blocked with 5% BSA in PBS 0.1% Tween 20 for 1 hour followed by overnight incubation with the primary antibody at 4°C. The Gα_z and β-actin antibodies were used at a 1:1000 dilution and the Gα_z antibody was raised against an epitope separate from the mutagenesis site. The membranes were then washed in PBS 0.1% Tween 20 and incubated with either anti-rabbit 800CW or anti-mouse 680RD secondary antibodies used at a dilution of 1:10,000 for 1 hour at 25°C. The membranes were then washed again in PBS 0.1% Tween 20 before detection with an Odyssey Classic infrared imaging system (LI-COR, Lincoln, NE, USA).

Data analysis

Concentration response curves were fit with the log(agonist) vs. response (three parameter) equation and functional rates were determined by fitting a one-phase association or decay in GraphPad Prism 7.02. All data was analysed by first pooling the experimental replicates together followed by curve fitting. Western blot micrographs were analysed with Fiji.

5.3 Results

Monitoring G protein activation at the D₂R

To investigate D₂R mediated activation of different G proteins in live cells we used a genetically encoded bioluminescence resonance energy transfer (BRET) sensor (Fig. 5.1A)(258). The BRET sensor monitors Gβγ release by utilising the pleckstrin homology domain of GRK3 (GRKct) that binds free Gβγ upon dissociation from the Gα subunit. While there are several methods for detection of G protein activation, this assay allows use of wild-type GPCRs and Gα subunits, hence it can be universally applied to any GPCR and Gα subunit. In addition, previous studies have demonstrated that the assay provides a robust signal-to-noise ratio and high temporal resolution (132,354).

We used Flp-In HEK 293 cells stably expressing the long isoform of the D₂R (Flp-In-293-D₂L_R) and transiently transfected the BRET sensor together with pertussis toxin (PTX) insensitive G α_i subfamily proteins or wild-type G α_z (that is natively PTX insensitive) followed by treatment with PTX to abolish any signal from endogenous G α_i coupling. The D₂R agonist ropinirole was used to probe G protein activation due to dopamine suffering from oxidation (355) and a potential lack of selectivity for dopamine D₂ type receptors over endogenously expressed adrenergic receptors (356). In addition, ropinirole is a useful reference as it displays similar efficacy and binding kinetics to dopamine at the D₂R (96,357). Upon stimulation of Flp-In-293-D₂R cells with ropinirole, we detected activation of all G α proteins known to couple to the D₂R, including G α_z (Fig. 5.1B). The measured responses 15 minutes after stimulation with increasing concentrations of ropinirole fit well to a sigmoidal concentration-response curve. Ropinirole was approximately 10-fold more potent at activating G α_{oA} , G α_{oB} and G α_z subunits compared to G α_{i2} , and 5-fold more potent than at G α_{i1} and G α_{i3} (Fig 5.1C-E, Fig S5.1A-C & Table 5.1). Additionally, ropinirole-induced activation of G α_{oA} , G α_{oB} and G α_z subunits produced a larger maximal effect (given as change in BRET ratio) compared to G α_{i1} , G α_{i2} and G α_{i3} subunits (Fig. 5.1B-E, Fig S5.1A-C & Table 5.1). While it has been demonstrated that the D₂R preferentially activates G α_{oA} subunits over G α_{i1} , G α_{i2} and G α_{i3} (139), the potency and maximal effect of ropinirole in the G α_z condition suggest that the D₂R is also efficiently coupled to this G protein.

Some studies using [³⁵S]GTP γ S binding assays to detect G protein coupling have failed to detect activation of some or all of G α_{i1} , G α_{i2} and G α_{i3} upon stimulation of the D₂R with partial agonists (137-139). Therefore, we next stimulated the Flp-In-293-D₂R cells with the partial agonist antipsychotic aripiprazole. Aripiprazole induced activation of G α_{i1} , G α_{i2} and G α_{i3} with approximately half the maximal effect of ropinirole, and induced activation of G α_{oA} , G α_{oB} and G α_z with responses almost equal to ropinirole's maximal effect (Fig. 5.1B-E, Fig S5.1A-C & Table 5.1). Detection of aripiprazole-induced responses at G α_{i1} , G α_{i2} and G α_{i3} suggest that the BRET-based G protein activation assay has superior sensitivity for detecting G protein coupling compared to the [³⁵S]GTP γ S binding assays used in previous studies.

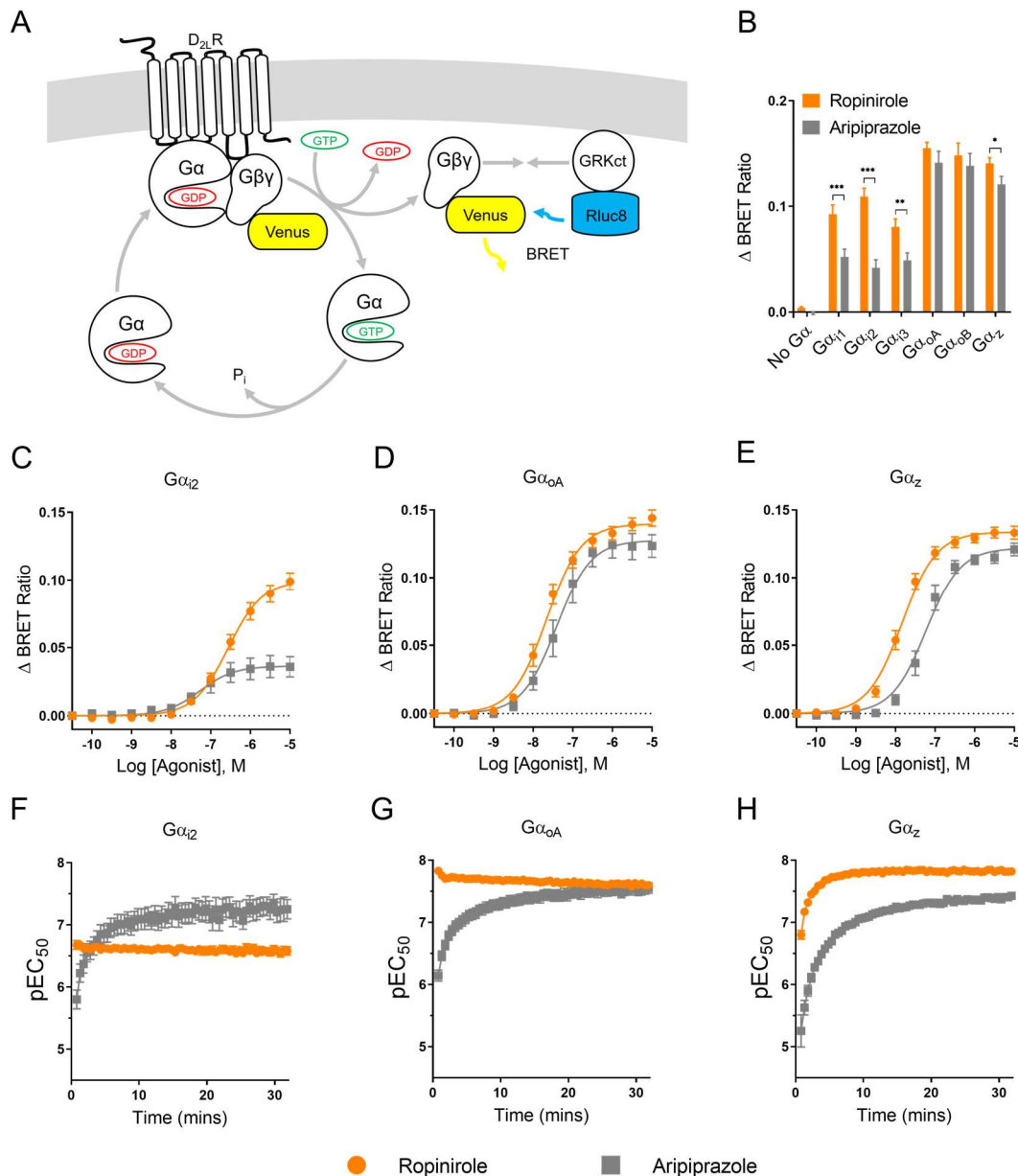


Figure 5.1: G protein activation assay accurately measures differences in agonist responses over time at the D_2R . (A) Diagram of the detection method for G protein activation by the D_2R . D_2R activation of $G\alpha_{i/o/z}$ - $G\beta\gamma$ -Venus heterotrimers induces a conformational change in the G protein that results in $G\alpha_{i/o/z}$ exchanging its bound GDP for GTP and dissociation of the $G\beta\gamma$ -Venus subunit. The myristoylated and RLuc8-tagged pleckstrin homology domain of GRK3 reversibly binds free $G\beta\gamma$ -Venus subunits such that when the $G\alpha$ subunit is inactive (GDP bound) it can outcompete the GRK3 domain for $G\beta\gamma$, yet once the $G\alpha$ subunit becomes active (exchanges GDP for GTP) the $G\alpha$ subunit dissociates from $G\beta\gamma$. (B) Quantification of increases in BRET ratio in response to 2.5 minutes of stimulation with 10 μ M ropinirole (orange bars) or 10 μ M aripiprazole (grey bars) for cells transfected with the G protein activation sensor together with the indicated $G\alpha$ subunit or $G\alpha$ -free control. (C, D & E) Concentration response curves of cells transfected with cDNA encoding the G protein activation sensor together with $G\alpha_{i2}$ (panel C), $G\alpha_{oA}$ (panel D) or $G\alpha_z$ (panel E) measured at 15 minutes in response to increasing concentrations of ropinirole (orange circles) or aripiprazole (grey squares). (F, G & H) Potency changes over 30 minutes of $G\alpha_{i2}$ (panel F), $G\alpha_{oA}$ (panel G) or $G\alpha_z$ (panel H) activation plotted as pEC_{50} parameter values estimated from concentration response curves fitted at each measurement interval after stimulation of increasing concentrations of ropinirole (orange circles) or aripiprazole (grey squares). All values are expressed as mean \pm SEM from 5-9 separate

experiments performed in single wells. Students unpaired t test was used to test for statistical significance between ropinirole and aripiprazole induced maximal values in panel B. * $P < 0.05$, ** $P < 0.01$, *** $P < 0.001$.

Table 5.1: Ropinirole and aripiprazole induced dissociation of various G proteins by the D₂R. Potency (pEC₅₀) and maximal effect (E_{\max} – BRET units) parameter values represent the mean \pm SEM from 5-9 separate experiments determined 15 minutes after stimulation

G α subunit	Ropinirole		Aripiprazole	
	pEC ₅₀	E_{\max}	pEC ₅₀	E_{\max}
G α_{i1}	6.95 \pm 0.09 ^a	8.44 \pm 0.34 $\times 10^{-2}$ ^a	7.14 \pm 0.12	4.40 \pm 0.23 $\times 10^{-2}$ ^b
G α_{i2}	6.56 \pm 0.06	9.95 \pm 0.30 $\times 10^{-2}$	7.28 \pm 0.18 ^b	3.64 \pm 0.28 $\times 10^{-2}$ ^b
G α_{i3}	6.90 \pm 0.07 ^a	7.45 \pm 0.26 $\times 10^{-2}$ ^a	7.19 \pm 0.13	4.27 \pm 0.23 $\times 10^{-2}$ ^b
G α_{oA}	7.65 \pm 0.04 ^a	13.97 \pm 0.25 $\times 10^{-2}$ ^a	7.41 \pm 0.08	12.76 \pm 0.43 $\times 10^{-2}$ ^{a, b}
G α_{oB}	7.54 \pm 0.08 ^a	13.18 \pm 0.45 $\times 10^{-2}$ ^a	7.47 \pm 0.09	12.05 \pm 0.42 $\times 10^{-2}$ ^a
G α_z	7.83 \pm 0.04 ^a	13.37 \pm 0.20 $\times 10^{-2}$ ^a	7.23 \pm 0.05 ^b	12.19 \pm 0.28 $\times 10^{-2}$ ^{a, b}

^a Significantly different ($P < 0.05$) from corresponding G α_{i2} value within the column as determined by one-way analysis of variance with Dunnett's multiple comparisons test

^b Significantly different ($P < 0.05$) from corresponding ropinirole parameter value within the row as determined by student's t-test

Temporal patterns of G protein activation change depending on the agonist and the G α subunit

Having accurately detected G protein activation, we then analysed agonist action over time by fitting concentration response curves to the data at each measurement interval over a time-course of 30 minutes (Fig. S5.2). We were then able to plot potencies (pEC₅₀) values over time to compare ropinirole and aripiprazole at each G protein (Fig. 5.1F-H, Fig. S5.1D-F). We have previously demonstrated that aripiprazole displays a fast association rate and a slow dissociation rate for the D₂R such that upon addition of aripiprazole, the equilibrium between the bound and free species of the D₂R will slowly be reached (96). Therefore, the potency in a functional assay is expected to increase over time as the occupancy of aripiprazole at the receptor increases. As predicted, aripiprazole displayed a large increase in potency over time for each of the different G proteins. In contrast, ropinirole is a fast dissociating agonist such that binding at the D₂R will rapidly reach equilibrium. In agreement with ropinirole's binding kinetics at the D₂R, the potency for G α_{i1} , G α_{i2} , G α_{i3} , G α_{oA} and G α_{oB} activation remained constant over time. However, ropinirole displayed a 10-fold increase in potency over time at G α_z . Additionally, aripiprazole displayed a larger increase in potency over time for G α_z than any other G α subunit, suggesting a ligand-independent difference at the level of the G α_z G protein. This was surprising as G protein activation is thought to occur on the millisecond-second timescale and thus might be expected to be limited by the rate of agonist binding to the D₂R (11).

Gα subunit-specific cAMP inhibition reflects G protein activation

The Gα_i subfamily proteins, including Gα_z, inhibit the production of cAMP by binding to and negatively modulating adenylate cyclases. This property allowed us to investigate if any downstream consequences result from the different temporal patterns seen at the level of G protein activation. Measurements of relative intracellular cAMP concentrations in Flp-In-293-D₂R cells were determined with a conformational BRET sensor based on Epac1 (Fig. 5.2A) (358). We used the same rationale as the G protein activation assay to measure G protein-specific signalling whereby the G protein cDNA (PTX insensitive Gα_i subunits or wild-type Gα_z) was transfected together with the BRET sensor followed by overnight treatment with PTX. Gα_{i2} was used as a representative subunit for the Gα_{i1}, Gα_{i2} and Gα_{i3} subunits, and Gα_{oA} was used as a representative of the Gα_{oA} and Gα_{oB} isoforms. Similar to the G protein activation assay, we observed that ropinirole was more potent at stimulating Gα_{oA} and Gα_z mediated cAMP inhibition than Gα_{i2} (Fig. 5.2B, D & F & Table 5.2). Aripiprazole also showed maximal responses closer to ropinirole at Gα_{oA} and Gα_z but produced approximately half the maximal effect of ropinirole when measuring Gα_{i2} dependent cAMP inhibition. Measuring potency over time showed that aripiprazole increased in potency over time for each of the three Gα subunits, consistent with its binding kinetics to the D₂R (Fig. 5.2C, E & G). We then observed an increase in ropinirole's potency for Gα_z-dependent cAMP inhibition but not for Gα_{i2} or Gα_{oA}. Accordingly, all measurements of D₂R mediated cAMP inhibition closely matched the G protein activation assay, confirming that the observed temporal signalling patterns are dependent on the agonist as well as the G protein. The cAMP measurements also confirmed that the pattern of changing potency over time was not an artefact associated with the methods or plasmid constructs used in the G protein activation assay.

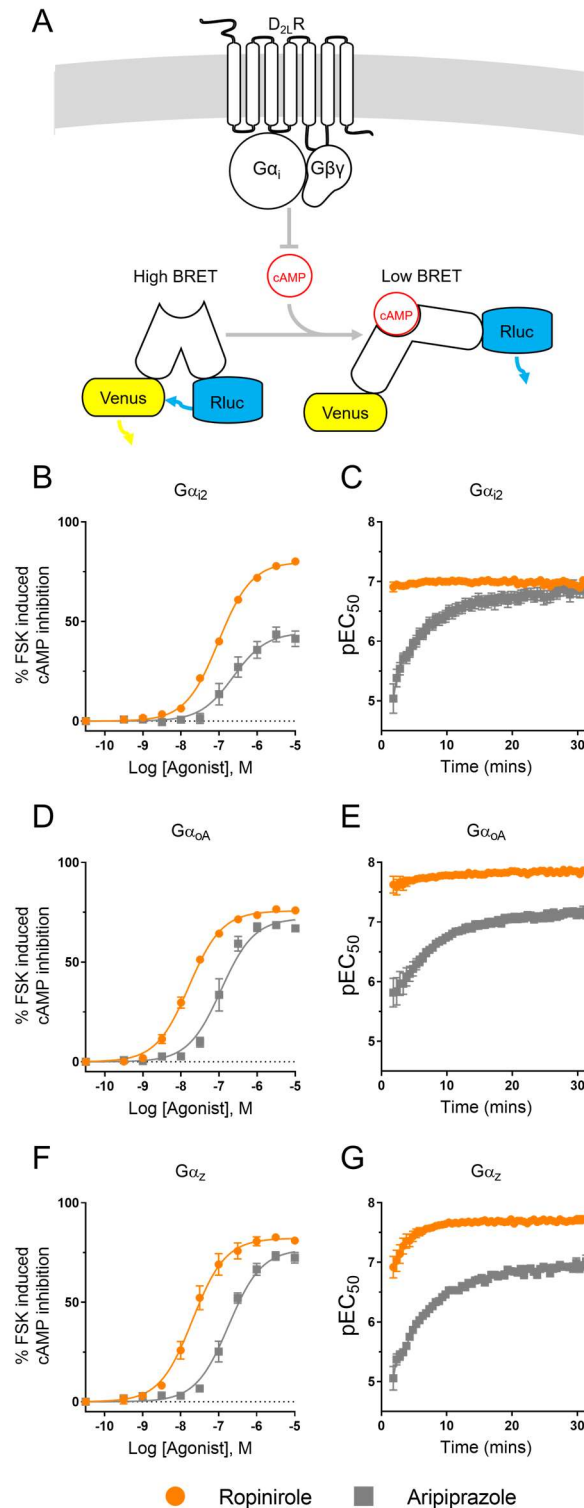


Figure 5.2: cAMP assay reports on individual G protein signalling kinetics. (A): Schematic of the intracellular cAMP detection method. Agonist activation of the D_2R results in coupling to $G\alpha_{i/o/z}$ subunits that inhibit the production of forskolin stimulated cAMP. The relative amount of cAMP within the live cells is then detected by the BRET-based cAMP sensor – CAMYEL, that undergoes a conformational change upon binding to cAMP resulting in increased proximity of the RLuc and Venus allowing for more efficient non-radiative energy transfer. Cells were transfected with the particular PTX-insensitive $G\alpha$ subunit of interest and treated with PTX to measure the cAMP inhibition mediated through the single $G\alpha$ species. **(B, D & F)** cAMP production inhibition concentration response curves of Flp-In-293- D_2R cells transfected with cDNA encoding the cAMP BRET sensor

together with G α_{i2} (B), G α_{oA} (D) or G α_z (F) measured at 15 minutes in response to increasing concentrations of ropinirole (orange circles) or aripiprazole (grey squares). (C, E & G) Potency changes over 30 minutes of G α_{i2} (C), G α_{oA} (E) or G α_z (G) dependent cAMP production inhibition plotted as pEC₅₀ parameter values estimated from concentration response curves fitted at each measurement interval after stimulation of increasing concentrations of ropinirole (orange circles) or aripiprazole (grey squares). All values are expressed as mean \pm SEM from 4-7 separate experiments performed in duplicate wells.

Table 5.2: Ropinirole and aripiprazole induced G protein-dependent cAMP inhibition by the D₂R.

Potency (pEC₅₀) and maximal effect (E_{max} – % Forskolin inhibition) parameter values represent the mean \pm SEM from 4-7 separate experiments determined 15 minutes after stimulation

G α subunit	Ropinirole		Aripiprazole	
	pEC ₅₀	E_{max}	pEC ₅₀	E_{max}
G α_{i2}	7.01 \pm 0.02	80.0 \pm 0.7	6.63 \pm 0.10 ^b	44.5 \pm 2.3 ^b
G α_{oA}	7.79 \pm 0.03 ^a	75.7 \pm 0.8	6.95 \pm 0.06 ^{a, b}	72.1 \pm 2.1 ^a
G α_z	7.69 \pm 0.05 ^a	82.2 \pm 1.6	6.738 \pm 0.05 ^b	76.8 \pm 1.8 ^a

^a Significantly different (P<0.05) from corresponding G α_{i2} value within the column as determined by one-way analysis of variance with Dunnett's multiple comparisons test

^b Significantly different (P<0.05) from corresponding ropinirole parameter value within the row as determined by student's t-test

Observed G protein activation rate at the D₂R is influenced by agonist efficacy

We next investigated the differences in G protein activation kinetics between ropinirole and aripiprazole on a faster timescale. To perform these experiments, we used a high concentration of the agonist that was calculated, using rate constants determined from our previously published binding experiments (96), to occupy >95% of receptors within 1.5 seconds. Upon injection of ropinirole, we observed that G α_{i2} , G α_{oA} and G α_z were all activated on a millisecond-second timescale consistent with what has been previously proposed for GPCR activation (Fig 5.3A, B & C) (359). Ropinirole-induced G α_{oA} activation was approximately 3-fold faster and 6-fold faster than ropinirole-induced activation of G α_{i2} and G α_z respectively (Table. 5.3). Stimulation with aripiprazole produced rates of activation for each G protein that were all considerably (>6-fold) slower than the ropinirole-induced rates (G α_{i2} , G α_{oA} & G α_z P <0.0001, student's t test), highlighting that a key determinant of the observed G protein activation rate at the D₂R is agonist efficacy. Furthermore, while ropinirole displayed 3-fold slower activation of G α_{i2} compared to G α_{oA} , the rates of activation of these two G proteins induced by aripiprazole was similar (Table 5.3). Moreover, aripiprazole produced a smaller total increase in BRET for G α_{i2} , consistent with its partial agonist action as detected by the concentration response curves measured at a later timepoint (Fig 5.1.). Therefore, activation of G α_{i2} by aripiprazole displays a unique temporal pattern whereby activation occurred almost as fast as observed for G α_{oA} , but it only produces a partial response.

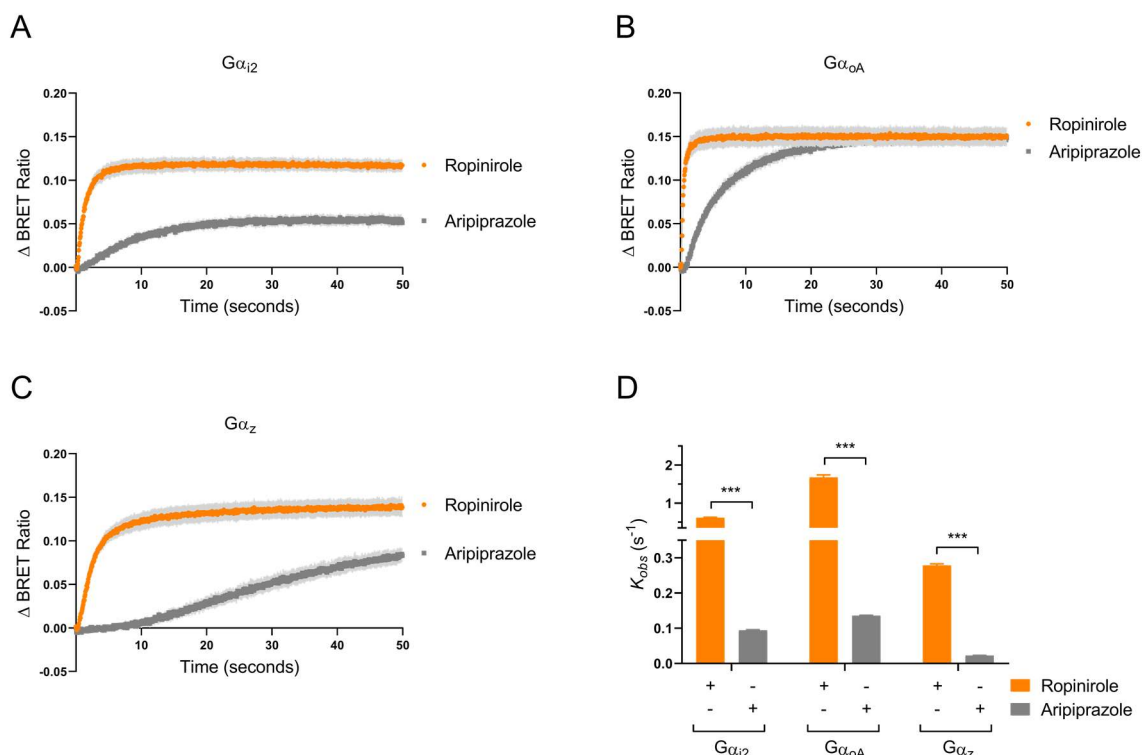


Figure 5.3: Differences in observed G protein activation rates in response to saturating concentrations of ropinirole and aripiprazole. (A) D₂R mediated Gα_{i2} activation response upon injection of 100 μM ropinirole (orange circles) or 10 μM aripiprazole (grey squares) over 50 seconds. All values represent the mean ± SEM (grey shading indicates error bars) of 5 separate experiments (ropinirole) or 3 separate experiments (aripiprazole). (B) D₂R mediated Gα_{oA} activation response upon injection of 100 μM ropinirole (orange circles) or 10 μM aripiprazole (grey squares) over 50 seconds. All values represent the mean ± SEM (grey shading indicates error bars) of 5 separate experiments (ropinirole) or 3 separate experiments (aripiprazole). (C) D₂R mediated Gα_z activation response upon injection of 100 μM ropinirole (orange circles) or 10 μM aripiprazole (grey squares) over 50 seconds. All values represent the mean ± SEM (grey shading indicates error bars) of 6 separate experiments (ropinirole) or 3 separate experiments (aripiprazole). (D) Ropinirole (orange bars) and aripiprazole (grey bars) stimulated D₂R dependent G protein activation rates determined by one phase association curve fit of the responses shown in panels A, B & C. Rate values are represented as mean ± SEM. Students unpaired t test was used to determine statistical significance between rates induced by ropinirole and aripiprazole. *** $P < 0.001$.

Table 5.3: Observed G protein activation rates induced by ropinirole and aripiprazole

K_{obs} (s⁻¹) values are determined from 3-6 separate experiments

Gα subunit	Ropinirole	Aripiprazole
Gα _{i2}	$6.18 \pm 0.12 \times 10^{-1}$	$9.46 \pm 0.14 \times 10^{-2}$ ^b
Gα _{oA}	$16.79 \pm 0.63 \times 10^{-1}$ ^a	$1.36 \pm 0.01 \times 10^{-1}$ ^{a, b}
Gα _z	$2.79 \pm 0.05 \times 10^{-1}$ ^a	$2.27 \pm 0.02 \times 10^{-2}$ ^{a, b}

^a Significantly different ($P < 0.05$) from corresponding Gα_{i2} value within the column as determined by one-way analysis of variance with Dunnett's multiple comparisons test

^b Significantly different ($P < 0.05$) from corresponding ropinirole value within the row as determined by student's t-test

Gα_z remains active for an extended period

High concentrations of ropinirole produced a rapid response at Gα_z (Fig. 5.3C), yet low concentrations of ropinirole produced responses that slowly increased over several minutes (Fig. S5.2, Panel C). This increase in response over time for low concentrations of agonist resulted in an increase in the potency of ropinirole over time. Furthermore, saturating concentrations of ropinirole produced a slower activation rate for Gα_z compared to Gα_{i2} and Gα_{oA}. Our previous ligand binding experiments revealed that the dissociation rate of ropinirole from the D₂R is fast such that this increase in potency over time cannot be related to an increase in receptor occupancy over time (96). Furthermore, this increase in potency is specific to Gα_z as no change in the potency of ropinirole is observed at the other Gα subunits. Thus, this difference must relate to a difference in the signalling properties of Gα_z compared to the other Gα_i subfamily G proteins. It is known that recombinant Gα_z purified from *Escherichia coli* displays a slow basal GTP hydrolysis rate when compared to other Gα subunits (19). We therefore hypothesized that once active, Gα_z may slowly hydrolyse its bound GTP in live cells, and thus remain in the active state for an extended period. This in turn would cause the active species of Gα_z to accumulate over time. The active species could make multiple interactions with effector proteins which may effectively amplify the signalling response. This would then result in an increase in potency over time as the active Gα_z species accumulates.

We first tested whether Gα_z remained active for an extended period by pre-stimulation with ropinirole followed by addition of a high concentration of the high affinity antagonist spiperone to rapidly stop the activation of the D₂R upon ropinirole dissociation. Upon addition of spiperone, Gα_z remained active for approximately 56-fold longer than Gα_{oA}, and 37-fold longer than Gα_{i2} as measured by a decrease in the BRET signal between Gβγ-venus and GRKct-Rluc8 (Table 5.4, Fig. 5.4A & B). We observed the same pattern when using the CAMYEL biosensor to measure changes in intracellular cAMP; the downstream rate of cAMP increase upon addition of spiperone in the Gα_z transfected condition was also significantly slower than that observed in the Gα_{i2} and Gα_{oA} conditions ($P=0.0001$ & $P<0.0001$ respectively, one-way ANOVA) (Table 5.4, Fig. 5.4C & D). Together these data indicate that, after activation, the Gα_z subunit remains in the active state for a longer time as compared to the other Gα_i subunits. However, the rate of inhibition of the Gα_{i2} and Gα_{oA} signals observed upon addition of spiperone were slower in the cAMP assay as compared to the rates detected using the direct G protein activation sensors. This suggests that the limiting step, at least for Gα_{i2} and Gα_{oA}-dependent cAMP inhibition lies at the level of adenylate cyclase whereas for Gα_z, it lies at the level of the G protein.

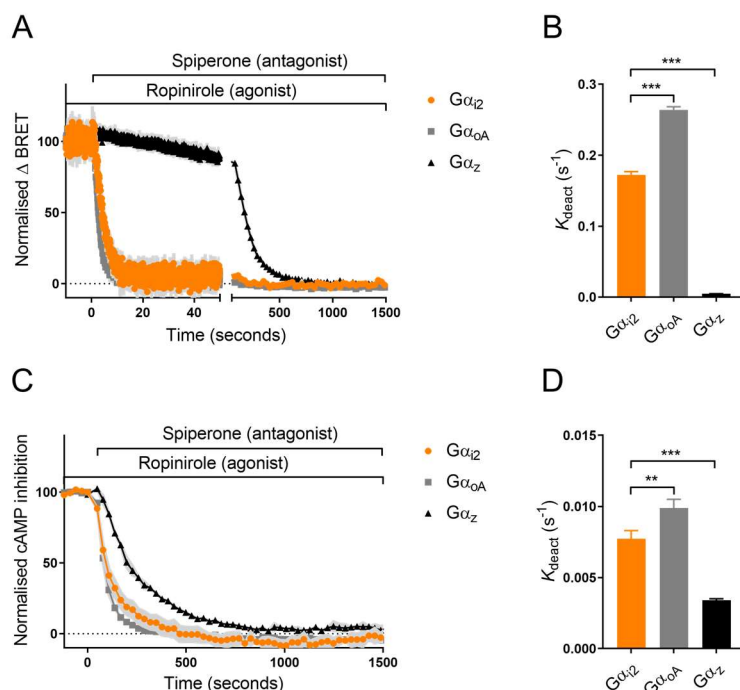


Figure 5.4: Gα_z exhibits an extended lifetime in the active state. (A) G protein deactivation of Gα_{i2} (orange circles), Gα_{oA} (grey squares) and Gα_z (black triangles) over time. Flp-In-293-D₂R cells transfected with the BRET sensor and specific Gα subunit were incubated for 18 minutes with 333nM ropinirole followed by injection with 20μM spiperone (antagonist) and changes in BRET were measured over time. All values represent mean ± SEM (light grey shading indicates error bars) of 4 separate experiments (Gα_{oA}) or 6 separate experiments (Gα_{i2} & Gα_z) performed in triplicate wells. (B) G protein deactivation rates for Gα_{i2} (orange bar), Gα_{oA} (grey bar) and Gα_z (black bar) determined by one phase decay curve fit of the responses shown in panel A. Rate values are represented as mean ± SEM. (C) Increase in intracellular cAMP concentration due to deactivation of Gα_{i2} (orange circles), Gα_{oA} (grey squares) and Gα_z (black triangles) over time. Flp-In-293-D₂R cells transfected with the BRET sensor and the Gα subunit of interest were incubated for 18 minutes with 100nM ropinirole followed by injection with 10μM spiperone (antagonist) and changes in BRET were measured over time. All values represent mean ± SEM (light grey shading indicates error bars) of 3 separate experiments performed in triplicate wells. (D) Rates of Gα specific increase in intracellular cAMP concentration for Gα_{i2} (orange bar), Gα_{oA} (grey bar) and Gα_z (black bar) determined by one phase decay curve fit of the responses shown in panel C. Rate values are represented as mean ± SEM. A one-way analysis of variance with Dunnett's multiple comparisons test was used to determine statistical significance between deactivation rates of Gα_{i2} and either Gα_{oA} or Gα_z. ** $P < 0.01$, *** $P < 0.001$.

Table 5.4: G protein deactivation rates determined by spiperone competition experiments
Values are determined from 3-6 separate experiments

Gα subunit	G protein sensor		cAMP sensor	
	K_{deact} (s ⁻¹)	$t_{1/2}$ (s)	K_{deact} (s ⁻¹)	$t_{1/2}$ (s)
Gα _{i2}	$17.24 \pm 0.18 \times 10^{-2}$	5.8	$7.72 \pm 0.34 \times 10^{-3}$	129.5
Gα _{oA}	$26.40 \pm 0.29 \times 10^{-2}$ ^a	3.8	$9.89 \pm 0.35 \times 10^{-3}$ ^a	101.2
Gα _z	$4.68 \pm 0.08 \times 10^{-3}$ ^a	213.9	$3.39 \pm 0.07 \times 10^{-3}$ ^a	294.6

^a Significantly different ($P < 0.05$) from corresponding Gα_{i2} value within the column as determined by one-way analysis of variance with Dunnett's multiple comparisons test

The unique signalling pattern of G α_z is dependent on serine 42

Many nucleotide binding proteins contain a conserved phosphate binding loop (P-loop) motif (360). For heterotrimeric G proteins in particular, it has been demonstrated through structural and biochemical studies on G α_{i1} , that a highly conserved glycine residue within the P-loop is required for the fast hydrolysis of GTP (Table 5.5) (361). G α_z is unique among the heterotrimeric G proteins, as it possesses a serine residue at this position (Ser42) (Table 5.5). Accordingly, we postulated that mutation of Ser42 to the glycine present in all other heterotrimeric G proteins will increase the G protein turnover kinetics in live cells. In our G protein activation assay, the S42G mutation lead to a modest 2-fold increase in the observed rate of activation upon stimulation with a saturating concentration of ropinirole ($K_{obs} = 5.90 \pm 0.17 \times 10^{-1} \text{ s}^{-1}$, Fig. 5.5A & B), while the expression levels of the G α_z -S42G mutant were similar to wild-type (Fig. 5.5C). Moreover, the deactivation rate was increased by approximately 20-fold ($K_{deact} = 9.99 \pm 0.01 \times 10^{-2} \text{ s}^{-1}$, (Fig. 5.5D & E), consistent with the hypothesis that serine 42 indeed governs the slow GTP hydrolysis rate of G α_z . This provides further evidence that it is not agonist dissociation rate from the D₂R that likely determines the rate of G α_z deactivation but, rather, the rate of GTP hydrolysis.

We then tested the effect of the S42G mutation on G protein activation response over time to increasing concentrations of ropinirole. Strikingly, this mutation completely abolished the increase in potency over time upon activation with ropinirole (Fig. 5.5G). Furthermore, the potency and maximal effect of ropinirole at G α_z -S42G was significantly decreased when measured 15 minutes after stimulation (Fig. 5.5F) ($pEC_{50} = 7.27 \pm 0.04$, $E_{max} = 8.884 \pm 0.13 \times 10^{-2}$ BRET units) ($P < 0.0001$ & $P < 0.0001$ respectively, student's t-test) as compared to that observed at G α_z wildtype ($pEC_{50} = 7.83 \pm 0.04$, $E_{max} = 13.37 \pm 0.20 \times 10^{-2}$ BRET units). Thus, the slow rate of GTP hydrolysis by G α_z is required for the increase in potency of ropinirole over time and may contribute to the higher potency observed at G α_z compared to G α_{i2} observed at later time-points.

Table 5.5: Alignment of G protein P-loop amino acid residues

G protein	Position	Sequence
G α_z	40	G T S N S G K S
G α_{i2}	40	G A G E S G K S
G α_{oA}	40	G A G E S G K S
G α_q	46	G T G E S G K S
G α_{12}	64	G A G E S G K S
G α_s	47	G A G E S G K S
H-Ras	10	G A G G V G K S
Ran	17	G D G G T G K T
RhoA	12	G D G A C G K T
Arf1	24	G L D A A G K T

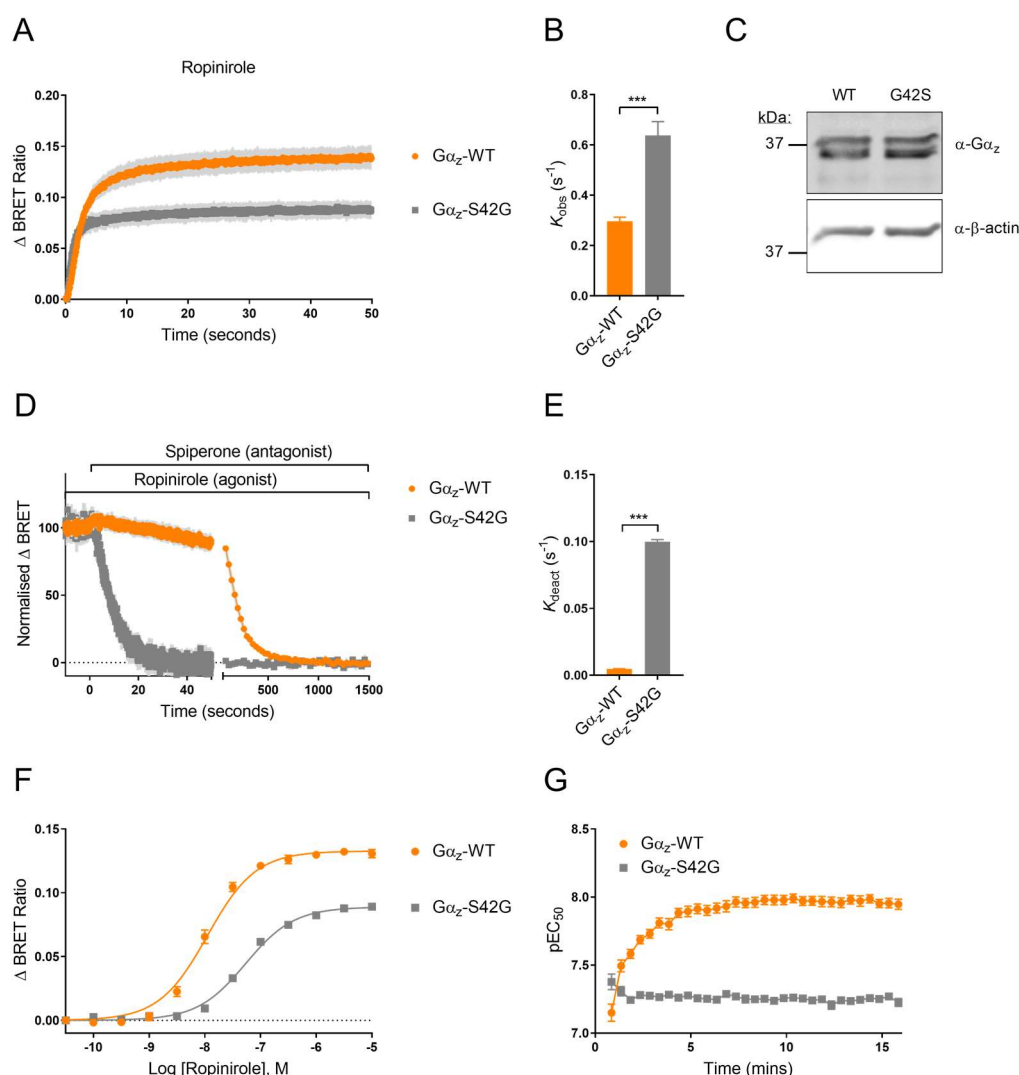


Figure 5.5: Mutation of serine 42 to glycine confers fast Gα_{i2} kinetics to Gα_z. (A) D₂R mediated G protein activation of Gα_z-WT (orange circles) and Gα_z-S42G (grey squares) over time. Flp-In-293-D₂R cells transfected with the BRET sensor and Gα_z-WT or Gα_z-S42G were injected with 100μM ropinirole and changes in BRET were measured over time. All values represent mean ± SEM (grey lines indicate error bars) of 6 separate experiments performed in triplicate wells. (B) D₂R mediated G protein activation rates for Gα_z-WT (orange bar) or Gα_z-S42G (grey bar) determined by one phase decay curve fit of the responses shown in panel A. Rate values are represented as mean ± SEM. (C) Expression levels of the different transfected Gα_z subunits in G protein activation assays were determined by western blotting. A representative western blot is shown from cell lysates of 3 experiments. (D) G protein deactivation of Gα_z-WT (orange circles) and Gα_z-S42G (grey squares) over time. Flp-In-293-D₂R cells transfected with the BRET sensor and Gα_z-wt or Gα_z-S42G were incubated for 18 minutes with 333nM ropinirole followed by injection with 20μM spiperone (antagonist) and changes in BRET were measured over time. All values represent mean ± SEM (light grey lines indicate error bars) of 6 (Gα_z-WT) or 4 (Gα_z-S42G) separate experiments performed in triplicate wells. (E) G protein deactivation rates the Gα_z-WT (orange bar) or Gα_z-S42G (grey bar) determined by one phase decay curve fit of the responses shown in panel D. Rate values are represented as mean ± SEM. (F) Concentration response curves for D₂R mediated activation of Gα_z-WT (orange circles) or Gα_z-S42G (grey squares) measured 15 minutes after addition of increasing concentrations of ropinirole. (G) Potency changes over 30 minutes of Gα_z-WT (orange circles) or Gα_z-S42G (grey squares) activation plotted as pEC₅₀ parameter values estimated from concentration response curves fitted at each measurement interval after stimulation of increasing concentrations of ropinirole. All values in panels F & G represent mean ± SEM of 4 separate experiments performed

in duplicate wells. Students unpaired t test was used to determine statistical significance between rates of $G\alpha_z$ -WT and $G\alpha_z$ -S42G. *** $P < 0.001$.

Next, we performed cAMP assays using cells expressing either $G\alpha_z$ -WT or $G\alpha_z$ -S42G. Similar to our observations in the G protein activation assay, we observed that the potency of ropinirole remained constant over time when the S42G mutant was expressed, while the potency increased in the presence of the WT G protein. Comparing concentration response curves obtained at a 15-minute timepoint we found that ropinirole displayed a statistically significant decrease in potency ($pEC_{50} = 6.95 \pm 0.1318$, $P = 0.00015$, student's t test) and maximal effect ($E_{max} = 65.44 \pm 4.014$ % FSK induced cAMP inhibition, $P = 0.0013$, student's t test) when $G\alpha_z$ -S42G was expressed as compared to the $G\alpha_z$ -WT condition (Fig. 5.6A & B). Expression levels of $G\alpha_z$ -S42G were comparable to wild-type in this assay (Fig. 5.6C). These data support our findings in the G protein activation assay; illustrating how the slow GTP hydrolysis rate of $G\alpha_z$ has a profound influence on agonist potency in a time-dependent manner.

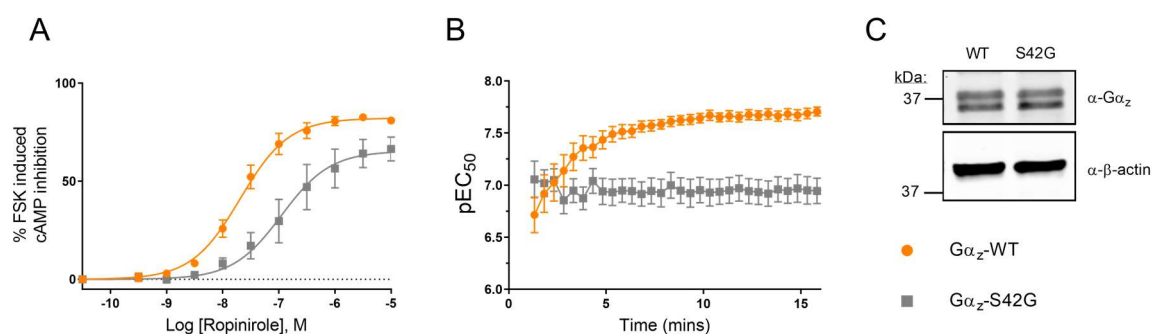


Figure 5.6: Mutation of serine 42 abolishes potency increase when measuring $G\alpha_z$ -dependent cAMP inhibition. (A) cAMP production inhibition concentration response curves of Flp-In-293- D_2R cells transfected with cDNA encoding the cAMP BRET sensor together with $G\alpha_z$ -WT (orange circles) or $G\alpha_z$ -S42G (grey squares) measured at 15 minutes after stimulation with increasing concentrations of ropinirole. (B) Potency changes of $G\alpha_z$ -WT (orange circles) or $G\alpha_z$ -S42G (grey squares) transduced cAMP production inhibition plotted as pEC_{50} parameter values estimated from concentration response curves fitted at each measurement interval after stimulation of increasing concentrations of ropinirole. Values in A & B represent mean \pm SEM of 7 ($G\alpha_z$ -WT) or 4 ($G\alpha_z$ -S42G) separate experiments performed in duplicate wells. (C) Expression levels of the different transfected $G\alpha_z$ subunits in cAMP production inhibition assays were determined by western blotting. A single representative western blot is shown from three separate experiments.

A mutation that decreases the GTP hydrolysis rate of $G\alpha_{i2}$ confers changes in agonist potency over time.

To demonstrate the relationship between GTP hydrolysis rate and time-dependent changes in agonist potency we replaced the conserved glycine residue within the P-loop of $G\alpha_{i2}$ with a serine

residue that is present in G α_z . We hypothesized that this mutation would confer a G α_z -like slow GTP hydrolysis rate that would in turn cause an increase in ropiniroles' potency over time. Indeed, estimates of potency increased over time in the G α_{i2} -G42S condition and no increase in ropiniroles' potency was observed in the WT G α_{i2} condition (Fig. 5.7B). This potency increase was analogous to ropinirole induced activation of wild type G α_z - albeit on a faster timescale (Fig. 5.7B). When measuring the G protein activation response after 15 minutes, the G42S mutation within the P-loop of G α_{i2} increased ropiniroles' potency by over 10-fold as well as increasing the maximal effect (pEC₅₀ = 7.64 ± 0.05 , $E_{\max} = 11.11 \pm 0.22 \times 10^{-2}$ BRET units) (Fig. 5.7A). Moreover, the rate of signal decay after competition of ropinirole with spiperone was slowed by approximately 20-fold ($K_{\text{deact}} = 8.31 \pm 0.30 \times 10^{-3} \text{ s}^{-1}$) compared to wild type G α_{i2} (Fig. 5.7C & D). In summary, upon replacement of glycine 42 for serine, the change in potency over time resembled that obtained in the presence of G α_z .

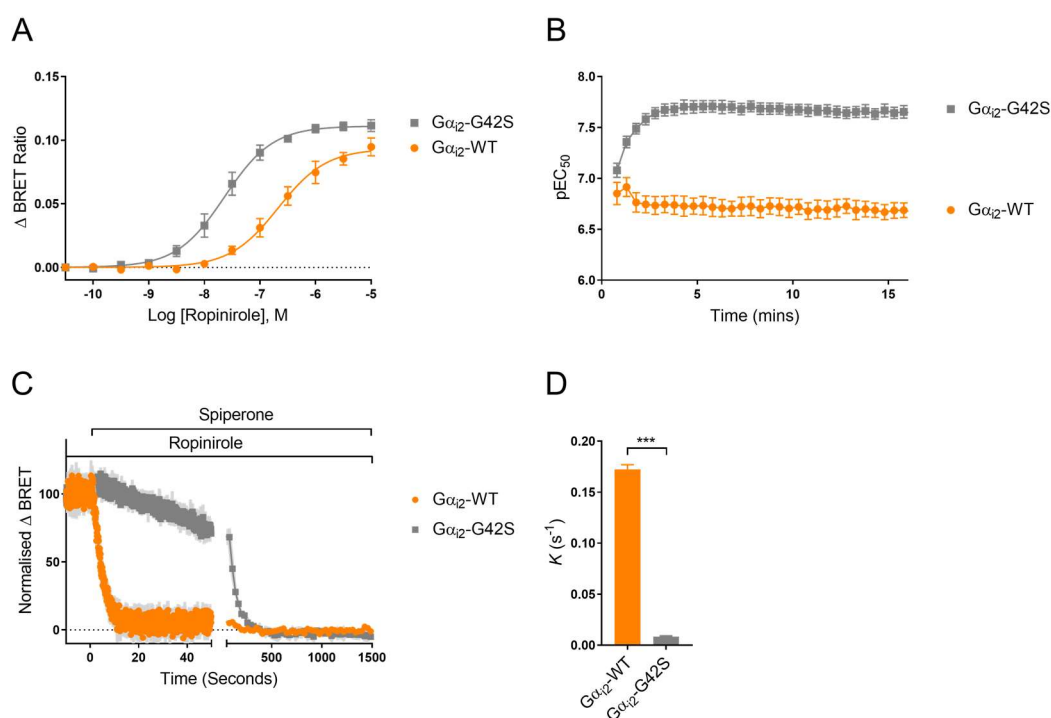


Figure 5.7: Mutation of glycine 42 to serine in G α_{i2} increases the active lifetime of the G protein. (A) Concentration response curves for D₂R mediated activation of G α_{i2} -WT (orange circles) or G α_{i2} -G42S (grey squares) measured 15 minutes after addition of increasing concentrations of ropinirole. (B) Potency changes over time of G α_{i2} -WT (orange circles) or G α_{i2} -G42S (grey squares) activation plotted as pEC₅₀ parameter values estimated from concentration response curves fitted at each measurement interval after stimulation of increasing concentrations of ropinirole. All values in panel A & B represent mean \pm SEM of 3 separate experiments performed in duplicate wells. (C) G protein deactivation of G α_{i2} -WT (orange circles) or G α_{i2} -G42S (grey squares) over time. Flp-In-293-D₂R cells transfected with the BRET sensor and G α_{i2} -WT or G α_{i2} -G42S were incubated for 18 minutes with 333nM ropinirole followed by injection with 20 μ M spiperone (antagonist) and changes in BRET were measured over time. All values represent mean \pm SEM (light grey lines indicate error bars) of 6 (G α_{i2} -WT) or 3 (G α_{i2} -G42S) separate experiments performed in triplicate wells. (D) G

protein deactivation rates of Gα_{i2}-WT (orange bar) or Gα_{i2}-G42S (grey bar) determined by one phase decay curve fit of the responses shown in panel C. Students unpaired t test was used to determine statistical significance between deactivation rates of Gα_{i2}-WT and Gα_{i2}-G42S. *** $P < 0.001$.

Co-expression of RGS proteins alters agonist potency over time

Having identified that the GTP hydrolysis rate of the Gα subunit is crucial in determining the agonist response over time, we were then interested in investigating the temporal effects that RGS proteins could have on the D₂R mediated responses. RGS proteins selectively bind to activated Gα-GTP subunits acting as GTPase-activating proteins (GAPs) to increase the Gα subunits' rate of GTP hydrolysis (362,363). By doing this, the RGS protein speeds up the rate of G protein deactivation within the G protein cycle. It is well appreciated that RGS proteins functioning in this manner can dampen the potency at a G protein-dependent signalling endpoint. Extending this, we wanted to determine the effect that RGS proteins have on the increase in agonist potency over time that we observe when measuring Gα_z activation. We therefore performed G protein activation assays where we co-expressed RGS9-2 or RGS20. RGS9-2 is an RGS9 splice variant that is strongly co-localised with the D₂R in the striatum where it regulates some D₂R functions (364,365). RGS20 is a member of the RGS-Z family of RGS proteins; RGS17, RGS19 and RGS20, that selectively act on Gα_z (366-369).

When assessing the responses 15 minutes after ropinirole stimulation, we observed that RGS9-2 and RGS20 had different effects depending on the Gα subunit being activated. When Gα_{i2} was activated, the maximal effect was significantly decreased in the presence of both RGS9-2 and RGS20 (Fig. 5.8A & Table 5.6). RGS20 also significantly reduced the potency of Gα_{i2} activation by approximately half a log-unit, while the small reduction in potency caused by RGS9-2 was not statistically significant. Measuring Gα_{oA} activation, we observed that both the maximal effect and the potency were significantly reduced by RGS9-2 and RGS20 (Fig. 5.8B & Table 5.6). Although, Gα_{oA} activation was more impacted in the presence of RGS9-2 than it was by RGS20. The largest effect we observed by any RGS protein acting on a Gα subunit was the potency decrease induced by RGS20 on Gα_z (Gα_z-pcDNA pEC₅₀ = 7.88 ± 0.05 , Gα_z-RGS20 pEC₅₀ = 6.81 ± 0.04 , mean ± SEM). RGS20 decreased the potency by approximately 10-fold, and also decreased the maximal effect of the response. Contrasting this, RGS9-2 had no effect on Gα_z activation relative to the pcDNA control (Fig. 5.8C & Table 5.6).

We next assessed the effect of RGS9-2 and RGS20 on potency estimates over time. Gα_{i2} and Gα_{oA} displayed altered potencies in the presence of either RGS9-2 and RGS20, however their potencies remained constant over time (Fig. 5.8D & E). This suggests that the Gα_{i2} and Gα_{oA} systems

quickly come to a condition that resembles a steady state. Furthermore, activation of G α_z in the pcDNA control condition displayed a large increase in potency over time that was consistent with our earlier experiments. The co-expression of RGS9-2 had no effect on this increase in potency. In contrast, however, in the presence of RGS20, the potency of ropinirole in the G α_z activation response did not increase in potency over time (Fig. 5.8F). This implies that GTP hydrolysis rate of G α_z was increased by RGS20, thus inhibiting the large accumulation of the active G α -GTP species that mediates the increase in agonist potency in the control condition.

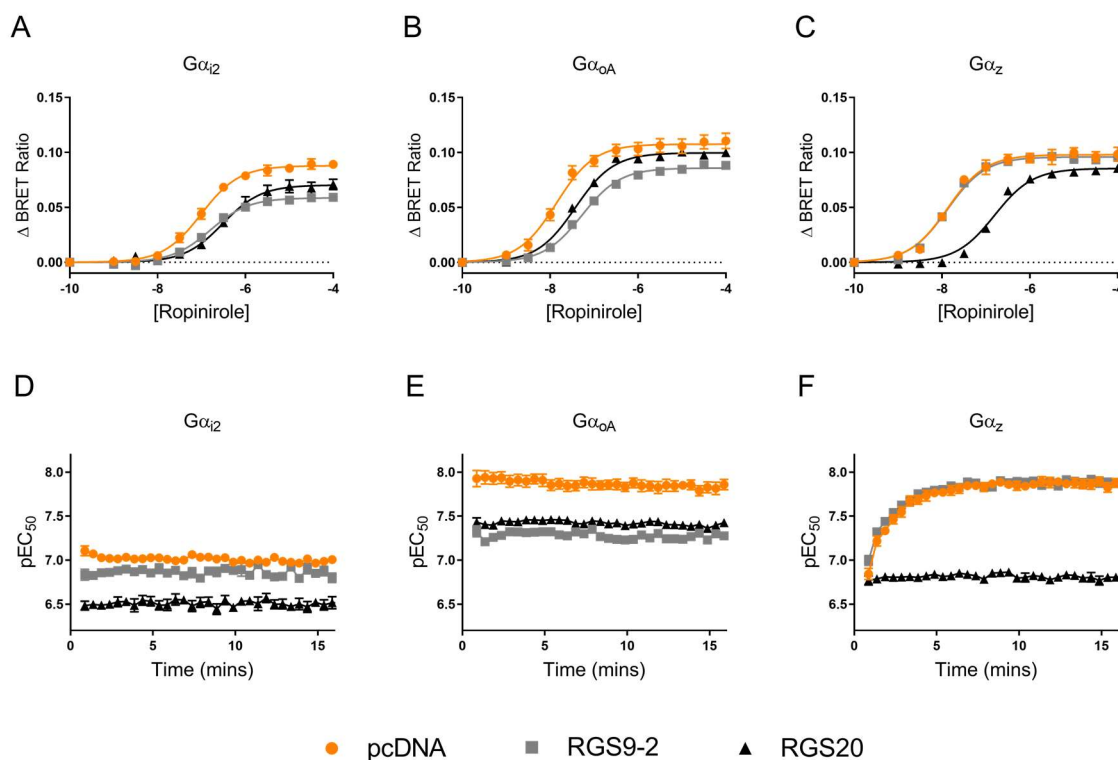


Figure 5.8: RGS protein co-expression alters D₂R mediated G α_{i2} , G α_{oA} and G α_z activation responses over time. (A, B & C) G α_{i2} (A), G α_{oA} (B) and G α_z (C) activation responses mediated by the D₂R 15 minutes after stimulation with increasing concentrations of ropinirole in the presence of transfected pcDNA control (orange circles), RGS9-2 (grey squares) or RGS20 (black triangles). Data represents the mean \pm SEM of 3 separate experiment for all. (D, E & F) Potency (pEC₅₀ parameter) values plotted over time after stimulation with ropinirole for G α_{i2} (D), G α_{oA} (E) and G α_z (F) activation in the presence of pcDNA control (orange circles), RGS9-2 (grey squares) or RGS20 (black triangles). Concentration response curves were determined at each timepoint as shown in panels A, B and C and the pEC₅₀ values were taken and plotted over time. Data represents the mean \pm SEM from 3 separate experiments for each data set. G β_5 s was co-transfected in all conditions for consistency as it forms a complex with RGS9-2.

Table 5.6: Ropinirole induced activation of G proteins by the D₂R in the presence of RGS proteins.

Potency (pEC₅₀) and maximal effect (E_{\max} – BRET units) parameter values were determined 15 minutes after ropinirole stimulation and represent the mean \pm SEM from 3 separate experiments

G α subunit	pcDNA		RGS9-2		RGS20	
	pEC ₅₀	E_{\max}	pEC ₅₀	E_{\max}	pEC ₅₀	E_{\max}
G α_{i2}	7.01 \pm 0.04	8.79 \pm 0.14 x10 ⁻²	6.80 \pm 0.05	5.86 \pm 0.12 x10 ⁻² b	6.52 \pm 0.07 b	7.03 \pm 0.20 x10 ⁻² b
G α_{oA}	7.86 \pm 0.06 a	10.75 \pm 0.20 x10 ⁻² a	7.28 \pm 0.03 a, b	8.58 \pm 0.08 x10 ⁻² a, b	7.43 \pm 0.03 a, b	9.96 \pm 0.11 x10 ⁻² a, b
G α_z	7.88 \pm 0.05 a	9.79 \pm 0.16 x10 ⁻² a	7.88 \pm 0.04 a	9.58 \pm 0.11 x10 ⁻² a	6.81 \pm 0.04 a, b	8.54 \pm 0.13 x10 ⁻² a, b

^a Significantly different (P<0.05) from corresponding G α_{i2} value within the column as determined by one-way analysis of variance with Dunnett's multiple comparisons test

^b Significantly different (P<0.05) from corresponding 'pcDNA condition' parameter value within the row as determined by one-way analysis of variance with Dunnett's multiple comparisons test

5.4 Discussion

A particular focus of the GPCR drug discovery field has been to ascertain how specific GPCRs can transmit unique intracellular signals while only activating a handful of communal effectors. In the present study, we reconstituted the D₂R with individual G α_i proteins in live cells to assess the G protein signalling in a temporal manner. Stimulation with two different agonists yielded varying G protein signalling profiles depending on the agonist efficacy and binding kinetics to the D₂R. In addition, G protein signalling was also highly dependent on the biochemical properties of the specific G protein α subunit. In this manner, we observed a D₂R-G α_z signalling wave that was kinetically distinct from G α_i or G α_o signalling.

The slow amplification of D₂R-G α_z signalling, manifesting as an increase in potency over time, occurs by a mechanism involving the slow GTP hydrolysis rate of G α_z that leads to an accumulation of the active G α_z -GTP species over time. Indeed, ropinirole and aripiprazole, when activating G α_z , increased in potency over time approximately 10- and 140-fold respectively. Such an increase in the potency of ropinirole and aripiprazole can only partly be attributed to the relatively slow dissociation rate from the D₂R of the latter and this mechanism could not explain the behaviour of ropinirole, a fast dissociating agonist. By rapidly 'switching off' the D₂R with an antagonist, we were able to monitor the deactivation rate of the different G protein α subunits. This revealed that G α_z slowly deactivates in live cells. This slow deactivation of G α_z has been observed before (354,370). We were able, through both mutagenesis of the P-loop as well as a secondary approach using co-expression with RGS20, to demonstrate that the slow deactivation of G α_z and the increase in agonist potency over time are due to its slow GTP hydrolysis rate. This was confirmed by

conferring the slow GTP hydrolysis rate into Gα_{i2} via mutagenesis, that conferred an increase in potency over time similar to that observed at Gα_z.

Our data demonstrate that the slow GTP hydrolysis rate of Gα_z occurs in live cells, implying that this characteristic may serve a physiological role. Indeed, the Ser42 residue of Gα_z that we demonstrate confers this slow hydrolysis rate is within the P-loop motif of the G protein α subunit. As a key determinant of the GTPase activity, the P-loop has significant evolutionary pressure on it, hence, it is highly conserved across all G proteins. Therefore, it must be evolutionarily favourable to harbour a G protein within an organisms' genome that has a slow deactivation rate for some particular function(s). We postulate that Gα_z may be upregulated and coupled to by GPCRs when a slow signalling pattern is desired as opposed to a fast signalling response. This may be a logical purpose for Gα_z considering that Gα_z has similar downstream effectors to the other Gα_i subfamily members and as such would not elicit a distinct biochemical response. Indeed, a previously suggested function of Gα_z has been that the sustained signalling pattern of Gα_z could be useful in regulating the slow control of the circadian clock by GPCRs such as GPR176 (371-373). Additionally, the expression of Gα_z mRNA in mice appears to be upregulated perinatally and decreases over time into adulthood (374). Therefore, the slow G protein signalling via Gα_z coupling to the D₂R may be dependent on developmental stage. Furthermore, studies have shown unique patterns of Gα_z expression in intracellular compartments (375-377). In addition to being localised to the plasma membrane, Gα_z in Purkinje cells was shown to be localised to the outer membrane of the nuclear envelope, the endoplasmic reticulum and microtubules (375). It has further been determined that Gα_z in the sciatic nerve can transport from the axon to the soma (retrograde axonal transport)(376,377). This leads one to hypothesise that the slow deactivation rate of Gα_z may allow GPCR-activated Gα_z to translocate from the plasma membrane to intracellular compartments for a sustained period to serve a distinct signalling role. Of course, this all must be considered in the context of RGS protein expression as our data illustrates that RGS20 can act on D₂R-activated Gα_z to increase the turnover rate. Thus, Gα_z may behave as a fast cycling G protein when co-expressed with specific RGS proteins or exist as a slow cycling G protein when no such RGS proteins are present. It is possible then, that the relative expression of Gα_z and its cognate RGS proteins may allow for fine tuning of temporal responses downstream of Gα_{i/o/z} coupled GPCRs in individual tissues.

The relative potency and maximal effect values suggest that perhaps there is an underappreciated role for the D₂R to signal through Gα_z in vivo. This contrasts with the most accepted view, that the D₂R predominantly exerts its' in vivo effects through the Gα_o isoforms (140). Certainly, in line with this historical view, our data showed that the D₂R couples more efficiently to Gα_{oA} and Gα_{oB} isoforms than to Gα_{i1}, Gα_{i2} and Gα_{i3} as previously reported (139). However, our concentration-

response curves demonstrated that the D₂R can be as efficiently coupled to Gα_z as it is to the Gα_o isoforms. While it was previously known that the D₂R can couple to Gα_z (378), the selectivity of the D₂R for all the Gα_i subunits had not been quantitatively assessed in the same system. This selectivity pattern implies that the D₂R may couple to Gα_z natively. Furthermore, the evidence supporting Gα_o as the main G protein transducer for the D₂R is largely based around one study by Jiang and colleagues (140). They reported that high affinity agonist binding at the D₂R was not present in membranes prepared from the brains of Gα_o knockout mice but it was present in the Gα_{i1}, Gα_{i2} and Gα_{i3} knockouts (140). Importantly, there are some limitations of this work: First, this study did not specifically investigate Gα_z coupling. Second, Gα_o is likely the most prevalent subunit in the brain and as such its effects are more easily measured than the other Gα subunits (141,142). Third, this direct agonist binding measurement provides an indication of agonist affinity for the receptor-G protein complex and as such, does not account for the proposed signal amplification associated with the longer lifetime of the active GTP-bound Gα_z G protein. Our data suggests that it is this step that contributes to the relatively high potency of agonists when the D₂R is coupled to Gα_z. Thus, Gα_z may have an unappreciated role in D₂R signalling that would not be detected by such an approach. D₂R-Gα_z coupling in vivo can be supported by data demonstrating that Gα_z is required for some D₂R mediated responses. For example, Van Den Buuse and colleagues (150), demonstrated that either amphetamine or apomorphine induced disruption of prepulse inhibition is enhanced in Gα_z knockout mice. The disruption of prepulse inhibition in mice induced by amphetamine and apomorphine is a D₂R dependent process (149,379). Therefore, this is direct evidence that D₂R signalling through Gα_z may play a role in sensorimotor gating. Moreover, in mice lacking Gα_z, the D₂-type selective agonist quinpirole is less effective at decreasing locomotor responses, inhibiting dopamine release in the nucleus accumbens, eliciting hypothermia and increasing plasma adrenocorticotrophic hormone (ACTH) (151). Additionally, Gα_z may couple to the D₂R in neuroendocrine systems. For example, Gα_z has been postulated to play a role in D₂R mediated inhibition of prolactin release from rat pituitary lactotrophs (148).

Having identified molecular and cellular evidence for a unique D₂R-Gα_z signalling wave, future studies could aim to investigate this in vivo and with additional GPCRs. Whole mouse genetic knockout studies have suggested a role for D₂R-Gα_z signalling in the brain (150,151). This may be a crude approach to investigate the dependence of Gα_z in some D₂R mediated behaviours. Given that we now recognise an important functional difference of Gα_z in its slow GTPase activity, a more targeted approach to investigate Gα_z could be to use gene editing technologies to alter the GTPase activity of Gα_z in vivo. D₂R-dependent behaviours could then be assessed to understand the role the slow GTP hydrolysis rate plays. Additionally, both the D₂R and Gα_z have separately been studied for

their role in metabolism. The D₂R and G α_z are expressed in pancreatic beta cells where they can modulate glucose-stimulated insulin secretion (146,147). Therefore, it could be worthwhile investigating whether the D₂R can couple to G α_z in such a system. Furthermore, given that the distinct D₂R-G α_z signalling wave we observed is in fact largely independent of the properties of the D₂R, other G α_z coupled receptors are worth investigating such as the serotonin, opioid, melatonin and α -adrenergic receptors (378,380-382). It would be of importance to determine whether an increase in potency over time is also observed upon activation of G α_z by these GPCRs.

Detailed measurement of agonist-stimulated D₂R-mediated G protein activation kinetics revealed that a saturating concentration of ropinirole stimulated activation of all tested G α subunits with an observed rate that was statistically faster than aripiprazole stimulation. This is consistent with previous studies of GPCRs in which increasing agonist efficacy has been associated with faster nucleotide exchange rates (383,384) as well as observed G protein dissociation rates (385). The data in this study, although confined to just one high efficacy and one partial agonist, is in agreement with such a relationship between G protein heterotrimer dissociation rate and agonist efficacy at the D₂R. Moreover, we found some nuances in the different agonist induced observed activation rates. Indeed, aripiprazole disproportionately activated G α_{i2} at a faster observed rate relative to G α_{oA} or G α_z subunits as compared to ropinirole's relative rate of activation of these subunits. It is important to understand that this observed rate is a multiple of the rates within the G protein cycle and not simply dependent on the GEF ability of the agonist bound D₂R. Consequently, we hypothesise that this faster relative rate of aripiprazole acting at G α_{i2} is due to the G protein cycle being less perturbed by aripiprazole, and therefore, it finds a new equilibrium more quickly. In line with this, aripiprazole displayed a lower maximal effect when activating G α_{i2} relative to ropinirole when compared to G α_{oA} or G α_z activation. Our estimated deactivation rate of G α_z was about 50-fold slower than G α_{oA} , whereas a previous study documented G α_z as having a 200-fold slower GTP hydrolysis rate (19). While the two assay readouts are different, the deactivation rate is entirely dependent on the GTPase rate. We believe this discrepancy may reflect differing experimental conditions in our BRET experiments as compared to the previous GTP hydrolysis assays (19). The experiments in this study, were performed in live mammalian cells at 37°C compared to the GTP hydrolysis assays performed at 30°C on G α_z purified from *E.coli* (19). Furthermore, being in live cells, our assays may be impacted by regulatory proteins within the cell and also the relative concentrations of all the signalling components within the system. We transfected constant amounts all components however it is difficult to have identical expression and localisation between the different transfection conditions. While the components within the GTP hydrolysis assays can be tightly controlled, the assays will be more influenced by the buffer conditions that can influence the G proteins differently.

‘Perfect’ biased agonism describes an observation where an agonist acting at a particular receptor can activate one signalling pathway while entirely avoiding activating another pathway whereas other non-biased agonists might display activity at all pathways. Such observations can be confounded by so called system bias. In this case a weak partial agonist might have robust activity at a particularly well coupled signalling endpoint but no measurable activity at a less efficiently coupled endpoint. While previous studies have suggested that ‘perfect’ biased agonism can occur at the D₂R, our measurements of the responses of the weak partial agonist aripiprazole are not consistent with this notion. To date the majority of studies investigating both agonist efficacy and G protein selectivity at the D₂R have used [³⁵S]GTPγS binding assays to measure G protein activation (19,386). [³⁵S]GTPγS assays have often failed to detect activation of either Gα_{i1}, Gα_{i2} or Gα_{i3} by the D₂R when stimulated with partial agonists even when overexpressing G proteins or using receptor-G protein fusions (137-139), inferring that some agonists can selectively activate Gα_o isoforms without activating Gα_i subunits. In contrast, we could detect robust responses induced by the weak partial agonist aripiprazole in the live cell BRET assay. We attribute this to the increased sensitivity in the new BRET assay as opposed to older methods. It would be interesting, therefore, to reassess such historical observations of bias using this more sensitive approach.

In conclusion, we showed that kinetically distinct G protein signalling waves transduced by the D₂R are determined by the nature of the agonist and the G protein. Agonists acting at the D₂R can induce distinct signalling patterns based on their efficacy and binding kinetics. On the other hand, we identified that the GTP hydrolysis rate of the G protein is crucial in determining the temporal response. In particular, we observed a distinct signalling wave mediated by Gα_z due to its considerably slower GTPase activity than all other Gα subunits. These findings bring increased importance to D₂R-Gα_z coupling as it may serve as a novel signalling platform to coordinate a unique response from the D₂R.

5.5 Supplementary Materials

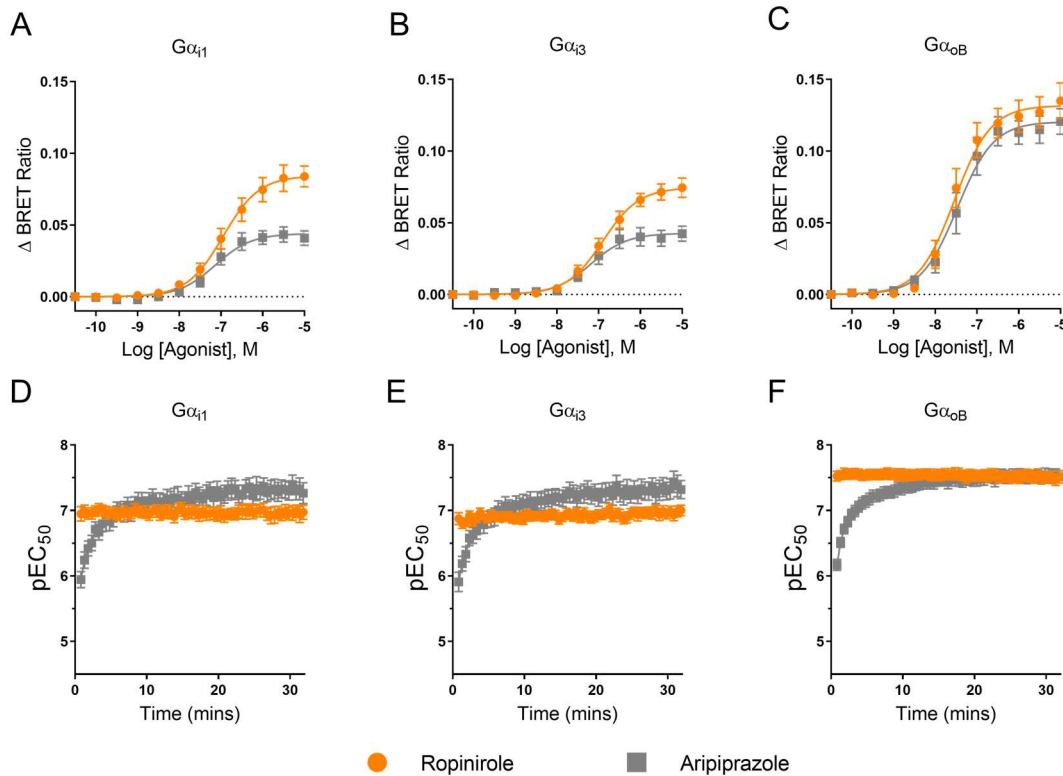


Figure S5.1: G protein activation of $G\alpha_{i1}$, $G\alpha_{i3}$ and $G\alpha_{oB}$ over time by the D₂R. (A, B & C) Concentration response curves of cells transfected with the G protein activation sensors together with $G\alpha_{i1}$ (A), $G\alpha_{i3}$ (B) or $G\alpha_{oB}$ (C) measured at 15 minutes in response to increasing concentrations of ropinirole (orange circles) or aripiprazole (grey squares). (D, E & F) Potency changes over 30 minutes of $G\alpha_{i1}$ (D), $G\alpha_{i3}$ (E) or $G\alpha_{oB}$ (F) activation plotted as pEC₅₀ parameter values estimated from concentration response curves fitted at each measurement interval after stimulation of increasing concentrations of ropinirole (orange circles) or aripiprazole (grey squares). All values are expressed as mean \pm SEM from 5 separate experiments performed in single wells.

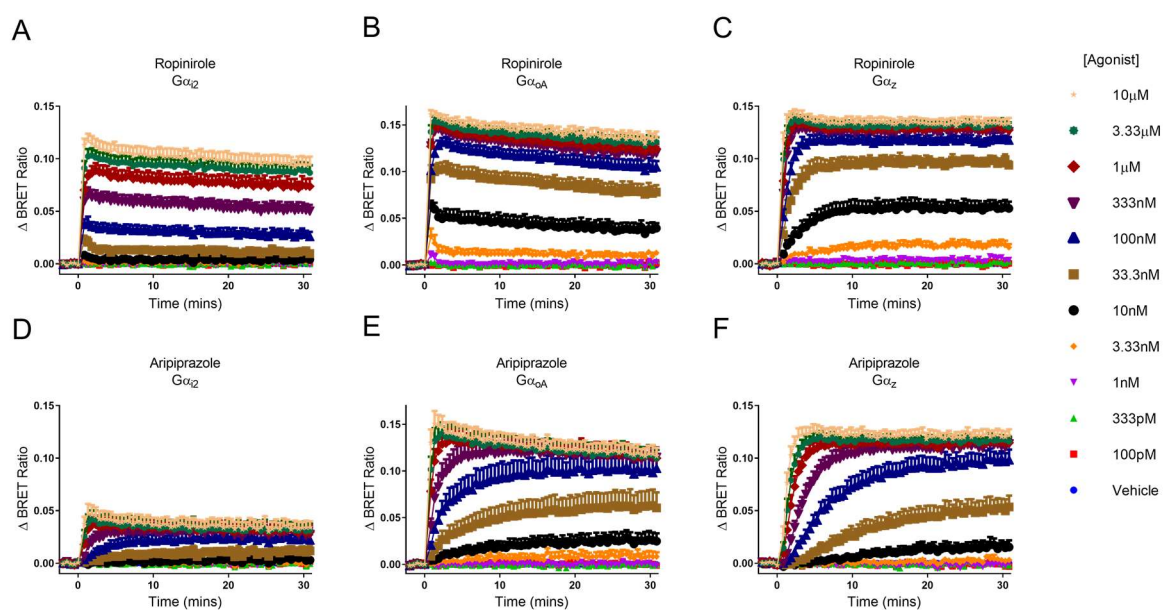


Figure S5.2: Examples of G protein activation increase in BRET responses over time used for potency estimates. (A, B & C) Ropinirole induced D₂R G protein activation responses over 30 minutes at G α_{i2} (A), G α_{oA} (B) or G α_z (C). (D, E & F) Aripiprazole induced D₂R G protein activation responses over 30 minutes at G α_{i2} (D), G α_{oA} (E) or G α_z (F). All values are expressed as mean \pm SEM from 5-9 separate experiments performed in single wells.

Chapter 6:

**A pertussis toxin-like protein tool for
occluding inhibitory G protein signalling
including $G\alpha_z$**

Abstract

Heterotrimeric G proteins are the main effector for G protein coupled receptors, including the D₂R. Consequently, understanding G proteins' functions is key to understanding how signalling responses and physiological effects of GPCRs emerge. A useful method for interrogating G proteins' functions has been to use bacterially derived AB₅ toxins, such as pertussis toxin, to inhibit their coupling and then evaluate the downstream changes. In chapter 3, some of the largest apparent biased agonism was observed between the well coupled G protein; G α_z , and the poorly coupled regulatory proteins. Additionally, we identified in chapter 5 that G α_z mediates a distinct signalling wave from the D₂R that is slow and sustained. Together these results advocated for further investigations of D₂R-G α_z signalling. However, G α_z signalling has been historically neglected due to a lack of inhibitor tools available to study it. Therefore, in the present chapter we develop a new pertussis toxin-like tool that can inhibit G α_i subfamily G proteins, including G α_z . In addition, we characterise G α subunits that are insensitive to the toxin to serve as tools in combination with the toxin. Used in the appropriate manner these tools will aid our laboratories' studies on D₂R-G α_z coupling. In addition, these tools should prove useful to the wider communities' general GPCR-G α_i and GPCR-G α_z signalling studies.

6.1 Introduction

Heterotrimeric guanine nucleotide-binding proteins (G proteins) are signalling transducers that link cell surface receptors to intracellular effectors. Heterotrimeric G proteins are localised to the intracellular side of the plasma membrane where they can be activated by G protein-coupled receptors (GPCRs). Agonists such as neurotransmitters, hormones, odorants or light can induce a conformational change in the transmembrane domains of GPCRs (7). This allows the G protein to couple to the GPCR, activate and then act on effectors downstream such as adenylyl cyclases, phospholipase C isotypes and ion channels (387-389).

Heterotrimeric G proteins consist of a $G\alpha$ subunit that has a guanine nucleotide-binding domain, as well as a $G\beta$ and $G\gamma$ subunit that function as an obligate dimer. The $G\alpha$ subunit is responsible, to a large degree, in determining the specificity of the interaction with the activated GPCR. Upon coupling, an important interaction is made between the carboxy-tail of the $G\alpha$ and the intracellular side of the active GPCR (8,9). Following this, the G protein becomes active by the $G\alpha$ subunit exchanging bound guanosine diphosphate (GDP) for guanosine triphosphate (GTP) and dissociating from, or rearranging relative to the $G\beta\gamma$ dimer (10,390). Having dissociated, the $G\alpha$ and $G\beta\gamma$ subunits are then able to act on downstream effectors (387-389).

$G\alpha$ subunits consist of four subfamilies ($G\alpha_s$, $G\alpha_i$, $G\alpha_q$ and $G\alpha_{12}$) based on sequence similarity. The functions of the $G\alpha$ subunits can be broadly generalised based on their subfamily classification. The stimulatory $G\alpha_s$ subfamily stimulates adenylyl cyclases to produce cyclic adenosine monophosphate (cAMP), in contrast, inhibitory $G\alpha_i$ subunits are able to inhibit adenylyl cyclases (349,387). The $G\alpha_q$ subfamily activates phospholipase C- β leading to increases in cytosolic Ca^{2+} , and the $G\alpha_{12}$ subfamily can activate Rho family GTPases that regulate cytoskeletal processes (388,391). However, the intricate functions of the individual subunits within each subfamily is far more complex than this. Understanding the details of how each subunit interacts with and regulates specific effectors is central to our comprehension of basic cellular signalling systems. Likewise, it is important to determine the role each individual $G\alpha$ subunit plays in controlling particular physiological processes.

One inhibitory $G\alpha$ subunit of interest is $G\alpha_z$ because it displays some divergent characteristics. $G\alpha_z$ is a $G\alpha_i$ subfamily member that was identified in 1988 (392,393), just prior to the $G\alpha_q$ and $G\alpha_{12}$ subfamilies (394,395). It was shown that $G\alpha_z$ has a slow GDP-GTP exchange rate, slow GTP hydrolysis rate, unique Mg^{2+} dependence, and a restricted pattern of expression (19,147,392,393). Despite these unique biochemical characteristics, only a handful of reports have shed light on the functions of $G\alpha_z$. While Kimple and colleagues have built a body of knowledge around $G\alpha_z$'s role in the pancreas (147,396-398), the functions of $G\alpha_z$ in other tissues largely remain elusive. This neglect of $G\alpha_z$ may be due to the lack of molecular tools for investigating its function.

AB₅-type toxins have been attractive tools for the interrogation of mechanisms of signalling. AB₅ toxins are virulence factors commonly secreted by pathogenic bacterial species. The toxins are characterised by a hetero-hexameric structure consisting of a single A subunit and pentameric ring of B subunits. The A subunit is an enzymatically active subunit that acts on a host protein within the cell to modulate the hosts' behaviour. The B subunits are responsible for recognition of host cell receptors on the cell surface, aiding in cellular entry. AB₅ toxins can have a varied functions on their targets to modulate host cell behaviour such as protease activity (399), RNA N-glycosidase activity (400) and NAD⁺-dependent ADP-ribosylation (401). While there are many AB₅ toxins with a range of host protein targets, there are currently only a few of known interest to the G protein signalling field. Cholera toxin (CTX) acts on the G α_s subfamily and renders G α_s subunits constitutively active (402). Pasteurella multocoda toxin (PMT) has been identified to deamidate members of the G α_i , G α_q and G α_{12} family, rendering them constitutively active (403). Pertussis toxin (PTX), from *Bordetella pertussis*, the organism responsible for whooping cough, can actively ADP-ribosylate the members of the G α_i subfamily, except for G α_z (404). The ADP-ribosylation by PTX occurs on a cysteine residue near the carboxy-tail of G α_i subunits, rendering them incapable of coupling to GPCRs. Cell signalling researchers have exploited the actions of CTX and PTX for decades to identify the G α subunits responsible for certain cell signalling and phenotypic phenomena.

A recent publication by Littler and colleagues (405), reported the identification and structural characterisation of a novel PTX-like protein derived from a uropathogenic *Escherichia coli*. The toxin has an active A subunit homologous to PTX and has maintained a similar overall structural fold (Fig. S6.1A & B). When using G α_{i2} as a substrate in vitro, the novel toxin was shown to have a distinct site of ADP-ribosylation from that of PTX (405). The toxin ADP-ribosylated an asparagine residue eight amino acids from the carboxy tail, as well as a lysine residue ten amino acids from the carboxy tail. Interestingly, the toxins' asparagine site - approximately one turn below PTXs' cysteine site - is conserved across several heterotrimeric G α subunits, suggesting that the toxin may have broader substrate specificity than PTX (Fig. 6.1A & B).

In the present study, we demonstrate that the newly described toxin can inhibit the coupling of all G α_i subfamily members tested, including G α_z . Thus, we refer to it as G α O, G α Z and G α I inhibiting ToXin, or in short; OZITX. Additionally, we show that OZITX abolishes all G α_i subfamily mediated downstream inhibition of cAMP production. The active A subunit also remains functional upon transfection into mammalian cells, allowing for experiments without the need for toxin expression and purification. Moreover, we generate members of the G α_i subfamily that are OZITX insensitive, and hence, can serve as tools in combination with OZITX treatment. Overall, we believe OZITX will be a useful molecular tool in the future.

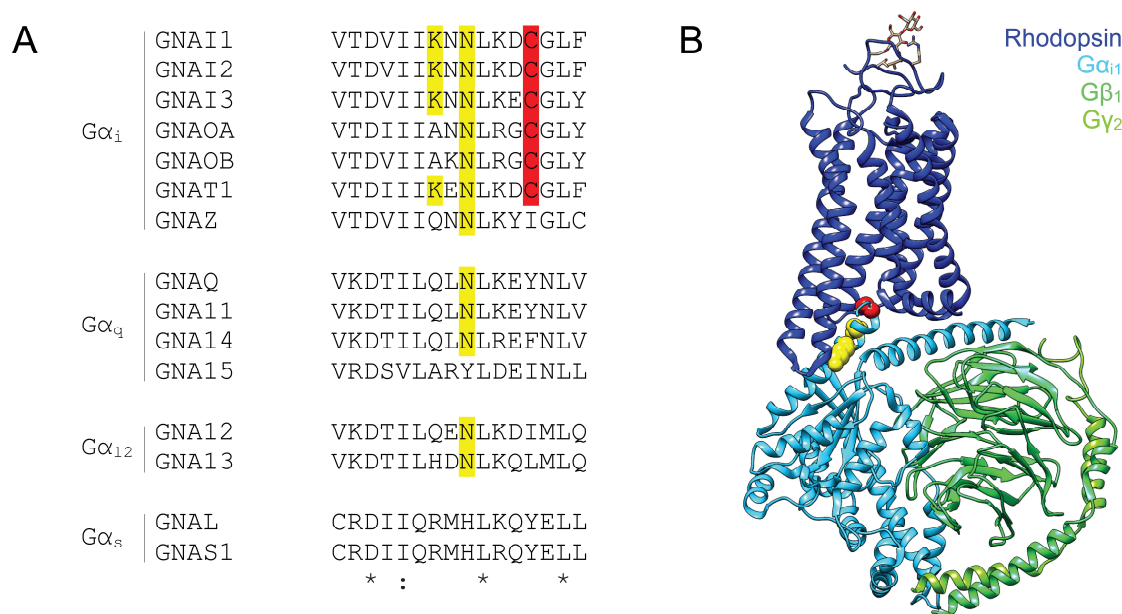


Figure 6.1: Identification of $G\alpha$ carboxy-tail amino acid residues that are putatively ADP-ribosylated by OZITX. (A) Amino acid sequence alignment of carboxy-terminal residues of heterotrimeric $G\alpha$ proteins. Cysteine residues ADP-ribosylated by PTX are indicated in red. Putative lysine and asparagine residues ADP-ribosylated by OZITX identified by Littler and colleagues(405) are indicated in yellow. The asparagine residue that is a putative substrate is conserved across many $G\alpha$ subunits. (B) The location of OZTX's and PTX's substrate amino acid sites within a GPCR-G protein complex. The structure of rhodopsin bound to $G\alpha_{i1}\beta_1\gamma_2$ is depicted in cartoon (PDB code 6CMO). Rhodopsin is shown in dark blue, $G\alpha_{i1}$ in light blue, $G\beta_1$ in green and $G\gamma_2$ in light green. The carboxy-terminal Cys³⁵¹ residue ADP-ribosylated by PTX is shown in red spheres. Lys³⁴⁵ and Asn³⁴⁷, the putative residues ADP-ribosylated by OZITX, are highlighted in yellow spheres. Graphic constructed using UCSF chimera.

6.2 Methods

Materials

Polyethylenimine (PEI), Linear (MW 25,000) was purchased from Polysciences, Inc. Ropinirole was purchased from BetaPharma (Shanghai) Co. Ltd. DAMGO ((D-Ala², N-Me-Phe⁴, Gly-ol⁵)-enkephalin)) was purchased from Mimotopes. SKF83822, neurotensin residues 8-13 (NT8-13), (-)-quinpirole hydrochloride (#1061), Acetylcholine chloride (#A2661), D-glucose (#G8270) and pertussis toxin (PTX) were purchased from Sigma-Aldrich. Isoproterenol (#1747) and endothelin-1 (#1160) was purchased from Tocris Bioscience (Bristol, UK). Coelenterazine-h was purchased from both NanoLight™ Technology and Dalton research molecules (#50303-86-9). Forskolin was purchased from Cayman Chemicals (#11018). Nano-Glo® luciferase assay system, containing the furimazine substrate, was purchased from Promega. Purified OZITX (EcPltAB) protein was a generous gift from Travis Beddoe, La Trobe University.

Plasmids

pcDNA3.1(+) encoding human constructs of: long isoform of the dopamine D₂ receptor (D₂LR), μ opioid receptor (MOPR), dopamine D₁ receptor (D₁R), neurotensin receptor 1 (NTS₁R), M₁ muscarinic acetylcholine receptor (M₁R), β_2 -adrenergic receptor (β_2 AR), endothelin A receptor (ET_AR), G α_{i1} , G α_{i2} , G α_{i3} , G α_{oA} , G α_{oB} , G α_z , G α_{sS} , G α_{sL} , G α_{olf} , G α_q , G α_{11} , G α_{14} , G α_{15} -EE, G α_{12} and G α_{13} were from the cDNA Resource Centre (cDNA.org). pcDNA3L-His-CAMYEL was purchased from ATCC (ATCC MBA-277). masGRK3ct-Nluc, masGRK3ct-Rluc8, venus-1-155-G γ_2 and venus-156-239-G β_1 were from Nevin Lambert, Augusta University. pCAGGS-Ric8A and pCAGGS-Ric8B were from Asuka Inoue, Tohoku University. The active S1 subunit of OZITX (*E_c*PltAB) was codon-optimized, synthesized and inserted into pcDNA3.1+. OZITX resistant mutations were made in G α_{i1} , G α_{i2} , G α_{i3} , G α_{oA} , G α_{oB} and G α_z using site directed mutagenesis. Primer sequences that were used for the mutagenesis can be found in Table 6.1.

Table 6.1: Primers for mutagenesis to create OZITX resistant G α subunits.

G α	C-terminal sequence	Primer Reverse with <i>Xho</i> I & <i>Xba</i> I digestion sites
G α_{i1}	TDV I IKN A LKDCGLF	CTAG C T C G A GTTAAAGAGACCACAATCTTTTAG A G C ATTTTTTA TGATGACATC
G α_{i2}	TDV I IKN A LKDCGLF	CTAG C T C G A GTTAAAGAGACCACAATCTTTTAG A G C ATTTTTTA TGATGACATC
G α_{i3}	TDV I IKN A LKECGLY	CTAG C T C G A GTCATAAAGTCCACATTCCTTTAA G G C GTTTTTAA TGATGACATC
G α_{oA}	TD I IIAN A LRGCGLY	CTAT C T A G A T C AGTACAAGCCGCAGCCCCGGAG G G C GTTGGCA ATGATGATG
G α_{oB}	TDV I IAK A LRGCGLY	CTAT C T A G A T C AGTAGAGTCCACAGCCCCGTAG G G C TTTGGCGA TGATGACATCTG
G α_z	TDV I IQN A LKYIGLC	CTAG C T C G A GTCAGCAAAGGCCAATGTACTTGAG A G C GTTCTGT ATGATGAC

OZITX resistant mutations were made by changing the eighth-last amino acid to an alanine (indicated in red) by using site-directed mutagenesis with the reverse primers used to the right, the alanine mutation change is shown in red and restriction site chosen in blue (*Xho*I) or green (*Xba*I). The constructs were inserted into pcDNA3.1+ with *Kpn*I and *Xho*I or *Xba*I as indicated.

Cell culture

HEK293T cells were purchased from ATCC (CRL-3216). HEK293A Δ G α -all CRISPR/Cas knockout cells and HEK293A Δ G $\alpha_{i/o}$ CRISPR/Cas knockout cells were a generous gift from Asuka Inoue, Tohoku University. HEK293T cells, HEK293A Δ G α -all cells and HEK293A Δ G $\alpha_{i/o}$ cells were cultured in T175 flasks with Dulbecco's Modified Eagle Medium (DMEM) + GlutaMAXTM-I (Gibco, Invitrogen, Paisley, UK) with 10% foetal bovine serum (Corning #35-010) and 1%

penicillin/streptomycin (Corning #30-002). All Cells were grown in a humidified incubator in 5% CO₂ at 37°C and sub-cultured at a ratio of 1/10-1/20.

Transfection

Briefly, cells were harvested from T175 flasks and plated into 6 well Nunc™ tissue culture plates at a density of 500,000 cells per well. The following day the media was removed and replaced with fresh media and transfected using PEI as the transfection reagent. The correct amounts of PEI and DNA were added to the buffer separately before mixing together, incubating for 20 minutes, and then adding dropwise on top of the cells in the fresh media.

For the G protein activation assays where the toxin was added exogenously: The HEK293A $\Delta G\alpha$ -all CRISPR knockout cells were transfected using PEI in a ratio of 6:1 PEI:DNA (w/w) in PBS. The cells were transfected with a cDNA mixture consisting of: 0.143 μ g GPCR, 0.286 μ g $G\alpha$, 0.143 μ g $G\beta_1$ -venus, 0.143 μ g $G\gamma_2$ -venus, 0.143 μ g masGRK3ct-Nluc and 0.143 μ g Ric8A or Ric8B or pcDNA3.1. The chaperone Ric8A was transfected together with $G\alpha_{14}$ and $G\alpha_{15}$ and Ric8B was transfected with $G\alpha_{olf}$.

For the cAMP BRET assays where the toxins were exogenously added: The HEK293A $\Delta G\alpha_{i/o}$ CRISPR knockout cells were transfected using PEI in a ratio of 6:1 PEI:DNA (w/w) in PBS. The cells were transfected with a cDNA mixture consisting of: 0.143 μ g D₂LR, 0.286 μ g $G\alpha_{i2}/G\alpha_{oA}/G\alpha_z$ /pcDNA3.1 and 0.429 μ g CAMYEL sensor.

Assays where the active A subunits of the toxins were transiently transfected had the following conditions: HEK293T cells were used and transfected using PEI in a ratio of 1.5 PEI: 1 DNA (w/w) mixed in 150mM NaCl. For the G protein activation assays the cells were transfected with $G\beta_1$, Venus- $G\gamma_2$ and masGRKctRluc8 as well as the $G\alpha$ subunit of interest together with a receptor suited for the specific G protein class and the chaperone proteins Ric8A for $G\alpha_{14}$ and $G\alpha_{15}$ and Ric8B for $G\alpha_{olf}$. For the cAMP production inhibition assays the cells were transfected with the CAMYEL sensor (ATCC MBA-277). For arrestin recruitment MeNArc assays (406), the cells were transfected with a membrane-anchor fused to the N-terminus of NanoLuc and β -arrestin-2 fused to the C-terminus, together with GRK2, D₂R and either the active subunit of PTX (PTX-S1), OZITX (OZITX-S1) or pcDNA3.1+ as a control.

G protein activation

G protein activation was measured using a BRET assay that monitors $G\beta\gamma$ release(257,258). The HEK293A $\Delta G\alpha$ -all cells were first transfected as described earlier and the following day the cells

were harvested and transferred into white 96 well CulturPlates (PerkinElmer) in DMEM +10% FBS. In the conditions where the cells were treated with OZITX or PTX, the cells were left to adhere before being treated in the 96 well plate 16-20 hours before performing the assay. The G protein activation assays were then performed approximately 24 hours after plating out the transfected cells. The media in each well was aspirated, washed with Hank's balanced salt solution pH7.4 (HBSS), replaced with HBSS and then kept at 37°C for the remainder of the assay. Furimazine was added with a multi-stepper pipette 15 minutes before agonist addition and left to equilibrate. The agonist was then added, and cells were incubated in a LUMIstar Omega (BMG Labtech) plate reader. The BRET measurements were then taken 2.5 minutes after agonist addition. Simultaneous dual emission filters were used in the LUMIstar Omega for detection of the luciferase at 445-505nm and venus at 505-565nm, all measured at 37°C. For G protein activation assays where the toxin active A subunit cDNAs were transfected, the same protocol was followed with some exceptions: HEK293T cells were used instead of CRISPR/Cas gene edited cells, DPBS + 5mM glucose was used as the assay buffer, 96 well black-white iso plates were used, and the plate was detected five minutes after agonist stimulation in a Pherastar FS (BMG Labtech). After acquiring the data, the ratio of the venus emission channel was then divided by the luciferase emission channel to determine the BRET ratio. The vehicle-subtracted raw BRET ratio (drug induced increase in BRET) is plotted for the G protein activation assay data.

cAMP production inhibition

The cAMP production inhibition assays' principle is based on the ability of a genetically encoded conformational BRET sensor to detect the relative concentrations of intracellular cAMP(358). Initially, the transfected HEK293A $\Delta G\alpha_{i/o}$ cells were harvested and transferred into white 96 well CulturPlates in DMEM +10% FBS 24 hours after the transient transfection. When the cells were treated with OZITX or PTX, this occurred in the 96 well plate after adherence and about 18 hours before the assay. Next, the cAMP inhibition assays were performed the following day after plating out the transfected cells and toxin or control treatment. On the day of the assay, the plate media was aspirated, washed once with HBSS pH 7.4 and replenished with HBSS pH 7.4 and then held at 37°C for the rest of the experiment. 5 μ M coelenterazine-h was added 15 minutes before agonist addition. 10 μ M Forskolin was added 10 minutes before agonist addition and the readings were then continuously taken in the live cells. Bioluminescence was detected on a LUMIstar Omega set to 37°C. Simultaneous dual emission filters were used for the BRET donor at 445-505nm and the acceptor at 505-565nm. The ratio of the acceptor channel was then divided by the donor channel to determine the BRET ratio. The data was then baseline-corrected to the vehicle control wells over

time. A slightly modified protocol was followed for the assays where the active subunit cDNAs of the toxins were transfected: HEK293T cells were used instead of the HEK293A $\Delta G\alpha_{i/o}$ cells, 96 well black-white isoplates were used, DPBS +5mM glucose was used as the assay buffer, a higher concentration of 30 μ M forskolin was used and this was co-added with the coelenterazine-h ten minutes prior to the addition of the agonist. The plate was then detected 20 minutes after agonist addition in a PHERAstar FS.

Arrestin recruitment

D₂R mediated β -arrestin-2 recruitment to the plasma membrane was conducted using the split luciferase complementation-based assay – MeNArC (406). HEK293T cells were co-transfected with multiple constructs as described earlier in the methods section. The cells were transfected with; D₂R, GRK2, a membrane-anchor fused to the N-terminal half of NanoLuc, β -arrestin-2 fused to the C-terminal half of NanoLuc and either the active subunit of PTX (PTX-S1), OZITX (OZITX-S1) or pcDNA3.1+ as a control. 48 hours after transfection the cells were washed with DPBS (Corning #21-031-CV), resuspended in DPBS +5 mM Glucose and seeded out into a 96 well black-white iso plate (Perkin-Elmer). Five minutes after the addition of 5 μ M coelenterazine-h, the D₂R agonist quinpirole was added and luminescence was read after 20 minutes in a Pherastar FS (BMG Labtech).

Data analysis

GraphPad Prism 8 was used for data analysis and performing statistical tests. Figures depicting molecular structures were constructed using ICM-Browser (MolSoft LLC) and UCSF Chimera (407).

6.3 Results

OZITX treatment abolishes GPCR mediated activation of all $G\alpha_i$ subfamily members, including $G\alpha_z$

$G\alpha_z$ displays divergent biochemistry and a more restricted expression profile compared to the other $G\alpha_i$ members (19,392,393). The significance of these characteristics, however, has not been realised partly due to the lack of molecular biological tools for $G\alpha_z$. We hypothesised that OZITX may serve as one such tool to investigate $G\alpha_z$ because we observed that $G\alpha_z$ possesses a conserved Asn³⁴⁸ residue eight amino acids from the carboxy tail that is thought to be ADP-ribosylated by OZITX (Fig. 6.1A) (405). Consequently, we sought to determine whether OZITX inhibits $G\alpha_z$

coupling to GPCRs. To achieve this, we used a previously described NanoBRET assay that measures the release of G $\beta\gamma$ subunits from the G α subunits upon activation of the heterotrimer (Fig. 6.2A) (257,258). While this assay provides a method for rapidly assessing G protein activation, the signal can potentially be partially contaminated by endogenously expressed G α subunits in the cells (257,354). We therefore, adapted the assay for use in newly edited HEK293A CRISPR/Cas Δ G α -all cells whereby all the G α subunits had been genetically knocked out (408). This allowed us to quickly monitor the G $\beta\gamma$ release from the activation of one particular G α subtype of interest that had been exogenously transfected.

The dopamine D₂ receptor (D₂R) was used as a prototypical G α_i subfamily coupled receptor to assess the effect of OZITX treatment on G α_i protein activation. The D₂R is an ideal GPCR to use for these experiments as it promiscuously couples to all of the G α_i subfamily, including G α_o isoforms and G α_z (186,267). Cells transiently expressing the D₂R were pre-incubated with PTX or OZITX followed by stimulation with the D₂-like receptor selective agonist ropinirole (409). When doing this, it was observed that OZITX completely blocked the activation of G α_{i1} , G α_{i2} , G α_{i3} , G α_{oA} and G α_{oB} (Fig. 6.2B). This finding demonstrates that OZITX can function essentially the same as PTX - a finding that was in fact previously reported by Littler and colleagues (405). We extended our studies to see the effect of OZITX treatment on G α_z activation. As predicted from the carboxy-tail Asn³⁴⁸ residue within G α_z , the D₂R was incapable of activating G α_z upon ropinirole stimulation of cells that were pre-incubated with OZITX (Fig. 6.2B). In contrast, G α_z was insensitive to inhibition by pre-treatment of cells with PTX, consistent with the absence of the required cysteine substrate site residue (Fig. 6.1A).

Next, the same set of experiments was performed with another G $\alpha_{i/o/z}$ coupled GPCR; the μ opioid receptor (MOPR). Cells expressing the MOPR were pre-incubated with either OZITX or PTX and then stimulated with the agonist DAMGO (Fig. 6.2C). OZITX again inhibited coupling to each of the G α_i subunits completely, including G α_z . (Fig. 6.2C). This showed that OZITX does not discriminate between GPCRs when inhibiting G protein activation and thus may serve as a universal GPCR tool. We then sought to further characterise the toxin by measuring the activation of G α_{i2} by the D₂R after exposure to OZITX at different timepoints. G α_{i2} activation decreased with increasing time of OZITX exposure until G α_{i2} activation was completely abolished approximately sixteen hours after the addition of OZITX (Fig. 6.2D). This is consistent with the characteristics of PTX and hence suggests that OZITX, like PTX, would be best utilised in the laboratory by incubating with the cells overnight.

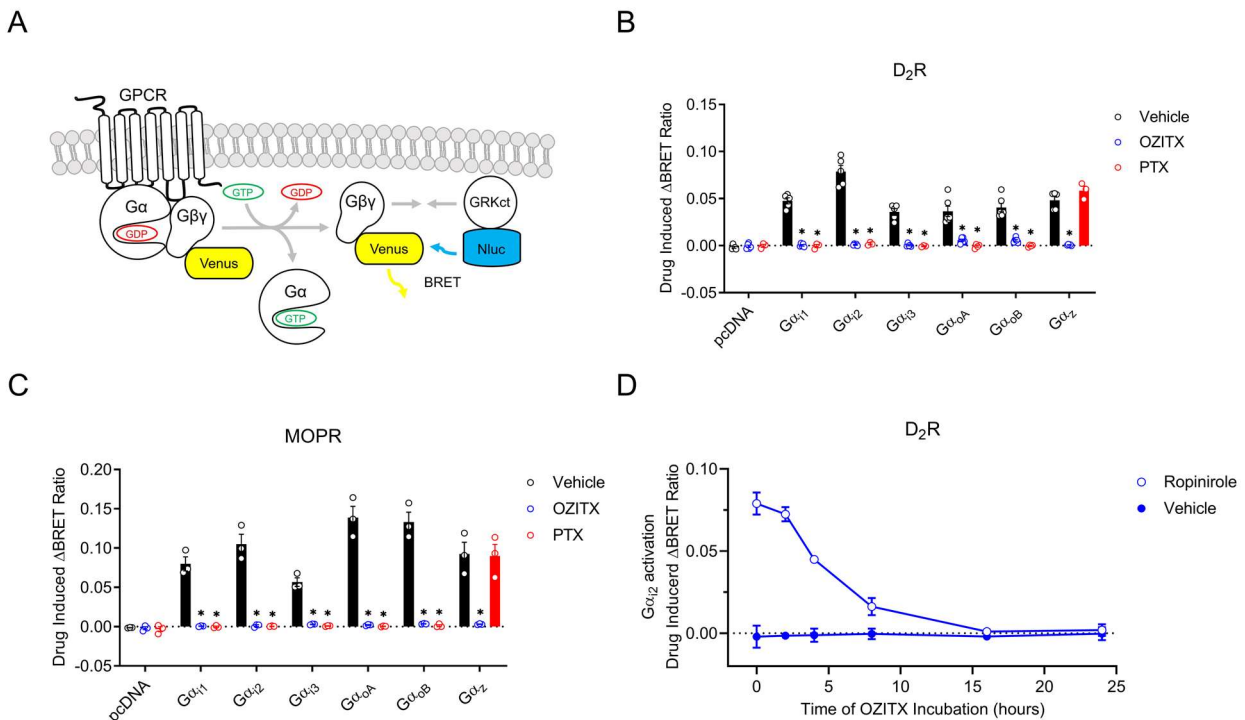


Figure 6.2: Activation of members of the Gα_i subfamily in the presence of OZITX and PTX. (A) Representation of the BRET sensors used for detection of G protein activation. Cells are transfected with DNA encoding a GPCR, Gα, venus156-239-Gβ1, venus1-155-Gγ2 and masGRK3ct-Nluc. The Gαβγ heterotrimer is activated through agonist binding to the GPCR. Active Gα exchanges the bound GDP for GTP and the Gα and Gβγ-venus dissociates. Free Gβγ-venus is bound by masGRK3ct-Nluc that serves as a BRET donor resulting in non-radiative energy transfer from Nluc to venus in the presence of the substrate furimazine. (B) D₂R mediated activation of Gα_i subfamily members in the presence of OZITX or PTX. Cells were pre-treated with either vehicle (black), OZITX (blue) or PTX (red) for 24 hours. Cells were then stimulated with 1μM ropinirole for 2.5 minutes followed by BRET detection. Data represents the mean drug induced increase in BRET ratio from vehicle ± SEM from 3-6 independent experiments. (C) MOPR mediated activation of Gα_i subfamily members in the presence of OZITX or PTX. Cells were pre-treated with either vehicle (black), OZITX (blue) or PTX (red) for 24 hours. Cells were then stimulated with 1μM DAMGO for 2.5 minutes followed by BRET detection. Data represents the mean drug induced increase in BRET ratio from vehicle ± SEM from 3 independent experiments. In (B) and (C), * represents where the response is significantly different ($P < 0.05$) from the respective vehicle toxin untreated control condition (black bar) as determined by a one-way ANOVA with Dunnett's multiple comparisons test. (D) Time course of OZITX treatment on G protein activation. HEK 293 ΔGα-all cells were transfected with cDNA encoding the D₂L_R, Gα_{i2} and G protein activation sensors. Cells were pre-treated with OZITX for the indicated times. BRET was measured 2.5 minutes after stimulation with 1μM ropinirole (blue open circles) or vehicle (blue filled circles). The basal BRET ratio prior to agonist stimulation has been subtracted to give the drug induced ΔBRET ratio. Data represents the mean ± SD from three separate experiments. * represents where the response is significantly different ($P < 0.05$) from the respective pcDNA control condition as determined by one-way ANOVA with Dunnett's multiple comparisons test.

G α_{i2} , G α_{oA} and G α_z mediated cAMP production inhibition is inhibited by OZITX

Cell surface receptor signalling is commonly amplified in the subsequent steps down the signalling cascade to increase the cells' sensitivity to extracellular stimuli. We wanted to confirm that OZITX also blocks the signalling at later stages in the cascade because a negligible response at the level of G protein activation could manifest as a larger signal further downstream. We therefore, assessed the effect of OZITX treatment on the downstream endpoint of intracellular cAMP since the G α_i subfamily are well-known to bind and inhibit adenylate cyclases (349,410). The intracellular cAMP levels were then monitored using CAMYEL; an intramolecular conformational BRET sensor based on EPAC (358). In these experiments, we used HEK293A cells that harboured a genetic knockout of all the G α_i subfamily members using CRISPR/Cas (HEK293A CRISPR/Cas Δ G α_i). Individual G α_i subunits of interest were then transfected into the cell background to monitor their ability to inhibit cAMP production. The cells were then treated with forskolin to stimulate adenylate cyclase, resulting in an increase in the levels of cAMP. This was then followed by treatment with ropinirole to stimulate the D $_2$ R, leading to activation of the G α_i subunit of interest. Importantly, in the absence of a transfected G α subunit, there was no detectable drug-induced inhibition of cAMP production, as observed by a lack of an increase in BRET ratio (Fig. 6.3A). When G α_{i2} or G α_{oA} were transfected, stimulation of the D $_2$ R produced a decrease in relative cAMP levels (indicated by an increase in BRET ratio) and this was completely abolished in cells treated with OZITX (Fig. 6.3B & C). In addition, cells transfected with G α_z also produced a decrease in cAMP, albeit to a slightly smaller amount, and this was again blocked in the presence of OZITX (Fig. 6.3D). This indicates that OZITX mediated ADP-ribosylation entirely occludes the G α_i protein members from coupling thus wholly preventing any downstream signalling.

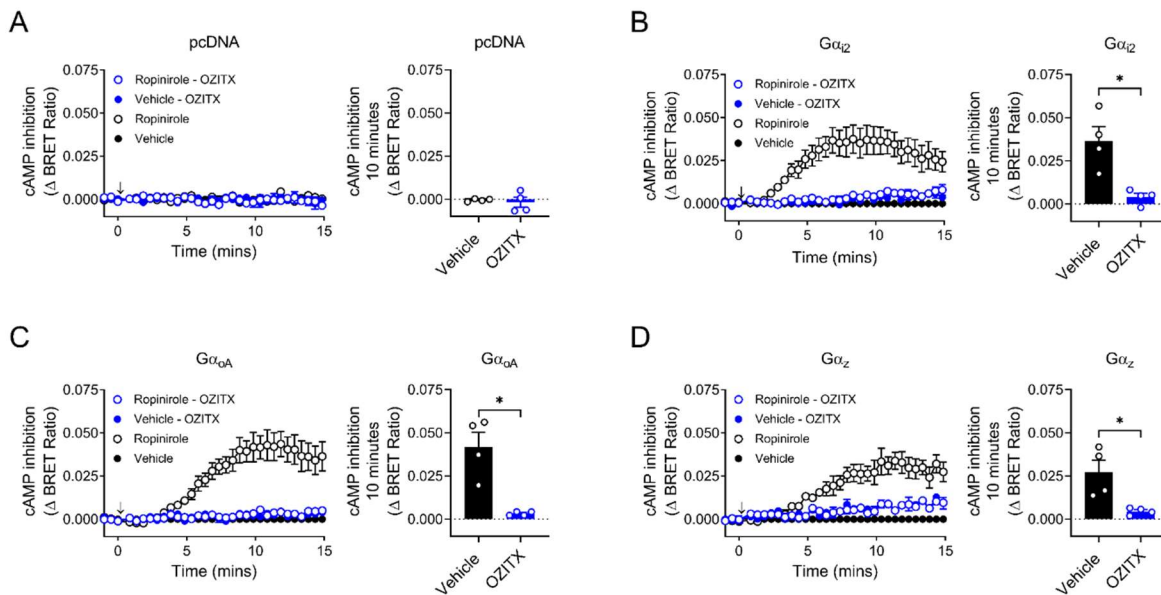


Figure 6.3: OZITX's effect on $G\alpha_{i2}$, $G\alpha_{oA}$ and $G\alpha_z$ mediated inhibition of cAMP production. Inhibition of forskolin stimulated cAMP production was detected in live cells using CAMYEL; a conformational BRET sensor based on EPAC. HEK 293 $\Delta G\alpha_{i/o}$ CRISPR cells were transfected with DNA encoding the D_2R , CAMYEL and either (A) pcDNA3.1+ control, (B) $G\alpha_{i2}$, (C) $G\alpha_{oA}$ or (D) $G\alpha_z$. Transfected cells were then incubated with either vehicle (black) or OZITX (blue) for 24 hours. Cells were then pre-stimulated with 10 μ M forskolin for 10 minutes before stimulation with either vehicle control (filled circles) or 1 μ M ropinirole (open circles). Data was baseline corrected to the cells not treated with OZITX or ropinirole and is shown as the mean \pm SEM from four separate experiments. Values were deemed significantly different using an unpaired student's t-test. * represents $P < 0.05$.

OZITX does not ablate $G\alpha_s$, $G\alpha_q$ or $G\alpha_{12}$ subfamily coupling

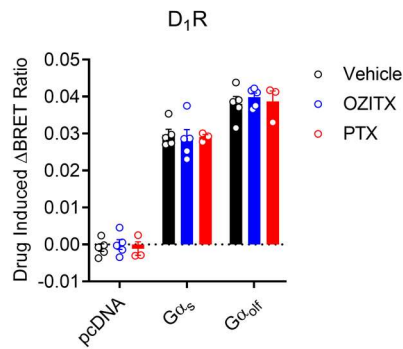
In addition to the $G\alpha_i$ subfamily, the asparagine residue eight amino acids upstream of the carboxy-terminus is also conserved across some other $G\alpha$ members (Fig. 6.1A). We therefore sought to further assess the substrate selectivity of OZITX as it could potentially be used as a tool to inhibit activation of a wider range of $G\alpha$ subunits. We first measured the $G\alpha_s$ subfamily activation after treatment with OZITX to serve as a negative control because the $G\alpha_s$ subfamily possess a histidine residue instead of an asparagine in this position. This was performed using the well-established $G\alpha_s$ coupled receptor, the dopamine D_1 receptor (D_1R) together with the D_1 -type selective agonist SKF83822 for activation (411-414). Indeed, overnight incubation with OZITX did not inhibit $G\alpha_s$ or $G\alpha_{olf}$ activation by the D_1R which was in line with our predicted mechanism of OZITX action (Fig. 6.4A).

Next, we measured the activation of the $G\alpha_q$ subfamily proteins using the $G\alpha_q$ coupled neurotensin receptor 1 (NTS_1R)(415,416). $G\alpha_q$, $G\alpha_{11}$, and $G\alpha_{14}$ but not $G\alpha_{15}$ possess an asparagine residue as their eighth last amino acid such that one would expect only the former three subunits to be substrates for OZITX and hence not be activated by NTS_1R in the presence of OZITX (Fig. 6.1A).

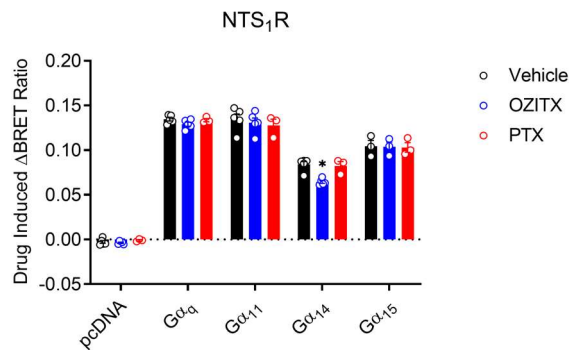
Upon stimulation of the NTS₁R with a truncated version of the endogenous agonist neurotensin (neurotensin residues 8-13 (NT8-13)), OZITX pre-treatment was incapable of completely inhibiting activation of any of the G α_q members (Fig. 6.4B). OZITX had no effect on G α_q , G α_{11} or G α_{15} although G α_{14} activation was partially decreased (vehicle control = 0.0840, OZITX treated = 0.0644, $P=0.0012$, one-way ANOVA with Dunnett's multiple comparisons test).

Moreover, both members of the G α_{12} subfamily; G α_{12} and G α_{13} , also harbour the putative asparagine site as their eighth-last amino acid (Fig. 6.1A). Consequently, we proceeded to assess the action of OZITX on the G α_{12} subfamily. We used the NTS₁R for activation again because it is known to also be capable of coupling to the G α_{12} subfamily (417). While we were successful in detecting robust activation of G α_{12} and G α_{13} by the NTS₁R, there was no inhibitory effect on the activation of either subunit when the cells were treated with OZITX (Fig. 6.4C). Taken together, despite the presence of the Asn residue with the G α_q and G α_{12} subfamilies, no detectable inhibitory action was observed with the exception of G α_{14} at which only partial inhibition was observed.

A



B



C

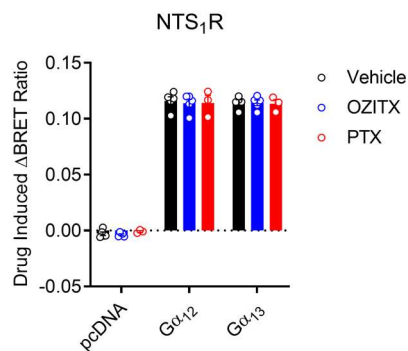


Figure 6.4: $G\alpha_s$, $G\alpha_q$ and $G\alpha_{12}$ subfamily activation in presence of OZITX and PTX. (A) Activation of $G\alpha_s$ subfamily members by D_1R in the presence of OZITX and PTX. (B) Activation of $G\alpha_q$ subfamily members by NTS_1R in the presence of OZITX and PTX. (C) Activation of $G\alpha_{12}$ subfamily members by NTS_1R in the presence of OZITX and PTX. HEK 293 $\Delta G\alpha$ -all CRISPR cells were transfected with cDNA encoding the particular GPCR and $G\alpha$ together with the G protein activation sensors as described the methods. The cells were pre-treated with either vehicle (black), OZITX (blue) or PTX (red) for 24 hours before stimulation with the GPCR agonists 100nM SKF83822 (D_1R) / 1 μ M NT8-13 (NTS_1R) for 2.5 minutes followed by BRET detection. The data is represented as the mean drug induced increase in BRET ratio from vehicle control \pm SEM from 3-5 separate experiments. * represents where the OZITX or PTX treated condition is significantly different ($P < 0.05$) from the vehicle treated condition (black) as determined by a one-way ANOVA with Dunnett's multiple comparisons test.

The active A subunit of OZITX can be transfected into mammalian cells to act as an inhibitor

In order to treat cells with AB₅ toxin protein complexes both expression and purification of this toxin is required (405). We therefore sought to determine if this process could be circumvented when using OZITX in order to increase its accessibility to laboratories. Accordingly, we tested whether the toxin would be functional upon transfection of the cDNA encoding the active A subunit on its own (OZITX-S1). Indeed, the active A subunit of PTX alone can be transiently expressed to act this way (418,419). The cDNA sequence of OZITX-S1 was codon optimised for high expression in human cells and ligated into pcDNA3.1+. The plasmid encoding OZITX-S1 was then co-transfected with the CAMYEL sensor into HEK293T cells to assess its effect in a cAMP production inhibition assay. Upon activation of the D₂R with the agonist quinpirole, cells that were transfected with the pcDNA control showed a concentration-dependent decrease in intracellular cAMP levels, whereas this response was completely blocked in cells transfected with the positive control PTX-S1 cDNA as well as the OZITX-S1 cDNA (Fig. 6.5A). This effect indicates that all endogenously expressing Gα_i subunits were ADP-ribosylated by transfected OZITX-S1 consistent with the action of the purified toxin described above. Having identified that transfected OZITX-S1 is functional, we then further monitored the activation of the other Gα subfamilies in OZITX-S1 transfected cells in order to confirm our previous results using treatment of the complete OZITX protein complex (Fig. S6.2 & Fig. 6.4). Indeed, OZITX-S1 transfection was ineffective in abolishing activation of Gα_s, Gα_q and Gα₁₂ subfamilies (Fig. S6.2).

We next were interested in assessing the effect of OZITX on arrestin recruitment to GPCRs. This is of importance considering many studies seeking to detect arrestin-dependent signalling do so by using PTX under the assumption that all Gα_i mediated signalling is blocked (420-426). We reasoned that OZITX may be more appropriately used in such situations given that PTX is an imperfect tool in such instances when the cells of interest express Gα_z and the GPCR of interest is coupled to this G protein. Accordingly, we examined the effect of OZITX on agonist-induced β-arrestin-2 (also termed arrestin-3) recruitment to the D₂R using a new MeNArC assay. We found that OZITX-S1 had a negligible effect on β-arrestin-2 recruitment to the D₂R, akin to the effect of transfected PTX-S1 (Fig. 6.5B). This illustrates that OZITX may be a useful tool to completely inhibit all Gα_i subfamily members while permitting the assessment of arrestin-dependent signalling.

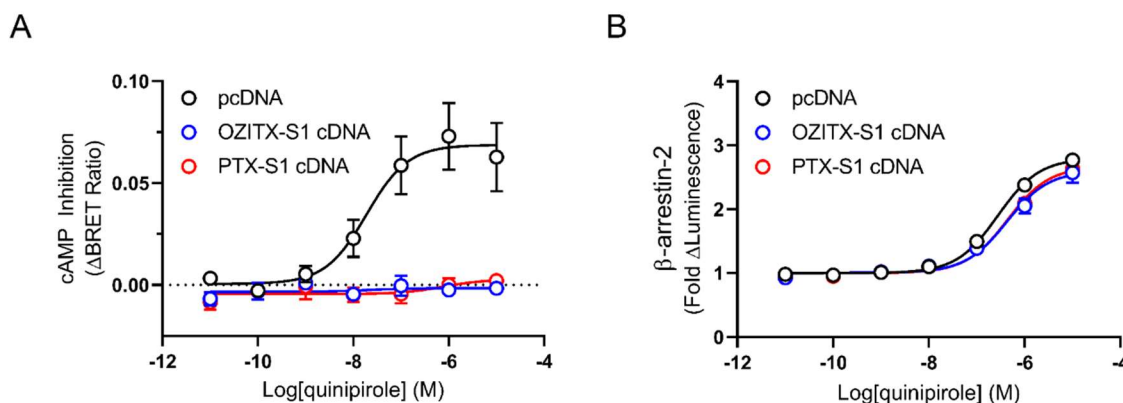


Figure 6.5: Effect of transfected cDNA encoding OZITX and PTX on cAMP inhibition and β -arrestin-2 recruitment. (A) D₂R mediated cAMP inhibition in the presence of OZITX and PTX cDNA. cAMP inhibition was performed after transfection of the either a pcDNA3.1+ control (black open circles), OZITX active subunit (OZITX-S1) (blue open circles), or PTX active subunit (PTX-S1) (red open circles) together with the D₂R and CAMYEL as described in methods. Cells were pre-treated with 30 μ M forskolin 5 minutes before stimulation with increasing concentrations of quinipirole followed by BRET detection. Data represents the mean \pm SEM of eight separate experiments. (B) Recruitment of β -arrestin-2 to the D₂R in the presence of OZITX and PTX cDNA. β -arrestin-2 recruitment was performed after transfection of the either a pcDNA3.1+ control (black open circles), OZITX active subunit (OZITX-S1) (blue open circles), or PTX active subunit (PTX-S1) (red open circles). β -arrestin-2 recruitment was measured in response to increasing concentrations of quinipirole using the MeNArc split luciferase complementation assay as outlined in the methods. Data represents the mean \pm SEM of four separate experiments.

G α_i subunits can be made OZITX insensitive

Understanding the actions of a single G α_i subtype has historically been challenging because there are usually multiple G α_i members expressed within any given cell type. A method that has permitted the investigation of a single G α_i subunit is to use cells expressing a PTX insensitive G α_i mutant in combination with PTX pre-treatment of the cells (427). This uncouples any endogenously expressed PTX sensitive G α_i subunits and allows GPCR mediated activation of only the PTX insensitive mutant of interest. Appreciating this, we followed the same rationale by attempting to generate OZITX insensitive G α_i mutants in the hope of increasing the scope of OZITX applications. To render the G $\alpha_{i/o/z}$ subunits insensitive to OZITX, we replaced the asparagine eight amino acids from the carboxy-terminus to an alanine (G α_{i1} -N347A, G α_{i2} -N348A, G α_{i3} -N347A, G α_{oA} -N347A, G α_{oB} -N347A and G α_z -N348A) as this was previously identified as the most likely substrate site using mass spectrometry (Fig. 6.1A) (405). We then performed G protein activation assays using the D₂R to activate each G α_i mutant in the presence or absence of PTX-S1 or OZITX-S1 (Fig. 6.6 & Fig. S6.3). In contrast to the activation of the wild-type G α_{i3} , G α_{oA} and G α_z that are all abolished by OZITX (Fig. 6.6A, B & C), activation of G α_{i3} -N347A, G α_{oA} -N347A and G α_z -N348A were OZITX insensitive (Fig. 6.6D, E & F). Additionally, it was observed that the N347A/N348A mutation did not impact the PTX sensitivity of the G α_i subunits (Fig. 6.6D, E & F). Likewise, the well-known PTX

insensitive mutation (C351I) introduced into $G\alpha_{i3}$ and $G\alpha_{oA}$, did not disturb the ability of OZITX to act on them (Fig. 6.6G & H). Having identified that the N347A/N348A mutation renders these $G\alpha_i$ members insensitive to OZITX without perturbation, the mutations were also extended into the remaining $G\alpha_i$ subunits and validated (Fig. S6.3).

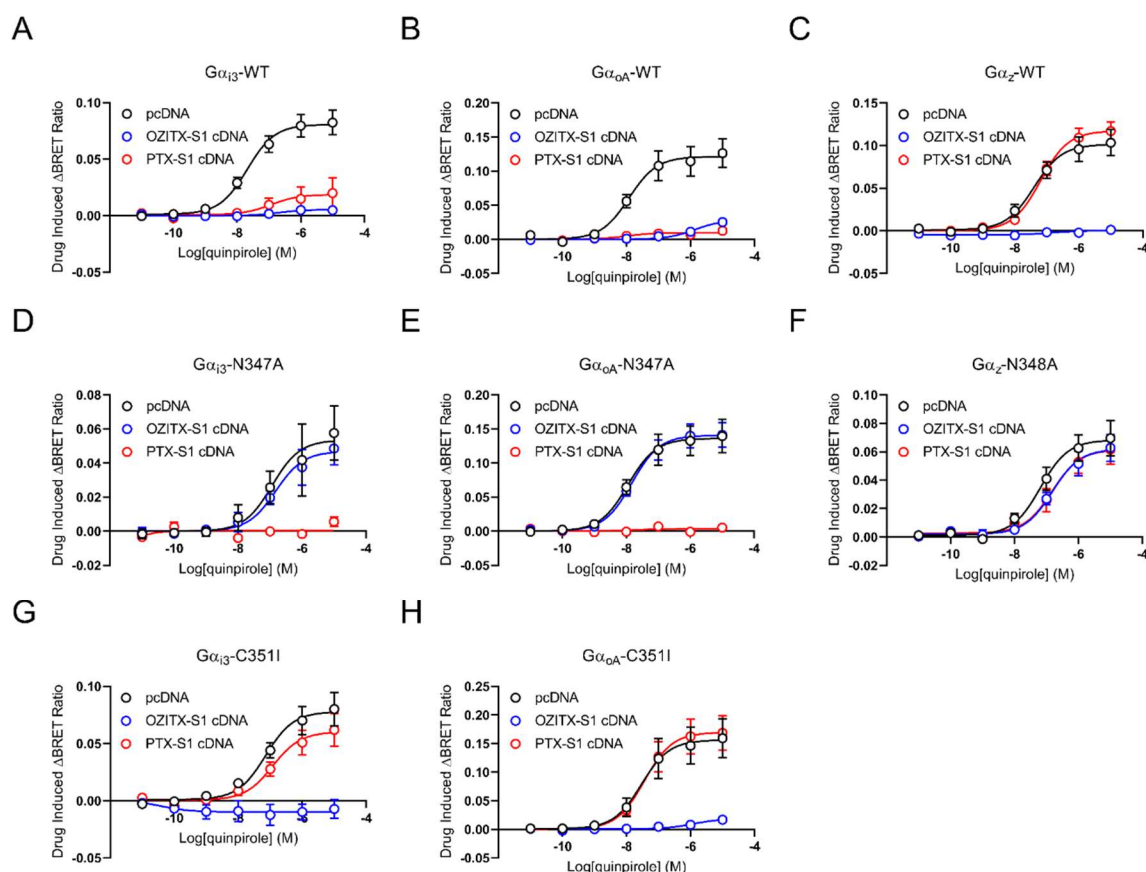


Figure 6.6: OZITX sensitivity of $G\alpha_i$ subfamily carboxy tail Asn347/348 mutants. (A) $G\alpha_{i3}$ -WT activation, $n=4-11$. (B) $G\alpha_{oA}$ -WT activation, $n=4$. (C) $G\alpha_z$ -WT activation, $n=5-6$. (D) $G\alpha_{i3}$ -N347A activation, $n=4$. (E) $G\alpha_{oA}$ -N347A activation, $n=4$. (F) $G\alpha_z$ -N347A activation, $n=6-8$. (G) $G\alpha_{i3}$ -C351I activation, $n=4-9$. (H) $G\alpha_{oA}$ -C351I activation, $n=4$. The G protein activation assay was performed on WT, Asn347Ala/Asn348Ala (putative OZITX site) and Cys351Ile (PTX insensitive) mutants. Cells were transfected with the D_2R , the particular $G\alpha$ mutant, the G protein activation sensors and either a pcDNA3.1+ control (black open circles), OZITX-S1 cDNA (blue open circles) or PTX-S1 cDNA (red open circles). Cells were then stimulated with increasing concentrations of quinpirole before BRET detection. Data represents the mean drug induced increase in BRET ratio from vehicle \pm SEM.

6.4 Discussion

PTX and CTX have been useful tools in GPCR signalling research to interrogate signalling pathways responsible for particular physiological processes. Here we have demonstrated a new tool for the inhibition of GPCR mediated activation of the $G\alpha_i$ subfamily, including $G\alpha_z$, through the use of a recently identified PTX-like protein - OZITX. OZITX has a distinct substrate site from that of PTX, enabling it to act on $G\alpha_z$ in addition to all the PTX sensitive $G\alpha$ subunits. The unique substrate

site was shown to be an asparagine residue eight amino acids from the carboxy-tail, yet, harbouring the asparagine residue was insufficient in rendering the $G\alpha_q$ and $G\alpha_{12}$ subfamilies sensitive to OZITX. Moreover, we showed that the transfected OZITX-S1 subunit is functional in mammalian cells, allowing for a more economical method of intracellular inhibitor delivery. Using this method of delivery, we finally showed that mutation of the Asn³⁴⁷ or Asn³⁴⁸ substrate site within $G\alpha_i$ subunits maintains their ability to couple to GPCRs while engendering them insensitive to OZITX.

While OZITX inhibits the other $G\alpha_i$ subunits, we showed that OZITX can be used for the total prevention of GPCR- $G\alpha_z$ signalling. Used in this fashion, OZITX is a tool distinct from all the prior methods that have been used to interrogate $G\alpha_z$ signalling. Previous studies have relied on inventive strategies to inhibit $G\alpha_z$ signalling such as; overexpression of $G\alpha_z$ -specific RGS proteins (147), $G\alpha_z$ -directed siRNA (428), and $G\alpha_z$ de-activation via PKC phosphorylation (148). However, these approaches do not completely block all activation of $G\alpha_z$. This property is crucial for reliable results because any amplification in the signal transduction system may mask the partial inhibition that occurred upstream. Therefore, an ideal molecular tool can completely block all signalling via the pathway of interest. Genetic knockouts of the gene that encodes $G\alpha_z$ have been used for this reason (150,396). The genetic knockout approach is more robust than the earlier described methods, however, it is technically challenging compared to OZITX treatment. Additionally, OZITX can be used in a more acute manner by overnight treatment whereas gene-editing technologies provide greater time for compensatory mechanisms by the cell potentially leading to uncertain results. While a complete genetic knockout may be advantageous in some circumstances, post-translational modification is likely to have less off-target cellular effects because it occurs at a later stage - the level of the protein.

Our results suggest that OZITX could serve as a replacement to PTX in most experimental paradigms aimed at interrogating $G\alpha_{i/o/z}$ signalling moving forward. One of the early demonstrations of PTX's utility was to aid in identifying the $G\alpha_i$ subfamily by distinguishing it from the $G\alpha_s$ subfamily (349). PTX was shown to block the inhibitory effect that $G\alpha_i$ proteins have on adenylyl cyclases, thus building evidence for a separate $G\alpha$ species with distinct functionality to $G\alpha_s$. Since then, PTX has been widely used with the same rationale, that is, to differentiate GPCR responses mediated by $G\alpha_i$ proteins from other signal transducers (429). However, it has been known for decades that it is imperfect due to its lack of action on $G\alpha_z$ (392,393). We have now shown that this contrasts with OZITX, we determined that it can inhibit $G\alpha_z$ in addition to inhibiting $G\alpha_{i1}$, $G\alpha_{i2}$, $G\alpha_{i3}$ and the $G\alpha_o$ isoforms. Considering this, it should be recognised that the replacement of PTX by OZITX will occur assuming OZITX also inhibits the visual and taste $G\alpha$ subunits; $G\alpha_{t1}$, $G\alpha_{t2}$ and $G\alpha_{gust}$. We have not evaluated whether OZITX inhibits the coupling of these $G\alpha$ subunits in the

present study. One would expect ADP-ribosylation by OZITX to occur on $G\alpha_{t1}$, $G\alpha_{t2}$ and $G\alpha_{gust}$ since they harbour an asparagine as their eighth-last amino acid residue in addition to having high sequence homology to the other $G\alpha_i$ subunits.

While OZITX is expected to often replace PTX, one would consider that PTX will not become redundant because the reasons for using PTX will evolve. There are likely be cases where PTX is still required due to its contrast in $G\alpha$ specificity. For example, disentangling the functions of $G\alpha_z$ from the other $G\alpha$ subunits will require both the use of PTX and OZITX. Indeed, performing an experiment with an OZITX treated, a PTX treated and an untreated condition in parallel, would enable the signalling mediated by $G\alpha_z$, PTX sensitive $G\alpha_i$ subunits and toxin insensitive $G\alpha$ subunits to be separately measured.

OZITX lacked the ability to abolish the coupling of the $G\alpha_q$ and $G\alpha_{12}$ subfamily, despite the $G\alpha_q$ and $G\alpha_{12}$ subfamilies carrying the conserved asparagine substrate site in their carboxy α -helix. OZITX only had a small effect on $G\alpha_{14}$ activation and there was a lack of any effect on all the remaining $G\alpha_q$ and $G\alpha_{12}$ subunits. This result complicated our predicted mechanism of action as we had presumed that the conserved asparagine residue was the main determinant for OZITX specificity. In line with our thinking, PTX can act on all the $G\alpha$ subunits that contain the Cys^{351/352} substrate site. Certainly, our initial results supported this mechanism because the $G\alpha_s$ subfamily was not inhibited and it does not possess an asparagine in the appropriate position for ADP-ribosylation. However, our results together suggested that $G\alpha_{14}$ is a very poor substrate for OZITX and that the $G\alpha_q$ and $G\alpha_{12}$ subfamilies are not the target of OZITX. Curiously, these findings can be explained when considering prior literature reporting that swapping the five carboxy-terminal residues of $G\alpha_{12}$ or $G\alpha_{oA}$ onto $G\alpha_q$ does not produce a $G\alpha$ subunit that is sensitive to PTX, even though the modified $G\alpha_q$ contains the required cysteine residue four amino acids from the carboxy-termini (430). This indicates that carrying the required substrate amino acid site alone is not enough to render the a $G\alpha$ subunit sensitive to the PTX-like protein. In the case of OZITX, this hypothesis could be further supported by determining whether introducing the conserved asparagine residue into the $G\alpha_s$ subfamily has any effect on the subfamilies' OZITX insensitivity. Furthermore, our results using OZITX together with previous findings using PTX would imply that the site of ADP-ribosylation is distinct from the binding recognition site of the PTX-like protein. Future studies could investigate the structural basis for the recognition of specific $G\alpha$ subunits by OZITX and PTX.

It was determined that the OZITX-S1 cDNA can be transfected for a more practical and economical approach to inhibit $G\alpha_{i/o/z}$ signalling as compared to use of the purified toxin. This means that the whole protein complex does not need to be expressed and purified, instead obtaining DNA that encodes the active A subunit is adequate. Previous studies have demonstrated that transfected

PTX-S1 can be used to reduce the time and cost associated with acquiring the purified protein (418,419). Indeed, this suggests that most ADP-ribosylating active subunits from PTX-like proteins will remain functional when transfected. Furthermore, we also demonstrated that using transfected OZITX does not prevent β -arrestin-2 recruitment to the D₂R. Accordingly, OZITX may be used as a method for blocking any unwanted $G\alpha_i$ subfamily signalling when seeking to exclusively assess arrestin-dependent signalling.

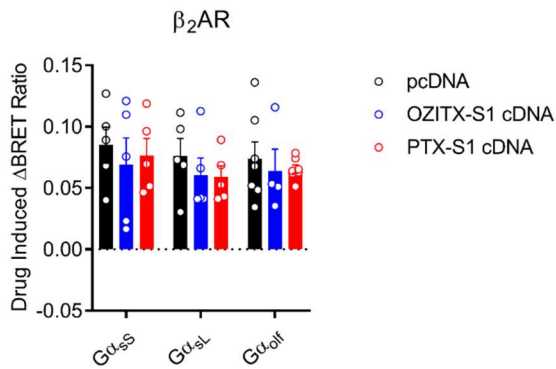
We showed that $G\alpha_i$ subunits can be made OZITX insensitive through an N347A/N348A mutation in the eighth-last amino acid position. Further studies may seek to check the alanine mutant and, if required, potentially swap the alanine with another residue that continues to prevent ADP-ribosylation while more closely matching the biochemistry of the wild type protein. Mutations like this have previously been generated for the PTX insensitive $G\alpha_i$ subunits by changing the initially discovered PTX insensitive C351G/C352G mutation to the preferred C351I/C352I mutation (431). Nonetheless, the OZITX insensitive mutants can serve as a useful tool in combination with OZITX treatment to investigate single $G\alpha_i$ proteins in an endogenous $G\alpha_i$ null background. Building on this, OZITX insensitive $G\alpha$ mutants and PTX insensitive mutants could be complementary to each other. For example, it could be of use to transfect both an OZITX insensitive $G\alpha$ mutant and a PTX insensitive $G\alpha$ mutant into the same cells and either treat with OZITX or PTX to assess the effect of one subunit in identical cellular conditions.

Moreover, it was interesting that in our hands, mutation of the Asn^{347/348} residue alone was sufficient to render $G\alpha_{i1}$, $G\alpha_{i2}$ and $G\alpha_{i3}$ resistant to OZITX. This is because these $G\alpha$ subunits contain a lysine residue as their tenth-last amino acid (Lys^{345/346}) that was suggested to be a site for OZITX by Littler and colleagues (Fig. 6.1A) (405). These results may suggest that this Lys^{345/346} site is a poor secondary substrate site that is very minimally ADP-ribosylated. Alternatively, another scenario may be that ADP-ribosylation of the Lys^{345/346} site may have no effect on the G protein coupling ability. However, this is less probable given that the Lys^{345/346} site would appear to have quite close proximity to the GPCR upon coupling.

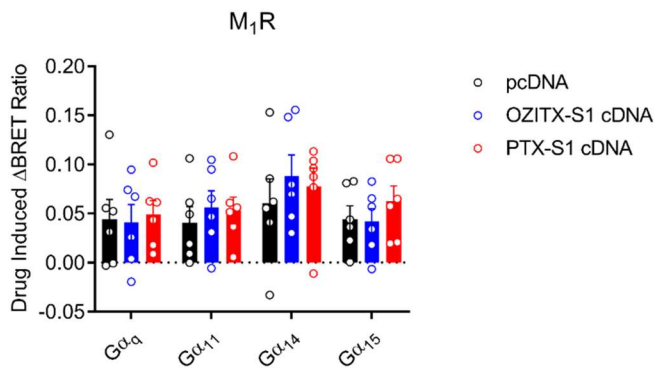
Finally, we have helped support the overarching idea that there is continuing value in the characterisation and use of novel AB₅ toxins as laboratory tools. Host-pathogen arms races are hotspots of molecular evolution that result in proteins with extraordinary functionality. This is exemplified in the diversity of ADP-ribosylating AB₅ toxins. At present, an unknown number of these toxins remain as a large untapped resource. Some ADP-ribosylating AB₅ toxins that have been well characterised, such as PTX and CTX, have been widely used as tools in G protein signal transduction research. Here, we have now validated the use of OZITX and hence, it can be added to the ADP-

ribosylating AB₅ protein tool kit. Indeed, OZITX will be particularly useful when investigating aspects of G α_z signalling.

A



B



C

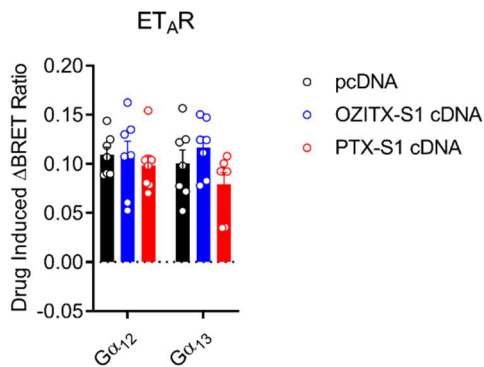


Figure S6.2: Gα_s, Gα_q and Gα₁₂ subfamily activation upon transfection of OZITX active subunit. (A) β₂AR activation of Gα_{ss}, Gα_{sl} and Gα_{olf}, n=4-7. (B) M₁R activation of Gα_q, Gα₁₁, Gα₁₄ and Gα₁₅, n=6. (C) ET_AR activation of Gα₁₂ and Gα₁₃, n=7. HEK 293T cells were transfected with cDNA encoding the particular GPCR, the Gα, the G protein activation sensors and either pcDNA3.1+ control (black), OZITX-S1 cDNA (blue) or PTX-S1 cDNA (red) as described in the methods. 48 hours after transfection the BRET assay was performed, stimulation of the cells was carried out by adding the agonists isoproterenol (β₂AR) / acetylcholine (M₁R) / endothelin 1 (ET_AR) for 5 minutes followed by BRET detection. The data is represented as the mean ± SEM drug induced increase in BRET ratio from the vehicle control.

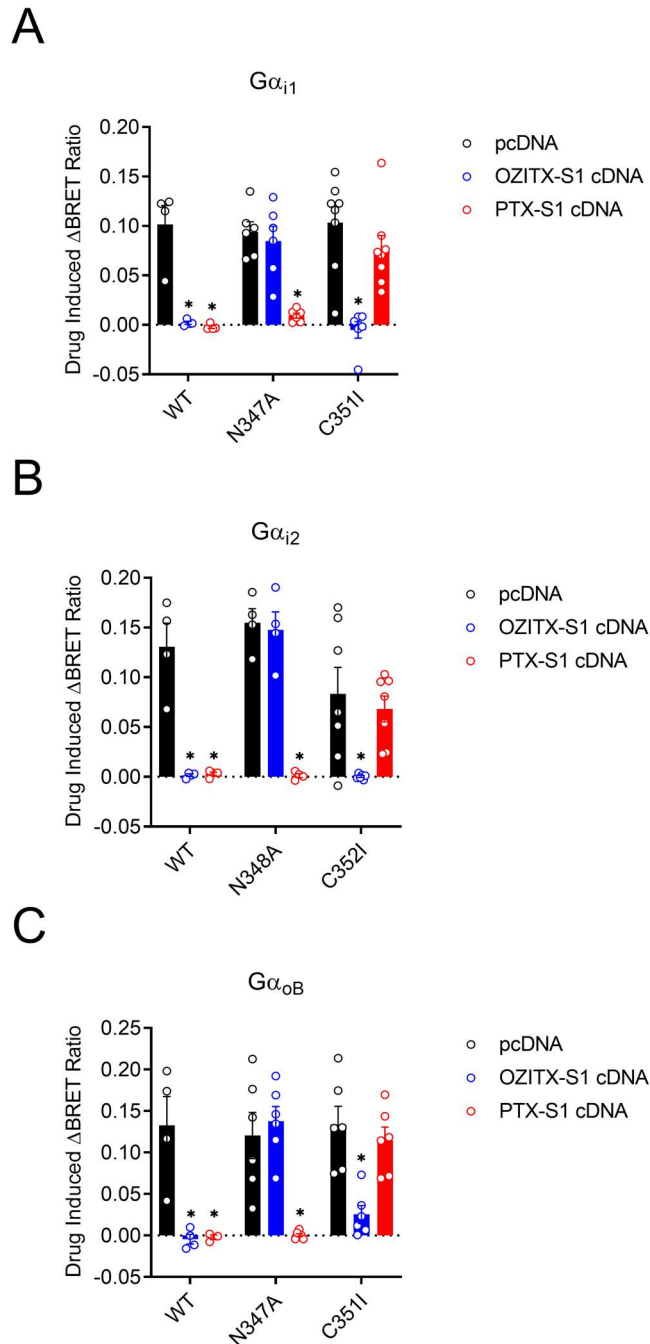


Figure S6.3: OZITX Resistant mutants of $G\alpha_{i1}$, $G\alpha_{i2}$ and $G\alpha_{oB}$ can be engineered. (A) Activation of $G\alpha_{i1}$ -WT, $G\alpha_{i1}$ -N347A and $G\alpha_{i1}$ -C351I, $n=4-8$. (B) Activation of $G\alpha_{i2}$ -WT, $G\alpha_{i2}$ -N348A and $G\alpha_{i2}$ -C352I, $n=4-7$. (C) Activation of $G\alpha_{oB}$ -WT, $G\alpha_{oB}$ -N347A and $G\alpha_{oB}$ -C352I, $n=4-6$. G protein activation was performed in the presence of either transfected pcDNA3.1+ control (black), OZITX-S1 cDNA (blue) and PTX-S1 cDNA (red). HEK 293 cells were transfected with the $G\alpha$ mutant subunit of interest, G protein activation sensors, the D_2R and either a pcDNA3.1+ control, OZITX-S1 cDNA or PTX-S1 cDNA. Cells were then stimulated with quinpirole and the drug induced increase in BRET ratio baseline subtracted from the vehicle wells is represented. Data is shown as the mean \pm SEM. * represents the response is significantly different from the respective pcDNA (non-toxin transfected) control response (black bar) using a one-way ANOVA with Dunnett's multiple comparisons test.

Chapter 7:

General Discussion

More clinically approved small molecules target GPCRs than any other protein family (2,432). Before the approval of a GPCR drug, lead molecules are selected for in a drug discovery process that is typically based on equilibrium estimates of affinity and potency. However, a drug's concentration in the body is usually in a constant state of change due to multiple physiological processes such as drug distribution, dosing regime, tissue absorption, hepatic metabolism and excretion (53,54). Therefore, this drug discovery process may be an inefficient means because a drug's binding kinetic rates for the GPCR can often better predict its efficacy in vivo (52,55,56,60).

The D₂R is one such GPCR where ligand binding kinetics has been related to clinical outcomes. The D₂R is a target to treat many neuropsychiatric and neurological disorders (103,433). D₂R antagonist kinetics are thought to be important for determining the side effect profile of antipsychotic drugs (61,187,218). In the case of D₂R agonists, differing binding kinetics has been linked to distinct functional effects including some observations of apparent biased agonism (96,189). However, the precise mechanisms as to how these findings arise are largely unclear.

Given that G protein signalling, regulation by GRKs, desensitisation and trafficking of the D₂R all occur over different timescales (96,102,153,261,434), the lifetime of the agonist-receptor complex could differently influence the ability of effectors to bind and function in these processes. Therefore, the primary hypothesis of this thesis was to determine whether differences in the residence time (or dissociation rate) of D₂R agonists can function as a mechanism to manifest biased agonism. Before examining this however, we first wanted to determine whether ligands could have their binding kinetics rationally modulated. We aimed to do this by determining different ligand's amino acid interactions along their binding pathway into the pocket of the D₂R. After having investigated these first two aims, we appreciated that to wholly understand the mechanisms of biased agonism, one must first understand the drivers of the signalling systems. We consequently developed secondary questions in this area. We aimed to ascertain the role GRK regulation plays in determining bias, and also, the influence G protein signalling kinetics has on shaping agonist action.

We made many key findings addressing the aims outlined in the above paragraph. Firstly, we observed that amino acid residue mutants in the extracellular regions of the D₂R can alter ligand binding kinetic rates in a ligand-specific manner. This was encouraging as it suggests that in the future ligands can have their structure logically modified to tune their binding kinetics. When next assessing the primary aim of this thesis however, we observed no clear relationship between the agonist dissociation rate (or residence time) and biased agonism. The results were somewhat hampered by the small amount of statistically significant biased agonism that we observed. Nonetheless, we revealed that regulation by GRK2/3 phosphorylation is directly proportional to agonist efficacy in any D₂R response. Suggesting that GRK biased “switching” between G protein responses and arrestin

scaffolding may be unlikely at the D₂R. We then showed that the G protein Gα_z can produce a distinct signalling wave by the D₂R that is largely independent of the properties of the agonist but instead dependent on the hydrolysis rate of Gα_z. We therefore had thoroughly examined D₂R biased agonism *in vitro*. We next wanted to take steps to examine D₂R bias in a more relevant context. One of the key challenges to further investigate D₂R biased agonism phenomena in relevant cells or tissues is how to isolate and measure G protein versus arrestin signalling or indeed signalling from specific G protein subunits given the promiscuity of the D₂R to activate all inhibitory G proteins. Therefore, we developed the pertussis toxin-like protein OZITX to inhibit all of the D₂R mediated Gα_{i/o} subfamily signalling, including Gα_z.

Showing that each ligand's binding kinetics can be differently influenced by particular amino acid residues in the extracellular vestibule may be an important step for D₂R drug discovery. For example, in Chapter 2 we were able to show that Trp100^{ECL1} and Leu94^{2,64} had dramatic effects on the dissociation rate of most tested ligands although, risperidone appeared to be less influenced than others. The extracellular vestibule is generally less conserved between GPCRs and as such can offer receptor subtype selectivity (65). Consequently, we may be able to rationally design D₂R drugs through medicinal chemistry such that they can make the sought-after interactions with extracellular vestibule residues. These interactions would tune the binding kinetics of the ligand while the ligand remains selective for the D₂R receptor subtype. If the ability of a D₂R agonist to activate particular signalling pathways is indeed related to its residence time, then one might be able to rationally modulate the agonist kinetics as a mechanism to design biased D₂R drugs. However, our functional data in Chapter 3 and 4 do not support that such pathway bias can be achieved in this way. Nonetheless, there is a strong link between antagonist dissociation rate and the propensity to cause extrapyramidal side effects (61,187,218). Indeed, the “gold standard” treatment for schizophrenia remains as the second generation antagonist clozapine and not the third generation partial agonist antipsychotics (175,435). Therefore, developing antagonists with an even better binding kinetics profile than clozapine may be possible in the future.

It would be exciting to extend these studies in Chapter 2 by performing assessments on a larger set of ligands as well as a larger number of D₂R mutants to get coverage of the complete ligand binding site and pathway. Before doing this however, it would be necessary to develop the assay to a point where large-scale high throughput determinations of ligand binding kinetics can be conducted. Sykes and colleagues have shown that the injection time of the receptors with the cocktail of tracer and unlabelled competitor is very important for accurately determining binding kinetics rates with this assay (245). Additionally, the instrument detection cycle time that determines the temporal resolution is also crucial for determining fast dissociating ligands (245). Currently, each mutant and

ligand combination require careful optimisation in order to be able to acquire meaningful rate constants. Having done this, it could then be coupled with molecular dynamics simulations to wholly understand the binding entry and exit pathways of D₂R ligands.

In Chapter 3, we observed no clear relationship between the agonist's binding kinetics and their biased agonism (of the panel of agonists that were tested). This was the primary result of the thesis that we set out to determine. This was achieved by assessing correlations between the binding kinetics and the relative transduction coefficients ($\Delta\text{Log } \tau/K_A$) from an operational model of agonism (86,87). While some correlations were observed between affinity estimates and biased agonism, the results were largely uncertain in regard to the mechanism behind this. However, we can make some definitive conclusions from our findings. Paton's rate theory argues for a positive relationship between the association rate and the efficacy of an agonist (90). We saw no relationship between any binding kinetic parameters and efficacy. This means that we can rule out rate theory or the opposite of rate theory (anti-rate theory - efficacy mediated by dissociation rate). Some recent reports suggest that anti-rate theory may explain efficacy at the M₃R and A_{2A}R as shown by a correlation between agonist dissociation rate and efficacy (91,93). However, based on our results at the D₂R we suspect that this is not a common property shared between all GPCRs. Furthermore, in the examples of the M₃R and A_{2A}R, human selection in the drug discovery process may have selected for high affinity/potency and consequently, slower dissociating agonists, as well as selected for increased efficacy. Therefore, the results showing anti-rate theory at these receptors could potentially be due to this selective pressure.

This also highlights a potential limitation in our study related to human selection. Klein-Herenbrink et al (96) showed that apparent biased agonism occurs between slowly dissociating agonists and fast dissociating agonists at the D₂R. Yet, all the slowly dissociating agonists in their study were low efficacy partial agonists (96). Therefore, in our study we deliberately incorporated both low efficacy (third generation antipsychotics) and high efficacy drugs. This reduced a confounder in our study and provided a wider range of efficacy to draw correlations. However, by potentially selecting compounds based on their efficacy we may have artificially influenced our correlations. Future work could seek to investigate this further by performing correlations where less human intervention is involved. We tested eleven separate compounds when the D₂R has a whole library of agonists available to assess because it is such a popular drug target. Therefore, selecting a larger and a random sample of ligands with D₂R activity may be a better approach. Similarly, future work could not only perform similar experiments on larger numbers of ligands but could also do this in a completely "receptor naïve" manner. This means, performing a large screen of a number of ligands with unknown efficacy at the D₂R. If millions of compounds could be screened and a panel

have agonism at the D₂R, then determining their transduction coefficient and determining their binding kinetics with identical methods to the ones we describe here could test this. This would mean that a random sample of agonists is selected with varying structure and efficacy.

In Chapters 3 and 4 only very minimal biased agonism is observed. Almost no biased agonism is observed between G protein subunits in Chapter 3 and no statistically significant biased agonism is reported for the putative biased agonists MLS1547 and UNC9994 in Chapter 4 (184,251). When looking back through the examples of bias at the D₂R our data here appears to follow a similar pattern that has occurred over the years: In 2002, dihydrexidine was the first reported biased agonist at the D₂R (436,437). However, this ligand is generally no longer under investigation as a biased agonist, and, in fact, it was recently reported as a D₁R biased agonist (285). Further, S-3PPP was reported soon after as another biased agonist at the D₂R. This compound was reported as a “protean agonist” through GTPγS binding with different G proteins showing that it lacked the ability to activate some poorly coupled Gai/o subunits (138,139). Subsequent BRET-based G protein activation assays that exhibit increased sensitivity have demonstrated that S-3PPP is capable of activating G proteins and is better defined as a partial agonist (96). Next, aripiprazole was identified as a biased agonist referred as “functionally selective” before biased agonism was the commonly recognised term (438,439). Aripiprazole displayed bias for arachidonic acid release compared to MAPK activity (438). Again aripiprazole was proven to act more so as a partial agonist than a biased agonist with more sensitive assays and also applying a model of agonist action to account for system bias (440). Moreover, UNC9975 and UNC9994 were identified as arrestin biased agonists and MLS1547 was said to be G protein biased (184,251). We here observe no statistically significant bias for these compounds. Interestingly, from literature it would appear that the order with which the putative biased agonists are reported aligns with their efficacy (dihydrexidine > S-3PPP > aripiprazole > UNC9994). This likely indicates that as more sensitive assay techniques were developed, weaker responses could be detected and agonists that originally displayed no activity in a particular pathway appear to act as partial agonists. Whether this pattern continues in the future will be fascinating to see.

If one can expect that a biased D₂R agonist found today will likely be re-characterised as a partial agonist in the future due to more sensitive laboratory techniques and more modern analytical approaches, then where does this leave D₂R drug discovery? And what role does this have in the future for the pharmacological management of psychiatric and neurological diseases? For D₂R drug discovery, it leaves two obvious options moving forwards; firstly, to go back to more traditional methods of small molecule drug discovery or, secondly, to harness system bias (system bias will be discussed in later paragraphs). In terms of going back to more traditional methods of pharmacology, this means focussing on classic parameters such as efficacy, binding kinetics rates and selectivity.

Therefore, for targeting the D₂R in schizophrenia, the best approach will be to design drugs that are antagonists with a fast dissociation rate from the D₂R and the appropriate receptor selectivity profile. Overall current guidelines should advocate for the use of clozapine as opposed to the approval and use of any existing reported biased agonist in the treatment of schizophrenia symptoms. For targeting the D₂R in diseases where agonism is wanted, then the ideal amount of efficacy should be determined based on the particular indication. Regarding Parkinson's disease, the results in this thesis show that dopamine is the most efficacious agonist when measuring regulatory responses. Given that L-DOPA is considered the most efficacious treatment clinically, this likely suggests that higher agonist efficacy *in vitro* corresponds to higher efficacy *in vivo*. Therefore, agonists could be developed that are higher efficacy than dopamine as an attempt to create even more efficacious drugs for the treatment of Parkinson's disease. In terms of current treatment for Parkinson's, the results in this thesis would suggest that L-DOPA should remain first line treatment, rotigotine also appears to offer superior agonist efficacy to other agonists and as such may be a good alternative to L-DOPA.

This pattern also appears to match biased agonism studies for at least some other GPCRs. Indeed, a similar pattern to the one we observe at the D₂R also seems to emerge when examining the history of biased agonism at the MOPR (441). The first reports of biased agonists later turned out to be partial agonists when further scrutinised (441). In addition, subsequent purported biased agonists such as PZM21, actually have never been shown to display any statistically significant biased agonism when using the Black/Leff operational model to quantify the bias (80,82). Moreover, the angiotensin II type-I receptor (AT₁R) may follow a similar narrative. The first reported biased agonist at the AT₁R; [Sar¹, Ile⁴, Ile⁸] Angiotensin II or SII - was reported to be arrestin biased and lack any ability to stimulate the G protein dependent responses IP accumulation and [³⁵S]GTPγS binding (442). Later, SII has proven to be a partial agonist at G protein mediated pathways and direct G protein activation (281,443). The discrepancies in these results may reflect the increased sensitivity of the BRET assays used in later studies investigating SII. Further, it would be fascinating to observe whether this pattern occurs for reported biased agonists at other GPCRs as their signalling pathways and pharmacology become better characterised. If this pattern continues to emerge then it will be clear that the field needs to revise early stage GPCR drug discovery pipelines to workflows that focus less heavily on biased agonism.

In Chapters 3 and 4 we observe apparent bias between some agonists. Ligand bias, system bias and observational bias are the three main drivers of bias observations. It is commonplace to assume that these can be separated by using methods that the field has developed such as reference agonists and reference pathways. However, this may be more challenging than initially thought. Certainly, in our studies in this thesis it is often not clear which type of bias we are observing and

whether it could be a combination of the three types. We therefore propose that the three bias mediators may overlap or be dependent on each other (Fig. 7.1).

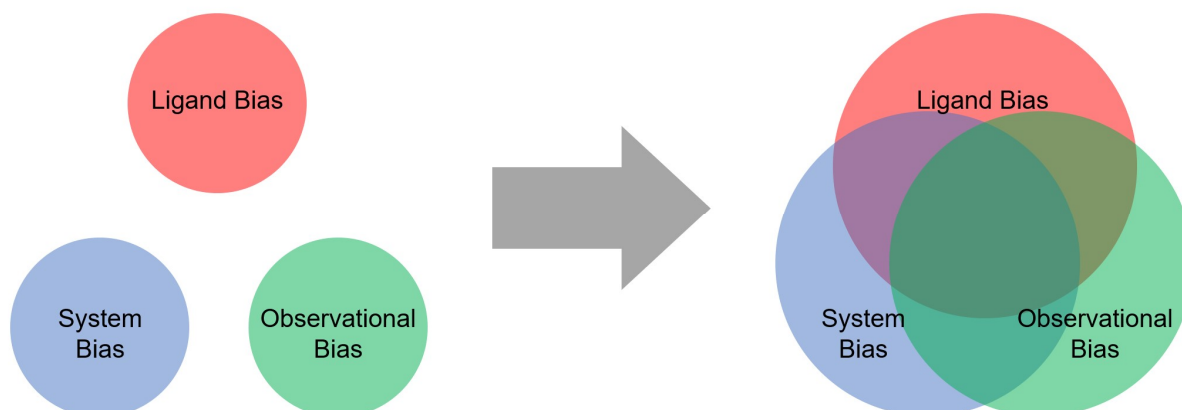


Figure 1. Biased agonism components may not be separated.

In our studies in Chapter 3 and 4 the statistically significant bias was generally detected between similar pathways and in the same direction. That is, we observed bias between a well coupled G protein pathways and a poorly coupled regulatory pathway and the biased agonism was usually directed towards the regulatory pathway. Therefore, this apparent bias is either due to all ligands acting in a similar manner or potentially the system is hard-wired to disproportionately amplify one pathway more than another. If this is system bias, then it is interesting as it may still be able to be harnessed. For example, Marcott and colleagues (144) have proposed that the D₂R couples to G α_o in the nucleus accumbens and G α_i in the dorsal striatum. The D₂R more efficiently couples to G α_o than G α_i such that all agonists are effectively full agonists at G α_o whereas partial agonism can be observed at G α_i (shown in Chapters 3, 4 and 5) (139,267). Therefore, by using either a full agonist or a partial agonist, the dorsal striatum will be activated to a different extent but the nucleus accumbens will have similar activity depending on the agonist.

Another example where system bias could be employed without the need for ligand bias is at the D₁R. A report by Yano et al (285) reveals agonists acting at the D₁R that display bias at G α_s relative to G α_{olf} . The D₁R has broad expression in the brain, the authors highlight G α_{olf} has the widest expression in the striatum whereas G α_s is expressed in the cortex and other brain regions (444). Therefore, the biased agonists are able to achieve brain region selectivity. However, system bias could have already been harnessed to achieve at least some tissue selectivity. It is shown that the D₁R preferentially couples to G α_s relative to G α_{olf} (285). Agonists with lower efficacy display more robust responses and increased potencies at G α_s . Therefore, if it is desired to selectively target D₁R signalling in the striatum then it can be achieved with a partial agonist, whereas if wanting to target both brain regions, a full agonist could be used.

We observed in both Chapter 3 and Chapter 4 that ergot agonists at the D₂R displayed bias. This was unexpected particularly considering we carried along previously reported biased agonists in Chapter 4, with their bias being overshadowed. While the ergot agonists share common structural similarities, it is not entirely clear how this bias emerged. It requires further investigation into how this may manifest.

In Chapter 5 we were able to convincingly show that an increase in potency at Gα_z is due to its slow GTP hydrolysis rate which leads to an accumulation of the active Gα_z-GTP species over time. Based on this work, we propose that the D₂R temporal responses may be regulated depending on Gα_{i/o} protein expression patterns (Fig. 7.2). At a neuronal synapse, dopamine is released and then rapidly taken up by dopamine transporters and broken down by MOA-B. Dopamine has a rapid dissociation rate from the D₂R (96). Therefore, as dopamine is taken up, the dopamine will leave the receptor and the receptor will be rapidly deactivated. If a Gα_i or Gα_o subtype is expressed, then the G protein signal will be rapidly switched off as the G protein hydrolyses the bound GTP. Yet, if Gα_z is expressed the it will continue to be active for several minutes (Fig. 7.2). Moreover, if there is sustained dopamine release or activation by exogenous agonists such as those in the treatment of Parkinson's disease, then arrestins may couple to sterically occlude G protein coupling and turn off the signal. Similarly, Gα_z will have already coupled and, based on our data in Chapter 5, it will again remain active in live cells for several minutes. We believe this model is highly plausible based on work in knockout mice demonstrating many D₂R dependent behaviours are altered and additionally that the D₂R has been suggested to couple to the Gα_z in rat pituitary tissues (148,150,151). However, the model needs to be considered in light of RGS proteins that regulate G proteins responses such as RGS9-2, known to regulate the D₂R in some instances (152). Furthermore, if this model does hold true this could also be a situation where natural system bias is harnessed.

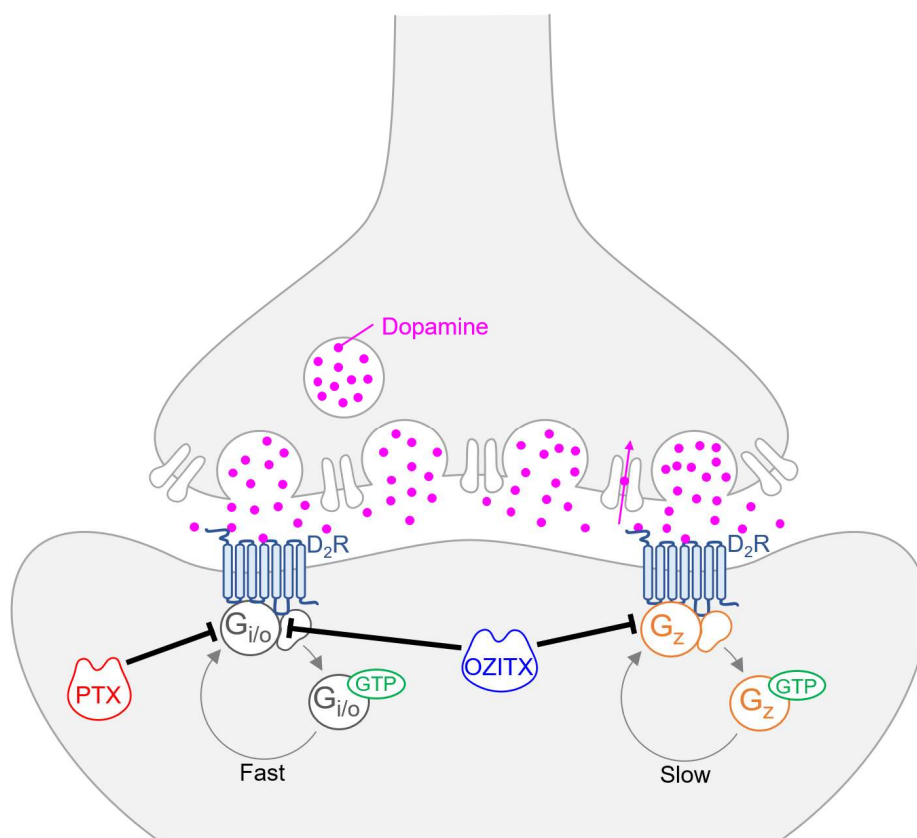


Figure 7.2: Identification of a novel D₂R G protein signalling wave and a new toxin for its inhibition. Dopamine is released from a neuron and can bind postsynaptic D₂Rs. This leads to a rapid yet short period of activation of the D₂R as dopamine dissociates and is then taken up by dopamine transporters and/or broken down by MOA-B. The D₂R can produce a short and sharp signalling wave upon coupling to G_{αi} or G_{αo} subunits as their GTP hydrolysis rates are fast and thus will be deactivated shortly after the receptor deactivates. In contrast, G_{αz} coupling will produce a sustained signalling wave due to its slow GTP hydrolysis rate even though dopamine has dissociated from the D₂R and the D₂R is no longer active. This slow and sustained G_{αz} signalling wave may produce distinct physiological effects. Moreover, PTX is able to act on G_{αi/o} proteins to inhibit the rapid signalling wave produced by these proteins whereas the newly characterised OZITX can block these proteins in addition to the G_{αz} signalling, providing a new tool to study this largely unexplored signalling.

Finally, in Chapter 6 we were able to demonstrate that a new AB₅ toxin – OZITX, could completely abolish G_{αz} activation and G_{αz} dependent cAMP inhibition. Thus, this is the first pan G_{αi/o} inhibitor that importantly acts on G_{αz} (Fig. 7.2). OZITX can be used by the scientific community in many ways. Of relevance to the work in Chapter 5, OZITX could be used in combination with PTX to disentangle D₂R signalling through G_{αz} from D₂R signalling through other G_{αi/o} subunits. Additionally, OZITX can be used as a replacement for PTX when it is used to block G_{αi/o} signalling to assess arrestin dependent signalling. PTX is commonly used in this manner even though it lacks the ability to block G_{αz} (426). Any study that has not recognised that G_{αz} signalling is a potential contaminant should be re-assessed in this context. Furthermore, the Chapter also presents the idea that AB₅ toxins are underutilised tools. Some of the first work describing G protein signalling relied

heavily on the use of AB₅ toxins such as PTX and CTX (349). These tools are underappreciated because they completely abolish coupling due to the covalent modifications that they make on the G protein. Other peptide and small molecule inhibitors for Gα_{q/11} and Gα_{s/olf} are available, however, their inhibition is dependent on the concentration of the inhibitor that can be achieved within the cell (445,446).

The use of BRET as a detection technique in Chapters 2, 3, 4 and 5 provides several advantages. These include high sensitivity, moderate throughput, ability to measure temporally, perform experiments at physiological temperatures and measure in live cells. Yet, BRET sensors generally require over-expression of the sensors. This may alter the stoichiometry of the interactions between effectors in some cases. This is as a potential limitation when examining biased agonism. However, this is likely not a major issue within the thesis because any over expression of the effectors should bias the signalling allosterically towards that pathway such that when assessing biased agonism the bias may be larger than in native cells. Very little biased agonism was observed in this research and therefore this effect is likely not a contributor.

In conclusion, the studies presented here provide a detailed kinetic insight into D₂R ligand binding, activation and regulation. Further, we propose a novel D₂R Gα_z signalling wave and we provide the first tool to entirely abolish Gα_z activation – a pan Gα_{i/o} acting toxin. Overall, the findings here should help guide future drug discovery efforts aiming to rationally develop biased agonists at the D₂R.

References

1. Rosenbaum, D. M., Rasmussen, S. G. F., and Kobilka, B. K. (2009) The structure and function of G-protein-coupled receptors. *Nature* **459**, 356-363
2. Hauser, A. S., Attwood, M. M., Rask-Andersen, M., Schiöth, H. B., and Gloriam, D. E. (2017) Trends in GPCR drug discovery: new agents, targets and indications. *Nature reviews Drug discovery* **16**, 829
3. Fredriksson, R., Lagerström, M. C., Lundin, L.-G., and Schiöth, H. B. (2003) The G-protein-coupled receptors in the human genome form five main families. Phylogenetic analysis, paralogon groups, and fingerprints. *Molecular pharmacology* **63**, 1256-1272
4. Schiöth, H. B., and Fredriksson, R. (2005) The GRAFS classification system of G-protein coupled receptors in comparative perspective. *General and comparative endocrinology* **142**, 94-101
5. Lagerstrom, M. C., and Schioth, H. B. (2008) Structural diversity of G protein-coupled receptors and significance for drug discovery. *Nat Rev Drug Discov* **7**, 339-357
6. Kniazeff, J., Prézeau, L., Rondard, P., Pin, J.-P., and Goudet, C. (2011) Dimers and beyond: The functional puzzles of class C GPCRs. *Pharmacology & therapeutics* **130**, 9-25
7. Farrens, D. L., Altenbach, C., Yang, K., Hubbell, W. L., and Khorana, H. G. (1996) Requirement of rigid-body motion of transmembrane helices for light activation of rhodopsin. *Science (New York, N.Y.)* **274**, 768-770
8. Sullivan, K. A., Miller, R. T., Masters, S. B., Beiderman, B., Heideman, W., and Bourne, H. R. (1987) Identification of receptor contact site involved in receptor–G protein coupling. *Nature* **330**, 758
9. Hamm, H. E., Deretic, D., Arendt, A., Hargrave, P. A., Koenig, B., and Hofmann, K. P. (1988) Site of G protein binding to rhodopsin mapped with synthetic peptides from the alpha subunit. *Science (New York, N.Y.)* **241**, 832-835
10. Digby, G. J., Lober, R. M., Sethi, P. R., and Lambert, N. A. (2006) Some G protein heterotrimers physically dissociate in living cells. *Proceedings of the National Academy of Sciences* **103**, 17789-17794
11. Bünemann, M., Frank, M., and Lohse, M. J. (2003) Gi protein activation in intact cells involves subunit rearrangement rather than dissociation. *Proceedings of the National Academy of Sciences* **100**, 16077-16082
12. Luttrell, L. M. (2008) Reviews in Molecular Biology and Biotechnology: Transmembrane Signaling by G Protein-Coupled Receptors. *Molecular Biotechnology* **39**, 239-264
13. Dohlman, H. G., and Thorner, J. (1997) RGS proteins and signaling by heterotrimeric G proteins. *Journal of Biological Chemistry* **272**, 3871-3874
14. Khan, S. M., Sleno, R., Gora, S., Zylbergold, P., Laverdure, J. P., Labbe, J. C., Miller, G. J., and Hebert, T. E. (2013) The expanding roles of Gbetagamma subunits in G protein-coupled receptor signaling and drug action. *Pharmacological reviews* **65**, 545-577
15. R K Sunahara, C W Dessauer, a., and Gilman, A. G. (1996) Complexity and Diversity of Mammalian Adenylyl Cyclases. *Annual Review of Pharmacology and Toxicology* **36**, 461-480
16. Exton, J. H. (1996) Regulation of Phosphoinositide Phospholipases by Hormones, Neurotransmitters, and Other Agonists Linked to G Proteins. *Annual Review of Pharmacology and Toxicology* **36**, 481-509
17. Worzfeld, T., Wettschureck, N., and Offermanns, S. (2008) G12/G13-mediated signalling in mammalian physiology and disease. *Trends in pharmacological sciences* **29**, 582-589
18. Milligan, G., and Kostenis, E. (2006) Heterotrimeric G-proteins: a short history. *British journal of pharmacology* **147**, S46-S55
19. Casey, P. J., Fong, H. K., Simon, M. I., and Gilman, A. G. (1990) Gz, a guanine nucleotide-binding protein with unique biochemical properties. *Journal of Biological Chemistry* **265**, 2383-2390
20. Gurevich, E. V., Tesmer, J. J. G., Mushegian, A., and Gurevich, V. V. (2012) G protein-coupled receptor kinases: more than just kinases and not only for GPCRs. *Pharmacology & therapeutics* **133**, 40-69

21. Gurevich, V. V., and Gurevich, E. V. (2019) The structural basis of the arrestin binding to GPCRs. *Molecular and cellular endocrinology*
22. Kang, Y., Zhou, X. E., Gao, X., He, Y., Liu, W., Ishchenko, A., Barty, A., White, T. A., Yefanov, O., and Han, G. W. (2015) Crystal structure of rhodopsin bound to arrestin by femtosecond X-ray laser. *Nature* **523**, 561-567
23. Staus, D. P., Hu, H., Robertson, M. J., Kleinhenz, A. L., Wingler, L. M., Capel, W. D., Latorraca, N. R., Lefkowitz, R. J., and Skiniotis, G. (2020) Structure of the M2 muscarinic receptor- β -arrestin complex in a lipid nanodisc. *Nature* **579**, 297-302
24. Lohse, M. J., Benovic, J. L., Codina, J., Caron, M. G., and Lefkowitz, R. J. (1990) β -Arrestin: a protein that regulates β -adrenergic receptor function. *Science (New York, N.Y.)* **248**, 1547-1550
25. Ferguson, S. S. G., Downey, W. E., III, Colapietro, A.-M., Barak, L. S., and et al. (1996) Role of β -arrestin in mediating agonist-promoted G protein-coupled receptor internalization. *Science (New York, N.Y.)* **271**, 363
26. Goodman, O. B., Krupnick, J. G., Santini, F., Gurevich, V. V., Penn, R. B., Gagnon, A. W., Keen, J. H., and Benovic, J. L. (1996) β -Arrestin acts as a clathrin adaptor in endocytosis of the β 2-adrenergic receptor. *Nature* **383**, 447-450
27. Jean-Alphonse, F., and Hanyaloglu, A. (2011) Regulation of GPCR signal networks via membrane trafficking. *Molecular and cellular endocrinology* **331**, 205-214
28. Cattaneo, F., Parisi, M., Fioretti, T., Esposito, G., and Ammendola, R. (2016) Intranuclear Signaling Cascades Triggered by Nuclear GPCRs. *J Cell*
29. Irannejad, R., Tomshine, J. C., Tomshine, J. R., Chevalier, M., Mahoney, J. P., Steyaert, J., Rasmussen, S. G., Sunahara, R. K., El-Samad, H., and Huang, B. (2013) Conformational biosensors reveal GPCR signalling from endosomes. *Nature* **495**, 534-538
30. Navratil, A. M., Bliss, S. P., Berghorn, K. A., Haughian, J. M., Farmerie, T. A., Graham, J. K., Clay, C. M., and Roberson, M. S. (2003) Constitutive localization of the gonadotropin-releasing hormone (GnRH) receptor to low density membrane microdomains is necessary for GnRH signaling to ERK. *Journal of Biological Chemistry* **278**, 31593-31602
31. Mullershausen, F., Zecri, F., Cetin, C., Billich, A., Guerini, D., and Seuwen, K. (2009) Persistent signaling induced by FTY720-phosphate is mediated by internalized S1P1 receptors. *Nature chemical biology* **5**, 428-434
32. Ferrandon, S., Feinstein, T. N., Castro, M., Wang, B., Bouley, R., Potts, J. T., Gardella, T. J., and Vilardaga, J.-P. (2009) Sustained cyclic AMP production by parathyroid hormone receptor endocytosis. *Nature chemical biology* **5**, 734-742
33. Calebiro, D., Nikolaev, V. O., Gagliani, M. C., De Filippis, T., Dees, C., Tacchetti, C., Persani, L., and Lohse, M. J. (2009) Persistent cAMP-signals triggered by internalized G-protein-coupled receptors. *PLoS Biol* **7**, e1000172
34. Stoeber, M., Jullié, D., Lobingier, B. T., Laeremans, T., Steyaert, J., Schiller, P. W., Manglik, A., and von Zastrow, M. (2018) A genetically encoded biosensor reveals location bias of opioid drug action. *Neuron* **98**, 963-976. e965
35. Wehbi, V. L., Stevenson, H. P., Feinstein, T. N., Calero, G., Romero, G., and Vilardaga, J.-P. (2013) Noncanonical GPCR signaling arising from a PTH receptor-arrestin-G β y complex. *Proceedings of the National Academy of Sciences* **110**, 1530-1535
36. Gutkind, J. S., and Kostenis, E. (2018) Arrestins as rheostats of GPCR signalling. *Nature Reviews Molecular Cell Biology* **19**, 615-616
37. Miller, W. E., and Lefkowitz, R. J. (2001) Expanding roles for β -arrestins as scaffolds and adapters in GPCR signaling and trafficking. *Current opinion in cell biology* **13**, 139-145
38. Xiao, K., McClatchy, D. B., Shukla, A. K., Zhao, Y., Chen, M., Shenoy, S. K., Yates, J. R., and Lefkowitz, R. J. (2007) Functional specialization of β -arrestin interactions revealed by proteomic analysis. *Proceedings of the National Academy of Sciences* **104**, 12011-12016
39. Evron, T., Daigle, T. L., and Caron, M. G. (2012) GRK2: multiple roles beyond G protein-coupled receptor desensitization. *Trends in pharmacological sciences* **33**, 154-164
40. Tolkovsky, A. M., and Levitzki, A. (1978) Coupling of a single adenylate cyclase of two receptors: adenosine and catecholamine. *Biochemistry* **17**, 3811-3817

41. Halls, M. L. (2012) Constitutive formation of an RXFP1-signalosome: a novel paradigm in GPCR function and regulation. *British journal of pharmacology* **165**, 1644-1658
42. Spooren, A., Rondou, P., Debowska, K., Lintermans, B., Vermeulen, L., Samyn, B., Skieterska, K., Debyser, G., Devreese, B., Vanhoenacker, P., Wojda, U., Haegeman, G., and Van Craenenbroeck, K. (2010) Resistance of the dopamine D4 receptor to agonist-induced internalization and degradation. *Cellular Signalling* **22**, 600-609
43. Guo, W., Shi, L., and Javitch, J. A. (2003) The fourth transmembrane segment forms the interface of the dopamine D2 receptor homodimer. *Journal of Biological Chemistry* **278**, 4385-4388
44. Lane, J. R., Donthamsetti, P., Shonberg, J., Draper-Joyce, C. J., Dentry, S., Michino, M., Shi, L., López, L., Scammells, P. J., and Capuano, B. (2014) A new mechanism of allostery in a G protein-coupled receptor dimer. *Nature chemical biology* **10**, 745-752
45. Ferre, S., Von Euler, G., Johansson, B., Fredholm, B. B., and Fuxe, K. (1991) Stimulation of high-affinity adenosine A2 receptors decreases the affinity of dopamine D2 receptors in rat striatal membranes. *Proceedings of the National Academy of Sciences* **88**, 7238-7241
46. Canals, M., Marcellino, D., Fanelli, F., Ciruela, F., De Benedetti, P., Goldberg, S. R., Neve, K., Fuxe, K., Agnati, L. F., and Woods, A. S. (2003) Adenosine A2A-dopamine D2 receptor-receptor heteromerization qualitative and quantitative assessment by fluorescence and bioluminescence energy transfer. *Journal of Biological Chemistry* **278**, 46741-46749
47. Trifilieff, P., Rives, M.-L., Urizar, E., Piskorowski, R. A., Vishwasrao, H. D., Castrillon, J., Schmauss, C., Slättman, M., Gullberg, M., and Javitch, J. A. (2011) Detection of antigen interactions ex vivo by proximity ligation assay: endogenous dopamine D2-adenosine A2A receptor complexes in the striatum. *Biotechniques* **51**, 111-118
48. Fenu, S., Pinna, A., Ongini, E., and Morelli, M. (1997) Adenosine A2A receptor antagonism potentiates L-DOPA-induced turning behaviour and c-fos expression in 6-hydroxydopamine-lesioned rats. *European journal of pharmacology* **321**, 143-147
49. Koschatzky, S., Tschammer, N., and Gmeiner, P. (2011) Cross-receptor interactions between dopamine D2L and neurotensin NTS1 receptors modulate binding affinities of dopaminergics. *ACS chemical neuroscience* **2**, 308-316
50. Borroto-Escuela, D. O., Ravani, A., Tarakanov, A. O., Brito, I., Narvaez, M., Romero-Fernandez, W., Corrales, F., Agnati, L. F., Tanganelli, S., Ferraro, L., and Fuxe, K. (2013) Dopamine D2 receptor signaling dynamics of dopamine D2-neurotensin 1 receptor heteromers. *Biochemical and Biophysical Research Communications* **435**, 140-146
51. Dziedzicka-Wasylewska, M., Faron-Górecka, A., Andrecka, J., Polit, A., Kusmider, M., and Wasylewski, Z. (2006) Fluorescence studies reveal heterodimerization of dopamine D1 and D2 receptors in the plasma membrane. *Biochemistry* **45**, 8751-8759
52. Guo, D., Hillger, J. M., IJzerman, A. P., and Heitman, L. H. (2014) Drug-Target Residence Time—A Case for G Protein-Coupled Receptors. *Medicinal research reviews* **34**, 856-892
53. Vauquelin, G. (2016) Effects of target binding kinetics on in vivo drug efficacy: koff, kon and rebinding. *British journal of pharmacology* **173**, 2319-2334
54. Vauquelin, G., and Charlton, S. J. (2010) Long-lasting target binding and rebinding as mechanisms to prolong in vivo drug action. *British journal of pharmacology* **161**, 488-508
55. de Witte, W. E., Danhof, M., van der Graaf, P. H., and de Lange, E. C. (2016) In vivo target residence time and kinetic selectivity: the association rate constant as determinant. *Trends in pharmacological sciences* **37**, 831-842
56. Copeland, R. A. (2016) The drug-target residence time model: a 10-year retrospective. *Nature Reviews Drug Discovery* **15**, 87
57. Sykes, D. A., Stoddart, L. A., Kilpatrick, L. E., and Hill, S. J. (2019) Binding kinetics of ligands acting at GPCRs. *Molecular and cellular endocrinology*
58. Tautermann, C. S. (2016) Impact, determination and prediction of drug-receptor residence times for GPCRs. *Current Opinion in Pharmacology* **30**, 22-26
59. Abrahamsson, T., Karp, L., Brandt-Eliasson, U., Morsing, P., Renberg, L., and SJOeQUIST, P.-O. (2000) Candesartan Causes Long-lasting Antagonism of the Angiotensin II Receptor-mediated Contractile Effects in Isolated Vascular Preparations: a

- Comparison with Irbesartan, Losartan and its Active Metabolite (EXP-3174). *Blood pressure* **9**, 52-52
60. Hothersall, J. D., Brown, A. J., Dale, I., and Rawlins, P. (2016) Can residence time offer a useful strategy to target agonist drugs for sustained GPCR responses? *Drug discovery today* **21**, 90-96
 61. Sykes, D. A., Moore, H., Stott, L., Holliday, N., Javitch, J. A., Lane, J. R., and Charlton, S. J. (2017) Extrapyramidal side effects of antipsychotics are linked to their association kinetics at dopamine D2 receptors. *Nature Communications* **8**, 763
 62. Miller, D. C., Lunn, G., Jones, P., Sabnis, Y., Davies, N. L., and Driscoll, P. (2012) Investigation of the effect of molecular properties on the binding kinetics of a ligand to its biological target. *Medchemcomm* **3**, 449-452
 63. Guo, D., Xia, L., van Veldhoven, J. P., Hazeu, M., Mocking, T., Brussee, J., IJzerman, A. P., and Heitman, L. H. (2014) Binding kinetics of ZM241385 derivatives at the human adenosine A2A receptor. *ChemMedChem* **9**, 752-761
 64. Alonso, J. A., Andrés, M., Bravo, M., Buil, M. A., Calbet, M., Castro, J., Eastwood, P. R., Esteve, C., Ferrer, M., and Forns, P. (2014) Structure–activity relationships (SAR) and structure–kinetic relationships (SKR) of bicyclic heteroaromatic acetic acids as potent CRTh2 antagonists III: The role of a hydrogen-bond acceptor in long receptor residence times. *Bioorganic & medicinal chemistry letters* **24**, 5127-5133
 65. Dror, R. O., Pan, A. C., Arlow, D. H., Borhani, D. W., Maragakis, P., Shan, Y., Xu, H., and Shaw, D. E. (2011) Pathway and mechanism of drug binding to G-protein-coupled receptors. *Proceedings of the National Academy of Sciences* **108**, 13118-13123
 66. Haga, K., Kruse, A. C., Asada, H., Yurugi-Kobayashi, T., Shiroishi, M., Zhang, C., Weis, W. I., Okada, T., Kobilka, B. K., and Haga, T. (2012) Structure of the human M2 muscarinic acetylcholine receptor bound to an antagonist. *Nature* **482**, 547-551
 67. Kruse, A. C., Hu, J., Pan, A. C., Arlow, D. H., Rosenbaum, D. M., Rosemond, E., Green, H. F., Liu, T., Chae, P. S., Dror, R. O., Shaw, D. E., Weis, W. I., Wess, J., and Kobilka, B. K. (2012) Structure and dynamics of the M3 muscarinic acetylcholine receptor. *Nature* **482**, 552-556
 68. Disse, B., Reichl, R., Speck, G., Traunecker, W., Rominger, K. L., and Hammer, R. (1993) Ba 679 BR, A novel long-acting anticholinergic bronchodilator. *Life Sciences* **52**, 537-544
 69. Tautermann, C. S., Kiechle, T., Seeliger, D., Diehl, S., Wex, E., Banholzer, R., Gantner, F., Pieper, M. P., and Casarosa, P. (2013) Molecular Basis for the Long Duration of Action and Kinetic Selectivity of Tiotropium for the Muscarinic M3 Receptor. *Journal of medicinal chemistry* **56**, 8746-8756
 70. Violin, J. D., and Lefkowitz, R. J. (2007) β -Arrestin-biased ligands at seven-transmembrane receptors. *Trends in pharmacological sciences* **28**, 416-422
 71. Palanche, T., Ilien, B., Zoffmann, S., Reck, M.-P., Bucher, B., Edelstein, S. J., and Galzi, J.-L. (2001) The neurokinin A receptor activates calcium and cAMP responses through distinct conformational states. *Journal of Biological Chemistry* **276**, 34853-34861
 72. Swaminath, G., Xiang, Y., Lee, T. W., Steenhuis, J., Parnot, C., and Kobilka, B. K. (2004) Sequential Binding of Agonists to the β_2 Adrenoceptor KINETIC EVIDENCE FOR INTERMEDIATE CONFORMATIONAL STATES. *Journal of Biological Chemistry* **279**, 686-691
 73. Kenakin, T. (2007) Collateral efficacy in drug discovery: taking advantage of the good (allosteric) nature of 7TM receptors. *Trends in pharmacological sciences* **28**, 407-415
 74. Okude, J., Ueda, T., Kofuku, Y., Sato, M., Nobuyama, N., Kondo, K., Shiraishi, Y., Mizumura, T., Onishi, K., and Natsume, M. (2015) Identification of a Conformational Equilibrium That Determines the Efficacy and Functional Selectivity of the μ -Opioid Receptor. *Angewandte Chemie* **127**, 15997-16002
 75. Liu, J. J., Horst, R., Katritch, V., Stevens, R. C., and Wüthrich, K. (2012) Biased Signaling Pathways in β_2 -Adrenergic Receptor Characterized by 19F-NMR. *Science (New York, N.Y.)* **335**, 1106-1110
 76. Strachan, R. T., Sun, J.-p., Rominger, D. H., Violin, J. D., Ahn, S., Thomsen, A. R. B., Zhu, X., Kleist, A., Costa, T., and Lefkowitz, R. J. (2014) Divergent transducer-specific molecular

- efficacies generate biased agonism at a G protein-coupled receptor (GPCR). *Journal of Biological Chemistry* **289**, 14211-14224
77. Wacker, D., Wang, C., Katritch, V., Han, G. W., Huang, X.-P., Vardy, E., McCorvy, J. D., Jiang, Y., Chu, M., Siu, F. Y., Liu, W., Xu, H. E., Cherezov, V., Roth, B. L., and Stevens, R. C. (2013) Structural Features for Functional Selectivity at Serotonin Receptors. *Science (New York, N.Y.)* **340**, 615-619
 78. Bohn, L. M., Gainetdinov, R. R., Lin, F.-T., Lefkowitz, R. J., and Caron, M. G. (2000) μ -Opioid receptor desensitization by β -arrestin-2 determines morphine tolerance but not dependence. *Nature* **408**, 720-723
 79. Viscusi, E. R., Webster, L., Kuss, M., Daniels, S., Bolognese, J. A., Zuckerman, S., Soergel, D. G., Subach, R. A., Cook, E., and Skobieranda, F. (2016) A randomized, phase 2 study investigating TRV130, a biased ligand of the μ -opioid receptor, for the intravenous treatment of acute pain. *Pain* **157**, 264-272
 80. Manglik, A., Lin, H., Aryal, D. K., McCorvy, J. D., Dengler, D., Corder, G., Levit, A., Kling, R. C., Bernat, V., and Hübner, H. (2016) Structure-based discovery of opioid analgesics with reduced side effects. *Nature* **537**, 185-190
 81. Schmid, C. L., Kennedy, N. M., Ross, N. C., Lovell, K. M., Yue, Z., Morgenweck, J., Cameron, M. D., Bannister, T. D., and Bohn, L. M. (2017) Bias factor and therapeutic window correlate to predict safer opioid analgesics. *Cell* **171**, 1165-1175. e1113
 82. Hill, R., Disney, A., Conibear, A., Sutcliffe, K., Dewey, W., Husbands, S., Bailey, C., Kelly, E., and Henderson, G. (2018) The novel μ -opioid receptor agonist PZM21 depresses respiration and induces tolerance to antinociception. *British journal of pharmacology* **175**, 2653-2661
 83. Kliewer, A., Schmiedel, F., Sianati, S., Bailey, A., Bateman, J., Levitt, E., Williams, J., Christie, M., and Schulz, S. (2019) Phosphorylation-deficient G-protein-biased μ -opioid receptors improve analgesia and diminish tolerance but worsen opioid side effects. *Nature communications* **10**, 1-11
 84. Kliewer, A., Gillis, A., Hill, R., Schmidel, F., Bailey, C., Kelly, E., Henderson, G., Christie, M. J., and Schulz, S. (2020) Morphine-induced respiratory depression is independent of β -arrestin2 signalling. *British journal of pharmacology*
 85. Michel, M. C., and Charlton, S. J. (2018) Biased agonism in drug discovery—is it too soon to choose a path? *Molecular pharmacology* **93**, 259-265
 86. Black, J., and Leff, P. (1983) Operational models of pharmacological agonism. *Proceedings of the Royal Society of London B: Biological Sciences* **220**, 141-162
 87. Kenakin, T., Watson, C., Muniz-Medina, V., Christopoulos, A., and Novick, S. (2012) A simple method for quantifying functional selectivity and agonist bias. *ACS chemical neuroscience* **3**, 193-203
 88. Birdsong, W. T., Arttamangkul, S., Clark, M. J., Cheng, K., Rice, K. C., Traynor, J. R., and Williams, J. T. (2013) Increased agonist affinity at the μ -opioid receptor induced by prolonged agonist exposure. *The Journal of Neuroscience* **33**, 4118-4127
 89. DeVree, B. T., Mahoney, J. P., Vélez-Ruiz, G. A., Rasmussen, S. G., Kuszak, A. J., Edwald, E., Fung, J.-J., Manglik, A., Masureel, M., and Du, Y. (2016) Allosteric coupling from G protein to the agonist-binding pocket in GPCRs. *Nature* **535**, 182-186
 90. Paton, W. D. M. (1961) A theory of drug action based on the rate of drug-receptor combination. *Proceedings of the Royal Society of London. Series B. Biological Sciences* **154**, 21-69
 91. Sykes, D. A., Dowling, M. R., and Charlton, S. J. (2009) Exploring the mechanism of agonist efficacy: a relationship between efficacy and agonist dissociation rate at the muscarinic M3 receptor. *Molecular pharmacology* **76**, 543-551
 92. Deng, H., Sun, H., and Fang, Y. (2013) Label-free cell phenotypic assessment of the biased agonism and efficacy of agonists at the endogenous muscarinic M 3 receptors. *J. Pharmacol. Toxicol. Methods* **68**, 323-333
 93. Guo, D., Mulder-Krieger, T., IJzerman, A. P., and Heitman, L. H. (2012) Functional efficacy of adenosine A2A receptor agonists is positively correlated to their receptor residence time. *British journal of pharmacology* **166**, 1846-1859

94. Hoeren, M., Brawek, B., Mantovani, M., Löffler, M., Steffens, M., van Velthoven, V., and Feuerstein, T. J. (2008) Partial agonism at the human $\alpha 2A$ -autoreceptor: role of binding duration. *Naunyn-Schmiedeberg's archives of pharmacology* **378**, 17
95. Rosethorne, E. M., Bradley, M. E., Gherbi, K., Sykes, D. A., Sattikar, A., Wright, J. D., Renard, E., Trifilieff, A., Fairhurst, R. A., and Charlton, S. J. (2016) Long Receptor Residence Time of C26 Contributes to Super Agonist Activity at the Human $\beta 2$ Adrenoceptor. *Molecular pharmacology* **89**, 467-475
96. Klein-Herenbrink, C., Sykes, D. A., Donthamsetti, P., Canals, M., Coudrat, T., Shonberg, J., Scammells, P. J., Capuano, B., Sexton, P. M., and Charlton, S. J. (2016) The role of kinetic context in apparent biased agonism at GPCRs. *Nature communications* **7**
97. Wacker, D., Wang, S., McCorvy, J. D., Betz, R. M., Venkatakrishnan, A. J., Levit, A., Lansu, K., Schools, Z. L., Che, T., Nichols, D. E., Shoichet, B. K., Dror, R. O., and Roth, B. L. (2017) Crystal Structure of an LSD-Bound Human Serotonin Receptor. *Cell* **168**, 377-389.e312
98. Kaiser, A., Wanka, L., Ziffert, I., and Beck-Sickinger, A. G. (2020) Biased agonists at the human Y 1 receptor lead to prolonged membrane residency and extended receptor G protein interaction. *Cellular and Molecular Life Sciences*, 1-17
99. D'Souza, U. M. (2010) Gene and Promoter Structures of the Dopamine Receptors. in *The Dopamine Receptors*, Springer. pp 23-46
100. Dal Toso, R., Sommer, B., Ewert, M., Herb, A., Pritchett, D. B., Bach, A., Shivers, B. D., and Seeburg, P. H. (1989) The dopamine D2 receptor: two molecular forms generated by alternative splicing. *The EMBO journal* **8**, 4025
101. Lindgren, N., Usiello, A., Goiny, M., Haycock, J., Erbs, E., Greengard, P., Hökfelt, T., Borrelli, E., and Fisone, G. (2003) Distinct roles of dopamine D2L and D2S receptor isoforms in the regulation of protein phosphorylation at presynaptic and postsynaptic sites. *Proceedings of the National Academy of Sciences* **100**, 4305-4309
102. Namkung, Y., Dipace, C., Javitch, J. A., and Sibley, D. R. (2009) G Protein-coupled Receptor Kinase-mediated Phosphorylation Regulates Post-endocytic Trafficking of the D2 Dopamine Receptor. *Journal of Biological Chemistry* **284**, 15038-15051
103. Beaulieu, J.-M., and Gainetdinov, R. R. (2011) The Physiology, Signaling, and Pharmacology of Dopamine Receptors. *Pharmacological reviews* **63**, 182-217
104. Seeman, P. (2006) Targeting the dopamine D2 receptor in schizophrenia. *Expert Opinion on Therapeutic Targets* **10**, 515-531
105. Uitti, R. J., and Ahlskog, J. E. (1996) Comparative Review of Dopamine Receptor Agonists in Parkinson's Disease. *CNS Drugs* **5**, 369-388
106. Hening, W. A., Allen, R. P., Earley, C. J., Picchiatti, D. L., and Silber, M. H. (2004) An update on the dopaminergic treatment of restless legs syndrome and periodic limb movement disorder. *Sleep* **27**, 560-583
107. Tohen, M., and Vieta, E. (2009) Antipsychotic agents in the treatment of bipolar mania. *Bipolar Disorders* **11**, 45-54
108. Mansour, A., Meador-Woodruff, J., Bunzow, J., Civelli, O., Akil, H., and Watson, S. (1990) Localization of dopamine D2 receptor mRNA and D1 and D2 receptor binding in the rat brain and pituitary: an in situ hybridization-receptor autoradiographic analysis. *Journal of neuroscience* **10**, 2587-2600
109. Missale, C., Nash, S. R., Robinson, S. W., Jaber, M., and Caron, M. G. (1998) Dopamine receptors: from structure to function. *Physiological reviews* **78**, 189-225
110. Jackson, D. M., and Westlind-Danielsson, A. (1994) Dopamine receptors: molecular biology, biochemistry and behavioural aspects. *Pharmacology & therapeutics* **64**, 291-370
111. Jang, J. Y., Jang, M., Kim, S. H., Um, K. B., Kang, Y. K., Kim, H. J., Chung, S., and Park, M. K. (2011) Regulation of dopaminergic neuron firing by heterogeneous dopamine autoreceptors in the substantia nigra pars compacta. *Journal of neurochemistry* **116**, 966-974
112. Rubí, B., Ljubicic, S., Pournourmohammadi, S., Carobbio, S., Armanet, M., Bartley, C., and Maechler, P. (2005) Dopamine D2-like receptors are expressed in pancreatic beta cells and mediate inhibition of insulin secretion. *Journal of Biological Chemistry* **280**, 36824-36832

113. Li, Z. S., Schmauss, C., Cuenca, A., Ratcliffe, E., and Gershon, M. D. (2006) Physiological modulation of intestinal motility by enteric dopaminergic neurons and the D2 receptor: analysis of dopamine receptor expression, location, development, and function in wild-type and knock-out mice. *Journal of Neuroscience* **26**, 2798-2807
114. Wang, Q., Ji, T., Zheng, L.-F., Feng, X.-Y., Wang, Z.-Y., Lian, H., Song, J., Li, X.-F., Zhang, Y., and Zhu, J.-X. (2012) Cellular localization of dopamine receptors in the gastric mucosa of rats. *Biochemical and biophysical research communications* **417**, 197-203
115. Liu, L., Yuan, G., Cheng, Z., Zhang, G., Liu, X., and Zhang, H. (2013) Identification of the mRNA expression status of the dopamine D2 receptor and dopamine transporter in peripheral blood lymphocytes of schizophrenia patients. *PloS one* **8**
116. Castellano, C., Cestari, V., Cabib, S., and Puglisi-Allegra, S. (1991) Post-training dopamine receptor agonists and antagonists affect memory storage in mice irrespective of their selectivity for D1 or D2 receptors. *Behavioral and Neural Biology* **56**, 283-291
117. Cunningham, C. L., Howard, M. A., Gill, S. J., Rubinstein, M., Low, M. J., and Grandy, D. K. (2000) Ethanol-conditioned place preference is reduced in dopamine D2 receptor-deficient mice. *Pharmacology Biochemistry and Behavior* **67**, 693-699
118. Trifilieff, P., Feng, B., Urizar, E., Winiger, V., Ward, R. D., Taylor, K. M., Martinez, D., Moore, H., Balsam, P. D., and Simpson, E. H. (2013) Increasing dopamine D2 receptor expression in the adult nucleus accumbens enhances motivation. *Molecular psychiatry* **18**, 1025-1033
119. Ben-Jonathan, N., and Hnasko, R. (2001) Dopamine as a prolactin (PRL) inhibitor. *Endocrine reviews* **22**, 724-763
120. Baskerville, T. A., and Douglas, A. J. (2008) Interactions between dopamine and oxytocin in the control of sexual behaviour. *Progress in brain research* **170**, 277-290
121. Chien, E. Y., Liu, W., Zhao, Q., Katritch, V., Han, G. W., Hanson, M. A., Shi, L., Newman, A. H., Javitch, J. A., and Cherezov, V. (2010) Structure of the human dopamine D3 receptor in complex with a D2/D3 selective antagonist. *Science (New York, N.Y.)* **330**, 1091-1095
122. Wang, S., Wacker, D., Levit, A., Che, T., Betz, R. M., McCorvy, J. D., Venkatakrishnan, A., Huang, X.-P., Dror, R. O., and Shoichet, B. K. (2017) D4 dopamine receptor high-resolution structures enable the discovery of selective agonists. *Science (New York, N.Y.)* **358**, 381-386
123. Wang, S., Che, T., Levit, A., Shoichet, B. K., Wacker, D., and Roth, B. L. (2018) Structure of the D2 dopamine receptor bound to the atypical antipsychotic drug risperidone. *Nature* **555**, 269
124. Fan, L., Tan, L., Chen, Z., Qi, J., Nie, F., Luo, Z., Cheng, J., and Wang, S. (2020) Haloperidol bound D 2 dopamine receptor structure inspired the discovery of subtype selective ligands. *Nature Communications* **11**, 1-11
125. Lane, J. R., Abramyan, A. M., Adhikari, P., Keen, A. C., Lee, K.-H., Sanchez, J., Verma, R. K., Lim, H. D., Yano, H., and Javitch, J. A. (2020) Distinct inactive conformations of the dopamine D2 and D3 receptors correspond to different extents of inverse agonism. *eLife* **9**, e52189
126. Thomas, T., Fang, Y., Yuriev, E., and Chalmers, D. K. (2016) Ligand binding pathways of clozapine and haloperidol in the dopamine D2 and D3 receptors. *Journal of chemical information and modeling* **56**, 308-321
127. Javitch, J. A., Fu, D., Chen, J., and Karlin, A. (1995) Mapping the binding-site crevice of the dopamine D2 receptor by the substituted-cysteine accessibility method. *Neuron* **14**, 825-831
128. Tresadern, G., Bartolome, J. M., Macdonald, G. J., and Langlois, X. (2011) Molecular properties affecting fast dissociation from the D2 receptor. *Bioorganic & medicinal chemistry* **19**, 2231-2241
129. Dyhring, T., Nielsen, E. Ø., Sonesson, C., Pettersson, F., Karlsson, J., Svensson, P., Christophersen, P., and Waters, N. (2010) The dopaminergic stabilizers pridopidine (ACR16) and (-)-OSU6162 display dopamine D2 receptor antagonism and fast receptor dissociation properties. *European journal of pharmacology* **628**, 19-26

130. Fyfe, T. J., Kellam, B., Sykes, D. A., Capuano, B., Scammells, P. J., Lane, J. R., Charlton, S. J., and Mistry, S. N. (2019) Structure–Kinetic Profiling of Haloperidol Analogues at the Human Dopamine D2 Receptor. *Journal of medicinal chemistry* **62**, 9488-9520
131. Shi, L., and Javitch, J. A. (2004) The second extracellular loop of the dopamine D2 receptor lines the binding-site crevice. *Proceedings of the National Academy of Sciences of the United States of America* **101**, 440-445
132. Masuho, I., Ostrovskaya, O., Kramer, G. M., Jones, C. D., Xie, K., and Martemyanov, K. A. (2015) Distinct profiles of functional discrimination among G proteins determine the actions of G protein–coupled receptors. *Sci. Signal.* **8**, ra123-ra123
133. Obadiah, J., Avidor-Reiss, T., Fishburn, C. S., Carmon, S., Bayewitch, M., Vogel, Z., Fuchs, S., and Levavi-Sivan, B. (1999) Adenylyl Cyclase Interaction with the D2 Dopamine Receptor Family; Differential Coupling to Gi, Gz, and Gs. *Cellular and Molecular Neurobiology* **19**, 653-664
134. Stoof, J., and Kebabian, J. (1981) Opposing roles for D-1 and D-2 dopamine receptors in efflux of cyclic AMP from rat neostriatum. *Nature* **294**, 366-368
135. Cardozo, D. L., and Bean, B. P. (1995) Voltage-dependent calcium channels in rat midbrain dopamine neurons: modulation by dopamine and GABAB receptors. *Journal of neurophysiology* **74**, 1137-1148
136. Schinelli, S., Paolillo, M., and Corona, G. L. (1994) Opposing Actions of D1 and D2-Dopamine Receptors on Arachidonic Acid Release and Cyclic AMP Production in Striatal Neurons. *Journal of neurochemistry* **62**, 944-949
137. Cordeaux, Y., Nickolls, S. A., Flood, L. A., Graber, S. G., and Strange, P. G. (2001) Agonist Regulation of D2 Dopamine Receptor/G Protein Interaction: EVIDENCE FOR AGONIST SELECTION OF G PROTEIN SUBTYPE. *Journal of Biological Chemistry* **276**, 28667-28675
138. Gazi, L., Nickolls, S. A., and Strange, P. G. (2003) Functional coupling of the human dopamine D2 receptor with Gai1, Gai2, Gai3 and Gao G proteins: evidence for agonist regulation of G protein selectivity. *British journal of pharmacology* **138**, 775-786
139. Lane, J. R., Powney, B., Wise, A., Rees, S., and Milligan, G. (2007) Protean agonism at the dopamine D2 receptor:(S)-3-(3-hydroxyphenyl)-N-propylpiperidine is an agonist for activation of Go1 but an antagonist/inverse agonist for Gi1, Gi2, and Gi3. *Molecular pharmacology* **71**, 1349-1359
140. Jiang, M., Spicher, K., Boulay, G., Wang, Y., and Birnbaumer, L. (2001) Most central nervous system D2 dopamine receptors are coupled to their effectors by Go. *Proceedings of the National Academy of Sciences* **98**, 3577-3582
141. Sternweis, P. C., and Robishaw, J. D. (1984) Isolation of two proteins with high affinity for guanine nucleotides from membranes of bovine brain. *Journal of Biological Chemistry* **259**, 13806-13813
142. Neer, E. J., Lok, J., and Wolf, L. (1984) Purification and properties of the inhibitory guanine nucleotide regulatory unit of brain adenylate cyclase. *Journal of Biological Chemistry* **259**, 14222-14229
143. Albert, P. R. (2002) G protein preferences for dopamine D2 inhibition of prolactin secretion and DNA synthesis in GH4 pituitary cells. *Molecular Endocrinology* **16**, 1903-1911
144. Marcott, P. F., Gong, S., Donthamsetti, P., Grinnell, S. G., Nelson, M. N., Newman, A. H., Birnbaumer, L., Martemyanov, K. A., Javitch, J. A., and Ford, C. P. (2018) Regional heterogeneity of D2-receptor signaling in the dorsal striatum and nucleus accumbens. *Neuron* **98**, 575-587. e574
145. Kimple, M. E., Hultman, R. C., and Casey, P. J. (2010) Signaling through Gz. in *Handbook of Cell Signaling*, Elsevier. pp 1649-1653
146. Farino, Z. J., Morgenstern, T. J., Maffei, A., Quick, M., De Solis, A. J., Wiriyasermkul, P., Freyberg, R. J., Aslanoglou, D., Sorisio, D., and Inbar, B. P. (2019) New roles for dopamine D 2 and D 3 receptors in pancreatic beta cell insulin secretion. *Molecular psychiatry*, 1
147. Kimple, M. E., Nixon, A. B., Kelly, P., Bailey, C. L., Young, K. H., Fields, T. A., and Casey, P. J. (2005) A role for Gz in pancreatic islet β -cell biology. *Journal of Biological Chemistry* **280**, 31708-31713

148. Gonzalez-Iglesias, A. E., Murano, T., Li, S., Tomić, M., and Stojilkovic, S. S. (2007) Dopamine inhibits basal prolactin release in pituitary lactotrophs through pertussis toxin-sensitive and-insensitive signaling pathways. *Endocrinology* **149**, 1470-1479
149. Ralph, R. J., Varty, G. B., Kelly, M. A., Wang, Y.-M., Caron, M. G., Rubinstein, M., Grandy, D. K., Low, M. J., and Geyer, M. A. (1999) The dopamine D2, but not D3 or D4, receptor subtype is essential for the disruption of prepulse inhibition produced by amphetamine in mice. *Journal of Neuroscience* **19**, 4627-4633
150. van den Buuse, M., Martin, S., Brosda, J., Leck, K.-J., Matthaei, K., and Hendry, I. (2005) Enhanced effect of dopaminergic stimulation on prepulse inhibition in mice deficient in the alpha subunit of Gz. *Psychopharmacology* **183**, 358-367
151. Leck, K. J., Blaha, C. D., Matthaei, K. I., Forster, G. L., Holgate, J., and Hendry, I. A. (2006) Gz proteins are functionally coupled to dopamine D2-like receptors in vivo. *Neuropharmacology* **51**, 597-605
152. Cabrera-Vera, T. M., Hernandez, S., Earls, L. R., Medkova, M., Sundgren-Andersson, A. K., Surmeier, D. J., and Hamm, H. E. (2004) RGS9-2 modulates D2 dopamine receptor-mediated Ca²⁺ channel inhibition in rat striatal cholinergic interneurons. *Proceedings of the National Academy of Sciences of the United States of America* **101**, 16339-16344
153. Namkung, Y., Dipace, C., Urizar, E., Javitch, J. A., and Sibley, D. R. (2009) G Protein-coupled Receptor Kinase-2 Constitutively Regulates D2 Dopamine Receptor Expression and Signaling Independently of Receptor Phosphorylation. *Journal of Biological Chemistry* **284**, 34103-34115
154. Skinbjerg, M., Ariano, M. A., Thorsell, A., Heilig, M., Halldin, C., Innis, R. B., and Sibley, D. R. (2009) Arrestin3 mediates D2 dopamine receptor internalization. *Synapse (New York, NY)* **63**, 621
155. Beaulieu, J.-M., Sotnikova, T. D., Marion, S., Lefkowitz, R. J., Gainetdinov, R. R., and Caron, M. G. (2005) An Akt/ β -arrestin 2/PP2A signaling complex mediates dopaminergic neurotransmission and behavior. *Cell* **122**, 261-273
156. Namkung, Y., and Sibley, D. R. (2004) Protein Kinase C Mediates Phosphorylation, Desensitization, and Trafficking of the D2 Dopamine Receptor. *Journal of Biological Chemistry* **279**, 49533-49541
157. Jeanneteau, F., Diaz, J., Sokoloff, P., and Griffon, N. (2004) Interactions of GIPC with dopamine D2, D3 but not D4 receptors define a novel mode of regulation of G protein-coupled receptors. *Molecular biology of the cell* **15**, 696-705
158. Nadine, K., Mathew, P. W., Jacob, C. N., and Robert, L. (2012) Dopamine Receptor Interacting Proteins: Targeting Neuronal Calcium Sensor-1/D2 Dopamine Receptor Interaction for Antipsychotic Drug Development. *Current Drug Targets* **13**, 72-79
159. Kabbani, N., Negyessy, L., Lin, R., Goldman-Rakic, P., and Levenson, R. (2002) Interaction with neuronal calcium sensor NCS-1 mediates desensitization of the D2 dopamine receptor. *The Journal of neuroscience* **22**, 8476-8486
160. Smith, F. D., Oxford, G. S., and Milgram, S. L. (1999) Association of the D2 dopamine receptor third cytoplasmic loop with spinophilin, a protein phosphatase-1-interacting protein. *Journal of Biological Chemistry* **274**, 19894-19900
161. Schmieg, N., Rocchi, C., Romeo, S., Maggio, R., Millan, M. J., and Mannoury la Cour, C. (2016) Dysbindin-1 modifies signaling and cellular localization of recombinant, human D3 and D2 receptors. *Journal of neurochemistry* **136**, 1037-1051
162. Liu, Y., Buck, D. C., and Neve, K. A. (2008) Novel Interaction of the Dopamine D2 Receptor and the Ca²⁺ Binding Protein S100B: Role in D2 Receptor Function. *Molecular Pharmacology* **74**, 371-378
163. Saha, S., Chant, D., Welham, J., and McGrath, J. (2005) A systematic review of the prevalence of schizophrenia. *PLoS medicine* **2**
164. Messias, E. L., Chen, C.-Y., and Eaton, W. W. (2007) Epidemiology of schizophrenia: review of findings and myths. *Psychiatric Clinics of North America* **30**, 323-338
165. Andreasen, N. C., Arndt, S., Alliger, R., Miller, D., and Flaum, M. (1995) Symptoms of schizophrenia: Methods, meanings, and mechanisms. *Archives of general psychiatry* **52**, 341-351

166. Howes, O. D., and Kapur, S. (2009) The dopamine hypothesis of schizophrenia: version III—the final common pathway. *Schizophrenia bulletin* **35**, 549-562
167. Keibadian, J. W., and Greengard, P. (1971) Dopamine-sensitive adenyl cyclase: possible role in synaptic transmission. *Science (New York, N.Y.)* **174**, 1346-1349
168. Keibadian, J. W., Petzold, G. L., and Greengard, P. (1972) Dopamine-sensitive adenylate cyclase in caudate nucleus of rat brain, and its similarity to the “dopamine receptor”. *Proceedings of the National Academy of Sciences* **69**, 2145-2149
169. Carlsson, A., and Lindqvist, M. (1963) Effect of chlorpromazine or haloperidol on formation of 3-methoxytyramine and normetanephrine in mouse brain. *Acta pharmacologica et toxicologica* **20**, 140-144
170. Seeman, P., Lee, T., Chau-Wong, M., and Wong, K. (1976) Antipsychotic drug doses and neuroleptic/dopamine receptors. *Nature* **261**, 717-719
171. Keibadian, J. W., and Calne, D. B. (1979) Multiple receptors for dopamine. *Nature* **277**, 93-96
172. Seeman, P., Chau-Wong, M., Tedesco, J., and Wong, K. (1975) Brain receptors for antipsychotic drugs and dopamine: direct binding assays. *Proceedings of the National Academy of Sciences* **72**, 4376-4380
173. Roth, B. L., Sheffler, D. J., and Kroeze, W. K. (2004) Magic shotguns versus magic bullets: selectively non-selective drugs for mood disorders and schizophrenia. *Nature reviews Drug discovery* **3**, 353-359
174. Behere, P. B., Das, A., and Behere, A. P. (2019) Antipsychotics. in *Clinical Psychopharmacology*, Springer. pp 39-87
175. Hippius, H. (1999) A historical perspective of clozapine. *The Journal of clinical psychiatry*
176. Seeman, P. (2002) Atypical antipsychotics: mechanism of action. *The Canadian Journal of Psychiatry* **47**, 29-40
177. Kikuchi, T., Tottori, K., Uwahodo, Y., Hirose, T., Miwa, T., Oshiro, Y., and Morita, S. (1995) 7-(4-[4-(2, 3-Dichlorophenyl)-1-piperazinyl] butyloxy)-3, 4-dihydro-2 (1H)-quinolinone (OPC-14597), a new putative antipsychotic drug with both presynaptic dopamine autoreceptor agonistic activity and postsynaptic D2 receptor antagonistic activity. *Journal of Pharmacology and Experimental Therapeutics* **274**, 329-336
178. Inoue, T., Domae, M., Yamada, K., and Furukawa, T. (1996) Effects of the novel antipsychotic agent 7-(4-[4-(2, 3-dichlorophenyl)-1-piperazinyl] butyloxy)-3, 4-dihydro-2 (1H)-quinolinone (OPC-14597) on prolactin release from the rat anterior pituitary gland. *Journal of Pharmacology and Experimental Therapeutics* **277**, 137-143
179. Newman-Tancredi, A. (2010) The importance of 5-HT_{1A} receptor agonism in antipsychotic drug action: rationale and perspectives. *Current opinion in investigational drugs (London, England: 2000)* **11**, 802-812
180. Mailman, R. B., and Murthy, V. (2010) Third generation antipsychotic drugs: partial agonism or receptor functional selectivity? *Current pharmaceutical design* **16**, 488-501
181. Beaulieu, J.-M., Sotnikova, T. D., Yao, W.-D., Kockeritz, L., Woodgett, J. R., Gainetdinov, R. R., and Caron, M. G. (2004) Lithium antagonizes dopamine-dependent behaviors mediated by an AKT/glycogen synthase kinase 3 signaling cascade. *Proceedings of the National Academy of Sciences of the United States of America* **101**, 5099-5104
182. Emamian, E. S., Hall, D., Birnbaum, M. J., Karayiorgou, M., and Gogos, J. A. (2004) Convergent evidence for impaired AKT1-GSK3 β signaling in schizophrenia. *Nature genetics* **36**, 131-137
183. Masri, B., Salahpour, A., Didriksen, M., Ghisi, V., Beaulieu, J.-M., Gainetdinov, R. R., and Caron, M. G. (2008) Antagonism of dopamine D2 receptor/ β -arrestin 2 interaction is a common property of clinically effective antipsychotics. *Proceedings of the National Academy of Sciences* **105**, 13656-13661
184. Allen, J. A., Yost, J. M., Setola, V., Chen, X., Sassano, M. F., Chen, M., Peterson, S., Yadav, P. N., Huang, X.-p., Feng, B., Jensen, N. H., Che, X., Bai, X., Frye, S. V., Wetsel, W. C., Caron, M. G., Javitch, J. A., Roth, B. L., and Jin, J. (2011) Discovery of β -Arrestin-Biased Dopamine D2 Ligands for Probing Signal Transduction Pathways Essential for

- Antipsychotic Efficacy. *Proceedings of the National Academy of Sciences* **108**, 18488-18493
185. Park, S. M., Chen, M., Schmerberg, C. M., Dulman, R. S., Rodriguiz, R. M., Caron, M. G., Jin, J., and Wetsel, W. C. (2016) Effects of β -arrestin-biased dopamine D2 receptor ligands on schizophrenia-like behavior in hypoglutamatergic mice. *Neuropsychopharmacology* **41**, 704-715
 186. Donthamsetti, P., Gallo, E. F., Buck, D. C., Stahl, E. L., Zhu, Y., Lane, J. R., Bohn, L. M., Neve, K. A., Kellendonk, C., and Javitch, J. A. (2018) Arrestin recruitment to dopamine D2 receptor mediates locomotion but not incentive motivation. *Molecular psychiatry*, 1-15
 187. Kapur, S., and Seeman, P. (2001) Does fast dissociation from the dopamine D2 receptor explain the action of atypical antipsychotics?: A new hypothesis. *American Journal of Psychiatry* **158**, 360-369
 188. Kapur, S., Zipursky, R., Jones, C., Remington, G., and Houle, S. (2000) Relationship between dopamine D2 occupancy, clinical response, and side effects: a double-blind PET study of first-episode schizophrenia. *American Journal of Psychiatry* **157**, 514-520
 189. Carboni, L., Negri, M., Michielin, F., Bertani, S., Delle Fratte, S., Oliosi, B., and Cavanni, P. (2012) Slow dissociation of partial agonists from the D2 receptor is linked to reduced prolactin release. *International Journal of Neuropsychopharmacology* **15**, 645-656
 190. Mateus, C., and Coloma, J. (2013) Health economics and cost of illness in Parkinson's disease. *Eur Neurol Rev* **8**, 6-9
 191. Bohingamu Mudiyansele, S., Watts, J. J., Abimanyi-Ochom, J., Lane, L., Murphy, A. T., Morris, M. E., and Iansek, R. (2017) Cost of living with Parkinson's disease over 12 months in Australia: a prospective cohort study. *Parkinson's Disease* **2017**
 192. Schapira, A. H., Chaudhuri, K. R., and Jenner, P. (2017) Non-motor features of Parkinson disease. *Nature Reviews Neuroscience* **18**, 435
 193. Surmeier, D. J., Obeso, J. A., and Halliday, G. M. (2017) Selective neuronal vulnerability in Parkinson disease. *Nat Rev Neurosci* **18**, 101-113
 194. Bellucci, A., Mercuri, N. B., Venneri, A., Faustini, G., Longhena, F., Pizzi, M., Missale, C., and Spano, P. (2016) Review: Parkinson's disease: from synaptic loss to connectome dysfunction. *Neuropathology and Applied Neurobiology* **42**, 77-94
 195. Halliday, G. M., Leverenz, J. B., Schneider, J. S., and Adler, C. H. (2014) The neurobiological basis of cognitive impairment in Parkinson's disease. *Movement Disorders* **29**, 634-650
 196. Freire, C., and Koifman, S. (2012) Pesticide exposure and Parkinson's disease: epidemiological evidence of association. *Neurotoxicology* **33**, 947-971
 197. Scheperjans, F. (2018) The prodromal microbiome. *Movement disorders* **33**, 5-7
 198. Ben-Joseph, A., Marshall, C. R., Lees, A. J., and Noyce, A. J. (2019) Ethnic Variation in the Manifestation of Parkinson's Disease: A Narrative Review. *Journal of Parkinson's Disease*, 1-15
 199. Polymeropoulos, M. H., Lavedan, C., Leroy, E., Ide, S. E., Dehejia, A., Dutra, A., Pike, B., Root, H., Rubenstein, J., and Boyer, R. (1997) Mutation in the α -synuclein gene identified in families with Parkinson's disease. *Science (New York, N. Y.)* **276**, 2045-2047
 200. Paisán-Ruiz, C., Jain, S., Evans, E. W., Gilks, W. P., Simón, J., Van Der Brug, M., De Munain, A. L., Aparicio, S., Gil, A. M. n., and Khan, N. (2004) Cloning of the gene containing mutations that cause PARK8-linked Parkinson's disease. *Neuron* **44**, 595-600
 201. Zimprich, A., Biskup, S., Leitner, P., Lichtner, P., Farrer, M., Lincoln, S., Kachergus, J., Hulihan, M., Uitti, R. J., and Calne, D. B. (2004) Mutations in LRRK2 cause autosomal-dominant parkinsonism with pleomorphic pathology. *Neuron* **44**, 601-607
 202. Valente, E. M., Abou-Sleiman, P. M., Caputo, V., Muqit, M. M., Harvey, K., Gispert, S., Ali, Z., Del Turco, D., Bentivoglio, A. R., and Healy, D. G. (2004) Hereditary early-onset Parkinson's disease caused by mutations in PINK1. *Science (New York, N. Y.)* **304**, 1158-1160
 203. Sidransky, E., Nalls, M. A., Aasly, J. O., Aharon-Peretz, J., Annesi, G., Barbosa, E. R., Bar-Shira, A., Berg, D., Bras, J., and Brice, A. (2009) Multicenter analysis of

- glucocerebrosidase mutations in Parkinson's disease. *New England Journal of Medicine* **361**, 1651-1661
204. Chaudhuri, K. R., and Schapira, A. H. (2009) Non-motor symptoms of Parkinson's disease: dopaminergic pathophysiology and treatment. *The Lancet Neurology* **8**, 464-474
 205. Connolly, B. S., and Lang, A. E. (2014) Pharmacological treatment of parkinson disease: A review. *JAMA* **311**, 1670-1683
 206. Zanettini, R., Antonini, A., Gatto, G., Gentile, R., Tesei, S., and Pezzoli, G. (2007) Valvular heart disease and the use of dopamine agonists for Parkinson's disease. *New England Journal of Medicine* **356**, 39-46
 207. Andersohn, F., and Garbe, E. (2009) Cardiac and noncardiac fibrotic reactions caused by ergot-and nonergot-derived dopamine agonists. *Movement Disorders* **24**, 129-133
 208. Hutcheson, J. D., Setola, V., Roth, B. L., and Merryman, W. D. (2011) Serotonin receptors and heart valve disease—it was meant 2B. *Pharmacology & therapeutics* **132**, 146-157
 209. Stowe, R., Ives, N., Clarke, C. E., Ferreira, J., Hawker, R. J., Shah, L., Wheatley, K., and Gray, R. (2008) Dopamine agonist therapy in early Parkinson's disease. *Cochrane Database of Systematic Reviews*
 210. Glover, V., Sandler, M., Owen, F., and Riley, G. (1977) Dopamine is a monoamine oxidase B substrate in man. *Nature* **265**, 80-81
 211. Athauda, D., Maclagan, K., Skene, S. S., Bajwa-Joseph, M., Letchford, D., Chowdhury, K., Hibbert, S., Budnik, N., Zampieri, L., and Dickson, J. (2017) Exenatide once weekly versus placebo in Parkinson's disease: a randomised, double-blind, placebo-controlled trial. *The Lancet* **390**, 1664-1675
 212. Domenici, M. R., Ferrante, A., Martire, A., Chiodi, V., Pepponi, R., Tebano, M. T., and Popoli, P. (2019) Adenosine A2A receptor as potential therapeutic target in neuropsychiatric disorders. *Pharmacological research* **147**, 104338
 213. Lang, A. E., and Espay, A. J. (2018) Disease modification in Parkinson's disease: current approaches, challenges, and future considerations. *Movement Disorders* **33**, 660-677
 214. West, A. B. (2017) Achieving neuroprotection with LRRK2 kinase inhibitors in Parkinson disease. *Experimental neurology* **298**, 236-245
 215. Stoker, T. B., Torsney, K. M., and Barker, R. A. (2018) Emerging treatment approaches for Parkinson's disease. *Frontiers in neuroscience* **12**, 693
 216. Palfi, S., Gurruchaga, J. M., Lepetit, H., Howard, K., Ralph, G. S., Mason, S., Gouello, G., Domenech, P., Buttery, P. C., and Hantraye, P. (2018) Long-term follow-up of a phase I/II study of ProSavin, a lentiviral vector gene therapy for Parkinson's disease. *Human Gene Therapy Clinical Development* **29**, 148-155
 217. Tomlinson, C. L., Stowe, R., Patel, S., Rick, C., Gray, R., and Clarke, C. E. (2010) Systematic review of levodopa dose equivalency reporting in Parkinson's disease. *Movement Disorders* **25**, 2649-2653
 218. Kapur, S., and Seeman, P. (2000) Antipsychotic agents differ in how fast they come off the dopamine D2 receptors. Implications for atypical antipsychotic action. *Journal of Psychiatry and Neuroscience* **25**, 161
 219. Liggett, S. B. (2011) Phosphorylation Barcoding as a Mechanism of Directing GPCR Signaling. *Science Signaling* **4**, pe36-pe36
 220. Santos, R., Ursu, O., Gaulton, A., Bento, A. P., Donadi, R. S., Bologa, C. G., Karlsson, A., Al-Lazikani, B., Hersey, A., and Oprea, T. I. (2017) A comprehensive map of molecular drug targets. *Nature reviews Drug discovery* **16**, 19
 221. Motulsky, H. J., and Mahan, L. (1984) The kinetics of competitive radioligand binding predicted by the law of mass action. *Molecular pharmacology* **25**, 1-9
 222. Disse, B., Speck, G. A., Rominger, K. L., Witek Jr, T. J., and Hammer, R. (1999) Tiotropium (Spiriva™): mechanistical considerations and clinical profile in obstructive lung disease. *Life sciences* **64**, 457-464
 223. Silhavy, T. J., Szmelcman, S., Boos, W., and Schwartz, M. (1975) On the significance of the retention of ligand by protein. *Proceedings of the National Academy of Sciences* **72**, 2120-2124

224. Gopalakrishnan, M., Forsten-Williams, K., Cassino, T. R., Padro, L., Ryan, T. E., and Täuber, U. C. (2005) Ligand rebinding: self-consistent mean-field theory and numerical simulations applied to surface plasmon resonance studies. *European Biophysics Journal* **34**, 943-958
225. García-Nafria, J., and Tate, C. G. (2019) Cryo-electron microscopy: Moving beyond x-ray crystal structures for drug receptors and drug development. *Annual review of pharmacology and toxicology* **60**
226. Söldner, C. A., Horn, A. H., and Sticht, H. (2018) Binding of histamine to the H1 receptor—a molecular dynamics study. *Journal of molecular modeling* **24**, 346
227. Nguyen, A. T., Baltos, J.-A., Thomas, T., Nguyen, T. D., Muñoz, L. L., Gregory, K. J., White, P. J., Sexton, P. M., Christopoulos, A., and May, L. T. (2016) Extracellular loop 2 of the adenosine A1 receptor has a key role in orthosteric ligand affinity and agonist efficacy. *Molecular pharmacology* **90**, 703-714
228. Guo, D., Pan, A. C., Dror, R. O., Mocking, T., Liu, R., Heitman, L. H., Shaw, D. E., and IJzerman, A. P. (2016) Molecular basis of ligand dissociation from the adenosine A2A receptor. *Molecular pharmacology* **89**, 485-491
229. Bressan, R. A., and Crippa, J. A. (2005) The role of dopamine in reward and pleasure behaviour—review of data from preclinical research. *Acta Psychiatrica Scandinavica* **111**, 14-21
230. Boulay, D., Depoortere, R., Perrault, G., Borrelli, E., and Sanger, D. (1999) Dopamine D2 receptor knock-out mice are insensitive to the hypolocomotor and hypothermic effects of dopamine D2/D3 receptor agonists. *Neuropharmacology* **38**, 1389-1396
231. Seeman, P. (2010) Dopamine D2 receptors as treatment targets in schizophrenia. *Clinical schizophrenia & related psychoses* **4**, 56-73
232. Lim, E. (2005) A walk through the management of Parkinson s disease. *Ann Acad Med Singapore* **34**, 188-195
233. Mansour, A., Meng, F., Meador-Woodruff, J. H., Taylor, L. P., Civelli, O., and Akil, H. (1992) Site-directed mutagenesis of the human dopamine D2 receptor. *European Journal of Pharmacology: Molecular Pharmacology* **227**, 205-214
234. Shi, L., and Javitch, J. A. (2004) The second extracellular loop of the dopamine D2 receptor lines the binding-site crevice. *Proceedings of the National Academy of Sciences* **101**, 440-445
235. Klein Herenbrink, C., Verma, R., Lim, H. D., Kopinathan, A., Keen, A., Shonberg, J., Draper-Joyce, C. J., Scammells, P. J., Christopoulos, A., Javitch, J. A., Capuano, B., Shi, L., and Lane, J. R. (2019) Molecular Determinants of the Intrinsic Efficacy of the Antipsychotic Aripiprazole. *ACS Chemical Biology* **14**, 1780-1792
236. Zhou, Y., Cao, C., He, L., Wang, X., and Zhang, X. C. (2019) Crystal structure of dopamine receptor D4 bound to the subtype selective ligand, L745870. *eLife* **8**, e48822
237. Sykes, D. A., Lane, J. R., Szabo, M., Capuano, B., Javitch, J. A., and Charlton, S. J. (2018) Reply to 'Antipsychotics with similar association kinetics at dopamine D2 receptors differ in extrapyramidal side-effects'. *Nature Communications* **9**, 3568
238. Harrison, T. S., and Perry, C. M. (2004) Aripiprazole. *Drugs* **64**, 1715-1736
239. Wadenberg, M.-L. G. (2007) Bifeprunox: a novel antipsychotic agent with partial agonist properties at dopamine D2 and serotonin 5-HT1A receptors.
240. Parkes, D. (1979) Bromocriptine. *New England Journal of Medicine* **301**, 873-878
241. Möller, H.-J. (2005) Risperidone: a review. *Expert opinion on pharmacotherapy* **6**, 803-818
242. Janssen, P. A. (1974) Butyrophenones and diphenylbutylpiperidines. *Psychopharmacological agents* **3**, 129-158
243. Ballesteros, J. A., and Weinstein, H. (1995) [19] Integrated methods for the construction of three-dimensional models and computational probing of structure-function relations in G protein-coupled receptors. in *Methods in neurosciences*, Elsevier. pp 366-428
244. Cherezov, V., Rosenbaum, D. M., Hanson, M. A., Rasmussen, S. G., Thian, F. S., Kobilka, T. S., Choi, H.-J., Kuhn, P., Weis, W. I., and Kobilka, B. K. (2007) High-resolution crystal structure of an engineered human β 2-adrenergic G protein-coupled receptor. *Science (New York, N. Y.)* **318**, 1258-1265

245. Sykes, D. A., Jain, P., and Charlton, S. J. (2019) Investigating the Influence of Tracer Kinetics on Competition-Kinetic Association Binding Assays: Identifying the Optimal Conditions for Assessing the Kinetics of Low-Affinity Compounds. *Molecular pharmacology* **96**, 378-392
246. Swinney, D. C., Beavis, P., Chuang, K. T., Zheng, Y., Lee, I., Gee, P., Deval, J., Rotstein, D. M., Dioszegi, M., and Ravendran, P. (2014) A study of the molecular mechanism of binding kinetics and long residence times of human CCR 5 receptor small molecule allosteric ligands. *British journal of pharmacology* **171**, 3364-3375
247. Van Oijen, A. M. (2011) Single-molecule approaches to characterizing kinetics of biomolecular interactions. *Current opinion in biotechnology* **22**, 75-80
248. Gilman, A. G. (1987) G proteins: transducers of receptor-generated signals. *Annual review of biochemistry* **56**, 615-649
249. Gurevich, V. V., and Gurevich, E. V. (2019) GPCR signaling regulation: the role of GRKs and arrestins. *Frontiers in pharmacology* **10**, 125
250. Peterson, Y. K., and Luttrell, L. M. (2017) The diverse roles of arrestin scaffolds in G protein-coupled receptor signaling. *Pharmacological reviews* **69**, 256-297
251. Free, R. B., Chun, L. S., Moritz, A. E., Miller, B. N., Doyle, T. B., Conroy, J. L., Padron, A., Meade, J. A., Xiao, J., Hu, X., Dulcey, A. E., Han, Y., Duan, L., Titus, S., Bryant-Genevieve, M., Barnaeva, E., Ferrer, M., Javitch, J. A., Beuming, T., Shi, L., Southall, N. T., Marugan, J. J., and Sibley, D. R. (2014) Discovery and Characterization of a G Protein-Biased Agonist That Inhibits β -Arrestin Recruitment to the D2 Dopamine Receptor. *Molecular Pharmacology* **86**, 96-105
252. Bonifazi, A., Yano, H., Guerrero, A. M., Kumar, V., Hoffman, A. F., Lupica, C. R., Shi, L., and Newman, A. H. (2019) Novel and potent dopamine D2 receptor Go-protein biased agonists. *ACS pharmacology & translational science* **2**, 52-65
253. Waelbroeck, M., Boufrahi, L., and Swillens, S. (1997) Seven helix receptors are enzymes catalysing G protein activation. What is the agonist Kact? *Journal of theoretical biology* **187**, 15-37
254. Kinzer-Ursem, T. L., and Linderman, J. J. (2007) Both Ligand-and Cell-Specific parameters control ligand agonism in a kinetic model of G protein-coupled Receptor signaling. *PLoS computational biology* **3**
255. Woolf, P. J., and Linderman, J. J. (2003) Untangling ligand induced activation and desensitization of G-protein-coupled receptors. *Biophysical journal* **84**, 3-13
256. Shonberg, J., Herenbrink, C. K., López, L., Christopoulos, A., Scammells, P. J., Capuano, B., and Lane, J. R. (2013) A Structure-Activity Analysis of Biased Agonism at the Dopamine D2 Receptor. *Journal of medicinal chemistry* **56**, 9199-9221
257. Masuho, I., Martemyanov, K. A., and Lambert, N. A. (2015) Monitoring G Protein Activation in Cells with BRET. in *G Protein-Coupled Receptors in Drug Discovery: Methods and Protocols* (Filizola, M. ed.), Springer New York, New York, NY. pp 107-113
258. Hollins, B., Kuravi, S., Digby, G. J., and Lambert, N. A. (2009) The c-terminus of GRK3 indicates rapid dissociation of G protein heterotrimers. *Cellular signalling* **21**, 1015-1021
259. Donthamsetti, P., Quejada, J. R., Javitch, J. A., Gurevich, V. V., and Lambert, N. A. (2015) Using Bioluminescence Resonance Energy Transfer (BRET) to Characterize Agonist-Induced Arrestin Recruitment to Modified and Unmodified G Protein-Coupled Receptors. *Current Protocols in Pharmacology*, 2.14. 11-12.14. 14
260. Lan, T.-H., Liu, Q., Li, C., Wu, G., and Lambert, N. A. (2012) Sensitive and High Resolution Localization and Tracking of Membrane Proteins in Live Cells with BRET. *Traffic* **13**, 1450-1456
261. De Vries, L., Finana, F., Cathala, C., Ronsin, B., and Cussac, D. (2019) Innovative Bioluminescence Resonance Energy Transfer Assay Reveals Differential Agonist-Induced D2 Receptor Intracellular Trafficking and Arrestin-3 Recruitment. *Molecular pharmacology* **96**, 308-319
262. Maeda, K., Sugino, H., Akazawa, H., Amada, N., Shimada, J., Futamura, T., Yamashita, H., Ito, N., McQuade, R. D., and Mørk, A. (2014) Brexpiprazole I: in vitro and in vivo

- characterization of a novel serotonin-dopamine activity modulator. *Journal of Pharmacology and Experimental Therapeutics* **350**, 589-604
263. Calne, D., Teychenne, P., Claveria, L., Eastman, R., Greenacre, J., and Petrie, A. a. (1974) Bromocriptine in parkinsonism. *Br med J* **4**, 442-444
 264. Scheller, D., Ullmer, C., Berkels, R., Gwarek, M., and Lübbert, H. (2009) The in vitro receptor profile of rotigotine: a new agent for the treatment of Parkinson's disease. *Naunyn-Schmiedeberg's archives of pharmacology* **379**, 73-86
 265. Wood, M., Dubois, V., Scheller, D., and Gillard, M. (2015) Rotigotine is a potent agonist at dopamine D 1 receptors as well as at dopamine D 2 and D 3 receptors. *British journal of pharmacology* **172**, 1124-1135
 266. Blackburn, T. (2017) Orally-active, highly effective, fast-onset, long-acting dopamine D3/D2 agonists in translational experimental models of Parkinson's disease displays specific biased agonism profile. in *pA2 online - BPS Pharmacology 2017*, London, UK
 267. Lane, J. R., Powney, B., Wise, A., Rees, S., and Milligan, G. (2008) G protein coupling and ligand selectivity of the D2L and D3 dopamine receptors. *Journal of Pharmacology and Experimental Therapeutics* **325**, 319-330
 268. Lawler, C. P., Prioleau, C., Lewis, M. M., Mak, C., Jiang, D., Schetz, J. A., Gonzalez, A. M., Sibley, D. R., and Mailman, R. B. (1999) Interactions of the novel antipsychotic aripiprazole (OPC-14597) with dopamine and serotonin receptor subtypes. *Neuropsychopharmacology* **20**, 612-627
 269. Brandt, D., and Ross, E. (1986) Catecholamine-stimulated GTPase cycle. Multiple sites of regulation by beta-adrenergic receptor and Mg²⁺ studied in reconstituted receptor-Gs vesicles. *Journal of Biological Chemistry* **261**, 1656-1664
 270. Klewe, I. V., Nielsen, S. M., Tarpø, L., Urizar, E., Dipace, C., Javitch, J. A., Gether, U., Egebjerg, J., and Christensen, K. V. (2008) Recruitment of β -arrestin2 to the dopamine D2 receptor: insights into anti-psychotic and anti-parkinsonian drug receptor signaling. *Neuropharmacology* **54**, 1215-1222
 271. Kim, K.-M., Valenzano, K. J., Robinson, S. R., Yao, W. D., Barak, L. S., and Caron, M. G. (2001) Differential Regulation of the Dopamine D2 and D3 Receptors by G Protein-coupled Receptor Kinases and β -Arrestins. *Journal of Biological Chemistry* **276**, 37409-37414
 272. Oakley, R. H., Laporte, S. A., Holt, J. A., Caron, M. G., and Barak, L. S. (2000) Differential affinities of visual arrestin, beta arrestin1, and beta arrestin2 for G protein-coupled receptors delineate two major classes of receptors. *Journal of Biological Chemistry* **275**, 17201-17210
 273. Kenakin, T. (2009) Quantifying biological activity in chemical terms: a pharmacology primer to describe drug effect. ACS Publications
 274. Luttrell, L. M., Maudsley, S., and Bohn, L. M. (2015) Fulfilling the promise of "biased" G protein-coupled receptor agonism. *Molecular pharmacology* **88**, 579-588
 275. White, K. L., Scopton, A. P., Rives, M.-L., Bikbulatov, R. V., Polepally, P. R., Brown, P. J., Kenakin, T., Javitch, J. A., Zjawiony, J. K., and Roth, B. L. (2014) Identification of novel functionally selective κ -opioid receptor scaffolds. *Molecular pharmacology* **85**, 83-90
 276. McAnally, D., Siddiquee, K., Sharir, H., Qi, F., Phatak, S., Li, J.-L., Berg, E., Fishman, J., and Smith, L. (2017) A systematic approach to identify biased agonists of the apelin receptor through high-throughput screening. *SLAS DISCOVERY: Advancing Life Sciences R&D* **22**, 867-878
 277. Frank, A., Kiss, D. J., Keserű, G. M., and Stark, H. (2018) Binding kinetics of cariprazine and aripiprazole at the dopamine D 3 receptor. *Scientific reports* **8**, 1-9
 278. Packeu, A., De Backer, J.-P., Van Liefde, I., Vanderheyden, P. M., and Vauquelin, G. (2008) Antagonist-radioligand binding to D2L-receptors in intact cells. *Biochemical pharmacology* **75**, 2192-2203
 279. Kessler, R. M., Votaw, J. R., de Paulis, T., Bingham, D. R., Ansari, M. S., Mason, N. S., Holburn, G., Schmidt, D. E., Votaw, D. B., and Manning, R. G. (1993) Evaluation of 5-[¹⁸F] fluoropropylepidepride as a potential PET radioligand for imaging dopamine D2 receptors. *Synapse* **15**, 169-176

280. Zimmerman, B., Beaudrait, A., Aguila, B., Charles, R., Escher, E., Claing, A., Bouvier, M., and Laporte, S. A. (2012) Differential β -Arrestin-Dependent Conformational Signaling and Cellular Responses Revealed by Angiotensin Analogs. *Sci. Signal.* **5**, ra33-ra33
281. Namkung, Y., LeGouill, C., Kumar, S., Cao, Y., Teixeira, L. B., Lukasheva, V., Giubilaro, J., Simões, S. C., Longpré, J.-M., and Devost, D. (2018) Functional selectivity profiling of the angiotensin II type 1 receptor using pathway-wide BRET signaling sensors. *Science signaling* **11**
282. Gundry, J., Glenn, R., Alagesan, P., and Rajagopal, S. (2017) A practical guide to approaching biased agonism at G protein coupled receptors. *Frontiers in neuroscience* **11**, 17
283. Onaran, H. O., Ambrosio, C., Uğur, Ö., Koncz, E. M., Grò, M. C., Vezzi, V., Rajagopal, S., and Costa, T. (2017) Systematic errors in detecting biased agonism: analysis of current methods and development of a new model-free approach. *Scientific reports* **7**, 1-17
284. Attramadal, H., Arriza, J. L., Aoki, C., Dawson, T. M., Codina, J., Kwatra, M. M., Snyder, S. H., Caron, M. G., and Lefkowitz, R. J. (1992) Beta-arrestin2, a novel member of the arrestin/beta-arrestin gene family. *Journal of Biological Chemistry* **267**, 17882-17890
285. Yano, H., Cai, N.-S., Xu, M., Verma, R. K., Rea, W., Hoffman, A. F., Shi, L., Javitch, J. A., Bonci, A., and Ferré, S. (2018) Gs-versus Golf-dependent functional selectivity mediated by the dopamine D 1 receptor. *Nature communications* **9**, 1-11
286. Bolognini, D., Moss, C. E., Nilsson, K., Petersson, A. U., Donnelly, I., Sergeev, E., König, G. M., Kostenis, E., Kurowska-Stolarska, M., and Miller, A. (2016) A novel allosteric activator of free fatty acid 2 receptor displays unique Gi-functional bias. *Journal of Biological Chemistry* **291**, 18915-18931
287. Inoue, A., and Nakata, Y. (2001) Strategy for modulation of central dopamine transmission based on the partial agonist concept in schizophrenia therapy. *Japanese journal of pharmacology* **86**, 376-380
288. McPherson, J., Rivero, G., Baptist, M., Llorente, J., Al-Sabah, S., Krasel, C., Dewey, W. L., Bailey, C. P., Rosethorne, E. M., and Charlton, S. J. (2010) μ -opioid receptors: correlation of agonist efficacy for signalling with ability to activate internalization. *Molecular pharmacology* **78**, 756-766
289. Beaulieu, J.-M. M., and Gainetdinov, R. R. (2011) The physiology, signaling, and pharmacology of dopamine receptors. *Pharmacol. Rev.* **63**, 182-217
290. Seeman, P. (2006) Targeting the dopamine D2 receptor in schizophrenia. *Expert Opin Ther Targets* **10**, 515-531
291. Namkung, Y., Dipace, C., Urizar, E., Javitch, J. A., and Sibley, D. R. (2009) G protein-coupled receptor kinase-2 constitutively regulates D2 dopamine receptor expression and signaling independently of receptor phosphorylation. *J. Biol. Chem.* **284**, 34103-34115
292. Cho, D. I., Zheng, M., Min, C., Kwon, K. J., Shin, C. Y., Choi, H. K., and Kim, K. M. (2013) ARF6 and GASP-1 are post-endocytic sorting proteins selectively involved in the intracellular trafficking of dopamine D2 receptors mediated by GRK and PKC in transfected cells. *Br. J. Pharmacol.* **168**, 1355-1374
293. Allen, J. A., Yost, J. M., Setola, V., Chen, X., Sassano, M. F., Chen, M., Peterson, S., Yadav, P. N., Huang, X.-p., Feng, B., Jensen, N. H., Che, X., Bai, X., Frye, S. V., Wetsel, W. C., Caron, M. G., Javitch, J. A., Roth, B. L., and Jin, J. (2011) Discovery of β -Arrestin-Biased Dopamine D2 Ligands for Probing Signal Transduction Pathways Essential for Antipsychotic Efficacy. *Proc. Natl. Acad. Sci. U.S.A* **108**, 18488-18493
294. Namkung, Y., Dipace, C., Javitch, J. A., and Sibley, D. R. (2009) G Protein-coupled Receptor Kinase-mediated Phosphorylation Regulates Post-endocytic Trafficking of the D2 Dopamine Receptor. *J. Biol. Chem.* **284**, 15038-15051
295. DeWire, S. M., Ahn, S., Lefkowitz, R. J., and Shenoy, S. K. (2007) β -Arrestins and Cell Signaling. *Ann. Rev. Physiol.* **69**, 483-510
296. Beaulieu, J.-M., Gainetdinov, R. R., and Caron, M. G. (2007) The Akt-GSK-3 signaling cascade in the actions of dopamine. *Trends Pharmacol. Sci.* **28**, 166-172

297. Peterson, S. M., Pack, T. F., Wilkins, A. D., Urs, N. M., Urban, D. J., Bass, C. E., Lichtarge, O., and Caron, M. G. (2015) Elucidation of G-protein and β -arrestin functional selectivity at the dopamine D2 receptor. *Proc. Natl. Acad. Sci. U.S.A* **112**, 7097-7102
298. Donthamsetti, P., Gallo, E. F., Buck, D. C., Stahl, E. L., Zhu, Y., Lane, J. R., Bohn, L. M., Neve, K. A., Kellendonk, C., and Javitch, J. A. (2018) Arrestin recruitment to dopamine D2 receptor mediates locomotion but not incentive motivation. *Mol. Psychiatry*
299. Porter-Stransky, K. A., Petko, A. K., Karne, S. L., Liles, L. C., Urs, N. M., Caron, M. G., Paladini, C. A., and Weinshenker, D. (2019) Loss of β -arrestin2 in D2 cells alters neuronal excitability in the nucleus accumbens and behavioral responses to psychostimulants and opioids. *Addict. Biol.*, e12823
300. Urs, N. M., Peterson, S. M., and Caron, M. G. (2017) New Concepts in Dopamine D2 Receptor Biased Signaling and Implications for Schizophrenia Therapy. *Biol. Psychiatry* **81**, 78-85
301. Urban, J. D., Clarke, W. P., von Zastrow, M., Nichols, D. E., Kobilka, B., Weinstein, H., Javitch, J. A., Roth, B. L., Christopoulos, A., Sexton, P. M., Miller, K. J., Spedding, M., and Mailman, R. B. (2007) Functional Selectivity and Classical Concepts of Quantitative Pharmacology. *J. Pharmacol. Exp. Ther.* **320**, 1-13
302. Violin, J. D., Crombie, A. L., Soergel, D. G., and Lark, M. W. (2014) Biased ligands at G-protein-coupled receptors: promise and progress. *Trends Biochem. Sci.* **35**, 308-316
303. Free, B. R., Chun, L. S., Moritz, A. E., Miller, B. N., Doyle, T. B., Conroy, J. L., Padron, A., Meade, J. A., Xiao, J., Hu, X., Dulcey, A. E., Han, Y., Duan, L., Titus, S., Bryant-Genevieve, M., Barnaeva, E., Ferrer, M., Javitch, J. A., Beuming, T., Shi, L., Southall, N. T., Marugan, J. J., and Sibley, D. R. (2014) Discovery and Characterization of a G Protein-Biased Agonist That Inhibits β -Arrestin Recruitment to the D2 Dopamine Receptor. *Mol. Pharmacol.* **86**, 96-105
304. Doll, C., Poll, F., Peuker, K., Loktev, A., Gluck, L., and Schulz, S. (2012) Deciphering micro-opioid receptor phosphorylation and dephosphorylation in HEK293 cells. *Br. J. Pharmacol.* **167**, 1259-1270
305. Mann, A., Mouledous, L., Froment, C., O'Neill, P. R., Dasgupta, P., Gunther, T., Brunori, G., Kieffer, B. L., Toll, L., Bruchas, M. R., Zaveri, N. T., and Schulz, S. (2019) Agonist-selective NOP receptor phosphorylation correlates in vitro and in vivo and reveals differential post-activation signaling by chemically diverse agonists. *Sci. Signal.* **12**
306. Tobin, A. B., Butcher, A. J., and Kong, K. (2008) Location, location, location...site-specific GPCR phosphorylation offers a mechanism for cell-type-specific signalling. *Trends Pharmacol. Sci.* **29**, 413-420
307. Lehmann, A., Kliewer, A., Gunther, T., Nagel, F., and Schulz, S. (2016) Identification of Phosphorylation Sites Regulating sst3 Somatostatin Receptor Trafficking. *Mol. Endocrinol.* **30**, 645-659
308. Hollins, B., Kuravi, S., Digby, G. J., and Lambert, N. A. (2009) The c-terminus of GRK3 indicates rapid dissociation of G protein heterotrimers. *Cell. Signal.* **21**, 1015-1021
309. Günther, T., Culler, M., and Schulz, S. (2016) Research Resource: Real-Time Analysis of Somatostatin and Dopamine Receptor Signaling in Pituitary Cells Using a Fluorescence-Based Membrane Potential Assay. *Mol. Endocrinol.* **30**, 479-490
310. Klein-Herenbrink, C., Sykes, D. A., Donthamsetti, P., Canals, M., Coudrat, T., Shonberg, J., Scammells, P. J., Capuano, B., Sexton, P. M., and Charlton, S. J. (2016) The role of kinetic context in apparent biased agonism at GPCRs. *Nature communications* **7**, 10842
311. Donthamsetti, P., Quejada, J. R., Javitch, J. A., Gurevich, V. V., and Lambert, N. A. (2015) Using Bioluminescence Resonance Energy Transfer (BRET) to Characterize Agonist-Induced Arrestin Recruitment to Modified and Unmodified G Protein-Coupled Receptors. *Curr. Protoc. Pharmacol.*, 2.14. 11-12.14. 14
312. Clagett-Dame, M., and McKelvy, J. F. (1989) N-linked oligosaccharides are responsible for rat striatal dopamine D2 receptor heterogeneity. *Arch Biochem Biophys* **274**, 145-154
313. Ikeda, S., Keneko, M., and Fujiwara, S. (2007) CARDIOTONIC AGENT COMPRISING GRK INHIBITOR. (Takeda Pharmaceutical Company Ltd ed.

314. Benovic, J. L., Strasser, R. H., Caron, M. G., and Lefkowitz, R. J. (1986) Beta-adrenergic receptor kinase: identification of a novel protein kinase that phosphorylates the agonist-occupied form of the receptor. *Proc. Natl. Acad. Sci. U.S.A* **83**, 2797-2801
315. Masuho, I., Ostrovskaya, O., Kramer, G. M., Jones, C. D., Xie, K., and Martemyanov, K. A. (2015) Distinct profiles of functional discrimination among G proteins determine the actions of G protein-coupled receptors. *Sci. Signal.* **8**, ra123
316. Lane, J. R., Powney, B., Wise, A., Rees, S., and Milligan, G. (2007) Protean Agonism at the Dopamine D2 Receptor: (S)-3-(3-Hydroxyphenyl)-N-propylpiperidine Is an Agonist for Activation of Go1 but an Antagonist/Inverse Agonist for Gi1, Gi2, and Gi3. *Mol. Pharmacol.* **71**, 1349-1359
317. Wood, M., Dubois, V., Scheller, D., and Gillard, M. (2015) Rotigotine is a potent agonist at dopamine D 1 receptors as well as at dopamine D 2 and D 3 receptors. *Br. J. Pharmacol.* **172**, 1124-1135
318. Inoue, T., Domae, M., Yamada, K., and Furukawa, T. (1996) Effects of the novel antipsychotic agent 7-(4-[4-(2,3-dichlorophenyl)-1-piperazinyl]butyloxy)-3,4-dihydro -2(1H)-quinolinone (OPC-14597) on prolactin release from the rat anterior pituitary gland. *J. Pharmacol. Expt. Ther.* **277**, 137-143
319. Shapiro, D. A., Renock, S., Arrington, E., Chiodo, L. A., Liu, L.-X., Sibley, D. R., Roth, B. L., and Mailman, R. (2003) Aripiprazole, A Novel Atypical Antipsychotic Drug with a Unique and Robust Pharmacology. *Neuropsychopharmacology* **28**, 1400-1411
320. Urs, N. M., Gee, S. M., Pack, T. F., McCorvy, J. D., Evron, T., Snyder, J. C., Yang, X., Rodriguiz, R. M., Borrelli, E., Wetsel, W. C., Jin, J., Roth, B. L., O'Donnell, P., and Caron, M. G. (2016) Distinct cortical and striatal actions of a β -arrestin-biased dopamine D2 receptor ligand reveal unique antipsychotic-like properties. *Proc. Natl. Acad. Sci. U.S.A* **113**, E8178-E8186
321. Ågren, R., Århem, P., Nilsson, J., and Sahlholm, K. (2018) The beta-arrestin-biased dopamine D2 receptor ligand, UNC9994, is a partial agonist at G-protein-mediated potassium channel activation. *Int. J. Neuropsychopharmacol.* **21**, 1102-1108
322. Black, J. W., and Leff, P. (1983) Operational models of pharmacological agonism. *Proc. R. Soc. Lond. B.* **220**, 141-162
323. Just, S., Illing, S., Trester-Zedlitz, M., Lau, E. K., Kotowski, S. J., Miess, E., Mann, A., Doll, C., Trinidad, J. C., Burlingame, A. L., von Zastrow, M., and Schulz, S. (2013) Differentiation of opioid drug effects by hierarchical multi-site phosphorylation. *Mol. Pharmacol.* **83**, 633-639
324. Miess, E., Gondin, A. B., Yousuf, A., Steinborn, R., Mösslein, N., Yang, Y., Göldner, M., Ruland, J. G., Bünemann, M., Krasel, C., Christie, M. J., Halls, M. L., Schulz, S., and Canals, M. (2018) Multisite phosphorylation is required for sustained interaction with GRKs and arrestins during rapid μ -opioid receptor desensitization. *Sci. Signal.* **11**, eaas9609
325. Cho, D., Zheng, M., Min, C., Ma, L., Kurose, H., Park, J. H., and Kim, K.-M. (2010) Agonist-Induced Endocytosis and Receptor Phosphorylation Mediate Resensitization of Dopamine D2 Receptors. *Mol. Endocrinol* **24**, 574-586
326. Jeong, J., Park, Y.-U., Kim, D.-K., Lee, S., Kwak, Y., Lee, S.-A., Lee, H., Suh, Y.-H., Gho, Y. S., and Hwang, D. (2013) Cdk5 phosphorylates dopamine D2 receptor and attenuates downstream signaling. *PLoS one* **8**, e84482
327. Namkung, Y., and Sibley, D. R. (2004) Protein Kinase C Mediates Phosphorylation, Desensitization, and Trafficking of the D2 Dopamine Receptor. *J. Biol. Chem.* **279**, 49533-49541
328. Thibault, D., Albert, P. R., Pineyro, G., and Trudeau, L.-É. (2011) Neurotensin triggers dopamine D2 receptor desensitization through a protein kinase C and β -arrestin1-dependent mechanism. *J. Biol. Chem.* **286**, 9174-9184
329. Morris, S. J., Itzhaki Van-Ham, I., Daigle, M., Robillard, L., Sajedi, N., and Albert, P. R. (2007) Differential desensitization of dopamine D2 receptor isoforms by protein kinase C: The importance of receptor phosphorylation and pseudosubstrate sites. *Eur. J. Pharmacol.* **577**, 44-53

330. Nobles, K. N., Xiao, K., Ahn, S., Shukla, A. K., Lam, C. M., Rajagopal, S., Strachan, R. T., Huang, T.-Y., Bressler, E. A., Hara, M. R., Shenoy, S. K., Gygi, S. P., and Lefkowitz, R. J. (2011) Distinct Phosphorylation Sites on the $\beta(2)$ -Adrenergic Receptor Establish a Barcode That Encodes Differential Functions of β -Arrestin. *Science signaling* **4**, ra51-ra51
331. Free, R. B., Chun, L. S., Moritz, A. E., Miller, B. N., Doyle, T. B., Conroy, J. L., Padron, A., Meade, J. A., Xiao, J., Hu, X., Dulcey, A. E., Han, Y., Duan, L., Titus, S., Bryant-Genevieve, M., Barnaeva, E., Ferrer, M., Javitch, J. A., Beuming, T., Shi, L., Southall, N. T., Marugan, J. J., and Sibley, D. R. (2014) Discovery and Characterization of a G Protein-Biased Agonist That Inhibits β -Arrestin Recruitment to the D2 Dopamine Receptor. *Mol. Pharmacol.* **86**, 96-105
332. Szabo, M., Klein Herenbrink, C., Christopoulos, A., Lane, J. R., and Capuano, B. (2014) Structure-activity relationships of privileged structures lead to the discovery of novel biased ligands at the dopamine D₂ receptor. *J. Med. Chem.* **57**, 4924-4939
333. Möller, D., Kling, R. C., Skultety, M., Leuner, K., Hübner, H., and Gmeiner, P. (2014) Functionally selective dopamine D₂, D₃ receptor partial agonists. *J. Med. Chem.* **57**, 4861-4875
334. Hiller, C., Kling, R. C., Heinemann, F. W., Meyer, K., Hübner, H., and Gmeiner, P. (2013) Functionally selective dopamine D2/D3 receptor agonists comprising an enyne moiety. *J. Med. Chem.* **56**, 5130-5141
335. McCorvy, J. D., Butler, K. V., Kelly, B., Rechsteiner, K., Karpiak, J., Betz, R. M., Kormos, B. L., Shoichet, B. K., Dror, R. O., Jin, J., and Roth, B. L. (2017) Structure-inspired design of β -arrestin-biased ligands for aminergic GPCRs. *Nat. Chem. Biol.* **14**, 126-134
336. Bonifazi, A., Yano, H., Guerrero, A. M., Kumar, V., Hoffman, A. F., Lupica, C. R., Shi, L., and Newman, A. H. (2019) Novel and Potent Dopamine D2 Receptor Go-Protein Biased Agonists. *ACS Pharmacol. Transl. Sci.* **2**, 52-65
337. Shen, Y., McCorvy, J. D., Martini, M. L., Rodriguiz, R. M., Pogorelov, V. M., Ward, K. M., Wetsel, W. C., Liu, J., Roth, B. L., and Jin, J. (2019) D2 Dopamine Receptor G protein-biased Partial Agonists Based on Cariprazine. *J. Med. Chem.* **62**, 4755-4771
338. Urban, J. D., Vargas, G. A., von Zastrow, M., and Mailman, R. B. (2007) Aripiprazole has Functionally Selective Actions at Dopamine D2 Receptor-Mediated Signaling Pathways. *Neuropsychopharmacology* **32**, 66-77
339. Masri, B., Salahpour, A., Didriksen, M., Ghisi, V., Beaulieu, J.-M., Gainetdinov, R. R., and Caron, M. G. (2008) Antagonism of dopamine D2 receptor/ β -arrestin 2 interaction is a common property of clinically effective antipsychotics. *Proc. Natl. Acad. Sci. U.S.A* **105**, 13656-13661
340. Chen, X., McCorvy, J. D., Fischer, M. G., Butler, K. V., Shen, Y., Roth, B. L., and Jin, J. (2016) Discovery of G Protein-Biased D2 Dopamine Receptor Partial Agonists. *J. Med. Chem.* **59**, 10601-10618
341. Chun, L. S., Vekariya, R. H., Free, R. B., Li, Y., Lin, D.-T., Su, P., Liu, F., Namkung, Y., Laporte, S. A., Moritz, A. E., Aubé, J., Frankowski, K. J., and Sibley, D. R. (2018) Structure-Activity Investigation of a G Protein-Biased Agonist Reveals Molecular Determinants for Biased Signaling of the D2 Dopamine Receptor. *Front. Synaptic. Neuroscience* **10**, 2
342. Urs, N. M., Gee, S. M., Pack, T. F., McCorvy, J. D., Evron, T., Snyder, J. C., Yang, X., Rodriguiz, R. M., Borrelli, E., Wetsel, W. C., Jin, J., Roth, B. L., O'Donnell, P., and Caron, M. G. (2016) Distinct cortical and striatal actions of a β -arrestin-biased dopamine D2 receptor ligand reveal unique antipsychotic-like properties. *Proc. Natl. Acad. Sci. U.S.A* **113**, E8178-E8186
343. Scarduzio, M., Zimmerman, C. N., Jaunarajs, K. L., Wang, Q., Standaert, D. G., and McMahon, L. L. (2017) Strength of cholinergic tone dictates the polarity of dopamine D2 receptor modulation of striatal cholinergic interneuron excitability in DYT1 dystonia. *Exp. Neurol.* **295**, 162-175
344. Haga, K., and Haga, T. (1990) Dual regulation by G proteins of agonist-dependent phosphorylation of muscarinic acetylcholine receptors. *FEBS letters* **268**, 43-47

345. Haga, K., and Haga, T. (1992) Activation by G protein beta gamma subunits of agonist-or light-dependent phosphorylation of muscarinic acetylcholine receptors and rhodopsin. *Journal of Biological Chemistry* **267**, 2222-2227
346. Koch, W. J., Inglese, J., Stone, W., and Lefkowitz, R. (1993) The binding site for the beta gamma subunits of heterotrimeric G proteins on the beta-adrenergic receptor kinase. *Journal of Biological Chemistry* **268**, 8256-8260
347. Jiang, M., Spicher, K., Boulay, G., Wang, Y., and Birnbaumer, L. (2001) Most central nervous system D2 dopamine receptors are coupled to their effectors by Go. *Proc. Natl. Acad. Sci. U.S.A* **98**, 3577-3582
348. Rask-Andersen, M., Almén, M. S., and Schiöth, H. B. (2011) Trends in the exploitation of novel drug targets. *Nature Reviews Drug Discovery* **10**, 579
349. Hildebrandt, J. D., Sekura, R. D., Codina, J., Iyengar, R., Manclark, C. R., and Birnbaumer, L. (1983) Stimulation and inhibition of adenylyl cyclases mediated by distinct regulatory proteins. *Nature* **302**, 706
350. Pfaffinger, P. J., Martin, J. M., Hunter, D. D., Nathanson, N. M., and Hille, B. (1985) GTP-binding proteins couple cardiac muscarinic receptors to a K channel. *Nature* **317**, 536
351. Sokolov, M., Lyubarsky, A. L., Strissel, K. J., Savchenko, A. B., Govardovskii, V. I., Pugh Jr, E. N., and Arshavsky, V. Y. (2002) Massive light-driven translocation of transducin between the two major compartments of rod cells: a novel mechanism of light adaptation. *Neuron* **34**, 95-106
352. Kenakin, T. (2016) Theoretical aspects of GPCR–ligand complex pharmacology. *Chemical reviews*
353. McCorvy, J. D., Butler, K. V., Kelly, B., Rechsteiner, K., Karpiak, J., Betz, R. M., Kormos, B. L., Shoichet, B. K., Dror, R. O., Jin, J., and Roth, B. L. (2017) Structure-inspired design of β -arrestin-biased ligands for aminergic GPCRs. *Nature Chemical Biology* **14**, 126
354. Masuho, I., Xie, K., and Martemyanov, K. A. (2013) Macromolecular Composition Dictates Receptor and G Protein Selectivity of Regulator of G Protein Signaling (RGS) 7 and 9-2 Protein Complexes in Living Cells. *Journal of Biological Chemistry* **288**, 25129-25142
355. Sutor, B., and ten Bruggencate, G. (1990) Ascorbic acid: A useful reductant to avoid oxidation of catecholamines in electrophysiological experiments in vitro? *Neuroscience Letters* **116**, 287-292
356. Atwood, B. K., Lopez, J., Wager-Miller, J., Mackie, K., and Straiker, A. (2011) Expression of G protein-coupled receptors and related proteins in HEK293, AtT20, BV2, and N18 cell lines as revealed by microarray analysis. *BMC Genomics* **12**, 14
357. Coldwell, M. C., Boyfield, I., Brown, T., Hagan, J. J., and Middlemiss, D. N. (1999) Comparison of the functional potencies of ropinirole and other dopamine receptor agonists at human D2(long), D3 and D4.4 receptors expressed in Chinese hamster ovary cells. *British journal of pharmacology* **127**, 1696-1702
358. Jiang, L. I., Collins, J., Davis, R., Lin, K.-M., DeCamp, D., Roach, T., Hsueh, R., Rebres, R. A., Ross, E. M., Taussig, R., Fraser, I., and Sternweis, P. C. (2007) Use of a cAMP BRET Sensor to Characterize a Novel Regulation of cAMP by the Sphingosine 1-Phosphate/G13 Pathway. *Journal of Biological Chemistry* **282**, 10576-10584
359. Vilardaga, J.-P., Bünemann, M., Krasel, C., Castro, M., and Lohse, M. J. (2003) Measurement of the millisecond activation switch of G protein–coupled receptors in living cells. *Nature Biotechnology* **21**, 807
360. Walker, J. E., Saraste, M., Runswick, M. J., and Gay, N. J. (1982) Distantly related sequences in the alpha- and beta-subunits of ATP synthase, myosin, kinases and other ATP-requiring enzymes and a common nucleotide binding fold. *The EMBO Journal* **1**, 945-951
361. Raw, A. S., Coleman, D. E., Gilman, A. G., and Sprang, S. R. (1997) Structural and Biochemical Characterization of the GTP γ S-, GDP \cdot Pi-, and GDP-Bound Forms of a GTPase-Deficient Gly42 \rightarrow Val Mutant of G α 1. *Biochemistry* **36**, 15660-15669
362. Koelle, M. R., and Horvitz, H. R. (1996) EGL-10 regulates G protein signaling in the C. elegans nervous system and shares a conserved domain with many mammalian proteins. *Cell* **84**, 115-125

363. Sjögren, B. (2017) The evolution of regulators of G protein signalling proteins as drug targets – 20 years in the making: IUPHAR Review 21. *British journal of pharmacology* **174**, 427-437
364. Rahman, Z., Schwarz, J., Gold, S. J., Zachariou, V., Wein, M. N., Choi, K.-H., Kovoov, A., Chen, C.-K., DiLeone, R. J., and Schwarz, S. C. (2003) RGS9 modulates dopamine signaling in the basal ganglia. *Neuron* **38**, 941-952
365. Kovoov, A., Seyffarth, P., Ebert, J., Barghshoon, S., Chen, C.-K., Schwarz, S., Axelrod, J. D., Cheyette, B. N., Simon, M. I., and Lester, H. A. (2005) D2 dopamine receptors colocalize regulator of G-protein signaling 9-2 (RGS9-2) via the RGS9 DEP domain, and RGS9 knock-out mice develop dyskinesias associated with dopamine pathways. *Journal of Neuroscience* **25**, 2157-2165
366. Wang, J., Tu, Y., Woodson, J., Song, X., and Ross, E. M. (1997) A GTPase-activating Protein for the G Protein Gαz: IDENTIFICATION, PURIFICATION, AND MECHANISM OF ACTION. *Journal of Biological Chemistry* **272**, 5732-5740
367. Mao, H., Zhao, Q., Daigle, M., Ghahremani, M. H., Chidiac, P., and Albert, P. R. (2004) RGS17/RGS22, a Novel Regulator of Gi/o, Gz, and Gq Signaling. *Journal of Biological Chemistry* **279**, 26314-26322
368. De Vries, L., Mousli, M., Wurmser, A., and Farquhar, M. G. (1995) GAIP, a protein that specifically interacts with the trimeric G protein G αi3, is a member of a protein family with a highly conserved core domain. *Proceedings of the National Academy of Sciences* **92**, 11916-11920
369. De Vries, L., Elenko, E., Hubler, L., Jones, T. L. Z., and Farquhar, M. G. (1996) GAIP is membrane-anchored by palmitoylation and interacts with the activated (GTP-bound) form of Gα_i subunits. *Proceedings of the National Academy of Sciences* **93**, 15203-15208
370. Jeong, S.-W., and Ikeda, S. R. (1998) G Protein α Subunit Gαz Couples Neurotransmitter Receptors to Ion Channels in Sympathetic Neurons. *Neuron* **21**, 1201-1212
371. Doi, M., Murai, I., Kunisue, S., Setsu, G., Uchio, N., Tanaka, R., Kobayashi, S., Shimatani, H., Hayashi, H., Chao, H.-W., Nakagawa, Y., Takahashi, Y., Hotta, Y., Yasunaga, J.-i., Matsuoka, M., Hastings, M. H., Kiyonari, H., and Okamura, H. (2016) Gpr176 is a Gz-linked orphan G-protein-coupled receptor that sets the pace of circadian behaviour. *Nature Communications* **7**, 10583
372. Goto, K., Doi, M., Wang, T., Kunisue, S., Murai, I., and Okamura, H. (2017) G-protein-coupled receptor signaling through Gpr176, Gz, and RGS16 tunes time in the center of the circadian clock [Review]. *Endocrine Journal* **64**, 571-579
373. Vancura, P., Abdelhadi, S., Csicsely, E., Baba, K., Tosini, G., Iuvone, P. M., and Spessert, R. (2017) Gnaz couples the circadian and dopaminergic system to G protein-mediated signaling in mouse photoreceptors. *PloS one* **12**, e0187411
374. Kelleher, K. L., Matthaei, K. I., Leck, K. J., and Hendry, I. A. (1998) Developmental expression of messenger RNA levels of the α subunit of the GTP-binding protein, Gz, in the mouse nervous system. *Developmental brain research* **107**, 247-253
375. Hinton, D., Blanks, J., Fong, H., Casey, P., Hildebrandt, E., and Simons, M. (1990) Novel localization of a G protein, Gz-α, in neurons of brain and retina. *The Journal of Neuroscience* **10**, 2763-2770
376. Hendry, I. A., Johanson, S. O., and Heydon, K. (1995) Retrograde axonal transport of the α subunit of the GTP-binding protein Gz to the nucleus of sensory neurons. *Brain Research* **700**, 157-163
377. Crouch, M. F., Heydon, K., Garnaut, S. M., Milburn, P. J., and Hendry, I. A. (1994) Retrograde Axonal Transport of the α-Subunit of the GTP-binding Protein Gz in Mouse Sciatic Nerve: a Potential Pathway for Signal Transduction In Neurons. *European Journal of Neuroscience* **6**, 626-631
378. Wong, Y., Conklin, B., and Bourne, H. (1992) Gz-mediated hormonal inhibition of cyclic AMP accumulation. *Science (New York, N.Y.)* **255**, 339-342

379. Curzon, P., and Decker, M. W. (1998) Effects of phencyclidine (PCP) and (+)MK-801 on sensorimotor gating in CD-1 mice. *Progress in Neuro-Psychopharmacology and Biological Psychiatry* **22**, 129-146
380. Serres, F., Li, Q., Garcia, F., Raap, D. K., Battaglia, G., Muma, N. A., and Van de Kar, L. D. (2000) Evidence that Gz-proteins couple to hypothalamic 5-HT_{1A} receptors in vivo. *Journal of Neuroscience* **20**, 3095-3103
381. Garzón, J., Martínez-Peña, Y., and Sánchez-Blázquez, P. (1994) Dissimilar efficacy of opioids to produce μ -mediated analgesia: Role of Gx/z and G12 transducer proteins. *Life Sciences* **55**, PL205-PL212
382. Chan, A. S. L., Lai, F. P. L., Lo, R. K. H., Voyno-Yasenetskaya, T. A., Stanbridge, E. J., and Wong, Y. H. (2002) Melatonin mt1 and MT2 receptors stimulate c-Jun N-terminal kinase via pertussis toxin-sensitive and -insensitive G proteins. *Cellular Signalling* **14**, 249-257
383. Traynor, J. R., Clark, M. J., and Remmers, A. E. (2002) Relationship between Rate and Extent of G Protein Activation: Comparison between Full and Partial Opioid Agonists. *Journal of Pharmacology and Experimental Therapeutics* **300**, 157-161
384. Furness, S. G. B., Liang, Y.-L., Nowell, C. J., Halls, M. L., Wookey, P. J., Dal Maso, E., Inoue, A., Christopoulos, A., Wootten, D., and Sexton, P. M. (2016) Ligand-Dependent Modulation of G Protein Conformation Alters Drug Efficacy. *Cell* **167**, 739-749.e711
385. Nikolaev, V. O., Hoffmann, C., Bünnemann, M., Lohse, M. J., and Vilardaga, J.-P. (2006) Molecular Basis of Partial Agonism at the Neurotransmitter α 2A-Adrenergic Receptor and Gi-protein Heterotrimer. *Journal of Biological Chemistry* **281**, 24506-24511
386. Barr, A. J., Brass, L. F., and Manning, D. R. (1997) Reconstitution of Receptors and GTP-binding Regulatory Proteins (G Proteins) in Sf9 Cells: A DIRECT EVALUATION OF SELECTIVITY IN RECEPTOR-G PROTEIN COUPLING. *Journal of Biological Chemistry* **272**, 2223-2229
387. Northup, J. K., Sternweis, P. C., Smigel, M. D., Schleifer, L. S., Ross, E. M., and Gilman, A. G. (1980) Purification of the regulatory component of adenylate cyclase. *Proceedings of the National Academy of Sciences* **77**, 6516-6520
388. Taylor, S. J., Smith, J. A., and Exton, J. H. (1990) Purification from bovine liver membranes of a guanine nucleotide-dependent activator of phosphoinositide-specific phospholipase C. Immunologic identification as a novel G-protein alpha subunit. *Journal of Biological Chemistry* **265**, 17150-17156
389. Hescheler, J., Rosenthal, W., Trautwein, W., and Schultz, G. (1987) The GTP-binding protein, Go9 regulates neuronal calcium channels. *Nature* **325**, 445
390. Lee, E., Taussig, R., and Gilman, A. G. (1992) The G226A mutant of Gs alpha highlights the requirement for dissociation of G protein subunits. *Journal of Biological Chemistry* **267**, 1212-1218
391. Buhl, A. M., Johnson, N. L., Dhanasekaran, N., and Johnson, G. L. (1995) G α 12 and G α 13 stimulate Rho-dependent stress fiber formation and focal adhesion assembly. *Journal of Biological Chemistry* **270**, 24631-24634
392. Fong, H., Yoshimoto, K. K., Eversole-Cire, P., and Simon, M. I. (1988) Identification of a GTP-binding protein alpha subunit that lacks an apparent ADP-ribosylation site for pertussis toxin. *Proceedings of the National Academy of Sciences* **85**, 3066-3070
393. Matsuoka, M., Itoh, H., Kozasa, T., and Kaziro, Y. (1988) Sequence analysis of cDNA and genomic DNA for a putative pertussis toxin-insensitive guanine nucleotide-binding regulatory protein alpha subunit. *Proceedings of the National Academy of Sciences* **85**, 5384-5388
394. Strathmann, M., Wilkie, T. M., and Simon, M. I. (1989) Diversity of the G-protein family: sequences from five additional alpha subunits in the mouse. *Proceedings of the National Academy of Sciences* **86**, 7407-7409
395. Strathmann, M., and Simon, M. I. (1990) G protein diversity: a distinct class of alpha subunits is present in vertebrates and invertebrates. *Proceedings of the National Academy of Sciences* **87**, 9113-9117

396. Kimple, M. E., Joseph, J. W., Bailey, C. L., Fueger, P. T., Hendry, I. A., Newgard, C. B., and Casey, P. J. (2008) Gaz negatively regulates insulin secretion and glucose clearance. *Journal of Biological Chemistry* **283**, 4560-4567
397. Brill, A. L., Wisinski, J. A., Cadena, M. T., Thompson, M. F., Fenske, R. J., Brar, H. K., Schaid, M. D., Pasker, R. L., and Kimple, M. E. (2016) Synergy between Gaz deficiency and GLP-1 analog treatment in preserving functional β -cell mass in experimental diabetes. *Molecular Endocrinology* **30**, 543-556
398. Fenske, R. J., Cadena, M. T., Harenda, Q. E., Wienkes, H. N., Carbajal, K., Schaid, M. D., Laundre, E., Brill, A. L., Truchan, N. A., and Brar, H. (2017) The Inhibitory G Protein α -Subunit, Gaz, Promotes Type 1 Diabetes-Like Pathophysiology in NOD Mice. *Endocrinology* **158**, 1645-1658
399. Ng, N. M., Littler, D. R., Paton, A. W., Le Nours, J., Rossjohn, J., Paton, J. C., and Beddoe, T. (2013) EcxAB is a founding member of a new family of metalloprotease AB5 toxins with a hybrid cholera-like B subunit. *Structure* **21**, 2003-2013
400. Endo, Y., Tsurugi, K., Yutsudo, T., Takeda, Y., Ogasawara, T., and Igarashi, K. (1988) Site of action of a Vero toxin (VT2) from *Escherichia coli* O157: H7 and of Shiga toxin on eukaryotic ribosomes: RNA N-glycosidase activity of the toxins. *European Journal of Biochemistry* **171**, 45-50
401. Katada, T., and Ui, M. (1982) Direct modification of the membrane adenylate cyclase system by islet-activating protein due to ADP-ribosylation of a membrane protein. *Proceedings of the National Academy of Sciences* **79**, 3129-3133
402. Cassel, D., and Pfeuffer, T. (1978) Mechanism of cholera toxin action: Covalent modification of the guanyl nucleotide-binding protein of the adenylate cyclase system. *Proceedings of the National Academy of Sciences* **75**, 2669-2673
403. Orth, J. H., Preuss, I., Fester, I., Schlosser, A., Wilson, B. A., and Aktories, K. (2009) *Pasteurella multocida* toxin activation of heterotrimeric G proteins by deamidation. *Proceedings of the National Academy of Sciences* **106**, 7179-7184
404. Katada, T., and Ui, M. (1982) ADP ribosylation of the specific membrane protein of C6 cells by islet-activating protein associated with modification of adenylate cyclase activity. *Journal of Biological chemistry* **257**, 7210-7216
405. Littler, D. R., Ang, S. Y., Moriel, D. G., Kocan, M., Kleifeld, O., Johnson, M. D., Tran, M. T., Paton, A. W., Paton, J. C., Summers, R. J., Schembri, M. A., Rossjohn, J., and Beddoe, T. (2017) Structure–function analyses of a pertussis-like toxin from pathogenic *Escherichia coli* reveal a distinct mechanism of inhibition of trimeric G-proteins. *Journal of Biological Chemistry* **292**, 15143-15158
406. Pedersen, M. H., Pham, J., Mancebo, H., Inoue, A., and Javitch, J. A. (2020) A novel luminescence-based β -arrestin membrane recruitment assay for unmodified GPCRs. *bioRxiv*
407. Pettersen, E. F., Goddard, T. D., Huang, C. C., Couch, G. S., Greenblatt, D. M., Meng, E. C., and Ferrin, T. E. (2004) UCSF Chimera—a visualization system for exploratory research and analysis. *Journal of computational chemistry* **25**, 1605-1612
408. Bowin, C.-F., Inoue, A., and Schulte, G. (2019) WNT-3A–induced β -catenin signaling does not require signaling through heterotrimeric G proteins. *Journal of Biological Chemistry* **294**, 11677-11684
409. Eden, R., Costall, B., Domeney, A., Gerrard, P., Harvey, C., Kelly, M., Naylor, R., Owen, D., and Wright, A. (1991) Preclinical pharmacology of ropinirole (SK&F 101468-A) a novel dopamine D2 agonist. *Pharmacology Biochemistry and Behavior* **38**, 147-154
410. Hildebrandt, J., Hanoune, J., and Birnbaumer, L. (1982) Guanine nucleotide inhibition of cyc-S49 mouse lymphoma cell membrane adenylyl cyclase. *Journal of Biological Chemistry* **257**, 14723-14725
411. Dearry, A., Gingrich, J. A., Falardeau, P., Fremeau Jr, R. T., Bates, M. D., and Caron, M. G. (1990) Molecular cloning and expression of the gene for a human D1 dopamine receptor. *Nature* **347**, 72

412. Zhou, Q.-Y., Grandy, D. K., Thambi, L., Kushner, J. A., Van Tol, H. H., Cone, R., Pribnow, D., Salon, J., Bunzow, J. R., and Civelli, O. (1990) Cloning and expression of human and rat D₁ dopamine receptors. *Nature* **347**, 76
413. Seeman, P., and Niznik, H. (1988) Dopamine D₁ receptor pharmacology. *ISI Atlas Sci Pharmacol* **2**, 161-170
414. Andersen, P. H., and Jansen, J. A. (1990) Dopamine receptor agonists: selectivity and dopamine D₁ receptor efficacy. *European Journal of Pharmacology: Molecular Pharmacology* **188**, 335-347
415. Wu, T., Li, A., and Wang, H.-L. (1995) Neurotensin increases the cationic conductance of rat substantia nigra dopaminergic neurons through the inositol 1, 4, 5-trisphosphate-calcium pathway. *Brain research* **683**, 242-250
416. Wang, H.-L., and Wu, T. (1996) G_q11 mediates neurotensin excitation of substantia nigra dopaminergic neurons. *Molecular brain research* **36**, 29-36
417. Besserer-Offroy, É., Brouillette, R. L., Lavenus, S., Froehlich, U., Brumwell, A., Murza, A., Longpré, J.-M., Marsault, É., Grandbois, M., and Sarret, P. (2017) The signaling signature of the neurotensin type 1 receptor with endogenous ligands. *European journal of pharmacology* **805**, 1-13
418. Vivaudou, M., Chan, K. W., Sui, J.-L., Jan, L. Y., Reuveny, E., and Logothetis, D. E. (1997) Probing the G-protein Regulation of GIRK1 and GIRK4, the Two Subunits of the KACH Channel, Using Functional Homomeric Mutants. *Journal of Biological Chemistry* **272**, 31553-31560
419. Castro, M. G., McNamara, U., and Carbonetti, N. H. (2001) Expression, activity and cytotoxicity of pertussis toxin S1 subunit in transfected mammalian cells. *Cellular microbiology* **3**, 45-54
420. Shenoy, S. K., Drake, M. T., Nelson, C. D., Houtz, D. A., Xiao, K., Madabushi, S., Reiter, E., Premont, R. T., Lichtarge, O., and Lefkowitz, R. J. (2006) β -Arrestin-dependent, G protein-independent ERK1/2 activation by the β 2 adrenergic receptor. *Journal of Biological Chemistry* **281**, 1261-1273
421. Quan, W., Kim, J.-H., Albert, P. R., Choi, H., and Kim, K.-M. (2008) Roles of G protein and β -arrestin in dopamine D₂ receptor-mediated ERK activation. *Biochemical and biophysical research communications* **377**, 705-709
422. Hunton, D. L., Barnes, W. G., Kim, J., Ren, X.-R., Violin, J. D., Reiter, E., Milligan, G., Patel, D. D., and Lefkowitz, R. J. (2005) β -Arrestin 2-dependent angiotensin II type 1A receptor-mediated pathway of chemotaxis. *Molecular pharmacology* **67**, 1229-1236
423. Friedman, J., Babu, B., and Clark, R. B. (2002) β 2-Adrenergic Receptor Lacking the Cyclic AMP-Dependent Protein Kinase Consensus Sites Fully Activates Extracellular Signal-Regulated Kinase 1/2 in Human Embryonic Kidney 293 Cells: Lack of Evidence for Gs/Gi Switching. *Molecular pharmacology* **62**, 1094-1102
424. Wang, J., Hanada, K., Staus, D. P., Makara, M. A., Dahal, G. R., Chen, Q., Ahles, A., Engelhardt, S., and Rockman, H. A. (2017) G α i is required for carvedilol-induced β 1 adrenergic receptor β -arrestin biased signaling. *Nature communications* **8**, 1706
425. Nogueras-Ortiz, C., Roman-Vendrell, C., Mateo-Semidey, G. E., Liao, Y.-H., Kendall, D. A., and Yudowski, G. A. (2017) Retromer stops beta-arrestin 1-mediated signaling from internalized cannabinoid 2 receptors. *Molecular biology of the cell* **28**, 3554-3561
426. Grundmann, M., Merten, N., Malfacini, D., Inoue, A., Preis, P., Simon, K., Rüttiger, N., Ziegler, N., Benkel, T., and Schmitt, N. K. (2018) Lack of beta-arrestin signaling in the absence of active G proteins. *Nature communications* **9**, 341
427. Senogles, S. E. (1994) The D₂ dopamine receptor isoforms signal through distinct Gi alpha proteins to inhibit adenylyl cyclase. A study with site-directed mutant Gi alpha proteins. *Journal of Biological Chemistry* **269**, 23120-23127
428. Doi, M., Murai, I., Kunisue, S., Setsu, G., Uchio, N., Tanaka, R., Kobayashi, S., Shimatani, H., Hayashi, H., and Chao, H.-W. (2016) Gpr176 is a Gz-linked orphan G-protein-coupled receptor that sets the pace of circadian behaviour. *Nature communications* **7**, 10583
429. Reisine, T. (1990) Pertussis toxin in the analysis of receptor mechanisms. *Biochemical pharmacology* **39**, 1499-1504

430. Joshi, S. A., Fan, K. P., Ho, V. W., and Wong, Y. H. (1998) Chimeric G α q mutants harboring the last five carboxy-terminal residues of G α i2 or G α o are resistant to pertussis toxin-catalyzed ADP-ribosylation. *FEBS letters* **441**, 67-70
431. Bahia, D. S., Wise, A., Fanelli, F., Lee, M., Rees, S., and Milligan, G. (1998) Hydrophobicity of residue 351 of the G protein G α i1 α determines the extent of activation by the α 2A-adrenoceptor. *Biochemistry* **37**, 11555-11562
432. Rask-Andersen, M., Masuram, S., and Schiöth, H. B. (2014) The druggable genome: evaluation of drug targets in clinical trials suggests major shifts in molecular class and indication. *Annual review of pharmacology and toxicology* **54**, 9-26
433. Bonci, A., and Hopf, F. W. (2005) The dopamine D2 receptor: new surprises from an old friend. *Neuron* **47**, 335-338
434. Krasel, C., Vilardaga, J.-P., Bünemann, M., and Lohse, M. (2004) Kinetics of G-protein-coupled receptor signalling and desensitization. Portland Press Ltd.
435. Volavka, J. (2012) Clozapine is gold standard, but questions remain. *International Journal of Neuropsychopharmacology* **15**, 1201-1204
436. Mottola, D. M., Kilts, J. D., Lewis, M. M., Connery, H. S., Walker, Q. D., Jones, S. R., Booth, R. G., Hyslop, D. K., Piercey, M., and Wightman, R. M. (2002) Functional selectivity of dopamine receptor agonists. I. Selective activation of postsynaptic dopamine D2 receptors linked to adenylate cyclase. *Journal of Pharmacology and Experimental Therapeutics* **301**, 1166-1178
437. Kilts, J. D., Connery, H. S., Arrington, E. G., Lewis, M. M., Lawler, C. P., Oxford, G. S., O'Malley, K. L., Todd, R. D., Blake, B. L., and Nichols, D. E. (2002) Functional selectivity of dopamine receptor agonists. II. Actions of dihydroxidine in D2L receptor-transfected MN9D cells and pituitary lactotrophs. *Journal of Pharmacology and Experimental Therapeutics* **301**, 1179-1189
438. Urban, J. D., Vargas, G. A., Von Zastrow, M., and Mailman, R. B. (2007) Aripiprazole has functionally selective actions at dopamine D2 receptor-mediated signaling pathways. *Neuropsychopharmacology* **32**, 67
439. Mailman, R. B. (2007) GPCR functional selectivity has therapeutic impact. *Trends in pharmacological sciences* **28**, 390-396
440. Tschammer, N., Bollinger, S., Kenakin, T., and Gmeiner, P. (2011) Histidine 6.55 is a major determinant of ligand-biased signaling in dopamine D2L receptor. *Molecular pharmacology* **79**, 575-585
441. Conibear, A. E., and Kelly, E. (2019) A biased view of μ -opioid receptors? *Molecular pharmacology* **96**, 542-549
442. Wei, H., Ahn, S., Shenoy, S. K., Karnik, S. S., Hunyady, L., Luttrell, L. M., and Lefkowitz, R. J. (2003) Independent β -arrestin 2 and G protein-mediated pathways for angiotensin II activation of extracellular signal-regulated kinases 1 and 2. *Proceedings of the National Academy of Sciences* **100**, 10782-10787
443. Saulière, A., Bellot, M., Paris, H., Denis, C., Finana, F., Hansen, J. T., Altié, M.-F., Seguelas, M.-H., Pathak, A., and Hansen, J. L. (2012) Deciphering biased-agonism complexity reveals a new active AT1 receptor entity. *Nature chemical biology* **8**, 622-630
444. Herve, D., Levi-Strauss, M., Marey-Semper, I., Verney, C., Tassin, J., Glowinski, J., and Girault, J. (1993) G (olf) and Gs in rat basal ganglia: possible involvement of G (olf) in the coupling of dopamine D1 receptor with adenylyl cyclase. *Journal of Neuroscience* **13**, 2237-2248
445. Taniguchi, M., Suzumura, K.-i., Nagai, K., Kawasaki, T., Saito, T., Takasaki, J., Suzuki, K.-i., Fujita, S., and Tsukamoto, S.-i. (2003) Structure of YM-254890, a novel Gq/11 inhibitor from Chromobacterium sp. QS3666. *Tetrahedron* **59**, 4533-4538
446. Dai, S. A., Hu, Q., Gao, R., Lazar, A., Zhang, Z., von Zastrow, M., Suga, H., and Shokat, K. M. (2020) A GTP-state specific cyclic peptide inhibitor of the GTPase Gas. *bioRxiv*

Appendix 1:

Molecular determinants of the intrinsic efficacy of the antipsychotic aripiprazole

Molecular Determinants of the Intrinsic Efficacy of the Antipsychotic Aripiprazole

Carmen Klein Herenbrink,^{†,∇} Ravi Verma,^{§,∇} Herman D. Lim,[†] Anitha Kopinathan,[‡] Alastair Keen,[†] Jeremy Shonberg,[‡] Christopher J. Draper-Joyce,[†] Peter J. Scammells,[‡] Arthur Christopoulos,[†] Jonathan A. Javitch,^{||,⊥} Ben Capuano,[‡] Lei Shi,^{*,§} and J. Robert Lane^{*,#,ⓐ}

[†]Drug Discovery Biology and [‡]Medicinal Chemistry, Monash Institute of Pharmaceutical Sciences, Monash University (Parkville campus), 399 Royal Parade, Parkville, VIC 3052, Australia

[§]Computational Chemistry and Molecular Biophysics Unit, National Institute on Drug Abuse-Intramural Research Program, National Institutes of Health, 333 Cassell Drive, Baltimore, Maryland 21224, United States

^{||}Departments of Psychiatry and Pharmacology, Vagelos College of Physicians and Surgeons, Columbia University, New York, New York 10032, United States

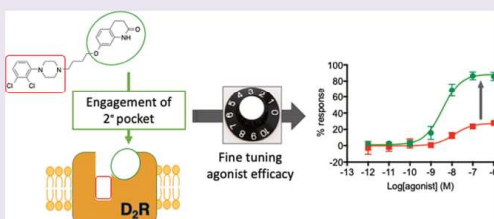
[⊥]Division of Molecular Therapeutics, New York State Psychiatric Institute, New York, New York 10032, United States

[#]Division of Pharmacology, Physiology and Neuroscience, School of Life Sciences, Queen's Medical Centre, University of Nottingham, Nottingham NG7 2UH, U.K.

[ⓐ]Centre of Membrane Protein and Receptors, Universities of Birmingham and Nottingham, Nottingham, United Kingdom

Supporting Information

ABSTRACT: Partial agonists of the dopamine D₂ receptor (D₂R) have been developed to treat the symptoms of schizophrenia without causing the side effects elicited by antagonists. The receptor–ligand interactions that determine the intrinsic efficacy of such drugs, however, are poorly understood. Aripiprazole has an extended structure comprising a phenylpiperazine primary pharmacophore and a 1,2,3,4-tetrahydroquinolin-2-one secondary pharmacophore. We combined site-directed mutagenesis, analytical pharmacology, ligand fragments, and molecular dynamics simulations to identify the D₂R–aripiprazole interactions that contribute to affinity and efficacy. We reveal that an interaction between the secondary pharmacophore of aripiprazole and a secondary binding pocket defined by residues at the extracellular portions of transmembrane segments 1, 2, and 7 determines the intrinsic efficacy of aripiprazole. Our findings reveal a hitherto unappreciated mechanism for fine-tuning the intrinsic efficacy of D₂R agonists.



The dopamine D₂ receptor (D₂R), a class A G protein-coupled receptor (GPCR), is the target of drugs that relieve symptoms of Parkinson's disease (agonists) and schizophrenia (partial agonists/antagonists).¹ The antipsychotics aripiprazole, brexpiprazole, and cariprazine are D₂R partial agonists.^{2–4} They are thought to act as functional antagonists in the striatum, where excessive dopamine activity is thought to cause positive symptoms, but to show agonist activity in the mesocortical pathway, where reduced dopamine activity is thought to be associated with negative symptoms and cognitive impairment. A partial agonist may also avoid the complete blockade of the nigrostriatal or tuberoinfundibular pathways that is associated with the extrapyramidal symptoms and elevated prolactin levels caused by typical antipsychotics.⁵ However, why these partial agonists display antipsychotic efficacy while other D₂R partial agonists have failed to do so remains unclear. It has been proposed that the low level of intrinsic activity elicited by aripiprazole gives sufficient

functional antagonism for antipsychotic efficacy whereas other partial agonists with higher intrinsic activity, such as bifeprunox, failed in clinical development.⁶ Furthermore, the intrinsic activity of aripiprazole is apparently sufficient to avoid motor side effects and prolactinemia.

The crystal structures of the D₂R, D₃R, and D₄R, in complex with the antagonists risperidone, eticlopride, and nemonapride, respectively, reveal the location of an orthosteric binding site (OBS) comprised of residues that are conserved in the dopamine D₂-like receptors and are consistent with earlier findings of mutagenesis and molecular modeling studies.^{7–10} Despite the therapeutic utility of D₂R full and partial agonists, our understanding of the ligand–receptor contacts that

Received: May 1, 2019

Accepted: July 24, 2019

Published: July 24, 2019

Table 1. Effects of Mutations in the OBS and ECL2 of the D₂R on the Affinity and Functional Activity of Selected Agonists^a

construct	ropinirole			dopamine			aripiprazole		
	p <i>K_i</i> (fold Δ)	log(<i>τ</i> / <i>K_A</i>) (fold Δ)	p <i>K_i</i> (fold Δ)	log(<i>τ</i> / <i>K_A</i>) (fold Δ)	p <i>K_i</i> (fold Δ)	log(<i>τ</i> / <i>K_A</i>) (fold Δ)	p <i>K_A</i> (fold Δ)	log <i>r</i> (fold Δ)	
WT	5.18 ± 0.04 (1.0)	8.29 ± 0.06 (1.0)	4.94 ± 0.03 (1.0)	8.51 ± 0.05 (1.0)	9.92 ± 0.02 (1.0)	8.45 ± 0.06 (1.0)	7.75 ± 0.14	0.69 ± 0.15	
V115 ³³³ A	4.73 ± 0.20 (2.8)	6.78 ± 0.15* (33)	4.06 ± 0.15* (7.7)	7.32 ± 0.12* (16)	9.07 ± 0.04* (7.1)	7.70 ± 0.17* (5.6)	7.83 ± 0.20 (0.8)	−0.19 ± 0.04* (8)	
C118 ³³⁶ A	5.43 ± 0.09 (0.6)	ND	4.40 ± 0.16* (3.5)	5.94 ± 0.09* (370)	9.36 ± 0.03* (3.6)	ND	ND	ND	
T119 ³³⁷ A	5.37 ± 0.16 (0.7)	6.47 ± 0.08* (67)	4.84 ± 0.04 (1.3)	ND	9.68 ± 0.10 (1.7)	ND	ND	ND	
I122 ³⁴⁰ A	5.11 ± 0.04 (1.2)	ND	5.21 ± 0.10 (0.5)	ND	10.11 ± 0.09 (0.6)	ND	ND	ND	
L174 ^{ECL2} A	5.65 ± 0.13 (0.3)	8.21 ± 0.09 (1.2)	5.24 ± 0.12 (0.5)	8.22 ± 0.06 (1.9)	10.16 ± 0.07 (0.6)	8.43 ± 0.19 (1.0)	7.95 ± 0.14 (0.6)	0.48 ± 0.11 (1.6)	
E181 ^{ECL2} A	5.52 ± 0.03 (0.5)	7.94 ± 0.19 (2.2)	5.02 ± 0.01 (0.8)	8.63 ± 0.17 (0.8)	9.88 ± 0.05 (1.1)	8.20 ± 0.22 (1.8)	8.00 ± 0.16 (0.6)	0.19 ± 0.08 (3)	
I183 ^{ECL2} A	5.50 ± 0.02 (0.5)	8.51 ± 0.18 (0.6)	5.02 ± 0.03 (0.8)	8.75 ± 0.10 (0.6)	9.50 ± 0.08 (2.7)	8.05 ± 0.24 (2.5)	7.61 ± 0.23 (1.4)	0.44 ± 0.01 (1.8)	
I184 ^{ECL2} A	5.18 ± 0.06 (1.0)	7.36 ± 0.16* (8.5)	4.40 ± 0.07* (3.5)	7.06 ± 0.05* (28)	9.45 ± 0.12 (3.0)	7.93 ± 0.05 (3.3)	7.65 ± 0.07 (1.3)	0.27 ± 0.09 (2.6)	
A185 ^{ECL2} S	5.69 ± 0.03* (0.3)	8.39 ± 0.08 (0.8)	5.37 ± 0.11* (0.4)	8.61 ± 0.09 (0.8)	10.06 ± 0.13 (0.7)	8.65 ± 0.06 (0.6)	7.87 ± 0.15 (0.8)	0.79 ± 0.11 (0.8)	
N186 ^{ECL2} A	5.01 ± 0.10 (1.5)	7.67 ± 0.07 (4.2)	4.54 ± 0.09 (2.5)	8.01 ± 0.06 (3.2)	9.60 ± 0.21 (2.1)	8.10 ± 0.20 (2.2)	7.63 ± 0.12 (1.6)	0.47 ± 0.11 (1.6)	
S193 ⁴³² A	4.00 ± 0.05* (15)	5.32 ± 0.12* (930)	2.86 ± 0.09* (120)	5.30 ± 0.14* (1600)	10.41 ± 0.06* (0.3)	8.82 ± 0.11 (0.4)	7.29 ± 0.16 (2.9)	1.53 ± 0.15* (0.1)	
S194 ⁴³² A	5.01 ± 0.11 (1.5)	6.99 ± 0.09* (20)	4.39 ± 0.08* (3.6)	7.48 ± 0.12* (11)	9.66 ± 0.17 (1.8)	8.42 ± 0.09 (1.1)	7.72 ± 0.07 (1.1)	0.71 ± 0.30 (1)	
S197 ⁴³⁶ A	5.07 ± 0.04 (1.3)	8.08 ± 0.14 (1.6)	4.47 ± 0.03* (3.0)	ND	9.21 ± 0.07* (5.1)	8.58 ± 0.06 (0.7)	7.82 ± 0.10 (0.9)	0.80 ± 0.10 (0.8)	
F202 ⁴⁵¹ A	4.91 ± 0.07 (1.9)	6.21 ± 0.21* (120)	4.15 ± 0.04* (6.2)	6.30 ± 0.10* (160)	9.40 ± 0.10* (3.3)	ND	ND	ND	
F360 ⁶⁵¹ A	ND	ND	ND	ND	ND	ND	ND	ND	
F361 ⁶⁵² A	ND	7.36 ± 0.15* (8.6)	ND	7.65 ± 0.18* (72)	ND	8.03 ± 0.23 (2.6)	7.29 ± 0.18 (2.8)	0.73 ± 0.13 (0.9)	
H364 ⁶⁵³ A	5.39 ± 0.05 (0.6)	7.52 ± 0.25* (5.9)	4.33 ± 0.08* (4.1)	6.67 ± 0.21* (69)	10.22 ± 0.03 (0.5)	8.58 ± 0.16 (0.7)	7.64 ± 0.24 (1.3)	0.89 ± 0.07 (0.6)	
H364 ⁶⁵⁵ F	5.11 ± 0.09 (1.2)	6.26 ± 0.11* (110)	4.63 ± 0.05 (2.1)	7.06 ± 0.07* (28)	9.74 ± 0.05 (1.5)	8.43 ± 0.12 (1.0)	7.50 ± 0.14 (1.8)	0.93 ± 0.19 (0.6)	
N367 ⁶⁵⁸ A	5.28 ± 0.07 (0.8)	7.71 ± 0.08 (3.8)	4.45 ± 0.06* (3.1)	7.51 ± 0.03* (10)	9.91 ± 0.04 (1.0)	8.29 ± 0.13 (1.4)	7.93 ± 0.10 (0.7)	0.20 ± 0.04 (3.0)	
I368 ⁶⁵⁹ A	5.41 ± 0.09 (0.6)	7.58 ± 0.16* (5.2)	5.45 ± 0.11* (0.3)	8.59 ± 0.19 (0.8)	9.62 ± 0.07 (2.0)	8.49 ± 0.10 (0.9)	7.89 ± 0.14 (0.7)	0.60 ± 0.12 (1.2)	
S380 ⁷³⁶ A	5.57 ± 0.01 (0.4)	8.00 ± 0.13 (2.0)	5.06 ± 0.10 (0.8)	8.68 ± 0.16 (0.7)	9.92 ± 0.10 (1.0)	8.23 ± 0.26 (1.7)	8.41 ± 0.18 (0.22)	0.87 ± 0.19 (0.66)	
T383 ⁷³⁹ A	5.36 ± 0.04 (0.7)	6.83 ± 0.06* (29)	4.87 ± 0.04 (1.2)	7.91 ± 0.10 (4)	10.13 ± 0.14 (0.6)	9.09 ± 0.07 (0.2)*	7.99 ± 0.10 (0.6)	1.09 ± 0.13 (0.40)	

^aBinding affinity values were obtained in competition binding experiments using the radioligand [³H]spiperone. Functional affinities, efficacies, and transduction ratios were determined in an assay measuring inhibition of forskolin-induced intracellular cAMP production. Values are expressed as means ± the standard deviation from three (binding) or four (cAMP) separate experiments. ND indicates no specific binding or agonist activity could be determined. **p* < 0.05, significantly different from that of the wild-type receptor determined by one-way analysis of variance, with Dunnett's post hoc test.

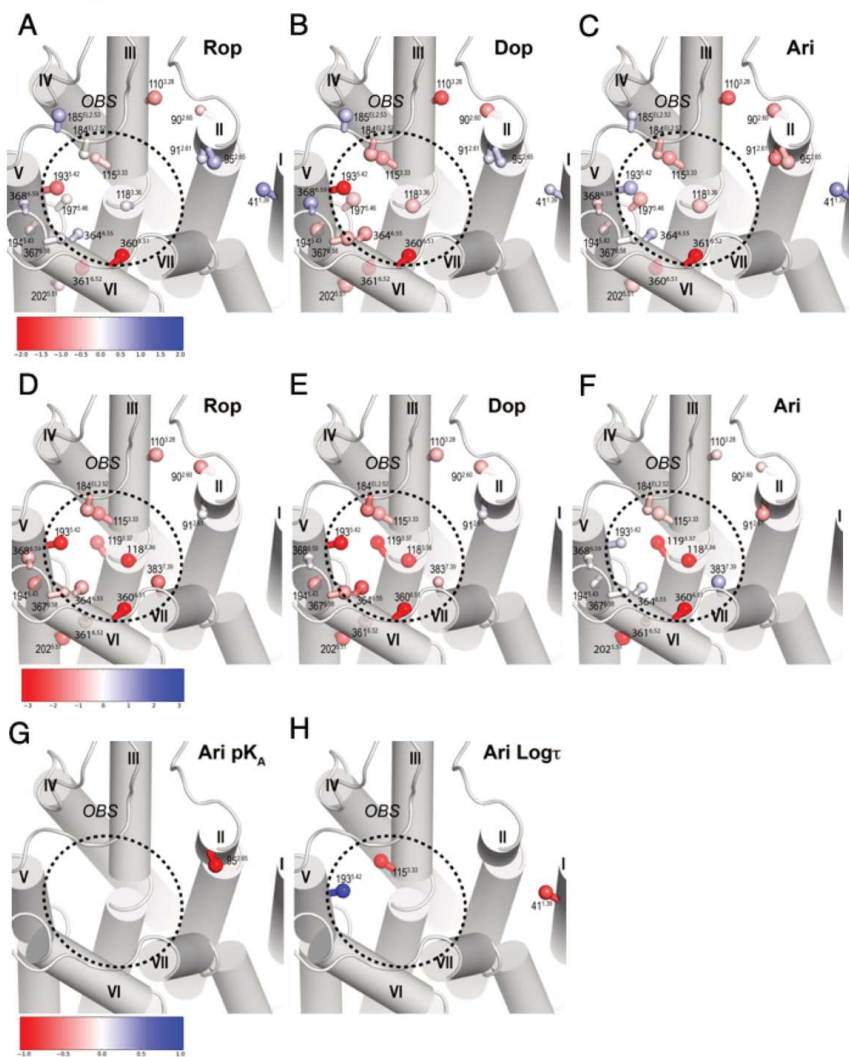


Figure 1. Mutations of residues within the OBS and SBP have distinct effects on the affinity and efficacy of aripiprazole as compared to those of dopamine and ropinirole. WT and mutant D₂Rs were stably expressed in FlpIN CHO cells. The change in affinity (pK_A) of (A) ropinirole, (B) dopamine, and (C) aripiprazole for each mutant was determined in competition binding experiments. The ability to increase the concentration of each agonist to activate the WT or mutant D₂Rs was determined in an assay measuring the inhibition of cAMP production. These data were fit to an operational model of agonism, and changes in the transduction coefficient (τ/K_A) were determined for (D) ropinirole, (E) dopamine, and (F) aripiprazole for each mutant. Changes in (G) functional affinity (pK_A) and (H) efficacy (τ) were also determined for aripiprazole. Mutations that cause significant increases (one-way analysis of variance with Dunnett's post hoc test; $p < 0.05$; blue) or decreases (red) for each parameter for the mutant receptor as compared to that of the WT are highlighted on a homology model of the D₂R.

determine the degrees of intrinsic efficacy is limited. Agonist-bound class A GPCR crystal structures reveal different patterns of agonist–receptor interactions but common structural rearrangements in the extracellular part of the transmembrane (TM) bundle near the OBS upon receptor activation.^{11,12} These are translated into larger rearrangements at the cytoplasmic side of the receptor, including translation and

rotation of TM5 and TM6 and relocation of TM3 and TM7. In particular, comparisons of class A GPCR crystal structures in active and inactive states, combined with molecular dynamics (MD) simulations, have highlighted the movement of a cluster of residues, Pro^{5.50}, Ile^{3.40}, and Phe^{6.44} (termed the “PIF motif”, Ballesteros and Weinstein numbering system¹³), along with Leu/Val^{5.51} and Trp^{6.48} on receptor activation. The

reconfigurations of these residues couple the conformational changes in the binding pocket to those at the intracellular coupling interface.^{14–16}

Aripiprazole is comprised of a 4-(2,3-dichlorophenyl)-piperazine primary pharmacophore (PP) and a 1,2,3,4-tetrahydroquinolin-2-one secondary pharmacophore (SP) linked by a flexible butoxy linker. This extended structure is typical of ligands that are selective for dopamine D₂-like receptors.^{7,17} Using the D₃R crystal structure,⁷ we revealed a secondary binding pocket (SBP) that extended away from the OBS toward the extracellular ends of TM1–TM3 and TM7 and demonstrated that the interaction between this SBP and the aryl tail moiety of phenylpiperazine derivatives not only was an important determinant of subtype selectivity but could also modulate ligand efficacy through reorientation of the phenylpiperazine core within the SBP.^{18,19} Surprisingly, however, little is known about the binding mode of aripiprazole at the D₂R and how this might determine its agonist efficacy. To address this, we combined MD simulations, mutagenesis, and analytical pharmacology to quantify agonist action in terms of both efficacy (τ) and functional affinity (K_A). Together, our studies reveal that the interaction between the 1,2,3,4-tetrahydroquinolin-2-one SP and the D₂R SBP is a determinant of aripiprazole's intrinsic efficacy.

RESULTS AND DISCUSSION

Aripiprazole and Dopamine Show Distinct Sensitivities to OBS Mutations. To interrogate the ligand–receptor interactions involved in agonist binding and the subsequent activation of the D₂R, we mutated residues within the OBS, the SBP, and the transmission switch of the D₂R. An enzyme-linked immunosorbent assay (ELISA) revealed no significant difference between the cell surface expression levels of the mutant and wild-type (WT) receptors (Supplementary Figure 1). We then determined the effect of each mutation on the dissociation constant (pK_d) of [³H]spiperone and/or [³H]raclopride. A homologous competition binding assay revealed that none of the mutations had a significant effect on the pK_d of [³H]spiperone (Supplementary Table 2) with the exception of V91^{2,61}A, F360^{6,51}A, and F361^{6,52}A, for which no detectable binding was observed. Of these three mutants, [³H]raclopride bound V91^{2,61}A with WT affinity but was unable to bind F360^{6,51}A and F361^{6,52}A (Supplementary Table 2).

The binding affinities (K_i) of the agonists at the D₂R were determined in competition binding experiments (Table 1). To measure the functional impact of the mutations, we used inhibition of forskolin-induced cAMP production as a measure of D₂R G $\alpha_{i/o}$ G protein signaling. Many OBS mutations, however, abrogated the binding and/or functional activity of dopamine, which prevented us from quantifying the relative effect of these mutations on aripiprazole. We, therefore, extended our studies to ropinirole, an agonist that retained activity at many OBS mutations. We designed a sensitive cAMP assay using a low (300 nM) concentration of forskolin to give a greater dynamic range with which to quantify the deleterious effects of receptor mutants. In this assay, aripiprazole displayed a robust partial maximal response (80%) relative to that of dopamine. This contrasts with the results of previous studies of aripiprazole using the same CHO cell background for which a much weaker relative maximal response was observed.^{2,20} Such differences reflect different receptor expression levels and assay sensitivities. Our data were

fitted with an operational model of agonism to derive a transduction coefficient (τ/K_A) of all three agonists, comprised of agonist efficacy (τ) and the functional affinity of the receptor when coupled to a specific signaling pathway (K_A).²¹ Although we could not define these two separate parameters for the full agonists dopamine and ropinirole, in the case of the partial agonist aripiprazole, we could determine separate values of affinity and efficacy [K_A = 17 nM, and τ = 5 (Table 1)].

We first investigated the role of OBS residues (Table 1). Asp114^{3,32} forms a salt bridge interaction with the positively charged nitrogen of dopaminergic ligands, and the D114^{3,32}A mutation ablates agonist and antagonist binding.²² Val^{3,33}, Cys^{3,36}, and Thr^{3,37} line the OBS in the D₂R, D₃R, and D₄R structures, respectively.^{7,9,10} V115^{3,33}A reduced the binding affinity of dopamine and aripiprazole but not that of ropinirole and decreased the transduction coefficients (τ/K_A) of all ligands (Table 1). In the case of aripiprazole, this effect was caused by a significant 8-fold decrease in efficacy (τ). C118^{3,36}A or T119^{3,37}A had little effect on binding affinity (K_i) but significantly reduced the functional effect of all ligands, causing a >50-fold decrease in transduction coefficients (τ/K_A) or abrogating activity altogether (Table 1).

The conserved TMS serine residues have been shown to be important for agonist binding and action at all DR subtypes.^{23–27} In agreement with these previous studies, the binding affinity of dopamine was significantly reduced at S193^{5,42}A, S194^{5,43}A, and S197^{5,46}A by 120-, 4-, and 3-fold, respectively (Figure 1 and Table 1). The transduction coefficient of dopamine was reduced at S193^{5,42}A (1600-fold) and S194^{5,43}A (11-fold), whereas S197^{5,46}A abolished its functional effect entirely (Figure 1 and Table 1). The binding affinity and transduction coefficient of ropinirole were also significantly reduced at S193^{5,42}A by 15- and 930-fold, respectively. S194^{5,43}A had no effect on ropinirole affinity but caused a 20-fold decrease in the transduction coefficient, whereas S197^{5,46}A had no effect. Interestingly, mutation of the TMS serines did not decrease the efficacy (τ) of aripiprazole (Figure 1). Rather, S193^{5,42}A caused a 3-fold increase in binding affinity and a 10-fold increase in efficacy, whereas S197^{5,46}A caused a 5-fold decrease in binding affinity with no effect on the functional response (Figure 1 and Table 1).

Residues within ECL2 form part of the D₂R and D₃R OBS.^{7,28} I184^{ECL2}A significantly reduced the binding affinity and transduction coefficient of dopamine (4- and 28-fold, respectively) (Table 1). None of the ECL2 mutations affected the binding affinity, functional affinity, or efficacy of aripiprazole (Table 1).

Residues 6.51 and 6.52 interact with the substituted aromatic ring of eticlopride in the D₃R and the methoxy benzamide ring of nemonapride in the D₄R.^{7,9} None of the agonists displayed functional activity at F360^{6,51}A, and F361^{6,52}A caused a significant decrease in the transduction coefficients of both ropinirole (9-fold) and dopamine (7-fold) (Figure 1 and Table 1). Residue 6.55 has been shown to be important for agonist binding and efficacy at the D₂R and D₃R.^{7,27,29,30} H364^{6,55}A decreased the binding affinity (4-fold) and transduction coefficient (69-fold) of dopamine and the transduction coefficient (6-fold) of ropinirole but not its affinity. The H364^{6,55}F mutation reduced the transduction coefficient of ropinirole (110-fold) and dopamine (28-fold), indicating that the imidazole side chain of His364^{6,55} is important for the agonist action of these ligands (Table 1). Residues 6.58 and 6.59 line the OBS.³⁰ In the 5HT_{2B} receptor,

these residues form hydrophobic contacts with ergotamine that are important for its biased action.³¹ N367^{6,58}A caused a 3-fold decrease in the binding affinity and a 10-fold decrease in the transduction coefficient of dopamine only (Table 1). I368^{6,59}A decreased the transduction coefficient of ropinirole by 5-fold. Notably, mutation of these TM6 residues (F361^{6,52}A, H364^{6,55}A/F, N367^{6,58}A, or I368^{6,59}A) did not change the affinity or efficacy of aripiprazole (Figure 1 and Table 1). Mutation of Thr383^{7,39}, a residue shown to contribute to aminergic receptor ligand binding,⁸ did not change the binding affinity of the three agonists but decreased the transduction coefficient of ropinirole (29-fold) while it increased that of aripiprazole 5-fold.

In summary, we identified OBS residues that contribute to the efficacy of all three agonists but found mutations in ECL2 (I184^{ECL2}A), TM5 (S193^{5,42}A, S194^{5,43}A, and S197^{5,46}A), and TM6 (F361^{6,52}A, H364^{6,55}A, N367^{6,58}A, or I368^{6,59}A) that had deleterious effects on the functional effect of dopamine and ropinirole but no effect on the efficacy of aripiprazole. Differential engagements of the TM5 serines (at positions 5.42, 5.43, and 5.46) and His^{6,55} by D₂R agonists have been suggested to underlie differences in efficacy through the stabilization of distinct receptor conformations.^{27,29} In the case of aripiprazole, rather than deleterious effects, the S^{5,46}A, F^{6,52}A, and H^{6,55}A mutations caused a modest increase in efficacy. Interestingly, S^{5,42}A and S^{5,46}A mutations caused decreases in the affinity and transduction coefficient of dopamine, in agreement with previous studies, whereas the S^{5,46}A mutation had no effect on ropinirole. In a previous study, our MD simulations found that N-1 of sumanirole, an agonist that is structurally similar to ropinirole, forms a hydrogen bond with the side chain of Ser^{5,42} but no interaction with Ser^{5,46} was observed.³² Ropinirole might adopt a similar orientation, but further simulations are required to confirm this hypothesis.

Transmission Switch Residues Are Required for Agonist Action at the D₂R. Comparison of the active and inactive structures of rhodopsin and the adenosine A_{2A}, β_2 adrenergic, and μ opioid receptors revealed rearrangement of a cluster of hydrophobic and aromatic residues (including residues 3.40, 5.50, 5.51, 6.44, and 6.48) in the TM3–TM5–TM6 motif as a common feature of class A GPCR activation.^{11,12,15} I122^{3,40} is part of the conserved P^{5,50}-I^{3,40}-P^{6,44} motif that undergoes structural rearrangement upon receptor activation to allow the outward movement of TM6. The I122^{3,40}A mutation had no significant effect on the binding affinity of the agonists but abrogated functional activity. The F202^{5,51}A mutation caused a significant reduction in the binding affinity of dopamine and aripiprazole [6- and 3-fold, respectively (Table 1)]. Aripiprazole displayed no agonism with this mutation, and ropinirole and dopamine displayed >100-fold lower transduction coefficients (Table 1). Thus, all three D₂R agonists require conformational rearrangement of transmission switch residues to exert their agonistic effect. While F202^{5,51} does not form part of the OBS, the F202^{5,51}A mutation may modulate the conformation of the OBS causing the loss of affinity of dopamine and aripiprazole but not that of ropinirole. Interestingly, the recent D₂R crystal structure obtained in complex with the antagonist risperidone included the I122^{3,40}A mutation as one of three thermostabilizing mutations.¹⁰ This mutation likely exerts its thermostabilizing effect by preventing the isomerization of the receptor into the active state.

Molecular Dynamics Simulations Reveal an Extended Pose of Aripiprazole. To characterize and dissect the contributions of residues from the OBS and SBP to the binding pose of aripiprazole, we performed a computational modeling and simulation study of D₂R models in complex with aripiprazole. From the initial docking results, we chose several poses of aripiprazole with its quinoline moiety oriented in various directions in the extracellular vestibule (EV) of D₂R (see Methods). We then collected multiple MD trajectories for each pose (Supplementary Table 1) and sought to identify a convergent trend of the ligand dynamics in the binding site.

Similar to the partial agonists with a 2,3-diCl-phenylpiperazine PP that we have characterized previously in D₃R models,¹⁸ the PP of aripiprazole adopts a pose that is relatively parallel to the membrane and close to Ser193^{5,42} but does not form an H-bond with Ser193^{5,42}. In all our simulations, Ser197^{5,46} forms a H-bond to the backbone carbonyl of Ser193^{5,42}. Thus, the S193^{5,42}A mutation may lead to an optimized hydrophobic interaction and slightly improve the affinity, whereas the Ser197^{5,46}A mutation disrupts the local conformation of TM5 and results in a slightly decreased affinity. In such a pose, both rings of 2,3-diCl-phenylpiperazine are tightly packed with Phe360^{6,51}, and it is expected that the F360^{6,51}A mutation would destabilize the observed orientation of the phenylpiperazine. Thus, this pose of the PP within the D₂R OBS is in agreement with our mutagenesis results.

For the SP and the flexible butoxy linker, however, we found that our simulations from different starting poses and multiple trajectories converged to two distinct poses in the EV, depending on the orientation of the highly conserved Trp384^{7,40}. When Trp384^{7,40} faces the lipid as in the D₃R structure, the quinoline ring occupies a cavity at the interface among TM1, TM2, and TM7 and is in contact with Leu41^{1,39}, Val91^{2,61}, and Trp384^{7,40} (Figure 2C). In contrast, when the indole ring of Trp384^{7,40} rotates inward between the side chains of Val91^{2,61} and Leu41^{1,39}, the quinoline ring can no longer extend into this cavity but rather tilts toward ECL2 and TM3, forming a weak interaction with Glu95^{2,65} (Figure 2D). Such an inward orientation of Trp384^{7,40} is observed in most of the crystal structures of aminergic receptors.³³ While Trp384^{7,40} of the D₃R faces the lipid, that of the D₂R structure is in an intermediate position, and in our simulations, we observed that this residue can adopt both inward and outward orientations.^{7,10}

The SP of Aripiprazole Confers an Increase in Efficacy. To explore how the interaction of the SP of aripiprazole with the D₂R SBP might influence affinity and efficacy, we characterized a series of progressively extended fragments of aripiprazole incorporating either the PP or the SP. The introduction of the alkyl or alkoxy spacers (compounds 2–4) into the PP 2,3-dichlorophenylpiperazine fragment (DCPP, 1) conferred 32–115-fold increases in binding affinity (Figure 3 and Table 2). Incorporation of the 1,2,3,4-tetrahydroquinolin-2-one (THQ) moiety of aripiprazole enhanced the binding affinity by a further 22-fold compared to that of the methoxybutyl-substituted derivative (4). Fragments containing the SP were able to displace the radioligand only upon inclusion of an ionizable nitrogen atom within its structure (Supplementary Table 3). In functional studies, this time using a bioluminescence resonance energy transfer (BRET) biosensor to measure cAMP levels, the incorporation of alkyl or alkoxy spacers conferred a ≤ 17 -fold increase in functional affinity as compared to that of DCPP,

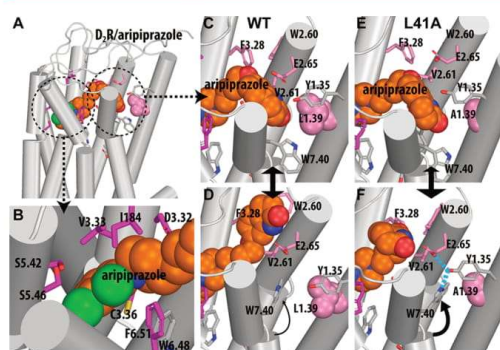


Figure 2. Molecular modeling and simulations reveal that aripiprazole adopts an extended orthosteric pose at the D₂R. (A) Molecular modeling and docking experiments using a homology model of the D₂R followed by MD simulations reveal that aripiprazole adopts an extended orthosteric pose within the D₂R and interacts with residues within the OBS and SBP. (B) Within the OBS, the 2,3-diC-phenylpiperazine PP of aripiprazole adopts a pose parallel to the membrane oriented toward TMS. Within the SBP, the 1,2,3,4-tetrahydroquinolin-2-one “tail” moiety and the flexible butoxy linker adopt two distinct poses depending on the orientation of Trp384^{7,40}. (C) When this residue faces lipids, the quinalinone ring occupies a cavity within the SBP contacting residues from TM1, TM2, and TM7. (D) When Trp384^{7,40} rotates inward, the quinalinone ring can no longer occupy the SBP but instead tilts toward TM3 and ECL2. (E and F) The L41^{1,39}A mutation increases the propensity for Trp384^{7,40} to rotate inward, allowing Trp384^{7,40}, Tyr37^{1,35}, and Glu95^{2,65} to interact.

although a further increase in functional affinity was not observed upon incorporation of the THQ moiety. The DCPD fragment of aripiprazole displayed a weak intrinsic efficacy, in agreement with previously published data,¹⁸ an effect conferred through interaction of the PP with the OBS as shown by our MD simulations. The incorporation of a propyl linker (2) caused a 2-fold decrease in efficacy, whereas the butyl linker (3) and butoxy linker (4) derivatives displayed a level of efficacy similar to that of DCPD (Figure 3 and Table 2). Strikingly, the incorporation of the THQ moiety (to generate aripiprazole) caused a 10-fold increase in efficacy.

In our previous study, we observed that the DCPD core of R22 could be replaced with a 2-methoxyphenylpiperazine (2MeOPP) core with little change in efficacy or affinity at the D₂R.¹⁸ We hypothesized that addition of the 7-butoxy-1,2,3,4-tetrahydroquinolin-2-one substituent of aripiprazole to the 2MeOPP core (11) would cause an increase in both affinity and efficacy (τ). The addition of an *N*-butyl substitution conferred a 32-fold increase in affinity, whereas the addition of the 7-butoxy-1,2,3,4-tetrahydroquinolin-2-one substituent (13) conferred a 2600-fold higher affinity than the 2MeOPP core to yield an extended ligand with the same affinity as aripiprazole (Figure 2 and Table 2). Importantly, we observed that the addition of the 7-butoxy-1,2,3,4-tetrahydroquinolin-2-one substituent caused 26- and 10-fold increases in efficacy (τ) as compared to those of the 2MeOPP (11) and the *N*-butyl substituent (12), respectively (Figure 3 and Table 2). Thus, the linking of the 7-butoxy-1,2,3,4-tetrahydroquinolin-2-one SP to the 2MeOPP PP to generate a novel partial agonist results in increases in both efficacy and affinity.

Interaction with SBP Residues Determines the Efficacy of Aripiprazole.

Our results show that the interaction of the SP with the SBP contributes to the affinity and, more surprisingly, the efficacy of aripiprazole. We used mutagenesis to explore the SBP residues that contribute to this interaction. In agreement with the interaction of the SP with SBP residues, the binding affinity of aripiprazole was significantly reduced by SBP mutations W90^{2,60}A (5-fold), V91^{2,61}A (8-fold), and E95^{2,65}A (3-fold) (Table 3). The V91^{2,61}A mutation caused a 11-fold reduction in the transduction coefficient of aripiprazole, whereas the E95^{2,65}A mutation resulted in a 11-fold reduction in its functional affinity (K_A) (Figure 1 and Table 3). While the V91^{2,61}A and E95^{2,65}A mutations had no effect on the two smaller agonists, the W90^{2,60}A mutation reduced the transduction coefficients of ropinirole (14-fold) and dopamine (6-fold) and the binding affinity of dopamine (6-fold). The E95^{2,65}A, V91^{2,61}A, and L41^{1,39}A mutations did not change the affinity of the DCPD fragment (Table 2). The F110^{3,28}A mutation significantly reduced the binding affinity of all three agonists and the transduction coefficients of dopamine and ropinirole but not that of aripiprazole (Table 3). The L41^{1,39}A mutation increased the binding affinity of ropinirole and aripiprazole (5-fold) but had no significant effect on the binding affinity of dopamine (Figure 1 and Table 3). Strikingly, this mutation caused a 5-fold decrease in the efficacy (τ) of aripiprazole, whereas the transduction coefficients of the smaller agonists were not significantly changed (Table 3). Val91^{2,61} and Phe110^{3,28} are in close contact with the butoxy linker of aripiprazole in both of the SP poses obtained with our MD simulations (Figure 2), and these interactions can be correlated to the negative impact of the V91^{2,61}A or F110^{3,28}A mutation on aripiprazole affinity. We extended our MD simulations to compare the pose of aripiprazole at the WT and L41^{1,39}A mutant. The L41^{1,39}A mutation is associated with a higher propensity for inward rotation of Trp384^{7,40} (Figure 2E,F and Supplementary Figure 1), which affects the orientation of Glu95^{2,65} and Tyr37^{1,35}. Interestingly, Trp384^{7,40}, Tyr37^{1,35}, and Glu95^{2,65} form an interaction network only in the mutant simulations (Figure 2F and Supplementary Figure 1). Thus, our simulations indicate that the orientation of the SP toward ECL2 and TM3 is favored in the L41^{1,39}A mutant.

To allow us to compare the effect of the L41^{1,39}A mutation with the functional data obtained with the various fragments of aripiprazole (Table 2), we repeated these experiments using the BRET biosensor to measure the inhibition of cAMP. In this assay, dopamine and aripiprazole displayed significant 4- and 5-fold decreases in transduction coefficients at the L41^{1,39}A mutant, respectively (Figure 4 and Supplementary Table 4). The latter effect was caused by a 5-fold decrease in aripiprazole efficacy (τ) (Figure 4J), similar to changes observed in the Alphascreen cAMP assay. It is noteworthy that the efficacy of aripiprazole at this mutant was equivalent to that of the DCPD fragment at the WT receptor, suggesting that the increase in efficacy conferred by the SP of aripiprazole requires Leu41^{1,39}. To determine whether the decreased transduction coefficient of dopamine at L41^{1,39}A was caused by a decrease in functional affinity or efficacy, we treated cells with increasing concentrations of phenoxybenzamine to alkylate cell surface D₂Rs prior to stimulation with an agonist. We applied the operational model of agonism to these data to determine the functional affinity and efficacy of dopamine and ropinirole (Figure 4 and Supplementary Table 4). The L41^{1,39}A mutation

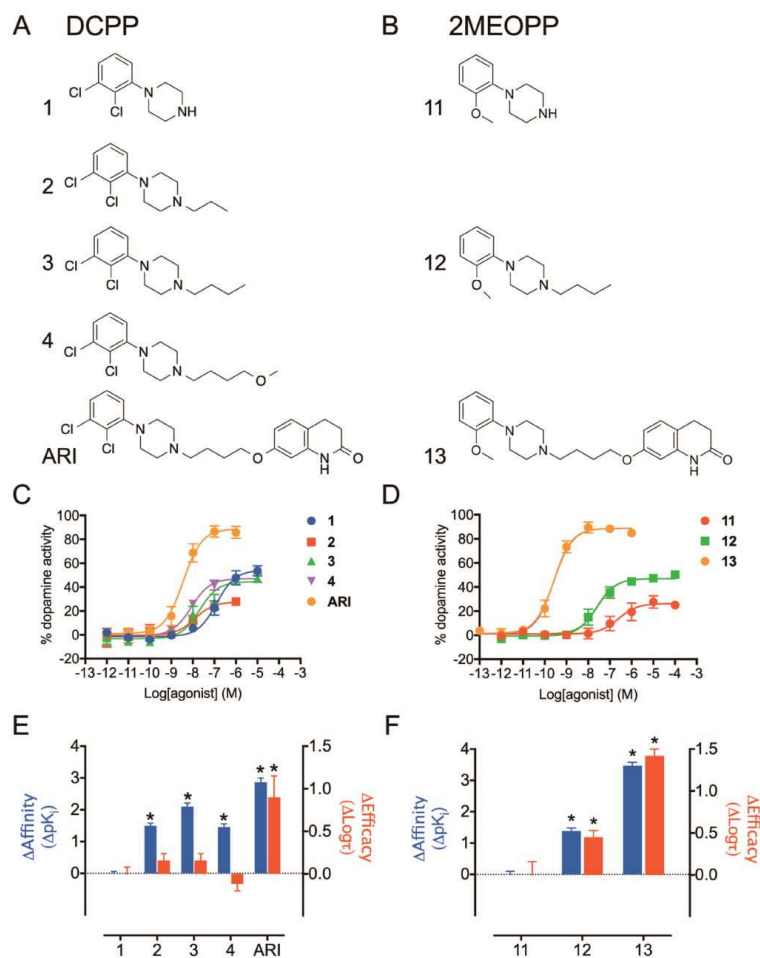


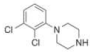
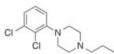
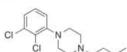
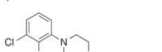
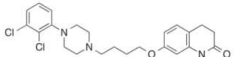
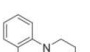
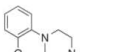
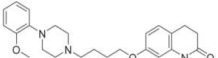
Figure 3. 7-Butoxy-1,2,3,4-tetrahydroquinolin-2-one substitution of a phenylpiperazine core confers an increase in efficacy and affinity. Two series of substituted phenylpiperazine fragments and extended compounds were synthesized, (A) one that incorporates the 2,3-dichlorophenylpiperazine (DCPP) core that includes aripiprazole and (B) one that incorporates the 2-methoxyphenylpiperazine core (2MeOPP). The ability of increasing concentrations of each compound in (C and E) the DCPP series or (D and F) the 2MeOPP series to activate the WT $D_{2S}Rs$ was determined through an assay measuring the inhibition of forskolin-stimulated cAMP production using a BRET biosensor. (E and F) These data were fit to an operational model of agonism, and changes in functional affinity or efficacy were determined as compared to the that of phenylpiperazine core of each series. An asterisk indicates a significant change in the parameter as compared to that of the core of each series (one-way analysis of variance with Dunnett's post hoc test; $p < 0.05$).

caused a 10-fold decrease in dopamine functional affinity (K_A) but no change in efficacy (τ) (Figure 4H,K and Supplementary Table 4). The functional affinity and efficacy of ropinirole were unaffected by this mutation (Figure 4I,L and Supplementary Table 4).

As described above, Leu41^{1.39} directly affects the rotation of Trp384^{7.40} (Figure 2). To explore the interaction between Trp384^{7.40} and Leu41^{1.39}, either Trp384^{7.40} or both residues were mutated to alanine. The action of all agonists was compromised at the double mutant because of its low level of cell surface expression (Supplementary Figure 3). The

W384^{7.40}A mutation caused significant decreases in dopamine (5-fold) and ropinirole (3-fold) transduction coefficients but had no effect on that of aripiprazole (Figure 4 and Supplementary Table 4). This is consistent with our proposal that the aripiprazole pose shown in Figure 2C may be more relevant to its intrinsic efficacy, as the W384^{7.40}A mutation is unlikely to have a negative impact on this pose when Trp384 faces lipids. In addition, the preference of the aripiprazole pose in the L41^{1.39}A mutant, which is coordinated with the inward rotation of Trp384 (Figure 2F), supports the idea that the

Table 2. Binding Affinities and Functional Action of Phenylpiperazine Fragments and Extended Compounds at the D₂R^a

Compound	pK _i ± SEM [³ H]spiperone			pK _i ± SEM [³ H]raclopride		cAMP (BRET Biosensor)	
	WT	L41 ^{1,39} A (fold)	E95 ^{2,65} A (fold)	WT	V91 ^{2,61} A (fold)	pK _A	Log τ
1 	6.24 ± 0.04 [#]	6.80 ± 0.16 (0.3)	6.29 ± 0.16 (0.9)	7.45 ± 0.31	7.59 ± 0.17 (0.7)	6.49 ± 0.18	0.12 ± 0.06 [#]
2 	7.74 ± 0.07 [#]	-	-	-	-	7.50 ± 0.28	-0.30 ± 0.07 [#]
3 	8.30 ± 0.10 [#]	-	-	-	-	7.20 ± 0.24	-0.04 ± 0.06 [#]
4 	7.70 ± 0.09 [#]	-	-	-	-	7.72 ± 0.19	0.00 ± 0.05 [#]
Aripiprazole 	9.11 ± 0.12	-	-	-	-	7.41 ± 0.30	1.02 ± 0.24
11 	5.64 ± 0.07 [*]	6.23 ± 0.15 [*] (0.4)	6.12 ± 0.13 [*] (0.3)	6.49 ± 0.19	6.43 ± 0.24 (1.1)	6.51 ± 0.42 [*]	-0.42 ± 0.11 [*]
12 	7.03 ± 0.05 [*]	-	-	-	-	7.31 ± 0.20 [*]	-0.03 ± 0.05 [*]
13 	9.11 ± 0.08	10.4 ± 0.09 [*] (0.1)	9.34 ± 0.16 (0.6)	10.3 ± 0.22	8.41 ± 0.26 [*] (77)	8.56 ± 0.26	1.00 ± 0.22

^aBinding affinity (K_i) determined by competition binding experiments using radiolabeled antagonist [³H]spiperone or [³H]raclopride at WT or mutant SNAP-D₂R. Functional affinity (K_A) and efficacy (τ) determined in an assay measuring inhibition of forskolin-stimulated cAMP production. Values are expressed as means ± the standard deviation from three separate experiments. ^{*}Values significantly different from that of the WT as determined by one-way analysis of variance (Dunnett's post hoc test; $p < 0.05$). [#]Values significantly different from that of aripiprazole as determined by one-way analysis of variance (Dunnett's post hoc test; $p < 0.05$).

impact of this remote TM1 mutation may be partially mediated by Trp384^{7,40}.

We explored the effect of adding bulk and aromaticity to the SBP by mutating both V91^{2,61} and L41^{1,39} to phenylalanine. L41^{1,39}F had no effect. V91^{2,61}F caused 35-, 30-, and 170-fold decreases in the transduction coefficients of dopamine, ropinirole, and aripiprazole, respectively (Figure 4F and Supplementary Table 4). This mutation caused decreases in the functional affinity (14-fold) and efficacy (11-fold) of aripiprazole. Leu41^{1,39} and Val91^{2,61} directly interact (Figure 2C). The double mutation (L41^{1,39}A/V91^{2,61}A) caused a 10-fold decrease in the transduction coefficient of dopamine and ropinirole but a much greater 49-fold decrease in that of aripiprazole, driven by a 42-fold decrease in efficacy (Figure 4I and Supplementary Table 4). In contrast, this double mutation decreased the functional affinity (Figure 4H and Supplemen-

tary Table 4) of dopamine by 5-fold and had no significant effect on dopamine efficacy.

Together, these data indicate that the direct interaction of the SP of aripiprazole with the D₂R SBP contributes to its intrinsic efficacy. The addition of the SP to the phenylpiperazine PP conferred a significant increase in efficacy, and mutations within the SBP modulated the activity of aripiprazole. The mutation of Leu41^{1,39}, a SBP residue distal to the OBS, significantly decreased the efficacy of aripiprazole in all signaling pathways but increased its binding affinity. Furthermore, the increase in efficacy conferred by the addition of the SP to the SBP was lost at the L41^{1,39}A mutant. Thus, the increase in efficacy caused by the interaction of the SP with the SBP appears to be dependent on Leu41^{1,39}. Our MD simulations predicted two distinct orientations of the SP, one in which the SP occupies the SBP (contacting Leu41^{1,39}, Val91^{2,61}, and Glu95^{2,65}) and one in which the SP extends

Table 3. Effects of Mutations in the SBP of the D₂R on the Binding Affinities and Functional Activities of Selected Agonists^a

construct	ropinirole			dopamine			aripiprazole		
	pK _i (fold Δ)	log(τ/K _d) (fold Δ)	pK _i (fold Δ)	pK _i (fold Δ)	log(τ/K _d) (fold Δ)	pK _i (fold Δ)	log(τ/K _d) (fold Δ)	pK _i (fold Δ)	log(τ/K _d) (fold Δ)
WT	5.18 ± 0.04	8.29 ± 0.06	4.94 ± 0.03	8.51 ± 0.05	9.92 ± 0.02	8.45 ± 0.06	7.75 ± 0.14	0.69 ± 0.15	0.03 ± 0.07*
WT [#]	5.83 ± 0.12	8.09 ± 0.16 (1.6)	5.78 ± 0.13	7.89 ± 0.27 (4.2)	9.86 ± 0.11	10.61 ± 0.04* (0.2)	8.07 ± 0.16 (0.5)	0.37 ± 0.08 (2.0)	0.12 ± 0.22 (3.7)
L41 ^{1,39} A	5.85 ± 0.10*	7.14 ± 0.18* (14)	5.29 ± 0.02 (0.5)	7.71 ± 0.20* (6.4)	10.61 ± 0.04* (0.2)	8.13 ± 0.16 (2.1)	7.74 ± 0.10 (1.0)	0.78 ± 0.10 (0.8)	0.03 ± 0.07*
W90 ^{2,60} A	4.90 ± 0.14 (1.9)	8.32 ± 0.12 (1.0)	4.17 ± 0.05* (5.9)	8.69 ± 0.20 (0.7)	9.18 ± 0.08* (5.5)	7.41 ± 0.26* (11)	7.29 ± 0.36 (2.8)	0.12 ± 0.22 (3.7)	0.03 ± 0.07*
V91 ^{2,61} A [#]	6.03 ± 0.02 (0.6)	8.16 ± 0.11 (1.4)	6.03 ± 0.08 (0.6)	8.22 ± 0.11 (2.0)	8.96 ± 0.04* (8.1)	7.87 ± 0.15 (3.8)	7.71 ± 0.21* (11)	0.16 ± 0.24 (0.3)	0.03 ± 0.07*
E95 ^{2,65} A	5.68 ± 0.08* (0.3)	8.16 ± 0.11 (1.4)	5.24 ± 0.06 (0.5)	7.58 ± 0.19* (8.6)	9.41 ± 0.06* (3.2)	8.08 ± 0.11 (2.3)	7.30 ± 0.16 (2.8)	0.03 ± 0.07*	0.03 ± 0.07*
F110 ^{3,28} A	4.37 ± 0.15* (6.5)	7.19 ± 0.13* (13)	3.57 ± 0.08* (24)	7.58 ± 0.19* (8.6)	8.68 ± 0.06* (17)	8.08 ± 0.11 (2.3)	7.30 ± 0.16 (2.8)	0.03 ± 0.07*	0.03 ± 0.07*

^aBinding affinity values were obtained in competition binding experiments using the radioligand [³H]spiperone unless otherwise stated. Functional affinities, efficacies, and transduction ratios were determined in an assay measuring inhibition of forskolin-induced intracellular cAMP production. [#]Binding affinity values are obtained in competition binding experiments using the radioligand [³H]raclopride. Values are expressed as means ± the standard deviation from three (binding) or four (cAMP) separate experiments. * *p* < 0.05, significantly different from that of the wild-type receptor determined by a one-way analysis of variance, with Dunnett's post hoc test.

toward TM3. Our simulations show that the L41^{1,39}A mutation promotes the latter orientation (Figure 2). The mutation of V91^{2,61} and E95^{2,65} also caused significant losses of aripiprazole's affinity and a functional effect, consistent with the loss of SBP interactions. We propose that the interaction of the SP with the SBP promotes a higher intrinsic efficacy whereas the orientation of the SP toward TM3 appears to be associated with a lower efficacy but a higher binding affinity. The combination of the V91^{2,61}A mutation with the L41^{1,39}A mutation, which we postulate would further promote the orientation of the SP toward TM3 over the SBP pose, caused an even greater (44-fold) loss of efficacy. In our recent studies of extended 2,3-diCl-phenylpiperazine derivatives, we found that the structures of both the SP and the linker can modulate ligand efficacy. We proposed a mechanism whereby the interaction of the linker and SP with the SBP modulated the conformation of the PP in the OBS, leading to changes in ligand efficacy.¹⁸ The relationship between distinct binding orientations of a single ligand at a receptor and efficacy has been explored in studies of extended bitopic ligands that bind the muscarinic M₂ acetylcholine receptor.³⁴ In this study, it is proposed that such ligands can bind the receptor in two distinct orientations, one that occupies the OBS and one purely allosteric mode that does not.³⁴ The relative propensity of such ligands to occupy the receptor in an orthosteric versus an allosteric orientation determined the intrinsic efficacy. In the study presented here, we find no evidence that aripiprazole can bind the D₂R in a purely allosteric mode. Rather, we propose that the PP of aripiprazole occupies the OBS in a rather stable pose in both orientations of the ligand and that the direct interaction of the SP of aripiprazole with the SBP confers an increase in efficacy. We have also shown that the interaction of the SP of a D₂R negative allosteric modulator with a similar SBP was required for allosteric pharmacology, whereas the PP of this ligand acted as a competitive antagonist.³⁵ Together with the study presented here, this illustrates that the interaction of SP of extended ligands with the SBP of the D₂R can confer changes in pharmacology relative to that which results from binding of the primary pharmacophore alone in the orthosteric binding site.

Mutation of SBP residues also influenced the binding and functional affinity of small orthosteric agonists not expected to interact with the SBP. The effects of these mutants upon aripiprazole compared to their effects on the smaller agonists were, however, distinct. In the case of SBP mutations that affected the action of all three agonists (V91^{2,61}F and L41^{1,39}A/V91^{2,61}A), the effect on aripiprazole was much stronger. It should be noted, however, that while the L41^{1,39}A mutation or the L41^{1,39}A/V91^{2,61}A double mutation did not affect the efficacy of dopamine or ropinirole, each caused a decrease in the functional affinity of dopamine. The functional affinity presumably reflects the affinity of dopamine for the receptor when coupled to signaling effectors.³⁶ In contrast, the binding affinity of dopamine, which was unchanged relative to that of WT, reflects the affinity of dopamine for the uncoupled state of the receptor. Dopamine cannot make direct contacts with this SBP residue when bound in the OBS. Thus, this mutation appears to modulate the affinity with which dopamine binds to a coupled receptor state but does not affect the efficiency with which it stimulates receptor-mediated G protein activation. In addition, the indirect effect of this mutation upon dopamine's functional affinity is distinct from the effect upon aripiprazole efficacy that we propose is caused by modulation of the

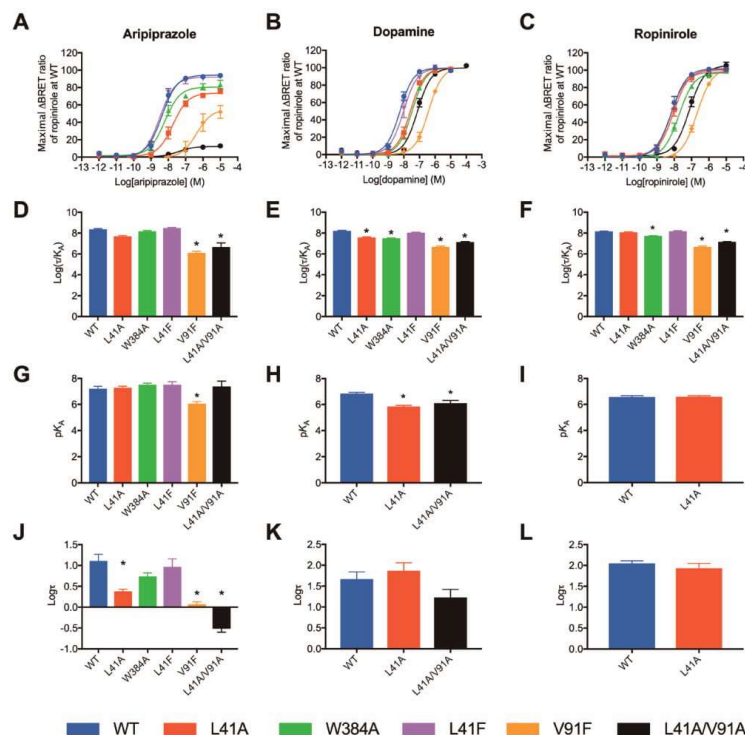


Figure 4. Mutation of SBP residues decreases the efficacy of aripiprazole but not that of dopamine. The ability of increasing concentrations of (A) aripiprazole, (B) dopamine, or (C) ropinirole to activate the WT or mutant (L41¹⁻³⁹A, W384⁷⁻⁴⁰A, L41F, V91F, and L41¹⁻³⁹A/V91¹⁻⁶¹A) SNAP-tagged D₂Rs was determined in a BRET assay measuring the inhibition of forskolin-stimulated cAMP production. These data were fit to an operational model of agonism and estimates of the (D–F) transduction coefficients and (G–I) functional affinities and (J–L) efficacies at the WT and mutant receptors. An asterisk indicates a significant change in the parameter for each agonist relative to WT (one-way analysis of variance with Dunnett's post hoc test; $p < 0.05$).

interaction between the SP and the SBP. Nonetheless, our data indicate that residues within the SBP can influence the binding of even small agonists to the OBS. This effect is dependent upon the structure of the orthosteric agonist as the L41¹⁻³⁹A mutation had no effect on ropinirole. This is difficult to reconcile with a global effect of this mutation, such as the impairment of the transition to an active receptor state, as one would envisage that all agonists would be affected in a similar manner. Dopamine and ropinirole were shown to display distinct sensitivities to the mutation of OBS residues; for example, the S197⁵⁻⁴⁶A mutation ablated dopamine's functional activity but had no effect on ropinirole. Thus, they are likely to have distinct patterns of interaction with the OBS. The mutation of L41¹⁻³⁹ may modulate the conformation of the OBS in a manner that affects the functional affinity of some but not all agonists and is dependent upon their structure and the residues they engage to exert their effect. Consistent with the idea of changes in the conformation of the SBP modulating the binding of agonists to the OBS, we have previously shown that a SP fragment of an extended D₂R ligand acted as a negative allosteric modulator and that its binding was sensitive to SBP.³⁷ Moreover, allosteric modulators of the muscarinic

receptor interact with residues that align with those forming the D₂R SBP.^{38,39} A SBP defined by residues of extracellular TM1, TM2, and TM7 has also been implicated in the agonist binding and/or activation of the chemokine CCR5, nicotinic acid (GPR109A), and angiotensin 1 receptors.^{40–42} Thus, the SBP defined in this study is likely to be important for the modulation of agonist action in other GPCRs.

The Biased Agonism of Aripiprazole Is Unchanged in OBS or SBP Mutants. Previously, we have shown that aripiprazole displays biased agonism toward inhibition of cAMP over phosphorylation of ERK1/2.^{43,44} In our pERK1/2 assay, aripiprazole displayed a maximal response of 29% of ropinirole at the WT D₂R, corresponding to a τ of 0.39, 12-fold lower than that observed in the cAMP assay (Figure 5 and Supplementary Table 5). We quantified the biased agonism of dopamine and aripiprazole between inhibition of cAMP production and ERK1/2 phosphorylation using ropinirole as the reference agonist.²¹ Consistent with our previous results, aripiprazole was biased toward the inhibition of cAMP production over ERK1/2 phosphorylation whereas dopamine was not (Supplementary Table 6).⁴³ None of the OBS or SBP mutations caused a significant change in this bias. Note,

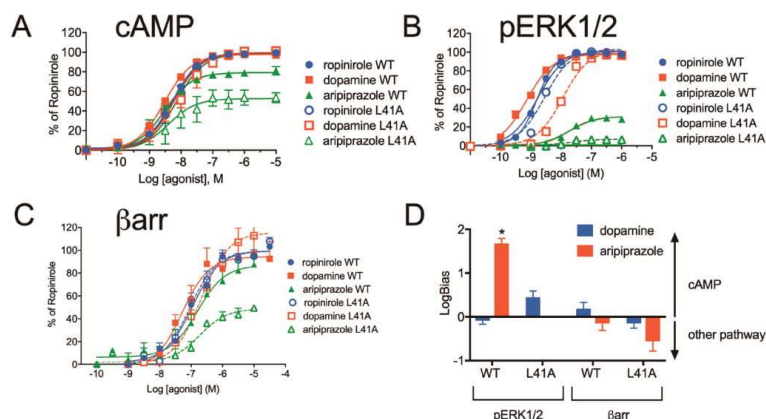


Figure 5. Mutation L41³⁹A decreases the intrinsic efficacy of aripiprazole at multiple signaling pathways. The ability of increasing concentrations of each agonist to activate the WT or L41³⁹A D₂Rs was determined through an Alphascreen assay measuring the inhibition of (A) forskolin-stimulated cAMP production, (B) ERK1/2 phosphorylation, and (C) β-arrestin translocation. (D) These data were fit to an operational model of agonism, and bias factors between each pathway were determined for dopamine and aripiprazole relative to ropinirole. An asterisk indicates significant bias toward one pathway (two-tailed, unpaired Student's *t* test; *p* < 0.05).

however, that the window in which the deleterious effects of a mutation can be detected is smaller in the pERK1/2 assay because of the lower efficacy of aripiprazole at the WT D₂R as compared to that obtained in the cAMP assay. Accordingly, we were unable to quantify a change in bias for the mutations that abrogated aripiprazole action in the pERK1/2 assay but that also had a deleterious effect in the cAMP assay (for example, L41³⁹A and V91²⁶¹A). While previous studies have shown that aripiprazole does not display bias between cAMP and β-arrestin recruitment,^{43,45} we were curious to see whether L41³⁹A might change this. In a β-arrestin translocation assay that measures the movement of a β-arrestin-2-Venus to the cell surface, aripiprazole acted as a partial agonist at the WT D₂R [*E*_{max} = 86% of maximal response of ropinirole (Figure 5 and Supplementary Table 7)]. Aripiprazole displayed a significant 6-fold decrease in efficacy in the L41³⁹A mutant as compared to that of WT. No bias between cAMP and β-arrestin-2 translocation was observed for dopamine or aripiprazole relative to ropinirole at the WT or L41³⁹A D₂R (Figure 5 and Supplementary Table 7).

Conclusions. The weak intrinsic efficacy of D₂R partial agonists such as aripiprazole is thought to determine both their antipsychotic effect and their low propensity to cause extrapyramidal side effects and hyperprolactinemia as compared to those of typical antipsychotics. Our results reveal the molecular interactions that are important for this intrinsic efficacy. Aripiprazole's structure is typical of many D₂-like DR subtype-selective ligands, namely a substituted piperazine PP and a lipophilic SP.^{7,17} Previous studies have revealed that the addition of a SP to a piperazine PP can confer gains in affinity and subtype selectivity through interaction with a SBP defined by the extracellular ends of TM1, TM2, and TM7.^{7–10,18,33,46,47} In this study, we find that the interaction of the quinalinone SP of aripiprazole with the SBP is a key determinant of the intrinsic efficacy of this drug. Addition of aripiprazole's SP to the 2,3-diCl-phenylpiperazine PP or a distinct 2-methoxyphenylpiperazine PP fragment conferred

gains in both affinity and efficacy. These data, combined with our previous study that found that the interaction of an SP with a distinct indole structure with the SBP caused a decrease in intrinsic efficacy,¹⁸ provide a means of designing D₂R partial agonists with the desired intrinsic efficacy.

METHODS

Materials. Aripiprazole was synthesized in house as previously described and shown to be >98% pure.⁴³ Ropinirole was purchased from BetaPharma Co. Ltd. (Wujiang, China) and was >98% pure as described by the supplier. All novel compounds were synthesized as described in the Supporting Information. pcDNA3.1-His-CAMYEL was purchased from ATCC. Dulbecco's modified Eagle's medium (DMEM), hygromycin B, and FlpIn CHO cells were purchased from Invitrogen (Carlsbad, CA). Fetal bovine serum (FBS) was purchased from ThermoTrace (Melbourne, Australia). [³H]Spiperone, [³H]-raclopride, AlphaScreen reagents, Ultima gold scintillation cocktail, 384-well optiplates, and 384-well proxiplates were purchased from PerkinElmer (Boston, MA). All of the other reagents were purchased from Sigma-Aldrich (Castle Hill, Australia).

Molecular Biology and Generation of Cell Lines. The molecular biology and generation of cell lines were performed as described previously.⁴³ Full details are given in the Supporting Information. cDNA in pcDNA3.1+ encoding the short isoform of the wild-type human dopamine D₂ receptor with an N-terminal SNAP tag was obtained from Cisbio (Bagnols-sur-Cèze, France).

ELISA and Cell Signaling Assays. The ELISA protocol, ERK1/2 phosphorylation assay, cAMP Alphascreen assay, and BRET assays measuring intracellular cAMP and β-arrestin-2 recruitment to the plasma membrane were performed as described previously.^{43,48} Full details are given in the Supporting Information.

Membrane Preparation and Radioligand Binding Assays. Radioligand binding assays were performed as described previously.⁴³ Full details are given in the Supporting Information.

Data Analysis. The results were analyzed using Prism 6.0 (GraphPad Software Inc., San Diego, CA). Full details of data analysis are given in the Supporting Information. All affinity (*pK_i*, *pK_D*, or *pK_A*), potency (*pEC₅₀*), and transduction ratio [*log(τ/K_A)*] parameters were estimated as logarithms, where fold changes were calculated using the corresponding antilog values. We have previously demonstrated that the distribution of the antilog parameters does not

conform to a normal (Gaussian) distribution whereas the logarithm is approximately Gaussian. Thus, because the application of *t* tests and analyses of variance assume a Gaussian distribution, estimating the parameters as logarithms allows valid statistical comparison. All results are expressed as means \pm the standard deviation. We performed a Brown–Forsythe test (GraphPad Prism 6.0) to ensure ourselves of equal variance when such parameters are compared.

MD Simulations. Full details of the protocol are provided in the Supporting Information.

■ ASSOCIATED CONTENT

Supporting Information

The Supporting Information is available free of charge on the ACS Publications website at DOI: 10.1021/acscchembio.9b00342.

Supplementary methods, including chemical synthesis, Supplementary Figures 1–3, Supplementary Tables 1–7, and supplementary references (PDF)

■ AUTHOR INFORMATION

Corresponding Authors

*Centre of Membrane Proteins and Receptors, Compare Office C101a, School of Life Sciences, Queens Medical Centre, University of Nottingham, Nottingham NG7 2UH, U.K. E-mail: rob.lane@nottingham.ac.uk. Telephone: +44 (0)115 8230468.

*Computational Chemistry and Molecular Biophysics Unit, National Institute on Drug Abuse-Intramural Research Program, National Institutes of Health, 333 Cassell Dr., Baltimore, MD 21224. E-mail: lei.shi2@nih.gov. Telephone: +1(443)740-2774.

ORCID

Peter J. Scammells: 0000-0003-2930-895X

Ben Capuano: 0000-0001-5434-0180

J. Robert Lane: 0000-0002-7361-7875

Author Contributions

†C.K.H. and R.V. contributed equally to this work.

Notes

The authors declare no competing financial interest.

■ ACKNOWLEDGMENTS

This research was supported by Project Grant 1049564 from the National Health and Medical Research Council (NHMRC) and the National Institute on Drug Abuse-Intramural Research Program (Z1A DA000606-03) (L.S.).

■ REFERENCES

- (1) Beaulieu, J.-M., and Gainetdinov, R. R. (2011) The Physiology, Signaling, and Pharmacology of Dopamine Receptors. *Pharmacol. Rev.* 63, 182–217.
- (2) Burris, K. D. (2002) Aripiprazole, a Novel Antipsychotic, Is a High-Affinity Partial Agonist at Human Dopamine D2 Receptors. *J. Pharmacol. Exp. Ther.* 302, 381–389.
- (3) Oshiro, Y., Sato, S., Kurahashi, N., Tanaka, T., Kikuchi, T., Tottori, K., Uwahodo, Y., and Nishi, T. (1998) Novel antipsychotic agents with dopamine autoreceptor agonist properties: synthesis and pharmacology of 7-[4-(4-phenyl-1-piperazinyl)butoxy]-3,4-dihydro-2(1H)-quinolinone derivatives. *J. Med. Chem.* 41, 658–667.
- (4) Kiss, B., Horvath, A., Nemethy, Z., Schmidt, E., Laszlovsky, I., Bugovics, G., Fazekas, K., Hornok, K., Orosz, S., Gyertyan, I., Agai-Csongor, E., Domany, G., Tihanyi, K., Adham, N., and Szombathelyi, Z. (2010) Cariprazine (RGH-188), a Dopamine D3 Receptor-Preferring, D3/D2 Dopamine Receptor Antagonist-Partial Agonist

Antipsychotic Candidate: In Vitro and Neurochemical Profile. *J. Pharmacol. Exp. Ther.* 333, 328–340.

(5) Lieberman, J. A. (2004) Dopamine Partial Agonists: A New Class of Antipsychotic. *CNS Drugs* 18, 251–267.

(6) Natesan, S., Reckless, G. E., Barlow, K. B. L., Nobrega, J. N., and Kapur, S. (2011) Partial agonists in schizophrenia—why some work and others do not: insights from preclinical animal models. *Int. J. Neuropsychopharmacol.* 14, 1165–1178.

(7) Chien, E. Y. T., Liu, W., Zhao, Q., Katritch, V., Won Han, G., Hanson, M. A., Shi, L., Newman, A. H., Javitch, J. A., Cherezov, V., and Stevens, R. C. (2010) Structure of the Human Dopamine D3 Receptor in Complex with a D2/D3 Selective Antagonist. *Science* 330, 1091–1095.

(8) Shi, L., and Javitch, J. A. (2002) The binding site of aminergic G protein-coupled receptors: the transmembrane segments and second extracellular loop. *Annu. Rev. Pharmacol. Toxicol.* 42, 437–467.

(9) Wang, S., Wacker, D., Levit, A., Che, T., Betz, R. M., McCorvy, J. D., Venkatakrishnan, A. J., Huang, X.-P., Dror, R. O., Shoichet, B. K., and Roth, B. L. (2017) D4 dopamine receptor high-resolution structures enable the discovery of selective agonists. *Science* 358, 381–386.

(10) Wang, S., Che, T., Levit, A., Shoichet, B. K., Wacker, D., and Roth, B. L. (2018) Structure of the D2 dopamine receptor bound to the atypical antipsychotic drug risperidone. *Nature* 555, 269–273.

(11) Venkatakrishnan, A. J., Deupi, X., Lebon, G., Tate, C. G., Schertler, G. F., and Babu, M. M. (2013) Molecular signatures of G-protein-coupled receptors. *Nature* 494, 185–194.

(12) Deupi, X., and Standfuss, J. (2011) Structural insights into agonist-induced activation of G-protein-coupled receptors. *Curr. Opin. Struct. Biol.* 21, 541–551.

(13) Ballesteros, J. A., and Weinstein, H. (1995) *Methods in Neuroscience*, pp 366–428, Elsevier.

(14) Huang, W., Manglik, A., Venkatakrishnan, A. J., Laeremans, T., Feinberg, E. N., Sanborn, A. L., Kato, H. E., Livingston, K. E., Thorsen, T. S., Kling, R. C., Granier, S., Gmeiner, P., Husbands, S. M., Traynor, J. R., Weis, W. I., Steyaert, J., Dror, R. O., and Kobilka, B. K. (2015) Structural insights into μ -opioid receptor activation. *Nature* 524, 315–321.

(15) Latorraca, N. R., Venkatakrishnan, A. J., and Dror, R. O. (2017) GPCR Dynamics: Structures in Motion. *Chem. Rev.* 117, 139–155.

(16) Dror, R. O., Arlow, D. H., Maragakis, P., Mildorf, T. J., Pan, A. C., Xu, H., Borhani, D. W., and Shaw, D. E. (2011) Activation mechanism of the β_2 -adrenergic receptor. *Proc. Natl. Acad. Sci. U. S. A.* 108, 18684–18689.

(17) Löber, S., Hübner, H., Tschammer, N., and Gmeiner, P. (2011) Recent advances in the search for D3- and D4-selective drugs: probes, models and candidates. *Trends Pharmacol. Sci.* 32, 148–157.

(18) Newman, A. H., Beuming, T., Banala, A. K., Donthamsetti, P., Pongetti, K., LaBounty, A., Levy, B., Cao, J., Michino, M., Luedtke, R. R., Javitch, J. A., and Shi, L. (2012) Molecular determinants of selectivity and efficacy at the dopamine D3 receptor. *J. Med. Chem.* 55, 6689–6699.

(19) Michino, M., Boateng, C. A., Donthamsetti, P., Yano, H., Bakare, O. M., Bonifazi, A., Ellenberger, M. P., Keck, T. M., Kumar, V., Zhu, C., Verma, R., Deschamps, J. R., Javitch, J. A., Newman, A. H., and Shi, L. (2017) Toward Understanding the Structural Basis of Partial Agonism at the Dopamine D3 Receptor. *J. Med. Chem.* 60, 580–593.

(20) Tadori, Y., Miwa, T., Tottori, K., Burris, K. D., Stark, A., Mori, T., and Kikuchi, T. (2005) Aripiprazole's low intrinsic activities at human dopamine D2L and D2S receptors render it a unique antipsychotic. *Eur. J. Pharmacol.* 515, 10–19.

(21) Kenakin, T., Watson, C., Muniz-Medina, V., Christopoulos, A., and Novick, S. (2012) A Simple Method for Quantifying Functional Selectivity and Agonist Bias. *ACS Chem. Neurosci.* 3, 193–203.

(22) Mansour, A., Meng, F., Meador-Woodruff, J. H., Taylor, L. P., Civelli, O., and Akil, H. (1992) Site-directed mutagenesis of the human dopamine D2 receptor. *Eur. J. Pharmacol., Mol. Pharmacol. Sect.* 227, 205–214.

- (23) Chemel, B. R., Bonner, L. A., Watts, V. J., and Nichols, D. E. (2012) Ligand-Specific Roles for Transmembrane 5 Serine Residues in the Binding and Efficacy of Dopamine D1 Receptor Catechol Agonists. *Mol. Pharmacol.* 81, 729–738.
- (24) Woodward, R., Coley, C., Daniell, S., Naylor, L. H., and Strange, P. G. (1996) Investigation of the role of conserved serine residues in the long form of the rat D2 dopamine receptor using site-directed mutagenesis. *J. Neurochem.* 66, 394–402.
- (25) Sartania, N., and Strange, P. G. (1999) Role of conserved serine residues in the interaction of agonists with D3 dopamine receptors. *J. Neurochem.* 72, 2621–2624.
- (26) Wilcox, R. E., Huang, W. H., Brusniak, M. Y., Wilcox, D. M., Pearlman, R. S., Teeter, M. M., DuRand, C. J., Wiens, B. L., and Neve, K. A. (2000) CoMFA-based prediction of agonist affinities at recombinant wild type versus serine to alanine point mutated D2 dopamine receptors. *J. Med. Chem.* 43, 3005–3019.
- (27) Fowler, J. C., Bhattacharya, S., Urban, J. D., Vaidehi, N., and Mailman, R. B. (2012) Receptor Conformations Involved in Dopamine D2L Receptor Functional Selectivity Induced by Selected Transmembrane-5 Serine Mutations. *Mol. Pharmacol.* 81, 820–831.
- (28) Shi, L., and Javitch, J. A. (2004) The second extracellular loop of the dopamine D2 receptor lines the binding-site crevice. *Proc. Natl. Acad. Sci. U. S. A.* 101, 440–445.
- (29) Tschammer, N., Bollinger, S., Kenakin, T., and Gmeiner, P. (2011) Histidine 6.55 Is a Major Determinant of Ligand-Biased Signaling in Dopamine D2L Receptor. *Mol. Pharmacol.* 79, 575–585.
- (30) Javitch, J., Ballesteros, J., Weinstein, H., and Chen, J. (1998) A cluster of aromatic residues in the sixth membrane-spanning segment of the dopamine D2 receptor is accessible in the binding-site crevice. *Biochemistry* 37, 998–1006.
- (31) Wacker, D., Wang, C., Katritch, V., Han, G. W., Huang, X.-P., Vardy, E., McCorvy, J. D., Jiang, Y., Chu, M., Siu, F. Y., Liu, W., Xu, H. E., Cherezov, V., Roth, B. L., and Stevens, R. C. (2013) Structural features for functional selectivity at serotonin receptors. *Science* 340, 615–619.
- (32) Zou, M.-F., Keck, T. M., Kumar, V., Donthamsetti, P., Michino, M., Burzynski, C., Schweppe, C., Bonifazi, A., Free, R. B., Sibley, D. R., Janowsky, A., Shi, L., Javitch, J. A., and Newman, A. H. (2016) Novel Analogues of (R)-5-(Methylamino)-5,6-dihydro-4H-imidazo[4,5,1-ij]quinolin-2(1H)-one (Sumanitrolol) Provide Clues to Dopamine D2/D3 Receptor Agonist Selectivity. *J. Med. Chem.* 59, 2973–2988.
- (33) Michino, M., Beuming, T., Donthamsetti, P., Newman, A. H., Javitch, J. A., and Shi, L. (2015) What can crystal structures of aminergic receptors tell us about designing subtype-selective ligands? *Pharmacol. Rev.* 67, 198–213.
- (34) Bock, A., Chirinda, B., Krebs, F., Messerer, R., Bätz, J., Muth, M., Dallanocce, C., Klingenthal, D., Tränkle, C., Hoffmann, C., De Amici, M., Holzgrave, U., Kostenis, E., and Mohr, K. (2014) Dynamic ligand binding dictates partial agonism at a G protein-coupled receptor. *Nat. Chem. Biol.* 10, 18–20.
- (35) Lane, J. R., Donthamsetti, P., Shonberg, J., Draper-Joyce, C. J., Dentry, S., Michino, M., Shi, L., López, L., Scammells, P. J., Capuano, B., Sexton, P. M., Javitch, J. A., and Christopoulos, A. (2014) A new mechanism of allosterism in a G protein-coupled receptor dimer. *Nat. Chem. Biol.* 10, 745–752.
- (36) Kenakin, T. (2014) What is pharmacological “affinity?” Relevance to biased agonism and antagonism. *Trends Pharmacol. Sci.* 35, 434–441.
- (37) Mistry, S. N., Shonberg, J., Draper-Joyce, C. J., Klein Herenbrink, C., Michino, M., Shi, L., Christopoulos, A., Capuano, B., Scammells, P. J., and Lane, J. R. (2015) Discovery of a Novel Class of Negative Allosteric Modulator of the Dopamine D2 Receptor Through Fragmentation of a Bitopic Ligand. *J. Med. Chem.* 58, 6819–6843.
- (38) Dror, R. O., Green, H. F., Valant, C., Borhani, D. W., Valcourt, J. R., Pan, A. C., Arlow, D. H., Canals, M., Lane, J. R., Rahmani, R., Baell, J. B., Sexton, P. M., Christopoulos, A., and Shaw, D. E. (2013) Structural basis for modulation of a G-protein-coupled receptor by allosteric drugs. *Nature* 503, 295–299.
- (39) Abdul-Ridha, A., Lane, J. R., Mistry, S. N., Lopez, L., Sexton, P. M., Scammells, P. J., Christopoulos, A., and Canals, M. (2014) Mechanistic Insights into Allosteric Structure-Function Relationships at the M1Muscarinic Acetylcholine Receptor. *J. Biol. Chem.* 289, 33701–33711.
- (40) Rosenkilde, M. M., Bølle, T., Frimur, T. M., and Schwartz, T. W. (2010) The minor binding pocket: a major player in 7TM receptor activation. *Trends Pharmacol. Sci.* 31, 567–574.
- (41) Govaerts, C., Blanpain, C., Deupi, X., Ballet, S., Ballesteros, J. A., Wodak, S. J., Vassart, G., Pardo, L., and Parmentier, M. (2001) The TXP motif in the second transmembrane helix of CCR5. *J. Biol. Chem.* 276, 13217–13225.
- (42) Reis, R. I., Santos, E. L., Pesquero, J. B., Oliveira, L., Schanstra, J. P., Bascands, J.-L., Pecher, C., Paiva, A. C. M., and Costa-Neto, C. M. (2007) Participation of transmembrane proline 82 in angiotensin II AT1 receptor signal transduction. *Regul. Pept.* 140, 32–36.
- (43) Klein Herenbrink, C., Sykes, D. A., Donthamsetti, P., Canals, M., Coudrat, T., Shonberg, J., Scammells, P. J., Capuano, B., Sexton, P. M., Charlton, S. J., Javitch, J. A., Christopoulos, A., and Lane, J. R. (2016) The role of kinetic context in apparent biased agonism at GPCRs. *Nat. Commun.* 7, 10842.
- (44) Szabo, M., Klein Herenbrink, C., Christopoulos, A., Lane, J. R., and Capuano, B. (2014) Structure-Activity Relationships of Privileged Structures Lead to the Discovery of Novel Biased Ligands at the Dopamine D2 Receptor. *J. Med. Chem.* 57, 4924–4939.
- (45) Allen, J. A., Yost, J. M., Setola, V., Chen, X., Sassano, M. F., Chen, M., Peterson, S., Yadav, P. N., Huang, X.-P., Feng, B., Jensen, N. H., Che, X., Bai, X., Frye, S. V., Wetsel, W. C., Caron, M. G., Javitch, J. A., Roth, B. L., and Jin, J. (2011) Discovery of β -arrestin-biased dopamine D2 ligands for probing signal transduction pathways essential for antipsychotic efficacy. *Proc. Natl. Acad. Sci. U. S. A.* 108, 18488–18493.
- (46) Simpson, M. M., Ballesteros, J. A., Chiappa, V., Chen, J., Suehiro, M., Hartman, D. S., Godel, T., Snyder, L. A., Sakmar, T. P., and Javitch, J. A. (1999) Dopamine D4/D2 receptor selectivity is determined by a divergent aromatic microdomain contained within the second, third, and seventh membrane-spanning segments. *Mol. Pharmacol.* 56, 1116–1126.
- (47) Michino, M., Donthamsetti, P., Beuming, T., Banala, A., Duan, L., Roux, T., Han, Y., Trinquet, E., Newman, A. H., Javitch, J. A., and Shi, L. (2013) A single glycine in extracellular loop 1 is the critical determinant for pharmacological specificity of dopamine d2 and d3 receptors. *Mol. Pharmacol.* 84, 854–864.
- (48) Donthamsetti, P., Quejada, J. R., Javitch, J. A., Gurevich, V. V., and Lambert, N. A. (2015) Using Bioluminescence Resonance Energy Transfer (BRET) to Characterize Agonist-Induced Arrestin Recruitment to Modified and Unmodified G Protein-Coupled Receptors. *Curr. Protoc. Pharmacol.* 70, 2.14.1–2.14.14.

Supporting Information

Molecular determinants of the intrinsic efficacy of the antipsychotic aripiprazole.

Carmen Klein Herenbrink^{1#}, Ravi Kumar Verma^{3#}, Herman D. Lim¹, Anitha Kopinathan², Alastair Keen¹, Jeremy Shonberg², Christopher Draper-Joyce¹, Peter J. Scammells², Arthur Christopoulos¹, Jonathan A. Javitch^{5,6}, Ben Capuano², Lei Shi^{3*}, J. Robert Lane^{7,8*},

¹Drug Discovery Biology and ²Medicinal Chemistry, Monash Institute of Pharmaceutical Sciences, Monash University (Parkville campus), 399 Royal Parade, Parkville, VIC 3052, Australia

³Computational Chemistry and Molecular Biophysics Unit, National Institute on Drug Abuse – Intramural Research Program, National Institutes of Health, 333 Cassell Drive, Baltimore, Maryland 21224, United States

⁵Departments of Psychiatry and Pharmacology, Vagelos College of Physicians and Surgeons, Columbia University, and ⁶Division of Molecular Therapeutics, New York State Psychiatric Institute, New York, New York 10032, United States

⁷Division of Pharmacology, Physiology and Neuroscience, School of Life Sciences, Queen's Medical Centre, University of Nottingham, Nottingham NG7, 2UH, U.K.

⁸Centre of Membrane Protein and Receptors, Universities of Birmingham and Nottingham, United Kingdom.

[#]these authors contributed equally

*To whom correspondence should be addressed:

Dr. Rob Lane, Centre of Membrane Proteins and Receptors, Compare Office C101a, School of Life Sciences, Queens Medial Centre, University of Nottingham, Nottingham, NG7 2UH, UK, Tel: +44 (0)115 8230468

Email: rob.lane@nottingham.ac.uk

Dr. Lei Shi, Computational Chemistry and Molecular Biophysics Unit, National Institute on Drug Abuse – Intramural Research Program, National Institutes of Health, 333 Cassell Drive, Baltimore, Maryland 21224, United States. Tel: +1(443)740-2774, Email: lei.shi2@nih.gov

Supplementary Methods

Chemistry.

All solvents and chemicals were purchased from standard suppliers and were used without any further purification. ^1H NMR and ^{13}C NMR spectra were acquired at 400.13 (^1H spectra) and 100.62 (^{13}C spectra) MHz, respectively, on a Bruker Avance III Nanobay 400 MHz NMR spectrometer coupled to the BACS 60 automatic sample changer and equipped with a 5 mm PABBO BB-1H/ D Z-G RD probe. All spectra obtained was processed using MestReNova software (v.6.0). Chemical shifts (δ) for all ^1H spectra are reported in parts per million (ppm) using tetramethylsilane (TMS, 0 ppm) as the reference. The data for all spectra are reported in the following format: chemical shift (δ), (multiplicity, coupling constants J (Hz), integral), where the multiplicity is defined as s = singlet, d = doublet, t = triplet, q = quartet, p = pentet, and m = multiplet. ^{13}C NMR were routinely carried out as J -modulated spin-echo experiments (JMOD), all ^{13}C δ are reported in ppm and assignment of carbon signals were abbreviated as: C = quaternary carbon, CH = methine carbon, CH_2 = methylene carbon, and CH_3 = methyl carbon. Thin layer chromatography (TLC) was carried out routinely on silica gel 60F254 precoated plates (0.25 mm, Merck). Flash column chromatography was carried out using Davisil LC60A silica gel, 40-63 μm .

Liquid chromatography mass spectroscopy (LCMS) was detected on one of two instruments; either an Agilent 6100 Series Single Quad LC/MS or an Agilent 1200 Series HPLC (equipped with a 1200 Series G1311A Quaternary Pump, G1329A Thermostatted Autosampler, and a G1314B Variable Wavelength Detector) and the data was processed using LC/MSD Chemstation Rev.B.04.01 SP1 coupled with Easy Access Software. Both systems were equipped with a Reverse Phase Luna C₈(2) (5 μm , 50 \times 4.6 mm, 100 Å) column maintained at 30 °C. An MeCN gradient (5-100%) was used to obtain optimal separation, where 4 min were required for the gradient to reach 100% MeCN and maintained for a further 3 min before requiring 3 min to return to the initial gradient of 5% MeCN (total run time = 10 min). Solvent A = 0.1% aqueous formic acid; Solvent B = MeCN/ 0.1% formic acid.

The purity and retention time of final products were determined using analytical HPLC and high-resolution mass spectroscopy (HRMS). Analytical HPLC was carried out using an Agilent 1260 Infinity Analytical HPLC fitted with a Zorbax Eclipse Plus C18 Rapid Resolution column (100 mm \times 4.60 mm, 3.5 μm) using a binary solvent system: solvent A of 0.1% aqueous trifluoroacetic acid; solvent B of 0.1% TFA in MeCN. Gradient elution was achieved over 10 min using 95% A + 5% B to 100% B over 9 min, and 100% B maintained for 1 min at a flow rate of 1 mL/min monitored at both 214 and 254 nm. HRMS were conducted on an Agilent 6224 TOP LC/MS Mass Spectrometer coupled to an Agilent 1290 Infinity. All data was

acquired and reference mass corrected via dual-spray electrospray ionisation (ESI) source. Each scan or data point on the total ion chromatogram (TIC) is average of 13700 transients, producing one spectrum per second. Mass spectra were created by averaging the scans across each peak and background subtracted against the first 10 sec of the TIC. Data acquisition was carried out using the Agilent Mass Hunter Data Acquisition software version B.05.00 Build 5.0.5042 and analysis was performed using Mass Hunter Qualitative Analysis version B.05.00 Build 5.0.519.13.

General Procedure A (Reductive Alkylation)

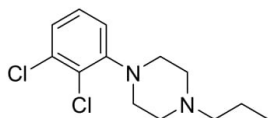
The amine (1 equiv) and aldehyde (1 equiv) were dissolved in dry 1,2- DCE (15 mL). $\text{NaBH}(\text{OAc})_3$ (1.5 equiv) was added and stirred under an atmosphere of N_2 for 24 h. LCMS was used to confirm completion of the reaction. The mixture was then diluted in DCM (20 mL), and washed with 1 M K_2CO_3 (3×20 mL) and brine, then dried over anhydrous Na_2SO_4 and evaporated to dryness. The crude material was then purified using flash chromatography (MeOH: DCM 3:97) unless otherwise stated.

General procedure B (Deprotection of *tert*-butyl carbamate and HATU Amide Coupling)

To a stirring solution of protected amine (1 equiv) and DCM (5 mL) at rt was added an excess of TFA (2 mL). The solution was stirred overnight and then diluted with DCM (20 mL). 1 M K_2CO_3 or 1 M NaOH was added to bring the mixture to pH 12. The product was then extracted using DCM (2×20 mL). The combined organic extracts were washed with brine, dried over anhydrous Na_2SO_4 then concentrated *in vacuo* to yield the free amine. Following confirmation of product formation via TLC or LCMS, the resulting amine (1 equiv), carboxylic acid (1.2 equiv) and the coupling reagent, 1-[bis(dimethylamino)methylene]-1*H*-1,2,3-triazolo[4,5-*b*]pyridinium 3-oxid hexafluorophosphate (HATU) (1.2-2 equiv) were stirred in a minimal volume of anhydrous DMF (3 mL). To this, an excess of DIPEA (2 equiv) was added and the reaction was left to stir between 2 and 24 hours. The reaction was ceased upon confirmation of complete consumption of the amine via LCMS. The mixture was then diluted with 1:1 mixture of a saturated sodium bicarbonate (NaHCO_3) solution and water (30 mL) and left to stir for 30 min. The resulting precipitate was filtered and washed or the product was extracted from the

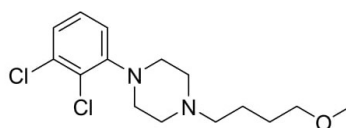
aqueous using EtOAc (3 × 20 mL) if precipitation had not occurred and concentrated under vacuum. Any further purification was as specified.

1-(2,3-Dichlorophenyl)-4-propylpiperazine (2).¹



1-(2,3-Dichlorophenyl)piperazine hydrochloride (803 mg, 3.00 mmol), 1-bromopropane (273 μ L, 3.00 mmol) and K_2CO_3 (1.24 g, 9.00 mmol) were stirred in acetone under reflux for 16 hours. The resultant mixture was then concentrated *in vacuo* and the resultant residue was diluted with EtOAc, washed with H_2O (2 × 50 mL) and brine (50 mL), and dried over anhydrous Na_2SO_4 . The solution was then reduced under pressure and purified via column chromatography (1:9 MeOH: $CHCl_3$) to afford 1-(2,3-dichlorophenyl)-4-propylpiperazine as a colourless oil (444 mg, 54%). 1H NMR ($CDCl_3$) δ 7.14 (m, 2H), 6.96 (m, 1H), 3.07 (br s, 4H), 2.67 (br s, 4H), 2.38 (m, 2H), 1.55 (m, 2H), 0.93 (t, J = 7.4 Hz, 3H). ^{13}C NMR ($CDCl_3$) δ 151.5 (C), 134.1 (C), 127.6 (C), 127.5 (CH), 124.6 (CH), 118.71 (CH), 60.8 (CH_2), 53.5 (CH_2), 51.5 (CH_2), 20.2 (CH_2), 12.1 (CH_3). HPLC: t_R 5.93 min, >95% purity. HRMS (m/z): $[M+H]^+$ calcd for $C_{13}H_{19}Cl_2N_2$ requires 273.0920; found 273.0923.

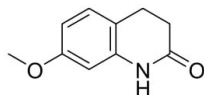
1-(2,3-Dichlorophenyl)-4-(4-methoxybutyl)piperazine (4).



1-(2,3-Dichlorophenyl)piperazine hydrochloride (500 mg, 1.87 mmol), 1-bromo-4-methoxybutane (244 μ L, 1.87 mmol) and K_2CO_3 (1.24 g, 9.00 mmol) were stirred in acetone at reflux for 16 h. The mixture was then concentrated *in vacuo* and the resultant residue was diluted with EtOAc, washed with H_2O (2 × 50 mL) and brine (50 mL), and dried over anhydrous Na_2SO_4 . The solution was then reduced under pressure and purified via column chromatography (3:2 EtOAc: Hexane) to obtain 1-(2,3-dichlorophenyl)-4-(4-methoxybutyl)piperazine as a yellow oil (240 mg, 40%). 1H NMR ($CDCl_3$) δ 7.15 (m, 2H), 6.96 (m, 1H), 3.41 (app t, J = 6.1 Hz, 2H), 3.34 (s, 3H), 3.07 (br s, 4H), 2.64 (br s, 4H), 2.38

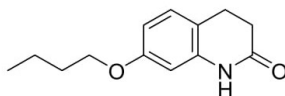
(app t, $J = 7.3$ Hz, 2H), 1.65 (m, 4H). ^{13}C NMR (CDCl_3) δ 151.3 (C), 134.0 (C), 127.5 (C), 127.4 (CH), 124.5 (CH), 118.6 (CH), 72.7 (CH_2), 58.6 (CH_3), 58.4 (CH_2), 53.3 (CH_2), 51.3 (CH_2), 27.7 (CH_2), 23.6 (CH_2). HPLC: t_R 5.85 min, >95% purity. HRMS (m/z): $[\text{M}+\text{H}]^+$ calcd for $\text{C}_{15}\text{H}_{23}\text{Cl}_2\text{N}_2\text{O}$ requires 317.1182; found 317.1182.

7-Methoxy-3,4-dihydroquinolin-2(1H)-one (5).²



To an rbf containing 7-hydroxy-3,4-dihydroquinolin-2(1H)-one (200 mg, 1.23 mmol) and K_2CO_3 (186 mg, 1.35 mmol), DMF (10 mL) was added and left to stir until completely dissolved. Methyl iodide (76.3 μL , 1.23 mmol) was then added to the mixture and the reaction was stirred at room temperature for 16 h. The mixture was then poured into water (100 mL) and neutralised with 1 M HCl. The compound was extracted with EtOAc (6×20 mL) and the combined organic phases were washed with water (2×100 mL) and brine (100 mL). After the organic phase was dried over anhydrous Na_2SO_4 and concentrated *in vacuo*. The crude product was purified via column chromatography (1:1 EtOAc: Pet. Spirits) to yield 7-methoxy-3,4-dihydroquinolin-2(1H)-one as an opaque, white solid (471 mg, 72%). ^1H NMR (CDCl_3) δ 7.55 (br s, 1H), 7.06 (d, $J = 8.3$ Hz, 1H), 6.54 (dd, $J = 8.3$ Hz, 2.5 Hz, 1H), 6.29 (d, $J = 2.5$ Hz, 1H), 3.78 (s, 3H), 2.97 – 2.81 (m, 2H), 2.62 (m, 2H). ^{13}C NMR (101 MHz, CDCl_3) δ 171.79 (C), 159.23 (C), 138.15 (C), 128.71 (CH), 115.82 (C), 108.14 (CH), 101.59 (CH), 55.46 (CH_3), 31.09 (CH_2), 24.58 (CH_2). HPLC: t_R 5.16 min, >95% purity. HRMS (m/z): $[\text{M}+\text{H}]^+$ calcd for $\text{C}_{10}\text{H}_{12}\text{NO}_2$ requires 177.0863; found 177.0863.

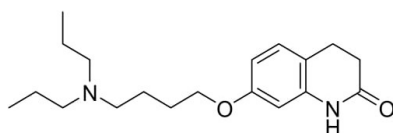
7-butoxy-3,4-dihydroquinolin-2(1H)-one (6).



The phenol (200 mg, 1.23 mmol) was taken up in acetone (15 mL) and added to the solution was potassium carbonate (339 mg, 2.45 mmol) and 1-bromobutane (248 μL , 2.45 mmol), and the reaction mixture heated at reflux for 16 h. After this time, the solvents were removed in *vacuo*, then the mixture taken up in 1 M sodium hydroxide solution (15 mL) and the product

extracted into chloroform (2×20 mL). The combined organic layers were washed with brine (10 mL) then dried over anhydrous sodium sulfate, and evaporated to dryness to reveal a yellow waxy solid. The crude material was then purified by gradient flash column chromatography (1:4 1:1 EtOAc: Pet. Spirits) to give the title compound as a colourless oil (65 mg, 24% yield). ^1H NMR (CDCl_3) δ 8.92 (br s, 1H, NH), 7.03 (d, $J = 8.3$ Hz, 1H), 6.52 (dd, $J = 8.3, 2.4$ Hz, 1H), 6.39 (d, $J = 2.4$ Hz, 1H), 3.93 (t, $J = 6.5$ Hz, 2H), 2.94 – 2.84 (m, 2H), 2.62 (dd, $J = 8.3, 6.7$ Hz, 2H), 1.79 – 1.69 (m, 2H), 1.55 – 1.38 (m, 2H), 0.97 (t, $J = 7.4$ Hz, 3H). ^{13}C NMR (CDCl_3) δ 172.4 (C), 159.0 (C), 138.3 (C), 128.7 (CH), 115.7 (C), 108.9 (CH), 102.4 (CH), 68.0 (CH_2), 31.4 (CH_2), 31.3 (CH_2), 24.7 (CH_2), 19.3 (CH_2), 14.0 (CH_3). HPLC: $t_R = 10.0$ min, >95% purity.

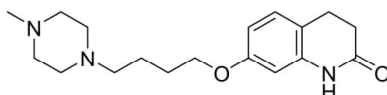
7-(4-(dipropylamino)butoxy)-3,4-dihydroquinolin-2(1H)-one (7).



The alkyl halide (300 mg, 1.01 mmol) was taken up in acetone (30 mL), then potassium carbonate (278 mg, 2.01 mmol), sodium iodide (533 mg, 3.56 mmol) and di-*N*-propylamine (550 μL , 4.02 mmol) were added to the stirred mixture. The reaction mixture was heated at reflux for 2 days, after which point complete consumption of starting material was evident by LCMS. The mixture was evaporated to dryness and taken up in water (20 mL) and ethyl acetate (2×20 mL). The organic phase was then washed with 1 M potassium carbonate solution (15 mL), then the product was extracted into 1 M hydrogen chloride solution (2×15 mL). The acidic aqueous phase was then neutralised with ammonium hydroxide solution to pH = 10, and then the product extracted back into ethyl acetate (2×25 mL). The final organic phases were combined, washed with brine (10 mL), then dried over anhydrous sodium sulfate and evaporated to dryness to give the product as a colourless oil (310 mg, 97% yield). ^1H NMR (CDCl_3) δ 9.14 (s, 1H), 7.02 (d, $J = 8.3$ Hz, 1H), 6.51 (dd, $J = 8.3, 2.4$ Hz, 1H), 6.41 (d, $J = 2.4$ Hz, 1H), 3.93 (t, $J = 6.4$ Hz, 2H), 2.89 (t, $J = 7.5$ Hz, 2H), 2.67 – 2.56 (m, 2H), 2.51 – 2.42 (m, 2H), 2.40 – 2.32 (m, 4H), 1.83 – 1.70 (m, 2H), 1.64 – 1.52 (m, 2H), 1.51 – 1.38 (m, 4H), 0.93 – 0.81 (m, 6H). ^{13}C NMR (CDCl_3) δ 172.0 (C), 158.3 (C), 138.5 (C), 128.7 (CH), 116.2 (C), 108.8 (CH), 102.5 (CH), 67.2 (CH_2), 54.4 (CH_2), 52.6 (CH_2), 50.8 (CH_2), 31.2 (CH_2), 26.6

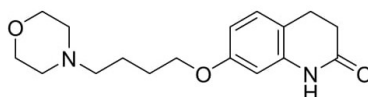
(CH₂), 24.7 (CH₂), 20.8 (CH₂), 17.3 (CH₂), 11.4 (CH₃). HPLC (λ = 254 nm) t_R = 7.85 min, >95% purity. LCMS (m/z): [M+H]⁺ 319.2.

7-(4-(4-methylpiperazin-1-yl)butoxy)-3,4-dihydroquinolin-2(1H)-one (8).



The alkyl halide (160 mg, 539 μ mol) was taken up in acetone (15 mL), and added to the solution was potassium carbonate (124 mg, 899 μ mol), sodium iodide (135 mg, 899 μ mol) and 1-methylpiperazine (49.8 μ L, 449 μ mol). The mixture was heated at reflux for 16 h, after which point LCMS confirmed the complete consumption of all piperazine starting material. The mixture was evaporated of solvents in vacuo, and then taken up in chloroform (20 mL) and washed with 1 M potassium carbonate solution (2 \times 15 mL). The organic extract was then washed with brine (15 mL), dried over anhydrous sodium sulfate, and evaporated to dryness to give a yellow oil. The product was then purified by column chromatography (1:4 MeOH:CHCl₃) to give the title compound as a colourless oil (74 mg, 52% yield). ¹H NMR (CDCl₃) δ 9.12 (s, 1H), 7.03 (d, J = 8.3 Hz, 1H), 6.51 (dd, J = 8.3, 2.4 Hz, 1H), 6.39 (d, J = 2.4 Hz, 1H), 3.94 (t, J = 6.3 Hz, 2H), 2.89 (t, J = 7.5 Hz, 2H), 2.61 (dd, J = 8.4, 6.7 Hz, 2H), 2.58 – 2.42 (m, 8H), 2.40 (d, J = 7.6 Hz, 2H), 2.30 (s, 3H), 1.84 – 1.72 (m, 2H), 1.72 – 1.59 (m, 2H). ¹³C NMR (CDCl₃) δ 172.4 (C), 158.7 (C), 138.3 (C), 128.6 (CH), 115.7 (C), 108.8 (CH), 102.3 (CH), 67.9 (CH₂), 58.2 (CH₂), 55.2 (CH₂), 53.2 (CH₂), 46.1 (CH₃), 31.2 (CH₂), 27.3 (CH₂), 24.6 (CH₂), 23.5 (CH₂). HPLC (λ = 254 nm) t_R = 5.65 min, >95% purity. LCMS (m/z): [M+H]⁺ 318.2.

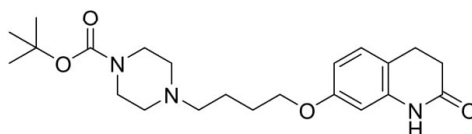
7-(4-Morpholinobutoxy)-3,4-dihydroquinolin-2(1H)-one (9).³



A suspension of morpholine (201 μ L, 2.30 mmol), 7-(4-bromobutoxy)-3,4-dihydroquinolin-2(1H)-one (570 mg, 1.91 mmol) and potassium carbonate (789 mg, 5.73 mmol) in acetone was left to stir under reflux overnight. The resultant mixture was then concentrated *in vacuo* to yield

a white precipitate. The solid product was taken up in 1 M HCl (30 mL) and EtOAc (30 mL) and the aqueous layer was collected. Sat. Na₂CO₃ was used to basify the solution to pH 13 and the product was extracted using EtOAc (4 × 20 mL). The combined organic fractions were then washed with water (2 × 50 mL) brine (50 mL) and dried over anhydrous Na₂SO₄. The product was concentrated *in vacuo* to yield 7-(4-morpholinobutoxy)-3,4-dihydroquinolin-2(1*H*)-one as a yellow oil (422 mg, 72%). ¹H NMR (CDCl₃) δ 7.90 (br s, 1H), 7.04 (d, *J* = 8.0 Hz, 1H), 6.52 (dd, *J* = 8.0 Hz, 4.0 Hz, 1H), 6.30 (d, *J* = 2.0 Hz, 1H), 3.95 (t, *J* = 6.3 Hz, 2H), 3.72 (app t, *J* = 4.0 Hz, 4H), 2.90 (app t, *J* = 6.0 Hz, 2H), 2.62 (m, 2H), 2.41 (m, 6H), 1.79 (m, 2H), 1.67 (m, 2H). ¹³C NMR (CDCl₃) δ 171.6 (C), 158.7 (C), 138.1 (C), 128.7 (CH), 115.8 (C), 108.6 (CH), 102.1 (CH), 67.9 (CH₂), 67.0 (CH₂), 58.6 (CH₂), 53.7 (CH₂), 31.0 (CH₂), 27.2 (CH₂), 24.6 (CH₂), 23.1 (CH₂). HPLC: *t*_R 4.36 min, >95% purity. HRMS (*m/z*): [M+H]⁺ calcd for C₁₇H₂₅N₂O₃ requires 305.1860; found 305.1862.

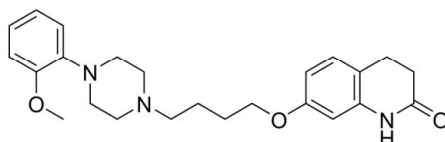
***tert*-Butyl 4-(4-((2-oxo-1,2,3,4-tetrahydroquinolin-7-yl)oxy)butyl)piperazine-1-carboxylate (10).**



A suspension of *tert*-butyl piperazine-1-carboxylate (300 mg, 1.61 mmol), 7-(4-bromobutoxy)-3,4-dihydroquinolin-2(1*H*)-one (320 mg, 1.07 mmol) and potassium carbonate (594 mg, 4.30 mmol) in acetone (20 mL) was heated and stirred at reflux overnight. The resultant mixture was taken up in 20 mL EtOAc and washed with water (2 × 30 mL) and brine. The organic mixture was then dried over anhydrous Na₂SO₄ and concentrated *in vacuo*. Column chromatography (1:19 MeOH: DCM) was then used to yield *tert*-butyl 4-(4-((2-oxo-1,2,3,4-tetrahydroquinolin-7-yl)oxy)butyl)piperazine-1-carboxylate as a yellow oil (196 mg, 45%). ¹H NMR (CDCl₃) δ 8.20 (br s, 1H), 7.04 (d, *J* = 8.0 Hz, 1H), 6.52 (dd, *J* = 8.3, 2.4 Hz, 1H), 6.33 (d, *J* = 2.4 Hz, 1H), 3.94 (t, *J* = 6.2 Hz, 2H), 3.43 (app t, *J* = 6.0 Hz, 4H), 2.90 (app t, *J* = 6.0 Hz, 2H), 2.63 (app dd, *J* = 8.3, 6.7 Hz, 2H), 2.41 (m, 6H), 1.80 (m, 2H), 1.67 (m, 2H), 1.46 (s, 9H). ¹³C NMR (CDCl₃) δ 171.8 (C), 158.6 (C), 154.8 (C), 138.1 (C), 128.7 (CH), 115.7 (C), 108.7 (CH), 102.2 (CH), 79.6 (CH₂), 67.8 (2 CH₂), 58.2 (2 CH₂), 53.0 (CH₂), 31.1 (2 CH₂),

28.4 (3 CH₃), 27.2 (CH₂), 24.6 (CH₂), 23.3 (CH₂). HPLC: *t*_R 5.46 min, > 95% purity. HRMS (*m/z*): [M+H]⁺ calcd for C₂₂H₃₄N₃O₄ requires 404.2544; found 404.2550.

7-(4-(4-(2-Methoxyphenyl)piperazin-1-yl)butoxy)-3,4-dihydroquinolin-2(1H)-one (13).



An rbf containing 1-(2-methoxyphenyl)piperazine hydrochloride (320 mg, 1.40 mmol), 7-(4-bromobutoxy)-3,4-dihydroquinolin-2(1H)-one (500 mg, 1.68 mmol) and K₂CO₃ (193 mg, 1.40 mmol) in MeCN (30 mL) was stirred at reflux for 72 h. The resultant mixture was concentrated *in vacuo* and purified using column chromatography (1:9 MeOH: DCM). The product obtained was a yellow oil (389 mg, 68%). ¹H NMR (CDCl₃) δ 9.33 (s, 1H), 7.03 – 6.82 (m, 5H), 6.50 (dd, *J* = 8.3, 2.4 Hz, 1H), 6.40 (d, *J* = 2.3 Hz, 1H), 3.94 (t, *J* = 6.1 Hz, 2H), 3.84 (s, 3H), 3.10 (br s, 4H), 2.87 (t, *J* = 7.5 Hz, 2H), 2.62 (m, 6H), 2.47 (t, *J* = 7.5 Hz, 2H), 1.86 – 1.65 (m, 4H). ¹³C NMR (CDCl₃) δ 172.5 (C), 158.7 (C), 152.3 (C), 141.4 (C), 138.3 (C), 128.5 (CH), 122.9 (CH), 121.0 (CH), 118.2 (CH), 115.6 (C), 111.2 (CH), 108.8 (CH), 102.3 (CH), 67.9 (CH₂), 58.3 (CH₂), 55.4 (CH₃), 53.5 (CH₂), 50.7 (CH₂), 31.1 (CH₂), 27.3 (CH₂), 24.6 (CH₂), 23.4 (CH₂). HPLC: *t*_R 5.50 min, >95% purity. HRMS (*m/z*): [M+H]⁺ calcd for C₂₄H₃₂N₃O₃ requires 410.2438; found 410.2443.

Molecular Biology

cDNA in pcDNA3.1+ encoding the short isoform of the wild-type human dopamine D2 receptor with an N-terminal SNAP tag was obtained from Cisbio (Bagnols-sur-Ce'ze, France). Oligonucleotides were purchased from GeneWorks (Hindmarsh, Australia). The receptor construct in pcDNA3.1+ was transferred into the pEF5/frt/V5/dest vector using Gateway cloning strategy (Invitrogen). Desired mutations were introduced using the Quikchange site-directed mutagenesis kit (Agilent).

Cell Lines and Transfection

Flp-In-CHO cells were grown in DMEM supplemented with 10% fetal bovine serum and maintained at 37°C in a humidified incubator containing 5% CO₂. The Flp-In-CHO cells were transfected with the pOG44 vector encoding Flp recombinase and the pDEST vector encoding the wild-type or mutant SNAP-D₂₅R at a ratio of 9:1 using polyethylenimine as transfection reagent. 24 hours after transfection the cells were subcultured and the medium was supplemented with 700 µg/ml hygromycin B as selection agent to obtain cells stably expressing the SNAP-D₂₅R.

ELISA

125,000 cells/well were plated into 48-well culture plates. After 7h, cells were washed with phosphate-buffered saline (PBS) and incubated in serum-free DMEM overnight. The next day cells were washed with Tris-buffered saline (TBS), fixed in 3.7% v/v paraformaldehyde for 30 minutes, then washed with TBS and blocked on a shaker o/n at 4°C in blocking buffer (0.1M NaHCO₃ pH8.6, 1% fat free milk). The blocking buffer was aspirated, and primary antibody added in TBS + 0.1% BSA (1:1000, SNAP Antibody, ThermoFisher) for 4hrs at RT. After washing with TBS, cells were incubated or 2h (RT) with the secondary antibody (1:2000, HRP-linked anti-rabbit IgG, Cell Signaling Technology). Cells were washed with TBS and peroxidase substrate (SIGMAFAST™ OPD, 0.4mg/ml). The reaction was terminated by the addition of 1M HCl. The coloured reaction product was detected at 490nm in a multi-label plate reader (EnVision, PerkinElmer Life Sciences).

ERK1/2 Phosphorylation Assay

ERK1/2 phosphorylation was measured using the Alphascreen™ SureFire ERK kit (PerkinElmer, Waltham, USA). Cells were seeded into 96-well plates at a density of 50,000 cells/well. After 5-7h, cells were washed with phosphate-buffered saline (PBS) and incubated in serum-free DMEM overnight before assaying. Dose-response experiments were performed for each ligand at 37°C in the presence of 0.1% ascorbic acid. Stimulation of the cells was terminated after 5 minutes of agonist stimulation by removing the media and the addition of 100 µl of SureFire lysis buffer to each well. The plate was shaken for 5 minutes at room temperature before transferring 5 µl of the lysates to a white 384-well Proxiplate (PerkinElmer, Waltham, USA). Then 8 µl of a 240:1440:7:7 mixture of Surefire activation buffer: Surefire reaction buffer: Alphascreen acceptor beads: Alphascreen donor beads was added to the

samples and incubated in the dark at 37°C for 1.5 h. Plates were read using a Fusion-TM plate reader (PerkinElmer, Waltham, USA).

cAMP Alphascreen™ Assay

Flp-In-CHO cells stably expressing the wild-type or mutant SNAP-D_{2S}R were grown overnight in 96-well plates at a density of 50,000 cells/well. After pre-incubating the cells for 45 minutes with stimulation buffer (Hank's buffered salt solution: 0.14 M NaCl, 5.4 mM KCl, 0.8 µM MgSO₄, 1.3 mM CaCl₂, 0.2 mM Na₂HPO₄, 0.44 mM KH₂PO₄, 5.6 mM D-glucose, 1 mg/ml BSA, 0.5mM 3-isobutyl-1-methylxanthine, and 5 mM HEPES, pH 7.4) the cells were stimulated simultaneously with drug and 300 nM forskolin for 30 minutes at 37°C. Stimulation of cells was terminated by the removal of the stimulation buffer and the addition of 50 µl ice-cold 100% EtOH. The plates containing the cell lysates were then incubated at 37°C without lid to allow complete evaporation of the EtOH. After all the EtOH was evaporated, 50 µl of detection buffer (1 mg/ml BSA, 0.3% Tween-20, and 5 mM HEPES, pH 7.4) was added to each well. The plate was shaken for 5 minutes to ensure complete and even suspension of the cell material. 5 µl of the samples was then transferred into a white 384-well Optiplate (PerkinElmer, Waltham, USA). Anti-cAMP acceptor beads (0.2 units/µl) diluted in stimulation buffer were added to all samples and incubated in the dark at room temperature for 30 minutes before addition of 15 µl of the donor beads/biotinylated cAMP (0.07 units/ul) mixture made up in detection buffer. Following a 1 hour incubation at RT, plates were read using a Fusion-TM plate reader (PerkinElmer, Waltham, USA).

Bioluminescence Resonance Energy Transfer (BRET) cAMP assay

Flp-In-CHO cells stably expressing the wild-type or mutant SNAP-D_{2S}R were seeded at a density of 2,000,000 cells per 10 cm dish and were transfected the following day using polyethylenimine as transfection reagent. The cells were transfected with 3 µg CAMYEL to allow the detection of cAMP levels within the cells. 24 h after transfection the cells were plated into 96-well CulturPlates (PerkinElmer) and grown overnight. The cells were equilibrated in Hank's balanced salt solution at 37°C before starting the experiment. The cells were co-stimulated with the agonists and 300nM forskolin for the indicated timeframes when the BRET readings were captured. Coelenterazine (Promega) was added at a final concentration of 5µM at least 5 min prior to measurement. The signals were detected at 445-505 and 505-565 nm using a LUMIstar Omega instrument (BMG LabTech, Offenburg, Germany). Net BRET was determined by subtraction of the vehicle control co-added with 10µM forskolin.

Phenoxybenzamine-treatment was performed out in Flp-In-CHO cells stably expressing the wild-type or mutant SNAP-D_{2S}R. The cells were treated with 0.1, 0.3 or 1 μ M of Phenoxybenzamine (Sigma Aldrich) and equilibrated at 37 °C for 30 mins prior to the commencement of the assay.

β -arrestin-2 recruitment to the plasma membrane

Measurement of β -arrestin-2 recruitment to the plasma membrane was achieved through BRET by co-transfecting SNAP-D_{2S}R-WT or SNAP-D_{2S}R-L41A with β -arrestin-2-venus as well as Rluc8-KRasct which anchors to the plasma membrane serving as a localised BRET donor⁴.

Flp-In-HEK 293 cells were initially seeded into 10cm dishes at a density of 2,000,000 cells in DMEM supplemented with 10% foetal bovine serum. The following day cells were transfected with 2 μ g SNAP-D_{2S}R-WT or SNAP-D_{2S}R-L41A, 2 μ g GRK2, 5.5 μ g β -arrestin-2-venus and 0.5 μ g Rluc8-KRasct using polyethylenimine (PEI) as a transfection reagent in a ratio of 5:1 μ g/ μ L (PEI:DNA). 24 hours after transfection cells were harvested and transferred into poly-D-lysine coated 96-well white CulturPlates (PerkinElmer). The following day cells were washed once and equilibrated with Hank's balanced salt solution for 30 minutes at 37°C before starting the experiment. Cells were then treated with increasing concentrations of dopamine, ropinirole or aripiprazole for 30 minutes at 37°C before detection. Coelenterazine h (Nanolight Technology) was added 15 minutes before detection to make a final concentration of 5 μ M. The emission signals of Rluc8 and venus were detected simultaneously at wavelengths of 445-505nm (Rluc8) and 505-565nm (venus) using a PHERAstar FS Omega microplate reader (BMG LabTech, Offenburg, Germany). The data was quantified by dividing the venus acceptor signal by the Rluc8 donor signal to give a BRET ratio that was then baseline-normalised to the vehicle control wells.

Membrane preparation

Flp-In-CHO cells stably expressing the dopamine wild-type or mutant SNAP-D_{2S}R were grown to 90% confluency in 175 cm² cell culture flasks. The cells were harvested in PBS containing 2mM EDTA and centrifuged at 300 g for 3 min. The resulting pellet was resuspended in ice-cold assay buffer (20 mM HEPES, 100 mM NaCl, 6 mM MgCl₂, 1 mM EGTA and 1 mM EDTA, pH 7.4) and the centrifugation step was repeated. The intact cell

pellet was then resuspended in assay buffer and homogenized using a Polytron homogenizer. After centrifugation (1000g, 10 min) the pellet was discarded, and the supernatant was recentrifuged at 30,000g for 1h at 4°C using a Sorvall Evolution RC ultracentrifuge (Thermo Scientific). The resulting pellet was resuspended in assay buffer and stored in 250 µl aliquots at -80°C. Membrane protein concentration was determined using the method of Bradford.

[³H]Spiperone and [³H]Raclopride Binding Assays

All radioligand binding experiments were conducted in a 1 ml reaction volume in assay buffer (20mM HEPES, 100mM NaCl, 6mM MgCl₂, 1mM EGTA and 1mM EDTA, pH 7.4) containing 100µM GppNHp and 0.1% ascorbic acid. In all cases non-specific binding was determined in the presence of 10µM haloperidol. To obtain affinity estimates of unlabelled agonists, competition binding experiments were performed at equilibrium. The ability of increasing concentrations of the agonists to compete with 0.1nM [³H]spiperone or 1nM [³H]raclopride for binding to the wild-type or mutant SNAP-D_{2S}R was tested. Raclopride binding is entropy driven at temperatures up to 30°C and enthalpy driven at 37°C, consequently the binding affinity of raclopride at 37°C is lower⁵. The binding experiments with [³H]raclopride were therefore conducted at 25°C, whereas those with [³H]spiperone were conducted at 37°C. The membranes (5µg) were incubated with the drugs for 3h at 37°C ([³H]spiperone) or 25°C ([³H]raclopride). After this incubation period, bound and free radioligand were separated by fast-flow filtration through GF/B filters using a brandel harvester followed by three washes with ice-cold 0.9% NaCl. Filter bound radioactivity was measured by scintillation spectrometry after the addition of 3.5 ml of Ultima Gold (PerkinElmer) using a Tri-Carb 2900TR liquid scintillation counter (PerkinElmer).

Data analysis

Dose-response curves were fitted using the following three-parameter equation

$$response = bottom + \frac{top - bottom}{1 + 10^{(\log EC_{50} - \log[A])}} \quad (1)$$

where top and bottom represent the maximal and minimal asymptote of the dose response curve, [A] is the molar concentration of agonist, and EC₅₀ is the molar concentration of agonist required to give a response half way between bottom and top.

To compare profiles between the WT and mutant D₂R, agonist concentration response curves were also fitted to the operational model of agonism⁶ below,

$$Y = \frac{E_m - basal}{1 + \left(\frac{K_A + [A]}{\tau[A]} \right)^n} \quad (2)$$

Where E_m is the maximal possible response of the system, basal is the basal level of response, K_A represents the equilibrium dissociation constant of the agonist (A) and τ is an index of the signalling efficacy of the agonist that is defined as R_T/K_E , where R_T is the total number of receptors and K_E is the coupling efficiency of each agonist-occupied receptor, and n is the slope of the transducer function that links occupancy to response. The analysis assumes that the transduction machinery utilized for a given cellular pathway are the same for all agonists, such that the E_m and transducer slope (n) are shared between agonists. Data for aripiprazole for each pathway were fit globally to determine values of K_A and τ . In cases where the expression level of the mutant D₂R was different to WT the corrected τ values (τ_c) were normalized to WT cell surface expression obtained by ELISA as follows.

$$\tau_c = \frac{\tau}{\text{normalized receptor expression}} \quad (3)$$

To obtain values of K_A and τ for dopamine and ropinirole, agonists that produced the maximal system response, we treated cells with phenoxybenzamine to irreversibly block cell surface D₂Rs as described above. This resulted in significant reductions in the maximal response. Given the proportional relationship of R_T to measured τ , K_A is invariant with receptor depletion. Hence estimates of K_A and τ could be obtained by operational fitting of the family of concentration response curves for each agonist at WT and mutant D₂Rs. Dose-response data were also fitted to the following form of the operational model of agonism⁷ to allow the quantification of biased agonism.

$$Y = basal + \frac{(E_m - basal) \left(\frac{\tau}{K_A} \right)^n [A]^n}{[A]^n \left(\frac{\tau}{K_A} \right)^n + \left(1 + \frac{[A]}{K_A} \right)^n} \quad (4)$$

Biased agonism was quantified as previously described^{8,9}. In short, to exclude the impact of cell-dependent and assay-dependent effects on the observed agonism at each pathway, the

$\log(\tau/K_A)$ value of a reference agonist, in this case ropinirole, is subtracted from the $\log(\tau/K_A)$ value of the agonists of interest to yield $\Delta\log(\tau/K_A)$. The relative bias can then be calculated for each agonist at the two different signalling pathways by subtracting the $\Delta\log(\tau/K_A)$ of one pathway from the other to give a $\Delta\Delta\log(\tau/K_A)$ value which is a measure of bias. A lack of biased agonism will result in values of $\Delta\Delta\log(\tau/K_A)$ not significantly different from 0 between pathways.

For radioligand saturation binding data, the following equation was globally fitted to nonspecific and total binding data:

$$Y = \frac{B_{\max}[A]}{[A] + K_A} + NS[A] \quad (5)$$

where Y is radioligand binding, B_{\max} is the total receptor density, [A] is the free radioligand concentration, K_A is the equilibrium dissociation constant of the radioligand and NS is the fraction of nonspecific radioligand binding. The concentration of agonist that inhibited half of the [³H]spiperone or [³H]raclopride binding (IC_{50}) was determined using the following equation:

$$Y = \frac{Bottom + (Top - Bottom)}{1 + 10^{(X - \log IC_{50})n_H}} \quad (6)$$

where Y denotes the percentage specific binding, Top and Bottom denote the maximal and minimal asymptotes, respectively, IC_{50} denotes the X value when the response is midway between Bottom and Top, and n_H denotes the Hill slope factor. IC_{50} values obtained from the inhibition curves were converted to K_i values using the Cheng and Prusoff equation.

MD simulations

We docked the aripiprazole molecule into our established D₂R model^{1,10-12} with the induced-fit docking protocol^{1,13} implemented in Schrödinger suite (release 2017-2, Schrödinger, LLC: New York, NY). From the initial docking results, we chose several poses that have the 2,3-diCl-phenylpiperazine moiety bound in the OBS with the positively charged amine forming a salt bridge with Asp114^{3,32}, and the flexible butoxy linker oriented with the quinoline moiety in various directions in the extracellular vestibule (EV) of D₂R. To investigate the effect of the

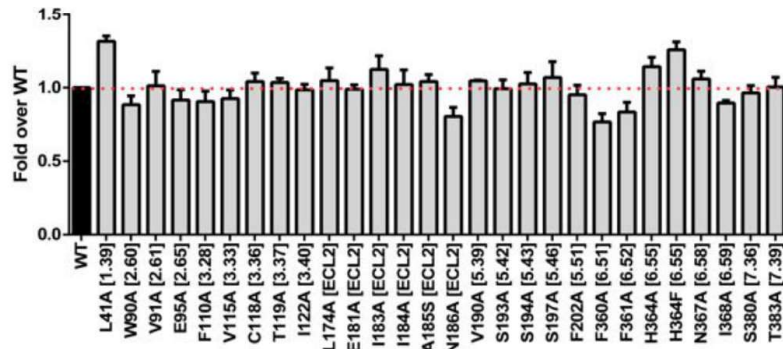
L41^{1,39}A mutation, Leu41^{1,39} was mutated to Ala in representative frames from equilibrated WT trajectories.

The D₂R/aripiprazole complex was immersed in the explicit water and 1-palmitoyl-2-oleoylphosphatidylcholine (POPC) lipid bilayer environment. The system charges were neutralized, and 150 mM NaCl was added. The total system size was ~112000 atoms. We used both the CHARMM36 force field¹⁴⁻¹⁷ together with TIP3P water model, and OPLS3 force field¹⁸, together with SPC water model. For the CHARMM36 simulations, the aripiprazole parameters were obtained through the GAAMP server¹⁹ with the initial force field based on CGenFF assigned by ParamChem²⁰. For the OPLS3 simulations, the aripiprazole parameters were based on the default atom typing of OPLS3, which were further optimized by the force field builder (Schrodinger release 2017-2).

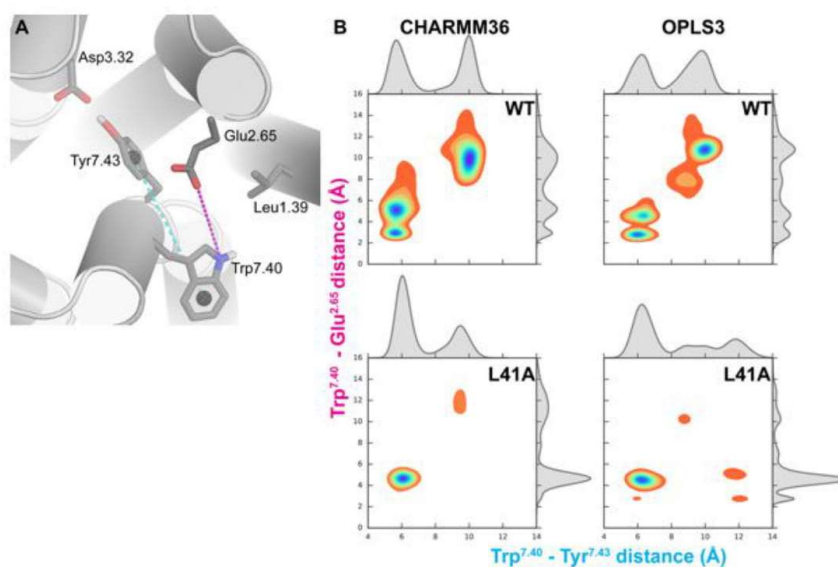
The MD simulations were carried out with Desmond (version 5.0; D. E. Shaw Research, New York, NY). Each system was first minimized and then equilibrated with restraints on the ligand heavy atoms and protein backbone atoms, followed by production runs in an isothermal–isobaric (NPT) ensemble at 310 K with all atoms unrestrained, as described previously^{10,13}. We then collected multiple MD trajectories at the microsecond scale for each pose (Supplementary Table 1).

While this manuscript was being prepared, the D₂R/risperidone (PDB 6CM4) became available²¹. In a separate study, we observed the extracellular loop 2 (EL2), which shows the most drastic difference between the structures of the highly homologous D₂R and D₃R, can spontaneously transition from the helical conformation in the D₂R structure to an extended conformation similar to that in the D₃R structure²². Thus, the D₂R structure is not necessarily a significantly better starting point for this study. The transition and dynamics of the EL2 add an extra layer of complexity for adequate sampling in the simulations, which is beyond the scope of this study.

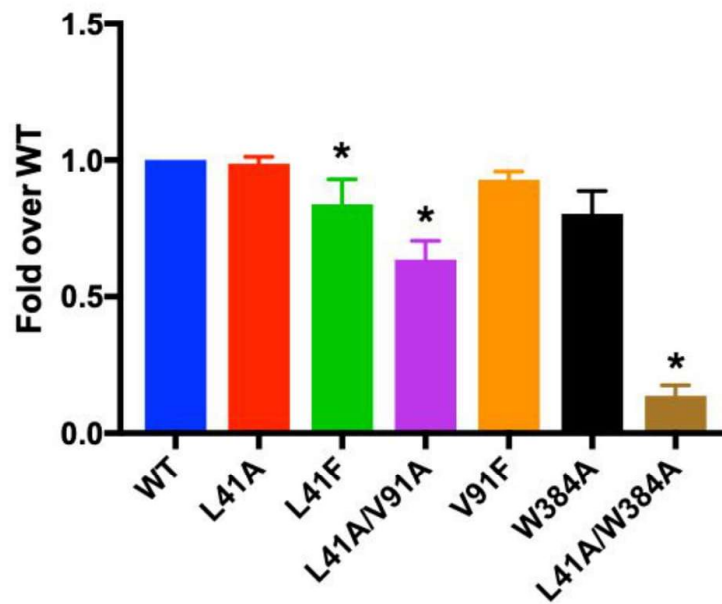
Supplementary Figure 1. Cell surface expression levels of the stably expressed mutant and wild-type receptors in FlpIn CHO cells determined by an ELISA experiment. Values are expressed as mean \pm S.E.M. from three independent experiments. No significant differences were observed ($P < 0.01$) in cell surface expression levels between the wild-type and mutant receptor constructs as determined by a one-way ANOVA, Dunnett post-hoc test.



Supplementary Figure 2. The L41¹⁻³⁹A mutation affects Trp^{7.40} side chain rotamer preferences. Panel **A** shows the two distances being evaluated, i.e., the distance between the centers of mass of Trp^{7.40} and Tyr^{7.43} 6-member rings (cyan), and the minimum distance between the indole nitrogen atom of Trp^{7.40} and the sidechain carboxyl oxygen atoms of Glu^{2.65} (magenta). **(B)** Distributions of these two distances in the indicated conditions.



Supplementary Figure 3. Cell surface expression levels of the stably expressed SBP mutant and wild-type receptors in FlpIn CHO cells determined by an ELISA experiment. Values are expressed as mean \pm S.E.M. from three independent experiments. Significant differences were observed ($P < 0.01$) in cell surface expression levels between the wild-type and mutant receptor constructs as determined by a one-way ANOVA, Dunnett post-hoc test.



Supplementary Table 1: Summary of MD simulations

D₂R Construct	Force Field	Number of trajectories	Simulation lengths (μs)
WT	CHARMM36	27	37.5
	OPLS3	8	7.2
L41A	CHARMM36	27	31.5
	OPLS3	7	5.6
Total		69	81.8

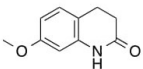
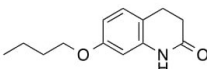
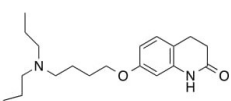
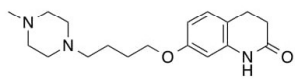
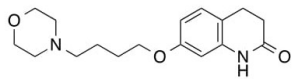
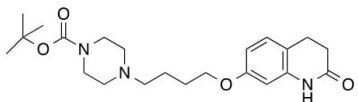
Supplementary Table 2. The affinities of [³H]spiperone and [³H]raclopride at the wild-type and mutant dopamine D₂ receptors determined with a homologous competition binding assay. Values are expressed as mean ± S.E.M. from three separate experiments. No significant differences were observed between the pK_d values of the different constructs according to one-way ANOVA, Dunnett post-hoc test ([³H]spiperone) or Student's unpaired two-tailed t-test ([³H]raclopride)

Construct	pK _d (fold)	pK _d (fold)
	[³ H]Spiperone	[³ H]Raclopride
WT	10.37 ± 0.14 (1.0)	8.76 ± 0.06 (1.0)
L41^{1.39}A	10.46 ± 0.28 (0.8)	-
W90^{2.60}A	10.22 ± 0.20 (1.4)	-
V91^{2.61}A	ND ^a	8.83 ± 0.09 (0.9)
E95^{2.65}A	10.26 ± 0.22 (1.3)	-
F110^{3.28}A	10.62 ± 0.18 (0.6)	-
V115^{3.33}A	10.22 ± 0.26 (1.4)	-
C118^{3.36}A	10.10 ± 0.14 (1.9)	-
T119^{3.37}A	9.43 ± 0.17 (8.7)	-
I122^{3.40}A	9.76 ± 0.12 (4.1)	-
L174^{ECL2}A	10.57 ± 0.28 (0.6)	-
E181^{ECL2}A	10.58 ± 0.21 (0.6)	-
I183^{ECL2}A	10.73 ± 0.15 (0.4)	-
I184^{ECL2}A	10.43 ± 0.18 (0.9)	-
A185^{ECL2}S	10.35 ± 0.24 (1.0)	-
N186^{ECL2}A	10.28 ± 0.22 (1.2)	-
V190^{5.39}A	10.58 ± 0.23 (0.6)	-
S193^{5.42}A	10.23 ± 0.24 (1.4)	-
S194^{5.43}A	10.41 ± 0.24 (0.9)	-
S197^{5.46}A	10.13 ± 0.22 (1.7)	-
F202^{5.51}A	9.80 ± 0.20 (3.7)	-
F360^{6.51}A	ND	ND
F361^{6.52}A	ND	ND
H364^{6.55}A	10.27 ± 0.23 (1.3)	-
H364^{6.55}F	10.36 ± 0.27 (1.0)	-

N367^{6.58}A	10.64 ± 0.36 (0.5)	-
I368^{6.59}A	10.21 ± 0.19 (1.4)	-
S380^{7.36}A	10.10 ± 0.17 (1.9)	-
T383^{7.39}A	10.52 ± 0.13 (0.7)	-

ND = no specific binding was detected

Supplementary Table 3. Binding affinities of THQ fragments at the WT SNAP-D₂R expressed in FlpIn CHO cells. Binding affinity (K_i) determined by competition binding experiments using radiolabelled antagonist [³H]spiperone. Values are expressed as mean \pm S.E.M. from three separate experiments. #Values significantly different from aripiprazole as determined by one-way ANOVA (Dunnett's post-hoc test) ($p < 0.05$).

	$pK_i \pm \text{SEM}$
	(K_i , nM)
5	
	< 5
6	
	< 5
7	
	< 5
8	
	< 5
9	
	< 5
10	
	6.05 ± 0.08 #

Supplementary Table 4. The effect of mutations in the SBP of the D₂R on the functional activity of selected agonists. Values of functional affinity, efficacy and transduction ratios were determined in an assay measuring inhibition of forskolin-induced intracellular cAMP production using a BRET CAMYEL biosensor. Values are

expressed as mean \pm S.E.M. four separate experiments. - Values not obtained. # Values of efficacy (τ) normalized for receptor expression levels using data from supplementary figure 3. * $P < 0.05$, significantly different from the value obtained for that agonist at the wild-type receptor determined by a one-way ANOVA, Dunnett post-hoc test.

Agonist	Receptor construct	pK _A (fold Δ)	Log τ (fold Δ)	Log(τ /K _A) (fold Δ)
aripiprazole	WT	7.22 \pm 0.18	1.11 \pm 0.16	8.36 \pm 0.06
	L41 ^{1.39} A	7.29 \pm 0.11 (0.9)	0.38 \pm 0.05* (5.4)	7.69 \pm 0.08 (4.7)
	W384 ^{7.40} A	7.51 \pm 0.13 (0.5)	0.74 \pm 0.08 (2.3) [#]	8.18 \pm 0.07 (1.5)
	L41 ^{1.39} F	7.51 \pm 0.23 (0.5)	1.04 \pm 0.19 (1.2) [#]	8.48 \pm 0.06 (0.8)
	V91 ^{2.61} F	6.05 \pm 0.17*(14)	0.07 \pm 0.06* (11)	6.12 \pm 0.14*(170)
	L41 ^{1.39} A/V91 ^{2.61} A	7.38 \pm 0.41 (0.7)	-0.52 \pm 0.08* (42) [#]	6.67 \pm 0.39* (49)
dopamine	WT	6.83 \pm 0.12	1.67 \pm 0.17	8.22 \pm 0.04
	L41 ^{1.39} A	5.84 \pm 0.10* (9.8)	1.87 \pm 0.19 (0.63)	7.58 \pm 0.05* (4.4)
	W384 ^{7.40} A	-	-	7.50 \pm 0.03* (5.2)
	L41 ^{1.39} F	-	-	8.04 \pm 0.04 (1.5)
	V91 ^{2.61} F	-	-	6.68 \pm 0.07* (35)
	L41 ^{1.39} A/V91 ^{2.61} A	6.10 \pm 0.21* (5.4)	1.23 \pm 0.19 (2.8) [#]	7.14 \pm 0.04* (12)
ropinirole	WT	6.57 \pm 0.09	2.05 \pm 0.06	8.16 \pm 0.04
	L41 ^{1.39} A	6.59 \pm 0.07 (1.0)	1.93 \pm 0.12 (1.3)	8.07 \pm 0.05 (1.2)
	W384 ^{7.40} A	-	-	7.72 \pm 0.04* (2.8)
	L41 ^{1.39} F	-	-	8.19 \pm 0.05 (0.9)
	V91 ^{2.61} F	-	-	6.68 \pm 0.07* (30)
	L41 ^{1.39} A/V91 ^{2.61} A	-	-	7.15 \pm 0.03* (10)

Supplementary Table 5. The effect of mutations to the D₂R upon the action of selected agonists measured using an ERK1/2 phosphorylation assay. Values of functional affinity, efficacy and transduction ratios were determined in an assay measuring ERK1/2 phosphorylation. ND = no agonist activity detected. *P<0.05, significantly different from the wild-type receptor determined by a one-way ANOVA, Dunnett post-hoc test.

Construct	<i>Ropinirole</i>	<i>Dopamine</i>	<i>Aripiprazole</i>		
	Log(τ/K_A)	Log(τ/K_A)	Log(τ/K_A)	pK _A	Log(τ)
	(fold Δ)	(fold Δ)	(fold Δ)	(fold Δ)	(fold Δ)
WT	8.80 ± 0.04	9.11 ± 0.08	7.27 ± 0.12	7.68 ± 0.13	-0.41 ± 0.10
L41^{1.39}A	8.61 ± 0.09 (1.5)	7.96 ± 0.05* (14)	ND	ND	ND
W90^{2.60}A	7.99 ± 0.05* (6.5)	8.41 ± 0.03* (5.0)	7.20 ± 0.17 (1.1)	7.64 ± 0.12 (1.1)	-0.44 ± 0.10 (1.1)
V91^{2.61}A	9.03 ± 0.05 (0.6)	9.47 ± 0.08 (0.4)	ND	ND	ND
E95^{2.65}A	8.63 ± 0.02 (1.5)	9.01 ± 0.13 (1.3)	6.98 ± 0.02 (1.9)	6.98 ± 0.02* (5.0)	-0.17 ± 0.06 (0.6)
F110^{3.28}A	7.32 ± 0.04* (30)	7.76 ± 0.15* (22)	7.30 ± 0.12 (0.9)	7.12 ± 0.13 (3.6)	-0.30 ± 0.09 (0.8)
V115^{3.33}A	6.78 ± 0.08* (104)	7.04 ± 0.05* (117)	ND	ND	ND
I122^{3.40}A	ND	ND	ND	ND	ND
C118^{3.36}A	ND	ND	ND	ND	ND
T119^{3.37}A	ND	ND	ND	ND	ND
L174^{ECL2}A	8.27 ± 0.06* (3.4)	8.61 ± 0.09* (3.2)	ND	ND	ND
E181^{ECL2}A	8.75 ± 0.07 (1.1)	9.00 ± 0.06 (1.3)	6.94 ± 0.12 (2.1)	7.63 ± 0.12 (1.1)	-0.69 ± 0.06 (1.9)
I183^{ECL2}A	8.77 ± 0.06 (1.1)	9.21 ± 0.08 (0.8)	6.30 ± 0.24* (9.3)	6.87 ± 0.25* (6.5)	-0.57 ± 0.10 (1.4)

I184^{ECL2A}	7.46 ± 0.11* (22)	7.24 ± 0.07* (74)	5.77 ± 0.22* (32)	6.97 ± 0.19* (5.1)	-1.20 ± 0.12* (6.2)
A185^{ECL2S}	8.67 ± 0.04 (1.3)	9.07 ± 0.10 (1.1)	7.03 ± 0.03 (1.7)	7.70 ± 0.07 (1.0)	-0.67 ± 0.04 (1.8)
N186^{ECL2A}	7.85 ± 0.07* (8.9)	8.38 ± 0.12* (5.4)	6.27 ± 0.07* (10)	7.06 ± 0.07 (4.2)	-0.79 ± 0.08 (2.4)
S193^{5.42A}	5.49 ± 0.07* (2040)	5.35 ± 0.10* (5750)	7.04 ± 0.06 (1.7)	7.05 ± 0.05 (4.3)	-0.01 ± 0.10 (0.4)
S194^{5.43A}	7.41 ± 0.02* (25)	7.82 ± 0.10* (19)	7.01 ± 0.09 (1.8)	7.27 ± 0.06 (2.6)	-0.25 ± 0.03 (0.7)
S197^{5.46A}	8.52 ± 0.04 (1.9)	ND	7.70 ± 0.11 (0.4)	7.44 ± 0.14 (1.7)	0.27 ± 0.08* (0.2)
F202^{5.51A}	ND	ND	ND	ND	ND
F361^{6.52A}	7.93 ± 0.07* (7.0)	8.16 ± 0.05* (8.9)	7.77 ± 0.09 (0.3)	7.73 ± 0.05 (0.9)	0.04 ± 0.11* (0.4)
H364^{6.55A}	7.84 ± 0.07* (9.0)	6.74 ± 0.04* (234)	7.60 ± 0.11 (0.5)	7.32 ± 0.11 (2.3)	0.29 ± 0.01* (0.2)
H364^{6.55F}	6.71 ± 0.02* (120)	7.27 ± 0.10* (69)	7.45 ± 0.11 (0.7)	7.14 ± 0.16 (3.5)	0.31 ± 0.07* (0.2)
S380^{7.36A}	8.78 ± 0.07 (1.0)	9.44 ± 0.16 (0.5)	7.03 ± 0.12 (1.7)	7.33 ± 0.11 (2.2)	-0.30 ± 0.07 (0.8)
N367^{6.58A}	8.27 ± 0.06* (3.4)	7.74 ± 0.06* (23)	7.13 ± 0.25 (1.4)	7.83 ± 0.16 (0.7)	-0.70 ± 0.11 (2.0)
I368^{6.59A}	8.55 ± 0.17 (1.8)	9.36 ± 0.14 (0.6)	7.84 ± 0.16 (0.3)	7.97 ± 0.10 (0.5)	-0.13 ± 0.12 (0.5)
T383^{7.39A}	7.03 ± 0.09* (59)	8.04 ± 0.07* (12)	7.38 ± 0.15 (0.8)	7.08 ± 0.22 (4.0)	0.30 ± 0.07* (0.2)

Supplementary Table 6. Calculation of biased agonism ($\Delta\Delta\text{Log}(\tau/K_A)$) of the selected ligands between the inhibition of forskolin-induced cAMP production and ERK1/2 phosphorylation at the wild-type and mutant D₂Rs. Biased agonism was calculated utilizing the difference in ‘transduction coefficient’, $\text{log}(\tau/K_A)$. Ropinirole was used as the reference agonist. Values are expressed as mean \pm S.E.M. from four separate experiments. ND = no agonist activity detected in the ERK1/2 phosphorylation assay and/or cAMP assay by the ligand in question or the reference agonist ropinirole. No significance from the wild-type receptor as determined by a one-way ANOVA, Dunnett post-hoc test.

Construct	$\Delta\Delta\text{Log}(\tau/K_A)$	
	Dopamine	Aripiprazole
WT	-0.09 \pm 0.08	1.68 \pm 0.11
L41 ^{1.39} A	0.45 \pm 0.14	ND
W90 ^{2.60} A	0.15 \pm 0.13	1.77 \pm 0.23
V91 ^{2.61} A	-0.07 \pm 0.16	ND
E95 ^{2.65} A	-0.33 \pm 0.18	1.53 \pm 0.12
F110 ^{3.28} A	-0.05 \pm 0.16	1.39 \pm 0.22
V115 ^{3.33} A	0.06 \pm 0.09	ND
C118 ^{3.36} A	ND	ND
T119 ^{3.37} A	ND	ND
I122 ^{3.40} A	ND	ND
L174 ^{ECL2} A	-0.32 \pm 0.12	ND
E181 ^{ECL2} A	0.46 \pm 0.11	2.07 \pm 0.23
I183 ^{ECL2} A	-0.01 \pm 0.16	2.09 \pm 0.30
I184 ^{ECL2} A	-0.11 \pm 0.21	2.23 \pm 0.26
A185 ^{ECL2} S	-0.10 \pm 0.14	1.94 \pm 0.10
N186 ^{ECL2} A	-0.29 \pm 0.16	1.95 \pm 0.21
S193 ^{5.42} A	-0.34 \pm 0.21	1.93 \pm 0.16
S194 ^{5.43} A	0.06 \pm 0.14	1.82 \pm 0.15
S197 ^{5.46} A	ND	1.30 \pm 0.15

F202^{5,51}A	-0.52 ± 0.11	ND
F360^{6,51}A	ND	ND
F361^{6,52}A	0.05 ± 0.15	0.82 ± 0.17
H364^{6,55}A	0.21 ± 0.25	1.29 ± 0.19
H364^{6,55}F	0.12 ± 0.19	1.35 ± 0.14
N367^{6,58}A	0.31 ± 0.10	1.69 ± 0.22
I368^{6,59}A	0.39 ± 0.27	1.45 ± 0.21
S380^{7,36}A	0.54 ± 0.19	1.99 ± 0.25
T383^{7,39}A	-0.02 ± 0.14	1.86 ± 0.15

Supplementary Table 7. The action of selected agonists in a β -arrestin-2 translocation assay at the wild-type and L41^{1.39}A D₂R.

Values of transduction coefficient $\text{Log}(\tau/K_A)$, functional affinity and efficacy were determined for each agonist in a BRET assay measuring β -arrestin-2 translocation to the plasma membrane. Values are expressed as mean \pm S.E.M. from four separate experiments. *P<0.05, significantly different from the wild-type receptor as determined by a two-tailed unpaired Student's t-test.

	<i>WT</i>			L41^{1.39}A (fold Δ from WT)		
	Rop	Dopa	Aripip	Rop	Dopa	Aripip
$\text{Log}(\tau/K_A)$	6.98 \pm 0.10	7.17 \pm 0.10	6.83 \pm 0.13	6.91 \pm 0.08 (1.1)	6.76 \pm 0.08 (2.6)*	6.35 \pm 0.21 (3.0)
pK_A	-	-	5.95 \pm 0.30	-	-	6.51 \pm 0.20 (0.8)
$\text{Log}(\tau)$	-	-	0.80 \pm 0.23	-	-	-0.02 \pm 0.06 (6.0)*
$\text{LogBias}_{\text{cAMP-}\beta\text{arr}}$	0.00 \pm 0.14	0.19 \pm 0.14	-0.15 \pm 0.16	0.00 \pm 0.11 (1.0)	-0.15 \pm 0.11 (2.1)	-0.56 \pm 0.22 (2.5)
$(\Delta\Delta\text{Log}(\tau/K_A))$						

Supplementary References

- (1) Newman, A. H., Beuming, T., Banala, A. K., Donthamsetti, P., Pongetti, K., LaBounty, A., Levy, B., Cao, J., Michino, M., Luedtke, R. R., Javitch, J. A., and Shi, L. (2012) Molecular determinants of selectivity and efficacy at the dopamine D3 receptor. *J. Med. Chem.* 55, 6689–6699.
- (2) Felpin, F.-X., Coste, J., Zakri, C., and Fouquet, E. (2009) Preparation of 2-quinolones by sequential Heck reduction-cyclization (HRC) reactions by using a multitask palladium catalyst. *Chemistry* 15, 7238–7245.
- (3) Lan, Y., Chen, Y., Xu, X., Qiu, Y., Liu, S., Liu, X., Liu, B.-F., and Zhang, G. (2014) Synthesis and biological evaluation of a novel sigma-1 receptor antagonist based on 3,4-dihydro-2(1H)-quinolinone scaffold as a potential analgesic. *Eur. J. Med. Chem.* 79, 216–230.
- (4) Donthamsetti, P., Quejada, J. R., Javitch, J. A., Gurevich, V. V., and Lambert, N. A. (2015) Using Bioluminescence Resonance Energy Transfer (BRET) to Characterize Agonist-Induced Arrestin Recruitment to Modified and Unmodified G Protein-Coupled Receptors. *Curr. Protoc. Pharmacol.* 70, 2.14.1–14.
- (5) Hall, H., Wedel, I., and Sällemark, M. (1988) Effects of Temperature on the in Vitro Binding of 3H-Raclopride to Rat Striatal Dopamine-D 2 Receptors. *Pharmacol. Toxicol.* 63, 118–121.
- (6) Black, J. W., and Leff, P. (1983) Operational models of pharmacological agonism. *Proc. R. Soc. Lond., B, Biol. Sci.* 220, 141–162.
- (7) Kenakin, T. (2009) Quantifying Biological Activity in Chemical Terms: A Pharmacology Primer To Describe Drug Effect. *ACS Chem. Biol.* 4, 249–260.
- (8) Kenakin, T., Watson, C., Muniz-Medina, V., Christopoulos, A., and Novick, S. (2012) A Simple Method for Quantifying Functional Selectivity and Agonist Bias. *ACS Chem. Neurosci.* 3, 193–203.
- (9) Klein Herenbrink, C., Sykes, D. A., Donthamsetti, P., Canals, M., Coudrat, T., Shonberg, J., Scammells, P. J., Capuano, B., Sexton, P. M., Charlton, S. J., Javitch, J. A., Christopoulos, A., and Lane, J. R. (2016) The role of kinetic context in apparent biased agonism at GPCRs. *Nat Commun* 7, 10842.
- (10) Michino, M., Boateng, C. A., Donthamsetti, P., Yano, H., Bakare, O. M., Bonifazi, A., Ellenberger, M. P., Keck, T. M., Kumar, V., Zhu, C., Verma, R., Deschamps, J. R., Javitch, J. A., Newman, A. H., and Shi, L. (2017) Toward Understanding the Structural Basis of Partial Agonism at the Dopamine D3 Receptor. *J. Med. Chem.* 60, 580–593.
- (11) Michino, M., Donthamsetti, P., Beuming, T., Banala, A., Duan, L., Roux, T., Han, Y., Trinquet, E., Newman, A. H., Javitch, J. A., and Shi, L. (2013) A single glycine in extracellular loop 1 is the critical determinant for pharmacological specificity of dopamine d2 and d3 receptors. *Mol. Pharmacol.* 84, 854–864.
- (12) Michino, M., Free, R. B., Doyle, T. B., Sibley, D. R., and Shi, L. (2015) Structural basis for Na(+)-sensitivity in dopamine D2 and D3 receptors. *Chem. Commun. (Camb.)* 51, 8618–8621.
- (13) Sherman, W., Day, T., Jacobson, M. P., Friesner, R. A., and Farid, R. (2006) Novel Procedure for Modeling Ligand/Receptor Induced Fit Effects. *J. Med. Chem.* 49, 534–553.
- (14) Klauda, J. B., Venable, R. M., Freites, J. A., O'Connor, J. W., Tobias, D. J., Mondragon-Ramirez, C., Vorobyov, I., MacKerell, A. D., and Pastor, R. W. (2010) Update of the CHARMM all-atom additive force field for lipids: validation on six lipid types. *J. Phys. Chem. B* 114, 7830–7843.

- (15) MacKerell, D. A., Brooks, B., Brooks, C. L., Nilsson, L., Roux, B., Won, Y., and Karplus, M. CHARMM: The Energy Function and Its Parameterization. John Wiley & Sons, Inc.
- (16) MacKerell, A. D., Feig, M., and Brooks, C. L. (2004) Extending the treatment of backbone energetics in protein force fields: limitations of gas-phase quantum mechanics in reproducing protein conformational distributions in molecular dynamics simulations. *J. Comput. Chem.* 25, 1400–1415.
- (17) Best, R. B., Zhu, X., Shim, J., Lopes, P. E. M., Mittal, J., Feig, M., and MacKerell, A. D. (2012) Optimization of the additive CHARMM all-atom protein force field targeting improved sampling of the backbone ϕ , ψ and side-chain $\chi(1)$ and $\chi(2)$ dihedral angles. *J. Chem. Theory Comput.* 8, 3257–3273.
- (18) Harder, E., Damm, W., Maple, J., Wu, C., Reboul, M., Xiang, J. Y., Wang, L., Lupyan, D., Dahlgren, M. K., Knight, J. L., Kaus, J. W., Cerutti, D. S., Krilov, G., Jorgensen, W. L., Abel, R., and Friesner, R. A. (2016) OPLS3: A Force Field Providing Broad Coverage of Drug-like Small Molecules and Proteins. *J. Chem. Theory Comput.* 12, 281–296.
- (19) Huang, L., and Roux, B. (2013) AUTOMATED FORCE FIELD PARAMETERIZATION FOR NON-POLARIZABLE AND POLARIZABLE ATOMIC MODELS BASED ON AB INITIO TARGET DATA. *J. Chem. Theory Comput.* 9, 3543–3556
- (20) Vanommeslaeghe, K., Hatcher, E., Acharya, C., Kundu, S., Zhong, S., Shim, J., Darian, E., Guvench, O., Lopes, P., Vorobyov, I., and Mackerell, A. D. (2010) CHARMM general force field: A force field for drug-like molecules compatible with the CHARMM all-atom additive biological force fields. *J. Comput. Chem.* 31, 671–690.
- (21) Wang, S., Che, T., Levit, A., Shoichet, B. K., Wacker, D., and Roth, B. L. (2018) Structure of the D2 dopamine receptor bound to the atypical antipsychotic drug risperidone. *Nature* 555, 269–273.
- (22) Lane, J. R., Abramyan, A. M., Verma, R. K., Lim, H. D., Javitch, J. A., and Shi, L. (2019, July 16) Distinct antagonist-bound inactive states underlie the divergence in the structures of the dopamine D2 and D3 receptors. *BioRxiv*.

Appendix 2: Distinct inactive conformations of the dopamine D2 and D3 receptors correspond to different extents of inverse agonism

Distinct inactive conformations of the dopamine D₂ and D₃ receptors correspond to different extents of inverse agonism

J Robert Lane^{1,2*}, Ara M Abramyan³, Pramisha Adhikari³, Alastair C Keen^{1,2,4}, Kuo-Hao Lee³, Julie Sanchez^{1,2}, Ravi Kumar Verma³, Herman D Lim⁴, Hideaki Yano³, Jonathan A Javitch^{5,6,7*}, Lei Shi^{3*}

¹Division of Pharmacology, Physiology and Neuroscience, School of Life Sciences, Queen's Medical Centre, University of Nottingham, Nottingham, United Kingdom; ²Centre of Membrane Protein and Receptors, Universities of Birmingham and Nottingham, Nottingham, United Kingdom; ³Computational Chemistry and Molecular Biophysics Unit, National Institute on Drug Abuse - Intramural Research Program, National Institutes of Health, Baltimore, United States; ⁴Drug Discovery Biology, Department of Pharmacology and Medicinal Chemistry, Monash Institute of Pharmaceutical Sciences, Monash University, Parkville, Australia; ⁵Department of Psychiatry, Vagelos College of Physicians and Surgeons, Columbia University, New York, United States; ⁶Division of Molecular Therapeutics, New York State Psychiatric Institute, New York, United States; ⁷Department of Pharmacology, Vagelos College of Physicians and Surgeons, Columbia University, New York, United States

*For correspondence:

Rob.Lane@nottingham.ac.uk (JRL);
 jaj2@cumc.columbia.edu (JAJ);
 lei.shi2@nih.gov (LS)

Competing interests: The authors declare that no competing interests exist.

Funding: See page 23

Received: 25 September 2019

Accepted: 24 January 2020

Published: 27 January 2020

Reviewing editor: Yibing Shan, DE Shaw Research, United States

© This is an open-access article, free of all copyright, and may be freely reproduced, distributed, transmitted, modified, built upon, or otherwise used by anyone for any lawful purpose. The work is made available under the [Creative Commons CC0 public domain dedication](#).

Abstract By analyzing and simulating inactive conformations of the highly homologous dopamine D₂ and D₃ receptors (D₂R and D₃R), we find that eticlopride binds D₂R in a pose very similar to that in the D₃R/eticlopride structure but incompatible with the D₂R/risperidone structure. In addition, risperidone occupies a sub-pocket near the Na⁺ binding site, whereas eticlopride does not. Based on these findings and our experimental results, we propose that the divergent receptor conformations stabilized by Na⁺-sensitive eticlopride and Na⁺-insensitive risperidone correspond to different degrees of inverse agonism. Moreover, our simulations reveal that the extracellular loops are highly dynamic, with spontaneous transitions of extracellular loop 2 from the helical conformation in the D₂R/risperidone structure to an extended conformation similar to that in the D₃R/eticlopride structure. Our results reveal previously unappreciated diversity and dynamics in the inactive conformations of D₂R. These findings are critical for rational drug discovery, as limiting a virtual screen to a single conformation will miss relevant ligands.

Introduction

G-protein-coupled receptors (GPCRs) are important therapeutic targets for numerous human diseases. Our understanding of GPCR functional mechanisms has evolved from a simple demarcation of single active and inactive states to the appreciation and detection of multiple active states responsible for partial or biased agonism (Latorraca *et al.*, 2017; Venkatakrishnan *et al.*, 2013; Weis and Kobilka, 2018). High-resolution crystal structures of these proteins are vital for structure-based (rational) drug discovery (RDD) efforts designed to tailor selectivity and efficacy (Congreve *et al.*, 2014; Michino *et al.*, 2015a). While considerable efforts have been directed at

eLife digest Almost a third of prescribed drugs work by acting on a group of proteins known as GPCRs (short for G-protein coupled receptors), which help to transmit messages across the cell's outer barrier. The neurotransmitter dopamine, for instance, can act in the brain and body by attaching to dopamine receptors, a sub-family of GPCRs. The binding process changes the three-dimensional structure (or conformation) of the receptor from an inactive to active state, triggering a series of molecular events in the cell.

However, GPCRs do not have a single 'on' or 'off' state; they can adopt different active shapes depending on the activating molecule they bind to, and this influences the type of molecular cascade that will take place in the cell. Some evidence also shows that classes of GPCRs can have different inactive structures; whether this is also the case for the dopamine D₂ and D₃ receptors remained unclear. Mapping out inactive conformations of receptors is important for drug discovery, as compounds called antagonists can bind to inactive receptors and interfere with their activation.

Lane et al. proposed that different types of antagonists could prefer specific types of inactive conformations of the dopamine D₂ and D₃ receptors. Based on the structures of these two receptors, the conformations of D₂ bound with the drugs risperidone and eticlopride (two dopamine antagonists) were simulated and compared. The results show that the inactive conformations of D₂ were very different when it was bound to eticlopride as opposed to risperidone. In addition D₂ and D₃ showed a very similar conformation when attached to eticlopride. The two drugs also bound to the inactive receptors in overlapping but different locations. These computational findings, together with experimental validations, suggest that D₂ and D₃ exist in several inactive states that only allow the binding of specific drugs; these states could also reflect different degrees of inactivation. Overall, the work by Lane et al. contributes to a more refined understanding of the complex conformations of GPCRs, which could be helpful to screen and develop better drugs.

the development of biased agonists that couple preferentially to a particular effector pathway (Free et al., 2014; Manglik et al., 2016; McCorvy et al., 2018), less attention has been dedicated to the possibility that different antagonist scaffolds with differing efficacy of inverse agonism might lead to different receptor conformations and hence different 'inactive' states. Such a possibility could have a major impact on RDD for antagonists, since a GPCR crystal structure stabilized by a particular antagonist might represent an invalid docking target for an antagonist that prefers a different inactive conformation. Although substantial differences in antagonist binding mode and position of the binding pockets have been revealed among different aminergic receptors, no conformational differences has been detected for the inactive state in any individual aminergic receptor (Michino et al., 2015a). In particular, although a number of antagonists derived from different scaffolds have been co-crystallized with the β₂ adrenergic receptor, conformational differences among these crystal structures are minimal (Michino et al., 2015a).

Curiously, the inactive state structures of the highly homologous dopamine D₂ and D₃ receptors (D₂R and D₃R) revealed substantial differences on the extracellular side of the transmembrane domain, especially in TM6 (Figure 1), when bound with antagonists derived from different scaffolds (Chien et al., 2010; Wang et al., 2018). Specifically, the D₃R structure is in complex with eticlopride, a substituted benzamide (PDB: 3PBL) (Chien et al., 2010), while the D₂R structure is bound with risperidone, a benzisoxazole derivative (PDB: 6CM4) (Wang et al., 2018). The binding poses of the two ligands differ substantially. Risperidone is oriented relatively perpendicular to the membrane plane with its benzisoxazole ring penetrating into a hydrophobic pocket beneath the orthosteric binding site (OBS) of D₂R; in contrast, eticlopride is oriented relatively parallel to the membrane plane and contacts the extracellular portion of TM5 in D₃R, a sub-pocket that risperidone does not occupy in D₂R (Sibley and Shi, 2018; Wang et al., 2018). Nemonapride, another substituted benzamide, binds in the OBS of the slightly divergent D₄R (PDB: 5WIV) (Wang et al., 2017) in a manner very similar to that of eticlopride in the D₃R (Sibley and Shi, 2018).

Importantly, the co-crystallized ligands (risperidone, eticlopride, and nemonapride) display little subtype selectivity across D₂R, D₃R, and D₄R (Chien et al., 2010; Hirose and Kikuchi, 2005; Silvestre and Prous, 2005; Wang et al., 2017) (also see PDSP database; Roth et al., 2000). Given

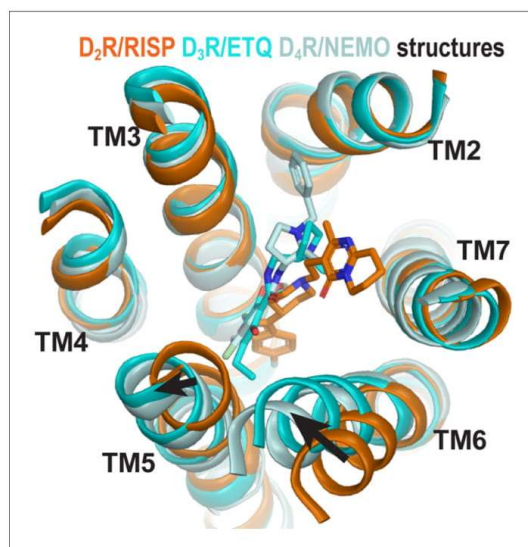


Figure 1. The structures of homologous D₂R, D₃R, and D₄R show different conformations in the extracellular vestibules. Superpositioning of D₂R, D₃R, and D₄R structures shows that the binding of eticlopride (ETQ, cyan) in D₃R and nemonapride (NEMO, pale cyan) in D₄R result in outward and inward rearrangements of the extracellular portions of TM5 and TM6, respectively, compared to the binding of risperidone (RISP, orange) in D₂R. The online version of this article includes the following figure supplement(s) for figure 1:

Figure supplement 1. Chemical structure alignments of the non-selective D₂-like receptors ligands.

the high homology among these D₂-like receptors, especially between D₂R and D₃R, the drastic conformational differences between the inactive state structures of these receptors may be better explained by different binding poses of antagonists bearing different scaffolds rather than inherent differences in the receptors. Thus, we hypothesized that different antagonist scaffolds may favor distinct inactive conformations of D₂R. To test this hypothesis, we carried out extensive molecular dynamics (MD) simulations of D₂R in complex with non-selective antagonists derived from different scaffolds to characterize the plasticity of the OBS and the extracellular loop dynamics in the inactive conformational state.

Results

The Ile^{3.40} sub-pocket is occupied by risperidone and spiperone but not eticlopride in D₂R

Compared to eticlopride bound in the D₃R structure, risperidone in the D₂R structure penetrates deeper into the binding site, with its benzisoxazole moiety occupying a sub-pocket that eticlopride does not reach. By examining the D₂R/risperidone structure, we found that the benzisoxazole moiety is enclosed by eight residues in D₂R, which are identical among all D₂-like receptors (i.e. D₂R, D₃R, and D₄R): Cys118^{3.36} (superscripts denote Ballesteros-Weinstein numbering *Ballesteros and Weinstein, 1995*), Thr119^{3.37}, Ile122^{3.40}, Ser197^{5.46}, Phe198^{5.47}, Phe382^{6.44}, Trp386^{6.48}, and Phe390^{6.52}. Notably, three of these residues (Ile122^{3.40}, Phe198^{5.47}, and Phe382^{6.44}) on the intracellular side of the OBS that we previously defined (*Michino et al., 2015a*), accommodate the F-substitution at the tip of the benzisoxazole ring in a small cavity (termed herein as the Ile^{3.40} sub-pocket) (*Figure 2a*). Both Ile122^{3.40} and Phe382^{6.44} of this Ile^{3.40} sub-pocket are part of the conserved Pro^{5.50}-Ile^{3.40}-Phe^{6.44} motif that undergoes rearrangement upon receptor activation (*Rasmussen et al., 2011*), and

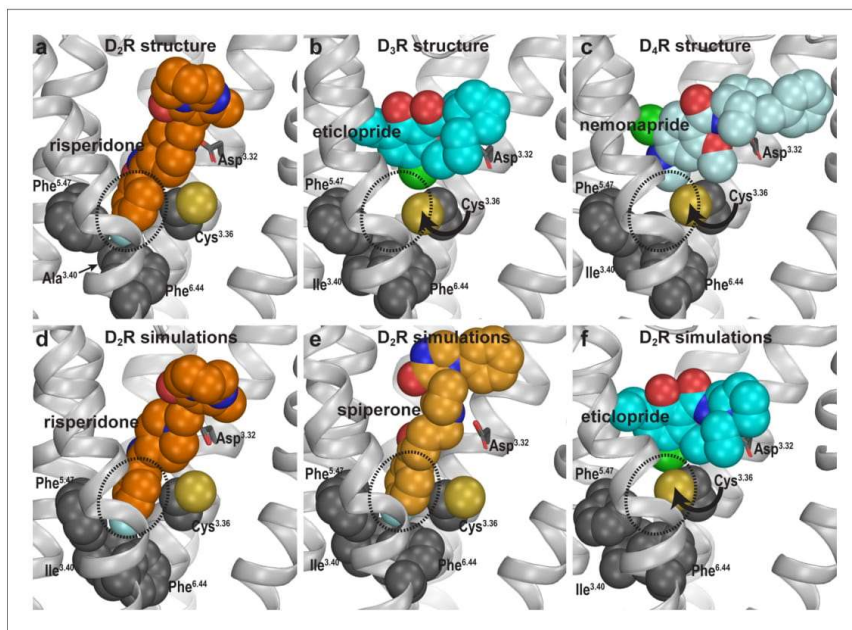


Figure 2. Divergent occupations of the Ile^{3.40} sub-pocket by non-selective ligands from different scaffolds. In the D₂R structure (a), the F-substitution on the benzisoxazole ring of risperidone occupies the Ile^{3.40} sub-pocket (dotted circle) enclosed by conserved Ile^{3.40} (mutated to Ala in the crystal structure to thermostabilize the receptor), Phe^{5.47}, and Phe^{6.44}. The same viewing angle shows that in the D₃R (b) and D₄R (c) structures, Cys^{3.36} rotates to fill in the Ile^{3.40} sub-pocket, and the substituted benzamides eticlopride and nemonapride cannot occupy the aligned sub-pockets. In our D₂R/risperidone simulations (d), risperidone maintains its pose revealed by the crystal structure. In the D₂R/spiperone simulations (e), the Ile^{3.40} sub-pocket is similarly occupied as in D₂R/risperidone. In the D₂R/eticlopride simulations (f), the Ile^{3.40} sub-pocket is collapsed as in the D₃R (b) and D₄R (c) structures (this trend is independent of the force field being used in the simulations).

The online version of this article includes the following figure supplement(s) for figure 2:

Figure supplement 1. Allosteric communication between the Ile^{3.40} sub-pocket and the Na⁺ binding site.

we have found that the I122^{3.40}A mutation renders D₂R non-functional (Klein Herenbrink *et al.*, 2019; Wang *et al.*, 2018). Interestingly, this Ile^{3.40} sub-pocket is collapsed in both the D₃R and D₄R structures (Sibley and Shi, 2018; Figure 2b,c). We noted that this collapse is associated with rotation of the sidechain of Cys^{3.36}: In the D₂R/risperidone structure, the sidechain of Cys^{3.36} faces the OBS, whereas in the D₃R/eticlopride and D₄R/nemonapride structures, it rotates downwards to partially fill the Ile^{3.40} sub-pocket (Figure 2a–c).

To test our hypothesis that these observed differences in the crystal structures are due to the binding of antagonists bearing different scaffolds but not intrinsic divergence of D₂-like receptors, we compared the binding modes of three non-selective antagonists in D₂R. We reverted three thermostabilizing mutations introduced for crystallography (I122^{3.40}A, L375^{6.37}A, and L379^{6.41}A) back to their WT residues, established WT D₂R models in complex with risperidone, spiperone, or eticlopride, and carried out extensive MD simulations (see Materials and methods, Figure 1—figure supplement 1 and Table 1).

In our prolonged MD simulations of the WT D₂R/risperidone complex (>65 μ s, Table 1), we observed that risperidone stably maintains the binding pose captured in the crystal structure, even without the thermostabilizing mutations (Figure 2d). Thus, the I122^{3.40}A mutation has minimal impact on the binding pose of risperidone. Interestingly, in the simulations of the WT D₂R model in

Table 1. Summary of molecular dynamics simulations.

Receptor	Ligand	Bound na ⁺	Number of OPLS3e trajectories	Number of CHARMM36 trajectories	Accumulated simulation time (ns)
D ₂ R	Risperidone	+	12		28410
		-	11		42240
	Spiperone	+	22		42000
		-	17		29550
	Eticlopride	+	5	12	51540
		-	7		11280
	(-)-Sulpiride	+	3		4500
		-	3		3600
	Aripiprazole	+	40		66660
D ₃ R	Eticlopride	+		3	13200
		-		4	6240
	R22	+		7	33600
	S22	-		7	59400
Total			120	33	392220

complex with spiperone, a butyrophenone derivative, the F-substitution on the butyrophenone ring similarly occupies the Ile^{3.40} sub-pocket as risperidone (**Figure 2e**). Note that the F-substitutions in risperidone and spiperone are located at similar distances to the protonated N atoms that interact with Asp^{3.32} (measured by the number of carbon atoms between them, **Figure 1—figure supplement 1**) and these two ligands appear to be optimized to occupy the Ile^{3.40} sub-pocket.

In contrast, in our simulations of the D₂R/eticlopride complex, the eticlopride pose revealed in the D₃R structure (PDB: 3PBL) is stable throughout the simulations and does not protrude into the Ile^{3.40} sub-pocket (**Figure 2f**). Consistent with the difference in the crystal structures noted above (**Figure 2a,b**), when risperidone and spiperone occupy the Ile^{3.40} sub-pocket, the sidechain of Cys118^{3.36} rotates away with its χ_1 rotamer in *gauche*-, while in the presence of the bound eticlopride, this rotamer is stable in *trans* (**Figure 2—figure supplement 1**).

To validate these computational findings regarding the occupation of the Ile^{3.40} sub-pocket, we mutated Ile122^{3.40} of WT D₂R to both Trp and Ala and characterized how these mutations affect the binding affinities for spiperone, risperidone, and eticlopride (**Table 2**). We hypothesized that the bulkier sidechain of Trp at position 3.40 would hamper the binding of spiperone and risperidone

Table 2. The effect of mutations on the binding affinities of selected D₂R ligands.

The affinities of [³H]spiperone were determined in saturation experiments at WT or mutant SNAP-tagged D₂Rs stably expressed in FlpIn CHO cells. Binding affinity values for risperidone and eticlopride were obtained in competition binding experiments. Means of *n* independent experiments performed in triplicate are shown with 95% confidence intervals.

SNAP-D ₂ R	[³ H]spiperone saturation binding		[³ H]spiperone competition binding			
	pK _d (K _d , nM) (95% CI)	N	Risperidone pK _i (K _i , nM) (95% CI)	N	Eticlopride pK _i (K _i , nM) (95% CI)	N
WT	9.74 (0.18) (9.36–10.14)	3	8.55 (2.8) (8.07–9.04)	8	9.84 (0.14) (9.10–10.58)	3
WT -Na ⁺	9.70 (0.20) (9.09–10.32)	3	8.96 (1.1) (8.84–9.08)	6	-	
I122 ^{3.40} A	9.74 (0.18) (9.09–10.38)	3	8.14 (7.9) (7.97–8.32)	8	10.33 (0.04) (10.22–10.44)	3
I122 ^{3.40} W	8.95 (1.15) (8.59–9.30)	3	7.43 (37) (7.11–7.75)	5	9.61 (0.25) (9.33–9.89)	4

since they occupy the Ile^{3.40} sub-pocket but have no effect on eticlopride binding, while the smaller Ala should not affect the binding of spiperone or risperidone. Consistent with this hypothesis, the I122W mutation decreased the binding affinities of risperidone (13-fold) and spiperone (6-fold) compared to WT but had no effect on that of eticlopride. In contrast, the I122A mutation did not affect the affinities of spiperone or risperidone, which is consistent with our simulation results that show the I122A mutation has minimal impact on risperidone binding. In contrast, I122A caused a threefold increase in the affinity of eticlopride, suggesting that the I122A mutation may promote an inactive conformation of D₂R that favors eticlopride binding. Together these results support our proposal that different antagonist scaffolds may favor distinct inactive conformations of D₂R.

Occupation of the Ile^{3.40} sub-pocket confers insensitivity to Na⁺ in antagonist binding

Ligand binding in D₂-like receptors can be modulated by Na⁺ bound in a conserved allosteric binding pocket coordinated by Asp^{2.50} and Ser^{3.39} (Michino et al., 2015b; Neve, 1991; Wang et al., 2017). Note that the aforementioned Cys^{3.36} and Ile^{3.40} are adjacent to the Na⁺ coordinating Ser^{3.39}; thus, we further hypothesized that the occupation of the Ile^{3.40} sub-pocket by spiperone or risperidone makes them insensitive to Na⁺. To test this hypothesis, we simulated D₂R/risperidone, D₂R/spiperone, D₂R/eticlopride, and D₂R/(-)-sulpiride complexes in the presence versus absence of bound Na⁺ (Table 1). Interestingly, the occupancy of the Ile^{3.40} sub-pocket by either spiperone or risperidone was unaffected by the presence or absence of bound Na⁺ (Figure 2—figure supplement 1). In contrast, while the poses of eticlopride and (-)-sulpiride are highly stable in the presence of bound Na⁺, they oscillated between different poses in the absence of Na⁺. These oscillations are associated with the sidechain of Cys^{3.36} swinging back and forth between the two rotamers, suggesting an important role of Na⁺ binding in stabilizing the poses of eticlopride and (-)-sulpiride and the configuration of the Ile^{3.40} sub-pocket (Figure 2—figure supplement 1). Interestingly, the previous MD simulations described by Wang et al. indicated that nemonapride's binding pose in D₄R is more stable in the presence of bound Na⁺ as well (Wang et al., 2017).

Consistent with these computational results, we have previously shown that spiperone binding is insensitive to the presence of Na⁺, while the affinities of eticlopride and sulpiride are increased in the presence of Na⁺ (Michino et al., 2015b). In this study, we performed binding experiments in the absence or presence of Na⁺ and found the affinity of risperidone to be unaffected, in accordance with this hypothesis (Table 2).

Together these findings support our hypothesis that the ability of a ligand to bind the Ile^{3.40} sub-pocket relates with its sensitivity to Na⁺ in binding, due to allosteric connections between the sub-pocket and the Na⁺ binding site.

Functional consequences of distinct antagonist-bound inactive conformations

To further investigate the functional impact of these conformational differences surrounding the OBS, we used a bioluminescence resonance energy transfer (BRET) assay, which measures conformational changes of the Go protein heterotrimer following activation by D₂R (Michino et al., 2017), to evaluate the inverse agonism activities of several representative D₂R ligands. These ligands can be categorized into two groups according to their sensitivities to Na⁺ in binding at D₂R, which have been characterized either in our current study or in previous studies (Michino et al., 2015b; Neve, 1991; Newton et al., 2016). While risperidone, spiperone, and (+)-butaclamol have been found to be insensitive to Na⁺ in binding, (-)-sulpiride, eticlopride, and raclopride show enhanced binding affinities in the presence of Na⁺. Using quinpirole as a reference full agonist, we found that the Na⁺ insensitive ligands display significantly greater inverse agonism (< -30% that of the maximal response of quinpirole) relative to the Na⁺-sensitive ligands (> -15% that of the maximal response of quinpirole, Figure 3). These observations are consistent with findings from earlier [³⁵S]GTPγS binding experiments of Roberts and Strange in which (+)-butaclamol, risperidone, and spiperone were found to inhibit significantly more [³⁵S]GTPγS binding than raclopride and (-)-sulpiride (Roberts and Strange, 2005). Of note, these [³⁵S]GTPγS-binding experiments were performed in the absence of Na⁺.

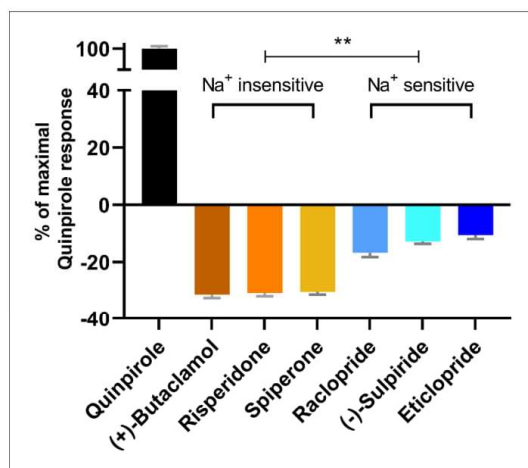


Figure 3. The extent of inverse agonism is negatively related with the Na⁺ sensitivity of ligand binding. In a D₂R-Go BRET assay, the maximal responses of the indicated ligands are normalized to that of the reference full agonist quinpirole. The ligands that are insensitive to Na⁺ in D₂R binding display significantly higher inverse agonism (in each case, **p<0.0001 using ordinary one-way ANOVA followed by Tukey's multiple comparisons test) than the Na⁺-sensitive ligands; however, within the Na⁺-sensitive group, raclopride is significantly different from eticlopride (p=0.005).

Based on these functional data together with the different binding modes revealed by our computational simulations, we propose that ligands that occupy the Ile^{3.40} sub-pocket exhibit a greater level of inverse agonism as compared to those that do not. Therefore, across the tested inverse agonists there is a negative relation between ligand sensitivity to Na⁺ and the extent of inverse agonism at D₂R. The differential occupation of the Ile^{3.40} sub-pocket is the structural basis for the Na⁺ sensitivity, which contributes significantly to the extent of inverse agonism of the tested ligands.

Plasticity of the ligand-binding site propagates to affect the overall receptor conformation

By occupying the Ile^{3.40} sub-pocket, the benzisoxazole moiety of risperidone pushes the conserved Phe^{6.52} away from the binding site in the D₂R/risperidone structure compared to its position in the D₃R/eticlopride structure. This interaction is responsible for positioning the aromatic cluster of TM6 and TM7 (Trp^{6.48}, Phe^{6.51}, Phe^{6.52}, His^{6.55}, and Tyr^{7.35}) in D₂R differently from its configurations in the D₃R and D₄R structures, resulting in an overall outward positioning of the extracellular portion of TM6 in D₂R (Figure 4—figure supplement 1). On the extracellular side of the OBS, the space near Ser^{5.42} and Ser^{5.43} that accommodates the bulky substitutions of the benzamide rings of the bound eticlopride and nemonapride in the D₃R and D₄R structures is not occupied by risperidone in D₂R, which is likely associated with the inward movement of the extracellular portion of TM5 in D₂R relative to those in the D₃R and D₄R structures (Figure 1).

To evaluate whether these conformational rearrangements are due to the minor divergence in these regions of the receptors or to the ligand-binding site plasticity that accommodates ligands bearing different scaffolds, we compared the resulting conformations of D₂R bound with risperidone or eticlopride. We observed the same trend of rearrangements of the transmembrane segments surrounding the OBS in the resulting receptor conformations from our D₂R/risperidone and D₂R/eticlopride simulations (Figure 4a), that is, an inward movement of TM6 and outward movement of TM5 in the presence of the bound eticlopride (Figure 4b,c). Without such movements in D₂R/eticlopride, Ser193^{5.42} and Ser194^{5.43} would clash with the bound eticlopride (Figure 4a). These

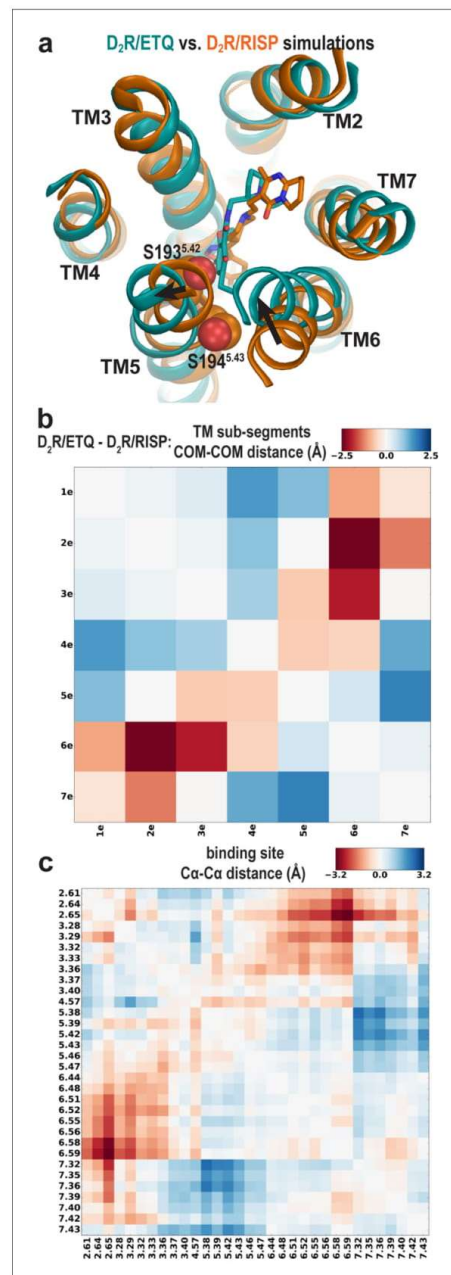


Figure 4. The different conformations in the extracellular vestibules of D_2R and D_3R are likely due to binding of non-selective ligands from different scaffolds. (a) Compared to the comparison of the crystal structures shown in Figure 1, superpositioning of representative frames of the D_2R/ETQ and $D_2R/RISP$ simulations shows a similarly trend of the outward and inward movements of TM5 and TM6, respectively, in the presence of the bound ETQ, Figure 4 continued on next page

Figure 4 continued

even when the simulations were started from the D₂R conformation stabilized by RISP. Note Ser193^{5,42} and Ser194^{5,43} would clash with the bound eticlopride if there was no conformational adjustment. (b, c) PIA-GPCR analysis (see Materials and methods) comparing the D₂R/ETQ and D₂R/RISP conformations. The analysis of the pairwise-distance differences among the subsegments (b) indicates that TM6e moves inward (smaller distance to TM2e, dark red pixel), while TM5e moves outward (larger distances to TM7e, dark blue pixel) in the D₂R/ETQ simulations. The analysis of pairwise-distance differences among the C α atoms of the ligand-binding residues (c) indicates significant changes near residues Phe189^{5,38}, Ser193^{5,42}, Asn367^{6,58}, and Ile368^{6,59} (darker colored pixels). The online version of this article includes the following figure supplement(s) for figure 4:

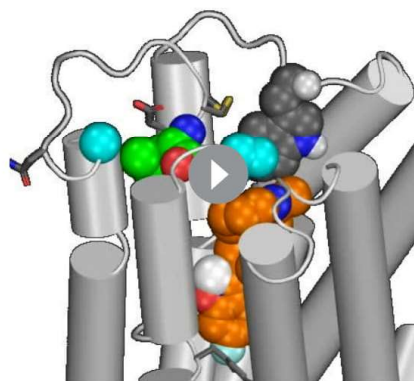
Figure supplement 1. The occupation of the Ile^{3,40} pocket by risperidone is associated with outward movement of the extracellular portion of TM6.

findings further support our inference that differences between the D₂R and D₃R inactive structures are largely due to the different scaffolds of the bound non-selective ligands.

The extracellular loop 2 (EL2) of D₂R/risperidone can spontaneously unwind

In addition to differences in the transmembrane segments surrounding the OBS, there are also substantial differences in the configuration of EL2 in the D₂R and D₃R structures. EL2 between TM4 and TM5 is connected to TM3 via a disulfide bond formed between Cys^{EL2,50} (see Materials and methods and *Figure 5—figure supplement 1* for the indices of EL1 and EL2 residues) and Cys^{3,25}. The conformation of EL2, the sequence of which is not conserved among aminergic GPCRs, is expected to be dynamic. Indeed, in the D₂R/risperidone structure, the sidechains of residues 176^{EL2,40}, 178^{EL2,46}, 179^{EL2,47}, and 180^{EL2,48}, which are distal to the OBS were not solved, likely due to their dynamic nature. Curiously, the portion of EL2 C-terminal to Cys182^{EL2,50} (residues 182^{EL2,50}-186^{EL2,54}), which forms the upper portion of the OBS that is in contact with ligand, is in a helical conformation in the D₂R/risperidone structure.

Strikingly, in our MD simulations of D₂R complexes, we found that this helical region showed a tendency to unwind (*Video 1*). The unwinding of EL2 involves a drastic rearrangement of the sidechain of Ile183^{EL2,51}, which dissociates from a hydrophobic pocket formed by the sidechains of Val111^{3,29}, Leu170^{4,60}, Leu174^{EL2,38}, and Phe189^{5,38}. Specifically, the unwinding process is initiated by the loss of a hydrogen-bond (H-bond) interaction between the sidechain of Asp108^{3,26} and the backbone amine group of Ile183^{EL2,51} formed in the D₂R/risperidone structure (*Figure 5—figure supplement 2b*, step (i)). When this interaction is broken, the orientation of residues 182^{EL2,50}-186^{EL2,54} deviates markedly from that of the crystal structure, losing its helical conformation (see below). Subsequently, the sidechain of Ile183^{EL2,51} rotates outwards and passes a small steric barrier of Gly173^{EL2,37} (*Figure 5—figure*



Video 1. A movie of a 4.2 μ s D₂R/risperidone trajectory collected using the OPLS3e force field shows spontaneous unwinding of EL2. The conformation of EL2 gradually transitions to an extended configuration similar to that in the D₃R structure. See *Figure 5—figure supplement 2* for the pathway of unwinding. Note that the extended conformation of EL2 stabilizes Trp100^{EL1,50}. The C α atom of Gly173^{EL2,37}, the sidechains of Trp100^{EL1,50}, Ile183^{EL2,51}, and Ile184^{EL2,52} and the bound risperidone are shown as spheres. Asp108^{3,26} and the disulfide bond between Cys107^{3,25} and Cys182^{EL2,50} are shown as sticks. The carbon atoms of Gly173^{EL2,37} and Ile184^{EL2,52} are colored in cyan, those of Ile183^{EL2,51} are in green, those of Trp100^{EL1,50}, Cys107^{3,25}, Asp108^{3,26}, Asn175^{EL2,39}, and Cys182^{EL2,50} are in dark gray; those of the bound ligand risperidone are in orange.

<https://elifesciences.org/articles/52189#video1>

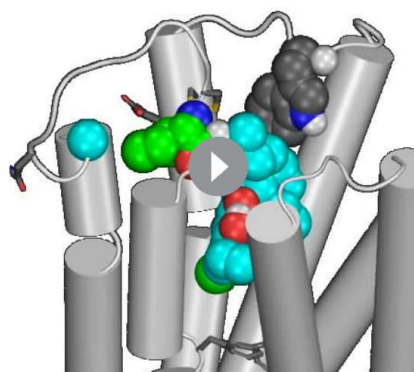
supplement 2b, step (ii), and in some trajectories makes a favorable hydrophobic interaction with the sidechain of Ala177^{EL2.45}. In a few long trajectories, Ile183^{EL2.51} rotates further toward the extra-cellular vestibule where it can make favorable interactions with hydrophobic or aromatic residues from the N terminus, or the bound risperidone (**Video 1**). Consequently, residues 182^{EL2.50}-186^{EL2.54} are in a fully extended loop conformation while Ile184^{EL2.52} tilts under EL2 (**Figure 5—figure supplement 2b**, step (iii)).

In the D₃R structure, the aligned residue for Asp108^{3.26} of D₂R is conserved as Asp104^{3.26}; its sidechain forms an interaction not with Ile182^{EL2.51} but rather with the sidechain of Asn173^{EL2.39}, which is also conserved in D₂R as Asn175^{EL2.39}. In the D₄R, the aligned two residues (Asp109^{3.26} and Asn175^{EL2.39}) are conserved as well, their sidechains are only 4.3 Å away in the D₄R structure, a distance slightly larger than the 3.2 Å in the D₃R structure. Even though these residues are conserved in D₂R, the interaction in D₃R (and potentially in D₄R), between Asp^{3.26}-Asn^{EL2.39}, is not present in the D₂R structure in which the aligned Asn175^{EL2.39} faces lipid (**Figure 5—figure supplement 2a**). However, in a few of our long D₂R simulations, Asn175^{EL2.39} gradually moves inwards and approaches Asp108^{3.26} (**Figure 5—figure supplement 2b**, step (iv)). At this point, the EL2 conformation of D₂R is highly similar to that of D₃R (**Figure 5—figure supplement 2c**), suggesting that EL2 is dynamic and can exist in both conformations.

We evaluated the tendency of the EL2 helix to unwind in each of the simulated D₂R complexes by measuring the stability of the backbone H-bond between Ile183^{EL2.51} and Asn186^{EL2.54}, a key stabilizing force of the helix (**Figure 5a**). When we plotted the Ile183^{EL2.51}-Asn186^{EL2.54} distance against the Asp108^{3.26}-Ile183^{EL2.51} distance for each D₂R complex (**Figure 5b**), we found that the loss of the Asp108^{3.26}-Ile183^{EL2.51} interaction increases the probability of breaking the Ile183^{EL2.51}-Asn186^{EL2.54} H-bond, that is the unwinding of EL2. Interestingly, in all our simulated D₂R complexes, EL2 has a clear tendency to unwind, regardless of the scaffold of the bound ligand (**Figure 5c,d**, **Videos 1–3**). Note that in the D₃R/eticlopride simulations, the aligned residues Ser182^{EL2.51} and Asn185^{EL2.54} do not form such a H-bond, and EL2 is always in an extended conformation (**Figure 5b–d**). This tendency of EL2 to transition toward the extended conformation is also present in our simulations of D₂R in complex with a partial agonist, aripiprazole, whereas EL2 in the D₃R complexes with partial agonists (R22 and S22) remains in the extended conformation (**Table 1** and **Figure 5—figure supplement 3**). Interestingly, Asp104^{3.26} and Ser182^{EL2.51} can move into interacting range in the D₃R/eticlopride simulations, and the Ser182^{EL2.51}-Asn185^{EL2.54} interaction can sporadically form in the D₃R/R22 simulations – both raise the possibility that the extended conformation of D₃R EL2 may transition to a helical conformation.

Interestingly, in one of our long MD trajectories of the D₂R/risperidone complex, EL2 evolved into a conformation that has a helical N-terminal portion and an extended C-terminal portion (**Video 4** and **Figure 5—figure supplement 4**). This conformation is not observed in either of the D₂R/risperidone and D₃R/eticlopride structures but is similar to that of the 5-HT_{2A}R/risperidone structure, further demonstrating the dynamics of this loop region (**Figure 5—figure supplement 4**).

In marked contrast to the obvious trend toward unwinding of EL2 in all our simulated D₂R complexes, in our recent simulations of MhsT, a transporter protein with a region found by crystallography to alternate between helical and unwound conformations (Malinauskaite et al., 2014), we failed to observe any spontaneous unwinding over a similar simulation timescale



Video 2. A movie of a 4.2 μs D₂R/eticlopride trajectory shows the dynamics of Trp100^{EL1.50} when the C-terminal portion of EL2 is in a helical conformation. Note that Trp100^{EL1.50} can be stabilized by interacting with the disulfide bond. The presentation and color scheme are similar to those in **Video 1**, except that the bound carbon atoms of the ligand eticlopride are colored in cyan.

<https://elifesciences.org/articles/52189#video2>

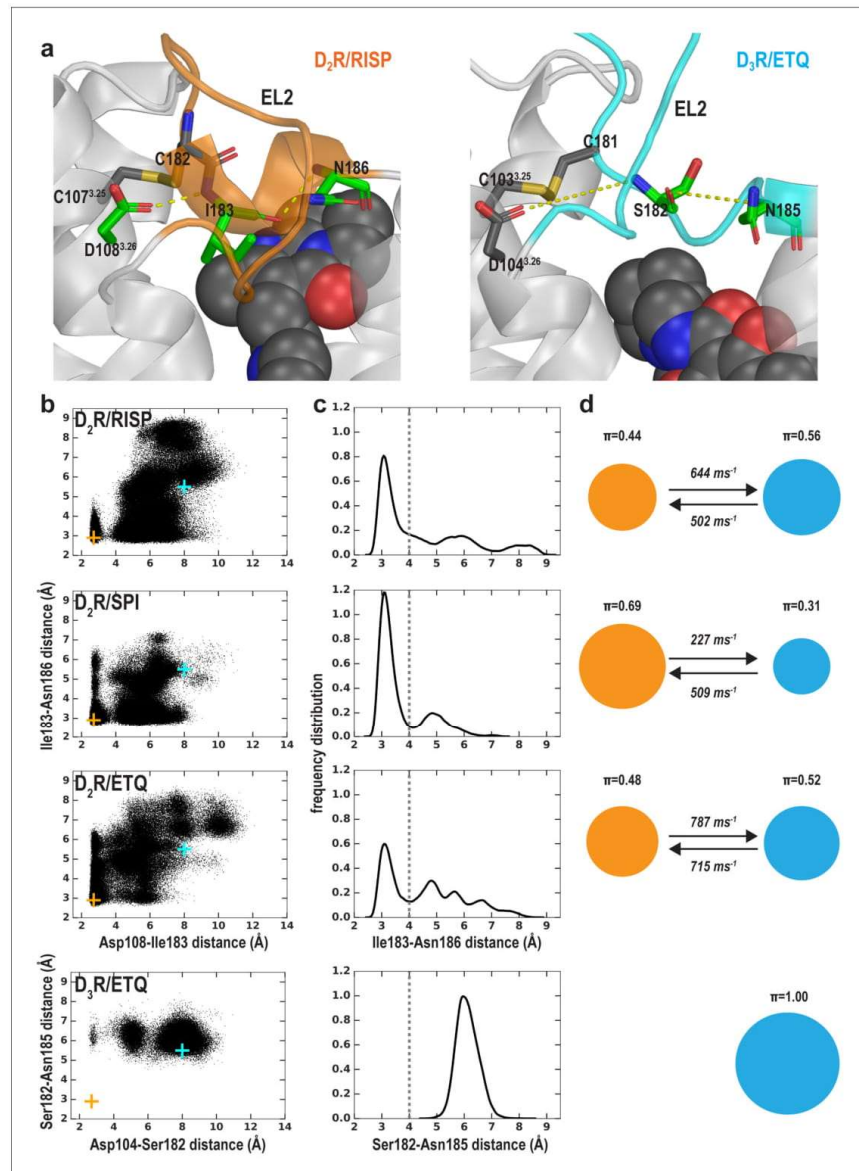


Figure 5. The helical conformation of EL2 in the D₂R/risperidone structure has a tendency to unwind in our simulations, regardless of the bound ligand. (a) The Ile183^{EL2.51}-Asn186^{EL2.54} backbone H-bond and the Ile183^{EL2.51}-Asp108^{3.26} interaction in D₂R and their aligned interactions in D₃R. (b) The scatter plots of the two distances in the indicated D₂R and D₃R complexes. The orange and cyan crosses indicated the distances in the D₂R/risperidone and D₃R/eticlopride structures, respectively. (c) The distributions of the EL2.51-EL2.54 distances in the indicated simulations. These distances were used to evaluate the tendency to unwind using Markov state model (MSM) analysis in (d). (d) The MSM analysis of the transition between the helical and extended conformational states of EL2. The area of each disk representing a state is proportional to the equilibrium probability. Figure 5 continued on next page

Figure 5 continued

probability (π) in each simulated condition. The values from the maximum likelihood Bayesian Markov model for π and transition rates from 500 Bayesian Markov model samples are shown. Thus, EL2 in all the D₂R complexes show significant tendencies to unwind, while that in D₃R/eticlopride remains extended.

The online version of this article includes the following figure supplement(s) for figure 5:

Figure supplement 1. Sequence alignment and residue indices of EL1 and EL2 for the receptors being compared in this study.

Figure supplement 2. The helical region of EL2 of D₂R can spontaneously unwind to an extended conformation similar to that of D₃R.

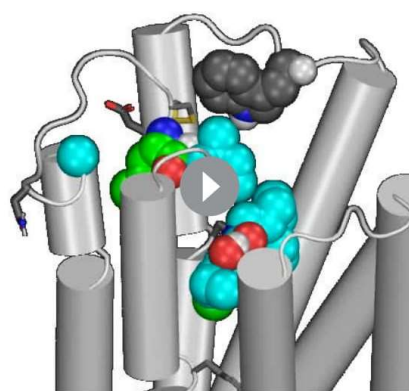
Figure supplement 3. The MSM analysis of Ile183-Asn186 distance in the simulations of the D₂R/aripiprazole, D₃R/S22, and D₃R/R22 complexes (Table 1).

Figure supplement 4. The distinct D₂R EL2 conformations revealed by the MD simulations are similar to those of homologous receptors.

Figure supplement 5. The accessibility pattern of EL2 revealed by previous SCAM studies in D₂R is more consistent with an extended EL2 conformation similar to that in the D₃R/eticlopride structure.

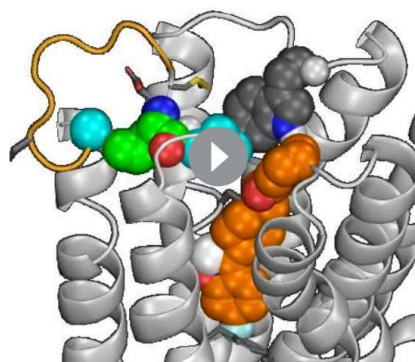
Figure supplement 6. Implied timescales (ITS) for the MSM analysis.

(with the longest simulations being ~5–6 μ s) when the region was started from the helical conformation (Abramyan et al., 2018; Stolzenberg et al., 2017). This shows how difficult it can be to capture known dynamics in simulations and suggests that the C-terminal helical conformation of EL2 in D₂R represents a higher energy state than the extended conformation, which allows for observation of the transitions in a simulation timescale not usually adequate to sample folding/unfolding events (Piana et al., 2011).



Video 3. A movie of a 3.6 μ s D₂R/eticlopride trajectory collected using the CHARMM36 force field shows another example of unwinding of EL2. Thus, considering the similar unwinding pathway as that in Video 1 (Figure 5—figure supplement 2), the unwinding does not depend on the force field used in the simulations or the identity of the antagonist bound in the OBS. Note the sidechain of Asn175^{EL2.39} rotates inward and approaches Asp108^{3.26} in this trajectory. The presentation and color scheme are the same as those in Video 2.

<https://elifesciences.org/articles/52189#video3>



Video 4. A movie of a 4.5 μ s D₂R/risperidone trajectory shows the N-terminal portion of EL2 can transition into a helical conformation when the C-terminal portion is extended. This is a novel EL2 conformation that has not been revealed by the D₂R, D₃R or D₄R structures but similar to those in the 5-HT_{2A}R/risperidone (Figure 5—figure supplement 4f), β_1 AR and β_2 AR structures. The presentation and color scheme are the same as those in Video 1.

<https://elifesciences.org/articles/52189#video4>

Both the EL2 conformation and ligand scaffold affect the EL1 conformation

We have previously shown that the divergence in both the length and number of charged residues in EL1 among D₂R, D₃R, and D₄R is responsible for the selectivity of more extended ligands (Michino *et al.*, 2013; Newman *et al.*, 2012). Another striking difference in the D₂R, D₃R, and D₄R structures is the position of the conserved Trp^{EL1.50} in EL1. Trp100^{EL1.50} is in a much more inward position in the D₂R structure, making a direct contact with the bound risperidone (Figure 6a), Trp101^{EL1.50} in D₄R interacts with the bound nemonapride that has an extended structure, whereas Trp96^{EL1.50} in D₃R is not in contact with eticlopride (Figure 6b). Thus, we asked whether these distinct positions of Trp^{EL1.50} are due to the divergence in EL1 among these receptors (Michino *et al.*, 2013) or due to the multiple inactive conformations that differentially accommodate the binding of non-selective ligands of divergent scaffolds.

When residues 182^{EL2.50}-186^{EL2.54} of EL2 are in a helical conformation, in the D₂R/risperidone simulations, we found that there is more room in the extracellular vestibule and the position of Trp100^{EL1.50} is flexible and can adopt several positions and orientations (Figure 6c,e,f). In the D₂R/eticlopride simulations, Trp100^{EL1.50}, which cannot interact with eticlopride, shows more flexibility than that observed in the presence of risperidone and can move to a similar position like that of Trp96^{EL1.50} in the D₃R structure (Figure 6—figure supplement 1 and Video 2). Interestingly, in this position, the conformation of Trp^{EL1.50} can be stabilized by the disulfide bond of EL2 (Joerger *et al.*, 1999) (as shown in Video 2) or by interaction with the N terminus, which was truncated in the receptor construct used in the determination of the crystal structure. In the D₂R/spiperone simulations, the phenyl substitution on the triazaspiro[4.5]decane moiety protrudes toward the interface between TM2 and TM3, and contacts Trp100^{EL1.50}, which is flexible as well and can adopt a position that is even further away from the OBS than that of Trp96^{EL1.50} in the D₃R structure (Figure 6—figure supplement 1).

In contrast, when EL2 is in an extended conformation like that in D₃R, it restricts the flexibility of Trp100^{EL1.50} (Video 3). This trend is consistent with the D₃R/eticlopride simulations in which we do not observe any significant rearrangement of Trp96^{EL1.50} (Figure 6d,e,f).

Thus, we infer that the distinct conformation of Trp100^{EL1.50} in the D₂R structure is a combined effect of the helical EL2 conformation and the favored interaction that Trp100^{EL1.50} can form with the bound risperidone in the crystal structure, the latter of which however, has a limited influence on the binding affinity of risperidone (Wang *et al.*, 2018), consistent with the unstable interaction between risperidone and Trp100^{EL1.50} in our simulations (Figure 6, Video 2). Indeed, in the fully extended EL2 conformation in which Ile183^{EL2.51} rotates to face the extracellular vestibule, Ile183^{EL2.51} makes a direct contact with the bound risperidone, whereas Trp100^{EL1.50} loses its interaction with the ligand entirely (Video 1). Nevertheless, risperidone retains all other contacts in the OBS. In the recently reported 5-HT_{2A}R/risperidone structure (PDB: 6A93) Kimura *et al.* (2019), risperidone has a very similar pose in the OBS as that in the D₂R structure, occupying the Ile^{3.40} sub-pocket as well. However, on the extracellular side of the OBS, EL2 in the 5-HT_{2A}R/risperidone complex is in an extended conformation and the EL2 residue Leu228^{EL2.51} contacting risperidone aligns to Ile183^{EL2.51} of D₂R, whereas the conserved Trp141^{EL1.50} does not interact with risperidone in the 5-HT_{2A}R. It is tempting to speculate that the EL2 and EL1 dynamics we observe in the D₂R/risperidone simulations represents a more comprehensive picture, as the divergent interactions shown in the extracellular loops of the 5-HT_{2A}R/risperidone and D₂R/risperidone structures may not result from differences in the protein sequences of this dynamic region between these two receptors but rather two different static snapshots due to differences in the crystallographic conditions (Note risperidone has similarly high affinities for both D₂R and 5HT_{2A}R; Kimura *et al.*, 2019; Wang *et al.*, 2018).

Thus, the plasticity of the OBS and the dynamics of the extracellular loops appear to be two relatively separated modules in ligand recognition. To the extent of our simulations, we did not detect strong ligand-dependent bias in the EL2 dynamics as we did for the OBS. However, when EL2 is helical, the EL1 dynamics are sensitive to the bound ligand (compare Figure 6 and Figure 6—figure supplement 1); when EL2 is extended, it restricts EL1 dynamics (Figure 6).

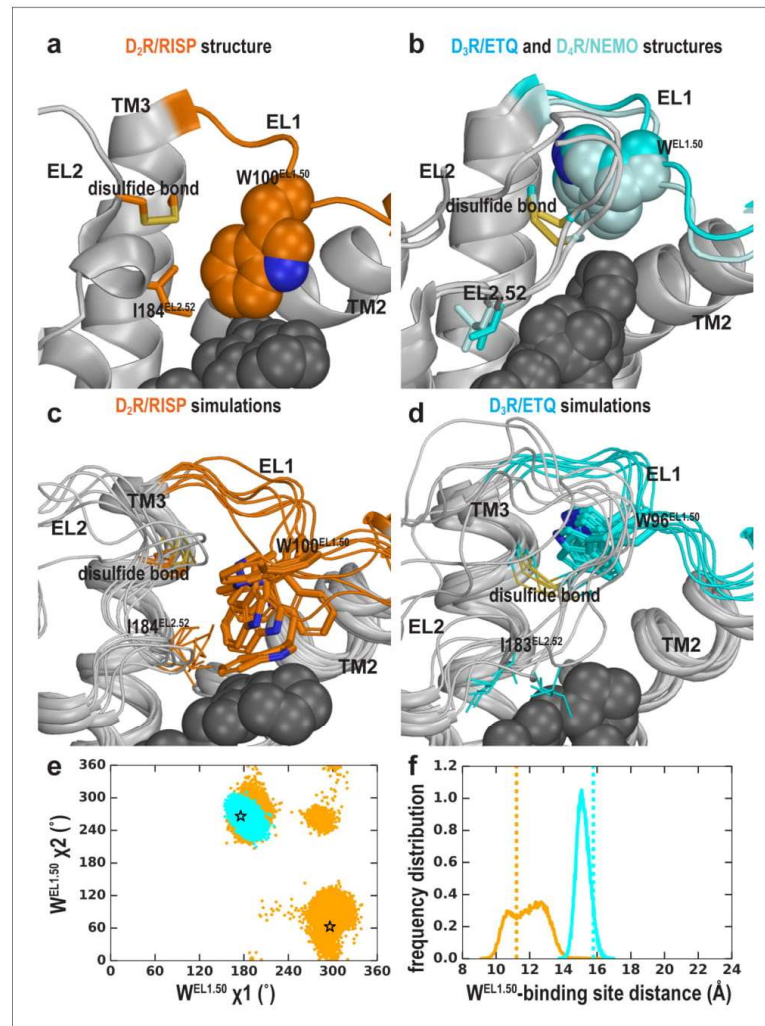


Figure 6. The EL2 conformation affects the EL1 conformation. Divergent EL1-EL2 interfaces among the D₂R (a), D₃R, and D₄R (b) structures. In the D₂R structure, the Trp100^{EL1.50} in EL1 forms a weak interaction with Ile184^{EL2.52}, while the aligned Trp96^{EL1.50} of D₃R and Trp101^{EL1.50} in D₄R are stabilized by their interactions with the disulfide bond – their passages toward the position of Trp100^{EL1.50} in D₂R are blocked by the extended EL2. In our simulations, Trp100^{EL1.50} in D₂R shows significant flexibility and can adopt multiple positions and orientations in D₂R/risperidone (c), while Trp96^{EL1.50} in D₃R is highly stable in D₃R/eticlopride (d). (e) The χ₁ and χ₂ dihedral angles of Trp100^{EL1.50} in the subset of the D₂R/risperidone simulations in which EL2 is still in a helical conformation (orange), are more widely distributed than those of Trp96^{EL1.50} in the D₃R/eticlopride simulations in which EL2 remains in extended conformations (cyan). These dihedral angle values in the D₂R and D₃R structures are indicated with the orange and cyan stars, respectively. (f) For the same two sets of simulations in e, the distance between the center of mass (COM) of the sidechain heavy atoms of Trp100 in D₂R and the COM of the Cα atoms of the ligand-binding site residues (excluding Trp100, see Materials and methods for the list of the residues) has wider distributions than the corresponding distance between Trp96^{EL1.50} in D₃R and its ligand binding site. These distances in the D₂R and D₃R structures are indicated with the orange and cyan dotted lines, respectively.

Figure 6 continued on next page

Figure 6 continued

The online version of this article includes the following figure supplement(s) for figure 6:

Figure supplement 1. EL1 is dynamic in the D₂R/eticlopride and D₂R/spiperone simulations when EL2 is helical.**Figure supplement 2.** Trp^{EL1.50} is closely associated with Leu^{2.64} regardless of the EL2 conformation.**The Ile184^{EL2.52}-Trp100^{EL1.50} interaction is not critical for risperidone binding**

To further investigate the dynamics and coordination of EL2 and EL1 loops, we mutated Leu94^{2.64}, Trp100^{EL1.50}, and Ile184^{EL2.52}, and evaluated the effects of the L94A, W100A, and I184A, mutations on the binding affinities of eticlopride, risperidone, and spiperone. As shown in **Figure 6—figure supplement 2**, Leu94^{2.64} and Trp100^{EL1.50} are closely associated in both the D₂R and D₃R structures, while Ile184^{EL2.52} interacts with Trp100^{EL1.50} only in the D₂R structure. In our time-resolved energy transfer (Tr-FRET) binding experiments, using a fluorescently labeled spiperone derivative (spiperone-d2) as a tracer ligand, we found that both L94A and W100A significantly reduced the affinities of all tested antagonists, whereas I184A only reduced the affinity of eticlopride while it improved that of risperidone (**Table 3**). Thus, the effects of the L94A and W100A mutations have similar trends, which appear independent of the effect of I184A. Indeed, for Trp100 to switch between the positions in the D₂R and D₃R structures, it must pass the steric hinderance of the sidechain of Leu94; thus, some effects of the L94A mutation may reflect its perturbation of the positioning of Trp100, and vice versa.

These findings support our conclusions that the close interaction between Ile184^{EL2.52} and Trp100^{EL1.50} revealed by the D₂R/risperidone crystal structure is not necessary for the stabilization of the risperidone pose. Indeed, in our simulations, EL2 has significant intrinsic dynamics and transitions from the helical to unwound conformation independent of the bound ligands (see above). When it is in an extended conformation, Ile184 is dissociated from Trp100.

The clustering of the binding site conformations

Virtual screening has been widely used as an initial step in drug discovery for novel ligand scaffolds. To this end, we found that D₂R can significantly change its binding site shape to accommodate antagonists bearing different scaffolds, while EL2 is intrinsically dynamic. Thus, it is necessary to comprehensively consider the binding site conformations in virtual screening campaigns against D₂R, because limiting the screening to only a single conformation will miss relevant ligands. Indeed,

Table 3. The effect of mutations on the binding affinities of selected D₂R ligands as determined in Tr-FRET-binding experiments. The affinities of the fluorescently labeled spiperone derivative (Spiperone-d2) or unlabeled antagonists were determined in saturation experiments at WT or mutant SNAP-tagged D₂Rs stably expressed in FlpIn CHO cells. Binding affinity values for risperidone and eticlopride were obtained in competition binding experiments. Means of n independent experiments are shown with 95% confidence intervals (CIs).

SNAP-D ₂ R	Spiperone-d2 saturation binding			Spiperone-d2 competition binding								
	pK_d (K_d , nM) (95% CI)	N	Mut/ WT	Eticlopride pK_i (K_i , nM) (95% CI)	N	Mut/ WT	Risperidone pK_i (K_i , nM) (95% CI)	N	Mut/ WT	Spiperone pK_i (K_i , nM) (95% CI)	N	Mut/ WT
WT	8.54 (2.88) (8.32–8.77)	9	1.0	10.06 (0.09) (9.90–10.21)	8	1.0	8.47 (3.34) (8.15–8.80)	7	1.0	9.96 (0.11) (9.76–10.18)	8	1.0
L94A	7.71 (19.5) (7.41–8.00)*	5	6.8	9.08 (0.83) (8.91–9.23)*	4	9.2	8.02 (9.54) (7.86–8.17)*	5	2.9	8.36 (4.37) (8.21–8.50)*	5	39.7
W100A	7.39 (40.7) (7.21–7.56)*	9	14.1	8.06 (8.71) (7.78–8.32)*	4	96.8	7.60 (25.1) (7.41–7.79)*	7	7.5	8.39 (4.07) (8.19–8.59)*	7	37.0
I184A	8.79 (1.62) (8.58–9.00)	5	0.6	9.34 (0.45) (8.94–9.75)*	4	5	9.33 (0.47) (9.18–9.48)*	5	0.1	9.78 (0.17) (9.51–10.05)	5	1.6

*=significantly different from WT value, p<0.05, one-way ANOVA with Dunnett's post-hoc test.

the strategy of ensemble docking, in which each ligand is docked to a set of receptor conformers, has been adapted in recent virtual screening efforts (Amaro *et al.*, 2018).

To characterize the OBS conformational ensemble sampled by D₂R in complex with ligands bearing different scaffolds in the context of EL2 dynamics, we clustered the OBS conformations in our representative D₂R/eticlopride and D₂R/risperidone MD trajectories in which EL2 transitioned from helical to unwound conformations (see Materials and methods). As expected, the OBS conformations in these two complexes are significantly different and can be easily separated into distinct clusters. For the clustering results shown in Table 4, the average pairwise RMSDs of the OBS residues (apRMSDs, see Materials and methods) between the D₂R/eticlopride and D₂R/risperidone clusters are >1.1 Å, which are similar to that between the D₂R and D₃R structures (1.2 Å), while the apRMSDs within each cluster is smaller than those between any two clusters (Figure 7). Interestingly, at this level of clustering, when the two clusters for each complex are ~0.8–0.9 Å apRMSD away from each other, the extended and helical conformations of EL2 are always mixed in a cluster (Table 4). This observation suggests that the helical versus extended EL2 conformations are not closely associated with the OBS conformations.

Thus, while the centroid frames from each cluster can form an ensemble for future virtual screening for the primary scaffold occupying the OBS, in order to discover novel extended ligands that protrude out of the OBS to interact with EL2 and EL1 residues (Michino *et al.*, 2015a), additional frames that cover both helical and extended EL2 conformations from each cluster will have to be used to screen for the optimal extensions of the primary scaffold.

Discussion

Our results highlight unappreciated conformational complexity of the inactive state of GPCRs and suggest that the risperidone bound D₂R structure represents only one of a number of possible inactive conformations of D₂R. Critically, this conformation is incompatible with the binding of other high-affinity D₂R ligands such as eticlopride. While distinct conformational states responsible for functional selectivity have garnered great attention, the potential existence of divergent inactive conformations is of critical importance as well. By combining *in silico* and *in vitro* findings, we propose that occupation of the Ile^{3.40} sub-pocket by antagonists confers a distinct D₂R conformation that is associated with both a greater degree of inverse agonism and Na⁺ insensitivity in binding, such that Na⁺ sensitivity is negatively related with the extent of inverse agonism for the tested ligands. However, other structural elements may also contribute to the extent of inverse agonism (Zhang *et al.*, 2014). Regardless, the distinct inactive conformations stabilized by antagonists with different scaffolds may reflect different degrees of inactivation.

In addition to advancing our mechanistic understanding of receptor function, our findings have implications for high-throughput virtual screening campaigns, as important hits would be missed by focusing on a single inactive state captured in a crystal structure that is stabilized by an antagonist bearing a specific scaffold. Moreover, rational lead optimization requires rigorous physical

Table 4. Clustering results of the OBS conformations sampled in the D₂R/eticlopride and D₂R/risperidone simulations.

The compositions in each cluster are shown as percentages of the frames randomly extracted for each complex (see Materials and methods), when sorted by either receptor/ligand complex or EL2 conformation.

Cluster ID	Percentage (%)							
	Complex				EL2 conformation			
	D ₂ R/eticlopride		D ₂ R/risperidone		Extended		Helical	
	Mean	Sd	Mean	Sd	Mean	Sd	Mean	Sd
1	38.4	0.7	0.0	0.0	4.9	0.4	33.5	0.5
2	61.6	0.7	0.0	0.0	45.1	0.4	16.5	0.6
3	0.0	0.0	43.7	1.0	2.5	0.4	41.3	0.8
4	0.0	0.0	56.3	1.0	47.5	0.4	8.7	0.8

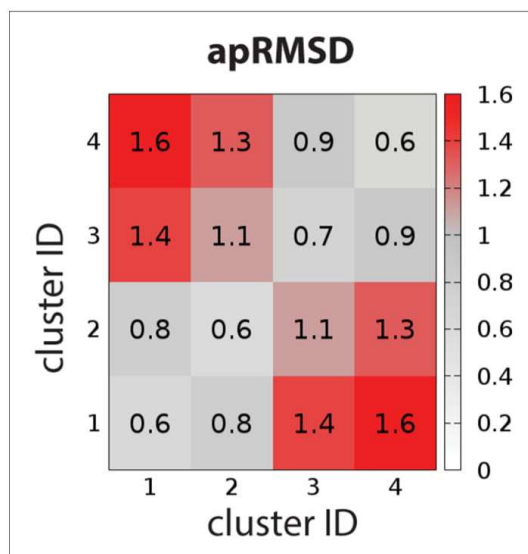


Figure 7. The average pairwise RMSDs of the clusters of the OBS conformations. The clustering level was chosen to be 4, so that the average pairwise RMSDs (apRMSDs) between the D₂R/eticlopride clusters (1 and 2, see Table 4 for the composition of each cluster) and D₂R/risperidone clusters (3 and 4) are similar to that between D₂R and D₃R structures (1.2 Å), while all the apRMSDs within a cluster are smaller than those between any given two clusters.

description of molecular recognition (Beuming and Shi, 2017), which depends on adequate understanding of the conformational boundary and flexibility of the targeted state. We have shown previously that both dopamine receptor subtype selectivity and modulation of agonist efficacy can be achieved through the design of ligands that extend from the OBS into an extracellular secondary binding pocket (SBP) (Michino et al., 2015a; Newman et al., 2012). We now show that one might consider the occupation of the Ile^{3.40} sub-pocket in the process of decorating an D₂R antagonist scaffold to attain a desired level of inverse agonism. Our findings also reveal allosteric communication between the Ile^{3.40} sub-pocket and the Na⁺-binding site. Thus, Na⁺ sensitivity in antagonist binding may provide useful mechanistic insights as part of such efforts.

The mutation of Trp100^{EL1.50} in D₂R to alanine, leucine or phenylalanine cause substantial increases in both the association and dissociation rate of risperidone (Wang et al., 2018). Curiously, both the dissociation and association rates of D₂R antagonists used as antipsychotics have been proposed to determine their propensity to cause extrapyramidal side-effects and hyperprolactinaemia (Seeman, 2014; Sykes et al., 2017). Our results indicate that both the EL2 conformation and antagonist scaffolds may influence the dynamics of Trp100^{EL1.50}, which in turn controls ligand access and egress to and from the OBS. Thus, understanding the relationship between the distinct inactive D₂R conformations stabilized by different antagonist scaffolds and these kinetic parameters will likely be important to facilitate the design of D₂R antagonists with an optimal kinetic profile that minimizes the risk of side effects.

Previously, using the substituted-cysteine accessibility method (SCAM) in D₂R (Javitch et al., 2000; Shi and Javitch, 2004), we found that G173^{EL2.37}C, N175^{EL2.39}C, and I184^{EL2.52}C were accessible to charged MTS reagents and that this accessibility could be blocked by the bound Na⁺-sensitive antagonist sulpiride, consistent with their water accessibility and involvement in ligand binding and not with a static orientation facing lipid, whereas A177^{EL2.45}C and I183^{EL2.51}C were accessible but not protected by sulpiride. Curiously, in the D₂R/risperidone structure, Ile184^{EL2.52} is only marginally in contact with the ligand, Ile183^{EL2.51} blocks the accessibility of Gly173^{EL2.37} to the OBS and

is itself buried in a hydrophobic pocket, whereas Asn175^{EL2.39} faces lipid, where it would be much less reactive. In the D₃R/eticlopride structure, Ile183^{EL2.52} is in close contact with the bound ligand, Ser182^{EL2.51} faces the extracellular vestibule, whereas the sidechain of Asn173^{EL2.39} is oriented toward the OBS (Figure 5—figure supplement 5). Thus, our analysis shows that the accessibility pattern of EL2 revealed by previous SCAM studies in D₂R are more consistent with the extended EL2 conformation revealed by the D₃R/eticlopride structure but not with the D₂R/risperidone structure. Indeed, we observed spontaneous transitions of EL2 from a helical to extended conformation in our D₂R simulations, which suggests that EL2 of D₂R exists in an ensemble of structured and unwound conformations, with substantial occupation of the configuration found in the D₃R structure. Such dynamics of EL2 suggest that the drastically different conformations between the D₂R and D₃R structures near EL2 are not related to the divergence of the receptors. Thus, the D₂R EL2 appears to have quite dramatic dynamics that are not captured by the crystal structure.

Taken together, our findings reveal that both the plasticity of the transmembrane domain in accommodating different scaffolds and the dynamics of EL2 and EL1 are important considerations in RDD targeting the inactive conformation of D₂R.

Materials and methods

Key resources table

Reagent type (species) or resource	Designation	Source or reference	Identifiers	Additional information
Cell line (<i>Cricetulus griseus</i>)	FlpIn CHO	Invitrogen	Cat# R75807	
Transfected construct (human)	SNAP-D ₂ R	Cisbio	Cat# pSNAPD2	
Transfected construct (human)	D ₂ R G _{αA} -RLuc8 Gβ1 Gγ2-Venus	Michino et al., 2017	N/A	
Commercial assay or kit	Spiperone-d2 SNAP-Lumi4-Tb 5x SNAP/CLIP labeling medium	Cisbio	Cat# L0002RED Cat# SSNPTBX Cat# LABMED	
Chemical compound, drug	Na bisulfite Glucose (+)-Butaclamol Risperidone Haloperidol	Sigma Aldrich	Cat# 243973 Cat# D9434 Cat# D033 Cat# R3030 Cat# H1512	
Chemical compound, drug	Spiperone	Cayman chemicals	Cat# 19769	
Chemical compound, drug	Eticlopride HCl Raclopride (-)-Sulpiride Quinpirole	Tocris Bioscience	Cat# 1847 Cat# 1810 Cat# 0895 Cat# 1061	
Chemical compound, drug	[³ H]spiperone	Perkin Elmer	Cat# NET1187250UC	
Chemical compound, drug	Polyethylenimine	Polysciences	Cat# 23966	
Chemical compound, drug	Coelenterazine-h	NanoLight Technology	Cat# 301-5	
Software, algorithm	Prism	GraphPad	v7.0 and v8.2.1	

Residue indices in EL1 and EL2

Based on a systematic analysis of aminergic receptors, we found a Trp in the middle of EL1 and the disulfide-bonded Cys in the middle of EL2 are the most conserved residues in each segment, and defined their residue indices as EL1.50 and EL2.50, respectively (Michino et al., 2015a). In this study, for the convenience of comparisons among D₂R, D₃R, and D₄R, and 5-HT_{2A}R, based on the

alignments of EL1 And EL2 shown in **Figure 5—figure supplement 1**, we index the EL1 and EL2 residues of each receptor in the same way as the Ballesteros-Weinstein numbering, for example the residues before and after the EL2.50 are EL2.49 and EL2.51, respectively. Note the indices for the shorter sequences are not necessarily be consecutive, given the gaps in the alignment.

Molecular modeling and docking

The D₂R models in this study are based on the corrected crystal structure of D₂R bound to risperidone (PDB: 6CM4) (Wang *et al.*, 2018). We omitted T4 Lysozyme fused into intracellular loop 3. Three thermostabilizing mutations (Ile122^{3.40}A, L375^{6.37}A, and L379^{6.41}A) were reverted to their WT residues. The missing N terminus in the crystal structure was built de novo using Rosetta (Bradley *et al.*, 2005), and then integrated with the rest of the D₂R model using Modeller (John and Sali, 2003). Using Modeller, we also extended two helical turns at the TM5 C terminus and three residues at the TM6 N terminus of the structure and connected these two ends with a 9 Gly loop, similar to our experimentally validated treatment of D₃R models (Michino *et al.*, 2017). The position of the Na⁺ bound in the canonical Na⁺-binding site near the negatively charged Asp^{2.50} was acquired by superimposing the Na⁺-bound structure of adenosine A_{2A} receptor (Liu *et al.*, 2012) to our D₂R models.

The binding poses of risperidone and eticlopride were taken according to their poses in the D₂R (Wang *et al.*, 2018) and D₃R (Chien *et al.*, 2010) structures, respectively. Docking of spiperone in our D₂R model was performed using the induced-fit docking (IFD) protocol (Sherman *et al.*, 2006) in the Schrodinger software (release 2017–2; Schrodinger, LLC: New York NY). Based on our hypothesis regarding the role of the Ile^{3.40} sub-pocket in the Na⁺ sensitivity (see text), from the resulting poses of IFD, we choose the spiperone pose with the F-substitution on the butyrophenone ring occupying the Ile^{3.40} sub-pocket. Note that in risperidone and spiperone the F-substitutions have similar distances to the protonated N atoms that interact with Asp^{3.32} (measured by the number of carbon atoms between them, **Figure 1—figure supplement 1**).

Molecular dynamics (MD) simulations

MD simulations of the D₂R and D₃R complexes were performed in the explicit water and 1-palmitoyl-2-oleoylphosphatidylcholine (POPC) lipid bilayer environment using Desmond MD System (version 4.5; D. E. Shaw Research, New York, NY) with either the OPLS3e force field (Roos *et al.*, 2019) or the CHARMM36 force field (Best *et al.*, 2012; Klauda *et al.*, 2010; MacKerell *et al.*, 1998; MacKerell *et al.*, 2004) and TIP3P water model. For CHARMM36 runs, the eticlopride parameters were obtained through the GAAMP server (Huang and Roux, 2013), with the initial force field based on CGenFF assigned by ParamChem (Vanommeslaeghe *et al.*, 2010). The system charges were neutralized, and 150 mM NaCl was added. Each system was first minimized and then equilibrated with restraints on the ligand heavy atoms and protein backbone atoms, followed by production runs in an isothermal-isobaric (NPT) ensemble at 310 K and one atm with all atoms unrestrained, as described previously (Michino *et al.*, 2017; Michino *et al.*, 2015b). We used Langevin constant pressure and temperature dynamical system (Feller *et al.*, 1995) to maintain the pressure and the temperature, on an anisotropic flexible periodic cell with a constant-ratio constraint applied on the lipid bilayer in the X-Y plane. For each condition, we collected multiple trajectories, the aggregated simulation length is ~392 μ s (**Table 1**).

While the majority of our D₂R simulations in this study used the OPLS3e force field, to compare with the D₃R simulations using CHARMM36 that have been continued from the previously reported shorter trajectories (Michino *et al.*, 2017; Michino *et al.*, 2015b), we carried out the D₂R/eticlopride simulations using both the OPLS3e and CHARMM36 force fields (see **Table 1**). We did not observe significant differences and pooled their results together for the analysis.

Conformational analysis

Distances and dihedral angles of MD simulation results were calculated with MDTraj (version 1.8.2) (McGibbon *et al.*, 2015) in combination with in-house Python scripts.

To characterize the structural changes in the receptor upon ligand binding, we quantified differences of structural elements between the D₂R/eticlopride and D₂R/risperidone conditions (using last 600 ns from a representative trajectory for each condition), by applying the previously described

pairwise interaction analyzer for GPCR (PIA-GPCR) (Michino *et al.*, 2017). The subsegments on the extracellular side of D₂R were defined as following: TM1e (the extracellular subsegment (e) of TM1, residues 31–38), TM2e (residues 92–96), TM3e (residues 104–113), TM4e (residues 166–172), TM5e (residues 187–195), TM6e (residues 364–369), and TM7e (residues 376–382).

For the PIA-GPCR analysis in Figure 4 and the distance analysis in Figure 6, we used the set of ligand-binding residues previously identified by our systematic analysis of GPCR structures. Specifically, for D₂R, they are residues 91, 94, 95, 100, 110, 111, 114, 115, 118, 119, 122, 167, 184, 189, 190, 193, 194, 197, 198, 353, 357, 360, 361, 364, 365, 367, 368, 376, 379, 380, 383, 384, 386, and 387; for D₃R, they are residues 86, 89, 90, 96, 106, 107, 110, 111, 114, 115, 118, 165, 183, 188, 189, 192, 193, 196, 197, 338, 342, 345, 346, 349, 350, 352, 353, 362, 365, 366, 369, 370, 372, and 373.

For the clustering of the OBS conformations, we used representative D₂R/eticlopride and D₂R/risperidone MD trajectories in which EL2 transitioned from the helical to unwound conformations. For each complex, using the Ile183-Asn186 distance as a criterion to differentiate the EL2 conformation (Figure 5), 1000 MD frames with helical EL2 conformations and another 1000 frames with extended EL2 conformations were randomly selected. For these 4000 frames, the pairwise RMSD of the backbone heavy atoms of the OBS residues defined in Michino *et al.* (2015a), except for Ile184^{EL2.52}, were calculated. The resulting 4000 × 4000 matrix was used to cluster these frames using the k-mean algorithm implemented in R. We chose *nstart* to be 20 to assure the convergence of cluster centroids and boundaries. We chose the clustering level to be 4, so that the average pairwise RMSDs (apRMSDs) between the D₂R/eticlopride and D₂R/risperidone clusters are similar to that between D₂R and D₃R structures (1.2 Å), while all the apRMSDs within a cluster are smaller than those between any given two clusters. The same frame selection and clustering procedure was repeated to 20 times. The averages of these 20 runs for the compositions of each cluster were reported in Table 4.

Markov State Model (MSM) analysis

The MSM analysis was performed using the pyEMMA program (version 2.5.5) (Scherer *et al.*, 2015). To characterize the dynamics of EL2 of D₂R, specifically the transitions between helical and extended conformations of its C-terminal portion, we focused on a key hydrogen bond formed in the helical conformation between the backbone carbonyl group of Ile183 and the backbone amine group of Asn186. Thus, for each of the simulated conditions, the distance of Ile183-Asn186 (Ser182-Asn185 in D₃R) was used as an input feature for the MSM analysis. We discretized this feature into two clusters – distances below and above 4 Å (i.e. EL2 forming a helical conformation and unwinding). Implied relaxation timescale (ITS) (Swope *et al.*, 2004) for the transition between these clusters was obtained as a function of various lag times. Convergences of ITS for the MSMs for all conditions was achieved at a lag time of 300 ns (Figure 5—figure supplement 6), which we further used to estimate Bayesian Markov models with 500 transition matrix samples (Trendelkamp-Schroer and Noé, 2013). The maximum likelihood transition matrix was used to calculate the transition and equilibrium probabilities (π) shown in Figure 5 and Figure 5—figure supplement 3.

Cell culture and cell line generation

Site-directed mutagenesis was performed using the Quickchange method using pEF5/DEST/FRT plasmid encoding FLAG-SNAP-D₂₅R as the DNA template. The mutagenesis was confirmed, and the full coding region was checked using Sanger sequencing at the DNA Sequencing Laboratory (University of Nottingham). Stable cell lines were generated using the Flp-In recombination system (Invitrogen).

[³H]spiperone binding assay

FlpIn CHO cells (Invitrogen) stably expressing WT or mutant SNAP-D₂₅s cells were cultured before the preparation of cell membrane as described before (Klein Herenbrink *et al.*, 2019). All stable cell lines were confirmed to be mycoplasma free. For saturating binding assays cell membranes (Mutant or WT SNAP-D₂₅-FlpIn CHO, 2.5 µg) were incubated with varying concentrations of [³H]spiperone and 10 µM haloperidol as a non-specific control, in binding buffer (20 mM HEPES, 100 mM NaCl, 6 mM MgCl₂, 1 mM EGTA, and 1 mM EDTA, pH 7.4) to a final volume of 200 µL and were incubated at 37°C for 3 hr. For competition binding assays, cell membranes (SNAP-D₂₅-FlpIn CHO,

2.5 µg) were incubated with varying concentrations of test compound in binding buffer containing 0.2 nM of [³H]spiperone to a final volume of 200 µL and were incubated at 37°C for 3 hr. Binding was terminated by fast-flow filtration using a Uniplate 96-well harvester (PerkinElmer) followed by five washes with ice-cold 0.9% NaCl. Bound radioactivity was measured in a MicroBeta2 LumiJET MicroBeta counter (PerkinElmer). Data were collected from at least three separate experiments performed in triplicate and analysed using non-linear regression (Prism 7, Graphpad software). For radioligand saturation binding data, the following equation was globally fitted to nonspecific and total binding data:

$$Y = \frac{B_{\max}[A]}{[A] + K_A} + NS[A] \quad (1)$$

where Y is radioligand binding, B_{max} is the total receptor density, [A] is the free radioligand concentration, K_A is the equilibrium dissociation constant of the radioligand, and NS is the fraction of non-specific radioligand binding. The B_{max} of the SNAP-tagged D2SRs were as follows; WT = 7.95 ± 1.63 pmol.mg⁻¹, 6.39 ± 1.04 pmol.mg⁻¹, 4.37 ± 0.92 pmol.mg⁻¹, 2.61 ± 0.50 pmol.mg⁻¹.

For competition binding assays, the concentration of ligand that inhibited half of the [³H]spiperone binding (IC₅₀) was determined by fitting the data to the following equation:

$$Y = \frac{Bottom + (Top - Bottom)}{1 + 10^{(X - LogIC_{50})n_H}} \quad (2)$$

where Y denotes the percentage specific binding, Top and Bottom denote the maximal and minimal asymptotes, respectively, IC₅₀ denotes the X-value when the response is midway between Bottom and Top, and n_H denotes the Hill slope factor. IC₅₀ values obtained from the inhibition curves were converted to K_i values using the Cheng and Prusoff equation. No statistical methods were used to predetermine sample size.

Bioluminescence resonance energy transfer (BRET) assay

The Go-protein activation assay uses a set of BRET-based constructs previously described (Michino *et al.*, 2017). Briefly, HEK293T cells were transiently co-transfected with pcDNA3.1 vectors encoding (i) D₂R, (ii) Gα_{oA} fused to Renilla luciferase 8 (RLuc8; provided by Dr. S. Gambhir, Stanford University, Stanford, CA) at residue 91, (iii) untagged Gβ1, and (iv) Gγ2 fused to mVenus. Transfections were performed using polyethyleneimine (PEI) at a ratio of 2:1 (PEI:total DNA; weight:weight), and cell culture was maintained as described previously (Bonifazi *et al.*, 2019). After ~48 hr of transfection, cells were washed with PBS and resuspended in PBS + 0.1% glucose + 200 µM Na Bisulfite buffer. Approximately 200,000 cells were then distributed in each well of the 96-well plates (White Lumitrac 200, Greiner bio-one). 5 µM Coelenterazine H, a luciferase substrate for BRET, was then added followed by addition of vehicle and test compounds using an automated stamp transfer protocol (Nimbus, Hamilton Robotics) from an aliquoted 96-well compound plate. Following ligands were used – quinpirole, eticlopride, raclopride, and (-)-sulpiride (Tocris Bioscience), (+)-butaclamol, dopamine, and risperidone (Sigma Aldrich), and Spiperone (Cayman chemicals). mVenus emission (530 nm) over RLuc 8 emission (485 nm) were then measured after 30 min of ligand incubation at 37°C using a PHERAstar FSX plate reader (BMG Labtech). BRET ratio was then determined by calculating the ratio of mVenus emission over RLuc eight emission.

Data were collected from at least nine independent experiments and analyzed using Prism 7 (GraphPad Software). Drug-induced BRET, defined by BRET ratio difference in the presence and absence of compounds, was calculated. Concentration response curves (CRCs) were generated using a non-linear sigmoidal dose-response analyses using Prism 7 (GraphPad Software). CRCs are presented as mean drug-induced BRET ± SEM. E_{max} bar graphs are plotted as the percentage of maximal drug-induced BRET by quinpirole ± SEM.

Tr-FRET ligand binding

Materials: Spiperone-d2, SNAP-Lumi4-Tb and 5x SNAP/CLIP labeling medium were purchased from Cisbio Bioassays. Eticlopride hydrochloride was purchased from Tocris Bioscience. Saponin was purchased from Fluka/Sigma-Aldrich. Bromocriptine, haloperidol, risperidone, spiperone, pluronic-F127,

Gpp(NH)p, DNA primers, Hanks Balanced Salt Solution H8264 (HBSS) and phosphate buffered saline (PBS) was purchased from Sigma-Aldrich.

Terbium cryptate labeling and membrane preparation

Terbium cryptate labeling of the SNAP-tagged receptors and membrane preparation was performed with minor changes to previously described methods (Klein Herenbrink *et al.*, 2016). Flp-In CHO-K1 cells stably expressing the mutant SNAP-D₂₅R constructs were grown in T175 flasks to approximately 90% confluency. Cell media was aspirated, and the cells were washed twice with 12 mL PBS. The cells were then incubated with terbium cryptate labeling reagent in 1xSNAP/CLIP labeling medium for 1 hr at in a humidified cell culture incubator with 5% CO₂ at 37°C. The terbium cryptate labeling reagent was then removed and the cells were washed once with 12 mL PBS. The labeled cells were then harvested in 10 mL PBS by cell scraping. Harvested cells were then collected by centrifugation at 300 g for 5 min and removal of the supernatant. The cell pellets were then frozen at –80°C for later membrane preparation. For cell membrane preparation, each cell pellet was removed from the –80°C freezer and thawed on ice. The pellet was then resuspended in 10 mL of ice-cold Buffer 1 (10mM HEPES 10 mM EDTA pH7.4). The pellet was then homogenised (IKA works T 10 basic Ultra-Turrax homogeniser) with eight bursts of 3 s on setting 4. The homogenized cells were transferred to an ultra-fast centrifuge tube and an additional 10 mL of Buffer one was added. The tube was then centrifuged at 48,000 g for 30 min at 4°C. The supernatant was discarded, 20 mL of Buffer one was added and the pellet was resuspended. The resuspension was then centrifuged a second time at 48,000 g for 30 min at 4°C. The supernatant was then removed, and the cell membrane pellet was collected by resuspension in 2 mL ice-cold Buffer 2 (10mM HEPES 0.1 mM EDTA pH 7.4). The resuspended membranes were then put through a syringe with a BD precision glide 26-gauge needle to make the solution uniform. Membrane protein concentration was determined by bicinchonic acid (BCA) assay detecting the absorbance at 562 nm on a CLARIOstar plate reader (BMG Labtech) using bovine serum albumin (BSA) as the protein standard. The cell membrane solution was then aliquoted and frozen at –80°C.

TR-FRET binding assay

All ligands were diluted in Binding Buffer (Hanks Balanced Salt Solution (Sigma H8264), 20 mM HEPES, 0.02% Pluronic-F127, 1% dimethyl sulfoxide, pH 7.4 (with KOH)). For competition binding experiments; 10 µL of spiperone-d2 in Binding Buffer was added to each well of a 384-well white optiplate LBS coated (PerkinElmer) at varied concentrations depending on the SNAP-D₂₅R mutant. 10 µL of increasing concentrations of unlabeled ligands were then added into the 10 µL of fluorescent ligand and mixed. A final concentration of 100 µM haloperidol was used to determine non-specific binding. Cell membranes were diluted to 0.075 µg/µL in Binding Buffer supplemented with 50 µg/mL saponin and 100 µM Gpp(NH)p.

TR-FRET measurements were acquired on a PHERAstar FS plate reader (BMG Labtech) at 37°C. The optiplate containing the ligand cocktails in the wells was incubated in the instrument for 6 min. The cell membrane solution was primed into the on-board injection system and incubated for 5 min. 20 µL of cell membrane solution was injected at 400 µL/s into the ligand cocktail wells to initiate the binding reaction. After 30-min incubation, the HTRF optic filter module was used to perform an excitation at 337 nm and simultaneous dual emission detection at 620 nm (terbium cryptate donor) and 665 nm (fluorescent ligand acceptor). The focal height was set to 10.4 mm. All experiments were performed in singlet wells. The TR-FRET binding values were determined by dividing the by the fluorescent ligand acceptor channel values by the terbium cryptate donor channel values and multiplying by 10,000. These values were then subtracted by the non-specific binding values determined in each experiment to give the specific HTRF ratio x 10,000. The data was then analysed with GraphPad Prism 8.2.1 using *Equations 1 and 2*.

Acknowledgements

Support for this research was provided by the National Institute on Drug Abuse–Intramural Research Program, Z1A DA000606-03 (LS), NIH grant MH54137 (JAJ) and National Health and Medical

Research Council (NHMRC) Project Grant APP1049564 (JRL). We thank Jackie Glenn for technical support in generating membrane preparations.

Additional information

Funding

Funder	Grant reference number	Author
National Institutes of Health	Z1A DA000606-03	Lei Shi
National Institutes of Health	MH54137	Jonathan A Javitch
National Health and Medical Research Council	APP1049564	J Robert Lane

The funders had no role in study design, data collection and interpretation, or the decision to submit the work for publication.

Author contributions

J Robert Lane, Conceptualization, Data curation, Formal analysis, Supervision, Funding acquisition, Investigation; Ara M Abramyan, Pramisha Adhikari, Ravi Kumar Verma, Herman D Lim, Hideaki Yano, Data curation, Formal analysis, Investigation; Alastair C Keen, Kuo-Hao Lee, Julie Sanchez, Formal analysis, Investigation; Jonathan A Javitch, Conceptualization, Investigation; Lei Shi, Conceptualization, Data curation, Formal analysis, Supervision, Funding acquisition, Investigation, Project administration

Author ORCIDs

Lei Shi  <https://orcid.org/0000-0002-4137-096X>

Decision letter and Author response

Decision letter <https://doi.org/10.7554/eLife.52189.sa1>

Author response <https://doi.org/10.7554/eLife.52189.sa2>

Additional files

Supplementary files

- Transparent reporting form

Data availability

All data generated or analysed during this study are included in the manuscript and supporting files.

References

- Abramyan AM, Quick M, Xue C, Javitch JA, Shi L. 2018. Exploring substrate binding in the extracellular vestibule of MhsT by atomistic simulations and markov models. *Journal of Chemical Information and Modeling* **58**:1244–1252. DOI: <https://doi.org/10.1021/acs.jcim.8b00175>, PMID: 29851339
- Amaro RE, Baudry J, Chodera J, Demir Ö, McCammon JA, Miao Y, Smith JC. 2018. Ensemble docking in drug discovery. *Biophysical Journal* **114**:2271–2278. DOI: <https://doi.org/10.1016/j.bpj.2018.02.038>, PMID: 29606412
- Ballesteros J, Weinstein H. 1995. Integrated methods for the construction of three-dimensional models of structure-function relations in G protein-coupled receptors. *Methods in Neurosciences* **25**:366–428. DOI: [https://doi.org/10.1016/S1043-9471\(05\)80049-7](https://doi.org/10.1016/S1043-9471(05)80049-7)
- Best RB, Zhu X, Shim J, Lopes PE, Mittal J, Feig M, Mackerell AD. 2012. Optimization of the additive CHARMM all-atom protein force field targeting improved sampling of the backbone ϕ , ψ and side-chain $\chi(1)$ and $\chi(2)$ dihedral angles. *Journal of Chemical Theory and Computation* **8**:3257–3273. DOI: <https://doi.org/10.1021/ct300400x>, PMID: 23341755
- Beuming T, Shi L. 2017. Editorial: computer aided Structure-based lead optimization. *Current Topics in Medicinal Chemistry* **17**:2575–2576. DOI: <https://doi.org/10.2174/156802661723170808161306>, PMID: 28889794

- Bonifazi A, Yano H, Guerrero AM, Kumar V, Hoffman AF, Lupica CR, Shi L, Newman AH. 2019. Novel and potent dopamine D₂ Receptor Go-Protein Biased Agonists. *ACS Pharmacology & Translational Science* **2**:52–65. DOI: <https://doi.org/10.1021/acspsci.8b00060>, PMID: 30775693
- Bradley P, Misura KM, Baker D. 2005. Toward high-resolution de novo structure prediction for small proteins. *Science* **309**:1868–1871. DOI: <https://doi.org/10.1126/science.1113801>, PMID: 16166519
- Chien EY, Liu W, Zhao Q, Katritch V, Han GW, Hanson MA, Shi L, Newman AH, Javitch JA, Cherezov V, Stevens RC. 2010. Structure of the human dopamine D₃ receptor in complex with a D₂/D₃ selective antagonist. *Science* **330**:1091–1095. DOI: <https://doi.org/10.1126/science.1197410>, PMID: 21097933
- Congreve M, Dias JM, Marshall FH. 2014. Structure-based drug design for G protein-coupled receptors. *Progress in Medicinal Chemistry* **53**:1–63. DOI: <https://doi.org/10.1016/B978-0-444-63380-4.00001-9>, PMID: 24418607
- Feller SE, Zhang Y, Pastor RW, Brooks BR. 1995. Constant pressure molecular dynamics simulation: the langevin piston method. *The Journal of Chemical Physics* **103**:4613–4621. DOI: <https://doi.org/10.1063/1.470648>
- Free RB, Chun LS, Moritz AE, Miller BN, Doyle TB, Conroy JL, Padron A, Meade JA, Xiao J, Hu X, Dulcey AE, Han Y, Duan L, Titus S, Bryant-Genevier M, Barnaeva E, Ferrer M, Javitch JA, Beuming T, Shi L, et al. 2014. Discovery and characterization of a G protein-biased agonist that inhibits β -arrestin recruitment to the D₂ dopamine receptor. *Molecular Pharmacology* **86**:96–105. DOI: <https://doi.org/10.1124/mol.113.090563>, PMID: 24755247
- Hirose T, Kikuchi T. 2005. Aripiprazole, a novel antipsychotic agent: dopamine D₂ receptor partial agonist. *The Journal of Medical Investigation* **52**:284–290. DOI: <https://doi.org/10.2152/jmi.52.284>, PMID: 16366516
- Huang L, Roux B. 2013. Automated force field parameterization for nonpolarizable and polarizable atomic models based on ab initio target data. *Journal of Chemical Theory and Computation* **9**:3543–3556. DOI: <https://doi.org/10.1021/ct4003477>
- Ioerger TR, Du C, Linthicum DS. 1999. Conservation of cys-cys trp structural triads and their geometry in the protein domains of immunoglobulin superfamily members. *Molecular Immunology* **36**:373–386. DOI: [https://doi.org/10.1016/S0161-5890\(99\)00032-2](https://doi.org/10.1016/S0161-5890(99)00032-2), PMID: 10444001
- Javitch JA, Shi L, Simpson MM, Chen J, Chiappa V, Visiers I, Weinstein H, Ballesteros JA. 2000. The fourth transmembrane segment of the dopamine D₂ receptor: accessibility in the binding-site crevice and position in the transmembrane bundle. *Biochemistry* **39**:12190–12199. DOI: <https://doi.org/10.1021/bi001069m>, PMID: 11015197
- John B, Sali A. 2003. Comparative protein structure modeling by iterative alignment, model building and model assessment. *Nucleic Acids Research* **31**:3982–3992. DOI: <https://doi.org/10.1093/nar/gkg460>, PMID: 12853614
- Kimura KT, Asada H, Inoue A, Kadji FMN, Im D, Mori C, Arakawa T, Hirata K, Nomura Y, Nomura N, Aoki J, Iwata S, Shimamura T. 2019. Structures of the 5-HT_{2A} receptor in complex with the antipsychotics risperidone and zotepine. *Nature Structural & Molecular Biology* **26**:121–128. DOI: <https://doi.org/10.1038/s41594-018-0180-z>
- Klauda JB, Venable RM, Freites JA, O'Connor JW, Tobias DJ, Mondragon-Ramirez C, Vorobyov I, MacKerell AD, Pastor RW. 2010. Update of the CHARMM all-atom additive force field for lipids: validation on six lipid types. *The Journal of Physical Chemistry B* **114**:7830–7843. DOI: <https://doi.org/10.1021/jp101759q>, PMID: 20496934
- Klein Herenbrink C, Sykes DA, Donthamsetti P, Canals M, Coudrat T, Shonberg J, Scammells PJ, Capuano B, Sexton PM, Charlton SJ, Javitch JA, Christopoulos A, Lane JR. 2016. The role of kinetic context in apparent biased agonism at GPCRs. *Nature Communications* **7**:10842. DOI: <https://doi.org/10.1038/ncomms10842>, PMID: 26905976
- Klein Herenbrink C, Verma R, Lim HD, Kopinathan A, Keen A, Shonberg J, Draper-Joyce CJ, Scammells PJ, Christopoulos A, Javitch JA, Capuano B, Shi L, Lane JR. 2019. Molecular determinants of the intrinsic efficacy of the antipsychotic aripiprazole. *ACS Chemical Biology* **14**:1780–1792. DOI: <https://doi.org/10.1021/acscchembio.9b00342>, PMID: 31339684
- Latorraca NR, Venkatakrishnan AJ, Dror RO. 2017. GPCR dynamics: structures in motion. *Chemical Reviews* **117**:139–155. DOI: <https://doi.org/10.1021/acs.chemrev.6b00177>, PMID: 27622975
- Liu W, Chun E, Thompson AA, Chubukov P, Xu F, Katritch V, Han GW, Roth CB, Heitman LH, IJzerman AP, Cherezov V, Stevens RC. 2012. Structural basis for allosteric regulation of GPCRs by sodium ions. *Science* **337**:232–236. DOI: <https://doi.org/10.1126/science.1219218>, PMID: 22798613
- MacKerell AD, Bashford D, Bellott M, Dunbrack RL, Evanseck JD, Field MJ, Fischer S, Gao J, Guo H, Ha S, Joseph-McCarthy D, Kuchnir L, Kuczera K, Lau FT, Mattos C, Michnick S, Ngo T, Nguyen DT, Prodhom B, Reiher WE, et al. 1998. All-atom empirical potential for molecular modeling and dynamics studies of proteins. *The Journal of Physical Chemistry B* **102**:3586–3616. DOI: <https://doi.org/10.1021/jp973084f>, PMID: 24889800
- MacKerell AD, Feig M, Brooks CL. 2004. Improved treatment of the protein backbone in empirical force fields. *Journal of the American Chemical Society* **126**:698–699. DOI: <https://doi.org/10.1021/ja036959e>, PMID: 14733527
- Malinauskaitė L, Quick M, Reinhard L, Lyons JA, Yano H, Javitch JA, Nissen P. 2014. A mechanism for intracellular release of Na⁺ by neurotransmitter/sodium symporters. *Nature Structural & Molecular Biology* **21**:1006–1012. DOI: <https://doi.org/10.1038/nsmb.2894>, PMID: 25282149
- Manglik A, Lin H, Aryal DK, McCorvey JD, Dengler D, Corder G, Levit A, Kling RC, Bernat V, Hübner H, Huang X-P, Sassano MF, Giguère PM, Löber S, Duan Da, Scherrer G, Koblika BK, Gmeiner P, Roth BL, Shoichet BK. 2016. Structure-based discovery of opioid analgesics with reduced side effects. *Nature* **537**:185–190. DOI: <https://doi.org/10.1038/nature19112>

- McCorvy JD, Butler KV, Kelly B, Rechsteiner K, Karpiak J, Betz RM, Kormos BL, Shoichet BK, Dror RO, Jin J, Roth BL. 2018. Structure-inspired design of β -arrestin-biased ligands for aminergic GPCRs. *Nature Chemical Biology* **14**:126–134. DOI: <https://doi.org/10.1038/nchembio.2527>, PMID: 29227473
- McGibbon RT, Beauchamp KA, Harrigan MP, Klein C, Swails JM, Hernández CX, Schwantes CR, Wang LP, Lane TJ, Pande VS. 2015. MDTraj: a modern open library for the analysis of molecular dynamics trajectories. *Biophysical Journal* **109**:1528–1532. DOI: <https://doi.org/10.1016/j.bpj.2015.08.015>, PMID: 26488642
- Michino M, Donthamsetti P, Beuming T, Banala A, Duan L, Roux T, Han Y, Trinquet E, Newman AH, Javitch JA, Shi L. 2013. A single glycine in extracellular loop 1 is the critical determinant for pharmacological specificity of dopamine D2 and D3 receptors. *Molecular Pharmacology* **84**:854–864. DOI: <https://doi.org/10.1124/mol.113.087833>, PMID: 24061855
- Michino M, Beuming T, Donthamsetti P, Newman AH, Javitch JA, Shi L. 2015a. What can crystal structures of aminergic receptors tell us about designing subtype-selective ligands? *Pharmacological Reviews* **67**:198–213. DOI: <https://doi.org/10.1124/pr.114.009944>, PMID: 25527701
- Michino M, Free RB, Doyle TB, Sibley DR, Shi L. 2015b. Structural basis for Na⁺-sensitivity in dopamine D2 and D3 receptors. *Chemical Communications* **51**:8618–8621. DOI: <https://doi.org/10.1039/c5cc02204e>
- Michino M, Boateng CA, Donthamsetti P, Yano H, Bakare OM, Bonifazi A, Ellenberger MP, Keck TM, Kumar V, Zhu C, Verma R, Deschamps JR, Javitch JA, Newman AH, Shi L. 2017. Toward understanding the structural basis of partial agonism at the dopamine D₃ Receptor. *Journal of Medicinal Chemistry* **60**:580–593. DOI: <https://doi.org/10.1021/acs.jmedchem.6b01148>, PMID: 27983845
- Neve KA. 1991. Regulation of dopamine D2 receptors by sodium and pH. *Molecular Pharmacology* **39**:570–578. PMID: 2017157
- Newman AH, Beuming T, Banala AK, Donthamsetti P, Pongetti K, LaBounty A, Levy B, Cao J, Michino M, Luedtke RR, Javitch JA, Shi L. 2012. Molecular determinants of selectivity and efficacy at the dopamine D3 receptor. *Journal of Medicinal Chemistry* **55**:6689–6699. DOI: <https://doi.org/10.1021/jm300482h>, PMID: 22632094
- Newton CL, Wood MD, Strange PG. 2016. Examining the effects of sodium ions on the binding of antagonists to dopamine D2 and D3 receptors. *PLoS ONE* **11**:e0158808. DOI: <https://doi.org/10.1371/journal.pone.0158808>, PMID: 27379794
- Piana S, Lindorff-Larsen K, Shaw DE. 2011. How robust are protein folding simulations with respect to force field parameterization? *Biophysical Journal* **100**:L47–L49. DOI: <https://doi.org/10.1016/j.bpj.2011.03.051>, PMID: 21539772
- Rasmussen SG, Choi HJ, Fung JJ, Pardon E, Casarosa P, Chae PS, Devree BT, Rosenbaum DM, Thian FS, Kobilka TS, Schnapp A, Konetzki I, Sunahara RK, Gellman SH, Pautsch A, Steyaert J, Weis WI, Kobilka BK. 2011. Structure of a nanobody-stabilized active state of the $\beta(2)$ adrenoceptor. *Nature* **469**:175–180. DOI: <https://doi.org/10.1038/nature09648>, PMID: 21228869
- Roberts DJ, Strange PG. 2005. Mechanisms of inverse agonist action at D2 dopamine receptors. *British Journal of Pharmacology* **145**:34–42. DOI: <https://doi.org/10.1038/sj.bjp.0706073>, PMID: 15735658
- Roos K, Wu C, Damm W, Reboul M, Stevenson JM, Lu C, Dahlgren MK, Mondal S, Chen W, Wang L, Abel R, Friesner RA, Harder ED. 2019. OPLS3e: extending force field coverage for Drug-Like small molecules. *Journal of Chemical Theory and Computation* **15**:1863–1874. DOI: <https://doi.org/10.1021/acs.jctc.8b01026>, PMID: 30768902
- Roth BL, Lopez E, Patel S, Kroeze WK. 2000. The multiplicity of serotonin receptors: uselessly diverse molecules or an embarrassment of riches? *The Neuroscientist* **6**:252–262. DOI: <https://doi.org/10.1177/107385840000600408>
- Scherer MK, Trendelkamp-Schroer B, Paul F, Pérez-Hernández G, Hoffmann M, Plattner N, Wehmeyer C, Prinz JH, Noé F. 2015. PyEMMA 2: a software package for estimation, validation, and analysis of markov models. *Journal of Chemical Theory and Computation* **11**:5525–5542. DOI: <https://doi.org/10.1021/acs.jctc.5b00743>, PMID: 26574340
- Seeman P. 2014. Clozapine, a fast-off-D2 antipsychotic. *ACS Chemical Neuroscience* **5**:24–29. DOI: <https://doi.org/10.1021/cn400189s>, PMID: 24219174
- Sherman W, Day T, Jacobson MP, Friesner RA, Farid R. 2006. Novel procedure for modeling ligand/receptor induced fit effects. *Journal of Medicinal Chemistry* **49**:534–553. DOI: <https://doi.org/10.1021/jm050540c>, PMID: 16420040
- Shi L, Javitch JA. 2004. The second extracellular loop of the dopamine D2 receptor lines the binding-site crevice. *PNAS* **101**:440–445. DOI: <https://doi.org/10.1073/pnas.2237265100>, PMID: 14704269
- Sibley DR, Shi L. 2018. A new era of rationally designed antipsychotics. *Nature* **555**:170–172. DOI: <https://doi.org/10.1038/d41586-018-02328-z>, PMID: 29517027
- Silvestre JS, Prous J. 2005. Research on adverse drug events. I. Muscarinic M3 receptor binding affinity could predict the risk of antipsychotics to induce type 2 diabetes. *Methods and Findings in Experimental and Clinical Pharmacology* **27**:289–304. DOI: <https://doi.org/10.1358/mf.2005.27.5.908643>
- Stolzenberg S, Li Z, Quick M, Malinauskaitė L, Nissen P, Weinstein H, Javitch JA, Shi L. 2017. The role of transmembrane segment 5 (TM5) in Na² release and the conformational transition of neurotransmitter:sodium symporters toward the inward-open state. *Journal of Biological Chemistry* **292**:7372–7384. DOI: <https://doi.org/10.1074/jbc.M116.757153>
- Swope WC, Pitera JW, Suits F. 2004. Describing Protein Folding Kinetics by Molecular Dynamics Simulations. 1. Theory ¹. *The Journal of Physical Chemistry B* **108**:6571–6581. DOI: <https://doi.org/10.1021/jp037421y>

- Sykes DA, Moore H, Stott L, Holliday N, Javitch JA, Lane JR, Charlton SJ. 2017. Extrapyramidal side effects of antipsychotics are linked to their association kinetics at dopamine D2 receptors. *Nature Communications* **8**:763. DOI: <https://doi.org/10.1038/s41467-017-00716-z>
- Trendelkamp-Schroer B, Noé F. 2013. Efficient bayesian estimation of markov model transition matrices with given stationary distribution. *The Journal of Chemical Physics* **138**:164113. DOI: <https://doi.org/10.1063/1.4801325>, PMID: 23635117
- Vanommeslaeghe K, Hatcher E, Acharya C, Kundu S, Zhong S, Shim J, Darian E, Guvench O, Lopes P, Vorobyov I, Mackerell AD. 2010. CHARMM general force field: a force field for drug-like molecules compatible with the CHARMM all-atom additive biological force fields. *Journal of Computational Chemistry* **31**:671–690. DOI: <https://doi.org/10.1002/jcc.21367>, PMID: 19575467
- Venkatakrisnan AJ, Deupi X, Lebon G, Tate CG, Schertler GF, Babu MM. 2013. Molecular signatures of G-protein-coupled receptors. *Nature* **494**:185–194. DOI: <https://doi.org/10.1038/nature11896>, PMID: 23407534
- Wang S, Wacker D, Levit A, Che T, Betz RM, McCorvy JD, Venkatakrisnan AJ, Huang XP, Dror RO, Shoichet BK, Roth BL. 2017. D₄ dopamine receptor high-resolution structures enable the discovery of selective agonists. *Science* **358**:381–386. DOI: <https://doi.org/10.1126/science.aan5468>, PMID: 29051383
- Wang S, Che T, Levit A, Shoichet BK, Wacker D, Roth BL. 2018. Structure of the D2 dopamine receptor bound to the atypical antipsychotic drug risperidone. *Nature* **555**:269–273. DOI: <https://doi.org/10.1038/nature25758>, PMID: 29466326
- Weis WI, Kobilka BK. 2018. The molecular basis of G Protein-Coupled receptor activation. *Annual Review of Biochemistry* **87**:897–919. DOI: <https://doi.org/10.1146/annurev-biochem-060614-033910>, PMID: 29925258
- Zhang B, Albaker A, Plouffe B, Lefebvre C, Tiberi M. 2014. Constitutive activities and inverse agonism in dopamine receptors. *Advances in Pharmacology* **70**:175–214. DOI: <https://doi.org/10.1016/B978-0-12-417197-8.00007-9>, PMID: 24931197

